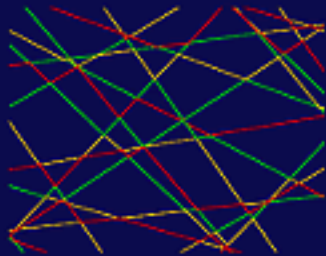# QUANTUM PHASE TRANSITIONS

QUANTUM PHASE TRANSITIONS

SUBIR SACHDEV

Professor of Physics,
Yale University,
New Haven, CT 06520-8120, USA

To
Menaka, Monisha and Usha

Contents

Preface

The last decade has seen a substantial rejuvenation of interest in the study of quantum phase transitions, driven by experiments on the cuprate superconductors, the heavy fermion materials, organic conductors and related compounds. Although quantum phase transitions in simple spin systems, like the Ising model in a transverse field, were studied in the early 70's, much of the subsequent theoretical work examined a particular example: the metal-insulator transition. While this is a subject of considerable experimental importance, the greatest theoretical progress was made for the case of the Anderson transition of non-interacting electrons, which is driven by the localization of the electronic states in the presence of a random potential. The critical properties of this transition of non-interacting electrons constituted the primary basis upon which most condensed matter physicists have formed their intuition on the behavior of the systems near a quantum phase transition. On the other hand, it is clear that strong electronic interactions play a crucial in the systems of current interest noted earlier, and simple paradigms for the behavior of such systems near quantum critical points are not widely known.

It is the purpose of this book to move interactions to center stage by describing and classifying the physical properties of the simplest interacting systems undergoing a quantum phase transition. The effects of disorder will be neglected for the most part, but will be considered in the concluding chapters. Our focus will be on the dynamical properties of such systems at non-zero temperature, and it shall become apparent that these differ substantially from the non-interacting case. We shall also be considering inelastic collision-dominated quantum dynamics and transport: this will apply to clean physical systems whose inelastic scattering time is much *shorter* than their disorder-induced elastic scattering

time. This is the converse of the usual theoretical situation in Anderson localization or mesoscopic system theory, where inelastic collision times are conventionally taken to be much *larger* than all other time scales.

One of the most interesting and significant regimes of the systems we shall study is one in which the inelastic scattering and phase coherence times are of order $\hbar/k_B T$, where T is the absolute temperature. The importance of such a regime was pointed out by Varma *et al.* [510, 511] by an analysis of transport and optical data on the cuprate superconductors. Neutron scattering measurements of Hayden *et al.* [220] and Keimer *et al.* [267] also supported such an interpretation in the low doping region. It was subsequently realized [440, 97, 424] that the inelastic rates are in fact a *universal number* times $k_B T/\hbar$, and are a robust property of the high temperature limit of renormalizable, interacting quantum field theories which are not asymptotically free at high energies. In the Wilsonian picture, such a field theory is defined by renormalization group flows away from a critical point describing a second order quantum phase transition. It is not essential for this critical point to be in an experimentally accessible regime of the phase diagram: the quantum field theory it defines may still be an appropriate description of the physics over a substantial intermediate energy and temperature scale. Among the implications of such an interpretation of the experiments was the requirement that response functions should have prefactors of anomalous powers of T and a singular dependence on the wavevector; recent observations of Aeppli *et al* [2], at somewhat higher dopings, appear to be consistent with this. These recent experiments also suggest that the appropriate quantum critical point may be one involving competition between an insulating state in which the holes have crystallized into a striped arrangement, and a d-wave superconductor. There is no theory yet for such quantum transitions, but we shall discuss numerous simpler models here which capture some of the basic features.

It is also appropriate to note here theoretical studies [341, 23, 504, 103, 104] on the relevance of finite temperature crossovers near quantum critical points of Fermi liquids [225] to the physics of the heavy fermion compounds.

A separate motivation for the study of quantum phase transitions is simply the value in having another perspective on the physics of an interacting many body system. A traditional analysis of such a system would begin from either a weak coupling Hamiltonian, and then build in interactions among the nearly free excitations, or from a strong-coupling limit, where the local interactions are well accounted for, but their coher-

ent propagation through the system is not fully described. In contrast, a quantum critical point begins from an intermediate coupling regime which straddles these limiting cases. One can then use the powerful technology of scaling, relevant and irrelevant operators, to set up a systematic expansion of physical properties away from the special critical point. For many low-dimensional strongly correlated systems, I believe that such an approach holds the most promise for a comprehensive understanding. Many of the vexing open problems are related to phenomena at intermediate temperatures, and this is precisely the region over which the influence of a quantum critical point is dominant. One of these open problems is the appearance of the so-called pseudo-gap in the high temperature superconductors, and, as we shall see in Chapters 7 and 8, pseudo-gap like features indeed appear over a wide temperature range in systems near quantum critical points. Related ideas also appear in recent discussions by Laughlin [293].

The particular quantum phase transitions that are examined in this book are undoubtedly heavily influenced by my own research. However, I do believe that my choices can also be justified on pedagogical grounds, and lead to a logical development of the main physical concepts in the simplest possible contexts. Throughout, I have also attempted to provide experimental motivations for the models considered: this is mainly in the form of a guide to the literature, rather than in-depth discussion of the experimental issues. A more experimentally oriented introduction to the subject of quantum phase transitions can be found in the excellent review article of Sondhi, Girvin, Carini and Shahar [469]. Readers may also be interested in a recent introductory article [520], intended for a general science audience.

Many important topics have been omitted from this book due to the limitations of space, time and my expertise. The reader may find discussion on the metal insulator transition of electronic systems in the presence of disorder and interactions in a number of reviews [299, 73, 149, 47, 237]. The fermionic Hubbard model, and its metal insulator transition is discussed in most useful treatises by Georges, Kotliar, Krauth and Rozenberg [177] and Gebhard [172]. I have also omitted discussions of quantum phase transitions in quantum Hall systems: these are reviewed by Sondhi *et al.* [469] by Huckenstein [230], and also in the collections edited by Prange and Girvin [393] and Das Sarma and Pinczuk [119] (however, some magnetic transitions in quantum Hall systems [377, 378] will be briefly noted). Quantum impurity problems are also not discussed, although these have been the focus of much recent theoretical

and experimental interest; useful discussions of significant developments may be found in Refs [368, 302, 525, 12, 144, 262, 303, 516, 106, 107, 374, 376].

Some recent books and review articles offer the reader a complementary perspective on the topics covered: I note the works of Fradkin [162], Auerbach [30], Continentino [103] ,Tsvelik [503] and Chakrabarti, Dutta and Sen [82], and I will occasionally make contact with some of them.

How to use this book

I wrote most of this book at a level which should be accessible to graduate students who have completed the standard core curriculum of courses required for a master's degree. In principle, I also do not assume a detailed knowledge of the renormalization group and its application to the theory of second-order phase transitions in classical systems at nonzero temperature. I provide a synopsis of the needed background in the context of quantum systems, but my treatment is surely too concise to be comprehensible to students who have not had a prior exposure to this well-known technology. I decided it would be counterproductive for me to enter into an in-depth discussion of topics for which numerous excellent texts are already available. In particular, the texts by Ma [318], Itzykson and Drouffe [247] and Goldenfeld [184], and the review article by Brézin *et al.* [63] can serve as useful companions to this book.

An upper level graduate course on quantum statistical mechanics can be taught on selected topics from this book, as I have done at Yale. I suggest that such a course begin by covering all of Part 1 (excluding Section 3.2), followed by Chapters 4, 5, and 8 from Part 2. The material in Chapter 8 should be supplemented by some of the readings on the renormalization group mentioned above. Depending upon student interest and time, I would then pick from Chapters 10–12 (as a group), Chapter 13 (until Section 13.3.1), and Chapter 14 from Part 3. A more elementary course should skip Chapters 8 and 10–12. The chapters not mentioned in this paragraph are at a more advanced level, and can serve as starting points for student presentations.

Readers who are newcomers to the subject of quantum phase transitions should read the chapters selected above first. More advanced readers should go through all the chapters in the order they appear.

Subir Sachdev

Acknowledgements

Part one

Introduction

1

Basic concepts

1.1 What is a quantum phase transition ?

Consider a Hamiltonian, $H(g)$, whose degrees of freedom reside on the sites of a lattice, and which varies as a function of a dimensionless coupling g. Let us follow the evolution of the ground state energy of $H(g)$ as a function of g. For the case of a finite lattice, this ground state energy will generically be a smooth, analytic function of g. The main possibility of an exception comes from the case when g couples only to a conserved quantity (*i.e.*, $H(g) = H_0 + gH_1$ where H_0 and H_1 commute). This means that H_0 and H_1 can be simultaneously diagonalized and so the eigenfunctions are independent of g even though the eigenvalues vary with g: then there can be a level crossing where an excited level becomes the ground state at $g = g_c$ (say), creating a point of non-analyticity of the ground state energy as a function of g (see Fig 1.1). The possibilities for an *infinite* lattice are richer. An avoided level-crossing between the ground and an excited state in a finite lattice could become progressively sharper as the lattice size increases, leading to a non-analyticity at $g = g_c$ in the infinite lattice limit. We shall identify any point of non-analyticity in the ground state energy of the infinite lattice system as a quantum phase transition: the non-analyticity could be either the limiting case of an avoided level crossing, or an actual level crossing. The first kind is more common, but we shall also discuss transitions of the second kind in Chapters 11 and 13. The phase transition is usually accompanied by a qualitative change in the nature of the correlations in the ground state, and describing this change shall clearly be one of our major interests.

Actually our focus shall be on a limited class of quantum phase transitions which are *second order*. Loosely speaking, these are transitions
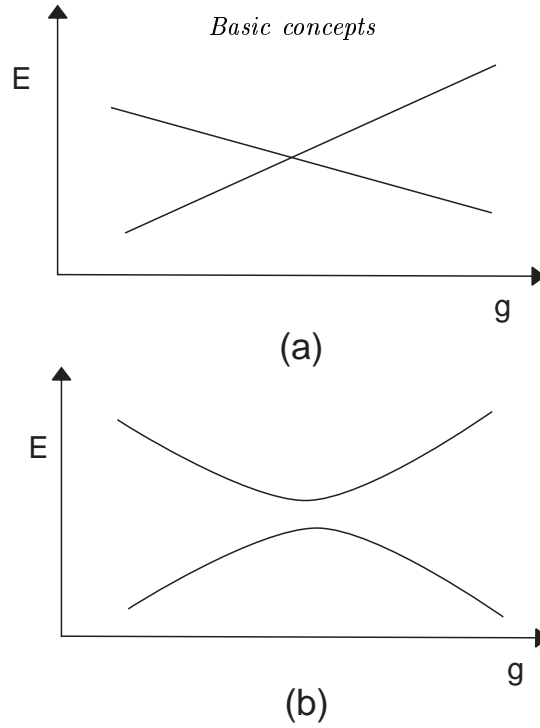
Fig. 1.1. Low eigenvalues, E, of a Hamiltonian $H(g)$ on a finite lattice, as a function of some dimensionless coupling g. For the case where $H(g) = H_0 + gH_1$, where H_0 and H_1 commute and are independent of g, there can be an actual level-crossing, as in (a). More generally, however, there is an "avoided level-crossing", as in (b).

at which the characteristic energy scale of fluctuations above the ground state vanishes as g approaches g_c. Let the energy Δ represent a scale characterizing some significant spectral density of fluctuations at zero temperature (T) for $g \neq g_c$. Thus Δ could be the energy of the lowest excitation above the ground state, if this is non-zero (*i.e.*, there is an energy gap Δ), or if there are excitations at arbitrarily low energies in the infinite lattice limit (*i.e.*, the energy spectrum is *gapless*), Δ is the scale at which there is a qualitative change in the nature of the frequency spectrum from its lowest frequency to its higher frequency behavior. In most cases, we will find that as g approaches g_c, Δ vanishes as

$$\Delta \sim J|g - g_c|^{z\nu} \tag{1.1}$$

(exceptions to this behavior appear in Section 14.2.6). Here J is the energy scale of a characteristic microscopic coupling, and $z\nu$ is a *critical*

exponent. The value of $z\nu$ is usually *universal, i.e.,* it is independent of most of the microscopic details of the Hamiltonian $H(g)$: we shall have much more to say about the concept of universality below, and in the following chapters. The behavior (1.1) holds both for $g > g_c$ and $g < g_c$ with the same value of the exponent $z\nu$, but with different non-universal constants of proportionality. We shall sometimes use the symbol Δ_+ (Δ_-) to represent the characteristic energy scale for $g > g_c$ ($g < g_c$).

In addition to a vanishing energy scale, second order quantum phase transitions invariably have a diverging characteristic length scale ξ: this could be the length scale determining the exponential decay of equal time correlations in the ground state, or the length scale at which some characteristic crossover occurs to the correlations at the longest distances. This length diverges as

$$\xi^{-1} \sim \Lambda|g - g_c|^{\nu}, \tag{1.2}$$

where ν is a critical exponent, and Λ is an inverse length scale (a 'momentum cutoff') of order the inverse lattice spacing. The ratio of the exponents in (1.1) and (1.2) is z, the dynamic critical exponent: the characteristic energy scale vanishes as the z'th power of the characteristic inverse length scale

$$\Delta \sim \xi^{-z}. \tag{1.3}$$

It is important to notice that the discussion above refers to singularities in the *ground state* of the system. So strictly speaking, quantum phase transitions occur only at zero temperature, $T = 0$. All experiments are necessarily at some non-zero, though possibly very small, temperature, and so a central task of the theory of quantum phase transitions is to describe the consequences of this $T = 0$ singularity on physical properties at $T > 0$. It turns out that working outward from the quantum critical point at $g = g_c$, and $T = 0$ is a powerful way of understanding and describing the thermodynamic and dynamic properties of numerous systems over a broad range of values of $|g - g_c|$ and T. Indeed, it is not even necessary that the system of interest ever have its microscopic couplings reach a value such that $g = g_c$: it can still be very useful to argue that there is a quantum critical point at a physically inaccessible coupling $g = g_c$, and to develop a description in the deviation $|g - g_c|$. It is one of the purposes of this book to describe the physical perspective that such an approach offers, and to contrast it from more
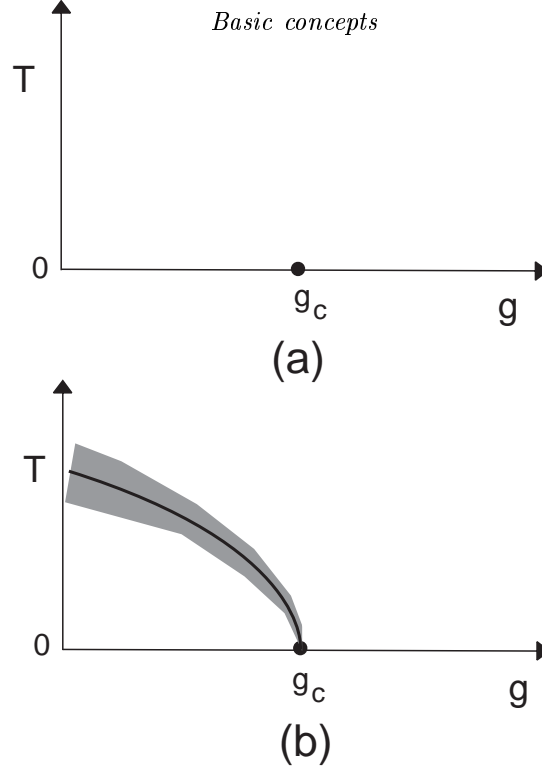
Fig. 1.2. Two possible phase diagrams of system near a quantum phase transition. In both cases there is a quantum critical point at $g = g_c$ and $T = 0$. In (b), there is a line of $T > 0$ second order phase transitions terminating at the quantum critical point. The theory of phase transitions in classical systems driven by thermal fluctuations can be applied with the shaded region of (b).

conventional expansions about very weak (say $g \to 0$) or very strong couplings (say $g \to \infty$).

1.2 Quantum versus classical phase transitions

There are two important possibilities for the $T > 0$ phase diagram of a system near a quantum critical point: these are shown in Fig 1.2, and we will meet examples of both kinds in this book. In the first, shown in Fig 1.2a, the thermodynamic singularity is present only at $T = 0$, and all $T > 0$ properties are analytic as a function of g near $g = g_c$. In the second, shown in Fig 1.2b, there is line of $T > 0$ second order phase transitions (this is a line at which the thermodynamic free energy is not analytic) which terminates at the $T = 0$ quantum critical point at $g = g_c$.

In the vicinity of such a line, we will find that the typical frequency at which the important long distance degrees of freedom fluctuate, ω_{typ}, satisfies

$$\hbar\omega_{\mathrm{typ}} \ll k_B T. \tag{1.4}$$

Under these conditions, it will be seen that a purely *classical* description can be applied to these important degrees of freedom—this classical description works in the shaded region of Fig 1.2b. Consequently, the ultimate critical singularity along the line of $T > 0$ phase transitions in Fig 1.2b is described by the theory of second order phase transitions in classical systems. This theory was developed thoroughly in last three decades and has been explained in many popular reviews and books [318, 63, 247, 184, 550]—we shall assume here that the reader has some familiarity with at least the basic concepts of this classical theory, and will occasionally refer to some of these sources for specific details. Notice that the shaded region of classical behavior in Fig 1.2b is within the wider window of the phase diagram, with moderate values of $|g - g_c|$ and T, which we asserted above should be described as an expansion about the quantum critical point at $g = g_c$ and $T = 0$. So our study of quantum phase transitions will also apply to the shaded region of Fig 1.2b, where it will yield information which is complementary to that available by directly thinking of the $T > 0$ phase transition in terms of purely classical models.

We note that phase transitions in classical models are driven only by thermal fluctuations, as classical systems usually freeze into a fluctuationless ground state at $T = 0$. In contrast, quantum systems have fluctuations driven by the Heisenberg uncertainty principle even in the ground state, and these can drive interesting phase transitions at $T = 0$. The $T > 0$ region in the vicinity of a quantum critical point therefore offers a fascinating interplay of effects driven by quantum and thermal fluctuations; sometimes, as in the shaded region of Fig 1.2b, we can find some dominant, effective degrees of freedom whose fluctuations are purely classical and thermal, and then the classical theory will apply. However, as already noted, our attention will not be limited to such regions, and we shall be interested in a broader section of the phase diagram.

1.3 Experimental examples

To make the concepts of the previous sections less abstract, let us mention some recent experimental studies of second order quantum phase transitions. All of the following examples will also be discussed further in this book.

- The low-lying magnetic excitations of the insulator $LiHoF_4$ consist of fluctuations of the Ho ions between two spin states which are aligned parallel and anti-parallel to a particular crystalline axis. These states can be represented by a two-state 'Ising' spin variable on each Ho ion. At $T = 0$, the magnetic dipolar interactions between the Ho ions cause all the Ising spins to align in the same orientation, so the ground state is a ferromagnet. Bitko *et al.* [55] placed this material in a magnetic field transverse to the magnetic axis. Such a field induces quantum tunneling between the two states of each Ho ion, and a sufficiently strong tunneling rate can eventually destroy the long-range magnetic order. Such a quantum phase transition was indeed observed [55], with the ferromagnetic moment vanishing continuously at a quantum critical point. Note that such a transition can, in principle, occur precisely at $T = 0$, when it is driven entirely by quantum fluctuations. We shall call the $T = 0$ state without magnetic order a *quantum paramagnet*. On the other hand, we can also destroy the magnetic order at a fixed transverse magnetic field (possibly zero), simply by raising the temperature, and undergoing a conventional Curie transition to a high temperature magnetically disordered state. Among the objectives of this book is to provide a description of the intricate crossover between the zero temperature quantum transition and the finite temperature transition driven partially by thermal fluctuations; we shall also delineate the important differences between the $T = 0$ quantum paramagnet and the high temperature 'thermal paramagnet'; see Chapters 5, 7 and 8.
- The heavy fermion material $CeCu_{6-x}Au_x$ [415, 479, 517, 447] has a magnetically ordered ground state, with the magnetic moments on the Ce ions arranged in a spin density wave with an incommensurate period (this simply means that the expectation value of the spin operator oscillates in a wave-like manner with a period which is not a rational number times a period of the crystalline lattice). This order is present at larger values of the doping x. By decreasing the value of x, or by placing the crystal under pressure, it is possible to destroy the magnetic order in a second order quantum phase transition. The

ground state then becomes a Fermi liquid with a rather large effective mass for the fermionic quasiparticles. This transition will be discussed in Chapter 12

- The two-dimensional electron gas in semiconductor heterostructures has a very rich phase diagram with a large number of quantum phase transitions. Let us describe a particular class of transitions which will be relevance to the theoretical development in this book. As is well known, the energy spectrum of electrons moving in two dimensions in the presence of a perpendicular magnetic field splits into discrete, equally spaced energy levels (Landau levels), with each level having the same fixed macroscopic degeneracy. Consider a two-dimensional electron gas in a magnetic field at density such that the lowest Landau level is precisely filled (filling factor $\nu = 1$). The electronic spins are then fully polarized in the direction of the field, and the ground state is a fully polarized ferromagnet. Actually, this ferromagnetic order is induced more by the ferromagnetic exchange interactions between the electrons than by the Zeeman coupling to the external field. Now imagine bringing two such ferromagnetic layers close to each other [385, 377, 445, 378, 310]. For large layer spacing, the two layers will have their ferromagnetic moments both aligned in the direction of the applied field. For smaller spacings, there turns out to be a substantial *antiferromagnetic* exchange between the two layers, so that ground state eventually becomes a spin singlet, created by a 'bonding' of electrons in opposite layers into spin singlet pairs [546, 120, 121]. The transition from a fully polarized ferromagnet to a spin singlet state actually happens through two second order quantum phase transitions via an intermediate state with 'canted' antiferromagnetic order: this shall be discussed in Section 13.4.

- The low energy spin fluctuations of the insulator La_2CuO_4 consist of quantum fluctuations in the orientations of $S = 1/2$ spins located on the sites of a square lattice. Each spin represents the magnetic states of the d-orbitals on a Cu ion. There is an antiferromagnetic exchange coupling between the spins which prefers an anti-parallel orientation for neighboring spins, and the resulting Hamiltonian is the square lattice $S = 1/2$ Heisenberg antiferromagnet (the modifier 'Heisenberg' indicates that the model has the full $SU(2)$ symmetry of rotations in spin space). The ground state of this model is a "Néel" state, in which the spins are polarized in opposite orientations on the two checkerboard sublattices of the square lattice. However, theoretically, we can consider a more general model with both first and second neighbor

antiferromagnetic exchange. As we shall discuss in Chapter 13, such a model can undergo a quantum phase transition in which the Néel order is destroyed, and the ground state becomes a quantum paramagnet with a gap to all spin excitations. While such a phase transition has not been observed experimentally so far, it still pays to consider the physics of this quantum critical point, and to understand the finite temperature crossovers in its vicinity. These crossovers also influence the behavior of the nearest neighbor model found in La_2CuO_4, and turn out to be a useful way of interpreting its magnetic properties at intermediate temperatures; see Chapters 5, 7 and 13.

1.4 Theoretical models

The physics underlying the quantum transitions discussed above is quite complex, and in many cases, not completely understood. Our strategy in this book will be to thoroughly analyze the physical properties of quantum phase transitions in two simple theoretical model systems in Part 2 — the quantum Ising and rotor models; fortunately, these simple models also have some direct experimental applications and these will be noted at numerous points in Part 2. Part 3 will then survey some important basic quantum phase transitions in other models of physical interest. Our motivation in dividing the discussion in this manner is mainly pedagogical: the quantum transitions of the Ising/rotor models have an essential simplicity, but their behavior is rich enough to display most of the basic phenomena we wish to explore. It will therefore pay to first meet the central physical ideas in this simple context.

We will introduce the quantum Ising and rotor models in turn, and discuss the nature of the quantum phase transitions in them.

1.4.1 Quantum Ising model

We begin by writing down the Hamiltonian of the quantum Ising model. It is

$$H_I = -Jg \sum_i \hat{\sigma}_i^x - J \sum_{\langle ij \rangle} \hat{\sigma}_i^z \hat{\sigma}_j^z \tag{1.5}$$

As in the general notation introduced above, $J > 0$ is an exchange constant which sets the microscopic energy scale, and $g > 0$ is a dimensionless coupling which will be used to tune H_I across a quantum phase transition. The quantum degrees of freedom are represented by

operators $\hat{\sigma}_i^{z,x}$ which reside on the sites, i, of a hypercubic lattice in d dimensions; the sum $\langle ij \rangle$ is over pairs of nearest neighbor sites i, j. The $\hat{\sigma}_i^{x,z}$ are the familiar Pauli matrices; the matrices on different sites i act on different spin states, and so matrices with $i \neq j$ commute with each other. In the basis where the $\hat{\sigma}_i^z$ are diagonal, these matrices have the well-known form

$$\hat{\sigma}^z = \begin{pmatrix} 1 & 0 \\ 0 & -1 \end{pmatrix} \;\; ; \;\; \hat{\sigma}^y = \begin{pmatrix} 0 & -i \\ i & 0 \end{pmatrix} \;\; ; \;\; \hat{\sigma}^x = \begin{pmatrix} 0 & 1 \\ 1 & 0 \end{pmatrix} \qquad (1.6)$$

on each site i. We will denote the eigenvalues of $\hat{\sigma}_i^z$ simply by σ_i^z, and so σ_i^z takes the values ± 1. We identify the two states with eigenvalues $\sigma_i^z = +1, -1$ as the two possible orientations of an 'Ising spin' which can oriented up or down in $|\uparrow\rangle_i, |\downarrow\rangle_i$. Consequently at $g = 0$, when H_I involves only the $\hat{\sigma}_i^z$, H_I will be diagonal in the basis of eigenvalues of $\hat{\sigma}_i^z$, and it reduces simply to the familiar classical Ising model. However, the $\hat{\sigma}_i^x$ are off-diagonal in the basis of these states, and therefore induce quantum-mechanical tunneling events which flip the orientation of the Ising spin on a site. The physical significance of the two terms in H_I should be clear in the context of our earlier discussion in Section 1.3 for LiHoF$_4$. The term proportional to J is the magnetic interaction between the spins which prefers their global ferromagnetic alignment; the actual interaction in LiHoF$_4$ has a long-range dipolar nature, but we have simplified this here to a nearest neighbor interaction. The term proportional to Jg is the external transverse magnetic field, which disrupts the magnetic order.

Let us make these qualitative considerations somewhat more precise. The ground state of H_I can depend only upon the value of the dimensionless coupling g, and so it pays to consider the two opposing limits $g \gg 1$ and $g \ll 1$.

First consider $g \gg 1$. In this case the first term in (1.5) dominates and, to leading order in $1/g$, the ground state is simply

$$|0\rangle = \prod_i | \rightarrow \rangle_i \qquad (1.7)$$

where

$$| \rightarrow \rangle_i = (|\uparrow\rangle_i + |\downarrow\rangle_i)/\sqrt{2}$$
$$| \leftarrow \rangle_i = (|\uparrow\rangle_i - |\downarrow\rangle_i)/\sqrt{2} \qquad (1.8)$$

are the two eigenstates of $\hat{\sigma}_i^x$ with eigenvalues ± 1. The values of σ_i^z on different sites are totally uncorrelated in the state (1.7), and so

$\langle 0 | \hat{\sigma}_i^z \hat{\sigma}_j^z | 0 \rangle = \delta_{ij}$. Perturbative corrections in $1/g$ will build in correlations in σ^z which increase in range at each order in $1/g$; for g large enough these correlations are expected to remain short-ranged, and we expect in general that

$$\langle 0 | \hat{\sigma}_i^z \hat{\sigma}_j^z | 0 \rangle \sim e^{-|x_i - x_j|/\xi} \tag{1.9}$$

for large $|x_i - x_j|$, where x_i is the spatial co-ordinate of site i, $|0\rangle$ is the exact ground state for large g, and ξ is the 'correlation length' introduced earlier above (1.2).

Next we consider the opposing limit $g \ll 1$. We will find that the nature of the ground state is qualitatively different from the large g limit above, and shall use this to argue that there must be a quantum phase transition between the two limiting cases at a critical $g = g_c$ of order unity. For $g \ll 1$, the second term in (1.5) coupling neighboring sites dominates; at $g = 0$ the spins are either all up or down (in eigenstates of σ^z):

$$|\!\uparrow\rangle = \prod_i |\uparrow\rangle_i \qquad |\!\downarrow\rangle = \prod_i |\downarrow\rangle_i \tag{1.10}$$

Turning on a small g will mix in a small fraction of spins of the opposite orientation, but in an infinite system the degeneracy will survive at any finite order in a perturbation theory in g: this is because there is an exact global Z_2 symmetry transformation (generated by the unitary operator $\prod_i \sigma_i^x$), which maps the two ground states into each other, under which H_I remains invariant:

$$\hat{\sigma}_i^z \to -\hat{\sigma}_i^z \qquad \hat{\sigma}_i^x \to \hat{\sigma}_i^x, \tag{1.11}$$

and there is no tunneling matrix element between the majority up and down spin sectors of the infinite system at any finite order in g. The mathematically alert reader will note that establishing the degeneracy to all orders in g, is not the same thing as establishing its existence for any small non-zero g, but more sophisticated considerations show that this is indeed the case. A thermodynamic system will always choose one or the other of the states as its ground states (which may be preferred by some infinitesimal external perturbation), and this is commonly referred to as a 'spontaneous breaking' of the Z_2 symmetry. As in the large g limit, we can characterize the ground states by the behavior of correlations of $\hat{\sigma}_i^z$; the nature of the states (1.10) and the small g perturbation theory suggest that

$$\lim_{|x_i - x_j| \to \infty} \langle 0 | \hat{\sigma}_i^z \hat{\sigma}_j^z | 0 \rangle = N_0^2, \tag{1.12}$$

where $|0\rangle$ is either of the ground states obtained from $|\uparrow\rangle$ or $|\downarrow\rangle$ by perturbation theory in g, and $N_0 \neq 0$ is the 'spontaneous magnetization' of the ground state. This identification is made clearer by the simpler statement

$$\langle 0|\hat{\sigma}_i^z|0\rangle = \pm N_0 \tag{1.13}$$

which also follows from the perturbation theory in g. We have $N_0 = 1$ for $g = 0$, but quantum fluctuations at small g reduce N_0 to a smaller, but non-zero, value.

Now we make the simple observation that it is not possible for states which obey (1.9) and (1.12) to transform unto each other analytically as a function of g. There must be a critical value $g = g_c$ at which the large $|x_i - x_j|$ limit of the two-point correlator changes from (1.9) to (1.12)—this is the position of the quantum phase transition, which shall the focus of intensive study in this book. Our arguments so far do not exclude the possibility that there could be *more* than one critical point, but this is known not to happen for H_I, and we will assume here that there is only one critical point at $g = g_c$. For $g > g_c$ the ground state is, as noted earlier, a *quantum paramagnet*, and (1.9) is obeyed. We will find that as g approaches g_c from above, the correlation length, ξ, diverges as in (1.2). Precisely at $g = g_c$, neither (1.9) nor (1.12) is obeyed, and we find instead a power-law dependence on $|x_i - x_j|$ at large distances. The result (1.12) holds for all $g < g_c$, when the ground state is *magnetically ordered.* The spontaneous magnetization of the ground state, N_0, vanishes as a power law as g approaches g_c from below.

Finally, a comment about the excited states of H_I. In finite lattice, there is necessarily a nonzero energy separating the ground state and the first excited state. However, this energy spacing can either remain finite or approach zero in the infinite lattice limit, the two cases being identified as having a gapped or gapless energy spectrum respectively. We will find that there is an energy gap Δ which is non-zero for all $g \neq g_c$, but that it vanishes upon approaching g_c as in (1.1), producing a gapless spectrum at $g = g_c$.

1.4.2 Quantum rotor model

We turn to the somewhat less familiar quantum rotor models. Elementary quantum rotors do not exist in nature; rather, each quantum rotor is an effective quantum degree of freedom for the low energy states of a small number of closely coupled electrons. We will first define the

quantum mechanics of a single rotor, and then briefly motivate how it might represent some physically interesting systems—more details on this physical mapping will appear later.

Each rotor can be visualized as a particle constrained to move on the surface of a (fictitious) ($N > 1$)-dimensional sphere. The orientation of each rotor is represented by an N-component unit vector $\hat{\mathbf{n}}_i$ which satisfies

$$\hat{\mathbf{n}}^2 = 1. \tag{1.14}$$

The caret on $\hat{\mathbf{n}}_i$ reminds us that the orientation of the rotor is a quantum mechanical operator, while i represents the site on which the rotor resides—we will shortly consider an infinite number of such rotors residing on the sites of a d-dimensional lattice. Each rotor has a momentum $\hat{\mathbf{p}}_i$, and the constraint (1.14) implies that this must be tangent to the surface of the N-dimensional sphere. The rotor position and momentum satisfy the usual commutation relations

$$[\hat{n}_\alpha, \hat{p}_\beta] = i\delta_{\alpha\beta} \tag{1.15}$$

on each site i; here $\alpha, \beta = 1 \ldots N$. (Here, and in the remainder of the book, we will always measure time in units in which

$$\hbar = 1, \tag{1.16}$$

unless stated explicitly otherwise. This is also a good point to note that we will also set Boltzmann's constant

$$k_B = 1 \tag{1.17}$$

by absorbing it into the units of temperature, T.) We will actually find it more convenient to work with the $N(N-1)/2$ components of the rotor angular momentum

$$\hat{L}_{\alpha\beta} = \hat{n}_\alpha \hat{p}_\beta - \hat{n}_\beta \hat{p}_\alpha \tag{1.18}$$

These operators are the generators of the group of rotation in N dimensions, denoted O(N). Their commutation relations follow straightforwardly from (1.15) and (1.18). The case $N = 3$ will be of particular interest to us: for this we define $\hat{L}_\alpha = (1/2)\epsilon_{\alpha\beta\gamma}L_{\beta\gamma}$ (where $\epsilon_{\alpha\beta\gamma}$ is totally antisymmetric tensor with $\epsilon_{123} = 1$), and then the commutation relation between the operators on each site are

$$[\hat{L}_\alpha, \hat{L}_\beta] = i\epsilon_{\alpha\beta\gamma}\hat{L}_\gamma$$
$$[\hat{L}_\alpha, \hat{n}_\beta] = i\epsilon_{\alpha\beta\gamma}\hat{n}_\gamma$$
$$[\hat{n}_\alpha, \hat{n}_\beta] = 0; \tag{1.19}$$

the operators with different site labels all commute.

The dynamics of each rotor is governed simply by its kinetic energy term; interesting effects will arise from potential energy terms which couple the rotors together, and these will be considered momentarily. Each rotor has the kinetic energy

$$H_K = \frac{J\widetilde{g}}{2}\hat{\mathbf{L}}^2 \tag{1.20}$$

where $1/J\widetilde{g}$ is the rotor moment of inertia (we have put a tilde over g as we wish to reserve g for a different coupling to be introduced below). The Hamiltonian H_K can be readily diagonalized for general values of N by well-known group theoretical methods. We quote the results for the physically important cases of $N = 2, 3$. For $N = 2$ the eigenvalues are

$$J\widetilde{g}\ell^2/2/2 \quad \ell = 0, 1, 2, \ldots \quad ; \quad \text{degeneracy} = 2 - \delta_{\ell,0}. \tag{1.21}$$

Note that there is a non-degenerate ground state with $\ell = 0$, while all excited states are two-fold degenerate corresponding to a left or right moving rotor. In physical applications, these states can be visualized as the low-lying energy levels of a superconducting quantum dot: ℓ measures the deviation in the number of Cooper pairs on the dot from the number found in the ground state, and $J\widetilde{g}$ is a measure of the inverse self-capacitance of the dot. More details on this physical application of $N = 2$ quantum rotors will appear in Chapter 10. For $N = 3$, the eigenvalues of H_K are

$$J\widetilde{g}\ell(\ell+1)/2 \quad \ell = 0, 1, 2, \ldots \quad ; \quad \text{degeneracy} = 2\ell + 1, \tag{1.22}$$

corresponding to the familiar angular momentum states in 3 dimension. These states can be viewed as representing the eigenstates of an even number of antiferromagnetically-coupled Heisenberg spins. The ground state is a spin singlet, as can be expected from an antiferromagnetic coupling which prefers spins in opposite orientations. This mapping will be discussed more explicitly in Section 5.1.1.1 and Chapter 13 where will see that there is a general and powerful correspondence between quantum antiferromagnets and $N = 3$ rotors. The O(3) quantum rotors also describe the double layer quantum Hall systems discussed in Section 1.3 [120, 121].

We are ready to write down the full quantum rotor Hamiltonian, which

shall be the focus of intensive study in Part 2. It is

$$H_R = \frac{J\widetilde{g}}{2} \sum_i \hat{\mathbf{L}}_i^2 - J \sum_{\langle ij \rangle} \hat{\mathbf{n}}_i \cdot \hat{\mathbf{n}}_j. \tag{1.23}$$

We have augmented the sum of kinetic energies of each site with a coupling, J, between rotor orientations on neighboring sites. This coupling energy is minimized by the simple 'magnetically ordered' state in which all the rotors are oriented in the same direction. In contrast, the rotor kinetic energy is minimized when the orientation of the rotor is maximally uncertain (by the uncertainty principle), and so the first term in H_R prefers quantum paramagnetic state in which the rotors do not have a definite orientation, *i.e.*, $\langle \mathbf{n} \rangle = 0$. Thus the roles of the two terms in H_R closely parallel those of the terms in the Ising model H_I. As in Section 1.4.1, for $\widetilde{g} \gg 1$, when the kinetic energy dominates, we expect a quantum paramagnet in which, following (1.9),

$$\langle 0 | \hat{\mathbf{n}}_i \cdot \hat{\mathbf{n}}_j | 0 \rangle \sim e^{-|x_i - x_j|/\xi}. \tag{1.24}$$

Similarly, for $\widetilde{g} \ll 1$, when the coupling term dominates, we expect a magnetically ordered state in which, as in (1.12),

$$\lim_{|x_i - x_j| \to \infty} \langle 0 | \hat{\mathbf{n}}_i \cdot \hat{\mathbf{n}}_j | 0 \rangle = N_0^2 \tag{1.25}$$

Finally, we can anticipate a second-order quantum phase transition between the two phases at $\widetilde{g} = \widetilde{g}_c$, and the behavior of N_0 and ξ upon approaching this point will be similar to that in the Ising case. These expectations turn out to be correct for $d > 1$, but we will see that they need some modifications for $d = 1$. In one dimension, we will show that $\widetilde{g}_c = 0$ for $N \geq 3$, and so the ground state is a quantum paramagnetic for all non-zero $\widetilde{g}$. The case $N = 2$, $d = 1$ is special: there is a transition at a finite $\widetilde{g}_c$, but the divergence of the correlation length does not obey (1.2) and the long-distance behavior of the correlation function $\widetilde{g} < \widetilde{g}_c$ differs from (1.25)—this case will not be considered until Section 14.3 in Part 3.

2

The mapping to classical statistical mechanics: single site models

This chapter will discuss the reason for the central importance of the quantum Ising and rotor models in the theory of quantum phase transitions, quite apart from any experimental motivations. It turns out that the quantum transitions in these models in d dimensions are intimately connected to certain well-studied finite temperature phase transitions in classical statistical mechanics models in $D = d + 1$ dimensions [134, 483, 382, 164, 537]. We will then be able to transfer much of the sophisticated technology developed to analyze these classical models to the quantum models of interest here.

We will discuss this mapping here in the simplest context of $d = 0$, $D = 1$: we will consider single site quantum Ising and rotor models, and explicitly discuss their mapping to classical statistical mechanics models in $D = 1$ (the cases $d > 0$ will then be discussed in Chapter 3). These very simple classical models in $D = 1$, actually do not have any phase transitions. Nevertheless, it is quite useful to examine them thoroughly as they do have regions in which the correlation 'length' ξ becomes very large: the properties of these regions are very similar to those in the vicinity of the phase transition points in higher dimensions. In particular, we will introduce the central ideas of the *scaling limit* and *universality* in this very simple context. We will then go on to map the classical models to equivalent zero-dimensional quantum models and demonstrate that this mapping becomes *exact in the scaling limit.*

The following sections will actually carry out the quantum-to-classical mapping in reverse. With the benefit of hindsight, we will begin by examining certain $D = 1$ classical statistical mechanics model and show that they are intimately related to single-site quantum Ising and rotor models. The classical models we shall study are the $D = 1$, N-component classical spin ferromagnets, and are surely familiar to most

readers in other contexts. We will consider the $N = 1, 2, 3$ case in the following sections in turn. The models with $N > 3$ are very similar to the case $N = 3$.

For a traditional, 'classical' perspective of these models, the reader is referred to the review by Thompson [490].

2.1 The classical Ising chain

Here we will consider the $D = 1$, $N = 1$ classical spin ferromagnet, more commonly known as the ferromagnetic Ising chain [242]. This chain has the partition function

$$\mathcal{Z} = \sum_{\{\sigma_i^z = \pm 1\}} \exp(-H) \tag{2.1}$$

where σ_i^z are Ising spins on sites i of a chain which take the values ± 1, and H is given by

$$H = -K \sum_{i=1}^{M} \sigma_i^z \sigma_{i+1}^z - h \sum_{i=1}^{M} \sigma_i^z. \tag{2.2}$$

In all our discussion of classical statistical mechanics models we absorb its 'temperature' into the definition of the coupling constants, as we have done above for K and h; in contrast, the temperature of quantum-mechanical models will always be explicitly indicated, and we will reserve the symbol T for it—as we will see below, the total length of the classical model will determine T. There are a total of M Ising spins (M large), and for convenience we have also added a uniform magnetic field h acting on all the spins. We will assume periodic boundary conditions, and therefore $\sigma_{M+1}^z \equiv \sigma_1^z$.

We will evaluate the partition function exactly following the original solution of Ising [242]. The trick is to write $\mathcal{Z}$ as a trace over a matrix product, with one matrix for every site on the chain. Notice that the partition functions involves the exponential of a sum of terms on the sites of the chain: rewrite this as the product of exponentials of each term, and we easily obtain

$$\mathcal{Z} = \sum_{\{\sigma_i^z\}} \prod_{i=1}^{M} T_1(\sigma_i^z, \sigma_{i+1}^z) T_2(\sigma_i^z) \tag{2.3}$$

where $T_1(\sigma_1^z, \sigma_2^z) = \exp(K\sigma_1^z \sigma_2^z)$ and $T_2(\sigma^z) = \exp(h\sigma^z)$. Now notice that (2.3) has precisely the structure of a matrix product, if we interpret

the two possible values of σ_i^z as the index labeling the rows and columns of a 2×2 matrix T_1; T_2 has only one index and so should be interpreted as a diagonal matrix. So we have

$$\mathcal{Z} = \text{Tr}\left(T_1 T_2 T_1 T_2 \cdots M \text{ times} \cdots\right) \qquad (2.4)$$

where the summation over the $\{\sigma_i^z\}$ has been converted to a matrix trace because of the periodic boundary conditions, and

$$T_1 = \begin{pmatrix} e^K & e^{-K} \\ e^{-K} & e^K \end{pmatrix} \qquad T_2 = \begin{pmatrix} e^h & 0 \\ 0 & e^{-h} \end{pmatrix}. \qquad (2.5)$$

The matrix $T_1 T_2$ is identified as the 'transfer matrix' of the Ising chain H (Eqn (2.2)), the nomenclature suggesting that it transfers the trace over spins from each site to its neighbor. We can manipulate (2.4) into

$$\begin{aligned} \mathcal{Z} &= \text{Tr}\left(T_1 T_2\right)^M \\ &= \text{Tr}\left(T_2^{1/2} T_1 T_2^{1/2}\right)^M \\ &= \epsilon_1^M + \epsilon_2^M \end{aligned} \qquad (2.6)$$

where $\epsilon_{1,2}$ are the eigenvalues of the symmetric matrix

$$T_2^{1/2} T_1 T_2^{1/2} = \begin{pmatrix} e^{K+h} & e^{-K} \\ e^{-K} & e^{K-h} \end{pmatrix}, \qquad (2.7)$$

given by

$$\epsilon_{1,2} = e^K \cosh(h) \pm \left(e^{2K}\sinh^2(h) + e^{-2K}\right)^{1/2}. \qquad (2.8)$$

With these eigenvalues, (2.6) leads to an exact result for the free energy $F = -\ln \mathcal{Z}$. We will return to interpreting this result for F momentarily.

Now, we show how the above approach can also lead to exact information on correlation functions. For simplicity, we will consider only the case $h = 0$ (the generalization to non-zero h is not difficult), and describe the two-point spin correlator

$$\langle \sigma_i^z \sigma_j^z \rangle = \frac{1}{\mathcal{Z}} \sum_{\{\sigma_i^z\}} \exp(-H)\sigma_i^z \sigma_j^z \qquad (2.9)$$

Going through exactly the same steps as those in the derivation of (2.6) we see that

$$\langle \sigma_i^z \sigma_j^z \rangle = \frac{1}{\mathcal{Z}} \text{Tr}\left(T_1^i \hat{\sigma}^z T_1^{j-i} \hat{\sigma}^z T_1^{M-j}\right), \qquad (2.10)$$

where we have assumed that $j \geq i$, and σ^z (without a site index) is also interpreted as a 2×2 diagonal Pauli matrix $\hat{\sigma}^z$ in (1.6). The trace in

(2.10) can be evaluated in closed form in the basis in which T_1 is diagonal. The eigenvectors of T_1 are the states in (1.8) and the corresponding eigenvalues are $\epsilon_1 = 2\cosh(K)$ and $\epsilon_2 = 2\sinh(K)$. Now using the matrix elements $\langle \rightarrow |\sigma^z| \rightarrow \rangle = \langle \leftarrow |\sigma^z| \leftarrow \rangle = 0$ and $\langle \rightarrow |\sigma^z| \leftarrow \rangle = \langle \rightarrow |\sigma^z| \leftarrow \rangle = 1$ we get from (2.6) and (2.10)

$$\langle \sigma_i^z \sigma_j^z \rangle = \frac{\epsilon_1^{M-j+i}\epsilon_2^{j-i} + \epsilon_2^{M-j+i}\epsilon_1^{j-i}}{\epsilon_1^M + \epsilon_2^M} \tag{2.11}$$

The equations (2.10) and (2.11) are our main results on the Ising chain with an arbitrary number of sites, M. While simple, they contain a great deal of useful information, as we will now show; much of the structure we will extract below generalizes to more complex models.

Let us examine the form of the correlations in (2.11) in the limit of an infinite chain ($M \rightarrow \infty$); then we have

$$\langle \sigma_i^z \sigma_j^z \rangle = (\tanh(K))^{j-i} \tag{2.12}$$

It is useful for the following discussion to label the spins not by the site index i, but by a physical length co-ordinate τ; we have chosen the symbol τ, rather than the more conventional x, because we will shortly interpret this 'length' as the imaginary time direction of a quantum problem. So if we imagine that the spins are placed on a lattice of spacing a, then $\sigma^z(\tau) \equiv \sigma_j^z$ where

$$\tau = ja. \tag{2.13}$$

With this notation, we can write (2.12) as

$$\langle \sigma^z(\tau)\sigma^z(0) \rangle = e^{-|\tau|/\xi} \tag{2.14}$$

where the correlation length, ξ, is given by

$$\frac{1}{\xi} = \frac{1}{a}\ln\coth(K). \tag{2.15}$$

We emphasize that the symbol ξ always represents the actual correlation length at $h = 0$; the actual correlation length for $h \neq 0$ will, of course, be different. In the large K limit, the correlation length becomes much larger than the lattice spacing, a:

$$\frac{\xi}{a} \approx \frac{1}{2}e^{2K} \gg 1 \qquad K \gg 1. \tag{2.16}$$

In the sequel, we shall primarily be interested in physics on the scale of order ξ, in the regime where ξ is much greater than a. It is precisely in this situation that the concepts of the scaling limit and universality become useful, and they are introduced in the following subsections.

2.1.1 The scaling limit

The simplest way to think of the scaling limit is to first divide all lengths into "large" and "small" lengths. For the Ising chain, we take the correlation length ξ, the observation scale τ, and the system size

$$L_\tau \equiv M a, \tag{2.17}$$

as our large lengths, and the lattice spacing, a, as the only small length. The scaling limit of an observable is then defined as its value when all corrections involving the ratio of small to large lengths are neglected.

There are two conceptually rather different, but equivalent, ways of thinking about the scaling limit. We can either send the small length a to zero while keeping the large lengths fixed (as particle physicists are inclined to do) or send all the large lengths to infinity while keeping a fixed (as is more common among condensed matter physicists). The physics can only depend upon the ratio of lengths, so it is clear that the two methods are equivalent. We shall choose among these points of view at our convenience, and show that it is often very useful to straddle this cultural divide and use the insights of both perspectives.

To complete the definition of the scaling limit, we also have to discuss the manner in which the parameters K and h must be treated. From (2.15), we see that K can be expressed in terms of the ratio of lengths ξ/a; we can use this to eliminate explicit dependence upon K, and then the scaling limit is specified by the already specified $\xi/a \to \infty$ limit. It remains to discuss the behavior of h. In general, there is no a priori way of determining this and one has to examine the structure of the correlation functions to determine the appropriate limit. Let us guess the answer here by a physical argument. The scaling limit involves the study of large K, when the spin correlation length becomes large. Under these conditions, spins a few lattice spacings apart invariable point in the same direction, and should there be sensitive to the mean magnetic field h per unit length. This is measured by $\widetilde{h}$, defined by

$$\widetilde{h} \equiv \frac{h}{a}. \tag{2.18}$$

So we take the scaling limit $a \to 0$ while keeping $\tilde{h}$ fixed; any other choice would result in a limiting theory with spins under the influence of a field with either infinite or vanishing strength. Alternatively stated, we have chosen $1/\tilde{h}$, a quantity with the dimensions of length, as one of our large length scales.

We have assembled all the necessary steps for the scaling limit. Ex-

press any observable in terms of the physical length τ, replace the number of sites M by L_τ/a, solve (2.15) to express K in terms of ξ/a, and use (2.18) to replace h by $\widetilde{h}$. Then take the limit $a \to 0$ at fixed τ, L_τ, ξ, and $\widetilde{h}$.

We first describe the results for the free energy F. The quantity with the finite scaling limit should clearly be the free energy density, $\mathcal{F}$,

$$\mathcal{F} = -(\ln \mathcal{Z})/Ma. \tag{2.19}$$

First, from (2.8) we get in the scaling limit

$$\epsilon_{1,2} \approx \left(\frac{2\xi}{a}\right)^{1/2} \left[1 \pm \frac{a}{2\xi}\left(1 + 4\widetilde{h}^2\xi^2\right)^{1/2}\right]. \tag{2.20}$$

Inserting this into (2.8), and using the identity $\lim_{y\to\infty}(1 + c/y)^y = e^c$, we get

$$\mathcal{F} = E_0 - \frac{1}{L_\tau}\ln\left[2\cosh\left(L_\tau\sqrt{1/(4\xi^2) + \tilde{h}^2}\right)\right] \tag{2.21}$$

where $E_0 = -K/a$ is the ground state energy per unit length of the chain in zero external field.

In a similar manner, we can take the scaling limit of the correlation function in (2.11), which recall was in zero external field $\widetilde{h} = 0$. We obtain

$$\langle\sigma^z(\tau)\sigma^z(0)\rangle = \frac{e^{-|\tau|/\xi} + e^{-(L_\tau - |\tau|)/\xi}}{1 + e^{-L_\tau/\xi}}. \tag{2.22}$$

The results (2.21), (2.22) are the main conclusions of this subsection.

2.1.2 Universality

The assertion of *universality* is that the results of the scaling limit are not sensitive to the precise microscopic model being used. This is can be seen as the formal consequence of the physically reasonable requirement that correlations at the scale of the large ξ should not depend upon the details of the interactions on the scale of the lattice spacing, a.

Let us describe this by an explicit example. Suppose, instead of using the model H in (2.2), we worked with a Hamiltonian H_1 with both first (K_1) and *second* (K_2) neighbor exchanges between the Ising spins σ^z. This model can also be solved by the transfer matrix methods (one needs a basis of 4 sites corresponding to the 4 states of two near-neighbor spins, and the transfer matrix is 4×4), but we will not present the explicit solution here. From the solution we can determine the correlation length,

ξ of H_1, which will be a function of both K_1 and K_2. Now, as in Section 2.3, express the free energy density in terms of ξ, and take the limit $a \to 0$ at fixed ξ, L_τ, and $\tilde{h}$. The implication of universality is that the result will be precisely identical to (2.21), with E_0 given by the ground state energy density of H_1 in zero field: $E_0 = -(K_1 + K_2)/a$. The reader is invited to check this assertion for this simple example.

We can make the above assertion more precise by introducing the concept of a *universal scaling function*. We write (2.21) in the form

$$\mathcal{F} = E_0 + \frac{1}{L_\tau}\Phi_{\mathcal{F}}\left(\frac{L_\tau}{\xi}, \tilde{h}L_\tau\right), \qquad (2.23)$$

where $\Phi_{\mathcal{F}}$ is the universal scaling function, whose explicit value can be easily deduced by comparing with (2.21). Notice that the arguments of $\Phi_{\mathcal{F}}$ are simply the two dimensionless ratios that can be made out of the three large lengths at our disposal: L_τ, ξ, and $1/\tilde{h}$. The prefactor, $1/L_\tau$, in front of $\Phi_{\mathcal{F}}$ is necessary because the free energy density has dimensions of inverse length.

As its name implies, the $\Phi_{\mathcal{F}}$ is independent of microscopic details. In contrast, E_0, the ground state energy of the Ising chain, clearly depends sensitively on the values of the microscopic exchange constants, and is therefore identified as a *non-universal* additive contribution to $\mathcal{F}$.

In a similar manner, we can introduce a universal scaling function of the two-point correlation function. We have

$$\langle\sigma^z(\tau)\sigma^z(0)\rangle = \Phi_\sigma\left(\frac{\tau}{L_\tau}, \frac{L_\tau}{\xi}, \tilde{h}L_\tau\right) \qquad (2.24)$$

where Φ_σ is another universal scaling function, and there is now no non-universal additive constant. Again Φ_σ is a function of all the independent dimensionless combinations of large lengths; there is no prefactor because the correlator is clearly dimensionless. We can read off the value of $\Phi_\sigma(y_1, y_2, 0)$ by comparing (2.24) with (2.22), but determining the full function $\Phi(y_1, y_2, y_3)$ requires knowledge of the lattice correlator in the presence of a non-zero h, which is somewhat tedious to obtain. A simpler method will become apparent in the following subsection.

2.1.3 Mapping to a quantum model: Ising spin in a transverse field

We will show the statistical mechanics of the Ising chain can be mapped onto the quantum mechanics of a *single* Ising spin [483, 164]. Further,

as stated in the introduction to this chapter, correlators of the quantum spin will precisely reproduce the scaling limit of the classical Ising chain.

Let us return to the expressions (2.4), (2.5), and write the transfer matrices T_1, T_2 in terms of ratios of "large" to small length scales. We have

$$
\begin{aligned}
T_1 &= e^K \left(1 + e^{-2K}\hat{\sigma}^x\right) \\
&\approx e^K \left(1 + (a/2\xi)\hat{\sigma}^x\right) \\
&\approx \exp\left(a(-E_0 + (1/2\xi)\hat{\sigma}^x\right). \\
T_2 &= \exp\left(a\tilde{h}\hat{\sigma}^z\right),
\end{aligned}
\tag{2.25}
$$

where $\hat{\sigma}^{x,z}$ are the Pauli matrices in (1.6). Notice that both $T_{1,2}$ have the form e^{aO}, where O is some operator, acting on the $|\uparrow,\downarrow\rangle$ states, which is independent of a. Using the fact that $e^{aO_1}e^{aO_2} = e^{a(O_1+O_2)}(1 + \mathcal{O}(a^2))$, we can write (2.4) in the limit $a \to 0$ as

$$
\begin{aligned}
T_1 T_2 &\approx \exp(-aH_Q) \\
\mathcal{Z} &= (T_1 T_2)^M \approx \mathrm{Tr}\,\exp(-H_Q/T)
\end{aligned}
\tag{2.26}
$$

where

$$
H_Q = E_0 - \frac{\Delta}{2}\hat{\sigma}^x - \tilde{h}\hat{\sigma}^z,
\tag{2.27}
$$

with

$$
T \equiv \frac{1}{L_\tau} \quad , \quad \Delta \equiv \frac{1}{\xi}.
\tag{2.28}
$$

We have introduced the fundamental *quantum* Hamiltonian H_Q. It describes the dynamics of a single Ising quantum spin, whose Hilbert space consists of the two states $|\uparrow,\downarrow\rangle$, and which is under the influence of a longitudinal field $\tilde{h}$, and a *transverse* field Δ; it is the single site version of (1.5) with an additional longitudinal field. Notice, from the first relation in (2.26), that the transfer matrix of the classical chain H is the quantum evolution operator $e^{-H_Q \tau}$ over an imaginary time $\tau = a$, the lattice spacing: so the transfer from one site to the next is similar to evolution in imaginary time, and length co-ordinates for the classical chain translate into imaginary time co-ordinates for the quantum model H_Q. The energy Δ is also the *gap* between the ground and excited state of H_Q in zero (longitudinal) field, and it is precisely equal to the inverse of the correlation length of the classical Ising chain, as expected from the length to time mapping. Further, the partition function of the quantum spin is taken at a temperature T which precisely equals the inverse of

the total length of the classical chain. These correspondences between a gap of a quantum system and a correlation length of the corresponding classical model along the 'time' direction, and between the temperature of the quantum system and the total length of the classical model, are extremely general, and will apply to essentially all of the models we shall consider in this book.

We can use (2.26) and (2.27) to quickly evaluate the free energy of the quantum spin, $\mathcal{F} = -T \ln \mathcal{Z}$. The eigenenergies of H_Q are $E_0 \pm \sqrt{(\Delta/2)^2 + \widetilde{h}^2}$, and we have

$$\mathcal{F} = E_0 - T \ln \left[2 \cosh \left(\sqrt{(\Delta/2)^2 + \tilde{h}^2} \right) \right] \qquad (2.29)$$

which agrees precisely with the scaling limit of the classical Ising chain (2.21). Indeed, the single spin quantum Hamiltonian H_Q is precisely *the* theory describing the universal scaling properties of the entire class of classical Ising chains with short range interactions. Statements of this type are often shortened to "H_Q is the scaling theory of H".

The correspondence between H_Q and H also extends to correlation functions. Let us define the *time-ordered* correlator, G of H_Q in imaginary time by

$$G(\tau_1, \tau_2) = \begin{cases} \frac{1}{\mathcal{Z}} \mathrm{Tr} \left(e^{-H_Q/T} \hat{\sigma}^z(\tau_1) \hat{\sigma}^z(\tau_2) \right) & \text{for } \tau_1 > \tau_2 \\ \frac{1}{\mathcal{Z}} \mathrm{Tr} \left(e^{-H_Q/T} \hat{\sigma}^z(\tau_2) \hat{\sigma}^z(\tau_1) \right) & \text{for } \tau_1 < \tau_2 \end{cases} , \qquad (2.30)$$

where $\hat{\sigma}^z(\tau)$ is defined by the imaginary time evolution under the H_Q:

$$\hat{\sigma}^z(\tau) \equiv e^{H_Q \tau} \hat{\sigma}^z e^{-H_Q \tau}. \qquad (2.31)$$

Now, upon carrying through the mapping described above for the free energy for the case of the correlation function, we find that

$$G(\tau_1, \tau_2) = \lim_{a \to 0} \langle \sigma^z(\tau_1) \sigma^z(\tau_2) \rangle_H , \qquad (2.32)$$

where we have emphasized by the subscript that the average on the right hand side is for the classical model with Hamiltonian H. The time-ordered functions appear in the quantum problem for the same reason we had to assume $j \geq i$ in (2.10): as the transfer matrix evolves the system from 'earlier' sites to 'later' sites, the earlier $\hat{\sigma}^z$ operators appear first in the trace.

The representation (2.30) also makes the origin of the mapping between the quantum gap, Δ, and the classical correlation length, ξ, in

(2.28) quite clear. We can evaluate (2.30) at $T = 0$ by inserting a complete set of H_Q eigenstates and obtain the general representation

$$G(\tau_1, \tau_2) = \sum_n |\langle 0|\sigma^z|n\rangle|^2 \, e^{-(E_n - E_0)|\tau_1 - \tau_2|}, \qquad (2.33)$$

where $|n\rangle$ are all the eigenstates of H_Q with eigenvalues E_n, and $|0\rangle$ is the ground state. For sufficiently large $|\tau_1 - \tau_2|$, the sum over n will be dominated by lowest energy state for which the matrix element is non-zero, and this gives an exponential decay of the correlation function over a 'length' $\xi = 1/(E_1 - E_0) = 1/\Delta$. Of course, in the present simple system there are only a total of two states, but this result is clearly more general.

It is quite easy to evaluate (2.30) for H_Q, and the direct quantum computation is much simpler than the use of the classical mapping in (2.32). We find

$$G(\tau_1, \tau_2) = \Phi_\sigma \left(T(\tau_1 - \tau_2), \frac{\Delta}{T}, \frac{\widetilde{h}}{T} \right) \qquad (2.34)$$

where Φ_σ is precisely the same scaling function that appeared in (2.24), and can be computed from (2.30) to be

$$\Phi_\sigma (y_1, y_2, y_3) = \frac{4y_3^2}{y_2^2 + 4y_3^2} + \frac{y_2^2}{y_2^2 + 4y_3^2} \frac{\cosh \left(\sqrt{y_2^2 + 4y_3^2}(1 - 2|y_1|)/2 \right)}{\cosh \left(\sqrt{y_2^2 + 4y_3^2}/2 \right)}$$

$$(2.35)$$

It can be checked that the $y_3 = 0$ case of this result agrees with the combination of (2.22) and (2.24).

2.2 The classical XY chain and a O(2) quantum rotor

We will consider the $D = 1$, $N = 2$ classical ferromagnet; this is also referred to as the XY ferromagnet. We generalize (2.1,2.2) to $N = 2$ by replacing σ_i^z by a two-component unit-length variable $\mathbf{n}_i$. This modifies (2.1) to

$$\mathcal{Z} = \prod_i \int D\mathbf{n}_i \delta (\mathbf{n}_i^2 - 1) \exp (-H) \, ; \qquad (2.36)$$

for H we modify (2.2) to

$$H = -K \sum_{i=1}^M \mathbf{n}_i \cdot \mathbf{n}_j - \sum_{i=1}^M \mathbf{h} \cdot \mathbf{n}_i, \qquad (2.37)$$

where, as in the Ising case, we have added a uniform field $\mathbf{h} = (h, 0)$. (3.3). It is convenient to parameterize the unit length classical spins, $\mathbf{n}_i$, by

$$\mathbf{n}_i = (\cos\theta_i, \sin\theta_i) \tag{2.38}$$

where the continuous angular variables θ_i, run from 0 to 2π. In these variables, H takes the form

$$H = -K\sum_{i=1}^{M}\cos(\theta_i - \theta_{i+1}) - h\sum_{i=1}^{M}\cos\theta_i, \tag{2.39}$$

and the partition function is

$$\mathcal{Z} = \int_0^{2\pi}\prod_{i=1}^{M}\frac{d\theta_i}{2\pi}\exp(-H). \tag{2.40}$$

We again assume periodic boundary conditions with $\theta_{M+1} \equiv \theta_1$. Notice that in zero field, H remains invariant if all the spins are rotated by the same angle ϕ, $\theta_i \rightarrow \theta_i + \phi$, and so our results will not depend upon the particular orientation chosen for $\mathbf{h}$. The partition function can be evaluated by transfer matrix methods [156, 255] quite similar to those used for the Ising chain. Although we will not use such a method to obtain our results, we nevertheless describe the main steps for completeness. First write $\mathcal{Z}$ in the form

$$\begin{aligned}
\mathcal{Z} &= \int_0^{2\pi}\prod_{i=1}^{M}\frac{d\theta_i}{2\pi}\langle\theta_1|\hat{T}|\theta_2\rangle\langle\theta_2|\hat{T}|\theta_3\rangle\cdots\langle\theta_M|\hat{T}|\theta_1\rangle \\
&= \mathrm{Tr}\hat{T}^M \tag{2.41}
\end{aligned}$$

where the symmetric transfer matrix operator $\hat{T}$ is defined by

$$\langle\theta|\hat{T}|\theta'\rangle = \exp\left(K\cos(\theta - \theta') + \frac{h}{2}(\cos\theta + \cos\theta')\right), \tag{2.42}$$

and the trace is clearly over continuous angular variable θ. As in the Ising case, we have to diagonalize the transfer matrix $\hat{T}$ by solving the eigenvalue equation

$$\int_0^{2\pi}\frac{d\theta'}{2\pi}\langle\theta|\hat{T}|\theta'\rangle\Psi_\mu(\theta') = \lambda_\mu\Psi_\mu(\theta) \tag{2.43}$$

for the eigenfunctions $\Psi_\mu(\theta)$ (with $\Psi_\mu(\theta + 2\pi) = \Psi_\mu(\theta)$), and corresponding eigenvalues λ_μ. Then the partition function $\mathcal{Z}$ is simply

$$\mathcal{Z} = \sum_\mu\lambda_\mu^M \tag{2.44}$$

where the sum extends over the infinite number of eigenvalues λ_μ. The solution of (2.43) is quite involved, and the present approach is a rather convoluted method of obtaining the universal properties of H.

Instead, it is useful to approach the problem with a little physical insight, and take the scaling limit at the earliest possible stage. We anticipate, from our experience with the Ising model, that the universal scaling behavior will emerge at large values of K. For this case, θ_i is not expected to vary much from one site to the next, suggesting that it should be useful to expand in terms of gradients of θ_i. So we define a continuous co-ordinate $\tau = ja$, where a is the lattice spacing, and the label τ anticipates its eventual interpretation as the imaginary time co-ordinate of a quantum problem. Then to lowest order in the gradients of the function $\theta(\tau = ja) \equiv \theta_j$, the Hamiltonian H takes the continuum form H_c:

$$H_c[\theta(\tau)] = \int_0^{L_\tau} d\tau \left[\frac{\xi}{4} \left(\frac{d\theta(\tau)}{d\tau} \right)^2 - \widetilde{h} \cos\theta(\tau) \right] \qquad (2.45)$$

where

$$\xi = 2Ka \qquad\qquad \widetilde{h} = \frac{h}{a}, \qquad (2.46)$$

and as before $L_\tau = Ma$. The coefficient of the gradient squared term is clearly a length (along the time direction) and we have written this length in terms of the symbol ξ: the parameterization anticipates some of our subsequent results where we will see that ξ is the $h = 0$ correlation length of an infinite XY chain. With this new form of H, the partition function becomes a functional integral

$$\mathcal{Z}_c = \sum_{p=-\infty}^{\infty} \int_{\theta(L_\tau)=\theta(0)+2\pi p} \mathcal{D}\theta(\tau) \exp\left(-H_c[\theta(\tau)] \right) \qquad (2.47)$$

The integral is taken over all functions $\theta(\tau)$ that satisfy the specified boundary conditions. As we can continuously follow the value of θ from $\tau = 0$ to $\tau = L_\tau$, its actual value, and not just the angle modulo 2π, becomes significant; so we allow for an overall phase winding by $2\pi p$ in the boundary conditions. This boundary condition is the only remnant of the periodicity of the original lattice problem as $\theta(\tau)$ is allowed to assume all real values. We have also absorbed an overall normalization factor into the definition of the functional integral, and will therefore not keep track of additive non-universal constants to the free energy like E_0 of Section 2.1.

We now assert that $\mathcal{Z}_c$ and H_c are the universal scaling theories of H and $\mathcal{Z}$ in (2.39,2.40). So if we started with a different microscopic model, its universal properties would also be described by $\mathcal{Z}_c$, with the only change being in the values of ξ and $\tilde{h}$. For instance if we had a Hamiltonian like (2.39), but with j'th neighbor interactions K_j, its continuum limit would also be H_c, with the same value for $\tilde{h}$, but ξ modified to

$$\xi = 2a \sum_{j=1}^{\infty} K_j j^2 \tag{2.48}$$

This continuum limit is valid for all models in which the summation over j in (2.48) converges. The universality of H_c also applies to models in which the constraint $\mathbf{n}_i^2 = 1$ is not imposed rigidly, and fluctuations in the amplitude of $\mathbf{n}_i$ are allowed about their mean value. The prescription for determining the input value of ξ is however still very simple: set the magnitude of $\mathbf{n}_i$ to its optimum value and measure the energy change of a uniform twist. Corrections due to the fluctuations in the magnitude of $\mathbf{n}_i$ about this optimum value will not modify the universal scaling theory (2.46).

Before turning to an evaluation of $\mathcal{Z}_c$ and its associated correlators, let us describe the scaling forms expected in the universal theory. These can be deduced by simple dimensional analysis. In the present case ξ, L_τ, and $\tilde{h}$ are the large lengths of the theory, and we simply make the appropriate dimensionless combinations. So we have for the free energy $\mathcal{F} = -(\ln \mathcal{Z}_c)/L_\tau$ and the two-point correlator:

$$
\begin{aligned}
\mathcal{F} &= \frac{1}{L_\tau} \Phi_{\mathcal{F}} \left(\frac{L_\tau}{\xi}, \tilde{h} L_\tau \right) \\
\langle \mathbf{n}(\tau) \cdot \mathbf{n}(0) \rangle &= \Phi_n \left(\frac{\tau}{L_\tau}, \frac{L_\tau}{\xi}, \tilde{h} L_\tau \right)
\end{aligned}
\tag{2.49}
$$

where $\Phi_{\mathcal{F}}$ and Φ_n are universal functions, portions of which will be determined explicitly below.

Let us evaluate $\mathcal{Z}_c$ in zero field $\tilde{h} = 0$. To satisfy the boundary conditions let us decompose

$$\theta(\tau) = \frac{2\pi p \tau}{L_\tau} + \theta'(\tau) \tag{2.50}$$

where $\theta'(\tau)$ satisfies periodic boundary conditions $\theta'(L_\tau) = \theta'(0)$. Inserting this into (2.45) we find that the cross term between the two pieces of $\theta(\tau)$ vanishes because of the periodic boundary conditions on θ', and

(2.47) becomes

$$\mathcal{Z}_c(\widetilde{h} = 0) = \left(\sum_{p=-\infty}^{\infty} \exp\left(-\frac{\pi^2 p^2 \xi}{L_\tau} \right) \right)$$

$$\times \int_{\theta'(L_\tau) = \theta'(0)} \mathcal{D}\theta'(\tau) \exp\left(-\frac{\xi}{4} \int_0^{L_\tau} d\tau \left(\frac{d\theta'}{d\tau} \right)^2 \right) \tag{2.51}$$

Now notice that the last functional integral is simply the familiar Feynman path integral for the amplitude of a single quantum mechanical free particle, of mass $\xi/2$ with co-ordinate θ', to return to its starting position after imaginary time L_τ. Using the standard expression for this we find finally

$$\mathcal{Z}_c(\widetilde{h} = 0) = \left(\frac{\xi}{4\pi L_\tau} \right)^{1/2} A(\pi \xi / L_\tau), \tag{2.52}$$

where $A(y)$ is the elliptic theta function defined by

$$A(y) = \sum_{p=-\infty}^{\infty} e^{-\pi p^2 y}. \tag{2.53}$$

This result is clearly consistent with the scaling form for the free energy density $\mathcal{F} = -(\ln \mathcal{Z}_c)/L_\tau$ in (2.49).

Let us push the analogy with the quantum mechanics of a particle a bit further, and complete the quantum-classical mapping by obtaining an explicit expression for the quantum Hamiltonian, H_Q, which describes the scaling limit. Note that $\mathcal{Z}_c$ in (2.47), with the summation over p included, can be interpreted as the Feynman path integral of a particle constrained to move on a *circle* of unit radius; the angular co-ordinate of the particle is θ, and p represents the number of times the particle winds around the circle in its motion from imaginary time $\tau = 0$ to $\tau = L_\tau$. The term proportional to $\widetilde{h}$ is then a potential energy term which preferentially locates the particle at $\theta = 0$. The Hamiltonian of this quantum particle is then

$$H_Q = -\Delta \frac{\partial^2}{\partial \theta^2} - \widetilde{h} \cos \theta \tag{2.54}$$

where, as we will see shortly, Δ is defined as in the Ising case to be the gap of H_Q in zero external field. As the mass of the quantum particle is $1/2\Delta$, we have by comparing with (2.45)

$$\Delta = \frac{1}{\xi}; \tag{2.55}$$

This is precisely of the form (2.28), and is another realization of the fact that the gap of the quantum model is equal to the correlation 'length' of the classical model along the imaginary time direction. For some of our subsequent discussion it is useful to express H_Q solely in terms of quantum operators. Let $\hat{\mathbf{n}}$ be the Heisenberg operator corresponding to $\mathbf{n}$. Let us also define $\hat{L}$ as the angular momentum operator of the rotor

$$\hat{L} = \frac{1}{i}\frac{\partial}{\partial\theta}. \tag{2.56}$$

Then we have the commutation relation

$$[\hat{L}, \hat{n}_\alpha] = i\epsilon_{\alpha\beta}\hat{n}_\beta \tag{2.57}$$

where α, β extend over the two co-ordinate axes, x, y in the spin plane, and $\epsilon_{xy} = -\epsilon_{yx} = 1$, with other components zero. These are precisely the $N = 2$ case of the commutation relations following from (1.15) and (1.18). The Hamiltonian H_Q is clearly

$$H_Q = \Delta\hat{L}^2 - \widetilde{\mathbf{h}}\cdot\hat{\mathbf{n}} \tag{2.58}$$

which is simply the quantum rotor model (1.20) in the presence of field $\widetilde{\mathbf{h}}$, $1/2\Delta$ is the moment of inertia of the rotor, and commutation relation (2.57) is the $N = 2$ analog of (1.19). We have established the needed result: the scaling limit of the $D = 1$ classical XY ferromagnet is given exactly by the Hamiltonian of a single O(2) quantum rotor.

The Hamiltonian H_Q is related to the transfer matrix $\hat{T}$ (in (2.42) of the lattice XY model by a relationship identical to that found in (2.26). By a gradient expansion of (2.42) the reader can verify that

$$\hat{T} \approx \exp(-aH_Q) \tag{2.59}$$

to leading order in the lattice spacing a. So again, the transfer matrix 'evolves' the system by an imaginary time a.

We can use the quantum-classical mapping, and obtain explicit expressions for the universal scaling functions of the classical problem in (2.49). First, using the mapping (3.13) $T = 1/L_\tau$, let us write down the scaling forms (2.49) in the quantum language

$$\mathcal{F} = T\Phi_{\mathcal{F}}\left(\frac{\Delta}{T}, \frac{\widetilde{h}}{T}\right)$$

$$\langle\mathbf{n}(\tau)\cdot\mathbf{n}(0)\rangle = \Phi_n\left(T\tau, \frac{\Delta}{T}, \frac{\widetilde{h}}{T}\right). \tag{2.60}$$

We see here a structure that was used in (2.34), and which shall be used

throughout the book. We characterize the universal properties by the "small" energy scales Δ, $\widetilde{h}$ (these are the analogs of the "large" length scales of the corresponding classical problem, while the non-universal behavior at "small" length scales in the classical system maps onto high energy physics in the quantum system which is not of interest here). These "small" energy scales then appear in universal scaling functions of dimensionless ratio of these energies with the physical temperature, T.

Let us turn to the evaluation of the scaling functions. The eigenstates, $\psi_\mu(\theta)$, and eigenvalues ϵ_μ of H_Q are determined by solving the Schrödinger equation

$$H_Q \psi_\mu(\theta) = \epsilon_\mu \psi_\mu(\theta) \tag{2.61}$$

subject to the boundary condition $\psi_\mu(0) = \psi_\mu(2\pi)$. The equation (2.61) can be considered as the continuum scaling limit of the eigenvalue equation (2.43) with the correspondences (2.59) and $\lambda_\mu \propto \exp(-a\epsilon_\mu)$. The continuum limit partition function $\mathcal{Z}_c$ can be expressed directly in terms of H_Q:

$$
\begin{aligned}
\mathcal{Z}_c &= \operatorname{Tr} \exp(-H_Q/T) \\
&= \sum_\mu \exp(-\epsilon_\mu/T), \tag{2.62}
\end{aligned}
$$

where $T = 1/L_\tau$. The two-point correlator of $\hat{n}$ can also be expressed in the quantum language

$$
\begin{aligned}
\langle \mathbf{n}(\tau) \cdot \mathbf{n}(0) \rangle &= \frac{1}{\mathcal{Z}_c} \operatorname{Tr} \left(e^{-H_Q/T} e^{H_Q \tau} \hat{\mathbf{n}} e^{-H_Q \tau} \cdot \hat{\mathbf{n}} \right) \\
&= \frac{1}{\mathcal{Z}_c} \sum_{\mu,\nu} |\langle \mu | \hat{\mathbf{n}} | \nu \rangle|^2 e^{-\epsilon_\mu/T} e^{-(\epsilon_\nu - \epsilon_\mu)\tau} \tag{2.63}
\end{aligned}
$$

where the summation over μ, ν extends over all the eigenstates of H_Q, and we have assumed $\tau > 0$.

The solution of (2.61), combined with (2.62), (2.63) provides the complete solution of the universal scaling properties of the classical XY chain. An elementary solution of the eigenvalue equation (2.61) is only possible at $\widetilde{h} = 0$, to which we will restrict our attention form now on. In zero field, the eigenstates are $\psi_m(\theta) \propto e^{im\theta}$, where m is an arbitrary integer, and the corresponding eigenvalues are Δm^2 (these are the states of (1.21)). The ground state has zero energy ($m = 0$), and, as promised, the gap to the lowest excited states ($m = \pm 1$) is Δ. We can therefore

evaluate the partition function

$$
\begin{aligned}
\mathcal{Z}_c(\widetilde{h} = 0) &= \sum_{m=-\infty}^{\infty} \exp\left(-\frac{\Delta m^2}{T}\right) \\
&= A(\Delta/\pi T), \tag{2.64}
\end{aligned}
$$

a result that satisfies (2.60); the function $A(y)$ was defined in (2.53). Comparing this with (2.52), and using (2.55), (2.28), it does not appear obvious that the two expressions for $\mathcal{Z}_c$ are equivalent. However, equality can be established by use of the following inversion identity, which the reader is invited to establish as a simple application of the Poisson summation formula:

$$
A(y) = \frac{A(1/y)}{\sqrt{y}}. \tag{2.65}
$$

In terms of the original classical model, the expression (2.52) for $\mathcal{Z}_c$ is useful for large ξ (or large values of K, corresponding to a low classical "temperature" which has been absorbed into the definition of K) when its series converges rapidly; conversely the dual expression (2.64) is most useful for small ξ (or small K and high classical "temperatures").

Let us also discuss the form of the correlation functions at $\widetilde{h} = 0$. Recalling (2.38), and the wavefunction $\psi_m(\theta) \propto e^{im\theta}$, we have the very simple matrix element

$$
|\langle m|\hat{\mathbf{n}}|m+1\rangle|^2 = 1 \tag{2.66}
$$

and all others vanish; the correlation function follows simply from (2.63), and it is clear that the result agrees with (2.60). In particular, at $T = 0$ or $L_\tau = \infty$ we have

$$
\langle \mathbf{n}(\tau) \cdot \mathbf{n}(0) \rangle = e^{-\Delta|\tau|}, \tag{2.67}
$$

which establishes, as in the Ising chain, the inverse of the gap Δ as the correlation length of the classical chain.

2.3 The classical Heisenberg chain and a O(3) quantum rotor

We now generalize the results of the previous section to the $D = 1$, $N = 3$ case. The $N = 3$ classical ferromagnet is also known as the classical Heisenberg chain. The partition function is still given by (2.36) and the classical Hamiltonian by (2.37), with the only change that $\mathbf{n}$ is now a three-component unit vector. Taking its continuum limit as for

$N = 2$ we replace (2.45) and (2.47) by the partition function

$$
\begin{aligned}
\mathcal{Z}_c &= \mathcal{D}\mathbf{n}(\tau)\delta(\mathbf{n}^2 - 1)\exp\left(-H_c[\mathbf{n}(\tau)]\right) \\
H_c[\mathbf{n}(\tau)] &= \int_0^{L_\tau} d\tau \left[\frac{(N-1)\xi}{4}\left(\frac{d\mathbf{n}(\tau)}{d\tau}\right)^2 - \widetilde{\mathbf{h}}\cdot\mathbf{n} \right], \quad (2.68)
\end{aligned}
$$

with $\mathbf{n}(0) = \mathbf{n}(L_\tau)$; now $\xi = 2Ka/(N-1)$ and $\widetilde{\mathbf{h}} = \mathbf{h}/a$ as in (2.46). We have chosen the definition of ξ by anticipating a later computation in which ξ will be seen to be the correlation length. We will only consider the case $N = 3$ in this subsection, and have quoted, without proof, the form for general N; notice that (2.68) agrees with (2.45) for $N = 2$. Unlike (2.45), it is not possible to evaluate the partition function (2.68) in this form. Recall that for the $N = 2$ case of (2.45) we had a simple angular parameterization in which H became purely quadratic in the angular variable: one could parameterize the 3-component $\mathbf{n}$ using spherical co-ordinates, but the resulting H is not simply quadratic.

Further progress towards the evaluation of $\mathcal{Z}_c$ can however be made after the quantum-classical mapping. To do this, note as in (2.51), the functional integral in (2.68) can be interpreted as the imaginary-time Feynman path integral for a particle moving in a 3-dimensional space with co-ordinate $\mathbf{n}$. Then the term with $(\partial\mathbf{n}/\partial\tau)^2$ is its kinetic energy and its mass is $1/\xi$, and the term proportional to $\widetilde{\mathbf{h}}$ is like a "gravitational potential energy". The constraint that $\mathbf{n}^2 = 1$ may be viewed as a very strong potential that prefers the particle move on the surface of a unit sphere. We can therefore perform the quantum-classical mapping simply by writing down the Schrödinger Hamiltonian, H_Q, for this particle. The restriction that the motion take place on the surface of a sphere simply means that the radial kinetic energy term of the particle should be dropped. The resulting H_Q generalizes (2.58) to $N = 3$

$$
H_Q = \frac{\Delta}{2}\hat{\mathbf{L}}^2 - \widetilde{\mathbf{h}}\cdot\mathbf{n} \tag{2.69}
$$

where the angular momentum operator $\hat{\mathbf{L}}$ has 3 components (in general it has $N(N-1)/2$ components); again this is simply the $N = 3$ single rotor model H_K in (1.20) in the presence of a field $\widetilde{\mathbf{h}}$. The operators $\hat{\mathbf{L}}$ and $\hat{\mathbf{n}}$ obey the commutation relations in (1.19). The parameter Δ is again the energy gap at $\widetilde{\mathbf{h}} = 0$, as we will see below, and is given by $\Delta = 1/\xi$, as in (2.55). If we determine all the eigenvalues ϵ_μ of H_Q then the explicit expression for $\mathcal{Z}_c$ is given by (2.62). Determination of the eigenvalues of H_Q can, for instance, be done by solving the Schrödinger

differential equation for a wavefunction $\psi_\mu(\mathbf{n})$ on the surface of a unit sphere. The Hamiltonian in Schrödinger's equation is given by H_Q, with $\hat{\mathbf{L}}$ a differential operator

$$L_\alpha = -i\epsilon_{\alpha\beta\gamma} n_\beta \frac{\partial}{\partial n_\gamma}. \tag{2.70}$$

So to summarize, the complete solution of the classical partition function $\mathcal{Z}_c$ is given by mapping the problem to the dynamics of a O(3) quantum rotor with Hamiltonian H_Q defined by (2.69,1.19,2.70), and the value of $\mathcal{Z}_c$ is given by (2.62).

We conclude this section by explicitly determining the eigenvalues for $\widetilde{\mathbf{h}} = 0$. In this case, it is evident that the eigenfunctions ψ_μ are simply the spherical harmonics, and the eigenvalues are

$$\Delta \ell(\ell+1) \qquad \ell = 0, 1, 2 \ldots \infty \tag{2.71}$$

with degeneracy $2\ell + 1$ (as in (1.22)), so that

$$
\begin{aligned}
\mathcal{Z}_c(\widetilde{\mathbf{h}} = 0) &= \mathrm{Tr} e^{-H_Q/T} \\
&= \sum_{\ell=0}^{\infty} (2\ell+1) \exp\left(-\frac{\Delta}{2T}\ell(\ell+1)\right),
\end{aligned} \tag{2.72}
$$

replacing (2.64), and as before $T = 1/L_\tau$. The ground state is the non-degenerate $\ell = 0$ state, and it can be checked that the energy gap is Δ. The correlations continue to obey (2.67), and so there is no long-range order in the classical Heisenberg chain, and the correlation length $= 1/\Delta$.

3

Overview

This chapter will begin by presenting the $D > 1$-dimensional classi-
cal statistical mechanical models which are 'equivalent' (in a sense to
be made precise) to the quantum Ising and rotor models introduced in
Chapter 1. The universal properties of these transitions will be discussed
and we will argue that these are described by certain continuum field
theories. At the level of the these continuum theories it will be argued
quite generally that, at least in a formal sense, there is a classical sta-
tistical mechanical model associated with every second order quantum
phase transition. The nature of this general quantum-classical mapping
will be discussed and its limitations and utility will be highlighted.

   We set the stage by simply writing down the D-dimensional clas-
sical statistical mechanical models which will be mapped onto the d-
dimensional quantum Ising and rotor models of Chapter 1, where

$$D = d + 1, \tag{3.1}$$

These models are the straightforward generalizations of the $D = 1$ mod-
els considered in Chapter 2. For $N = 1$, we consider the classical Ising
partition function (generalizing (2.1) and (2.2)

$$\mathcal{Z} = \sum_{\{\sigma_i^z = \pm 1\}} \exp\left(K \sum_{<i,j>} \sigma_i^z \sigma_j^z \right) \tag{3.2}$$

where K is a dimensionless coupling which characterizes the 'tempera-
ture' of the classical problem, the sum is over all 2^M possible configu-
rations of Ising spins in a system of M sites in D dimensions (we will
set the external field $h = 0$ in this chapter, although it is not difficult
to extend our considerations to include it). For $N > 1$, we generalize

36
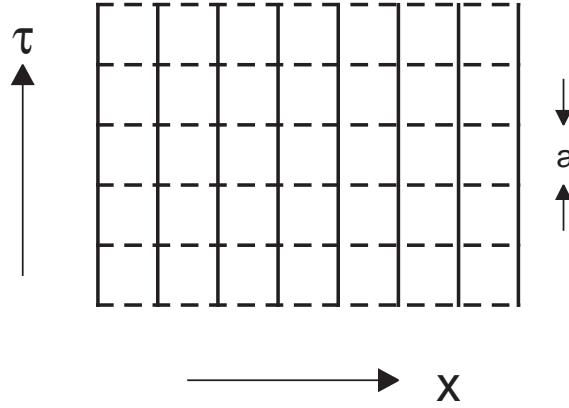
Fig. 3.1. *D*-dimensional lattice on which (3.2) and (3.3) are defined. The spatial co-ordinate *x* is a schematic for $d = D - 1$ directions. The mappings of Chapter 2 is performed independently on each of the columns represented by the full lines: this yields a *d*-dimensional lattice of quantum Ising spins (for (3.2) or quantum rotors (for (3.3) coupled to each other by the couplings on the dashed lines. The quantum operator $\exp(-aH_{I,R})$ is the transfer matrix of the classical models (3.2,3.3) from one *d*-dimensional 'row' to the next.

(2.36) and (2.37) to

$$\mathcal{Z} = \prod_i \int D\mathbf{n}_i \delta(\mathbf{n}_i^2 - 1) \exp\left(K \sum_{<i,j>} \mathbf{n}_i \cdot \mathbf{n}_j \right) \qquad (3.3)$$

where $\mathbf{n}_i$ is a $N \geq 2$ component unit vector on the sites, i, of a hypercubic lattice in D dimensions.

We can perform a close analog of the manipulations of Chapter 2 on the models (3.2) and (3.3), as illustrated in Fig 3.1. First, arbitrarily pick out one of the D directions as the quantum 'time' direction (the τ direction in Fig 3.1), and set up a transfer matrix formulation of the partition function. The transfer matrix would 'evolve' the configuration from one $d = D - 1$ dimensional plane to the next, just as the matrices in, *e.g.*, (2.41) couple two neighboring sites along the τ direction for the case $D = 1$. In other words, we perform the operations of Chapter 2 independently along each of the full lines of Fig. 3.1. The matrices therefore act on a space which is the direct tensor product of the spaces on each site in a *d*-dimensional spatial plane (a 'time slice'). The models (3.2) and (3.3) also have couplings within each time slice (represented by the dashed lines in Fig 3.1), but these merely contribute additional

diagonal terms to the transfer matrix. In this manner, we see that
the coupling K between two points separated by a full line in Fig 3.1
transforms into the transverse field term proportional to Jg in (1.5) for
$N = 1$ (as shown in Section 2.1), and into the term proportional to $J\widetilde{g}$
in (1.23) for $N \geq 2$ (as shown in Sections 2.2 and 2.3). Moreover, the
coupling K between two sites separated by a dashed line will simply go
along for the ride, and become the inter-site coupling proportional to
J in (1.5) and (1.23). Then the transfer matrix from one time slice to
the next is $\exp(-aH_{I,R})$ (as in (2.26)), while the full partition function
becomes

$$\mathcal{Z} \sim \mathrm{Tr}\exp\left(-H_{I,R}/T\right), \tag{3.4}$$

where $T = 1/L_\tau = 1/(Ma)$, with M the number of d-dimensional rows
along the τ direction (as in all the models of Chapter 2. We have now
established the advertised relationship between the D-dimensional clas-
sical partition functions (3.2,3.3) in a geometry which is of infinite extent
in $(D-1)$ dimensions and of finite length L_τ along the 'time' direction,
and the quantum partition functions of the d-dimensional Hamiltonians
in (1.5) and (1.23) at a temperature $T = 1/L_\tau$.

The above discussion gives a qualitative and intuitive picture of the
mapping, but it is not numerically precise, as it glossed over the limit
of lattice spacing $a \to 0$ we had to take in Chapter 2. However, as
in Chapter 2, the quantum-classical mapping can be made exact by
considerations of universal properties in an appropriate scaling limit of
both models. Such a scaling limit must clearly be taken in a regime
where the correlation length is much larger than the lattice spacing.
We have already discussed such regions of large correlation length in
Chapter 1 for the quantum Ising and rotor models. Let us now do the
same for the classical models (3.2) and (3.3).

The models (3.2) and (3.3) are central to the theory of finite temper-
ature phase transitions in classical statistical mechanics [63, 550, 247],
and readers should be already be familiar with the basic concepts (the
cited texts are good places to review these). For all values of N in $D > 2$,
and for $N = 1, 2$ in $D = 2$ these models display a phase transition be-
tween a low 'temperature' magnetically ordered phase for $K > K_c$ and
a high 'temperature' disordered phase for $K < K_c$. These phases are
characterized by correlations of the order parameter $\sigma^z, \mathbf{n}$ in a manner
closely analogous to the magnetically ordered and quantum paramag-
netic phases of Chapter 1. So in the $K < K_c$ disordered phase we have,

as in (1.24),

$$\langle \hat{\mathbf{n}}_i \cdot \hat{\mathbf{n}}_j \rangle \sim e^{-|x_i - x_j|/\xi}, \tag{3.5}$$

for large $|x_i - x_j|$, where the average is with respect to the classical partition function (3.3) and x_i is a D-dimensional co-ordinate. Similarly, for $K > K_c$ we have, in (1.25),

$$\lim_{|x_i - x_j| \to \infty} \langle 0 | \hat{\mathbf{n}}_i \cdot \hat{\mathbf{n}}_j | 0 \rangle = N_0^2, \tag{3.6}$$

where N_0 is the spontaneous magnetization (this does not apply to the special case $D = 2$, $N = 1$, where the behavior for $K > K_c$ will be discussed in Section 14.3). Similar results hold for the $N = 1$ case with the variable σ^z. Upon approaching K_c, N_0 vanishes as a power-law, and ξ diverges as

$$\xi^{-1} \sim a|K - K_c|^\nu, \tag{3.7}$$

with ν a critical exponent. Again, an exception to this is the case $N = 2$, $D = 2$ where the divergence of ξ has a different form. Also for the cases $N > 2$, $D = 2$ there is no phase transition at any finite K, but there is diverging correlation length for $K \to \infty$, and most of the considerations below apply to these cases too.

We can now make a precise statement of the quantum-classical mapping. The universal properties of the d-dimensional quantum Ising and rotor models in their region of large correlation length are identical to those of the D-dimensional classical models (3.2) and (3.3). Further, correlators of the classical model in D dimensions map onto imaginary time correlators of the d-dimensional quantum model, where one of the classical D dimensions behaves like the quantum imaginary time direction, and the remaining $D - 1$ classical directions map onto the d spatial directions of the quantum model. This assertion is justified by the considerations of Chapter 2, the arguments made in the paragraph following (3.3), and will be further supported by many of the computations in Part 2. The mapping has an immediate consequence: as the quantum imaginary time direction is simply one of the spatial directions of the classical model, we compare (3.7) and (1.1,1.2) and conclude that we must have the dynamic exponent $z = 1$ for the quantum Ising/rotor models.

Having identified the appropriate universal scaling limit of the quantum models, it is appropriate to ask (in the sense of the discussion below (2.29)): what is the quantum theory which describe these universal prop-

erties ? These turn out to be continuum quantum field theories which will be introduced in the following section.

3.1 Quantum field theories

The following discussion will be carried out in the language of the quantum Ising and rotor models. However, essentially the same arguments can also be made for the classical models (3.2) and (3.3), and these are discussed at considerable length in numerous excellent texts [63, 550, 247]; we will refer to these at the end of the following section.

We repeat the basic argument presented in Sections 2.1.1 and 2.1.2 for the $D = 1$ Ising chain, but apply it more generally. Returning to the notation of Section 1.1, let us consider the regime where $|g - g_c|$ is small, so that

$$\Delta \ll J \text{ and } \xi^{-1} \ll \Lambda. \tag{3.8}$$

Suppose further, that we are observing the system at a temperature T, a length scale x, and a frequency scale ω, and all of these are of order the temperature, length and energy scales that can be created out of Δ, ξ, and the fundamental constants. We will then be particularly interested in dynamic response functions of the system near a quantum critical point in the limit where the inequalities (3.8) are well satisfied. From a particle theorist's perspective, this means we are taking the limits $\Lambda \to \infty$ and $J \to \infty$ while keeping Δ, ξ, x, ω and T fixed. In terms of dimensionless parameters, this means we are sending $\Lambda\xi \to \infty$ and $J/\Delta \to \infty$, while keeping $\hbar\omega/\Delta$, x/ξ and $k_B T/\Delta$ fixed. A glance at (1.1) and (1.2) shows that these limits can only be taken while tuning g to become progressively closer to g_c. The complementary condensed matter theorist's perspective is that we are keeping Λ and J fixed and looking at the system's response at small Δ, large ξ and at long distances and times and low temperatures: the two approaches are clearly equivalent as the limits of the dimensionless ratios are the same. The resulting response functions can be considered to be correlators of a *quantum field theory*, which is now associated with a Hamiltonian defined in the continuum, and has no intrinsic short distance or high energy cutoff. A quantum field theory shares many of the characteristics of ordinary quantum mechanics, with a unitary time evolution operator defined by the continuum Hamiltonian, except that it has an infinite number of degrees of freedom per unit volume.

The physical utility of the quantum field theory relies mainly on its *universality*. As we have sent $\Lambda \to \infty$ and $J \to \infty$, it appears plausible that changes in the structure of $H(g)$ at the lattice scale will not modify the nature of the quantum field theory which eventually appears, and the only consequence is a change in the values of the dimensionful parameters Δ and ξ (this change happens due to modifications of the prefactors in (1.1) and (1.2), which, as we have already asserted, are non-universal). A general rule of thumb is that only essential qualitative features, like the symmetry of the order parameter, the dimensionality of space, and constraints placed by conservation laws survive the continuum limit, and the structure of the quantum field theory is severely constrained by these restrictions.

We have argued above that every second order quantum phase transition defines a quantum field theory in the continuum. Our attack on the quantum phase transition problem in this book can be considered as consisting of two essential steps. First we understand and classify the various quantum field theories that can arise out of quantum phase transitions in lattice Hamiltonians of physical interest. And second, we describe the dynamical properties of these quantum field theories at finite temperatures. The latter will then model the universal properties of the physical lattice Hamiltonians in the vicinity of the quantum critical point.

We can now answer the basic question: what are the quantum field theories associated with the second order quantum phase transitions in the quantum rotor model H_R in (1.23) and the quantum Ising model H_I in (1.5) ? It is possible to give a common treatment of H_I and H_R, with H_I simply being the $N = 1$ case of a general discussion for H_R. We attempt to write down a Feynman path integral for the partition function (we will explicitly include factors of $\hbar$ and k_B in the remainder of this chapter)

$$\mathcal{Z} = \mathrm{Tr} \exp\left(-\frac{H_{R,I}}{k_B T} \right), \qquad (3.9)$$

essentially by following the inverse of the mapping discussed in Chapter 2. This is expressed in terms of a functional integral over all possible time histories (the 'sum over histories' formulation of quantum mechanics) of the rotor co-ordinate $\mathbf{n}(\tau)$ over an imaginary time $0 \leq \tau \leq \hbar/k_B T$ (and similarly for σ_i^z for $N = 1$). If we think of this time axis as the one-dimensional axis of the classical models studied in Chapter 2, then this functional integral over time is simply the partition function of the

classical chain—we saw how to evaluate these in Chapter 2. The final quantum field theory is conveniently expressed in terms of a coarse-grained field $\phi_\alpha(x, \tau)$ defined by

$$\phi_\alpha(x, \tau) \sim \sum_{i \in \mathcal{N}(x)} n_{i\alpha}(\tau) \tag{3.10}$$

where x is a point in d-dimensional space, $\mathcal{N}(x)$ is a coarse-graining neighborhood of x, the index $\alpha = 1 \ldots N$, and the overall normalization of ϕ_α can be chosen at our convenience. For the case $N = 1$, we simply replace $n_{i\alpha}$ by σ_i^z. Because the $\mathbf{n}_i$ can point in different directions at each i, the magnitude of ϕ_α can vary over a wide range. Indeed, it seems reasonable that instead of placing a "hard" constraint like $\mathbf{n}_i^2 = 1$, we can view ϕ_α as a "soft" spin whose magnitude can vary freely over all positive values. A remnant of the hard constraint on the microscopic degrees of freedom is that we have a local effective potential $V(\phi_\alpha^2)$ which controls fluctuations of ϕ_α^2, and prevents it from becoming too large. We can also make a polynomial expansion for V, and it turns out to be adequate to truncate it at terms of order $(\phi_\alpha^2)^2$. In this manner, the quantum field theory obtained by considering the vicinity of the quantum critical points in $H_{R,I}$ is defined by the following imaginary time Feynman path integral over all possible time histories of the field $\phi_\alpha(x, \tau)$ for the partition function $\mathcal{Z}$:

$$\mathcal{Z} = \int \mathcal{D}\phi_\alpha(x, \tau) \exp(-\mathcal{S}_\phi)$$

$$\mathcal{S}_\phi = \int d^d x \int_0^{\hbar/k_B T} d\tau \left\{ \frac{1}{2} \left[(\partial_\tau \phi_\alpha)^2 + c^2 (\nabla_x \phi_\alpha)^2 + r\phi_\alpha^2(x) \right] \right.$$

$$\left. + \frac{u}{4!} (\phi_\alpha^2(x))^2 \right\}, \tag{3.11}$$

where c is a velocity, r and u are coupling constants, and the functional integral is over fields which are periodic in τ with period $\hbar/k_B T$, *i.e.*, $\phi_\alpha(x, \tau) = \phi_\alpha(x, \tau + \hbar/k_B T)$. The two non-gradient terms in (3.11) arise from the polynomial expansion of the potential $V(\phi_\alpha^2)$ noted above, the spatial gradient term represents the energy cost for the spatial variations in the orientation of the magnetic order. The time derivative term arises from the quantum-mechanical tunneling terms proportional to Jg ($J\tilde{g}$) in H_I (H_R), and we saw how they led to second-order time derivatives in Chapter 2. This quantum field theory undergoes a quantum phase transition by tuning the coupling r through a critical value r_c at $T = 0$.

An alternative formulation of this quantum field theory is sometimes

useful for analyzing H_R at small $\widetilde{g}$ and for low values of d; this formulation applies only for $N \geq 2$ and yields a field theory with precisely the same universal properties as the formulation in (3.11). The basic idea is that at small $\widetilde{g}$, the predominant fluctuations will be variations in the orientation of the local direction of $\mathbf{n}_i$. Also the orientation should not vary significantly from site to site, and we can therefore simply promote $\mathbf{n}_i(\tau)$ to a *unit length* continuum field $\mathbf{n}(x, \tau)$ and obtain

$$\mathcal{Z} = \int \mathcal{D}\mathbf{n}(x, \tau)\delta(\mathbf{n}^2(x, \tau) - 1)\exp(-\mathcal{S}_n)$$

$$\mathcal{S}_n = \frac{N}{2cg}\int d^d x \int_0^{\hbar/k_B T} d\tau \left[(\partial_\tau \mathbf{n})^2 + c^2(\nabla_x \mathbf{n})^2\right], \quad (3.12)$$

where the small $\widetilde{g}$ expressions for g and c are given in (5.14) and (5.17), and $\mathbf{n}(x, \tau)$ satisfies a periodicity condition similar to that for ϕ_α. This field theory is often called the O(N) quantum non-linear sigma model in d dimensions, for obscure historical reasons. The action is only quadratic in the field $\mathbf{n}(x, \tau)$, but the model is not a free field theory because of the constraint $\mathbf{n}^2(x, \tau) = 1$ which is imposed at each point in spacetime. Note also that (3.12) is the obvious higher dimensional generalization of the $D = 1$ field theory (2.68) studied in Chapter 2: instead of having only one 'quantum' τ directions, we also have d additional spatial directions labeled by x, along with the corresponding gradient squared term in the action.

The description of the universal dynamical properties of (3.11) and (3.12) will occupy a substantial portion of Part 2.

The field theories (3.11) and (3.12) can, of course, be obtained directly from the classical models (3.2) (3.3) in, perhaps, a somewhat more transparent manner. For example, by taking the naive continuum limit of (3.3), we directly obtain (3.12), where τ is now interpreted as one of the D spatial dimensions. Similar arguments can be made for (3.11), by motivating the introduction of 'soft' spins, as below (3.10). As we have mentioned earlier, notice that if we began with a classical model which was of infinite extent in all D dimensions, the resulting integral over τ in (3.11) and (3.12) would extend over an infinite range of τ—such classical models therefore map onto quantum systems at $T = 0$. To obtain quantum mechanics at finite temperature, consider models (3.2) and (3.3) in a particular 'slab' geometry. The slab is of infinite extent in $d = D - 1$ dimensions, but has a finite "length", L_τ, along the

temporal direction given by

$$L_\tau = \frac{\hbar}{k_B T}. \tag{3.13}$$

The classical fields obey periodic boundary conditions in this finite direction. Note that L_τ has the units of physical time: the time L_τ shall play a fundamental role in the dynamics of the quantum system near its critical point. So to reiterate, the imaginary time correlations of an infinite d-dimensional quantum system at a temperature T are simply related to the correlations of D-dimensional classical system which is infinite in d directions and of finite extent L_τ in one direction.

3.2 What's different about quantum transitions ?

The quantum-classical mapping discussed so far in Part 1 is in fact a very general result, and not a specific property of the Ising/rotor models. One can always reinterpret the imaginary time functional integral of a d-dimensional quantum field theory as the finite 'temperature' Gibbs ensemble of a D-dimensional classical field theory. We will often use this mapping between d-dimensional quantum mechanics and D-dimensional classical statistical mechanics, and refer to it as the $\mathcal{QC}$ mapping. However, in general, the resulting classical statistical mechanics problem will not be as simple as it was for the Ising/rotor models. Quantum critical points often have $z \neq 1$, and so correlators of the classical problem will scale differently along the x and τ directions. Furthermore, as we note below, there is no guarantee that the Gibbs weights are positive, and they could even be complex-valued.

Given this simple, and ubiquitous, quantum-classical mapping $\mathcal{QC}$, one can now legitimately raise the question: "Why does one need a separate theory of quantum phase transitions ? Is it not possible to simply lift results from the corresponding classical theory, and obtain all needed properties of the quantum system ?" The answer to the second question is an emphatic "no", and a direct treatment of the quantum problems is certainly needed. The reasons for this should become clearer to the reader as she proceeds through the book, but we note some important points here:

- Note that the quantum-classical mapping $\mathcal{QC}$ yields quantum correlation functions which are in *imaginary* time. The most interesting properties of the quantum critical point are often related to their *real* time dynamics, like their energy spectra, inelastic neutron scattering

cross sections, or relaxation rates as measured in NMR experiments. To obtain these, one needs to analytically continue the imaginary time results to real time. The crucial point is that this analytic continuation is an ill-posed problem, *i.e.,* it is possible to continue exact imaginary time results to real time, but anything short of an exact result leads to unreliable, and usually unphysical results. In particular, existing analytic results in the theory of classical critical phenomena (with the exception of a single exact result in two spatial dimensions we shall consider in Chapter 4) are totally inadequate for obtaining $T > 0$ dynamic properties of the corresponding quantum critical points. The problem is particularly severe for the long time limit $t \gg \hbar/k_B T$ which is usually of the greatest practical interest: these correlations are essentially impossible to reconstruct from the equivalent classical problem, which only yields imaginary time correlations in the domain $0 \leq \tau \leq \hbar/k_B T$. It is therefore of crucial importance that theory be constructed using the physical concepts of the quantum critical point, and that it formulate the dynamic analysis directly in real time at all stages.

• We will see in the following chapters that a fundamental new time scale characterizing the dynamic properties of systems near a quantum-critical point is the *phase coherence time*, τ_φ. Loosely speaking, τ_φ is the time over which the wavefunction of the many body system retains memory of its phase. Local measurements separated by times shorter than τ_φ will display quantum interference effects. Precise definitions of τ_φ have to be tailored to the physical situation at hand, and these will be presented later for the models and regimes considered. The phase coherence time has no analog near the corresponding classical critical point in D dimensions. Notice from (3.13), that an infinite D-dimensional classical system maps onto a d-dimensional quantum system at $T = 0$; in all the models we shall consider in this book, the latter will have either a unique ground state, or one with a degeneracy small enough that the entropy is not thermodynamically significant: under these circumstances we can expect that it always possible to define a τ_φ which is infinite at $T = 0$, and therefore the quantum system has perfect phase coherence at sufficiently low temperatures. From the infinite D-dimensional classical point of view, however, this result may seem extremely peculiar: most such systems have a high 'temperature' disordered phase in which there is no long-range order and all correlations decay exponentially over very short scales. Yet we are claiming that such a disordered state maps onto a correspond-

ing 'quantum-disordered' state which is characterized by correlations
which have an *infinite* correlation time (for related remarks from ex-
perimentalists' perspectives, the reader should see the recent articles
by Mason *et al.* [327] and Aeppli *et al.* [1]); for this reason we shall
eschew the commonly used 'quantum-disordered' appellation, and re-
fer to this state, as noted earlier, as a *quantum paramagnet*. This
peculiarity is closely related to the ill-posed nature of the analytic
continuation which was noted above. Quantum systems at $T = 0$
really do have a genuinely different long-range phase correlation in
time which is almost completely hidden once the mapping to imagi-
nary time and the corresponding classical system has been performed.
Only for $T > 0$ does the τ_φ of the quantum system become finite. An
important purpose of this book shall be to show how to introduce
a characterization of quantum states which demonstrates the perfect
coherence at $T = 0$, how to compute τ_φ for $T > 0$, and to highlight
the crucial role played by τ_φ in the structure of the dynamic correla-
tions. The manner in which $\tau_\varphi \to \infty$ as $T \to 0$ shall be an important
diagnostic in characterizing in the different $T > 0$ regions in vicinity
of the quantum critical point: we shall find that, in all of the models
we shall study, the time L_τ in (3.13) appears as a lower bound on τ_φ
on the rate of divergence of τ_φ as $T \to 0$, *i.e.*,

$$\tau_\varphi \geq \mathcal{C}\frac{\hbar}{k_B T} \quad \text{as } T \to 0, \tag{3.14}$$

where $\mathcal{C}$ is a number of order unity. Certain models will have regions
in which the inequality in (3.14) is saturated: these regions will be of
particular interest to us. Their dynamical properties have not been
studied until recently, and we will find that they have many remark-
ably universal characteristics even though their saturating the lower
bound on τ_φ implies that their physics is maximally incoherent.

• For a large class of interesting, physically relevant quantum critical
points, the corresponding classical critical points are rather artificial
and not of a class that have been studied earlier. In random systems,
the classical problems have disorder which is infinitely correlated along
the imaginary time direction. Moreover, even in non-random systems,
the classical problems often have complex-valued Boltzmann weights.
These complex weights are clearly a consequence of the underlying
quantum mechanics, and are often best understood as "Berry phase"
factors (see Ref [456] for an elementary introduction to Berry phases;
the Berry phases are complex even in imaginary time). We will study

quantum critical points of these types in Part 3 of this book. We will see that a whole new class of phenomena are then possible, which have no analogs in the classical theory.

- Even for those quantum critical points which do have well studied classical analogs, note that we need the classical correlation functions in a rather curious slab geometry: one which is infinite in $D - 1$ dimensions and of finite length L_τ in one directions. There are very few existing results in such a geometry, and one often has to reconstruct the needed correlators from scratch.

Despite these caveats, it should be evident that it will pay to push the quantum-classical mapping $\mathcal{QC}$ to the extent possible: this will allow us to get maximum mileage from the sophisticated and profound developments in the theory of classical critical phenomena. This shall be the strategy of this book. We will begin in Part 2 by thoroughly examining a class of quantum phase transitions which *do* have simple and well-studied classical analogs. In this manner, we will introduce many of the central concepts needed in a somewhat more familiar environment. Then, as noted above, we will proceed in Part 3 to many other physically important quantum phase transitions which involve Berry phases in a crucial way, and which do not have useful classical analogs.

There have also been discussions of the dynamical properties of quantum field theories at finite temperature in the particle physics literature [263, 56, 249, 386]. However, these are exclusively concerned with physics in $D = 4$ in models that do not satisfy 'hyperscaling' [63] properties, and this leads to significant differences from the systems we shall examine here. Some of these studies [56, 249] have examined the model $\mathcal{S}_\phi$ in (3.11) for the case $D = 4$, $N = 1$, which turns out to be essentially a free field theory at low energies: as a result inelastic, decoherence effects are rather weak and non-universal. This will be discussed further in Chapter 8. There is also interest in the high temperature dynamical properties of non-Abelian gauge theories [249, 386]: these are asymptotically free at high energies, (*i.e.,* scattering between the elementary excitations is negligibly small at high energies), and as a result the high temperature behavior is controlled by a Gaussian and classical fixed point. We will see an analogous phenomenon here in a much simpler context in Section 6.3; the simplicity will allow us to make greater progress than has so far been possible for the gauge theories. The models of primary interest in this book satisfy hyperscaling and are *not* asymp-

totically free at high energies: such models have not been studied in the particle physics literature.

Part two

Quantum Ising and Rotor Models

4

The Ising chain in a transverse field

This chapter will describe in considerable detail the quantum critical properties of the quantum $N = 1$ model in one spatial dimension. All of the results in this section are believed to be exact, but the physically oriented reader should not be turned off by this: we will keep technical details to a minimum, and show how the exact results can be obtained by physical arguments which do much to illustrate the main underlying principles. Most of the important concepts of this book will appear in the simple model under consideration: the remainder of the book is largely a description of similar phenomena in more complicated settings. This is thus one of the central chapters of this book, and a careful reading is urged.

We will study the $D = 1$ case of (1.5) which is

$$H_I = -J \sum_i \left(g\hat{\sigma}_i^x + \hat{\sigma}_i^z \hat{\sigma}_{i+1}^z \right). \tag{4.1}$$

As we have discussed in Part 1 and will establish in this chapter, H_I exhibits a phase transition at $T = 0$ between an ordered state with the Z_2 symmetry broken, and a quantum paramagnetic state where the symmetry remains unbroken. The quantum-classical mapping $\mathcal{QC}$ ensures that this transition will be in the universality class of the $D = 2$ classical Ising model.

There has been a great deal of theoretical work on the ground state correlations of H_I [306, 382, 336, 35]. However, properties of the order parameter $\hat{\sigma}_z$ at $T > 0$, which are our primary interest here, have been studied much less: methods relying upon knowledge of all the exact eigenstates and eigenfunctions of H_I do yield explicit results for equal-time correlators [306, 333, 38, 425], but results for unequal-time correlators have been restricted to $T = \infty$ [71, 380, 381] or to precisely

51

the critical coupling [337, 245] (seen below to be $g = 1$). There is also an approach which relies upon deriving non-linear partial differential equations satisfied by the $T > 0$ unequal time correlators [338, 281, 297] but these have not so far been solved to yield the physical correlators. Our discussion of the low T dynamics here will follow the intuitive phenomenological approach developed recently in Ref [442]: despite its seeming inexactness, its results are believed to be asymptotically exact, and this will be supported by evidence from numerical computations.

We will use our discussion of the quantum critical point of H_I and its vicinity to introduce some basic concepts and tools. These include the central idea of a *scaling transformation* to characterize the scaling limit theory of the quantum critical point, the *scaling dimension* of operators and coupling constants about the critical theory, and the *dynamic critical exponent z*. Another very useful, but much less familiar concept, is that of the *reduced scaling function*, and it will be introduced as an essential tool towards understanding the mechanism of emergence of classical behavior in limiting regimes of the phase diagram.

We will describe the properties of H_I by focusing on an especially important observable: the dynamic two-point correlations of the order parameter $\hat{\sigma}^z$ (as discussed in Section 3.1, correlators of the field ϕ in (3.11) will be similar to those of $\hat{\sigma}^z$)

$$
\begin{aligned}
C(x_i, t) &\equiv \langle \hat{\sigma}^z(x_i, t) \hat{\sigma}^z(0, 0) \rangle \\
&= \mathrm{Tr}\left(e^{-H_I/T} e^{iH_I t} \hat{\sigma}_i^z e^{-iH_I t} \hat{\sigma}_0^z\right)/\mathcal{Z}
\end{aligned}
\tag{4.2}
$$

where $\mathcal{Z} = \mathrm{Tr}(e^{-H_I/T})$ is the partition function, and $x_i = ia$ is the x-coordinate of the i'th spins with a the lattice spacing. Here, and in the remainder of this book, we will always use the symbol t to represent real physical time. Occasionally we will also find it convenient to consider the correlation at an imaginary time τ; this is defined by the analytic continuation $it \to \tau$ from (4.2) with $\tau > 0$

$$
C(x_i, \tau) = \mathrm{Tr}\left(e^{-H_I/T} e^{H_I \tau} \hat{\sigma}_i^z e^{-H_I \tau} \hat{\sigma}_0^z\right)/\mathcal{Z}.
\tag{4.3}
$$

Compare this definition with (2.30); from the discussion in Chapter 2 it should be clear that $C(x, \tau)$ is the correlator of the classical $D = 2$ Ising model (3.2) on an infinite strip of width $1/T$ and periodic boundary conditions along the 'imaginary time' direction. In all our subsequent discussion on the correlators like C, we will consistently use the argument t when referring to real time correlators as in (4.2), and the argument τ for imaginary time correlators as in (4.3). We will also deal with the

dynamic structure factor, $S(k, \omega)$, which is simply the Fourier transform of $C(x, t)$ to wavevectors and frequencies

$$S(k, \omega) = \int dx \int dt \, C(x, t) e^{-i(kx - \omega t)}. \qquad (4.4)$$

This is a useful quantity because it is directly proportional to the cross section in scattering experiments in which the probe (usually neutrons) couples to σ^z. If energy of the scattered neutron is integrated over, then the cross section in proportional to the *equal-time structure factor*, $S(k)$, defined by

$$S(k) \equiv \int \frac{d\omega}{2\pi} S(k, \omega), \qquad (4.5)$$

which is clearly also the spatial Fourier transform of $C(x, 0)$. The number of arguments of S will specify whether we are referring to the dynamic or equal-time structure factor. The identity $(\hat{\sigma}_i^z)^2 = 1$ implies that $C(0, 0) = 1$, and leads to the following sum rule for the dynamic structure factor

$$\int \frac{dk \, d\omega}{(2\pi)^2} S(k, \omega) = 1. \qquad (4.6)$$

Finally, also useful is the corresponding *dynamic susceptibility* $\chi(k, \omega_n)$ which is most conveniently defined by a Fourier transform in imaginary time

$$\chi(k, \omega_n) \equiv \int_0^{1/T} d\tau \int dx \, C(x, \tau) e^{-i(kx - \omega_n \tau)} \qquad (4.7)$$

where $\omega_n = 2\pi n T$, n integer, is the usual Matsubara imaginary frequency arising from the restriction to periodic functions along the imaginary time direction. We may also perform the analytic continuation to real frequencies by $i\omega_n \to \omega + i\delta$ (where δ is a positive infinitesimal) and obtain the *dynamic susceptibility*, $\chi(k, \omega)$. As was the case for C, it will be symbol for the frequency (ω_n or ω) which will distinguish whether we are referring to the imaginary or real frequency susceptibility. The dynamic susceptibility measures the response of the magnetization σ^z to an external field which couples linearly to σ^z and is oscillating at a wavevector k and frequency ω. In the limit that the external field becomes time-independent, the response is given by the *static susceptibility*, $\chi(k)$ defined by

$$\chi(k) \equiv \chi(k, \omega = 0). \qquad (4.8)$$

Again, the number of arguments of χ will specify whether we are referring to the dynamic or static susceptibility.

From (4.2), (4.3), (4.4) and (4.7) it is clear that there should be a relationship between the two real frequency correlators $S(k, \omega)$ and $\chi(k, \omega)$. This is the so-called *fluctuation-dissipation* theorem, and is established by expressing all the above correlators in terms of the (possibly unknown) exact eigenstates of H_I and their matrix elements; such an analysis may be found in many text books, and we will not reproduce it here (see, *e.g.*, Ref. [146]). It is conventional to decompose $\chi(k, \omega)$ into its real and imaginary parts by $\chi(k, \omega) = \mathrm{Re}\chi(k, \omega) + i\mathrm{Im}\chi(k, \omega)$, and the required relationship is then

$$S(k, \omega) = \frac{2}{1 - e^{-\omega/T}} \mathrm{Im}\chi(k, \omega). \tag{4.9}$$

A Kramers-Kronig transform also connects the real and imaginary parts of $\chi(k, \omega)$:

$$\mathrm{Re}\chi(k, \omega) = \mathcal{P} \int_{-\infty}^{\infty} \frac{d\Omega}{\pi} \frac{\mathrm{Im}\chi(k, \Omega)}{\Omega - \omega}, \tag{4.10}$$

where $\mathcal{P}$ labels the principal part. The spectral analysis also shows that $\mathrm{Im}\chi(k, \omega)$ is an odd function of ω, while $\mathrm{Re}\chi(k, \omega)$ is an even function of ω. From (4.9), the dynamic structure factor satisfies $S(k, -\omega) = e^{-\omega/T} S(k, \omega)$.

We will begin this chapter by developing a simple physical picture of the possible ground and excited states of H_I by examining the large and small g limits in Section 4.1. The exact spectrum will be determined in Section 4.2 and this will show the existence of a quantum critical point at $g = 1$. The universal continuum quantum theory of the vicinity of $g = 1$ will be obtained in Section 4.3. Equal time correlators for $T > 0$ will be discussed in Section 4.4, and the dynamical properties of the different $T > 0$ regimes will be examined in Section 4.5.

We note that the reader may also wish to examine the recent book by Chakrabarti, Dutta and Sen [82] which discusses aspects of quantum Ising models in one and higher dimensions.

4.1 Limiting cases at $T = 0$

We begin by examining the spectrum of H_I under strong $(g \gg 1)$ and weak $(g \ll 1)$ coupling limits, which were discussed briefly in Section 1.4.1. The analysis is relatively straightforward in these limits, and two very different physical pictures emerge. The exact solution, to be

discussed later, shows that there is a critical point exactly at $g = 1$, but that the qualitative properties of the ground states for $g > 1$ ($g < 1$) are very similar to those for $g \gg 1$ ($g \ll 1$). One of the two limiting descriptions is therefore always appropriate, and only the critical point $g = 1$ has genuinely different properties at $T = 0$.

4.1.1 *Strong coupling* $g \gg 1$

The $g = \infty$ ground state was presented in (1.7), where we also discussed the nature of the $1/g$ corrections. We found a quantum paramagnetic ground state, invariant under the Z_2 symmetry (1.11), with exponentially decaying $\hat{\sigma}^z$ correlations as in (1.9).

What about the excited states ? For $g = \infty$ these can also be listed exactly. The lowest excited states are

$$|i\rangle = |\leftarrow\rangle_i \prod_{j \neq i} |\rightarrow\rangle_j, \tag{4.11}$$

obtained by flipping the state on site i to the other eigenstate of $\hat{\sigma}^x$ (the eigenstates of $\hat{\sigma}^x$ were defined in (1.8)). All such states are degenerate, and we will refer to them as the "single-particle" states. Similarly, the next degenerate manifold of states are the two-particle states $|i, j\rangle$, obtained by flipping the states at sites i and j, and so on to the general n-particle states. To first order in $1/g$, we can neglect the mixing between states between different particle number, and just study how the degeneracy within each manifold is lifted. For the one-particle states, the exchange term $\hat{\sigma}_i^z \hat{\sigma}_{i+1}^z$ in H_I is not diagonal in the basis of the $|\rightarrow\rangle$, $|\leftarrow\rangle$ states, and leads only to the off-diagonal matrix element

$$\langle i | H_I | i + 1 \rangle = -J \tag{4.12}$$

which hops the 'particle' between nearest neighbor sites. As in the tight-binding models of solid state physics [27], the Hamiltonian is therefore diagonalized by going to the momentum space basis

$$|k\rangle = \frac{1}{\sqrt{N}} \sum_j e^{ikx_j} |j\rangle, \tag{4.13}$$

where N is the number of sites. This eigenstate has energy (we have added an overall constant to H_I to make the energy of the ground state zero)

$$\varepsilon_k = Jg \left[2 - (2/g) \cos(ka) + \mathcal{O}(1/g^2), \right] \tag{4.14}$$

where a is the lattice spacing. The lowest energy one-particle state is therefore at $\varepsilon_0 = 2g - 2J$

Now consider the two particle states. At $g = \infty$, the subspace of two particle states is spanned by the states (generalizing (4.11))

$$|i, j\rangle = |\leftarrow\rangle_i |\leftarrow\rangle_j \prod_{h \neq i,j} |\rightarrow\rangle_h, \qquad (4.15)$$

where $i \neq j$. Also notice that $|i, j\rangle = |j, i\rangle$, and so we may restrict our attention to $i > j$. Alternatively, we can say that the states are symmetric under interchange of the particle positions i, j and so we treat the particles as bosons. At first order in $1/g$, these states will be mixed by the matrix element (4.12); this will couple $|i, j\rangle$ to $|i\pm 1, j\rangle$ and $i, j \pm 1\rangle$ for all $i > j + 1$, while $|i, i-1\rangle$ will couple only to $|i+1, i-1\rangle$ and $|i, i-2\rangle$. For i and j well separated, we can ignore this last case, and the two particles will be independent of each other, with the matrix elements for each particle identical to those considered above for single particles. So the particles will acquire momenta k_1, k_2 (say), and the total energy of the two particle state will be $E_k = \varepsilon_k + \varepsilon'_k$, and its total momentum $k = k_1 + k_2$. However, when i and j approach each other, we will have to consider mixing between these momentum states arising from the restrictions in the matrix elements noted above. This is a problem in ordinary scattering theory, treated in many elementary quantum mechanics texts. (In this discussion, we are assuming that there are no two-particle bound states, a fact that can be verified by a full solution of the two-particle Schrödinger equation at order $1/g$.) The scattering of the two incoming particles with momenta k_1, k_2 will conserve total energy, and total momentum up to a reciprocal lattice vector. For small k_1, k_2 (which is our primary interest here), these conservation laws allow only one solution in $d = 1$: the momenta of the particles in the final state are also k_1 and k_2. The existence of a single final state is a special feature of $d = 1$, while a sum over an infinite number of momenta in the final state is required for the problems in $d > 1$ we will consider later. By this reasoning, we can conclude that the wavefunction of the two particle state will have the following wavefunction for $i \gg j$

$$\left(e^{i(k_1 x_i + k_2 x_j)} + S_{k_1 k_2} e^{i(k_2 x_i + k_1 x_j)} \right) |i, j\rangle. \qquad (4.16)$$

The quantity $S_{k_1 k_2}$ is of central importance, and is the S matrix for two particle scattering. Upon interpreting the stationary scattering state in (4.16) from the perspective of a time-dependent scattering problem, in

which particles scatter from an incoming wave corresponding to the first term in (4.16), to an outgoing wave corresponding to the second term, the S matrix can be related (just as in familiar scattering theory) to the time-evolution operator of H_I from the infinite past to the infinite future, and must therefore be a unitary matrix. In the present situation with a single final state, the S matrix is a complex number of unit modulus. The reader is urged to go through the simple exercise of computing the S matrix from the Schrödinger equation at order $1/g$. The result turns out to be remarkably simple; we find

$$S_{k_1 k_2} = -1, \tag{4.17}$$

for all momenta k_1, k_2. We will not give an explicit derivation of this result here (a detailed discussion of the computation of such S matrices in general spin models may be found in Ref [117]). Instead, will present a simple argument in the next paragraph which shows that a result like (4.17) holds in the limit of small k_1, k_2 for a generic Ising chain with additional further neighbor exchange couplings; the validity of (4.17) at all momenta is a special feature of the nearest neighbor exchange model (4.1). Our argument will also show that (4.17) continues to hold at higher orders in $1/g$ for small k_1, k_2.

Transform to the center of mass frame of the two particles, and consider the Schrödinger equation for their relative co-ordinates $x = x_i - x_j$. Taking for simplicity, a repulsive delta function potential $u\delta(x)$ between them (the result does not require this special form), we can write down the schematic Schrödinger equation

$$\left(-\frac{d^2}{dx^2} + u\delta(x) \right) \psi(x) = E\psi(x), \tag{4.18}$$

where x is their relative co-ordinate and $\psi(x)$ is the wavefunction in the center of mass frame. We make a simple argument based upon dimensional analysis. Notice from (4.18) that u has the dimensions of an inverse length. The S matrix is a dimensionless quantity, and can only be a function of u and the relative momentum $k = k_1 - k_2$. Dimensionally, this can only be of the form $S = f(u/k)$ where f is some unknown function. We are interested in the limit $k \to 0$, which is given by the value of $f(\infty)$. However, conceptually, it is much simpler to obtain $f(\infty)$ by taking $u \to \infty$ at fixed k. So to slowly moving particles, the potential appears effectively impenetrable. This means that $\psi(x)$ should vanish at $x = 0$, and its bosonic symmetry under particle exchange implies that it has the form $\psi \sim \sin(k|x|/2)$ for small x. Comparing with (4.16), we

conclude that $f(\infty) = -1$, and so (4.17) holds universally in the limit of small momenta.

We have now described the manner in which $1/g$ perturbations lift the degeneracy of the $g = \infty$ two particle eigenstates (4.15). The energy of a two-particle state with total momentum k is given by $E_k = \varepsilon_{k_1} + \varepsilon_{k_2}$ where $k = k_1 + k_2$. Notice that for a fixed k, there is still an arbitrariness in the single particle momenta $k_{1,2}$ and so the total energy E_k can take a range of values. There is thus no definite energy momentum relation, and we have instead a 'two-particle continuum'. It should be clear, however, that the lowest energy two-particle state in the infinite system (its "threshold") is at $2\varepsilon_0$. Similar considerations apply to the n-particle continua, which have thresholds at $n\varepsilon_0$.

At higher orders in $1/g$ we have to account for the mixing between states with differing numbers of particles. Non-zero matrix elements like

$$\langle 0|H_I|i, i+1\rangle = -J \qquad (4.19)$$

lead to a coupling between n and $n + 2$ particle states. It is clear that these will renormalize the one-particle energies ε_k. However qualitative features of the spectrum will not change, and we will still have renormalized one-particle states with a definite energy-momentum relationship, and renormalized $n \geq 2$ particle continua with thresholds at $n\varepsilon_0$. Note especially that the integrity and stability of the one particle states is not modified at any order in $1/g$: the one particle state with energy ε_k is the lowest energy state with a momentum k, and this protects it from decay.

Upon explicitly carrying out these higher order computations for the particular nearest neighbor model H_I, some rather 'miraculous' features emerge for this special Hamiltonian: as already noted, the result (4.17) holds not only at small k_1, k_2, but at all momenta and at all orders in $1/g$ (there are also no processes in which the number of outgoing particles does not equal the number of in-going ones). This remarkable fact appears quite mysterious at this stage, but will be explained rather simply in Section 4.2 using a mapping of H_I to fermionic variables.

The spectrum described above has important consequences for the dynamic structure factor $S(k, \omega)$. Inserting a complete sets of states between the operators in the definition (4.4) we see that $T = 0$

$$S(k, \omega) = 2\pi \sum_s |\langle 0|\hat{\sigma}^z(k)|s\rangle|^2 \delta(\omega - E_s), \qquad (4.20)$$

where the sum over s extends over all the eigenstates of H_I with en-
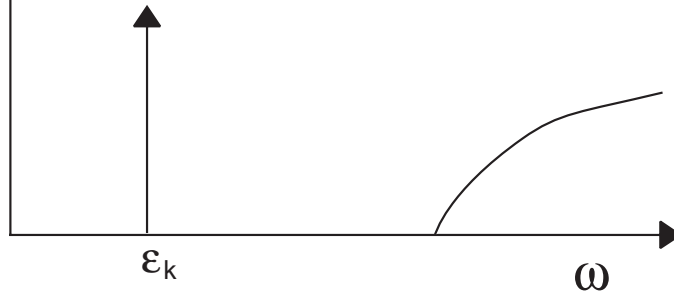
Fig. 4.1. Schematic of the dynamic structure factor $S(k, \omega)$ of H_I as a function of ω at $T = 0$ and a small k. There is a quasiparticle delta function at $\omega = \varepsilon_k$, and a three-particle continuum at higher frequencies. There are additional n-particle continua ($n \geq 5$ and odd) at higher energies which are not shown.

ergy $E_s > 0$, and so at $T = 0$, $S(k, \omega)$ is non-zero only for $\omega > 0$ (recall that we have chosen the ground state energy to be zero). The dynamic susceptibility can be obtained from (4.9), and equals $\mathrm{Im}\chi(k, \omega) = (\mathrm{sgn}(\omega)/2)S(k, |\omega|)$. The eigenstates and energies described above allow us to simply deduce the qualitative form of $S(k, \omega)$ which is sketched in Fig 4.1. The operator $\hat{\sigma}^z$ flips the state at a single site, and so the matrix element in (4.20) is non-zero for the single particle states: only the state with momentum k will contribute, and so there is an infinitely sharp delta function contribution to $S(k, \omega) \sim \delta(\omega - \varepsilon_k)$. This delta function is the "quasiparticle peak" and its co-efficient is the quasiparticle amplitude. At $g = \infty$ this quasiparticle peak is the entire spectral density which saturates the sum rule in (4.6), but for smaller g the quasiparticle amplitude decreases and the multiparticle states also contribute to the spectral density. The mixing between the one and three particle states discussed above, means that the next contribution to $S(k, \omega)$ occurs above the 3 particle threshold $\omega > 3\varepsilon_0$; because there are a continuum of such states, their contribution is no longer a delta function, but a smooth function of omega (apart from a threshold singularity), as shown in Fig 4.1. Similarly there are continua above higher odd number particle thresholds; only states with odd numbers of particles contribute because the matrix element in (4.20) vanishes for even numbers of particles.

4.1.2   *Weak coupling $g \ll 1$*

The $g = 0$ ground states were given in (1.10). They are two-fold degenerate, and posses long range correlations in the magnetic order parameter $\hat{\sigma}^z$. In the present notation, the result (1.12) implies

$$\lim_{|x| \to \infty} C(x, 0) = N_0^2 \neq 0, \tag{4.21}$$

where $C(x, t)$ was defined in (4.2). The spontaneous magnetization N_0 equals $\pm \langle \hat{\sigma}^z \rangle$ in the two ground states, corresponding to spontaneous breaking of the Z_2 symmetry (1.11). All of the statements made in this paragraph clearly hold for $g = 0$, and will hold for some $g > 0$ provided the perturbation theory in g has a non-zero radius of convergence. The exact solution of the model to be discussed later will verify that this is indeed the case.

The excited states can be described in terms of an elementary domain wall (or kink) excitation. For instance the state

$$\cdots |\uparrow\rangle_i \, |\uparrow\rangle_{i+1} \, |\downarrow\rangle_{i+2} \, |\downarrow\rangle_{i+3} \, |\downarrow\rangle_{i+4} \, |\uparrow\rangle_{i+5} \, |\uparrow\rangle_{i+6} \cdots$$

has domain walls, or nearest neighbor pairs of antiparallel spins, between sites $i + 1$, $i + 2$ and sites $i + 4$, $i + 5$. At $g = 0$ the energy of such a state is clearly $2J \times$ number of domain walls. The consequences of a small non-zero g are very similar to those due to $1/g$ corrections in the complementary large g limit: the domain walls become "particles" which can hop and form momentum eigenstates with excitation energy

$$\varepsilon_k = J \left(2 - 2g \cos(ka) + \mathcal{O}(g^2) \right). \tag{4.22}$$

The spectrum can be interpreted in terms n-particle scattering states, although it must be emphasized that the interpretation of the particle is very different from that in the large g limit. Again, the perturbation theory in g only mixes states which differ by even numbers of particles, although the matrix element in (4.20) is non-zero only for states s with an *even* number of particles; these assertions can easily be checked to hold in a perturbation theory in g. The structure factor $S(k, \omega)$ will have a delta function at $k = 0$, $\omega = 0$, from the term in (4.20) where $s =$ one of the ground states, indicating the presence of long-range order. Further, there is no single particle contribution, and the first finite ω spectral density is the continuum above the two particle threshold. So

$$S(k, \omega) = (2\pi)^2 N_0^2 \delta(k) \delta(\omega) + \text{continua of even numbers of particles.} \tag{4.23}$$

The absence of a single particle delta function is a special feature of

the $d = 1$ quantum Ising model, and is a consequence of the topological domain-wall nature of the excitations, in which all of the spins to the left (say) of a wall have to be flipped relative to the magnetically ordered state—so any local operator will not have a non-zero matrix element between states differing by an odd number of domain walls. It is not difficult to show [427] (using methods developed in Chapter 8) that $d > 1$ Ising models have a single-particle delta function in their dynamic structure function for *both* the magnetically ordered and quantum paramagnetic states.

The S matrix for the collision of two domain walls can be computed in a perturbation theory in g, and we find results very similar to those in the strong-coupling $1/g$ expansion: for the generic Ising chain we find $S_{kk'} = -1$ in the low momentum limit, but for the particular nearest-neighbor chain (4.1) we find that there is no particle production, and $S_{kk'} = -1$ at all momenta to all orders in g.

4.2 Exact spectrum

The qualitative considerations of the previous section are quite useful in developing an intuitive physical picture. We will now take a different route, and set up a formalism that will eventually lead to an exact determination of many physical correlators; these results will vindicate the approximate methods for $g > 1$, $g < 1$, and also provide an understanding of the novel physics at $g = 1$.

The essential tool in the solution is the Jordan-Wigner transformation [254, 306]. This is a very powerful mapping between models with spin-1/2 degrees of freedom and spinless fermions. The central observation is that there is a simple mapping between the Hilbert space of a system with a spin-1/2 degree of freedom per site, and that of spinless fermions hopping between sites with single orbitals. We may associate the spin up state with an empty orbital on the site, and a spin-down state with an occupied orbital. If the canonical fermion operator c_i annihilates a spinless fermion on site i, then this simple mapping immediately implies the operator relation

$$\hat{\sigma}_i^z = 1 - 2c_i^\dagger c_i \tag{4.24}$$

It is also clear that the operation of c_i is equivalent to flipping the spin from down to up, or the operation of $\hat{\sigma}_i^+ = (\hat{\sigma}_i^x + i\hat{\sigma}_i^y)/2$; similar creating a fermion by $c_i^\dagger$ is equivalent to lowering the spin by $\hat{\sigma}_i^- = (\hat{\sigma}_i^x - i\hat{\sigma}_i^y)/2$. While this equivalence works for a single site, we cannot yet equate

the fermion operators with the corresponding spin operators for the many site problem; this is because while two fermionic operators on different sites anticommute, two spin operators commute. The solution to this dilemma was found by Jordan and Wigner, who showed that the following representation satisfied both on-site and inter-site (anti)commutation relations:

$$
\begin{aligned}
\hat{\sigma}_i^+ &= \prod_{j<i} \left(1 - 2c_j^\dagger c_j\right) c_i \\
\hat{\sigma}_i^- &= \prod_{j<i} \left(1 - 2c_j^\dagger c_j\right) c_i^\dagger.
\end{aligned}
\tag{4.25}
$$

The naive single-site correspondence has been modified by a 'string' of operators, whose value is $+1$ (-1) if the total number of fermions on the sites to the left of site i are even (odd). Notice that the spin operators have a highly non-local representation in terms of the fermion operators. This feature is also found in the inverse of (4.25)

$$
\begin{aligned}
c_i &= \left(\prod_{j<i} \hat{\sigma}_j^z\right) \hat{\sigma}_i^+ \\
c_i^\dagger &= \left(\prod_{j<i} \hat{\sigma}_j^z\right) \hat{\sigma}_i^-.
\end{aligned}
\tag{4.26}
$$

It can be verified that (4.24,4.25,4.26) are consistent with the relations

$$
\begin{aligned}
\left\{c_i, c_j^\dagger\right\} &= \delta_{ij} \qquad \{c_i, c_j\} = \left\{c_i^\dagger, c_j^\dagger\right\} = 0 \\
[\hat{\sigma}_i^+, \hat{\sigma}_j^-] &= \delta_{ij}\hat{\sigma}_i^z \qquad [\hat{\sigma}_i^z, \hat{\sigma}_j^\pm] = \pm 2\delta_{ij}\hat{\sigma}_i^\pm,
\end{aligned}
\tag{4.27}
$$

where the curly brackets represent anticommutators, and square brackets are commutators.

The above formulation of the Jordan-Wigner transformation is the conventional one, but in the analysis of the Ising model it is convenient to rotate spin axes by 90 degrees about the y axis so that

$$
\hat{\sigma}^z \to \hat{\sigma}^x \quad , \quad \hat{\sigma}^x \to -\hat{\sigma}^z
\tag{4.28}
$$

The mapping becomes

$$
\begin{aligned}
\hat{\sigma}_i^x &= 1 - 2c_i^\dagger c_i \\
\hat{\sigma}_i^z &= -\prod_{j<i} \left(1 - 2c_j^\dagger c_j\right)(c_i + c_i^\dagger).
\end{aligned}
\tag{4.29}
$$

Inserting (4.29) into H_I, the resulting Hamiltonian is quadratic in the Fermi operators

$$H_I = -J \sum_i \left(c_i^\dagger c_{i+1} + c_{i+1}^\dagger c_i + c_i^\dagger c_{i+1}^\dagger + c_{i+1} c_i - 2g c_i^\dagger c_i - g \right) \quad (4.30)$$

This fermionic Hamiltonian has terms like $c^\dagger c^\dagger$ which violate the fermion conservation number; from (4.29), this means that $\sum_i \hat{\sigma}_i^x$ is not conserved and $|\rightarrow\rangle$ spins can be flipped in pairs under time evolution, as we saw in the perturbation theory in Section 4.1.1. So the eigenstates of H_I will not have a definite fermion number. Nevertheless, the new terms are still quadratic in the fermion operators, and H_I can be diagonalized by elementary means. First, use the momentum eigenstates

$$c_k = \frac{1}{\sqrt{M}} \sum_j c_j e^{-ik r_j}, \quad (4.31)$$

where M is the number of sites, to get

$$H_I = J \sum_k \left(2\left[g - \cos(ka)\right] c_k^\dagger c_k - i \sin(ka) \left[c_{-k}^\dagger c_k^\dagger + c_{-k} c_k \right] - g \right) \quad (4.32)$$

Next, use the Bogoliubov transformation to map into a new set of fermionic operators (γ_k) whose number is conserved. These new operators are defined by a unitary transformation on the pair $c_k, c_{-k}^\dagger$

$$\gamma_k = u_k c_k - i v_k c_{-k}^\dagger, \quad (4.33)$$

where u_k, v_k are real numbers satisfying $u_k^2 + v_k^2 = 1$, $u_{-k} = u_k$, and $v_{-k} = -v_k$. It can be checked that canonical fermion anticommutation relations for the c_k imply that the same relations are also satisfied by the γ_k, *i.e.*,

$$\left\{ \gamma_k, \gamma_{k'}^\dagger \right\} = \delta_{k,k'} \quad \left\{ \gamma_k^\dagger, \gamma_{k'}^\dagger \right\} = \{\gamma_k, \gamma_{k'}\} = 0. \quad (4.34)$$

We also note the inverse of (4.33)

$$c_k = u_k \gamma_k + i v_k \gamma_{-k}^\dagger \quad (4.35)$$

We insert (4.35) into (4.32), and demand that H_I not contain any terms like $\gamma^\dagger \gamma^\dagger$ which violate conservation of the γ fermions. The as yet undefined constants, u_k, v_k can always be chosen to ensure this: we define $u_k = \cos(\theta_k/2)$, $v_k = \sin(\theta_k/2)$, and a simple calculation then shows that the choice

$$\tan \theta_k = \frac{\sin(ka)}{\cos(ka) - g} \quad (4.36)$$

satisfies our requirements. The final form of H_I is

$$H_I = \sum_k \varepsilon_k (\gamma_k^\dagger \gamma_k - 1/2), \tag{4.37}$$

where

$$\varepsilon_k = 2J \left(1 + g^2 - 2g \cos k\right)^{1/2}. \tag{4.38}$$

is the single particle energy. As $\varepsilon_k \geq 0$, the ground state, $|0\rangle$, of H_I has no γ fermions and therefore satisfies $\gamma_k |0\rangle = 0$ for all k. The excited states are created by occupying the single particle states; they can clearly be classified by the total number of occupied states, and a n-particle state has the from $\gamma_{k_1}^\dagger \gamma_{k_2}^\dagger \cdots \gamma_{k_n}^\dagger |0\rangle$, with all the k_i distinct.

The above structure of the spectrum confirms the approximate considerations of Section 4.1. We have found that the particles are in fact free fermions, and two fermions will not scatter even when they are close to each other; alternatively they can be considered as hard-core bosons which have an S matrix which does not allow particle production, and which equals -1 at all momenta. We shall find it much more useful to take the latter point of view, as the bosonic particles have a simple, local, interpretation in terms of the underlying spin excitations: for $g \gg 1$ the bosons are simply spins oriented in the $|\leftarrow\rangle$ direction, while for $g \ll 1$ they are domain walls between the two ground states. The fermionic representation is useful for certain technical manipulations, but the bosonic point of view is much more useful for making physical arguments, as we shall see below.

It is also reassuring to see that the exact single-particle excitation energy (4.38) agrees with (4.14) in the limit $g \gg 1$, and with (4.22) in the limit $g \ll 1$.

4.3 Continuum theory and scaling transformations

The excitation energy ε_k in (4.38) is non-zero and positive for all k provided $g \neq 1$. The energy gap, or the minimum excitation energy, is always at $k = 0$ and equals $2J|1 - g|$. This gap vanishes at $g = 1$, and it is natural to expect that $g = 1$ is the phase boundary between the two qualitatively different phases discussed in Section 4.1. Precisely at $g = 1$, fermions with low momenta can carry arbitrarily low energy, and therefore must dominate the low temperature properties. These properties suggest that the state at $g = 1$ is critical, and there is a universal continuum quantum field theory which describes the critical properties in its vicinity.

We shall now obtain this critical theory. As the important excitations are near $k = 0$, we expect that a naive gradient expansion will yield the required theory. We define the continuum Fermi field

$$\Psi(x_i) = \frac{1}{\sqrt{a}} c_i \qquad (4.39)$$

where the normalization has been chosen so that Ψ has units of inverse square-root of length, and

$$\left\{ \Psi(x), \Psi^\dagger(x') \right\} = \delta(x - x'), \qquad (4.40)$$

with the right hand side a Dirac delta function in the continuum limit. We express H_I in terms of Ψ, and expand in spatial gradients, to obtain from (4.32) the continuum H_F:

$$H_F = E_0 + \int dx \left[\frac{c}{2} \left(\Psi^\dagger \frac{\partial \Psi^\dagger}{\partial x} - \Psi \frac{\partial \Psi}{\partial x} \right) + \Delta \Psi^\dagger \Psi \right] + \dots \qquad (4.41)$$

where the ellipses represent terms with higher gradients, and E_0 is an uninteresting additive constant. The coupling constants in H_F are

$$\Delta = 2J(1 - g) \qquad c = 2Ja. \qquad (4.42)$$

Notice that at the critical point $g = 1$, we have $\Delta = 0$, and we have $\Delta > 0$ in the magnetically ordered phase, and $\Delta < 0$ in the quantum paramagnet.

The continuum theory H_F in (4.41) can be viewed as having been obtained by replacing the dependence of the Hamiltonian on c_i, J, and g by Ψ, Δ and c, and then taking the limit $a \to 0$ at fixed Ψ, Δ and c. Notice from (4.42) that this limit requires $J \to \infty$ and $g \to 1$. Notice also the similarity to the discussion in Section 2.1.1.

It is convenient to perform our subsequent scaling analysis in a Lagrangean path integral representation of the dynamics of H_F. Using the standard Grassman path integral of canonical Fermi operators (see, *e.g.,* the book by Negele and Orland [360] or the text by Shankar [456]) we obtain for the partition function $\mathcal{Z} = \text{Tr} e^{-H_F/T}$

$$\mathcal{Z} = \int \mathcal{D}\Psi \mathcal{D}\Psi^\dagger \exp\left(- \int_0^{1/T} d\tau dx \, \mathcal{L}_I \right) \qquad (4.43)$$

where the functional integral is over complex Grassman fields Ψ, $\Psi^\dagger$ in space (x) and imaginary time (τ), and the Lagrangean density $\mathcal{L}_I$ is

$$\mathcal{L}_I = \Psi^\dagger \frac{\partial \Psi}{\partial \tau} + \frac{c}{2} \left(\Psi^\dagger \frac{\partial \Psi^\dagger}{\partial x} - \Psi \frac{\partial \Psi}{\partial x} \right) + \Delta \Psi^\dagger \Psi \qquad (4.44)$$

As we shall discuss in detail below, $\mathcal{L}_I$ is the required universal critical theory characterizing the critical point in H_I. In other words, if we modified the detailed form of H_I, *e.g.,* by including second neighbor coupling, the critical theory would still be $\mathcal{L}_I$ but with changes in the value of Δ and c. In general, it is not possible to determine the exact relationship between parameters characterizing the critical theory and microscopic couplings, as presented in (4.42), since the resulting microscopic Hamiltonian is not quadratic in Fermi fields. We then leave Δ and c as phenomenological parameters, to be determined by relating them to a physically measurable observable. The continuum theory $\mathcal{L}_I$ can be diagonalized much like the lattice model H_I, and the excitation energy now takes a "relativistic" form

$$\varepsilon_k = \left(\Delta^2 + c^2 k^2 \right)^{1/2} \tag{4.45}$$

which shows that $|\Delta|$ is the $T = 0$ energy gap (we chose the sign of Δ to be different on the two sides of the critical value of g), and c is the velocity of the excitations, both measurable quantities. The form of ε_k correctly suggests that $\mathcal{L}_I$ is invariant under Lorentz transformations. This can be made explicit by writing the complex Grassman field Ψ in terms of two real Grassman fields, when the action becomes what is known as the field theory of Majorana fermions of mass Δ/c^2 [247]; we will not explicitly display this here.

   The key to establishing that $\mathcal{L}_I$ is a *universal* critical theory is to examine its behavior under a *scaling transformation*. To obtain a physical picture of this transformation it is best to think of $\mathcal{L}_I$ as an effective theory of an underlying lattice problem, applicable only at length scales larger than some lattice spacing a, or momenta smaller than $\Lambda = \pi/a$. We are ultimately interested in long distance physics, and so it is useful to think of eliminating some short distance degrees of freedom from $\mathcal{L}_I$: say all modes of the field Ψ with momenta between Λ and $\Lambda e^{-\ell}$, where $e^{-\ell}$ is a dimensionless rescaling factor. As (4.43) involves only a Gaussian functional integral, integrating these modes out will only add an overall additive constant to the free energy (we will later meet situations, *e.g.,* in Section 6.1, where the consequences of integrating out the short distance modes is not so trivial). We are left with a new theory with the same action as $\mathcal{L}_I$, but valid only at length scales larger that ae^{ℓ}. We complete the scaling transformation by rescaling lengths, times and fields so that the resulting $\mathcal{L}_I$ has the same form and short distance

cutoff as the original $\mathcal{L}_I$. To this end we define

$$
\begin{aligned}
x' &= xe^{-\ell} \\
\tau' &= \tau e^{-z\ell} \\
\Psi' &= \Psi e^{\ell/2}.
\end{aligned}
\tag{4.46}
$$

The reader can easily check that new $\mathcal{L}_I$ expressed in terms of x', τ' and Ψ' has the same form, and the same short distance cutoff a, as the original $\mathcal{L}_I$ had in terms of x, τ and Ψ at the position of the quantum critical point $\Delta = T = 0$. The parameter z is the *dynamic critical exponent* and determines the relative rescaling factors of space and time. In the present case, only the choice $z = 1$ leaves the velocity c invariant. Indeed, all of the problems in Part 2 of this book will have $z = 1$ as they are related to classical problems which are fully isotropic in D spatial dimensions. When viewed as a transformation on the continuum theory, (*i.e.*, for the case $a \to 0$), it is evident that (4.46) is an exact invariance of $\mathcal{L}_I$, and this shall often be a useful point of view to take. However, the picture of a scaling transformation integrating out short distance degrees of freedom is also quite useful in developing physical intuition.

The invariance of $\mathcal{L}_I$ at $\Delta = T = 0$ under (4.46) means that all observable correlators must also be invariant under it. We will put this invariance to good use shortly. The reader should view the invariance (4.46) as playing the same role as, *e.g.*, invariance of the Hamiltonian of the hydrogen atom under spatial rotations. The latter allows one to classify observables under different representations of the rotation group, and we will shortly discuss how rescaling invariance classifies operators and couplings.

Let us move away from the critical point $\Delta = 0$, $T = 0$, by changing Δ but keeping $T = 0$. Under the rescaling (4.46) the action $\mathcal{L}_I$ remains invariant only if we introduce a new Δ'

$$
\Delta' = \Delta e^{\ell}.
\tag{4.47}
$$

Unlike at the critical point, it is necessary to redefine a coupling constant in $\mathcal{L}_I$. So at a fixed $\Delta \neq 0$, the correlators of $\mathcal{L}_I$ are not scale invariant. Nevertheless, the simple behavior of Δ under the rescaling transformation does place constraints on the allowed form of its correlators. We also find it useful to consider the consequences of repeated scaling transformations, in which case it is useful to define an ℓ-dependent $\Delta(\ell)$ which

satisfies the differential equation

$$\frac{d\Delta}{d\ell} = \Delta.$$

(4.48)

We see that any initially non-zero Δ grows indefinitely as one transforms to larger scales (larger ℓ), and such perturbations away from the scale-invariant quantum critical point are known as *relevant* perturbations. It is clear that they destroy scale-invariance at the largest scales and therefore must be included in any theory of the system.

This is a convenient place to introduce the concept of the *scaling dimension* of a coupling constant. This is simply the power to which the length rescaling factor e^ℓ must to raised to obtain the coupling constant's scaling transformation. The scaling dimension plays a role analogous to the angular momentum quantum number ℓ in systems with rotation invariance: the latter determines the specific action of the symmetry group and places restrictions on possible invariant combinations, and we will find the same for the former. We will denote the scaling dimension of Δ by $\dim[\Delta]$, and so

$$\dim[\Delta] = 1,$$

(4.49)

to ensure $\Delta' = \Delta(e^\ell)^{\dim[\Delta]}$. It is conventional to define the exponent ν as the inverse of the scaling dimension of the most relevant perturbation about a quantum critical point; in the present case, this will turn out to be Δ, and so

$$\nu = 1$$

(4.50)

We can also talk about the scaling dimension of an operator, and clearly from (4.46) we have

$$\dim[\Psi] = 1/2.$$

(4.51)

We may also talk of scaling dimensions of space and time themselves, which are clearly

$$\dim[x] = -1 \qquad \dim[\tau] = -z$$

(4.52)

The temperature, T, is just an inverse time, and therefore

$$\dim[T] = z.$$

(4.53)

This is positive, and so, not surprisingly, T is also a relevant perturbation at the quantum critical point. Let us also consider the scaling dimension of the free energy density $\mathcal{F}$ of the system (we always subtract out from $\mathcal{F}$ the ground state energy at the quantum critical point $\Delta = 0$

and consider the singular behavior of the remainder). This is given by $\mathcal{F} = -(T/V) \ln \mathcal{Z}$ where V is the volume, and $\mathcal{Z}$ is the partition function. As the logarithm is dimensionless, and clearly $\dim[V] = d \dim[x]$, we have

$$\dim[\mathcal{F}] = d + z. \qquad (4.54)$$

Finally, we also need the scaling dimension of the order parameter $\hat{\sigma}^z$. This is not a simple local function of the Fermi field Ψ, is therefore quite difficult to determine. We will describe a relatively elaborate calculation in Section 4.4 which shows that

$$\dim[\hat{\sigma}^z] = 1/8. \qquad (4.55)$$

This is the first example of what is known as an *anomalous dimension*. All previous scaling dimensions coincided with their so-called *engineering dimension*, *i.e.*, that obtained by the familiar dimensional analysis of lengths and times in meters and seconds, with the additional freedom to use powers of the velocity c to convert all times into lengths; the anomalous dimension is defined the *difference* of the scaling and engineering dimensions, and so all previous anomalous dimensions were 0. The engineering dimension of $\hat{\sigma}^z$, a dimensionless matrix, is clearly 0. Nevertheless, we will see that it has a non-zero scaling dimension. This can happen without violating equality of engineering dimensions (which must always be preserved) because we have the additional freedom to use powers of the lattice energy scale J (or the lattice spacing, a) in defining the continuum limit of observables. Indeed, (4.55) implies that it is only the combination $J^{1/8}\hat{\sigma}^z$ which has correlators which are finite in the continuum limit $a \to 0$ discussed below (4.42). Further discussion on anomalous dimensions can be found in texts [184] on phase transitions in classical statistical mechanics.

Armed with the knowledge of these scaling dimensions, we can put important general constraints on the structure of various universal scaling forms. We shall follow a simple, general convention in presenting these scaling forms. First pick the observable of interest and determine its scaling dimension. Then write down as a prefactor that power of T which has the same scaling dimension as the observable. This multiplies a dimensionless universal scaling function of a number of arguments; each argument should be a coupling or co-ordinate times a power of T so that the combination has net scaling dimension 0. Finally, powers of innocuous variables like c with zero scaling dimension are inserted so that the engineering dimensions of the expressions are consistent.

As an example of such considerations, let us consider the scaling form satisfied by the two-point correlator $C(x,t)$ defined in (4.2):

$$C(x,t) = ZT^{1/4}\Phi_I\left(\frac{Tx}{c}, Tt, \frac{\Delta}{T}\right).\qquad(4.56)$$

Here Z is an overall non-critical normalization constant, with zero scaling dimension, which depends on the details of the microscopic physics; its presence is related to the anomalous dimension of $\hat{\sigma}^z$ and consistency of (4.56) requires Z have engineering dimension $-1/4$. We will shortly relate Z to observable properties of the ground state. The scaling function Φ_I depends universally on its three arguments. The power of T in the front follows from (4.55) and (4.53). Notice that the physics depends completely on the ratio of two energy scales, that of the $T = 0$ energy gap to temperature: Δ/T. The central purpose of this chapter shall be a fairly complete description of the physical properties of Φ_I as a function of Δ/T.

It is very important to note that the scaling form (4.56) will *not* satisfy the relationship $C(0,0) = 1$, which is exactly obeyed by the lattice model: this is a short distance property which is lost once the continuum limit has been taken. Alternatively stated, the sum-rule (4.6) will not be obeyed by the Fourier transform of (4.56).

We can also describe rather explicitly the sense in which Φ_I is universal, *i.e.*, what happens if we generalize H_I or $\mathcal{L}_I$ to include other short range couplings ? There are two different types of perturbations to $\mathcal{L}_I$ that are possible. The first type arises from higher spatial gradients in the mapping from the particular Hamiltonian H_I, and the simplest of these is

$$\lambda_1\Psi^\dagger\frac{\partial^2\Psi}{\partial x^2}.\qquad(4.57)$$

The second type comes from additional terms we could add to H_I, like $\hat{\sigma}_i^x\hat{\sigma}_{i+1}^x$, which respect the symmetry (1.11), and are therefore not expected to modify qualitative features of the transition; after the Jordan-Wigner transformation, and expansion in spatial gradients, such a term induces in the continuum limit a term

$$\lambda_2\Psi^\dagger\frac{\partial\Psi^\dagger}{\partial x}\frac{\partial\Psi}{\partial x}\Psi;\qquad(4.58)$$

notice that two spatial gradients are required because the term with only one would vanish because of the Fermi statistics identity $\Psi^2 = 0$.

A simple computation shows that

$$\dim[\lambda_1] = -1 \qquad \dim[\lambda_2] = -2. \qquad (4.59)$$

These scaling dimensions are negative, and therefore when we integrate the analog of a flow equation like (4.48), we find that any initially non-zero $\lambda_{1,2}$ decrease indefinitely in absolute value upon transforming to larger scales. Such couplings are denoted as *irrelevant* as they can be neglected in a discussion of the leading long distance and low T properties.

The absence of other relevant perturbations at $\Delta = 0$ implies that $\mathcal{L}_I$ is the universal continuum quantum field theory describing crossovers near the $\Delta = 0$, $T = 0$ quantum-critical point. It is fortunate that this universal theory happens to be expressible as a free fermion model. Although our original motivation for examining H_I was its solvability, the arguments of this section have shown that this choice also happily coincides with that required for obtaining a universal critical theory.

There are two types of consequences of the irrelevant couplings. The first is that the values of the parameters Z, Δ and c appearing in the scaling form (4.56) change; this change is quite difficult to compute, and therefore we should consider Z, Δ and c to be defined by some experimental observable at $T = 0$—Δ defined to be the energy gap at $T = 0$, c is the velocity of excitations at $\Delta = 0$, and Z will be shown later to be related to certain amplitudes at $T = 0$. The second is that there are subleading corrections to the whole scaling form itself: the form of these corrections can be deduced from the general rules stated earlier, and we find that the result (4.56) has multiplicative corrections like

$$\left(1 + \lambda_1 T + \lambda_2 T^2 + \dots\right). \qquad (4.60)$$

These corrections are expected to be unimportant at low enough T.

Let us compute finite temperature correlators of the free fermion field Ψ. These correlators are not related to any local observable of the Ising chain, and therefore cannot be measured experimentally. Our main purpose in discussing them is to further illustrate the present scaling ideas in a simple context. The two-point Ψ correlators can be computed by performing the analog of the lattice Bogoliubov transformation on the continuum theory. We found for imaginary time $\tau > 0$

$$\left\langle \Psi(x,\tau)\Psi^\dagger(0,0) \right\rangle = \frac{1}{2} \int_{-\infty}^{\infty} \frac{dk}{2\pi} \frac{e^{ikx}}{e^{c|k|/T} + 1} \left(e^{c|k|(1/T - \tau)} + e^{c|k|\tau} \right)$$

$$= \left(\frac{T}{4c}\right)\left(\frac{1}{\sin(\pi T(\tau - ix/c))} + \frac{1}{\sin(\pi T(\tau + ix/c))}\right). \quad (4.61)$$

In a similar manner, we can find

$$\langle \Psi(x,\tau)\Psi(0,0)\rangle = \left(\frac{iT}{4c}\right)\left(\frac{1}{\sin(\pi T(\tau - ix/c))} - \frac{1}{\sin(\pi T(\tau + ix/c))}\right). \quad (4.62)$$

The results (4.61,4.64) have precisely the scaling forms that would have been expected under the scaling dimensions in (4.46). At $T = 0$, (4.61) simplifies to

$$\langle \Psi(x,\tau)\Psi^\dagger(0,0)\rangle = \frac{1}{4\pi}\left(\frac{1}{c\tau - ix} + \frac{1}{c\tau + ix}\right). \quad (4.63)$$

Now notice that the transformation

$$c\tau \pm ix \to \frac{c}{\pi T}\sin\left(\frac{\pi T}{c}(c\tau \pm ix)\right) \quad (4.64)$$

connects the $T = 0$ and $T > 0$ results. This mapping is actually an example of a very general connection between *all* $T = 0$ and $T > 0$ two-point correlators of the continuum theory $\mathcal{L}_I$. The existence of this mapping is due to a larger *conformal* symmetry of $\mathcal{L}_I$ [72]: the reader is referred to Ref [247] for further discussion on this point. Here we will defer discussion of this mapping to Chapter 14 where it will arise as a simple consequence of the bosonization method.

4.4 Equal time correlations of the order parameter

This section is of a technical nature. Its main purpose is to show how one may obtain the result (4.55) that $\dim[\hat{\sigma}^z] = 1/8$. We will also obtain explicit expressions for certain crossover functions which cannot be obtained otherwise. The limiting forms of these crossover functions, and all of the interesting dynamical properties of the system will be obtained again later in Section 4.5 using simple physical arguments that rely on the bosonic picture of the excitations developed in Section 4.1 using the large and small g expansions. Most readers may therefore glance at the next paragraph where we outline the main results, and omit the remainder of this section.

We will begin by writing down the main result, and then outline how it is obtained. The equal-time two-point correlation of the order parameter

has the following long distance limit at any $T > 0$ [425]

$$\lim_{|x| \to \infty} C(x, 0) = Z T^{1/4} G_I(\Delta/T) \exp\left(-\frac{T|x|}{c} F_I(\Delta/T) \right), \qquad (4.65)$$

where Z is the non-universal constant introduced earlier in (4.56), and $F_I(s)$ and $G_I(s)$ are universal scaling functions. Notice that (4.65) is completely consistent with the general scaling form (4.56). A crucial property of (4.65) is the prefactor of $T^{1/4}$, which establishes that $\dim[\hat{\sigma}^z] = 1/8$. A second important property is that the two-point correlations decay exponentially to zero at large enough x: so the $T = 0$ long-range-order discussed in Section 4.1.2 disappears at any $T > 0$: we will later give a simple physical explanation of this. The exponential decay defines a correlation length ξ which obeys

$$\xi^{-1} = \frac{T}{c} F_I\left(\frac{\Delta}{T} \right). \qquad (4.66)$$

The exact, self-contained expression for the universal function F_I is [425]

$$F_I(s) = |s|\theta(-s) + \frac{1}{\pi} \int_0^\infty dy \ln\coth\frac{(y^2 + s^2)^{1/2}}{2} \qquad (4.67)$$

The $s > 0$ ($s < 0$) portion of F_I describes the magnetically ordered (paramagnetic) side. Despite its appearance, the function $F_I(s)$ is smooth as a function of s for all real s, and is analytic at $s = 0$. The analyticity at $s = 0$ is required by the absence of any thermodynamic singularity at finite T for $\Delta = 0$. This is a key property, which was in fact used to obtain the answer in (4.67). The exact expression for the function $G_I(s)$ is also known [425]

$$\ln G_I(s) = \int_s^1 \frac{dy}{y} \left[\left(\frac{dF_I(y)}{dy} \right)^2 - \frac{1}{4} \right] + \int_1^\infty \frac{dy}{y} \left(\frac{dF_I(y)}{dy} \right)^2, \qquad (4.68)$$

and its analyticity at $s = 0$ follows from that of F_I. For the solvable model H_I, we chose the overall normalization of G_I such that $Z = J^{-1/4}$. In general, the value of Z is set by relating it to an observable, as we will show below. Also note that Z has no dependence on Δ, and is therefore non-singular at the quantum critical point.

We show a plot of the universal functions F_I and G_I in Fig 4.2. Notice that there are perfectly smooth at $\Delta = 0$ ($s = 0$).

We will outline how to establish (4.65). We will work with the lattice model H_I, and consider the evaluation of $\langle \hat{\sigma}_i^z \hat{\sigma}_{i+n}^z \rangle$. The continuum limit for the correlators of $\mathcal{L}_I$ can only be taken at a relatively late
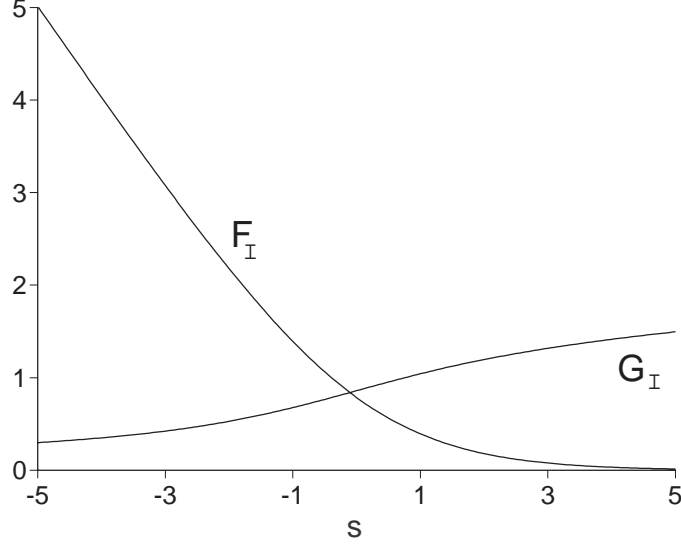
Fig. 4.2. The crossover functions for the correlation length (F_I) and the amplitude (G_I) as a function of $s = \Delta/T$.

stage. We use the fermionic representation (4.29) and the simple identity $1 - 2c_i^\dagger c_i = (c_i^\dagger + c_i)(c_i^\dagger - c_i)$, and obtain [306]

$$\langle \hat{\sigma}_i^z \hat{\sigma}_{i+n}^z \rangle = \left\langle (c_i^\dagger + c_i) \left[\prod_{j=i}^{i+n-1} (c_j^\dagger + c_j)(c_j^\dagger - c_j) \right] (c_{i+n}^\dagger + c_{i+n}) \right\rangle$$

$$= \left\langle (c_i^\dagger - c_i) \left[\prod_{j=i+1}^{i+n-1} (c_j^\dagger + c_j)(c_j^\dagger - c_j) \right] (c_{i+n}^\dagger + c_{i+n}) \right\rangle. \quad (4.69)$$

Notice that the string only extends between the sites i and $i + n$, with the operators on sites to the left of i having cancelled between the two strings. Now, using the notation

$$A_i = c_i^\dagger + c_i \quad , \quad B_i = c_i^\dagger - c_i \quad (4.70)$$

we have

$$\langle \hat{\sigma}_i^z \hat{\sigma}_{i+n}^z \rangle = \langle B_i A_{i+1} B_{i+1} \cdots A_{i+n-1} B_{i+n-1} A_{i+n} \rangle. \quad (4.71)$$

Since the expectation values are with respect to a free Fermi theory, the expression on the right hand side can be evaluated by the finite temperature Wick's theorem [146] which relates it to a sum over products

of expectation values of pairs of operators. The expectation value of any such pair is easily calculated

$$
\begin{aligned}
\langle A_i A_j \rangle &= \delta_{ij} \\
\langle B_i B_j \rangle &= -\delta_{ij} \\
\langle B_i A_j \rangle &= -\langle A_j B_i \rangle = D_{i-j+1}
\end{aligned}
\tag{4.72}
$$

with

$$
D_n \equiv \int_0^{2\pi} \frac{d\phi}{2\pi} e^{-in\phi} \widetilde{D}(e^{i\phi})
\tag{4.73}
$$

and

$$
\widetilde{D}(z = e^{i\phi}) \equiv \left(\frac{1 - gz}{1 - g/z} \right)^{1/2} \tanh \left[\frac{J}{T} ((1 - gz)(1 - g/z))^{1/2} \right] ; \quad (4.74)
$$

notice that the argument of the tanh (which arises from the thermal Fermi distribution function) is simply $\varepsilon_\phi / 2T$. In determining $\langle B_i A_j \rangle$, we have used the representation (4.35) and evaluated expectation values of the γ_k under the free fermion Hamiltonian (4.38). Collecting the terms in the Wick expansion, we find

$$
\langle \hat{\sigma}_i^z \hat{\sigma}_{i+n}^z \rangle = T_n \equiv
\begin{vmatrix}
D_0 & D_{-1} & \cdots & D_{-n+1} \\
D_1 & & & \\
\cdot & & & \\
\cdot & & & \\
\cdot & & D_0 & D_{-1} \\
D_{n-1} & & D_1 & D_0
\end{vmatrix}
\tag{4.75}
$$

We are now faced with the mathematical problem of evaluating the determinant T_n: to obtain the universal scaling limit answer we need to take the limit $n \to \infty$ while keeping the system close to its critical point. The expression for T_n is in a special class of determinants known as Toeplitz determinants, and the limit $T_{n\to\infty}$ can indeed be evaluated in closed form using a fairly sophisticated mathematical theory. We will not present the details of this evaluation here, and refer the reader to the literature [338, 333, 38, 425]. The final, universal, result has already been quoted at the beginning of this section.

4.5 Finite temperature crossovers

The key result of the previous section was that equal-time correlations of the order parameter, $C(x, 0)$, decay exponentially to zero at any $T > 0$.

The expression for the correlation length as a function of Δ/T was given in (4.66). From this result we can easily obtain the following important limiting forms; these will also be rederived in this section using simpler physical arguments

$$
\xi = \begin{cases}
c\sqrt{\dfrac{\pi}{2\Delta T}}\,e^{\Delta/T} & \text{for } \Delta \gg T \\[2em]
\dfrac{4c}{\pi T} & \text{for } |\Delta| \ll T \\[2em]
\dfrac{c}{|\Delta|} & \text{for } \Delta \ll -T
\end{cases}
\tag{4.76}
$$

Notice that for $\Delta > 0$, the correlation length diverges exponentially as $T \to 0$: as we will show explicitly in Section 4.5.1 below, this is a characteristic property of a state with long-range order at $T = 0$ which disappears at any nonzero T. Precisely at $\Delta = 0$, the correlation length diverges as $\sim 1/T$, which agrees with the naive analysis of scaling dimensions at a quantum critical point $\sim T^{-1/z}$. Finally for $\Delta < 0$, the correlation length reaches a finite value as $T \to 0$, suggesting a quantum paramagnetic ground state. These dependencies imply the important crossover phase diagram shown in Fig 4.3: there are three distinct universal regimes, characterized by the limiting forms in (4.76), determined by the largest of the two characteristic energy scales, Δ or T. A closely related phase diagram was discussed by Chakravarty, Halperin and Nelson [83] in the context of a model we shall study in Chapter 7, with a different terminology for the various regimes. We find our choices more appropriate and convenient, although we shall briefly recall their notation in the following subsections.

There are two low T regimes with $T \ll |\Delta|$. The one for $\Delta > 0$, on the magnetically ordered side, has an exponentially diverging correlation length ξ as $T \to 0$; it will be studied in Section 4.5.1. The other low T regime with $\Delta < 0$ has a correlation length which saturates at a finite value as $T \to 0$; it will be studied in Section 4.5.2. Then there is a novel continuum high T regime, $T \gg |\Delta|$, where the physics is controlled primarily by quantum critical point $\Delta = 0$ and its thermal excitations, and is described by the associated continuum quantum field theory: its properties will be discussed in Section 4.5.3. This is the analog of the "quantum-critical" regime of Ref. [83], but we prefer the term "high T" as a more accurate description of the dynamical properties of this regime. It is implicit in our high T limit here that we are not taking the
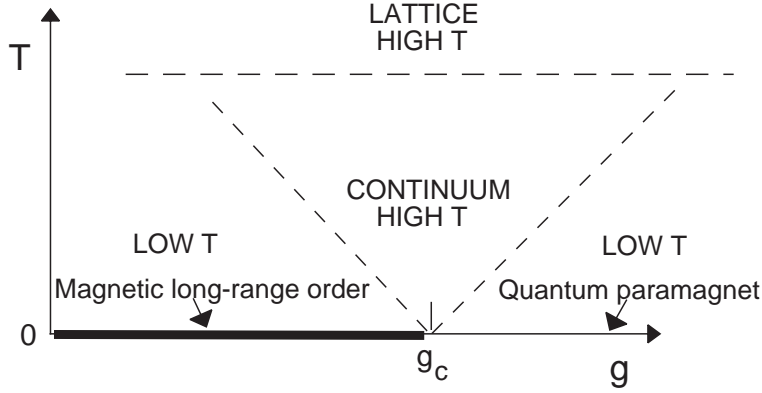
Fig. 4.3. Finite T phase diagram of the $d = 1$ quantum Ising model, H_I, as a function of the coupling g and temperature T. There is a quantum phase transition at $T = 0$ $g = g_c = 1$ with exponents $z = 1$, $\nu = 1$. Magnetic long-range order ($N_0 = \langle \hat{\sigma}_z \rangle \neq 0$) is present only for $T = 0$ and $g < g_c$. The ground state for $g > g_c$ is a quantum paramagnet. There is an energy gap above the ground state for all $g \neq g_c$. We use an energy scale $\Delta \sim g_c - g$ such that the energy gap is $|\Delta|$. The dashed lines are crossovers at $|\Delta| \sim T$. The low T region on the magnetically ordered side ($\Delta > 0$, $g < g_c$) is studied in Section 4.5.1, and low T region on the quantum paramagnetic side ($\Delta < 0$, $g > g_c$) is studied in Section 4.5.2. The continuum high T region is studied in Section 4.5.3; its properties are universal and determined by the continuum theory in (4.44). Finally there is also a "lattice high T" region with $T \gg J$ where the properties are non-universal and determined by the lattice scale Hamiltonian: this region shall not be studied here.

temperature so large that the mapping to the universal continuum model breaks down, and we have to allow for corrections like those in (4.60): this implies that we should always satisfy $T \ll J$. There is therefore a second, non-universal high T limit of the lattice model, also shown in Fig 4.3, where $T \gg J$: we shall have little to say about this regime here. The dynamic $T = \infty$ Ising model results of Ref [71, 380, 381] fall into this last regime; more generally discussions of dynamics at $T = \infty$ may be found in Ref [180] and references therein.

The three subsections below will describe the universal dynamics of the Ising chain in the regions of Fig 4.3. We will pay particular attention to the central concept of the phase coherence time τ_φ which was introduced in Section 3.2, where it was defined loosely as the time over which the wavefunction of the system retains phase memory, and so quantum interference is observable between local measurements separated by times up to τ_φ. We shall use more precise definitions here. We

shall show that τ_φ obeys

$$\tau_\varphi \quad \sim \quad \hbar/k_B T \quad \text{in the "Continuum High T" region, } T \gg \Delta$$
$$\tau_\varphi \quad \sim \quad (\hbar/k_B T)e^{|\Delta|/k_B T} \quad \text{in the "Low T" regions, } T \ll |\Delta| \quad (4.77)$$

Notice that τ_φ always diverges as $T \to 0$, for, as we argued in Section 3.2, the ground state of the system has perfect phase memory. On the magnetically ordered side ($\Delta > 0$, $g < 1$), the divergence of τ_φ is not surprising as it is also accompanied by the divergence of the correlation length, as we saw in (4.76). However, on the quantum paramagnetic side ($\Delta < 0$, $g > 1$), the correlation length saturates as $T \to 0$; this clearly does not give a complete physical picture as the divergence of τ_φ indicates a certain temporal coherence. Therefore, as already noted in Section 3.2, the commonly used description of the $\Delta < -T$ region as "quantum disordered" is quite misleading: there are quite precise long-range correlations in time which characterize the perfect coherence of paramagnetic ground state. Finally, in the continuum high T region, we see that the lower bound on τ_φ in (3.14) is saturated—this is therefore the most incoherent region.

4.5.1 Low T on the magnetically ordered side, $\Delta > 0$, $T \ll \Delta$

In their study of the model of Chapter 7, Chakravarty *et al.* [83] called the analogous regime "renormalized classical" [83]. The reasons for this name will become clear below; however, this is not the only regime which displays classical behavior, as we will see in Section 4.5.2.

First, let us consider the results for the equal-time correlations. Assuming that it is valid to interchange the limits $T \to 0$ and $x \to \infty$ in (4.65), we can use the limiting values $F_I(\infty) = 0$, $G_I(s \to \infty) = s^{1/4}$ to deduce that (recall (4.21)):

$$N_0^2 \equiv \lim_{|x|\to\infty} C(x,0) = Z\Delta^{1/4} \qquad \text{at } T = 0. \qquad (4.78)$$

Thus, as claimed earlier, there is long-range order in the $g < 1$ ground state of H_I, with the order parameter $N_0 = \langle \hat{\sigma}^z \rangle = Z^{1/2}\Delta^{1/8}$—notice that N_0 vanishes as g approaches g_c from below with the exponent $1/8$. We can also use the relationship (4.78) to relate the parameter Z to the observables N_0 and Δ. Turning next to non-zero T, for small $T \ll \Delta$, we obtain from the large s behavior of $F_I(s)$ (see (4.67)) that

$$C(x,0) = N_0^2 e^{-|x|/\xi_c} \quad \text{large } |x|, \qquad (4.79)$$

where the correlation length

$$\xi_c^{-1} = \left(\frac{2|\Delta|T}{\pi c^2} \right)^{1/2} e^{-|\Delta|/T}.$$

(4.80)

is finite at any non-zero T, showing that long-range order is present only precisely at $T = 0$. We have put a subscript c on the correlation length to emphasize that the system is expected to behave *classically* in this low temperature region. This is a crucial characteristic of this region and the reason for classical behavior is quite simple and familiar. The excitations consists of particles (the kinks and anti-kinks of Section 4.1) whose mean separation ($\sim \xi_c \sim e^{\Delta/T}$) is much larger than their de Broglie wavelengths ($\sim (c^2/\Delta T)^{1/2}$, which is obtained by equating the kinetic energy $\varepsilon_k - \Delta \sim c^2 k^2/2\Delta$ to the thermal equipartition value $T/2$) as $T \to 0$, which is precisely the canonical condition for the applicability of classical physics. It is also reassuring to note that (4.79) has the form of equal-time correlations in the classical Ising chain at low T, which were discussed in Section 2.1. The prefactor N_0^2 is the true ground state magnetization including the effects of quantum fluctuations, and this is the reason for the adjective "renormalized" in the name for this region.

We show that it is possible to give a simple physical interpretation for the value of ξ_c in (4.80). The energy of a domain wall with a small momentum k is $\Delta + c^2 k^2/2\Delta$, and therefore classical Boltzmann statistics tells us that their density, ρ, is

$$\rho = \int \frac{dk}{2\pi} e^{-(\Delta + c^2 k^2/2\Delta)/T} = \left(\frac{T\Delta}{2\pi c^2} \right)^{1/2} e^{-\Delta/T}.$$

(4.81)

Comparing with (4.80), we see that $\xi_c = 1/2\rho$. This result follows if we assume that the domain walls are classical *point* particles, which are distributed independently with a density ρ. Consider a system of size $L \gg |x|$, and let it contain M thermally excited particles; then $\rho = M/L$. Let q be the probability that a given particle will be between 0 and x. Clearly,

$$q = \frac{|x|}{L}.$$

(4.82)

The probability that a given set of j particles are the only ones between 0 and x is then $q^j(1-q)^{M-j}$: as each particle reverses the orientation of the ground state, in this case $\hat{\sigma}^z(x,0)\hat{\sigma}^z(0,0) = N_0^2(-1)^j$. Summing

over all possibilities we have

$$
\begin{aligned}
C(x,0) &= N_0^2 \sum_{j=0}^{M} (-1)^j q^j (1-q)^{M-j} \frac{M!}{j!(M-j)!} \\
&= N_0^2 (1-2q)^M \approx N_0^2 e^{-2qM} = N_0^2 e^{-2\rho|x|}, \quad (4.83)
\end{aligned}
$$

thus establishing the desired result.

This semiclassical picture can also be extended to compute unequal time correlations. In this computation it is essential to consider the collisions between the particles. Even though the particles are very dilute, they cannot really avoid each other in one dimension, and neighboring particles will always eventually collide (this is not true in higher dimensions where sufficiently dilute particles can be treated as non-interacting). During their collisions, the particles are certainly closer than their de Broglie wavelengths, and so the collisions must be treated quantum mechanically. Indeed, these collisions will be characterized by the two-particle S matrix which was considered earlier in Section 4.1: the diluteness does allow us to consider the collisions of only pairs of particles.

To study dynamic correlations, let us reexamine the explicit expression for $C(x,t)$ in (4.2). We will show how it can be evaluated essentially exactly using some simple physical arguments. The key is to recall that classical mechanics emerges from quantum mechanics as a stationary phase evaluation of a first-quantized Feynman path integral. We therefore attempt to evaluate the expression in (4.2) by such a path integral. It is clear that the integral is over a set of trajectories moving forward in time, representing the operator $e^{-iH_I t}$, and a second set moving backwards in time, corresponding to the action of $e^{iH_I t}$. In the semiclassical limit, stationary phase is achieved when the backward paths are simply the time reverse of the forward paths, and both sets are the classical trajectories. An example of a set of paths is shown in Fig 4.4. Now observe that

(i) the classical trajectories remain straight lines across collisions because the momenta before and after the collision are the same: this follows from the requirement of conservation of total momentum ($k_1 + k_2 = k_1' + k_2'$) and energy ($\varepsilon_{k_1} + \varepsilon_{k_2} = \varepsilon_{k_1'} + \varepsilon_{k_2'}$) in each two-particle collision, which has the unique solution $k_1 = k_1'$ and $k_2 = k_2'$ (or its equivalent permutation, which need not be considered separately because the particles are identical) in one dimension;

(ii) for each collision, the amplitude for the path acquires a phase $S_{k_1 k_2}$
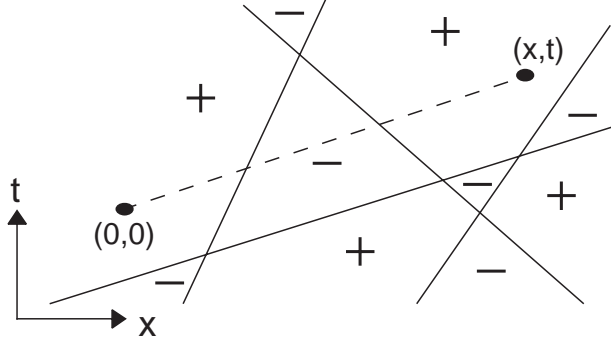
Fig. 4.4. A typical semiclassical contribution to the double time path integral for $\langle \hat{\sigma}^z(x,t)\hat{\sigma}^z(0,0)\rangle$. Full lines are thermally excited particles which propagate forward and backward in time. The $\pm$ signs are significant only for $g < g_c$ and denote the orientation of the order parameter. For $g > g_c$, the dashed line is a particle propagating only forward in time from $(0,0)$ to (x,t).

along the forward path and its complex conjugate along the backward path: the net factor for the collision is therefore $|S_{k_1k_2}|^2 = 1$.

These two facts imply that the trajectories are simply independently distributed straight lines, placed with a uniform density ρ along the x axis, with an inverse slope

$$v_k \equiv \frac{d\varepsilon_k}{dk}, \tag{4.84}$$

and with their momenta chosen with the Boltzmann probability density $e^{-\varepsilon_k/T}/\rho$ (Fig 4.4).

Computing dynamic correlators is now an exercise in classical probabilities. As each particle trajectory is the boundary between domains with opposite orientations of the spins, the value of $\hat{\sigma}^z(0,0)\hat{\sigma}^z(x,t)$ is the square of the magnetization renormalized by quantum fluctuations (N_0^2) times $(-1)^j$, where j is the number of trajectories intersecting the dashed line in Fig. 4.4. Now it remains to average $N_0^2(-1)^j$ over the classical ensemble of trajectories defined above. This average can be carried out in a manner quite similar to that in the equal-time computation earlier. Again choosing a system size $L \gg |x|$ with M particles, the probability q that a given particle with velocity v_k is between the points $(0,0)$ and (x,t) in Fig 4.4 is (compare (4.82))

$$q = \frac{|x - v_k t|}{L}. \tag{4.85}$$

We have to average over velocities, and then evaluate the summation in

(4.83). This gives one of the central results of this chapter [442]

$$
\begin{aligned}
C(x,t) &= N_0^2 R(x,t) \\
R(x,t) &\equiv \exp\left(-\int \frac{dk}{\pi} e^{-\varepsilon_k/T} \left|x - v_k t\right|\right).
\end{aligned} \tag{4.86}
$$

(This relaxation function also appeared in Refs [323] and [123] in a phenomenological analysis of related models by exponentiating a short-time expansion which ignored collisions.) The equal-time or equal-space form of the relaxation function $R(x,t)$ is quite simple:

$$
\begin{aligned}
R(x,0) &= e^{-|x|/\xi_c} \\
R(0,t) &= e^{-|t|/\tau_\varphi};
\end{aligned} \tag{4.87}
$$

for general x, t R also decreases monotonically with increasing $|x|$ or $|t|$, but the decay is not simply an exponential. The spatial correlation length ξ_c is given in (4.80). We have identified the equal-space correlation time as the phase coherence time for obvious reasons: the long-range order in the ground state is clearly a manifestation of phase coherence, and its decay in time is a natural measure of τ_φ. We can determine τ_φ from (4.86), and remarkably we find that τ_φ is independent of the functional form of ε_k and depends only on the gap:

$$
\begin{aligned}
\frac{1}{\tau_\varphi} &= \frac{2}{\pi} \int_0^\infty dk \frac{d\varepsilon_k}{dk} e^{-\varepsilon_k/T} \\
&= \frac{2}{\pi} \int_{|\Delta|}^\infty d\varepsilon_k e^{-\varepsilon_k/T} \\
&= \frac{2k_B T}{\pi \hbar} e^{-|\Delta|/k_B T}
\end{aligned} \tag{4.88}
$$

where we have momentarily inserted the fundamental constants $\hbar$, k_B in the last step to emphasize the universality of the result.

In the limit $T \ll \Delta$ we are now able to completely specify the form of the scaling function Φ_I in (4.56). The behavior of Φ_I is characterized by the concept of a *reduced scaling function* which is determined entirely by classical physics: we shall have several occasions to use this concept later in this book. Notice that the original function Φ_I had three arguments: the scales of space and time relative to T, and the ratio Δ/T. For $T \ll \Delta$ the last argument disappears, and we find that the scales of space and time are determined respectively by the large classical scales ξ_c and τ_φ respectively. By an analysis of (4.86) we find that the correlations can

be written in the following reduced classical scaling form

$$C(x, t) = N_0^2 \Phi_R \left(\frac{x}{\xi_c}, \frac{t}{\tau_\varphi} \right),$$ (4.89)

where clearly $R(x, t)$ satisfies the scaling form

$$R(x, t) = \Phi_R \left(\frac{x}{\xi_c}, \frac{t}{\tau_\varphi} \right).$$ (4.90)

These scaling forms are valid only for $T \ll \Delta$, and they must be consistent with the fully quantum Φ_I in (4.56) which is valid for all Δ/T. This requirement implies that the scales ξ_c and τ_φ must be *universal* functions of Δ/T, as we have already seen in the expressions (4.80) and (4.88). Evaluating (4.86) we can obtain an explicit closed form expression for Φ_R:

$$\ln \Phi_R(\bar{x}, \bar{t}) = -\bar{x} \, \mathrm{erf} \left(\frac{\bar{x}}{\bar{t}\sqrt{\pi}} \right) - \bar{t} e^{-\bar{x}^2/(\pi \bar{t}^2)}.$$ (4.91)

Notice that the characteristic time τ_φ and length ξ_c both diverge as $\sim e^{\Delta/T}$, and so we can define an effective classical dynamic exponent $z_c = 1$ (there is no fundamental reason why z_c and z should have the same value). We also note here that the classical dynamic scaling function obtained above is unrelated to the dynamic scaling functions associated with a popular classical statistical model for dynamics of Ising spins—the Glauber model [181]: the present underlying quantum dynamics leads to a rather different effective classical model in which energy and momentum conservation play a crucial role, the time evolution is deterministic, and the average is over the set of initial conditions.

All of the results above have been compared with exact numerical computations and the agreement is essentially perfect. We show a typical comparison in Fig 4.5. This agreement gives us confidence that the physical, 'hand-waving', quasi-classical particle approach to dynamical properties outlined above is in fact exact.

The Fourier transform of (4.89) and (4.91) yields the portion of the dynamic structure factor, $S(k, \omega)$ (defined in (4.4)), describing the $T > 0$ broadening of the $T = 0$ delta function in (4.23). We expect this broadening to occur on a frequency scale of order $1/\tau_\varphi$, and so the predominant weight in $S(k, \omega)$ is at frequencies $\omega \ll T$. Under this condition, some simplifications occur in the relationships between the response functions introduced in the opening of this chapter. In particular, for $\omega \ll T$, the fluctuation-dissipation theorem (4.9) reduces to its simpler, 'classical'
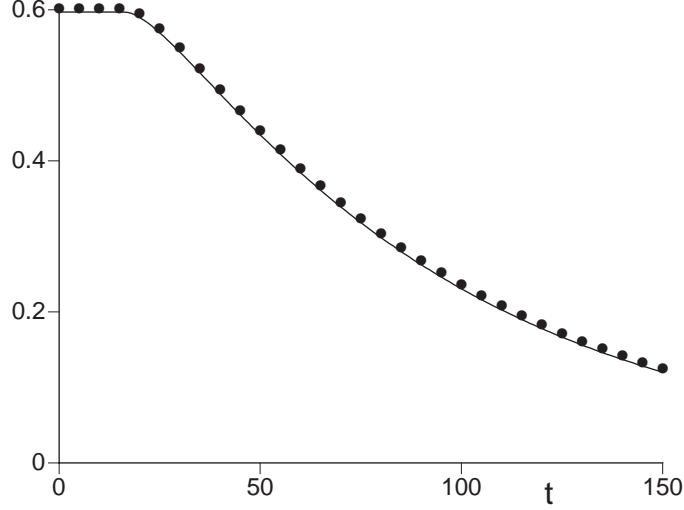
Fig. 4.5. Theoretical and numerical results from Ref. [442] for the real part of the correlator $\langle \hat{\sigma}^z(x,t)\hat{\sigma}^z(0,0) \rangle$ of H_I at $x = 20$ with $J = 1$, $g = 0.6$ (therefore $\Delta = 0.8$), $T = 0.3$ and so the system is in the low T region on the magnetically ordered side of Fig 4.3. The numerical data (shown in circles) was obtained for a lattice size $L = 512$ with free boundary conditions This is compared with the theoretical prediction in Eqn (4.86). The imaginary part of the correlator was numerically found to be negligibly small, and the semiclassical theoretical prediction is that it vanishes.

form

$$S(k,\omega) = \frac{2T}{\omega}\text{Im}\chi(k,\omega). \tag{4.92}$$

As $\text{Im}\chi(k,\omega)$ is always an odd function of ω, in the limit that (4.92) is obeyed, $S(k,\omega)$ becomes an even function of ω. Applying (4.92) to (4.5), we see that the equal-time structure factor is simply T times the static susceptibility

$$
\begin{aligned}
S(k) &= \int \frac{d\omega}{\pi}\frac{\text{Im}\chi(k,\omega)}{\omega} \\
&= T\chi(k),
\end{aligned}
\tag{4.93}
$$

where the second equation relies on the Kramers-Kronig transform in (4.10). So we see that the static, zero frequency response to an external field contains information on the equal-time spin correlations: it must be remembered that this is only true for effectively classical systems in which the predominant weight in the spectral density is at frequencies

smaller than T, and is *not* true in general. For the present situation, the value of $S(k)$ follows immediately from (4.86) and (4.87):

$$T\chi(k) = S(k) = N_0^2 \frac{2\xi_c}{1 + k^2 \xi_c^2} \tag{4.94}$$

So the delta function in $S(k)$ implied by (4.23) has been broadened on a momentum scale ξ_c^{-1}, and $S(0)$ takes an exponentially large value proportional to $\xi_c \sim e^{\Delta/T}$.

Turning to the broadening in $S(k, \omega)$, it is useful to introduce the parameterization

$$\frac{2T}{\omega} \text{Im}\chi(k, \omega) = S(k, \omega) = T\chi(k)\tau_\varphi \Phi_{Sc}(k\xi_c, \omega\tau_\varphi) \tag{4.95}$$

where Φ_{Sc} is a universal scaling function whose form follows from a Fourier transform of (4.91). We have inserted the prefactors in front of Φ_{Sc} because then it follows easily from (4.10) that its frequency integral has a fixed normalization

$$\int \frac{d\overline{\omega}}{2\pi} \Phi_{Sc}(\overline{k}, \overline{\omega}) = 1. \tag{4.96}$$

We will use scaling forms like (4.95) at several other occasions in this book. We performed a numerical Fourier transform of (4.91) and the result for Φ_{Sc} is shown in Fig 4.6. So the dynamic structure factor has a large peak of order $N_0^2 \xi_c \tau_\varphi \sim e^{2\Delta/T}$, and decays monotonically to zero on a frequency scale $\sim \tau_\varphi^{-1}$ and on a momentum scale $\sim \xi_c^{-1}$. The frequency width of Φ_{Sc} broadens with increasing wavevector, but its maximum remains at $\overline{\omega} = 0$.

The existence here of a classical reduced scaling function describing relaxation of the order parameter reflects an important underlying physical property: the clear separation of scales at which quantum and thermal fluctuations are dominant. Quantum fluctuations are paramount at distance scales up to c/Δ and these cause a reduction in the ordered moment from unity to N_0. The influence of thermal fluctuations is not felt until the much larger scale ξ_c, where the excitations behave classically except during collisions.

4.5.2 Low T on the quantum paramagnetic side, $\Delta < 0$, $T \ll |\Delta|$

In the study of the model of Chapter 7, Chakravarty *et al.* [83] called the analogous regime "quantum disordered" [83]. However, as we have
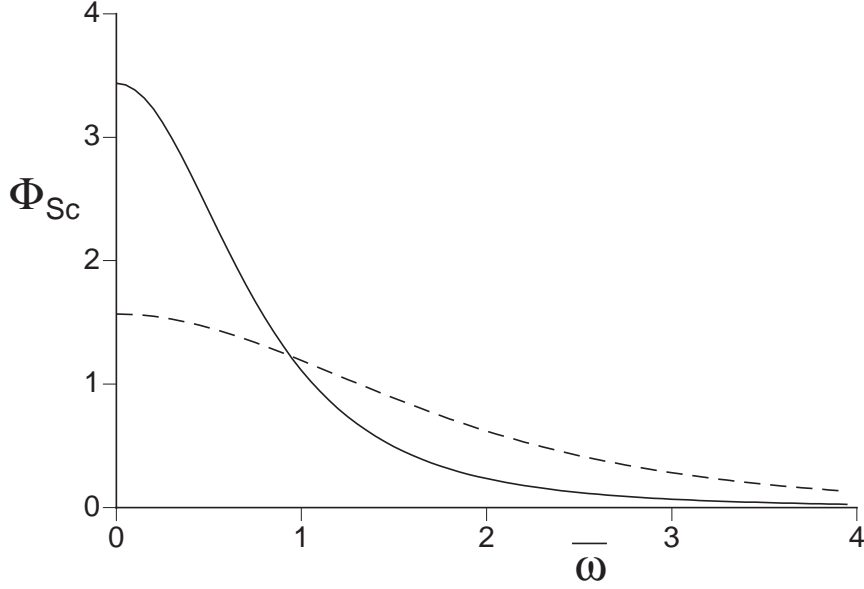
Fig. 4.6. Plot of the scaling function $\Phi_{Sc}(\overline{k}, \overline{\omega})$, appearing in (4.95), as a function of $\overline{\omega}$ at $\overline{k} = 0$ (full line) and $\overline{k} = 1.5$ (dashed line). This describes the broadening of the delta function in the dynamic structure factor in (4.23) at $0 < T \ll \Delta$.

already noted and as we will show below, this nomenclature does not capture the long range time correlations associated with the exponentially large τ_φ in this regime.

We begin by describing the equal-time correlations. We need to take the $s \to -\infty$ limit of the functions $F_I(s)$, $G_I(s)$; from these limits we find

$$C(x, 0) = \frac{ZT}{|\Delta|^{3/4}} e^{-|x|/\xi} \ , \ |x| \to \infty \text{ at fixed } 0 < T \ll |\Delta|, \qquad (4.97)$$

with the correlation length ξ given by

$$\xi^{-1} = \frac{|\Delta|}{c} + \left(\frac{2|\Delta|T}{\pi c^2}\right)^{1/2} e^{-|\Delta|/T} \qquad (4.98)$$

So correlations decay exponentially on a scale $\sim c/|\Delta|$, and there is no long-range order.

The equal time correlations at $T = 0$ behave in a similar manner, although the limits $T \to 0$ and $|x| \to \infty$ do not commute for the prefactor

of the exponential decay. Let us first use a simple argument to determine the overall large-x dependence of the $T = 0$ correlation. We already argued in the strong-coupling analysis of Section 4.1.1 that an important feature of the spectral density of the quantum paramagnet was the quasi-particle delta function shown in Fig 4.1. It is reasonable to expect that the leading term in the large x decay is determined simply by the contribution of this pole. We can combine this fact with the relativistic invariance of the continuum theory H_F in (4.61) to argue that near the quasi-particle pole the dynamic susceptibility must have the form

$$\chi(k, \omega) = \frac{\mathcal{A}}{c^2 k^2 + \Delta^2 - (\omega + i\delta)^2} + \dots \quad , \quad T = 0 \qquad (4.99)$$

where δ is a positive infinitesimal; the continuum of excitations above the three particle threshold in Fig 4.1 are represented by the ellipsis in (4.99). The scale-factor $\mathcal{A}$ is the quasi-particle residue, and we will obtain its value momentarily. First, we use (4.99) to deduce the $T = 0$ equal-time correlations. This is most simply done by first analytically continuing (4.99) to imaginary frequencies ω_n, and then using the inverse of the definition (4.7): this gives us

$$
\begin{aligned}
C(x, 0) &= \mathcal{A} \int \frac{d\omega}{2\pi} \int \frac{dk}{2\pi} \frac{e^{-ikx}}{\omega^2 + c^2 k^2 + \Delta^2} \\
&= \frac{\mathcal{A}}{\sqrt{8\pi c |\Delta||x|}} e^{-\Delta|x|/c} \quad , \quad |x| \to \infty \text{ at } T = 0. \quad (4.100)
\end{aligned}
$$

Comparing this result with (4.97) and (4.98), we see that the two results differ in the power of $|x|$ that appears in the prefactor of the exponential. This is acceptable because the two cases involve different orders of limits of $T \to 0$ and $|x| \to \infty$, and there is no mathematical requirement that the orders of limit commute: in (4.100) we have sent $T \to 0$ first, while the limit $|x| \to \infty$ was taken first in (4.97).

To complete the description of the equal-time correlators we need to specify the value of $\mathcal{A}$. This requires a microscopic lattice calculation of the type considered in Section 4.4; an analysis of the large n limit of T_n at $T = 0$ was carried out by McCoy [333] and Pfeuty [382], and comparing their results with (4.100) we can deduce that

$$\mathcal{A} = 2cZ|\Delta|^{1/4}, \qquad (4.101)$$

where we recall that $Z = J^{-1/4}$ for the nearest neighbor model H_I in (4.1). So the residue vanishes at the critical point $\Delta = 0$, where the

quasiparticle picture breaks down, and we will have a completely different structure of excitations. The relationship (4.101) also defines the value of Z on the quantum paramagnetic side in terms of the observables $\mathcal{A}$ and Δ; this complements the result (4.78) which defined Z on the magnetically ordered side.

The above is an essentially complete description of the correlations and excitations of the quantum paramagnetic ground state. We turn to the dynamic properties at $T > 0$. At nonzero T, there will be a small density of quasi-particle excitations which will behave classically for the same reasons as in Section 4.5.1: their mean spacing is much larger than their de Broglie wavelength. The collisions of these thermally excited quasi-particles will lead to a broadening of the delta function pole in (4.99): the form of this broadening can be computed exactly in the limit $T \ll |\Delta|$ using a semiclassical approach similar to that employed for the ordered side [442]. The argument again employs a semiclassical path-integral approach to evaluating the correlator in (4.2). The key observation is that we may consider the operator $\hat{\sigma}^z$ to be given by

$$\hat{\sigma}^z(x,t) = (2cZ|\Delta|^{1/4})^{1/2}(\psi(x,t) + \psi^\dagger(x,t)) + \dots \qquad (4.102)$$

where $\psi^\dagger$ is the operator which creates a single particle excitation from the ground state, and the ellipsis represent multi-particle creation or annihilation terms which are subdominant in the long time limit. This representation may also be understood from the $g \gg 1$ picture discussed earlier, in which the single-particle excitations where $|-\rangle$ spins: the $\hat{\sigma}^z$ operator flips spins between the $\pm x$ directions, and therefore creates and annihilates quasiparticles.

The computation of the nonzero T relaxation is best done in real space and time, so let us first write down the $T = 0$ correlations in this representation. We define $K(x,t)$ to be $T = 0$ correlator of the order parameter:

$$
\begin{aligned}
K(x,t) &\equiv \langle \hat{\sigma}^z(x,t)\hat{\sigma}^z(0,0)\rangle_{T=0} \\
&= \int \frac{dk}{2\pi} \frac{cZ|\Delta|^{1/4}}{\varepsilon_k} e^{i(kx-\varepsilon_k t)} \\
&= \frac{Z|\Delta|^{1/4}}{\pi} K_0(|\Delta|(x^2 - c^2 t^2)^{1/2}/c) \qquad (4.103)
\end{aligned}
$$

where K_0 is the modified Bessel function. This result is obtained by the Fourier transform of (4.99) and (4.9). Note that for $t > |x|/c$, the Bessel function has imaginary argument and is therefore complex and oscillatory. Indeed, (4.103) has the simple interpretation as the spacetime

Feynman propagator of a single relativistic particle in one dimension; this can be made more evident by looking at the non-relativistic limit of (4.103 well within the light cone $x \ll ct$—in this case (4.103) reduces to

$$K(x, t) = Z|\Delta|^{1/4} e^{i\Delta t} \left(\frac{1}{2\pi i \Delta t} \right)^{1/2} \exp\left(i \frac{|\Delta| x^2}{2 c^2 t} \right), \qquad (4.104)$$

which is the familiar Feynman propagator of a non-relativistic particle of mass $|\Delta|/c^2$; the leading oscillatory term $\sim e^{i\Delta t}$ represents the common "rest mass" energy of all the particles. Well outside the light-cone, $x \gg ct$, (4.103) reduces to the equal-time correlator obtained earlier in (4.100): here the correlations become exponentially small. Our primary interest shall be the $T > 0$ properties of the correlations within the light-cone, where the correlations are large and oscillatory (corresponding to the propagation of real particle), and display interesting semiclassical dynamics.

Now we consider the $T \neq 0$ evaluation of (4.2) in the same semiclassical path-integral approach that was employed earlier in Section 4.5.1. Again we are dealing with semiclassical particles, although the physical interpretation of these particles is quite different: they are quasiparticle excitations above a quantum paramagnet, and not domain walls between magnetically ordered regions. As in Section 4.5.1 the path integral representation of (4.2) leads to *two* sets of paths—forward and backwards in time. However there is a special trajectory that moves only forward in time: this is trajectory representing the particle which is created by the first $\hat{\sigma}_0^z$ and annihilated at the second $\hat{\sigma}_i^z$. The inverse process in which the first $\hat{\sigma}_0^z$ annihilates a preexisting thermally excited particle can be neglected as the probability of finding such a particle at a given location is exponentially small. Also as in the semiclassical limit, the forward and backward trajectories of the thermally excited particles are expected to be the same, the particle on the trajectory created by the $\hat{\sigma}_0^z$ must be annihilated at the $\hat{\sigma}_i^z$ for otherwise the initial and final states in the trace in (4.2) will not be the same. This reasoning leads to a space-time snapshot of the trajectories which is the same as in Fig 4.4, but its physical interpretation is very different. The dashed line represents the trajectory of a particle created at $(0,0)$ and annihilated at (x, t), and $\pm$ signs in the domains should be ignored. In the absence of any other particles this dashed line would contribute the $T = 0$ Feynman propagator above, $K(x, t)$, to $\langle \hat{\sigma}^z(x, t) \hat{\sigma}^z(0, 0) \rangle$. The scattering off the background thermally excited particles (represented by the full lines in Fig 4.4 (which are not domain walls)) introduces factors of the S matrix

element $S_{k_1 k_2}$ in (4.17) at each collision; as the dashed line only prop-
agates forward in time, the S matrix elements for collisions between
the dashed and full lines are not neutralized by a complex conjugate
partner. All other collisions occur both forward and backward in time,
and therefore contribute $|S_{k_1 k_2}|^2 = 1$. Using the low momentum value
$S_{k_1 k_2} = -1$, we see that the contribution to $\langle \hat{\sigma}^z(x,t)\hat{\sigma}^z(0,0) \rangle$ from the
set of trajectories in (4.4) equals $(-1)^j K(x,t)$ where j is the number of
full lines intersecting the dashed line. Remarkably, the $(-1)^j$ factor is
precisely the term that appeared in the analysis at low T on the magnet-
ically ordered side in Section 4.5.1, although for very different physical
reasons. We can carry out the averaging over all trajectories as in the
analysis leading to (4.86), and obtain one of our main results for low T
dynamic correlations on the paramagnetic side [442]

$$C(x,t) = K(x,t)R(x,t) \qquad (4.105)$$

with $K(x,t)$ is given by Eq. (4.103), and $R(x,t)$ again specified by the
second result (4.86). Now notice that in going from the magnetically or-
dered to the quantum paramagnetic side the only change in parameters
has been the change in sign of Δ. The dispersion spectrum ε_k is invariant
under this change of sign, and so we can use precisely the same expres-
sions for the relaxation function $R(x,t)$ as before: the result (4.87) still
applies, and we can continue to use the expression (4.91) for the scaling
function Φ_R. Further the characteristic space and time scales, ξ_c and τ_φ,
on which R varies are still given by (4.80) and (4.88) respectively: notice
that we were careful to insert the absolute value $|\Delta|$ in these expressions
even though that was not needed for the magnetically ordered side.

An interesting feature of the result (4.105) is that it clearly displays the
separation in scales at which quantum and thermal effects act. Quantum
fluctuations determine the oscillatory, complex function $K(x,t)$, which
gives the $T = 0$ value of the correlator. Exponential relaxation of spin
correlations occurs at longer scales $\sim \xi_c$, τ_φ, and is controlled by the
classical motion of particles and a purely real relaxation function. This
relaxation is expected to lead to a broadening of the quasi-particle pole
with widths of order ξ_c^{-1}, τ_φ^{-1} in momentum and energy space. We can
consider the presence of a quasi-particle delta function in the spectral
density of excitations above the ground state as a representation of the
perfect quantum coherence in the ground state, and so for $T > 0$ its
width in energy is a natural measure of the inverse phase relaxation
time $1/\tau_\varphi$. In Fig. 4.7 we compare the predictions of Eq. (4.105) with
numerical results on a lattice of size $L = 512$. As expected, there is a
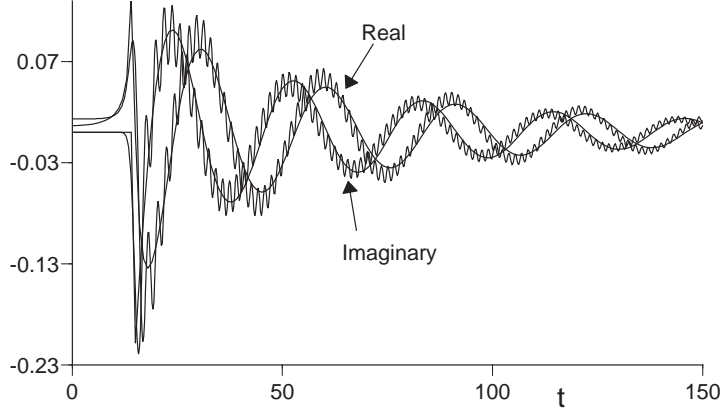
Fig. 4.7. Theoretical and numerical results from Ref. [442] for the correlator $\langle\hat{\sigma}^z(x,t)\hat{\sigma}^z(0,0)\rangle$ of H_I at $x=30$ with $J=1$, $g=1.1$ (therefore $\Delta=-0.2$), $T=0.1$ and so the system is in the low T region on the paramagnetic side of Fig 4.3. The numerical data was obtained for a lattice size $L=512$ with free boundary conditions; it has a "ringing" at high frequency due to the lattice cutoff. The theoretical prediction is from the continuum theory prediction in Eq. (4.105) and is represented by the smoother curve. The envelope of the numerical curve fits the theoretical prediction well.

rapid oscillatory part representing the Feynman propagator of a single particle, and an envelope which is exponentially decaying at a much slower rate. The theoretical curve was determined from the continuum expression for $K(x,t)$, but the full lattice form for ε_k was used. The theory agrees well with the numerics; some differences are visible for small x, outside the light cone, but this is outside the domain of validity of (4.105).

We can also compute the structure factor $S(k,\omega)$ from (4.105) by taking the Fourier transform as in (4.4). This will mainly have weight at positive frequencies $\omega\approx\varepsilon_k\approx|\Delta|+c^2k^2/(2|\Delta|)$, corresponding to the creation of a quasiparticle by the external probe. It is not possible to analytically perform the Fourier transform in general, but the leading term in an asymptotic expansion in $T/|\Delta|$ can be obtained in closed form. For reasons discussed in Ref [117], it turns out that because $\xi_c/c\tau_\varphi=(2T/\pi|\Delta|)^{1/2}\ll1$, the slower relaxation in time dominates the Fourier transform, and we can simply evaluate the Fourier transform while ignoring the x dependence of R:

$$S(k,\omega)\quad\approx\quad\int dt\int dx\,K(x,t)R(0,t)e^{-i(kx-\omega t)}$$

$$= \left(\frac{2cZ|\Delta|^{1/4}}{\varepsilon_k}\right) \frac{1/\tau_\varphi}{(\omega - \varepsilon_k)^2 + (1/\tau_\varphi)^2}. \qquad (4.106)$$

This result holds for k close enough to the band minimum, with $|k| \ll \sqrt{T\Delta}/c$; for larger k there is no alternative to complete numerical evaluation of the Fourier transform. The result (4.106) verifies our earlier expectation based upon the physical interpretation of $1/\tau_\varphi$: the $T > 0$ relaxation merely modifies the delta function into a Lorentzian of width $1/\tau_\varphi$ in energy space.

4.5.3 Continuum High T, $T \gg |\Delta|$

We turn finally to the universal continuum high T region of Fig 4.3, $T \gg |\Delta|$. We will not have anything to say about the lattice high T region, and so will implicitly assume that $T \ll J$.

In our study of the two low T regions of Fig 4.3 we found that it was possible to develop a semiclassical particle picture of phase relaxation because $1/\tau_\varphi \ll T$. The present high T region will turn out to be quite different. We will find that no effective classical model can provide an adequate description of the dynamics because the phase relaxation time is quite short: in particular we will find that $1/\tau_\varphi \sim T$, so that, as noted earlier, this regime is maximally incoherent. The de Broglie wavelength of the effective excitations will be of the same order as their spacing: this holds whether we consider the excitations to be the domain walls of the magnetically ordered phase, or the flipped spins of the quantum paramagnet. Consequently, it is difficult to disentangle quantum and thermal effects: they both play an equally important role. The large class of classical models discussed in the review of Hohenberg and Halperin [228] cannot, therefore, be applied in the present context. This novel regime of dynamics was first discussed in Refs [440, 97] in the context of the model of Chapter 7, and was dubbed *quantum relaxational*: we find it more convenient to introduce it in this book in the simpler context of the Ising chain.

As in the previous subsections, we begin by understanding the structure of the equal time correlations. Right at the critical point, $\Delta = 0$, $g = g_c$, this high T regime extends all the way down to $T = 0$. At the $T = 0$, $g = g_c$ quantum critical point, we can deduce the form of the correlator by a simple scaling analysis. As the ground state is scale invariant at this point, the only scale that can appear in the equal time correlator is the spatial separation x; from the scaling dimension of $\hat{\sigma}^z$

in (4.55), we then know that the correlator must have the form

$$C(x, 0) \sim \frac{1}{(|x|/c)^{1/4}} \qquad \text{at } T = 0, \, \Delta = 0. \qquad (4.107)$$

Actually, we can also include time-dependent correlations at this level without much additional work: we know that the continuum theory (4.44) is Lorentz invariant, and so we can easily extend (4.107) to the imaginary time result

$$C(x, \tau) \sim \frac{1}{(\tau^2 + x^2/c^2)^{1/8}} \qquad \text{at } T = 0, \, \Delta = 0. \qquad (4.108)$$

This result can also be understood by referring back to the classical $D = 2$ Ising model in (3.2): in this context (4.108) is simply the statement that correlations are isotropic with all D dimensions, and so the long distance correlations depend only upon the Euclidean distance between two points.

We extend the result (4.108) to $T > 0$ by a trick which we will quote without proof: later in Chapter 14 we will note an explicit derivation using the bosonization method. The basic point is that the $\Delta = 0$ continuum theory (4.44), in addition to being scale and Lorentz invariant, is also invariant under conformal transformations of spacetime [247]. Turning on a $T > 0$ is equivalent, in imaginary time, of placing the theory $\mathcal{L}_I$ on a spacetime manifold which is a cylinder of circumference $1/T$. However, it is known that one can conformally map the cylinder to the infinite plane, which allows one to obtain a remarkable and exact relationship between $T = 0$ and $T > 0$ correlators in imaginary time at the critical coupling $\Delta = 0$. This mapping was explicitly obtained in (4.64) where we simply noted it as an interesting property of a fermionic correlator we were able to obtain explicitly for $T > 0$. The implication of this discussion is that the same mapping can also be applied to (4.108), allowing us to obtain the correlators at $T > 0$:

$$C(x, \tau) \sim T^{1/4} \frac{1}{[\sin(\pi T (\tau - ix/c)) \sin(\pi T (\tau + ix/c))]^{1/8}} \qquad \Delta = 0. \tag{4.109}$$

We can obtain an independent confirmation of this result by specializing to the equal-time case again and comparing to our earlier results in Section 4.4; we have from (4.109)

$$C(x, 0) \quad \sim \quad \frac{T^{1/4}}{[\sinh(\pi T |x|/c)]^{1/4}}$$

$$\sim \quad T^{1/4} \exp\left(-\frac{\pi T |x|}{4c}\right) \qquad \text{as } |x| \to \infty. \quad (4.110)$$

Compare this with the precise results for this regime quoted earlier in (4.65), where using the values $F_I(0) = \pi/4$ (from evaluation of (4.67)) and $G_I(0) = 0.858714569\ldots$ we have

$$\lim_{|x|\to\infty} C(x,0) = ZT^{1/4} G_I(0) \exp\left(-\frac{\pi T |x|}{4c}\right) \quad \text{at } \Delta = 0. \quad (4.111)$$

The two results, obtained by very different methods, are in perfect agreement. We can combine (4.111) with (4.109) to determine the prefactor in (4.109), and so obtain our final closed-form result for the universal two-point correlator at $\Delta = 0$:

$$C(x,\tau) = ZT^{1/4} \frac{2^{-1/4} G_I(0)}{[\sin(\pi T(\tau - ix/c)) \sin(\pi T(\tau + ix/c))]^{1/8}}. \quad (4.112)$$

As expected, this result is of the scaling form (4.56), and indeed completely determines the function Φ_I for the case where its last argument is zero. It is the leading result everywhere in the continuum high T region of Fig 4.3. Notice that this result has been obtained in imaginary time. Normally, as we have noted earlier, such results are not terribly useful in understanding the long real-time dynamics at $T > 0$ because the analytic continuation in ill-posed. However, in the present case, we have the *exact* expression, and so the analytic continuation is a useful tool.

Now let us turn to a physical interpretation of the main result (4.112). Consider first the case $T = 0$. By a Fourier transformation of (4.108), and using the normalization constant implied by (4.112), we obtain the dynamic susceptibility

$$\chi(k,\omega) = Z(4\pi)^{3/4} G_I(0) \frac{\Gamma(7/8)}{\Gamma(1/8)} \frac{c}{(c^2 k^2 - (\omega + i\delta)^2)^{7/8}} \quad , \quad T = 0, \Delta = 0 \quad (4.113)$$

with δ a positive infinitesimal. Notice that this function has a *branch cut* in the complex ω plane at $\omega = ck$; this is to be contrasted with the simple pole-like structure which appeared in the quantum paramagnet at $T = 0$ in (4.99). In the present case the appearance of the branch cut at the quantum critical point is a direct consequence of the anomalous dimension of $\hat{\sigma}^z$ in (4.55), which led to the non-integer powers in (4.108) and (4.113). We plot $\text{Im}\chi(k,\omega)$ in Fig 4.8. There are no delta functions in the spectral density like there were in the quantum paramagnet (Fig 4.1), indicating that the $\hat{\sigma}^z$ operator has negligible overlap with
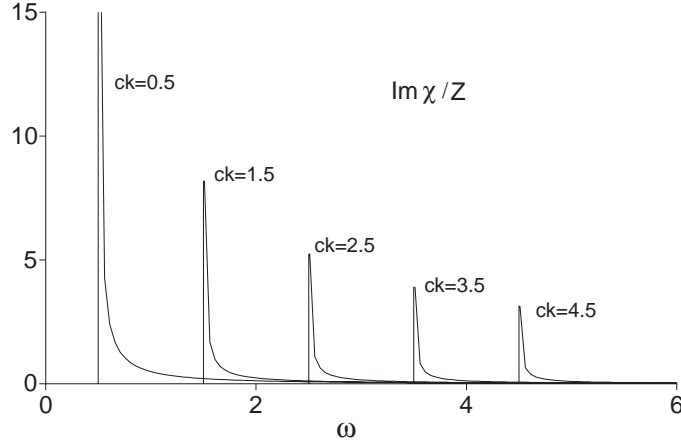
Fig. 4.8. Spectral density, $\text{Im}\chi(k,\omega)/Z$, of H_I at its critical point $g = 1$ ($\Delta = 0$) at $T = 0$, as a function of frequency ω, for a set of values of k.

the single fermion quasiparticle state of Section 4.2. Instead, we have a critical continuum above a branch cut arising from a superposition of states with an arbitrary number of fermionic quasiparticles. However, the presence of sharp thresholds and singularities indicates that there is still perfect phase coherence, as there must be in the ground state. It is also interesting to think about how the $T = 0$ spectral density crosses over from the form in Fig 4.1 characteristic of the quantum paramagnet, to the critical continuum in Fig 4.8. Consider for instance the case $k = 0$. In the quantum paramagnet, we have a quasi-particle delta function at $\omega = \Delta$, a continuum above the three-particle threshold at $\omega = 3\Delta$, another above the five-particle threshold at $\omega = 5\Delta$ and so on. As we approach the critical point with $\Delta \to 0$, all these continua come crashing down in energy and their limiting superposition leads to the critical form shown in Fig 4.8.

Now let us turn to $T > 0$. We Fourier transform (4.112) to obtain $\chi(k,\omega_n)$ at the Matsubara frequencies ω_n and then analytically continue to real frequencies. This gives us the leading result for $\chi(k,\omega)$ in the
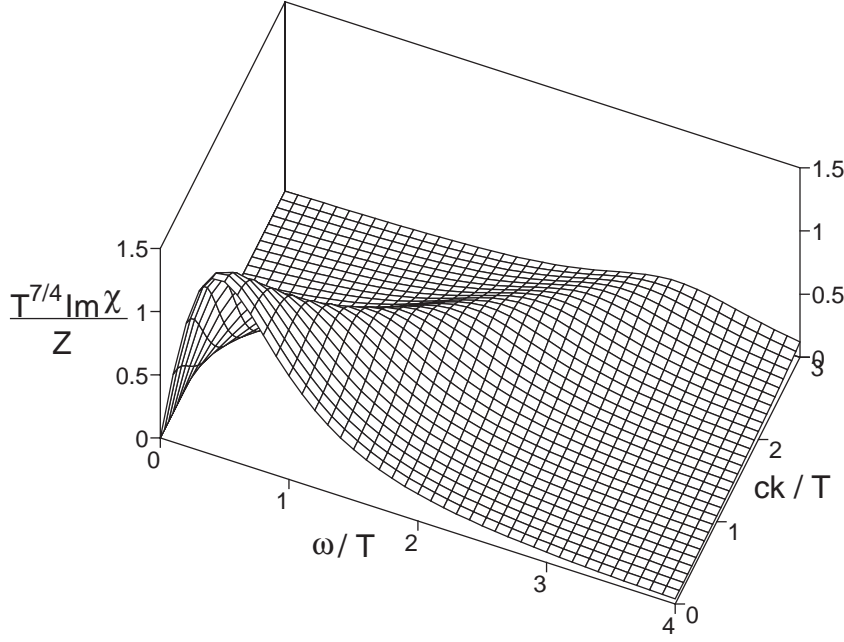
Fig. 4.9. The same observable as in Fig 4.8, $T^{7/4}\mathrm{Im}\chi(k,\omega)/Z$, but for $T \neq 0$. This is the leading result for $\mathrm{Im}\chi$ for $T \gg |\Delta|$, *i.e.*, in the high T region of Fig 4.3. All quantities are scaled appropriately with powers of T, and the absolute numerical values of both axes are meaningful.

high T region

$$\chi(k,\omega) = \frac{Zc}{T^{7/4}}\frac{G_I(0)}{4\pi}\frac{\Gamma(7/8)}{\Gamma(1/8)}\frac{\Gamma\left(\dfrac{1}{16} - i\dfrac{\omega + ck}{4\pi T}\right)\Gamma\left(\dfrac{1}{16} - i\dfrac{\omega - ck}{4\pi T}\right)}{\Gamma\left(\dfrac{15}{16} - i\dfrac{\omega + ck}{4\pi T}\right)\Gamma\left(\dfrac{15}{16} - i\dfrac{\omega - ck}{4\pi T}\right)}.$$

$$(4.114)$$

We show a plot of $\mathrm{Im}\chi$ in Fig 4.9. This result is the finite T version of Fig 4.8. Notice that the sharp features of Fig 4.8 have been smoothed out on the scale T, and there is non-zero absorption at all frequencies. For $\omega, k \gg T$ there is a well-defined 'reactive' peak in $\mathrm{Im}\chi$ at $\omega \approx ck$ (Fig 4.9) rather like the $T = 0$ critical behavior of Fig 4.8. However the low frequency dynamics is quite different, and for $\omega, k \ll T$ we cross-over to the *quantum relaxational* regime [97]. This is made clear by an examination of the quantity $\mathrm{Im}\chi(k,\omega)/\omega$ as a function of ω/T and ck/T; notice from (4.9) that for $\omega \ll T$ this quantity is proportional
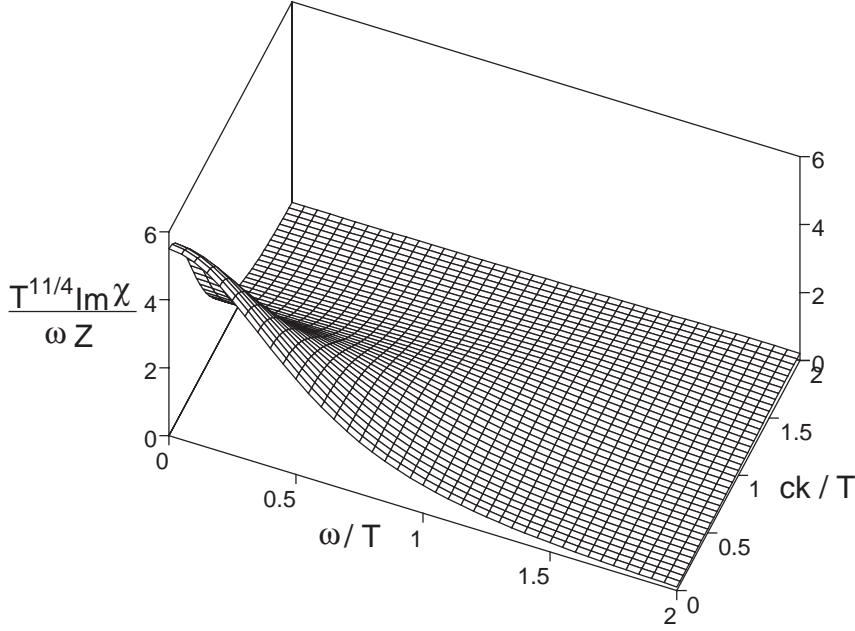
Fig. 4.10. Plot of the spectral density $T^{11/4}\mathrm{Im}\chi(k,\omega)/\omega Z$ as a function of ω/T and ck/T. Note that this is simply the quantity in Fig 4.9 divided by ω. The reactive peaks at $\omega \approx ck$ in Fig 4.9 are essentially invisible, and the plot is dominated by a large relaxational peak at zero wavevector and frequency.

to the dynamic structure factor, $S(k,\omega)$ (defined in (4.4)), which is in turn proportional to the neutron scattering cross section. (We prefer to work with $\mathrm{Im}\chi(k,\omega)/\omega$ rather than $S(k,\omega)$ because the former is an even function of the ω , while the latter is not; in any case, the two are practically indistinguishable for low frequencies.) We show a plot of $\mathrm{Im}\chi(k,\omega)/\omega$ in Fig 4.10 (notice that Fig 4.10 is simply Fig 4.9 divided by ω). Now the reactive peaks at $\omega \sim ck$ are just about invisible, and the spectral density is dominated by a large relaxational peak at zero frequency. We can understand the structure of Fig 4.10 by expanding the inverse of (4.114) in powers of k and ω; this expansion has the form

$$\chi(k,\omega) = \frac{\chi(0,0)}{1 - i(\omega/\omega_1) + k^2\widetilde{\xi}^2 - (\omega/\omega_2)^2}, \qquad (4.115)$$

where recall from (4.114) that $\chi(0,0) \sim T^{-7/4}$, and $\omega_{1,2}$ and $\widetilde{\xi}$ are parameters characterizing the expansion. For k not too large, the ω dependence in (4.115) is simply the response of a strongly damped har-
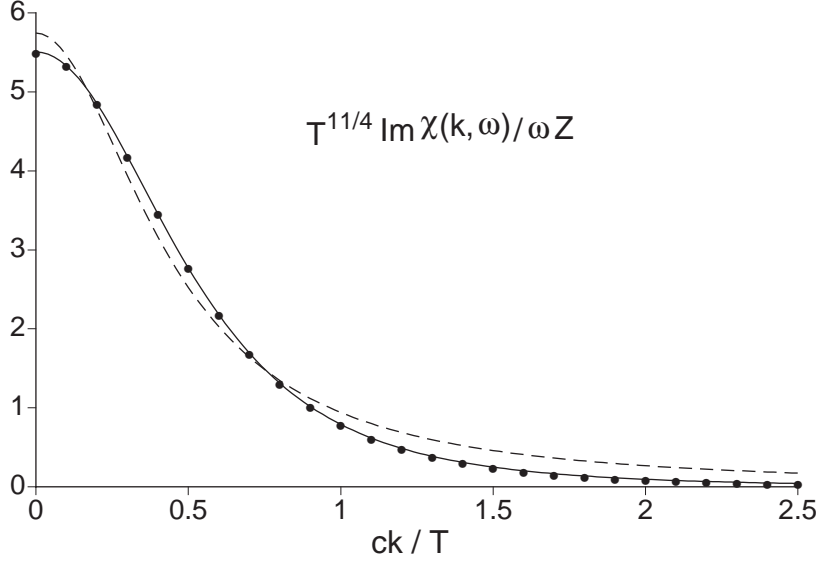
Fig. 4.11. Comparison of the predictions of (4.114) (dots) and (4.115) (solid line) for $\mathrm{Im}\chi(k,\omega)/\omega$ at $\omega = 0$ as a function of ck/T. The best fit parameters in (4.116) were used. The function (4.115) yields the *square* of a Lorentzian as a function of k; a best fit by just a Lorentzian is also shown (dashed line), and is much poorer.

monic oscillator: this is the reason we have identified the low frequency dynamics as "relaxational". The function in (4.115) provides an excellent description of the spectral response in Fig 4.10. We determined the best fit values of the parameters $\omega_{1,2}$ and $\widetilde{\xi}$ by minimizing the mean square difference between the values of $\mathrm{Im}\chi(k,\omega)/\omega$ given by (4.115) and (4.114) over the range $0 < \omega < 2T$ and $0 < ck < 2T$ and obtained

$$
\begin{aligned}
\omega_1 &= 0.396\,T \\
\omega_2 &= 0.795\,T \\
\widetilde{\xi} &= 1.280\,c/T.
\end{aligned}
\tag{4.116}
$$

The quality of the fit is shown in Figs 4.11 and 4.12 where we compare the predictions of (4.114) and (4.115) for $\mathrm{Im}\chi(k,\omega)/\omega$ at $\omega = 0$ as a function of ck/T, and at $ck/T = 0, 1.5$ as a function of ω/T respectively.

For $k = 0$ ($\omega = 0$) there is a large overdamped peak at $\omega = 0$ ($k = 0$), but a weak reactive peak at $\omega \sim ck$ does make an appearance at larger wavevectors or frequencies.
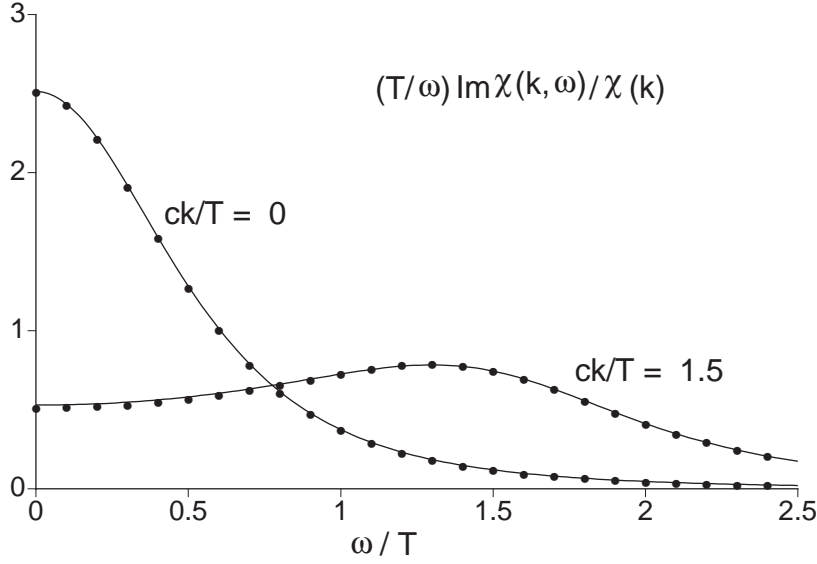
Fig. 4.12. Comparison of the predictions of (4.114) (dots) and (4.115) (solid line) for $(T/\omega)\text{Im}\chi(k,\omega)/\chi(k)$ as a function of ω/T at $ck/T = 0, 1.5$. The dispersion relation (4.10) implies that the area under both curves for $-\infty < \omega < \infty$ is exactly π. Notice also the similarity of the quantity plotted to the scaling function considered in (4.95) and Fig 4.6; however in the present case $S(k) \neq T\chi(k)$ as the dynamics is not effectively classical—in particular $S(0) = 1.058 T\chi(0)$. The overall magnitude of $\text{Im}\chi$ at $ck/T = 1.5$ is smaller than this figure would suggest, as $\chi(k = 1.5)/\chi(0) = 0.216$.

For an alternative, and more precise, characterization of the relaxational dynamics we can introduce the relaxation rate Γ_R defined by

$$\Gamma_R^{-1} \equiv i\chi(0) \left.\frac{\partial \chi^{-1}(0,\omega)}{\partial \omega}\right|_{\omega=0} = \frac{S(0,0)}{2T\chi(0)}, \qquad (4.117)$$

where the second relation follows from (4.9). We have chosen this definition because for the suggestive functional form (4.115), $\Gamma_R = \omega_1$, the frequency characterizing the damping. However, using (4.114) we determine:

$$\begin{aligned}
\Gamma_R &= \left(2\tan\frac{\pi}{16}\right)\frac{k_B T}{\hbar} \\
&\approx 0.397825\frac{k_B T}{\hbar}, \qquad (4.118)
\end{aligned}$$

where we have inserted physical units to emphasize the universality of

the result. Note that the value of Γ_R is quite close to the value of ω_1 which was determined by the least square minimization discussed above.

The rate Γ_R is a satisfactory measure of how thermal effects have rounded out the sharp, $T = 0$ phase-coherent structure in the dynamic susceptibility in Fig 4.8: we can therefore identify it with the phase coherence rate $1/\tau_\varphi$. At the scale of the characteristic rate Γ_R, the dynamics of the system involves intrinsic quantum effects which cannot be neglected. Description by an effective classical model (as was appropriate in both the low T regions of Fig 4.3) would require that $\Gamma_R \ll k_B T/\hbar$, which is thus not satisfied in the high T region of Fig 4.3 under discussion here. As noted earlier, the reason for the quantum nature of the relaxation is simply that the mean spacing between the thermally excited particles (considered either as the domain walls of the magnetically ordered state or the flipped spins of the quantum paramagnet) is of order their de Broglie wavelength, and so the classical thermal and quantum fluctuations must be treated on an equal footing. It is these quantum effects which lead to the intricate universal numerical relation between the relaxational and reactive parameters determining the response in (4.114) and (4.115).

4.5.4 Summary

Our detailed study of the $T > 0$ crossovers in the vicinity of the quantum-critical point of the Ising chain has led to a rich variety of different physical regimes, and so it is useful to summarize their main properties. Such a summary is contained in our earlier Fig 4.3 and in Figs 4.13 and 4.14.

At short enough times or distances in all three regions of Fig 4.3, the systems displays critical fluctuations characterized by the dynamic susceptibility (4.113). The regions are distinguished by their behaviors at the low frequencies and momenta. In both the low T regimes of Fig 4.3 (on the magnetically ordered and quantum paramagnetic sides), the long time dynamics is relaxational and is described by effective models of quasi-classical particles; however, the physical interpretation of the particles is quite different between the two low T regimes—they are domain walls on the magnetically ordered side, and flipped spins in the quantum paramagnet. The relaxation time, or equivalently, the phase coherence time, is of order $(\hbar/k_B T)e^{(\text{energy gap})/k_B T}$, and is therefore much longer than $\hbar/k_B T$; it is this condition which ensures that quantum thermal effects act at very different scales, and allows for a semiclassical description of the low frequency dynamics. In contrast, the dynamics in the

Low T (magnetically ordered)

Continuum high T

Low T (quantum paramagnetic)
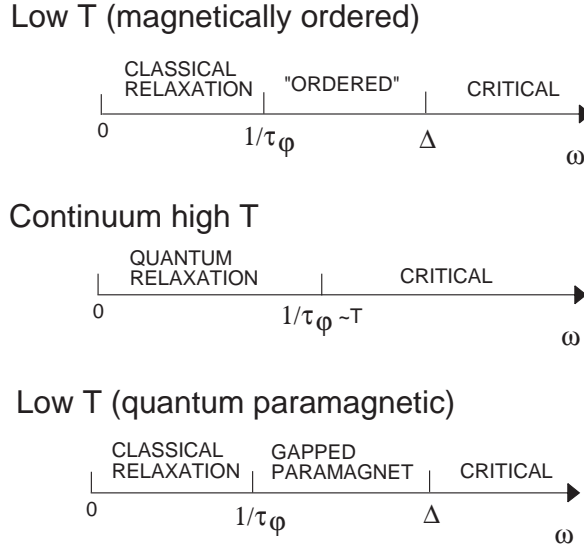
Fig. 4.13. Crossovers as a function of frequency for the Ising model in the different regimes of Fig 4.3. The high frequency critical fluctuations are present in all regimes and are characterized by (4.113). The two classical relaxational regimes are described by multiple collisions of thermally excited quasi-classical particles; the physical correlations in these two regimes are quite different but are described by the same relaxation function R in (4.86). The quantum relaxation is described by (4.114) and the relaxation rate (4.117). The "ordered" regime is in quotes, because there is no long-range order, and the system only appears ordered between spatial scales c/Δ and $c\tau_\varphi$. In the low T regions $1/\tau_\varphi \sim T e^{-|\Delta|/T}$.

high T region is also relaxational, but involves quantum effects in an essential way, as was described above. In this region, the spacing between the thermally excited particles is of order their de-Broglie wavelength, and the phase relaxation time is of order $\hbar/k_B T$.

The ease with which our expressions for the phase coherence times τ_φ in (4.88) and (4.118) have been obtained belies their remarkable nature. Notice that we have worked in a closed Hamiltonian system, evolving unitarily in time with the operator $e^{-iH_I t/\hbar}$, from an initial density matrix given by the Gibbs ensemble at a temperature T. Yet, we have obtained relaxational behavior at low frequencies, and determined *exact* values for a dissipation constant. In contrast, in the theory of dynamics near classical critical points [228], a statistical relaxation dynamics is postulated in a rather *ad hoc* manner, and the relaxational constants are

Fig. 4.14. Values of the correlation length, ξ (defined from the exponential decay of the equal-time correlations of the order parameter), and the phase coherence time, τ_φ (defined as discussed in the respective sections), in the different regimes of Fig 4.3. The two low T regimes have an interpretation in terms of quasi-classical particles, but the physical interpretation of the two particles are very different, as indicated.

	Low T (magnetically ordered). Quasi-classical particles —domain walls	Continuum high T (quantum critical).	Low T (quantum paramagnetic). Quasi-classical particles —flipped spins
ξ	$\left(\dfrac{\pi c^2}{2\Delta T}\right)^{1/2} e^{\Delta/T}$	$\dfrac{4c}{\pi T}$	$\dfrac{c}{\|\Delta\|}$
τ_φ	$\dfrac{\pi}{2T} e^{\Delta/T}$	$\dfrac{\cot(\pi/16)}{2T}$	$\dfrac{\pi}{2T} e^{\|\Delta\|/T}$

treated as phenomenological parameters to be determined by comparison with experiments. Our subsequent discussions of more complicated models in higher dimensions will also only consider deterministic unitary evolution from an initial density matrix, but we will only be able to obtain approximate values of dissipation constants.

It is also worth contrasting the small k, ω behavior of the dynamic structure factor, $S(k, \omega)$ in the three regimes of Fig 4.3. At low T on the quantum paramagnetic side, there is a sharp quasi-particle peak at $\omega \sim |\Delta|$ whose frequency width is exponentially small ($\sim T e^{-|\Delta|/T}$); this peak is only present for the case of energy absorption, $\omega > 0$, and has exponentially small weight on the energy emission side, $\omega < 0$. In the high T regime, the dominant peak of $S(k, \omega)$ moves towards $\omega = 0$ and has a width of order T. Finally, in the low T regime on the magnetically ordered side, the peak in $S(k, \omega)$ is at $\omega, k = 0$, but is now symmetric in ω, and has an exponentially large amplitude ($\sim e^{2\Delta/T}$) and exponentially small widths in frequency ($\sim T e^{-\Delta/T}$) and wavevector ($\sim (c/\sqrt{T\Delta}) e^{-\Delta/T}$).

4.6 Applications and extensions

We conclude this and subsequent chapters by making contact with other experimental or theoretical studies.

Detailed studies of one-dimensional Ising magnets have been carried out on the insulators $CsCoBr_3$ and $CsCoCl_3$. The Co ions form chains of *antiferromagnetically* interacting Ising spins. Their effective Hamiltonian is not the Ising chain in a transverse field, but the dynamics and structure of the domain-wall excitations above the magnetically ordered ground state [518] are essentially identical to our discussion in Section 4.5.1. Neutron scattering studies [536, 357, 183] have examined the temperature induced broadening of the $T = 0$ delta function in (4.23). Some interesting effects in the presence of a longitudinal magnetic field in these systems have been discussed recently [287].

The dynamical results of Section 4.5.3 are of considerable value, as these are the only known exact results for the low frequency response of a system in the continuum high T (or 'quantum critical') regime. We will discuss the $d = 2$ generalization of this regime in Chapters 7 and 8, where we will present approximate calculations which yield closely related dynamical results. Recent neutron scattering experiments by Aeppli *et al.* [2] on the high temperature superconductors have measured spin response functions whose T, k and ω dependencies are well fit by a functional form closely related to (4.115) and (4.116) (including the Lorentzian squared momentum dependence in Fig 4.11), suggesting the proximity of a quantum critical point to a ground state with long-range spin ordering; we will comment further on these experiments in Sections 7.4 and 8.4, after we have discussed the theory in $d = 2$.

5

Quantum rotor models: large N limit

This chapter turns to the models obtained by the quantum-classical mapping $\mathcal{QC}$ on the D-dimensional N-component classical ferromagnets in (3.3) with $N \geq 2$: these are the O(N) quantum rotor models in $d = D - 1$ dimensions, originally written down in (1.23).

The quantum Ising model studied previously had a discrete Z_2 symmetry. An important new ingredient in the rotor models will be the presence of a continuous symmetry: the physics is invariant under a uniform, global O(N) transformation on the orientation of the rotors, which is broken in the magnetically ordered state. We will introduce the important concept of the *spin stiffness*, which characterizes the rigidity of the ordered state, and determines the dispersion spectrum of the low energy 'spin-wave' excitations. Apart from this, much of the technology and the physical ideas introduced earlier for $d = 1$ Ising chain will generalize straightforwardly, although we will no longer be able to obtain exact results for crossover functions. The characterization of the physics in terms of three regions separated by smooth crossovers, the high T and the two low T regions on either side of the quantum critical point, will continue to be extremely useful, and will again be the basis of our discussion. Because we will consider models in spatial dimensions $d > 1$, it will be possible to have a thermodynamic phase transition at a non-zero temperature. We shall be particularly interested in the interplay between the critical singularities of the finite temperature transition and those of the quantum critical point.

The analysis will be carried out using a simple and important technical tool: the large N expansion [473, 316, 317, 64]. This chapter will largely confine itself to the results obtained at $N = \infty$. The results so obtained will give an adequate description of gross features of the phase diagram and some static observables, but will be quite inadequate for

dynamical properties at non-zero temperatures. The latter problems will be addressed in subsequent chapters.

We will examine here a slight extension of the quantum rotor model (1.23):

$$H_R = \frac{J\widetilde{g}}{2} \sum_i \hat{\mathbf{L}}_i^2 - J \sum_{\langle ij \rangle} \hat{\mathbf{n}}_i \cdot \hat{\mathbf{n}}_j - \mathbf{H} \cdot \sum_i \hat{\mathbf{L}}_i \qquad (5.1)$$

Recall that the N-component vector operators $\hat{\mathbf{n}}_i$, with $N \geq 2$, are of unit length, $\hat{\mathbf{n}}_i^2 = 1$, and represent the orientation of the rotors on the surface of a sphere in N-dimensional rotor space, and the operators $\hat{\mathbf{L}}_i$ are the $N(N-1)/2$ components of the angular momentum. We will phrase our physical discussion using the physically important case $N = 3$, in which case these operators satisfy the commutation relations (1.19) on each site (the operators on different sites commute); the generalization to other values of N is immediate but will not be discussed explicitly for simplicity. The form (5.1) for H_R differs from that in (1.23) by a field $\mathbf{H}$ which couples to the total angular momentum; this field should not be confused with the field $\widetilde{\mathbf{h}}$ in (2.69) which coupled to the rotor orientation $\mathbf{n}$. As we will see later, the field $\mathbf{H}$ does not have a familiar analog upon inverting the mapping to (3.3). It is however an important perturbation of the quantum rotor model which arises in many experimental applications. The total angular momentum is conserved in zero field as it commutes with H_R at $\mathbf{H} = 0$, and we will see that this has important implications for its scaling properties.

The study of the quantum rotor model H_R in (5.1) will occupy a substantial portion of Part 2 of this book. The motivation for this is primarily theoretical, but important experimental connections also exist. These will be discussed shortly in Section 5.1.1 below, but complete discussions are postponed to Chapters 10 and 13. We will also discuss contact with specific experiments in the concluding portion of chapters in Part 2.

As we already noted in Section 1.4.2, there is a strong analogy between the rotor Hamiltonian H_R in (5.1) and the Ising Hamiltonian H_I in (4.1). We will be looking at the transition between a magnetically ordered state with $\langle \hat{\mathbf{n}} \rangle \neq 0$ and O(N) symmetry broken, and a quantum paramagnet in which equal-time correlations of $\mathbf{n}$ are short ranged. As in the Ising model, it is the exchange term, proportional to J, that favors the ordered state, while the 'kinetic energy', proportional to $J\widetilde{g}$ leads to quantum fluctuations in the orientation of the order parameter and eventually to loss of long-range order. The similarity between the two models will

also be apparent in the strong (large $\widetilde{g}$) and weak coupling (small $\widetilde{g}$) analyses in the Section 5.1. We do not have the benefit of an exact analysis as was performed for the Ising chain, but will instead study the large N expansion in subsequent sections: the expansion will be setup in Section 5.2, followed by descriptions of the $N = \infty$ solution for $T = 0$ and $T > 0$ in Sections 5.3 and 5.4 respectively.

Most of our results will be expressed in terms of the dynamic susceptibility $\chi_{\alpha\beta}(\vec{k}, \omega)$ of the order parameter $\mathbf{n}$. As in (4.7) this is defined most conveniently in imaginary time

$$
\begin{aligned}
C_{\alpha\beta}(x, \tau) &\equiv \langle n_\alpha(\vec{x}, \tau) n_\beta(0, 0) \rangle \\
\chi_{\alpha\beta}(\vec{k}, \omega_n) &\equiv \int_0^{1/T} \int d^d x \, C_{\alpha\beta}(x, \tau) e^{-i(\vec{k}\cdot\vec{x} - \omega_n \tau)}
\end{aligned}
\tag{5.2}
$$

where $\mathbf{n}(x_i, i\tau)$ is the imaginary time representation of the quantum operator $\hat{\mathbf{n}}_i$. The dynamic structure factor $S_{\alpha\beta}(\vec{k}, \omega)$ is then defined as in (4.4) and related to $\chi_{\alpha\beta}$ by a relationship analogous to (4.9). For the most part, we will compute χ in zero field $H = 0$. Our analysis of the consequences of $\mathbf{H}$ will be restricted here to determining its linear response susceptibility: for reasons that will become evident when we consider the relationship between quantum rotors and quantum antiferromagnets, we will call this susceptibility the *uniform susceptibility*, χ_u. It is defined by the small H expansion of the free energy density $\mathcal{F} = -T \ln \mathcal{Z}$

$$
\mathcal{F}(\mathbf{H}) = \mathcal{F}(\mathbf{H} = 0) - \frac{1}{2}\chi_{u\alpha\beta}H_\alpha H_\beta + \dots
\tag{5.3}
$$

5.1 Limiting cases

The pictures which emerge in the following two perturbative analyses are expected to hold on either side of a quantum critical point at $\widetilde{g} = \widetilde{g}_c$, which separates the ordered and the quantum paramagnetic phases. We will see later that $\widetilde{g}_c = 0$ in $d = 1$, but $\widetilde{g}_c > 0$ for $d > 1$.

5.1.1 Strong coupling $\widetilde{g} \gg 1$

The strong coupling expansion was discussed in Ref. [208], and briefly noted in Section 1.4.2. At $\widetilde{g} = \infty$, the exchange term in H_R can be neglected, and the Hamiltonian decouples into independent sites, and can be diagonalized exactly. The eigenstates on each site are the eigenstates

of $\mathbf{L}^2$; for $N = 3$ these are the states of (1.22) and (2.71)

$$|\ell, m\rangle_i \quad \ell = 0, 1, 2, \ldots, \quad -\ell \leq m \leq \ell \tag{5.4}$$

and have eigenenergy $J\widetilde{g}\ell(\ell+1)/2$. The ground state of H_R in the large $\widetilde{g}$ limit consists of the quantum paramagnetic state with $\ell = 0$ on every site:

$$|0\rangle = \prod_i |\ell = 0, m = 0\rangle_i \tag{5.5}$$

Compare this with strong coupling ground state (1.7) of the Ising model. Indeed, the remainder of the strong coupling analysis of Section 4.1 can borrowed here for the rotor model, and we can therefore be quite brief. The lowest excited state is a 'particle' in which a single site has $\ell = 1$, and this excitation hops from site to site. An important difference from the Ising model is that this particle is three-fold degenerate at $\mathbf{H} = 0$, corresponding to the three allowed values $m = -1, 0, 1$. The single particle states are labeled by a momentum k and an azimuthal angular momentum m, and have energy

$$\varepsilon_{\vec{k}, m} = J\widetilde{g} \left(1 - (2/3\widetilde{g}) \sum_\mu \cos(k_\mu a) + \mathcal{O}(1/\widetilde{g}^2) \right) - Hm \tag{5.6}$$

for a field $\mathbf{H}$ oriented along the angular momentum quantization direction; the sum over μ extends over the d spatial directions. This result is the analog of (4.14). The dynamic susceptibility, χ, has a quasiparticle pole at the energy of this particle, and odd particle continua above the three particle threshold.

5.1.1.1 Mapping to double layer antiferromagnets

The present strong coupling expansion allows us to expose a simple and important connection between $O(3)$ quantum rotor models and a certain class of 'double layer' antiferromagnets. Actually the connection between rotor models and antiferromagnets is far more general than the present discussion may suggest, as we will see later in Chapter 13. However, this discussion should enable the reader to gain an intuitive feeling for the physical interpretation of the degrees of freedom of the rotor model.

Consider a system with two layers of 'Heisenberg spins' $\mathbf{S}_{1i}$ and $\mathbf{S}_{2i}$, where i is a site index within each layer, described by the Hamiltonian

$$H_d = K \sum_i \hat{\mathbf{S}}_{1i} \cdot \hat{\mathbf{S}}_{2i} + J \sum_{<ij>} \left(\hat{\mathbf{S}}_{1i} \cdot \hat{\mathbf{S}}_{1j} + \hat{\mathbf{S}}_{2i} \cdot \hat{\mathbf{S}}_{2j} \right). \tag{5.7}$$

The $\hat{\mathbf{S}}_{ni}$ ($n = 1, 2$ the layer index) are spin operators usually represent-
ing the total spin of a set of electrons in some localized atomic states.
On each site, the spins $\hat{\mathbf{S}}_{ni}$ obey the angular momentum commutation
relations

$$\left[\hat{S}_\alpha, \hat{S}_\beta \right] = i\epsilon_{\alpha\beta\gamma} \hat{S}_\gamma \tag{5.8}$$

(the site index has been dropped above), while spin operators on different
sites commute. These commutation relations are the same as those of the
$\hat{\mathbf{L}}$ operators in (1.19). However there is one crucial difference between
Hilbert space of states on which the quantum rotors and Heisenberg
spins act. For the rotor models we allowed states with arbitrary total
angular momentum ℓ on each site, as in (2.71): so there were an infinite
number of states on each site. For the present Heisenberg spins, however,
we will only allow states with total spin S on each site, and will permit
S to be integer or half-integer. Thus there are precisely $2S + 1$ states on
each site

$$|S, m\rangle \quad \text{with } m = -S \ldots S, \tag{5.9}$$

and the operator identity

$$\hat{\mathbf{S}}_{ni}^2 = S(S + 1) \tag{5.10}$$

holds for each i and layer n. Experimental realizations of the double-
layer model H_d include the spin-ladder compounds in $d = 1$ [34, 114]
and double-layer compounds in the family of the high temperature su-
perconductors in $d = 2$ [493, 494, 329, 342, 443, 444, 136].

Let us examine the properties of H_d in the limit $K \gg J$. As a first
approximation, we can neglect the J couplings entirely, and then H_d
splits into decoupled pairs of sites each with a strong antiferromagnetic
coupling K between two spins. The Hamiltonian for each pair can be
diagonalized by noting that $\mathbf{S}_{1i}$ and $\mathbf{S}_{2i}$ couple into states with total
angular momentum $0 \leq \ell \leq 2S$, and so we obtain the eigenenergies

$$(K/2)(\ell(\ell + 1) - 2S(S + 1)) \qquad \text{degeneracy } 2\ell + 1. \tag{5.11}$$

Note that these energies and degeneracies are in one-to-one correspon-
dence with those of a single quantum rotor in (5.4) and (2.71), apart
from the difference that the upper restriction on ℓ being smaller than
$2S$ is absent in the rotor model case. If one is interested primarily in
low energy properties, then it appears reasonable to represent each pair
of spins by a quantum rotor.

We have seen that the $K/J \to \infty$ limit of H_d closely resembles the

$\widetilde{g} \to \infty$ limit of H_R. To first order in $\widetilde{g}$ we saw above that the term proportional to J in H_R enabled hopping motion of the triplet excitation from one site to the next. However a simple computation shows that this is also the primary consequence of the J term in H_d. So we may conclude that the low energy properties of the two models are closely related for large K/J and $\widetilde{g}$. Somewhat different considerations in Chapter 13 will show that the correspondence also applies to the quantum critical point to the magnetically ordered phase.

The main lesson of the above analysis is that the O(3) quantum rotor model represents the low energy properties of quantum antiferromagnets of Heisenberg spins, with each rotor being an effective representation of a *pair* of antiferromagnetically coupled spins. The strong coupling spectra clearly indicate the operator correspondence $\hat{\mathbf{L}}_i = \hat{\mathbf{S}}_{1i} + \hat{\mathbf{S}}_{2i}$, and so the rotor angular momentum represents the total angular momentum of the underlying spin system. Examination of matrix elements in the large S limit shows that $\hat{\mathbf{n}}_i \propto \hat{\mathbf{S}}_{1i} - \hat{\mathbf{S}}_{2i}$: the rotor co-ordinate $\hat{\mathbf{n}}_i$ is the antiferromagnetic order parameter of the spin system. Magnetically ordered states of the rotor model with $\langle \hat{\mathbf{n}}_i \rangle \neq 0$, which we will encounter below, are therefore spin states with long range antiferromagnetic order, and have a vanishing total ferromagnetic moment. Quantum Heisenberg spin systems with a net ferromagnetic moment are *not* modeled by the quantum rotor model (5.1)–these will be studied in Section 13.2 by a different approach.

5.1.2 Weak coupling, $\widetilde{g} \ll 1$

At $\widetilde{g} = 0$, the ground state breaks O(N) symmetry, and all the $\hat{\mathbf{n}}_i$ vectors orient themselves in a common, but arbitrary direction. Excitations above this state consist of 'spin waves' which can have an arbitrarily low energy at $H = 0$, *i.e.,* they are 'gapless'. This is a crucial difference from the Ising model, in which there was an energy gap above the ground state. The presence of gapless spin excitations is a direct consequence of the continuous O(N) symmetry of H_R: we can make very slow deformations in the orientation of $\langle \hat{\mathbf{n}} \rangle$, and get an orthogonal state whose energy is arbitrarily close to that of the ground state. Explicitly, for $N = 3$, and a ground state polarized along $(0, 0, 1)$ we parameterize

$$\hat{\mathbf{n}}(x, t) = (\pi_1(x, t), \pi_2(x, t), (1 - \pi_1^2 - \pi_2^2)^{1/2}) \qquad (5.12)$$

where $|\pi_1|, |\pi_2| \ll 1$. In this limit, the commutation relations (1.19) become $[\hat{L}_1, \pi_2] = i$ and $[\hat{L}_2, \pi_1] = -i$, *i.e.,* π_1, $\hat{L}_2$ and π_2, $\hat{L}_1$ are

canonically conjugate pairs. We can determine the linearized Heisenberg equations of motion for π_1, π_2 at $\mathbf{H} = 0$:

$$\begin{aligned}
\frac{\partial \pi_1}{\partial t} &= J\widetilde{g}\hat{L}_2 \\
\frac{\partial L_2}{\partial t} &= Ja^2 \nabla^2 \pi_1
\end{aligned} \tag{5.13}$$

and similarly for the pair π_2, L_1 (we have taken the naive continuum limit on a hypercubic lattice here). These equations can be solved to yield two spin-wave normal modes with the dispersion $\varepsilon_k = ck$, where the spin-wave velocity

$$c = Ja\sqrt{\widetilde{g}}. \tag{5.14}$$

These normal modes can be quantized by the usual method for harmonic oscillators, and thereby obtain a wavefunction for the ground state and non-interacting spin-wave excited states. The reader should note the distinction between the *two* modes in the ordered phase with the *three* modes obtained in the quantum paramagnet in the strong coupling expansion above. In the ordered phase, rotations about the axis of $\langle \hat{\mathbf{n}} \rangle$ do not produce a new state, and so there are only two independent rotations about axes orthogonal to $\langle \hat{\mathbf{n}} \rangle$ which lead to gapless spin-wave modes.

The ground state wavefunction of the magnetically ordered state includes quantum zero-point motion of the spin waves about the fully polarized state. One consequence of the zero point motion is that ordered moment on each site is reduced at order $\widetilde{g}$:

$$\begin{aligned}
\langle \hat{n}_3 \rangle &= \left\langle (1 - \pi_1^2 - \pi_2^2)^{1/2} \right\rangle \\
&\approx 1 - (1/2) \left\langle \pi_1^2 + \pi_2^2 \right\rangle \\
&= 1 - \frac{\sqrt{\widetilde{g}}a^{d-1}}{2} \int \frac{d^d k}{(2\pi)^d} \frac{1}{k}.
\end{aligned} \tag{5.15}$$

In the last step we have evaluated the expectation value in the quantized harmonic oscillator wavefunctions implied by (5.13) by standard means. The integral over momenta k is cutoff at large k by the inverse lattice spacing, but there is no cutoff at small k. We therefore notice a small k divergence in $d = 1$, indicating an instability in the small $\widetilde{g}$ expansion: we will see that small $\widetilde{g}$ prediction of a state with magnetic long range order is never valid in $d = 1$, and the physical picture of the quantum paramagnet introduced by the large $\widetilde{g}$ expansion holds for all $\widetilde{g}$. In contrast, the small $\widetilde{g}$ expansion appears stable for $d > 1$, and we do expect magnetically ordered states to exist. In this case, comparison of

the small and large $\widetilde{g}$ expansions correctly suggests the existence of a quantum phase transition at intermediate $\widetilde{g}$.

The above was an analysis in the linearized, harmonic limit. The non-linearities neglected above lead to non-zero spin-wave scattering amplitudes, which we will show later are quite innocuous at low enough energies in dimensions $d > 1$. Precisely in $d = 1$, spin-wave interactions are very important, and destroy the long-range order of the ground state, as was already apparent from (5.15). For the classical ferromagnet (3.3), which the present model maps to, this corresponds to the absence of long-range order in $D = 2$, and is known as Hohenberg-Mermin-Wagner theorem.

5.2 Continuum theory and large N limit

Both the continuum analysis, and the study of the large N limit are most easily done in the imaginary time path integral. At $\mathbf{H} = 0$, the path integral can be derived by the inverse of the mapping discussed in Section 2.3, and indeed leads to the expression (3.12) already presented. The modification necessary for $\mathbf{H} \neq 0$ can be deduced by a simple trick which relies on the fact that $\mathbf{H}$ couples to the conserved total angular momentum. It is easy to see that the only effect of $\mathbf{H}$ is to cause a uniform Bloch precession of all the rotors, and that this precession can be 'removed' by transforming to a rotating reference frame. Because of a non-zero $\mathbf{H}$ each rotor acquires an additional precession $\delta \hat{n}_\alpha(t) = -\epsilon_{\alpha\beta\gamma} H_\beta \hat{n}_\gamma(t) \delta t$ in a small time δt. Including this extra precession in imaginary time in (3.12) we get the partition function

$$\mathcal{Z} = \mathrm{Tr} \exp\left(-\frac{H_R}{T}\right) \approx \int \mathcal{D}\mathbf{n}(x, \tau) \delta(\mathbf{n}^2 - 1) \exp(-\mathcal{S}_n)$$

$$\mathcal{S}_n = \frac{N}{2cg} \int d^d x \int_0^{1/T} d\tau \left[(\partial_\tau \mathbf{n} - i\mathbf{H} \times \mathbf{n})^2 + c^2 (\nabla_x \mathbf{n})^2 \right].$$

$$(5.16)$$

We have written the coupling to $\mathbf{H}$ in the form special for $N = 3$, but it should be clear that for general N one writes a term that generates rotations of $O(N)$. Notice also the i in the precession term, which therefore contributes a complex phase to the weights in the partition function: as a result the field $\mathbf{H}$ has no analog in classical statistical mechanics problems in D dimensions. We will be satisfied in this chapter, and in Part 2, by simply examining the linear response of the system to a small $\mathbf{H}$, as

specified by the susceptibility χ_u in (5.3). Properties beyond linear response require examining the partition function (5.16) with a non-zero H, including the complex weights: this problem is of a class we shall examine only in Part 3, and we will defer the analysis to Section 13.4. The coupling constant

$$g = N\sqrt{\tilde{g}}a^{d-1} \tag{5.17}$$

has the dimensions of $(\text{length})^{d-1}$, and will be the primary coupling we will change to vary the physical properties of the rotor model.

The above action is valid only at long distances and times, so there is an implicit cutoff above momenta of order $\Lambda \sim 1/a$ and frequencies of order $c\Lambda$. Our main interest here shall be the universal physics at scales much smaller than Λ. The following large N analysis will make it clear that such a universal regime does exist for $d < 3$, but that additional information on cutoff scale physics is necessary for $d \geq 3$. This identifies $d = 3$ as the so-called upper-critical dimension of the model. The large N analysis is especially suited for describing the universal physics in $d < 3$, and we will restrict our attention to these cases here. Properties in dimensions $d \geq 3$ are more easily analyzed by other methods, and will be discussed later.

The framework of the $N = \infty$ solution [112, 62, 223, 466, 390, 440, 96, 97, 86] is quite easy to set up, at least in the phase without long range order in the order parameter $\mathbf{n}$; we will consider the case with long range order later in this chapter. We impose the $\mathbf{n}^2 = 1$ constraint by a Lagrange multiplier, λ. The action (5.16) then becomes at $\mathbf{H} = 0$ (which is assumed throughout the remainder unless explicitly stated otherwise)

$$\mathcal{Z} = \int \mathcal{D}\mathbf{n}(x,\tau)\mathcal{D}\lambda(x,\tau)\exp(-\mathcal{S}_{n1})$$

$$\mathcal{S}_n = \frac{N}{2cg}\int d^dx \int_0^{1/T} d\tau \left[(\partial_\tau \mathbf{n})^2 + c^2\left(\nabla_x \mathbf{n}\right)^2 + i\lambda(\mathbf{n}^2 - 1)\right], \tag{5.18}$$

We rescale the $\mathbf{n}$ field to

$$\widetilde{\mathbf{n}} = \sqrt{N}\mathbf{n}, \tag{5.19}$$

and, as (5.18) is quadratic in the $\widetilde{\mathbf{n}}$ field, it can be integrated out to yield

$$\mathcal{Z} = \int \mathcal{D}\lambda(x,\tau)\exp\left[-\frac{N}{2}\left(\text{Tr}\ln(-c^2\nabla^2 - \partial_\tau^2 + i\lambda)\right.\right.$$

$$-\frac{i}{cg}\int_0^{1/T} d\tau \int d^dx\lambda\bigg)\bigg]. \qquad (5.20)$$

(See Ref [360] for further discussion on the interpretation of the functional determinant above.) The action has a prefactor of N, and the $N = \infty$ limit of the functional integral is therefore given exactly by its saddle point value. We assume that the saddle-point value of λ is space and time independent, and given by $i\lambda = m^2$. The saddle-point equation determining the value of the parameter m^2 is

$$\int^\Lambda \frac{d^dk}{(2\pi)^d}T\sum_{\omega_n}\frac{1}{c^2k^2+\omega_n^2+m^2} = \frac{1}{cg}, \qquad (5.21)$$

where the sum over ω_n extends over the Matsubara frequencies $\omega_n = 2n\pi T$, n integer. It is also not difficult to evaluate the order parameter susceptibility at $N = \infty$ by inserting an appropriate source term in (5.18): as expected the result is given simply by the propagator of the **n** field in (5.18) with λ replaced by its saddle-point value. The result obeys $\chi_{\alpha\beta} = \chi\delta_{\alpha\beta}$ where

$$\chi(k,\omega) = \frac{cg/N}{c^2k^2-(\omega+i\delta)^2+m^2}, \qquad (5.22)$$

is also the propagator of the **n** field. The large N limit of the uniform susceptibility, χ_u, can also be evaluated by first expanding $\mathcal{F}$ in powers of H, and evaluating the resulting 4 and 2 point correlators of **n** at tree level using the propagator in (5.22): this gives

$$\chi_u = 2T\sum_{\omega_n}\int\frac{d^dk}{(2\pi)^d}\frac{c^2k^2+m^2-\omega_n^2}{(c^2k^2+m^2+\omega_n^2)^2} \qquad (5.23)$$

The Eqns (5.21,5.22,5.23) apply only when the system does not have long-range spatial order (at $T = 0$ or $T > 0$), and O(N) symmetry is preserved; they are the central results of the $N = \infty$ theory, and most of the remainder of this chapter will be spent on analyzing their consequences. In spite of their extremely simple structure, these equations contain a great deal of information, and it takes a rather subtle and careful analysis to extract the universal information contained in them [440, 96, 97]. We will begin by characterizing the $T = 0$ ground states, and compare the results to the strong and weak coupling analyses noted earlier. Then we will turn to the finite temperature crossovers.

5.3 Zero temperature

At $T = 0$, we can make use of the relativistic invariance of the action (5.16) to simplify our analysis. The summation over Matsubara frequencies in (5.21) turns into an integral, and after introducing spacetime momentum $p \equiv (k, \omega/c)$, the constraint equation (5.21) becomes

$$\int^{\Lambda} \frac{d^{d+1}p}{(2\pi)^{d+1}} \frac{1}{p^2 + (m/c)^2} = \frac{1}{g} \qquad (5.24)$$

The integral on the left hand side increases monotonically with decreasing m; as $m \to 0$, it diverges as $\ln(1/m)$ in $d = 1$, and has a maximum finite value at $m = 0$ in $d > 1$. It is then clear that it is always possible to find a solution for (5.24) in $d = 1$, and for $d > 1$ there is no solution to (5.24) for $g < g_c$ where

$$\int^{\Lambda} \frac{d^{d+1}p}{(2\pi)^{d+1}} \frac{1}{p^2} = \frac{1}{g_c}. \qquad (5.25)$$

We have chosen the symbol g_c for the boundary point where the solution ceases to exist suggestively following the discussion in Chapter 4: as we will see shortly, the regime where the solution exists describes a quantum paramagnetic ground state, and g_c is the quantum critical point for a transition to the $g < g_c$ magnetically ordered state. In $d = 1$ a solution exists for all g, and so the general d discussion for $g > g_c$ below can be applied to all g in $d = 1$. This indicates that the $d = 1$ ground state is always a quantum paramagnet: this is a large N result and is manifestly incorrect for $N = 1$ as we saw in Chapter 4; it also not true at $N = 2$, but we will see that the large N theory leads to adequate results for all $N \geq 3$ in $d = 1$. For $g > g_c$ there is a unique solution of the saddle-point equation (5.24) describing a quantum paramagnetic ground state: we will study its properties in the following subsection and find that they are quite similar to those of quantum paramagnetic state of the Ising chain. The $d > 1$ critical point at $g = g_c$ will be studied in the next subsection. Determination of the $d > 1$ ground state for $g \leq g_c$ requires a reanalysis of the derivation of the large N saddle equation. This will be done in Section 5.3.3, where we find a state with magnetic long-range order and spontaneous breakdown of the O(N) symmetry.

5.3.1 Quantum paramagnet, $g > g_c$

For $d > 1$, subtract (5.24) from (5.25), and obtain

$$\frac{1}{g_c} - \frac{1}{g} = \int^{\Lambda} \frac{d^{d+1}p}{(2\pi)^{d+1}} \left(\frac{1}{p^2} - \frac{1}{p^2 + (m/c)^2} \right) \tag{5.26}$$

Now notice that for $d < 3$ it is possible to send the upper cut-off Λ to infinity and still obtain a finite result. Thus, provided we measure quantities in terms of deviations from their values at $g = g_c$, we see that observables are insensitive to the nature of the cut-off, *i.e.,* they are universal. For $d \geq 3$ it is necessary to retain the upper cut-off, and observables do have additional Λ dependence: as briefly noted earlier, this identifies $d = 3$ as the upper-critical dimension. The remaining analysis of this chapter will be implicitly restricted to $d < 3$, and we will examine $d \geq 3$ by other, more convenient, methods in subsequent chapters; in the language of the classical model (3.3), this restriction is equivalent to $D < 4$, where $D = 4$ is its upper-critical dimension. For $1 < d < 3$ we can evaluate the integral in (5.26) with an infinite cut-off and obtain

$$\frac{1}{g_c} - \frac{1}{g} = X_{d+1}(m/c)^{d-1}, \tag{5.27}$$

where the constant $X_d \equiv 2\Gamma((4-d)/2)(4\pi)^{-d/2}/(d-2)$; This equation can be easily solved to obtain the required value of m. In $d = 1$, we have $g_c = 0$, and evaluating (5.24) directly, we find for small m, g

$$\frac{1}{2\pi} \ln \left(\frac{c\Lambda}{m} \right) = \frac{1}{g}, \tag{5.28}$$

which also has a simple solution for $m = c\Lambda e^{-2\pi/g}$. Apart from the difference in the expression in the value of m above, the remaining discussion in this subsection will apply equally to $d = 1$ and $d > 1$.

A key step in the analysis of any ground state of a continuum theory, is the determination of an energy scale which characterizes it. In this case, the quantum paramagnet has a gap, Δ_+, given by

$$\Delta_+ \equiv m(T = 0). \tag{5.29}$$

We emphasize that, by definition, the gap Δ_+ is a temperature independent quantity, and equals the temperature dependent value of m only at $T = 0$. The presence of a gap is apparent in the structure of the spectral

density $\text{Im}\chi(k,\omega)$, which from (5.22) is given by

$$\text{Im}\chi(k,\omega) = \mathcal{A}\frac{\pi}{2\sqrt{c^2k^2 + \Delta_+^2}}\left(\delta(\omega - \sqrt{c^2k^2 + \Delta_+^2})\right.$$

$$\left. -\delta(\omega + \sqrt{c^2k^2 + \Delta_+^2})\right) \qquad (5.30)$$

which has weight only at frequencies greater than Δ_+. The spectral weight appears entirely in the form of delta functions which indicate the presence of magnon quasiparticles; the quantity

$$\mathcal{A} = \frac{cg}{N} \qquad (5.31)$$

is the quasi-particle residue. This magnon is obviously the same as the three-fold degenerate particle that appeared earlier in the strong-coupling analysis of the O(3) model in Section 5.1.1. The spectral density (5.30) is also identical in form to the exact result for the quantum paramagnetic phase of the Ising chain obtained by taking the imaginary part of (4.99). The n-particle continua ($n \geq 3$, odd) are absent here in the $N = \infty$ theory, but will appear later when we study fluctuation corrections.

We can also evaluate the uniform susceptibility χ_u by converting the frequency summation in (5.23) to an integral, and then evaluating the frequency integral. This gives the simple result

$$\chi_u = 0. \qquad (5.32)$$

This result could have been anticipated. The ground state is a spin singlet, the lowest excited state is a triplet which is separated by a gap. In a small field $\mathbf{H}$ there is no change in the energy of the singlet, while the one of the triplet states lowers its energy but remains above the singlet for $H < \Delta_+$. The ground state therefore remains unchanged and has vanishing uniform susceptibility.

Also justifying our identification of this phase as a quantum paramagnet, is that equal-time $\mathbf{n}$ correlations decay exponentially in space

$$\frac{1}{N}\langle \mathbf{n}(x,0)\cdot\mathbf{n}(0,0)\rangle = \frac{\mathcal{A}}{c}\int\frac{d^{d+1}p}{(2\pi)^{d+1}}\frac{e^{ip\cdot x}}{p^2 + (\Delta_+/c)^2}$$

$$= \frac{\mathcal{A}}{2c(2\pi)^{d/2}(\Delta_+/c)^{(2-d)/2}}\frac{e^{-x\Delta/c}}{x^{d/2}} \quad (5.33)$$

which identifies Δ/c as the inverse correlation length. Notice again the precise agreement of this result to that for the quantum paramagnetic

phase of the Ising chain in (4.100), where $2cZ\Delta^{1/4}$ played the role of the quasiparticle residue, $\mathcal{A}$.

5.3.2 Critical point, $g = g_c$

This subsection applies only for $1 < d < 3$. There is no critical point in $d = 1$, and there are violations of naive scaling hypotheses for $d \geq 3$.

As g approaches g_c from above, we see from (5.27) that the energy gap, Δ_+, vanishes as

$$\Delta_+ \sim (g - g_c)^{1/(d-1)} \tag{5.34}$$

The critical state at $g = g_c$ turns out to be scale-invariant at scales much longer than Λ^{-1}, as expected by analogy with the Ising model. The coupling g is the parameter which tunes the system away from this scale-invariant point, and as Δ_+ is an energy (inverse time) scale, the definition (4.52), the definition of the exponent ν above it, and the result (5.34) identifies the exponent

$$z\nu = \frac{1}{d-1} \tag{5.35}$$

The equal-time correlations decay as

$$\langle \mathbf{n}(x,0) \cdot \mathbf{n}(0,0) \rangle \quad \sim \quad \int \frac{d^{d+1}p}{(2\pi)^{d+1}} \frac{e^{ikx}}{p^2}$$

$$\sim \quad \frac{1}{x^{d-1}} \tag{5.36}$$

which is a power-law, as expected for a scale-invariant theory; the decay as a function of time has the same exponent, and so

$$z = 1, \tag{5.37}$$

as must be the case for a Lorentz-invariant theory. The application of the scaling transformation on (5.36), also tells us that

$$\dim[\mathbf{n}] = \frac{d-1}{2}. \tag{5.38}$$

This result can also be simply understood by demanding that the term $\int d^d x \int d\tau (\nabla \mathbf{n})^2$ in the action be invariant under the scaling transformation. The value of the exponent z is exact, as it is fixed by Lorentz invariance of the critical theory, but the values of ν and $\dim[\mathbf{n}]$ will have

corrections beyond the $N = \infty$ result, which will be discussed later. In general, it is conventional to parameterize

$$\dim[\mathbf{n}] = \frac{d + z - 2 + \eta}{2}, \qquad (5.39)$$

with η, the "anomalous dimension" of the field, accounting for deviations from the scaling dimension obtained by demanding invariance of the gradient squared term above for general z. Comparing with (5.38) we see that $\eta = 0$ in the $N = \infty$ theory. The exact solution of the Ising chain had $\eta = 1/4$, as that gives $\dim[\hat{\sigma}^z] = 1/8$. A non-zero, positive, value of η will appear upon consideration of fluctuation corrections, and has important physical consequences. In particular, it determines the scaling dimension of the quasiparticle residue $\mathcal{A}$: (5.39) implies that $\dim[\chi(k, \omega)] = -2 + \eta$, and demanding the consistency of this with the expression (5.30), we conclude $\dim[\mathcal{A}] = \eta$. Therefore, as g approaches g_c from above

$$\mathcal{A} \sim (g - g_c)^{\eta \nu}, \qquad (5.40)$$

i.e., in general, the quasiparticle residue vanishes as the system approaches the critical point. Again this scaling is consistent with the Ising model in which $\mathcal{A} = 2Z\Delta^{1/4} \sim (g - g_c)^{1/4}$ (see (4.101)). In the present $N = \infty$ theory, the quasiparticle residue $\mathcal{A}cg/N$ was non-zero all the way up to $g = g_c$, and this is consistent with $N = \infty$ result of $\eta = 0$—there is no dynamic scattering of the quasiparticle excitations at $N = \infty$ but such scattering will appear upon including $1/N$ corrections which will also induce a non-zero η.

If there are no quasiparticles for $\eta \neq 0$, what do the excitations look like ? As in the Ising chain, there is a critical continuum of excitations, whose spectral density is determined by η. Combining the Lorentz invariance of the theory with a simple analysis of scaling dimensions, we see that the dynamic susceptibility must have the form

$$\chi(k, \omega) \sim \frac{1}{(c^2 k^2 - \omega^2)^{1 - \eta/2}}, \qquad (5.41)$$

(compare (4.113)) and its imaginary part looks much like Fig 4.8. The $\eta = 0$ case is of course special, in that the spectral density has a single delta function at $\omega = ck$, and the critical excitations have a particle-like nature: this is clearly an artifact of the $N = \infty$ theory, and is one of its major failings.

We can also use simple scaling arguments to determine the exact scaling dimension of $\mathbf{H}$, and therefore from (5.3) that of χ_u. Notice that

in (5.16) **H** appears intimately coupled with a time derivative: as we discussed earlier, this is related to the fact that the only effect of **H** is to uniformly precess all the rotors, and this precession is not visible in a rotating reference frame. This is an exact property of theory, and therefore the precession angle must be invariant under scaling transformation. As a result the scaling dimension of **H** must be that of inverse time, which implies from (4.52) that

$$\dim[\mathbf{H}] = z, \qquad (5.42)$$

and using (4.54) and (5.3) that

$$\dim[\chi_u] = d - z \qquad (5.43)$$

5.3.3 Magnetically ordered ground state, $g < g_c$

This subsection necessarily applies only for $d > 1$, as there is no ordered state in $d = 1$.

Our analysis so far has shown no meaningful solution of the saddle-point equations in the large N limit for $g < g_c$. The culprit for this shortcoming lies in the step before (5.20), where we indiscriminately integrated out all N components of the **n** field [65]. As we expect a magnetically ordered phase to appear for $g < g_c$, it seems sensible to allow for the possibility that fluctuations of **n** along the direction of the ordered ground state will be different from those orthogonal to it. So we write

$$\mathbf{n} = (\sqrt{N}r_0, \pi_1, \pi_2 \dots \pi_{N-1}), \qquad (5.44)$$

where it is assumed that the order parameter is polarized along the 1 direction. Inserting this and (5.19) into (5.16), imposing the constraint with a Lagrange multiplier λ, and integrating out *only* the $\pi_{1\dots N-1}$ fields, we find

$$\mathcal{Z} = \int \mathcal{D}\lambda \mathcal{D}r_0 \exp\left[-\frac{N-1}{2}\mathrm{Tr}\ln(-c^2\partial_i^2 - \partial_\tau^2 + i\lambda) \right.$$
$$\left. +\frac{iN}{cg}\int_0^{1/T} d\tau \int d^dx\lambda(1 - r_0^2) \right] \qquad (5.45)$$

In the large N limit, we can ignore the difference between $N - 1$ and N, and obtain the saddle point equations with respect to variations in λ *and* r_0. As before, m^2 is taken to be the saddle-point value of $i\lambda$.

The mean value of r_0 will determine the spontaneous magnetization at $N = \infty$, which we denote by N_0; so

$$N_0 = \langle n_1 \rangle = \sqrt{N} r_0. \tag{5.46}$$

The saddle point equations are

$$N_0^2 + g \int^{\Lambda} \frac{d^{d+1}p}{(2\pi)^{d+1}} \frac{1}{p^2 + (m/c)^2} \;=\; 1$$
$$m^2 N_0 \;=\; 0 \tag{5.47}$$

where we have set $T = 0$. One solution of the second equation is $N_0 = 0$, but then the first equation for m becomes identical to the one considered earlier, and is known to fail for $g < g_c$. So we choose the other solution, where

$$m \;=\; 0$$
$$N_0^2 \;=\; 1 - g \int^{\Lambda} \frac{d^{d+1}p}{(2\pi)^{d+1}} \frac{1}{p^2}$$
$$\;=\; 1 - \frac{g}{g_c} \tag{5.48}$$

It is satisfying to find that N_0 is non-zero precisely for $g < g_c$, reinforcing our belief in the correctness of our procedure in finding the saddle point. Notice that N_0 vanishes as $(g_c - g)^{1/2}$ as g approaches g_c. It is conventional to define the critical exponent β by the dependence $N_0 \sim (g_c - g)^{\beta}$, and we therefore have $\beta = 1/2$ in the present $N = \infty$ theory. More generally, the scaling dimension of N_0 must be the same as the scaling dimension of $\mathbf{n}$, and we therefore have from (5.39) that

$$2\beta = (d + z - 2 + \eta)\nu, \tag{5.49}$$

an exponent relation that is satisfied by the $N = \infty$ theory.

The above approach also determines the two-point correlator of spin components orthogonal to the axis of the spontaneous magnetization. We denote the corresponding susceptibility by $\chi_\perp(k, \omega)$, and it is the Fourier transform of the n_2, n_2 correlator (say); we have at $N = \infty$

$$\chi_\perp(k, \omega) = \frac{cg/N}{c^2 k^2 - (\omega + i\delta)^2} \tag{5.50}$$

Notice that there is a quasiparticle pole at $\omega = ck$, and the energy of this excitation vanishes as $k \to 0$. These are the spin-wave excitations discussed earlier in the weak-coupling analysis. These spin waves survive

fluctuation corrections as $k \to 0$, although the nature of the spectral density becomes different at larger k, as we will discuss shortly.

As was the case on the disordered side, we need an energy scale to characterize the ordered ground state, and its distance from the critical point. A convenient choice is to build an energy out of the *spin stiffness*, ρ_s. This quantity is a measure of how easy it is to make smooth changes in the order parameter orientation. Imagine, if instead of the uniform condensate $\langle \mathbf{n} \rangle = N_0(1, 0, 0, 0, \ldots)$ the system would choose on its own, we constrain the magnetization to precess smoothly in the $1 - 2$ plane (say)

$$\langle \mathbf{n} \rangle = N_0(\cos \varphi(x), \sin \varphi(x), 0, 0, \ldots) \tag{5.51}$$

where $\varphi(x)$ is a very slowly varying function of x. A constant $\varphi(x)$ cannot change the ground state energy of the constrained system, so the change in energy can depend only $\nabla \varphi(x)$. By inversion symmetry in x, the change cannot be linear in $\nabla \varphi$, and so the lowest order term in the change in energy has to be of the form

$$\delta E = \frac{\rho_s}{2} \int d^d x (\nabla \varphi)^2 \tag{5.52}$$

The coefficient appearing in the expression above is defined to be the spin stiffness ρ_s. We emphasize that this stiffness is defined by changes in the ground state energy, and will always be assumed to be a $T = 0$ quantity, unless otherwise stated. The dimension of the stiffness under the scaling transformation of the $g = g_c$ point can now be easily deduced. The angle φ is a variable with period 2π, and therefore has both engineering and scaling dimension 0. By definition we have $\dim[\delta E] = z$, and therefore

$$\dim[\rho_s] = d + z - 2 \tag{5.53}$$

We can now construct the energy scale, which we denote Δ_-, which characterizes the ground state for $g < g_c$. The requirement is that Δ_- should have scaling dimension z, and physical units of $(\text{time})^{-1}$. Such an object has to made out of powers of ρ_s, whose scaling dimension is above, and whose physical units are $(\text{length})^{2-d}(\text{time})^{-1}$, and the velocity c, whose scaling dimension is 0 and physical units $(\text{length})(\text{time})^{-1}$; the unique combination is

$$\Delta_- \equiv (\rho_s/N)^{1/(d-1)} c^{(d-2)/(d-1)}. \tag{5.54}$$

The factor of N has been chosen for future convenience.

Knowledge of the spin stiffness allows us to make an exact statement

on the form of the static transverse susceptibility $\chi_\perp(k,0)$ in the limit $k \to 0$. This susceptibility is the response of the system to a very slowly varying static field, $h(x)$, which couples linearly to the 2 component (say). The system will respond to such an external field by a slowly varying shift in the angular orientation of the order parameter, and the net energy cost will then be

$$\delta E = \int d^d x \left[\frac{\rho_s}{2} (\nabla \varphi)^2 - h N_0 \sin \varphi \right] \tag{5.55}$$

Minimizing the energy cost with respect to variations in φ we get in Fourier space

$$\begin{aligned} \langle n_2(k) \rangle &\approx N_0 \varphi(k) \\ &= \frac{N_0^2}{\rho_s k^2} h(k). \end{aligned} \tag{5.56}$$

This gives us the exact result

$$\lim_{k \to 0} \chi_\perp(k, 0) = \frac{N_0^2}{\rho_s k^2} \tag{5.57}$$

Combining the $N = \infty$ results (5.48,5.50) with (5.57), we have

$$\rho_s = cN \left(\frac{1}{g} - \frac{1}{g_c} \right) \tag{5.58}$$

In general, from (5.53), ρ_s is expected to vanish as $(g_c - g)^{(d-1)\nu}$, and the result (5.58) is consistent with the $N = \infty$ values of the exponents.

We conclude this subsection by remarking on two features of the response functions of the ordered ground state which depend upon having a non-zero η, and are therefore absent in the $N = \infty$ theory. First, from (5.57), we deduce that the residue at the spin-wave pole (for $k \to 0$) is N_0^2/ρ_s; as g approaches g_c, this vanishes as $(g_c - g)^{\eta\nu}$, unlike the result (5.50) in which the spin-wave residue remains non-zero all the way up to g_c. Second, with energy scale Δ_- in hand, we can also define a corresponding length scale ξ_J

$$\xi_J = \frac{c}{\Delta_-}. \tag{5.59}$$

This is known as the Josephson length. The forms (5.57) and (5.50), which are characteristic long-wavelength transverse responses of a phase with spontaneously broken continuous symmetry, remain valid at length scales larger than ξ_J, and times longer than Δ_-^{-1}. At shorter scales, the responses crossover to the isotropic response of the critical points like in (5.41).
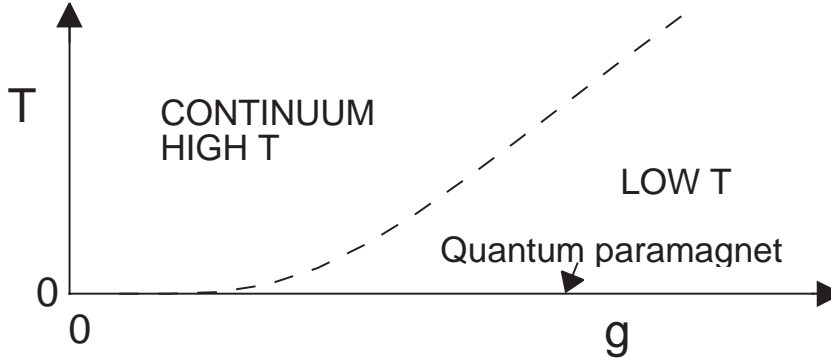
Fig. 5.1. Large N phase diagram for the O(N) rotor model in $d = 1$. This phase diagram applies for all $N \geq 3$. The dashed lines are crossovers. Our interest is in the two universal regions, which are the low and high T limits of the continuum quantum field theory. The crossover boundary is at $T \sim \Delta_+ \sim \exp(-2\pi/g)$.

5.4 Nonzero temperatures

We have shown in the previous section that (for $d > 1$) there are two distinct ground states separated by a quantum critical point at $g = g_c$, and each ground state is characterized by a single energy scale Δ_+ or Δ_- which vanishes as $|g - g_c|^{z\nu}$ near the critical point (in $d = 1$ we only have one phase characterized by Δ_+).

We can combine the insights gained from the solution of the Ising chain in Chapter 4 with some simple physical considerations, and also by partly anticipating some $N = \infty$ results to be discussed below, and sketch the $T > 0$ phase diagrams in Figs 5.1-5.3.

First we show the phase diagram for $d = 1$ in Fig 5.1 [253]. There is only one phase in $d = 1$: a quantum paramagnetic ground state with a gap Δ_+. The energy scale Δ_+ is the only one characterizing the universal physics, and therefore we expect a qualitative change in the nature of the physics at $T \sim \Delta_+ \sim \exp(-2\pi/g)$ (using (5.28)). We identify the region $T < \Delta_+$ as the low temperature limit of the continuum theory, which will be similar to the low T region on the quantum paramagnetic side of the Ising model in Fig 4.3. The region $\Delta_+ < T < J$ is the high temperature limit of the continuum theory: it differs from the high T region of the Ising chain in Fig 4.3, as we will see in the next chapter, by the presence of logarithmic corrections which modify some key dynamic properties and their physical interpretation. Finally there is a lattice
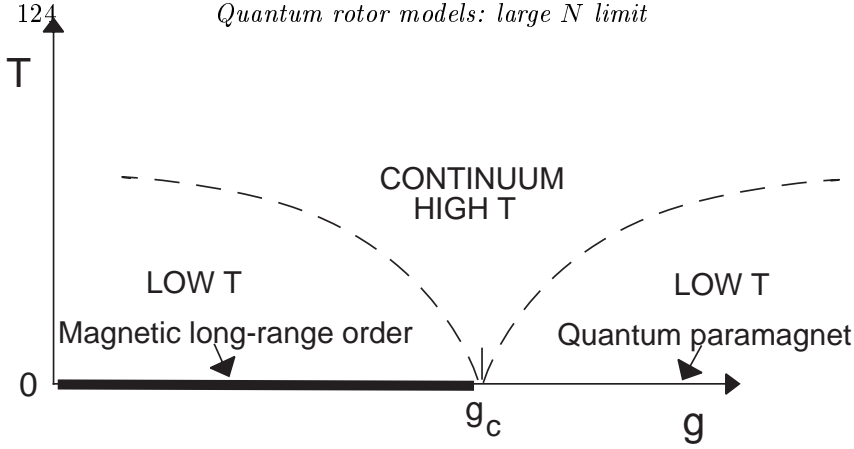
Fig. 5.2. Large N phase diagram for the O(N) rotor model in $d = 2$. As in Fig 5.1, this is expected to apply for all $N \geq 3$, and the lower dashed lines are crossovers determined by the conditions $\Delta_{\pm} \sim T$. As g approaches the critical coupling g_c, $\Delta_+ \sim (g - g_c)^{z\nu}$ for $g > g_c$, and $\Delta_- \sim (g_c - g)^{z\nu}$ for $g < g_c$. The physical interpretation of the regimes is identical to those for the Ising chain in Fig 4.3. As in Fig 4.3, there is also an additional, non-universal, lattice high T region for $T > J$ which is not shown here.

high T region, $T > J$, (not shown in Fig 5.1) where microscopic details matter: this region shall not be of interest to us here.

Turning next to $d = 2$, we show the anticipated large N phase diagram in Fig 5.2. The crossover phase boundaries and the physical interpretations of the regimes are essentially identical to those for the Ising chain in Fig 4.3. There is an ordered magnetic state at $T = 0$, but the long-range order disappears at any non-zero T. This is similar to the Ising chain, but the physics behind the destruction of long-range order by thermal fluctuations is quite different and will be discussed in more detail in the subsequent chapters.

Finally we also consider the large N limit for $2 < d < 3$ in Fig 5.3. Although these dimensions are unphysical, it is still useful to examine these cases as we can deal with systems whose long-range order survives until a non-zero temperature. Also the behavior for the physical cases $N = 1, 2$, $d = 2$ is quite similar to these large N limits. The non-zero T phase transition is within the region $T < \Delta_-$, and the nature of the singularity in its vicinity will be discussed below.

The crossovers in these phase diagrams can be described by scaling functions closely analogous to (4.56). It is more convenient to work in frequency and wavevector space, and we can obtain the scaling form
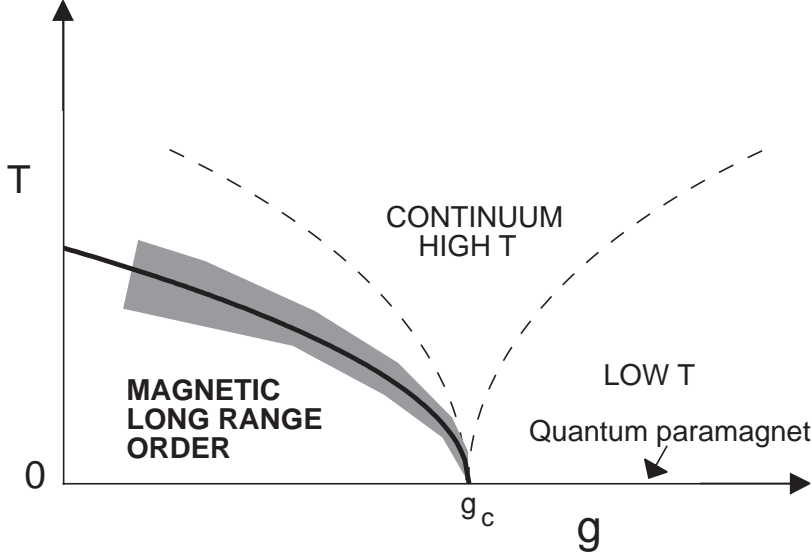
Fig. 5.3. Large N phase diagram for the O(N) rotor model with $2 < d < 3$. Qualitative features of the phase diagram apply for $N > 2$ and $2 < d < 3$, or $1 \leq N \leq 2$ and $2 \leq d < 3$. The dashed lines are crossovers determined by $\Delta_\pm \sim T$ ($\Delta_\pm \sim |g - g_c|^{z\nu}$), while the full line is the locus of finite temperature phase transitions with T_c given by (5.86). There is true magnetic long-range order at all temperatures below the full line. The shaded region is where the reduced classical scaling functions apply.

by arguments similar to those used to obtain (4.56). First, we can use the definition (5.2) and the scaling dimension (5.39) to conclude $\dim[\chi(k, \omega)] = 2\dim[\mathbf{n}] - d - z = -(2 - \eta)$. Then recalling $\dim[T] = z$, we can obtain the scaling form

$$\chi(k, \omega) = \frac{Z}{T^{(2-\eta)/z}} \Phi_\pm \left(\frac{ck}{T^{1/z}}, \frac{\omega}{T}, \frac{\Delta_\pm}{T} \right) \tag{5.60}$$

where the upper (lower) sign applies for $g \geq g_c$ ($g \leq g_c$). Also it should be clear that in $d = 1$ only the upper sign can apply. The functions $\Phi_\pm$ are completely universal and complex-valued, and are chosen to have finite limits at all k and ω as $\Delta_\pm \to 0$ at fixed T (there is an exception to this in $d = 1$, where, as will shall see in Chapter 6, the function Φ_+ diverges logarithmically as $\Delta_+/T \to 0$; this logarithm divergence is however absent in the present $N = \infty$ theory). There are strong restrictions that arise from the consistency of the two functions as they approach the common point $g = g_c$ from the two sides; not only their

values must agree, but also the fact that $\chi(k, \omega)$ must be *analytic* as a function of g at $g = g_c$ for $T > 0$ places many additional restrictions (the reasons for this analyticity, and its consequences will be discussed in more detail in Section 8.2.1). For the Ising chain we were able to work with a single function by defining a $\Delta = \Delta_+ > 0$ for $g \geq g_c$ and $\Delta = -\Delta_- < 0$ for $g \leq g_c$, but this is difficult to do in the present case as the definitions of $\Delta_\pm$ are quite different. Also, for the Ising chain, Δ was a simple, analytic linear function of g, so the analyticity requirement was simply that Φ was analytic as a function of Δ at $\Delta = 0$.

The prefactor Z is a non-universal constant which is non-singular at the $T = 0$ quantum critical point. It can be defined through (5.60) by relating it to some observable which depends upon the scale of the order parameter field. For $g > g_c$, we can, by demanding that the form of $\chi(k, \omega)$ near the quasi-particle pole at $T = 0$ in (5.30) (which holds even beyond $N = \infty$, as we saw in the Ising chain) be consistent with the scaling form (5.60), specify

$$Z = (\text{constant}) \frac{\mathcal{A}}{\Delta_+^{\eta/z}}. \tag{5.61}$$

The constant can be chosen at our convenience, and merely changes the definition of the $\Phi_\pm$. Alternatively, we could approach the critical point from $g < g_c$ and use (5.57) to define

$$Z = (\text{constant}) \frac{N_0^2 c^2}{\rho_s \Delta_-^{\eta/z}}. \tag{5.62}$$

A similar scaling form can be written down for the uniform susceptibility from the knowledge of the scaling dimension in (5.43):

$$\chi_u = \frac{T^{d/z-1}}{c^d} \Phi_{u\pm} \left(\frac{\Delta_\pm}{T} \right). \tag{5.63}$$

Unlike, (5.60), there is no non-universal prefactor like Z in front: this is because the unknown field scale, and the anomalous exponent η does not appear in the definition of χ_u: rather it is related by (5.3) to the free energy density.

The remainder of this section will present explicit results for these scaling functions at $N = \infty$. In this limit, the expressions in (5.22) and (5.23) specify χ and χ_u respectively. These are consistent with the scaling forms (5.60) and (5.63) for $\eta = 0$ and $z = 1$, if the Lagrange

multiplier m satisfies

$$m = TF_{\pm}\left(\frac{\Delta_{\pm}}{T}\right) \tag{5.64}$$

where $F_{\pm}$ are universal functions which will be obtained from the solution of (5.21), as we shall show below. The resulting predictions for the physical properties at $T > 0$ are quite simple. By Fourier transforming (5.22), we see that m/c is the correlation length. The imaginary part of (5.22) also implies that there is a gap in the spectrum equal to m. This feature is an artifact of the $N = \infty$ limit: the response of any interacting system at $T > 0$ has a non-zero spectral density at all frequencies (in certain cases, the response could vanish above some large ultraviolet cutoff $\sim c\Lambda$), as there are essentially no restrictions on the set of frequencies at which all the possible thermally excited states can absorb energy. A prominent objective of the remaining chapters in Part 2 is to describe a dynamical theory for the filling in of this gap at finite temperatures.

The uniform susceptibility is obtained by evaluating the frequency summation in (5.23) by standard methods which the reader can find in text books like Refs [146] and [321]; the result is

$$\chi_u = \frac{1}{2T}\int\frac{d^d k}{(2\pi)^d}\frac{1}{\sinh^2(\sqrt{c^2 k^2 + m^2}/2T)}, \tag{5.65}$$

with m given by (5.64).

We now determine the universal functions $F_{\pm}$, and will subsequently turn to a description of the physics in the various regions of Fig 5.1-5.3. The method used here introduces a number of useful tricks for the extraction of universal, cut-off independent crossover functions.

We present first the calculation on the disordered side $g \geq g_c$. The first step is to subtract from (5.21) the corresponding equation (5.24) at the same coupling constants at $T = 0$; this gives us

$$\int^{\Lambda}\frac{d^d k}{(2\pi)^d}T\sum_{\omega_n}\frac{1}{c^2 k^2 + \omega_n^2 + m^2} - \frac{1}{c}\int^{\Lambda}\frac{d^{d+1}p}{(2\pi)^{d+1}}\frac{1}{p^2 + (\Delta_+/c)^2} = 0 \tag{5.66}$$

where Δ_+ is the gap at the current value of g. A trick we shall often use is to subtract from the summation over frequencies of any quantity, the integration over frequencies of precisely the same function; so we rewrite (5.66) as

$$\int^{\Lambda}\frac{d^d k}{(2\pi)^d}\left(T\sum_{\omega_n}\frac{1}{c^2 k^2 + \omega_n^2 + m^2} - \int\frac{d\omega}{2\pi}\frac{1}{c^2 k^2 + \omega^2 + m^2}\right)$$

$$+\frac{1}{c}\int^{\Lambda}\frac{d^{d+1}p}{(2\pi)^{d+1}}\left(\frac{1}{p^2+(m/c)^2}-\frac{1}{p^2+(\Delta_+/c)^2}\right)=0. \quad (5.67)$$

Now we use the general relation

$$T\sum_{\omega_n}\frac{1}{\omega_n^2+a^2}-\int\frac{d\omega}{2\pi}\frac{1}{\omega^2+a^2}=\frac{1}{a}\frac{1}{e^{a/T}-1} \quad (5.68)$$

valid for any positive a (again this can be established by standard frequency summation methods [146, 321]). Notice that the right-hand side falls off exponentially as a becomes large. This is a key property, and was the reason for considering the combination in (5.68). Applying this identity to (5.67), we see that the first integration over k has an integrand which is exponentially small for large k, and hence is quite insensitive to Λ which can safely be sent to infinity. The integration over p in the second term is also ultraviolet convergent, again allowing Λ to be set to infinity. The resulting expression is then cutoff independent, and hence universal; we obtain for $d > 1$

$$\int\frac{d^dk}{(2\pi)^d}\frac{1}{\sqrt{c^2k^2+m^2}}\frac{1}{e^{\sqrt{c^2k^2+m^2}/T}-1}-\frac{X_{d+1}}{c^d}\left(m^{d-1}-\Delta_+^{d-1}\right)=0, \quad (5.69)$$

where the number X_d was defined below (5.27). In $d = 1$, this equation is modified to

$$\int\frac{dk}{(2\pi)}\frac{1}{\sqrt{c^2k^2+m^2}}\frac{1}{e^{\sqrt{c^2k^2+m^2}/T}-1}-\frac{\ln(m/\Delta_+)}{2\pi c}=0. \quad (5.70)$$

The solution of these equations is clearly of the form (5.64); after rescaling momenta by c/T in (5.69), we find that the function $F_+(s)$ is determined implicitly by solution of the equation

$$\int\frac{d^dk}{(2\pi)^d}\frac{1}{\sqrt{k^2+F_+^2}}\frac{1}{e^{\sqrt{k^2+F_+^2}}-1}-X_{d+1}\left(F_+^{d-1}-s^{d-1}\right)=0 \quad (5.71)$$

for $d > 1$, and similarly for $d = 1$. We will discuss asymptotic features of the solution of these equations in the subsections below. We note here that precisely in $d = 2$, the equation (5.71) has a simple, explicit solution [97]

$$F_+(s)=2\sinh^{-1}\left(\frac{e^{s/2}}{2}\right)\qquad d=2. \quad (5.72)$$

Now we turn to the ordered side, $g \leq g_c$, which implicitly means that we have $d > 1$. We assume that T is large enough that the magnetization is zero; the case of the magnetized state with $T \neq 0$ can be treated

similarly, and will be referred to below. Subtract from (5.21), the value of ρ_s/N in (5.58), and insert the value of $1/g_c$ in (5.25). Evaluating the frequency summation as above we find

$$\int \frac{d^d k}{(2\pi)^d} \frac{1}{\sqrt{c^2 k^2 + m^2}} \frac{1}{e^{\sqrt{c^2 k^2 + (m/c)^2}/T} - 1}$$
$$+ \frac{1}{c} \int \frac{d^{d+1} p}{(2\pi)^{d+1}} \left(\frac{1}{p^2 + m^2} - \frac{1}{p^2} \right) = \frac{\rho_s}{Nc^2}. \qquad (5.73)$$

The solution of this is also in the form (5.64), and the function $F_-(s)$ is given by

$$\int \frac{d^d k}{(2\pi)^d} \frac{1}{\sqrt{k^2 + F_-^2}} \frac{1}{e^{\sqrt{k^2 + F_-^2}} - 1} - X_{d+1} F_-^{d-1} - s^{d-1} = 0. \qquad (5.74)$$

Again, there is a simple explicit solution in $d = 2$ [97]

$$F_-(s) = 2 \sinh^{-1} \left(\frac{e^{-2\pi s}}{2} \right) \qquad d = 2 \qquad (5.75)$$

With expressions for the crossover functions $F_\pm$ in hand, let us discuss the physical properties of the system in different regimes of the g, T, plane for different values of d.

5.4.1 Low T on the quantum paramagnetic side, $g > g_c$, $T \ll \Delta_+$

The discussion here also applies in $d = 1$.

Properties of this phase are essentially identical to those of the low T quantum paramagnetic region of the Ising model in Section 4.5.2. The ground state has a gap, and non-zero T induces an exponentially small density of thermally excited triplet magnons. For the parameter m we have

$$m = \Delta_+ + \mathcal{O}(e^{-\Delta_+/T}). \qquad (5.76)$$

So there is a finite correlation length c/m which has exponentially small corrections from its $T = 0$ value c/Δ_+. The $N = \infty$ expression (5.22) has a quasi-particle peak that remains infinitely sharp at $T > 0$: this is clearly incorrect for finite N, as damping must be present, and will be described in subsequent chapters. The uniform susceptibility can be computed from (5.65), and we find that it is exponentially small

$$\chi_u = \mathcal{O}(e^{-\Delta_+/T}). \qquad (5.77)$$

5.4.2 High T, $T \gg \Delta_+, \Delta_-$

Again properties are the similar to those of the continuum high T region of the Ising chain as discussed in Section 4.5.3. Now we have, for $d > 1$

$$m = TF_+(0) = TF_-(0) \tag{5.78}$$

where $F_+(0)$, $F_-(0)$ are pure numbers. This represents a correlation length $\sim c/T$. In $d = 1$, the correlation length has an additional logarithmic correction [253], as can be seen from the solution of (5.70)

$$m = \frac{\pi T}{\ln(\mathcal{C}T/\Delta_+)}, \tag{5.79}$$

where

$$\mathcal{C} = 4\pi e^{-\gamma} = 7.055507955\ldots. \tag{5.80}$$

In a similar manner we find for the uniform susceptibility from (5.65) that in $d > 1$

$$\chi_u = \frac{T^{d-1}}{c^d}\Phi_{u+}(0) = \frac{T^{d-1}}{c^d}\Phi_{u-}(0), \tag{5.81}$$

where $\Phi_{u\pm}$ are universal pure numbers which can be determined by solutions of (5.65) and (5.69); in $d = 2$ we have the simple result $\Phi_{u\pm}(0) = (\sqrt{5}/\pi)\ln((\sqrt{5}+1)/2)$. Again, in $d = 1$ there are log corrections [253]

$$\chi_u = \frac{1}{\pi c}\ln(\mathcal{C}T/\Delta_+) \tag{5.82}$$

which will be better understood in the following chapter.

By analogy with the Ising chain we expect that the dynamics is quantum relaxational with a phase coherence time $\sim 1/T$. However damping and relaxation are completely absent at $N = \infty$ and will be further discussed later.

5.4.3 Low T on the magnetically ordered side, $g < g_c$, $T \ll \Delta_-$

This section applies only for $d > 1$, as there is no such region for $d = 1$. The properties in $d = 1$ will be analogous to the low T ordered region of the Ising chain in Section 4.5.1, but there will be important differences for $2 < d < 3$.

Let us assume first that T is large enough so that $\langle \mathbf{n} \rangle = 0$ and so (5.74) can be used to determine F_-. For $d = 2$, one finds that there is a

solution of (5.74) for all T, and even as $T \to 0$ ($s = \Delta_-/T \to \infty$). We find that as $T \to 0$

$$m = T \exp(-2\pi\Delta_-/T) = T \exp(-2\pi\rho_s/NT). \qquad (5.83)$$

So the correlation length $\sim c/m$ diverges as $T \to 0$, but remains finite for all non-zero T. This was exactly the situation as in the Ising chain, and the phase diagram for this model is therefore as shown in Fig 5.2. We will see in subsequent chapters that, as in the case of the Ising chain, because of the very large correlation length, it is possible to develop an effective classical dynamical model of the system, and to express the result in terms of reduced scaling functions. Let us also note (from (5.65)) that the uniform susceptibility in $d = 2$ is given as $T \to 0$ by

$$\chi_u = \frac{2\Delta_-}{c^2} = \frac{2\rho_s}{Nc^2}. \qquad (5.84)$$

This is actually an exact result even for finite N, as we will see later.

Now let us consider the case $2 < d < 3$. Although there is no physical dimension in this region, the results obtained below will apply in $d = 3$ with cutoff-dependent logarithmic corrections we do not want to discuss here. Further, the physics of the quantum Ising model in $d = 2$ is expected to be similar to that of the large N solution with $2 < d < 3$. The key observation in this case is that there is no solution of (5.74) for $F_-(s)$ above a critical value $s = s_c$, where $F_-(s_c) = 0$. The value of s_c is given by

$$
\begin{aligned}
s_c^{d-1} &= \int \frac{d^dk}{(2\pi)^d} \frac{1}{k} \frac{1}{e^k - 1} \\
&= \frac{2\Gamma(d-1)\zeta(d-1)}{\Gamma(d/2)(4\pi)^{d/2}}. \qquad (5.85)
\end{aligned}
$$

Just as was the case in the $T = 0$ analysis at the beginning of Section 5.3, the absence of a solution for the Lagrange multiplier m (related to $F_-(s)$ by (5.64)) implies that there must be magnetic order for $s > s_c$ This defines a critical temperature T_c given precisely by

$$T_c \equiv \Delta_-/s_c \qquad (5.86)$$

such that the system is in the paramagnetic phase only for $T > T_c$: the resulting phase diagram is shown in Fig 5.3. There is a finite temperature phase transition at $T = T_c$, and a magnetically ordered phase for $T < T_c$. As T approaches T_c, the conventional classical phase transition theory becomes applicable in the region $|T - T_c| \ll T_c$. The classical

scaling functions of this transition emerge as reduced scaling functions of the quantum functions, in a manner very similar to the discussion on the quantum Ising chain in Section 4.5.1. One consequence of this behavior is that all the scale factors of the classical scaling functions, which are usually considered non-universal, are universally determined by the parameters Δ_-, c, and N_0 of the quantum crossover functions. We have already seen an example of this in (5.86), where T_c was universally determined by Δ_- [427].

Let us explicitly observe the collapse of the scaling function (5.64) in this classical region. As the primary quantum crossover function has only one argument, the reduced function would have no arguments, i.e., it is a pure power law. Indeed, solution of (5.74) for s close to but above s_c gives us

$$m = T_c \left[\left(\frac{T - T_c}{T_c} \right) \frac{(d-1)s_c^{d-1}}{X_d} \right]^{1/(d-2)} . \qquad (5.87)$$

The correlation length c/m diverges with the classical exponent $\nu_c = 1/(d-2)$ with an amplitude that is universal.

The above is part of a very general lesson. Quantum critical scaling forms like (5.60) hold everywhere in the vicinity of the quantum critical point, including at or close to any finite temperature phase transition lines that may be approaching the quantum critical point. The classical critical singularities of these finite temperature transition appear as singularities of the quantum critical scaling function. Further, the amplitudes of the classical transitions, which are normally non-universal, become universal when expressed in terms of the arguments of the quantum-critical scaling function.

5.5 Applications and extensions

We have already mentioned application to double-layer antiferromagnets in Section 5.1.1.1.

We indicated in Section 5.1.1.1 that the O(3) quantum rotor model describes a large class of Heisenberg antiferromagnets, and this connection will be established more generally in Chapter 13. Here we will discuss application of rotor model results to thermodynamic measurements of the uniform spin susceptibility, χ_u, of quantum antiferromagnets; implications for other physical properties of antiferromagnets will be noted in subsequent chapters. The rotor model predictions for χ_u are given by

(5.65) in the large N limit, but computations with $1/N$ corrections are also available [96, 97].

The $S = 1/2$ square lattice antiferromagnet, found in the parent insulating compounds of the high temperature superconductors (like La_2CuO_4), has its low energy properties described by the O(3) quantum rotor model [83]. Very accurate results for the thermodynamic properties of the former model have been obtained in precision Monte Carlo computations by Kim and Troyer [269]. In particular they obtained the T dependence of the uniform susceptibility, χ_u, for a wide range of temperatures; experimental measurements of χ_u on La_2CuO_4 are also available [252], but these are of lower precision than the numerical data, and as it is practically certain that La_2CuO_4 is a square lattice antiferromagnet, it is appropriate to use the numerical data. For $T \ll \rho_s$ their measurements are in good agreement with universal low temperature response of the continuum rotor model in (5.84) (the correction of order T/ρ_s to (5.84) will be derived later in (7.25) [97, 218], and this was used in the comparisons with the numerical data in Ref [269]). At larger T they observe a clear crossover which is in good agreement with the continuum high T behavior in (5.81) (the leading $1/N$ and ρ_s/T computed corrections [97] to (5.81) were used in this comparison). This evidence supports the proposal, made in Ref. [96], that the $S = 1/2$ square lattice antiferromagnet is close enough to a quantum critical point to display the continuum high T behavior of Fig 5.2 at higher temperatures.

The low energy properties of a double-layer model of two $S = 1/2$ square lattice antiferromagnets coupled to each other are also described by O(3) quantum rotor model, as should be clear from the discussion in Section 5.1.1.1. Moreover, by changing the ratio of exchange couplings in this model it is possible to tune the rotor model coupling g through g_cT [329, 342]. There have been a number of studies of the double-layer antiferromagnet near this critical point [443, 444, 330, 175, 136, 498, 331], and the numerical results for χ_u are in good agreement with the (5.81) and its $1/N$ corrections [97].

Normand and Rice [366, 367] have proposed an interesting recent experimental realization of the quantum critical point of the $d = 3$ quantum rotor model in $LaCuO_{2.5}$. This is a spin-ladder compound in which the ladders are moderately coupled in three dimensions. By varying the ratio of the intra-ladder to inter-ladder exchange it is possible to drive such an antiferromagnet across a $d = 3$ quantum critical point separating Néel ordered and quantum paramagnetic phases. The uniform susceptibility has a T^2 dependence at intermediate T, which is characteristic of

the "High T" dependence in (5.81) in $d = 3$. The entire T dependence of χ_u has been computed in Monte Carlo simulations of an $S = 1/2$ antiferromagnet on the $LaCuO_{2.5}$ lattice [500] and the results are in good agreement with quantum rotor model computations like those discussed here.

6

The $d = 1$, $\mathrm{O}(N \geq 3)$ rotor models

As we noted in the preface, this and the following chapter are at a more advanced level, and some readers may wish to skip ahead to Chapter 8.

In Chapter 5 we studied the $\mathrm{O}(N)$ quantum rotor model in the large N limit for a number of values of the spatial dimensionality, including $d = 1$. We noted that the results provided an adequate description of the static properties in $d = 1$ for $N \geq 3$: this will be justified in the present chapter where we will obtain a number of exact results for the same static observables. We also noted that the large N limit did a very poor job of describing dynamical properties at nonzero temperatures: this will be repaired in this chapter by simple physical arguments which lead to a fairly complete (and believed exact) description of the long-time behavior. Some of the discussion in this chapter will be specialized to the $\mathrm{O}(N = 3)$ model, which is also the case of greatest physical importance; the properties of the $\mathrm{O}(N > 3)$ models are very similar, and many of our results will be quoted for general N. Of the remaining cases, the $d = 1$, $N = 1$ model has been already considered in Chapter 4, and study of the $d = 1$, $N = 2$ model is postponed to Section 14.3.

The physical picture of the $T = 0$, $N = 3$ state which emerged in Chapter 5 was very simple. The ground state was a quantum paramagnet which did not break any symmetries. There was an energy gap, Δ_+, above the ground state, and the low-lying excitations were a triplet of particles with dispersion $\varepsilon_k = \sqrt{c^2 k^2 + \Delta_+^2}$; this picture will be verified here by a more complete renormalization group analysis in Section 6.1. These triplet particle excitations lead to a quasi-particle pole in the dynamic susceptibility $\chi(k, \omega)$, which has the form (5.30) near the pole. This form contains the quasiparticle residue, $\mathcal{A}$, which sets the overall scale of the order parameter field.
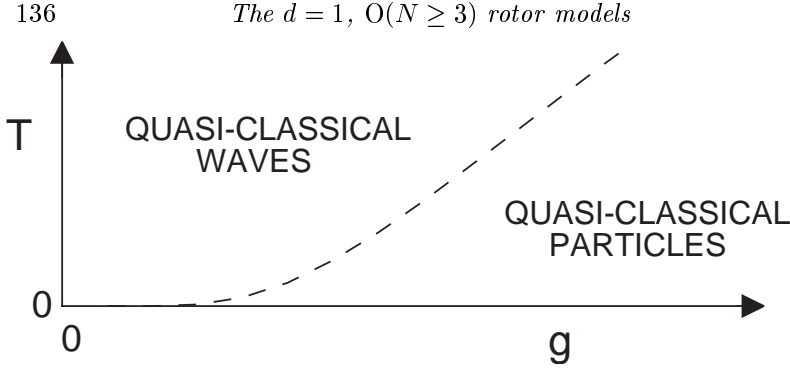
Fig. 6.1. Crossover phase diagram of the $d = 1$, $N \geq 3$ rotor model (5.1,5.16) as a function of the temperature and the coupling g. The continuum theory description fails above some T, as in Fig 4.3, but this has not been indicated. The quasi-classical particle model is developed in Section 6.2, while the quasi-classical wave model is discussed in Section 6.3.

Turning next to non-zero temperatures, we obtained the crossover phase diagram shown in Fig 5.1, a modified version of which has been reproduced in Fig 6.1. The primary purpose of this chapter is to give a fairly complete description of the dynamical properties in the two universal regions of Fig 5.1 and 6.1: these are the low T ($T \ll \Delta_+$) and high T ($\Delta_+ \ll T \ll J$) regions of the continuum quantum field theory. As indicated in Fig 6.1, the dynamics of the low T region will be described by an effective model of quasi-classical particles in Section 6.2, closely related to the particle model developed in Section 4.5.2 for the Ising chain. For the high T region, we will develop a new, 'dual', description in a model of quasi-classical *waves*, which shall be introduced in Section 6.3. As indicated in Section 5.1.1.1, and discussed more extensively in Chapter 13, the $d = 1$, O(3) rotor model describes a large class quantum spin chains. The low T regime of Fig 6.1 will be applicable to all such spin chains, while the high T, quasi-classical wave regime applies only if the continuum quantum field theory description for the lattice model holds at these elevated temperature—the precise restrictions this imposes are discussed in Ref [69], but will not be entered into here.

As we noted in Chapter 5, the dynamic susceptibility, $\chi(k, \omega)$ in the regions of Fig 6.1 is completely determined by the parameters $\mathcal{A}$, c, and Δ_+, and obeys the scaling form (5.60) with $\eta = 0$, $z = 1$. The uniform susceptibility, χ_u, depends only on Δ_+ and c as shown in (5.63). We shall also examine here an important new observable which characterizes the transport of the conserved angular momentum of the rotor model in

space: this is the *spin diffusion constant*, D_s. To compute this we will need spacetime dependent correlation functions of the angular momentum density $\mathbf{L}(x, t)$ (for a lattice model with spacing between sites, a, the continuum field $\mathbf{L}(x_i, t) = \hat{\mathbf{L}}_i(t)/a$); by analogy with (5.2) we define

$$
\begin{aligned}
C_{u,\alpha\beta}(x,\tau) &\equiv \langle L_\alpha(x,\tau)L_\beta(0,0)\rangle \\
\chi_{u,\alpha\beta}(k,\omega_n) &\equiv \int_0^{1/T}\int dx\, C_{u,\alpha\beta}(x,\tau)e^{-i(kx-\omega_n\tau)}.
\end{aligned} \qquad (6.1)
$$

Computations in this chapter will show that $\chi_{u,\alpha\beta}$ has the following form at small k and ω

$$
\chi_{u,\alpha\beta}(k,\omega) = \delta_{\alpha\beta}\chi_u \frac{D_s k^2}{-i\omega + D_s k^2}. \qquad (6.2)
$$

For simplicity, we have set the external field $\mathbf{H} = 0$: this will be done throughout this chapter, although it is not difficult to extend the results to a small $\mathbf{H} \neq 0$. The relationship (6.2) defines the value of the spin diffusion constant D_s. Actually the structure of (6.2) is a very general consequence of the conservation of $\mathbf{L}$, as we shall see in Chapter 9, and has been discussed in considerable detail in the book by Forster [161].

Notice that the static uniform susceptibility is defined by

$$
\chi_u \equiv \lim_{k\to 0}\lim_{\omega\to 0}\chi_u(k,\omega), \qquad (6.3)
$$

and the order of limits is important. It should also be clear that the full wavevector and frequency dependent $\chi_u(k,\omega)$ obeys a scaling form quite analogous to (5.63): one simply adds additional arguments of ω/T and $ck/T^{1/z}$ to (5.63). This in turn implies a scaling form for D_s

$$
D_s = c^2 T^{-2/z+1}\Phi_{D_s}\left(\frac{\Delta_+}{T}\right); \qquad (6.4)
$$

therefore, as we shall see in this chapter, the T dependence of D_s is also completely and universally specified by the values c and Δ_+ in the regions of Fig 5.1.

6.1 Scaling analysis at zero temperature

This section will briefly review a well-known argument [389, 65, 362] that the large N result for the $T = 0$ gap in (5.28), $\Delta_+ \sim c\Lambda\exp(-2\pi/g)$ is basically correct for all $N \geq 3$.

Our method will be to examine the behavior of the coupling g under a scaling transformation of the theory (5.16) at $\mathbf{H} = 0$. We considered

scaling transformations earlier in Section 4.3 where we examined the behavior of the simple free field theory H_F, (4.41), describing the Ising chain. The procedure is as before: consider the continuum theory (5.16) with a upper momentum cutoff Λ, first integrate out the degrees of freedom between Λ and $\Lambda e^{-\ell}$, and then perform the rescaling (4.46) to restore the cutoff to its original value. Finally we compare the relative values of the couplings before and after the transformation, and this allows us to extract a great deal of information. For the case of the Ising theory, (4.41), the first step was quite innocuous: (4.41) describes a free field theory, and integrating out high momentum modes merely multiplied the partition function by an overall constant. In contrast, we will find here that this step plays a crucial role in the scaling analysis of (5.16).

We will integrate out the degrees of freedom at momentum scales between $\Lambda e^{-\ell}$ and Λe^{ℓ} by the background field method of Polyakov [389, 390]. Let $\mathbf{n}_<(x, \tau)$ represent a 'background' configuration of fields with wavevectors less than $\Lambda e^{-\ell}$. The fluctuations in the scales between $\Lambda e^{-\ell}$ and Λ must not violate the constraint $\mathbf{n}^2 = 1$, and can therefore be parameterized by their $N-1$ components along the directions orthogonal to $\mathbf{n}_<(x, \tau)$. Specifically, we write

$$\mathbf{n}(x, \tau) = \sqrt{1 - \pi_a \pi_a}\, \mathbf{n}_<(x, \tau) + \sum_{a=1}^{N-1} \pi_a \mathbf{e}_a(x, \tau) \tag{6.5}$$

where $\vec{\pi}$ is a $N-1$ component field with wavevectors between $\Lambda e^{-\ell}$ and Λe^{ℓ}, and $\mathbf{e}_a(x, \tau)$, $\mathbf{n}_<(x, \tau)$ are N mutually orthogonal unit vectors in the N-dimensional rotor space. We insert (6.5) into (5.16) and expand the resulting action in powers of $\vec{\pi}$ at $\mathbf{H} = 0$: this gives the spatial gradient terms

$$\frac{cN}{2g}\left[(\nabla \mathbf{n}_<)^2(1 - \pi_a \pi_a) + (\nabla \pi_a)^2 + \pi_a \pi_b \nabla \mathbf{e}_a \cdot \nabla \mathbf{e}_b + 2\pi_a \nabla \pi_b \mathbf{e}_b \cdot \nabla \mathbf{e}_a\right]$$
$$\tag{6.6}$$

and also time derivative terms with an identical structure. Terms linear in π do not appear because they vanish upon spatial integration, as the momenta carried by the π_a is different from those of the background fields. Now the π_a fields are integrated out, and all terms containing up to two derivatives of the background fields are retained in the results. This results in an effective action for the fields $\mathbf{n}_<$ and $\mathbf{e}_a$; after using the orthonormality condition between these fields, all explicit dependence upon the $\mathbf{e}_a$ disappears, and the action for the $\mathbf{n}_<$ has precisely

the form of (5.16) but with a modified coupling g'. Finally, we perform the rescaling (4.46)—this has no effect on the coupling g, which is dimensionless in $d = 1$. We have now completed the required scaling transformation and it maps the original coupling g to a new coupling g' given by

$$\frac{1}{g'} = \frac{1}{g} - \frac{c(N-2)}{N} \int_{\Lambda e^{-\ell}}^{\Lambda} \frac{dk}{\pi} \int \frac{d\omega}{2\pi} \frac{1}{c^2 k^2 + \omega^2} + \mathcal{O}(g) \qquad (6.7)$$

The integrals in (6.7) can be easily carried out, and we can then represent the effects of successive application of this transformation (as in (4.48)) by the differential equation

$$\frac{dg}{d\ell} = \frac{N-2}{2\pi N} g^2 + \mathcal{O}(g^3) \qquad (6.8)$$

This is a key flow equation which will help us understand the properties of (5.16) at small g. By integrating (6.8) we can easily see that a system with a small initial value of g will flow into a system with a g of order unity at a scale

$$\ell = \frac{2\pi N}{(N-2)g} + \mathcal{O}(g^0) \qquad (6.9)$$

where the coefficient of the leading g^{-1} term does not depend upon the value of the order unity constant chosen, but that of the $\mathcal{O}(g)$ term does. Now we expect from the strong-coupling analysis of (5.1.1) that a system with a g of order unity, will have a gap Δ_+ of order its cutoff $c\Lambda'$. Undoing the rescaling transformation (4.46), we know that the original cutoff Λ is related to the new cutoff by $\Lambda'/\Lambda = e^{-\ell} \sim \Delta/c\Lambda$, and therefore from (6.9)

$$\ln\left(\frac{c\Lambda}{\Delta_+}\right) = \frac{2\pi N}{(N-2)g} + \mathcal{O}(g^0), \qquad (6.10)$$

where again, the uncertainty in the precise value of Δ_+ relative to Λ' does not modify the leading g^{-1} term. This result has precisely the same form as the large N result (5.28), establishing our earlier claims on the correctness of the large N theory for static and equal-time properties— the only change in the present exact treatment has been the replacement of $\Delta_+ \sim c\Lambda \exp(-2\pi/g)$ by $\Delta_+ \sim c\Lambda \exp(-2\pi N/(N-2)g)$. This also shows that the large N results breakdown badly at $N = 2$, but are quite reasonable for $N \geq 3$.

We have been rather sloppy in the above discussion about various constants of order unity. It is possible to be quite precise about these using a

more sophisticated field-theoretic renormalization group analysis, which
we will discuss later in this chapter.

6.2 Low temperature limit of continuum theory, $T \ll \Delta_+$

This $T > 0$ region was shown in Figs 5.1 and 6.1. All of the analysis of
this section will be specialized to $N = 3$, although the generalization to
other $N \geq 3$ is straightforward.

   The approach followed [433, 117] for $T \ll \Delta_+$ is very similar to that
taken for the corresponding low T region on the quantum paramagnetic
side of the Ising chain in Section 4.5.2. The central difference here is
that the quasi-particle excitations are triplets, and therefore have an
additional spin label, $m = -1, 0, 1$. This label is associated with the
eigenvalues of the conserved total angular momentum, and leads to im-
portant qualitative differences which will be discussed below.

   There are two key observations that allow our computation for $T \ll$
Δ_+. The first, as in the Ising chain, is that the density of thermally
excited particles is so low, that they can be treated, when well separated,
as classical particles. In particular, as their density $\sim e^{-\Delta_+/T}$, their
mean spacing $\sim e^{\Delta_+/T}$ is exponentially large at low T. On the other
hand, their thermal velocities are also small at low T, and so their typical
wavelength becomes large; however the divergence of the thermal de
Broglie wavelength is only $\sim c/\sqrt{T\Delta_+}$ and is therefore much smaller
than the particle spacing at low enough T. The density of particles with
each spin m ($m = -1, 0, 1$ for $N = 3$), ρ_m is given by the expression
(4.81), and the total density, ρ therefore equals $\rho_1 + \rho_0 + \rho_{-1}$, which is

$$\rho = 3 \left(\frac{T\Delta_+}{2\pi c^2} \right)^{1/2} e^{-\Delta_+/T}. \tag{6.11}$$

This classical picture also allows us to simply obtain the value of the
uniform susceptibility χ_u. In the presence of a field, the energy of a
particle with spin component m simply acquires the Zeeman shift of
$-mH$. This implies that in a field $\rho_m \to \rho_m e^{mH/T}$; expanding to linear
order in the field we obtain [501, 499, 433]

$$\chi_u = \frac{2\rho}{3T} = \frac{1}{c} \left(\frac{2\Delta_+}{\pi T} \right)^{1/2} e^{-\Delta_+/T}. \tag{6.12}$$

   Let us think about the dynamics of these classical particles. While
well-separated particles behave classically, in one dimension these par-
ticles are forced to collide with their near neighbors, and cannot avoid
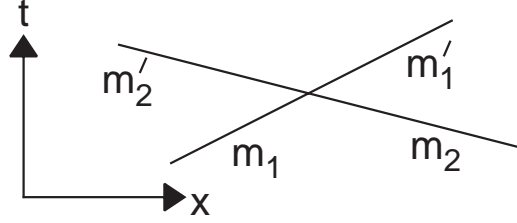
Fig. 6.2. Two particle collision described by the S matrix (6.13). The momenta before and after the collision are the same, so the figure also represents the spacetime trajectories of the particles.

each other even in the extremely dilute limit. The collision must clearly be treated quantum mechanically, and we therefore need the two-particle S matrix. Because of the presence of the particle labels m, this S matrix can be a rather complicated object, and not simply a pure phase-factor, as was the case in the Ising chain. Fortunately, we don't need the full S matrix, but only its value in the limit of vanishing momenta—the particles have thermal velocities which vanish, as noted above, in the low T limit as $v_T = c(T/\Delta_+)^{1/2}$. Furthermore, this zero-momentum S matrix turns out to have remarkably 'super-universal' structure in $d = 1$. For the process shown in Fig 6.2, the S matrix in the limit of vanishing momenta is

$$S^{m_1 m_2}_{m'_1, m'_2} = (-1)\delta_{m_1 m'_2}\delta_{m_2 m'_1}. \tag{6.13}$$

In other words, the excitations behave like impenetrable particles which preserve their spin in a collision. As in the Ising chain, energy and momentum conservation in $d = 1$ require that these particles simply exchange momenta across a collision (Fig 6.2). This result can be obtained in a variety of ways which are explored in some detail in Ref [117]. The simplest is to compute it in the strong-coupling expansion of Section 5.1.1: one solves the two-particle Schrödinger equation order-by-order in $1/g$, and finds that (6.13) holds at each order. Alternatively one can take the low-momentum limit of the exact S matrix obtained by Zamolodchikov and Zamolodchikov [543] for the continuum theory (5.16), and find that (6.13) is valid. The first method shows that (6.13) holds even for lattice models, and is not a special property of continuum relativistic theories. Indeed, (6.13) holds for practically every $d = 1$ model with a gap, and excitations which have a quadratic dispersion at low momenta; exceptions arise only in specially fine-tuned cases when
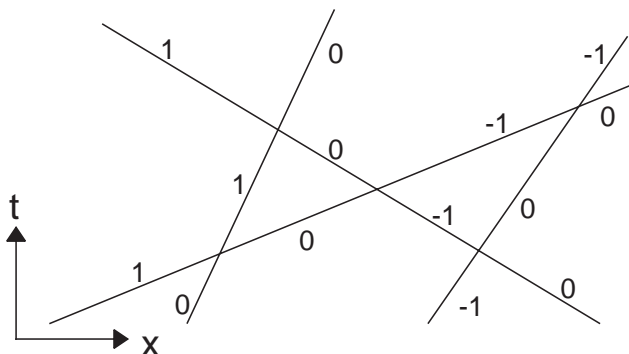
Fig. 6.3. A typical set of particle trajectories contributing to $C(x,t)$. Each trajectory represents paths moving both forward and backward in time, and the (-1) phase at each collision is neutralized by its time-reversed contribution. The particle co-ordinates are $x_k(t)$, with the labels k chosen so that $x_k(t) \leq x_l(t)$ for all t and $k < \ell$. Shown on the trajectories are the values of the particle spins m_k which are independent of t in the low T limit.

certain bound states happen to have exactly zero energy. The reasons for the 'super-universality' are explored in more detail elsewhere [117], but the underlying physics can be seen to be a simple consequence of the arguments made below (4.18) in Section 4.1.1. We argued there that to a slowly moving particle, with a very long wavelength, any short-range repulsive potential can be approximated by an *impenetrable* delta function (*i.e.*, a potential $u\delta(x)$ with $u \to \infty$). The wavefunctions of the two particles on either side of this potential therefore vanish as they approach $x = 0$. Exchange of spin requires actual overlap of the wavefunction, which we have shown becomes negligible in the low momentum limit. Hence the spins of the two particles are preserved and we have the result (6.13).

We can now proceed to the computation of correlation functions. As in Sections 4.5.1 and 4.5.2, we compute correlators as a 'double time' path integral, and in the classical limit, stationary phase is achieved when the trajectories of the particles are time-reversed pairs of classical paths as shown in Fig 6.3. Each trajectory has a spin label, m, which obeys (6.13) at each collision. The label, m, is assigned randomly at some initial time with equal probability, but then evolves in time as discussed above (Fig 6.3). We label the particles consecutively from left to right by an integer k; then their spins m_k are independent of t, and we denote their trajectories $x_k(t)$. The velocities of the particles are

chosen independently at the initial time from the classical Boltzmann distribution $P(v)$:

$$P(v) = \left(\frac{\Delta_+}{2\pi c^2 T} \right)^{1/2} \exp\left(-\frac{\Delta_+ v^2}{2c^2 T} \right) \tag{6.14}$$

We will first discuss evaluation of the correlations of the conserved angular momentum density, $C_{u,\alpha\beta}$, defined in (6.1); this has no analog in the Ising case, as the latter model did not have a conserved charge associated with a continuous symmetry. In the absence of an external field **H**, this correlator will be rotationally invariant, and it is convenient to compute the correlator of the component of the angular momentum whose eigenstates we labeled in Fig 6.3: we will therefore compute $C_{u,33}$. The operator L_3 has a particularly simple effect on the particle trajectories in Fig 6.3: it simply reports the azimuthal angular momentum of the particle it is operating on, but does not create or annihilate any particles (this is evident from the strong-coupling expansion of Section 5.1.1). We therefore only need to sum over the trajectories shown in Fig 6.3; for these every collision has a time-reversed pair, and therefore the -1's from the S matrix are completely neutralized. We are left then with a purely classical ensemble of point particles labeled with three 'colors' (the azimuthal angular momentum). The observable $L_3(x,t)$ can be written in this ensemble as

$$L_3(x,t) = \sum_k m_k \delta(x - x_k(t)) \tag{6.15}$$

We have to determine its correlators under average over a set of initial conditions of random, uncorrelated values of m_k and x_k, and velocities given by the distribution (6.14). In particular we have,

$$
\begin{aligned}
C_{u,33}(x - x', t - t') &= \sum_{k,k'} \langle m_k m'_k \delta(x - x_k(t)) \delta(x' - x_{k'}(t')) \rangle \\
&= \frac{2}{3} \sum_k \langle \delta(x - x_k(t)) \delta(x' - x_k(t')) \rangle .
\end{aligned}
\tag{6.16}
$$

In the second step (which is a crucial one) we have used the fact that the x'_k and $m'_k s$ are uncorrelated, and also that different $m'_k s$ are mutually independent. We are now left with a well-defined problem in classical statistical mechanics. Place point particles independently and uniformly along an infinite line with a density ρ. Give each an initial velocity from the distribution (6.14). Tag a particle, k, and determine its position autocorrelation function, averaged over the set of all possible

initial conditions: notice that such a particle tagging would seem quite unphysical apriori, but we have shown above how it is a natural consequence of the average over the spins m_k. This tagged particle problem can be solved exactly, as was first shown by Jepsen [251] and a little later by Lebowitz and Percus [295]. The following paragraph will present the exact evaluation of (6.16) using a method drawn from the latter authors.

The key to the solution is to notice that the trajectories in Fig 6.3 are quite simple: they are simply straight lines. Let us label the straight line 'trajectories' (as opposed to the 'particles') by the symbol μ. Then the μ'th trajectory is simply

$$x_\mu(t) = x_\mu + v_\mu t \tag{6.17}$$

where x_μ are the trajectory positions at $t = 0$, and v_μ are their velocities, and both of these have to be averaged over. Now, at a given time t, each trajectory μ will 'belong' to a particle $k_\mu(t)$, where k_μ is a rather complicated integer-valued function of time. Its explicit expression is

$$k_\mu(t) = \sum_{\mu'=1}^{M} \theta(x_\mu(t) - x_{\mu'}(t)) \tag{6.18}$$

where we have assumed there are a total of M trajectories (we will send $M \to \infty$ at a later stage), and $\theta(x)$ is the unit step function. It should be clear that (6.18) simply counts the trajectories to the left of a given trajectory at a time t, and this identifies the particle number. We can now rewrite (6.16) as a sum over trajectories, rather than particle number:

$$
\begin{aligned}
C_{u,33}(x,t) &= \sum_{\mu,\mu'=1}^{M} \left\langle \delta(x - x_\mu(t)) \delta(x_{\mu'}) \delta_{k_\mu(t),k_{\mu'}(0)} \right\rangle \\
&= \sum_{\mu,\mu'=1}^{M} \int_0^{2\pi} \frac{d\phi}{2\pi} \left\langle \delta(x - x_\mu(t)) \delta(x_{\mu'}) \right. \\
&\qquad \left. \times e^{i \sum_{\mu''} \left(\theta(x_\mu(t) - x_{\mu''}(t)) - \theta(x_{\mu'} - x_{\mu''}) \right)} \right\rangle
\end{aligned}
\tag{6.19}
$$

where in the second step we have introduced a Fourier representation of the Kronecker delta function. The average in (6.19) represents the multidimensional integral

$$\langle \cdot \rangle \equiv \prod_{\mu=1}^{M} \int_{-L/2}^{L/2} \frac{dx_\mu}{L} \int_{-\infty}^{\infty} dv_\mu \, P(v_\mu) \tag{6.20}$$

We have assumed the particles are on a line of length L, and are being quite sloppy about the boundary conditions. We ultimately want to take the limit $M \to \infty$, and $L \to \infty$ with the density $\rho = M/L$ fixed, and the result can be shown to be quite insensitive to the boundaries in this limit. Now the advantage of the Fourier representation in (6.19) should be quite evident: the $2M$ dimensional integral factorizes into products of M integrals. These integrals can be evaluated in closed form, and the subsequent limit $M \to \infty$, $L \to \infty$, $\rho = M/L$ fixed, easily taken. We will skip these intermediate steps, and present the final results.

The final results satisfy the scaling forms discussed below (6.3), but are, as expected, more usefully expressed in terms of reduced scaling forms which describe the semi-classical physics of the dilute gas of triplet magnons. The characteristic length and time scales of these reduced scaling functions are closely analogous to those found for the Ising chain in (4.80) and (4.88). In particular, we choose

$$
\begin{aligned}
\xi_c &= \frac{1}{\rho} = \frac{1}{3}\left(\frac{2\pi c^2}{T\Delta_+}\right)^{1/2} e^{\Delta_+/T} \\
\tau_\varphi &= \frac{\xi_c}{\sqrt{2}v_T} = \frac{\sqrt{\pi}}{3T} e^{\Delta_+/T}
\end{aligned}
\tag{6.21}
$$

Notice ξ_c is the mean spacing between the particles , and τ_φ is a typical time between particle collisions, which is naturally identified also as phase coherence time. The final result for C_u is then

$$
C_{u,\alpha\beta}(x,t) = \frac{2\rho^2}{3} F\left(\frac{|x|}{\xi_c}, \frac{|t|}{\tau_\varphi}\right) \delta_{\alpha\beta}
\tag{6.22}
$$

where F is a universal scaling function given by

$$
\begin{aligned}
F(\bar{x}, \bar{t}) = &\left[\left(2G_1(u)G_1(-u) + e^{-u^2}/(\bar{t}\sqrt{\pi})\right) I_0\left(2\bar{t}\sqrt{G_2(u)G_2(-u)}\right) \right. \\
&\left. + \frac{G_1^2(u)G_2(-u) + G_1^2(-u)G_2(u)}{\sqrt{G_2(u)G_2(-u)}} I_1\left(2\bar{t}\sqrt{G_2(u)G_2(-u)}\right) \right] \\
&\times \exp\left(-(G_2(u) + G_2(-u))\bar{t}\right)
\end{aligned}
\tag{6.23}
$$

with $u \equiv \bar{x}/\bar{t}$, $G_1(u) = \text{erfc}(u)/2$, and $G_2(u) = e^{-u^2}/(2\sqrt{\pi}) - uG_1(u)$. These expressions satisfy $\int_0^\infty d\bar{x} F(\bar{x}, \bar{t}) = 1/2$, which ensures the conservation of the total magnetization density with time, and yields

$$
\int dx \, C_{u,33}(x,t) = \frac{2\rho}{3} = T\chi_u
\tag{6.24}
$$

with the uniform susceptibility χ_u given by (6.12); this relationship between the spatial integral of C_u and χ_u from the conservation of total magnetization (which implies that the spatial integral of C_u is t independent), and the analog of the relation (4.93) (to be derived shortly) applied to correlators of the angular momentum density. For short times F has the ballistic form

$$F(\bar{x}, \bar{t}) \approx e^{-\bar{x}^2/\bar{t}^2}/\bar{t}\sqrt{\pi}, \qquad (6.25)$$

which is the auto-correlator of a classical ideal gas in $d = 1$, and holds for $|\bar{t}| \ll |\bar{x}| \ll 1$. In contrast, for $|\bar{t}| \gg 1, |\bar{x}|$ it crosses over to the *diffusive* form

$$F(\bar{x}, \bar{t}) \approx \frac{e^{-\sqrt{\pi}\bar{x}^2/2\bar{t}}}{(4\pi\bar{t}^2)^{1/4}} \qquad (6.26)$$

In the original dimensionful units, (6.21) and (6.26) imply a spin diffusion constant, D_s, given exactly by

$$D_s = \frac{c^2 e^{\Delta_+/T}}{3\Delta_+}. \qquad (6.27)$$

While this is exact spin diffusion co-efficient of the semiclassical model we have introduced above, it is not immediately clear that this result is also exact for the underlying quantum rotor model: there is a subtle question of orders of limits which makes the above less than rigorous, and reader is referred to Ref [117] for further discussion. Also, let us note that the Fourier transform of (6.26) yields the diffusive form (6.2) with the susceptibility χ_u given by (6.12).

We turn to the correlations of the order parameter field $\mathbf{n}(x, t)$. These are very closely related to the computations of the $N = 1$ case in Section 4.5.2. The basic observation is that, like $\hat{\sigma}^z$, the field $\mathbf{n}(x, t)$ is the creation and annihilation operator for magnon excitations above the ground state: in other words a relationship analogous to (4.102) holds. This can be seen explicitly from the strong-coupling expansion in Section 5.1.1. Then by arguments analogous to those in Section 4.5.2 we expect for the two-point correlator $C_{\alpha\beta} = C\delta_{\alpha\beta}$ in (5.2)

$$
\begin{aligned}
K(x, t) &\equiv C(x, t)|_{T=0} \\
&= \int \frac{dk}{2\pi} \frac{c\mathcal{A}}{2\varepsilon_k} e^{ikx - i\varepsilon_k t} \\
&= \frac{\mathcal{A}}{2\pi} K_0(\Delta_+ (x^2 - c^2 t^2)^{1/2}/c), \qquad (6.28)
\end{aligned}
$$

where $\mathcal{A}$ is the quasiparticle residue. The Bessel function is the Feynman

propagator of a relativistic particle, and its properties were discussed below (4.103). The $T > 0$ computation proceeds as in Section 4.5.2. We have to augment the trajectories in Fig 6.3 by an additional trajectory created and annihilated by the **n** fields. This is the only trajectory which moves only forward in time, and hence picks up additional -1 signs at each of its collisions. The $T > 0$ modification is then a matter of averaging over these -1 signs. Unlike the Ising case, this cannot be done analytically, as the 'colors' on the lines introduce additional complications. This problem and its numerical solution have been discussed elsewhere [117]; the answer has a structure closely analogous to that in Section 4.5.2. We find, as in (4.105), that

$$C(x,t) = K(x,t)R(x,t) \tag{6.29}$$

where $R(x,t)$ is a relaxation function very similar, although not exactly equal, to that found in (4.105): it obeys a scaling form identical to (4.90), and so R decays exponentially on the spatial scale $\sim \xi_c$, and on the temporal scale $\sim \tau_\varphi$. As in Section (4.5.2) we can also Fourier transform (6.29) to obtain the structure factor $S(k,\omega)$. This has to be done numerically, and it is found that for $|k| < \sqrt{\Delta T}/c$, the frequency dependence of the answer is reasonably well approximated by the following Lorentzian form

$$S(k,\omega) \approx \frac{\mathcal{A}}{\varepsilon_\parallel} \frac{0.72/\tau_\varphi}{(\omega - \varepsilon_k)^2 + (0.72/\tau_\varphi)^2}. \tag{6.30}$$

This result is the analog of (4.106).

6.3 High temperature limit of continuum theory, $\Delta_+ \ll T \ll J$

If we continue to push the analogy with the Ising chain further, we would expect that the present region (Figs 5.1 and 6.1) should be similar to the universal high T region of the Ising chain discussed in Section 4.5.3. There, we found a novel regime of 'quantum relaxational' dynamics for which no classical description was possible: the thermally excited particles had a spacing which was of the order of their de Broglie wavelength. The physics in the present region of the O(3) model is similar, but the presence of logarithms associated with the flow (6.8) does lead to a new twist. In particular, we will find that logarithms of $\ln(T/\Delta_+)$ make the classical thermal fluctuations marginally more important than the quantum fluctuations. If one is satisfied with results to leading logarithm accuracy, *i.e.*, where one neglects all corrections of order $1/\ln(T/\Delta_+)$,

then it is possible to develop an effective classical model of the dynamical properties. This classical model will be quite different from that of the low T region $T \ll \Delta_+$, where we had a description in terms of classical particles. In contrast, the present description will be in terms of *classical waves*. Our discussion here borrows heavily from the original analysis in Ref [117].

There are a number of ways to make the basic argument. One is to notice that the large N result (5.79) predicts a correlation length for $\mathbf{n}$ correlations

$$\xi \sim (c/T)\ln(T/\Delta_+). \tag{6.31}$$

(We will shortly obtain the exact correlation length to leading logarithmic accuracy, and this has the same form as (6.31)). At distances of order or shorter than this correlation length we may crudely expect that the weak-coupling, spin-wave picture of Section 5.1.2 will hold, and the typical spin-wave excitations will have energy of order or smaller than $c\xi^{-1}$, which is logarithmically smaller than the thermal energy T; in other words

$$\frac{c\xi^{-1}}{T} \sim \frac{1}{\ln(T/\Delta_+)} < 1 \tag{6.32}$$

So the occupation number of these spin-wave modes will then be

$$\frac{1}{e^{c\xi^{-1}/T} - 1} \approx \frac{T}{c\xi^{-1}} > 1 \tag{6.33}$$

The last occupation number is precisely that appearing in a classical description of thermally excited spin waves, which is the approach we shall follow here.

Another way to state the dominance of classical effects is to run the flow equation (6.8) backwards: going to higher T means that we are exploring shorter scales and higher energies, at which (6.10) implies an effective coupling $g \sim 1/\ln(T/\Delta_+)$, which is small. The coupling g controls the strength of the quantum fluctuations, and these are therefore expected to be subdominant. This latter argument will be made more precise in the following discussion.

We begin our analysis by first focusing on the static and thermodynamic correlations in this region. We shall use a method introduced by Luscher [312], and the same method will be of considerable use to us in subsequent chapters. The main idea is to develop an effective action for only the *zero Matsubara frequency* ($\omega_n = 0$) components of $\mathbf{n}$ after

integrating out all the $\omega_n \neq 0$ modes. We will do this first for the correlation length in this and the following subsection. We will turn to the thermodynamic uniform susceptibility in Section 6.3.2, and to the dynamical properties in Section 6.3.3.

The effective action for the zero frequency modes can be obtained in the same background field method discussed in Section 6.1: we just identify the $\mathbf{n}_<$ modes with the zero frequency components, and the $\vec{\pi}$ fields with all finite frequency components. Then it is easily seen that the effective action for $\mathbf{n}_<$ has precisely the same form as the $d = 1$ *classical ferromagnet* discussed in Section 2.3, with partition function (2.68) at $\widetilde{\mathbf{h}} = 0$; for our purposes we write this as

$$\mathcal{Z} = \int \mathcal{D}\mathbf{n}(x)\delta(\mathbf{n}^2 - 1)\exp\left(-\frac{(N-1)\xi}{4}\int dx \left(\frac{d\mathbf{n}(x)}{dx}\right)^2\right) \quad (6.34)$$

where ξ is already known from Section 2.3 to be the spatial correlation length. (Actually we have usually reserved ξ to be the symbol for the equal time correlations, while the present approach gives the correlation length for the zero frequency correlations; as we will see in Section 6.3.3, these two lengths are asymptotically equal because of the dominance of classical thermal fluctuations). Generalizing (6.7) to the present situation we have

$$\begin{aligned}
\frac{(N-1)\xi T}{2} &= \frac{cN}{g} - c^2(N-2)\int^\Lambda \frac{dk}{2\pi}T\sum_{\omega_n \neq 0}\frac{1}{c^2k^2 + \omega_n^2} + \cdots \\
&\approx \frac{cN}{g} - \frac{c(N-2)}{2\pi}\ln\left(\frac{\Lambda}{T}\right) \quad (6.35)
\end{aligned}$$

where in the second equation we have ignored constants on order unity. Now we can use (6.10) to eliminate Λ, and we find

$$\xi = \frac{c(N-2)\ln(T/\Delta_+)}{T\pi(N-1)}, \quad (6.36)$$

in agreement with (5.79). Notably, dependence on g has also disappeared. This is not an accident–the renormalization group was designed to make this happen order-by-order in g, and all physical properties depend only upon the measurable ratio Δ_+/T.

Actually, it is possible to be quite precise about the omitted constants of order unity in the argument of the logarithm in (6.36). To do this requires use of the field-theoretic renormalization group, and this will be done in the following Section 6.3.1. The same method will be applied to the uniform susceptibility, χ_u in Section 6.3.2.

6.3.1 Field-theoretic renormalization group

A full description of this sophisticated approach is already available in a number of reviews in the literature [63, 550, 247] (we especially recommend the article by Brezin *et al.* [63] for a physical exposition), and the uninitiated reader is referred to these works for an in-depth treatment. Here we will be satisfied by noting the essential points, and quickly reviewing the computations necessary for our purposes.

To understand the low energy and long-distance limit of the $d = 1$ O(N) rotor model, it is necessary to understand the behavior of the couplings under changes of the cut-off Λ. Computationally, it is advantageous to replace the cut-off by a new renormalization scale, μ, defined in the following manner. We define the coupling constants and the scale of the fields by relating them to the values of suitably chosen Green's functions (computed in the presence of a cut-off Λ) at external momenta proportional to μ. This statement is often shortened to "define the couplings at the scale μ". Now if we take an arbitrary observable, and re-express it in terms of couplings defined at the scale μ, we will find that the resulting expressions are finite in the limit $\Lambda \to \infty$ (this is a consequence of the 'renormalizability' of the field theory). So we take just this limit in all Green's function, and are left with Λ-independent expressions in which we no longer have to deal with the (messy) details of the short distance cutoff. As an added bonus, the independence of the underlying physics on the arbitrary scale μ also yields the required renormalization group equations. For the case of the O(N) rotor model, only two redefinitions of coupling constants or field scales ('renormalizations') are necessary [65]: one renormalizing the coupling g to $g_R(\mu)$, and the other rescaling the overall field scale (related to the quasiparticle residue $\mathcal{A}$) by a factor $\overline{Z}$. Let us consider just the coupling constant renormalization for now. There is a multiplicative factor which relates g_R to the bare coupling constant, g in the theory with a cut-off Λ; in an expansion in powers of g_R, this factor is a function of $\ln(\Lambda/\mu)$. However, it is advantageous to regulate the ultraviolet behavior by dimensional regularization (which means evaluating all momentum integrals in $d = 1 - \epsilon$ spatial dimensions), in which case the logarithms turn into poles in ϵ. The explicit relationship between the bare and renormalized coupling was shown by Brezin and Zinn-Justin [65] to be

$$g = g_R(\mu)\mu^{-\epsilon}\left(1 + \frac{N-2}{2\pi N}\frac{g_R(\mu)}{\epsilon} + \mathcal{O}(g_R^2)\right). \tag{6.37}$$

Similarly the field rescaling factor is shown to be [65]

$$\overline{Z} = 1 - \frac{N-1}{2\pi N} g_R(\mu) + \mathcal{O}(g_R^2). \qquad (6.38)$$

It is now possible to state the simple, field-theoretic recipe for computing correlators of (5.16) in $d = 1$. First, obtain formal expressions for any rotationally invariant, physically observable correlator of the bare theory in an expansion in powers of g, and leave all the Feynman integrals as formal, unevaluated expressions. Next, perform the substitution (6.37) to replace g by g_R, and also multiply the correlator by a power of $\overline{Z}^{-1}$ for each power of the field **n** in the correlator. Now, evaluate all the integrals in $d = 1 - \epsilon$ dimensions, in powers of ϵ. The constants in (6.37) and (6.38) have been cleverly chosen so that all poles in ϵ cancel. The resulting expressions for the correlators of the theory are now expressed in terms of g_R, and the momentum scale μ, with no explicit dependence on Λ.

It would seem that not much has been achieved with this rather sophisticated transformation. We began with a theory with a dimensionless coupling g and a cut-off Λ: this cut-off was rather hard to deal with in computing Feynman graphs, especially multi-loop ones. We have ended up with a closely related theory with the same universal low energy properties: this theory is expressed in terms of a dimensionless coupling g_R, and a scale μ which plays the physical role of an ultraviolet cut-off. The latter theory is much easier to compute with, and so it seems is that all we have done is to devise a clever and convenient short-distance regularization which allows us to compute properties to a high order in g_R.

However there is an additional advantage to the second approach: by using the independence of the original bare theory on μ, it is possible to easily derive an *exact* renormalization group equation for the flow of $g_R(\mu)$, and all observables, under rescalings of the 'cut-off' $\mu \to \mu e^\ell$. Indeed, simply differentiating (6.37) with respect to μ at a fixed g, gives us the flow equation

$$\frac{dg_R}{d\ell} = \frac{N-2}{2\pi N} g_R^2, \qquad (6.39)$$

which is of course the same equation obtained earlier in (6.8). We are dealing with the coupling g_R rather than g, but this is physically innocuous as it is simply the consequence of trading the momentum cutoff Λ for a renormalization scale μ (which effectively plays the role of the cutoff). Similarly, the field-scale renormalization, $\overline{Z}$ also implies an ex-

act statement on the behavior of correlation functions under changes of μ. (Again we are not terribly concerned with the physical consequences of changing the scale of correlators of $\mathbf{n}$ as we will eventually set the overall amplitude of the structure factor using the physically measurable quasiparticle amplitude $\mathcal{A}$.) This is also discussed by Brezin and Zinn-Justin [65]; for the two-point correlator of $\mathbf{n}$ defined in (5.2) their result takes the form

$$\overline{Z}^{-1} C(x, t; g_R(\mu_1), \mu_1) = \left[\ln\left(\frac{\mu_1}{\mu_2}\right)\right]^{\frac{(N-1)}{(N-2)}} \overline{Z}^{-1} C(x, t; g_R(\mu_2), \mu_2).$$

(6.40)

We will have several occasions to use this fundamental relation later.

Let us return to the physical problem of computing the correlation length using the present field-theoretic approach. The consequences of the above recipe are simple: we take the formal expression represented by the first equation in (6.35), perform the substitution in (6.37) to replace g by $g_R(\mu)$, and then evaluate the integrals in $d = 1 - \epsilon$ dimensions. Let us specify a few steps required in the latter evaluation:

$$T \sum_{\omega_n \neq 0} \int \frac{d^{1-\epsilon}k}{(2\pi)^{1-\epsilon}} \frac{1}{c^2 k^2 + \omega_n^2}$$

$$= \int \frac{d^{1-\epsilon}k}{(2\pi)^{1-\epsilon}} \left[T \sum_{\omega_n \neq 0} \frac{1}{c^2 k^2 + \omega_n^2} - \int \frac{d\omega}{2\pi} \frac{1}{c^2 k^2 + \omega^2 + T^2} \right]$$

$$+ c^{1-\epsilon} \int \frac{d^{2-\epsilon}p}{(2\pi)^{1-\epsilon}} \frac{1}{c^2 p^2 + T^2}$$

$$= \frac{1}{c} \left(\frac{T}{c}\right)^{-\epsilon} \left\{ \int \frac{d^{1-\epsilon}k}{(2\pi)^{1-\epsilon}} \left[\frac{1}{2k} \coth \frac{k}{2} - \frac{1}{k^2} - \frac{1}{2\sqrt{k^2+1}} \right] \right.$$

$$\left. + \frac{\Gamma(\epsilon/2)}{(4\pi)^{1-\epsilon/2}} \right\}$$

(6.41)

We are only interested in the poles in ϵ and the accompanying constants, and to this accuracy the first integral on the right hand side can be evaluated directly at $\epsilon = 0$, while the Γ function yields a $1/\epsilon$ term. Now inserting (6.41) and (6.37) into the first equation in (6.35), we find that all the poles in ϵ cancel in the resulting expression, and we get

$$\frac{(N-1)\xi T}{2c} = \frac{N}{g_R(\mu)} - \frac{(N-2)}{2\pi} \ln(\mu/T\sqrt{\mathcal{C}})$$

(6.42)

where the constant $\mathcal{C}$ was defined in (5.80). Rather than leave this expression in terms of μ and $g_R(\mu)$, it is conventional to express the

result in terms of the so-called 'renormalization group invariant $\Lambda_{\overline{MS}}$'. This is a somewhat unfortunate conventional notation for this quantity, as it suggests that $\Lambda_{\overline{MS}}$ is some sort of cutoff. In fact it is not, and is really a quantity which is closely analogous to the momentum scale Δ_+/c which is related to the energy gap, or the $T = 0$ correlation length. In the language of Section 2.1.1, $\Lambda_{\overline{MS}}^{-1}$ is a "large" length scale, rather than a "short" scale. The basic idea behind the definition of $\Lambda_{\overline{MS}}$ is as follows. Choose any physically measurable length scale associated with $d = 1$ rotor model at $T = 0$ you wish. By simple dimensional analysis, this scale must be of the form $(1/\mu) \times$ some function of $g_R(\mu)$. Now as this scale is physically measurable, it must not depend upon the choice of μ, *i.e.*, the resulting combination should be invariant under the flow equation (6.37). This turns out to be a very strong restriction: up to an arbitrary overall numerical factor, it turns out there is only one such function. We choose this overall factor by convention and call the result $\Lambda_{\overline{MS}}$: by integration of the two-loop version of the flow equation, we define, following Ref [312]

$$\Lambda_{\overline{MS}} = \mu\sqrt{\mathcal{C}} \left(\frac{(N-2)}{2\pi N} g_R \right)^{-1/(N-2)} \exp\left(-\frac{2\pi N}{g_R(N-2)} \right). \quad (6.43)$$

The constant $\mathcal{C}$ in the prefactor is purely for convenience and arbitrarily chosen.

Now the implication of the reasoning above is that *all* $T = 0$ measurable length scales are universal numbers times $\Lambda_{\overline{MS}}^{-1}$, and cannot depend separately upon μ and $g_R(\mu)$; similarly all measurable length scales at $T > 0$ are $\Lambda_{\overline{MS}}^{-1}$ times universal functions of the dimensionless ratio $c\Lambda_{\overline{MS}}/T$. It is easy to verify that this holds for our expression for the correlation length in (6.42): solving (6.43) for $g_R(\mu)$ and substituting in (6.42) we find

$$\xi(T) = \frac{c(N-2)}{T\pi(N-1)} \left\{ \ln\left[\frac{\mathcal{C}T}{c\Lambda_{\overline{MS}}} \right] \right.$$
$$\left. + \frac{1}{(N-2)} \ln\ln\frac{T}{c\Lambda_{\overline{MS}}} + \mathcal{O}\left(\frac{\ln\ln(T/c\Lambda_{\overline{MS}})}{\ln(T/c\Lambda_{\overline{MS}})} \right) \right\} (6.44)$$

As expected, the scale μ has completely dropped out.

However, the expression (6.44) is not very useful as it stands: it involves the scale $\Lambda_{\overline{MS}}$ which was defined by convention in the dimensional regularization scheme, and is not a priori known for any physical system. To make it useful, we need to relate $\Lambda_{\overline{MS}}$ to some other physical observable. We have consistently been using the $T = 0$ energy gap Δ_+

to characterize the ground state, and so it would be useful to know the universal dimensionless ratio $\Delta/c\Lambda_{\overline{MS}}$: this was computed recently by Hasenfratz and Niedermayer [216, 215] using the Bethe ansatz solution of the σ-model; they obtained

$$\frac{\Delta_+}{c\Lambda_{\overline{MS}}} = \frac{(8/e)^{1/(N-2)}}{\Gamma(1 + 1/(N-2))}. \tag{6.45}$$

The results (6.44,6.45) constitute the more precise form of (6.36). Explicitly, for the case $N = 3$ we have the exact leading result for the correlation length

$$\xi(T) = \frac{c}{2\pi T} \ln\left(\frac{32\pi e^{-(1+\gamma)}T}{\Delta_+}\right), \tag{6.46}$$

where γ is Euler's constant.

6.3.2 Computation of χ_u

This section will determine the uniform susceptibility, χ_u, by a strategy similar to that employed above in the computation of $\xi(T)$: place the system in an external magnetic field $\mathbf{H}$, integrate out the non-zero frequency modes, and then perform the average over the zero frequency fluctuations. We choose an $\mathbf{H}$ which rotates $\mathbf{n}$ in the 1–2 plane, and use (6.5) to integrate out the non-zero frequencies. Therefore the fields $\mathbf{n}_<$, $\mathbf{e}_a$ are independent of τ, while the π_a have no zero frequency components. It is also clear that the fields $\mathbf{n}_<(x)$ are simply the $\mathbf{n}(x)$ fields appearing in (6.34). We expand the partition function to quadratic order in $\mathbf{H}$, drop all terms proportional to the spatial gradients of $\mathbf{n}(x)$ or $\mathbf{e}_a(x)$ (these can be shown to yield logarithmically subdominant contributions to χ_u), and find that the $\mathbf{H}$ dependent terms in the free energy density are

$$-\frac{N\mathbf{H}^2}{2cg}\left[(n_1^2 + n_2^2)\left(1 - \sum_a \langle \pi_a^2 \rangle\right) + \sum_{ab}(e_{a1}e_{b1} + e_{a2}e_{b2})\langle \pi_a \pi_b \rangle\right.$$
$$-\frac{N}{cg}\sum_{abcd}(e_{a1}e_{b2} - e_{a2}e_{b1})(e_{c1}e_{d2} - e_{c2}e_{d1})$$
$$\left.\times \int dx d\tau \langle \pi_a \partial_\tau \pi_b(x, \tau); \pi_c \partial_\tau \pi_d(0, 0)\rangle\right] \tag{6.47}$$

Evaluating the expectation values of the π fields, and using orthonormality of the vectors $\mathbf{n}$, $\mathbf{e}_a$, the expression (6.47) simplifies to

$$-\frac{N\mathbf{H}^2}{2cg}\left[(n_1^2 + n_2^2)\left(1 - \frac{c(N-2)g}{N}T\sum_{\omega_n \neq 0}\int\frac{dk}{2\pi}\frac{1}{c^2k^2 + \omega_n^2}\right)\right.$$
$$\left.+\frac{2cg}{N}(1 - n_1^2 - n_2^2)T\sum_{\omega_n \neq 0}\int\frac{dk}{2\pi}\frac{c^2k^2 - \omega_n^2}{(c^2k^2 + \omega_n^2)^2}\right] \tag{6.48}$$

Finally to obtain the susceptibility χ_u, we have to evaluate the expectation value of the zero frequency field $\mathbf{n}$ under the partition function (6.34). This simply yields $\langle n_1^2 \rangle = \langle n_2^2 \rangle = 1/N$. The first frequency summation is precisely the same as that evaluated earlier for ξ in the first equation in (6.35), while the second is explicitly finite in $d = 1$ and can directly evaluated; in this manner we obtain our final result for χ_u:

$$\chi_u(T) = \frac{2}{N}\left[\frac{(N-1)T\xi}{2c^2} - \frac{(N-2)}{2\pi c}\right]$$
$$= \frac{(N-2)}{N\pi c}\ln\left(\frac{\mathcal{C}T}{c\Lambda_{\overline{MS}}e}\right) \tag{6.49}$$

We have omitted the form of the subleading logarithms, which are the same as those in (6.44). Again, let us quote the explicit expression for χ_u for $N = 3$:

$$\chi_u(T) = \frac{1}{3\pi c}\ln\left(\frac{32\pi e^{-(2+\gamma)}T}{\Delta_+}\right). \tag{6.50}$$

It is useful to compare the $T \gg \Delta_+$ expression (6.50) for χ_u with the $T \ll \Delta_+$ result in (6.12): the two expressions are roughly equal for $T \approx \Delta$ suggesting that one or the other of the two asymptotic limits is always reasonable.

6.3.3 Dynamics

We have now assembled all the ingredients necessary for a complete description of the low frequency dynamics. The key observation, made above (6.33), is that the energy, ω, of the characteristic excitation obeys $\omega \ll T$. We expect the spectral density, $\mathrm{Im}\chi(k,\omega)$ to be dominated by weight at such frequencies, and the fluctuation-dissipation theorem (4.9) then takes it 'classical' form in (4.92). We will work here with an effective theory in which (4.92) is obeyed exactly, and so the equal-time structure factor, $S(k)$, is related to the static susceptibility, $\chi(k)$, by

$S(k) = T\chi(k)$, as in (4.93). However, the static susceptibility is given by the two-point correlator of the $\omega_n = 0$ components of the $\mathbf{n}$ field, and these are determined by the effective action (6.34). So we arrive at the important conclusion that (6.34) yields the *equal-time* correlators of $\mathbf{n}$ in the limit that the classical fluctuation dissipation theorem in (4.92) is obeyed.

How do we extend (6.34) to unequal time correlations ? Recall that in classical statistical mechanics equal time correlations are given by an integral over configuration space (as in $\int dq$), while an extension to dynamics requires an integral over phase space (as in $\int dpdq$). Furthermore, the integral over the conjugate momenta simply factorizes, and for equal time correlations we can return to the configuration space formalism. So here, we need to extend (6.34) by finding the appropriate integral over conjugate momenta. The conjugate momentum of the rotor orientation $\mathbf{n}$ is clearly the rotor angular momenta $\mathbf{L}$. So we treat $\mathbf{L}$ also as a classical variable, and generalize (6.34) to a "$\int dqdp$" integral of the form (we will specialize the remainder of the discussion to the special case $N = 3$):

$$\mathcal{Z} = \int \mathcal{D}\mathbf{n}(x)\mathcal{D}\mathbf{L}(x)\delta(\mathbf{n}^2 - 1)\delta(\mathbf{L} \cdot \mathbf{n}) \exp\left(-\frac{\mathcal{H}_c}{T}\right)$$

$$\mathcal{H}_c = \frac{1}{2}\int dx\left[T\xi\left(\frac{d\mathbf{n}}{dx}\right)^2 + \frac{1}{\chi_{u\perp}}\mathbf{L}^2\right], \tag{6.51}$$

$\mathbf{L}$, $\mathbf{n}$ are classical commuting variables. The second term in $\mathcal{H}_c$ was absent in (6.34), and represents the kinetic energy of the classical rotors: integrating out $\mathbf{L}$ we obtain (6.34) as we should. The value of the coupling $\chi_{u\perp}$ in the kinetic energy can be determined by a simple argument. It is clear that an external field $\mathbf{H}$ will couple to the total angular momentum, and will therefore modify the classical Hamiltonian by

$$\mathcal{H}_c \rightarrow \mathcal{H}_c - \int dx\mathbf{H} \cdot \mathbf{L}. \tag{6.52}$$

Evaluating then linear response of (6.51) shows that

$$\chi_u = \frac{2}{N}\chi_{u\perp} \tag{6.53}$$

with $N = 3$ (we have given, without proof, the expression for general N); the factor of $2/3$ comes from the constraint $\mathbf{L} \cdot \mathbf{n} = 0$. Using (6.49), we then have the value of $\chi_{u\perp}$. It should also be clear from this discussion that $\chi_{u\perp}$ has a simple physical interpretation: it is the susceptibility to a

field oriented perpendicular to the local direction of the order parameter **n**.

Finally, to proceed to unequal time correlations, we need the equations of motion obeyed by the classical **n**, **L** fields. A direct approach is to compute the quantum equations of motion, and then to simply treat the quantum operators $\hat{\mathbf{n}}$ and $\hat{\mathbf{L}}$ as classical c-numbers: this is valid because the expectation value of any term will be dominated by large values as in (6.33), and any effects from non-commutativity will be suppressed. A quicker way to obtain the answer is to realize that the same result is obtained by replacing the quantum commutators by Poisson brackets, and generating the Hamilton-Jacobi equations of the Hamiltonian $\mathcal{H}_c$. The required Poisson brackets here are the continuum classical limit of the commutation relations (1.19):

$$
\begin{aligned}
\{L_\alpha(x), L_\beta(x')\}_{PB} &= \epsilon_{\alpha\beta\gamma} L_\gamma(x)\delta(x - x') \\
\{L_\alpha(x), n_\beta(x')\}_{PB} &= \epsilon_{\alpha\beta\gamma} n_\gamma(x)\delta(x - x') \\
\{n_\alpha(x), n_\beta(x')\}_{PB} &= 0.
\end{aligned}
\tag{6.54}
$$

From this, and (6.51), we obtain directly the equations of motion for the quasi-classical waves

$$
\begin{aligned}
\frac{\partial \mathbf{n}}{\partial t} &= \{\mathbf{n}, \mathcal{H}_c\}_{PB} \\
&= \frac{1}{\chi_{u\perp}} \mathbf{L} \times \mathbf{n} \\
\frac{\partial \mathbf{L}}{\partial t} &= \{\mathbf{L}, \mathcal{H}_c\}_{PB} \\
&= (T\xi)\mathbf{n} \times \frac{\partial^2 \mathbf{n}}{\partial x^2}.
\end{aligned}
\tag{6.55}
$$

To compute the needed unequal time correlation functions, pick a set of initial conditions for $\mathbf{n}(x)$, $\mathbf{L}(x)$ from the ensemble (6.51). Evolve these deterministically in time using the equations of motion (6.55). The value of the correlator is then the product of the appropriate time-dependent fields, averaged over the set of all initial conditions. We also note here that simple analysis of the differential equations (6.55) shows that small disturbances about a nearly ordered **n** configuration travel with a characteristic velocity $c(T)$ given by

$$
c(T) = (T\xi(T)/\chi_{u\perp}(T))^{1/2},
\tag{6.56}
$$

which is a basic relationship between thermodynamic quantities and the velocity $c(T)$. Notice from (6.44) and (6.49) that to leading logarithms

$c(T) \approx c$, but the second term in the first equation of (6.49) already shows that this result is not satisfied by the subleading terms.

Before relating the required correlators of the quantum model for $T \gg \Delta_+$ to the classical model defined above, we need to settle one final issue: that of the overall scale of the fields $\mathbf{n}$, $\mathbf{L}$. The scale of $\mathbf{L}$ is easy to set— it is specified completely by the coupling to the field $\mathbf{H}$ in (6.52), and by the first of the Poisson bracket relations in (6.54). These take the same values in the underlying quantum model and undergo no renormalization upon integrating out the finite frequency degrees of freedom. We have therefore

$$C_{u,\alpha\beta}(x, t) = \langle L_\alpha(x, t) L_\beta(0, 0) \rangle_c \tag{6.57}$$

where the subscript c represents the averaging procedure discussed below (6.55). The argument for the field scale of $\mathbf{n}$ is somewhat more subtle. So far the only parameter which has been sensitive to the scale of the order parameter has been the quasi-particle amplitude $\mathcal{A}$, which was defined from the residue of the quasi-particle pole at $T = 0$. In contrast, we need the overall scale of $\mathbf{n}$ at a temperature $T \gg \Delta_+$. The matching between these two scales can however be performed with the aid of the renormalization group invariance equation (6.40) which was noted earlier. Now the quasi-particle amplitude $\mathcal{A}$ is naturally defined at a scale $\mu_1 \sim \Delta_+$, where the coupling g_R is of order unity. On the other hand, the integration out of finite frequency modes and the derivation of the effective action for the zero frequency modes is most easily done at $\mu_2 \sim T$,as the coupling $g_R \sim 1/(\ln(T/\Delta_+))$ and the perturbation theory will be free of large logarithms. The two scales can be related via (6.40), and in this way we obtain the required result

$$C_{\alpha\beta}(x, t) = \mathcal{A}\widetilde{\mathcal{C}} \left[\ln \left(\frac{T}{\Delta_+} \right) \right]^{\frac{(N-1)}{(N-2)}} \langle n_\alpha(x, t) n_\beta(0, 0) \rangle_c \tag{6.58}$$

The constant $\widetilde{\mathcal{C}}$ is an unknown pure, universal number which cannot be obtained by the present methods. It could, in principle, be obtained from the Bethe-ansatz solution.

Let us now examine the structure of the classical dynamics problem defined by (6.51) and (6.55). It obeys that the crucial property of being free of all ultraviolet divergences: this is clear from the analysis of equal time correlations in Section 2.3, and the unequal time perturbation theory discussed in Ref [69]. Consequently, we may determine its characteristic length and time scales by simple engineering dimensional analysis, as no short distance cutoff scale is going to transform into an

anomalous dimension. Indeed, a straightforward analysis which shows that this classical problem is free of dimensionless parameters, and is a *unique*, parameter-free theory. This is seen by defining

$$
\begin{aligned}
\overline{x} &= \frac{x}{\xi} \\
\overline{t} &= \frac{t}{\tau_\varphi} \\
\overline{\mathbf{L}} &= \mathbf{L}\sqrt{\frac{\xi}{T\chi_{u\perp}}},
\end{aligned} \tag{6.59}
$$

where we have anticipated that the characteristic time, τ_φ, will be the phase coherence time, and it is given by

$$
\tau_\varphi = \sqrt{\frac{\xi\chi_{u\perp}}{T}}; \tag{6.60}
$$

then inserting these into (6.51) and (6.55), we find that all parameters disappear and the partition function and equations of motion acquire a unique, dimensionless form, given by setting $T = \xi = \chi_{u\perp} = 1$ in them.

The above transformations allow us to obtain scaling forms for the dynamic observables in terms of, as yet undetermined, universal functions.

First, consider the correlators of $\mathbf{n}$. The equal time two-point correlations of (6.34) are known from Section 2.3 to decay simply as $e^{-|x|/\xi}/3$; from these and (6.58), we deduce that the equal-time structure factor $S(k)$ (defined in (4.5)) is given by

$$
T\chi(k) = S(k) = \mathcal{A}\widetilde{\mathcal{C}}\left[\ln\left(\frac{T}{\Delta_+}\right)\right]^{\frac{(N-1)}{(N-2)}}\frac{2\xi/3}{(1+k^2\xi^2)}. \tag{6.61}
$$

For the dynamic structure factor, $S(k,\omega)$, (6.59) implies a scaling form similar to (4.95)

$$
\frac{2T}{\omega}\mathrm{Im}\chi(k,\omega) = S(k,\omega) = S(k)\tau_\varphi\Phi_{Sc}(k\xi,\omega\tau_\varphi), \tag{6.62}
$$

where Φ_{Sc} is a universal scaling function, normalized as in (4.96). Also, because the equations of motion are classical, the relation (4.92) is obeyed exactly, and Φ_{Sc} is an even function of $\overline{\omega}$. For further information on the structure of Φ_{Sc} we refer to a recent paper [69], which used a combination of analytic and numerical methods. At sufficiently large $k\xi$, we expect a pair of broadened, reactive, 'spin-wave' peaks at $\omega \approx c(T)k$ (with $c(T)$ given in (6.56)), which are similar to those found
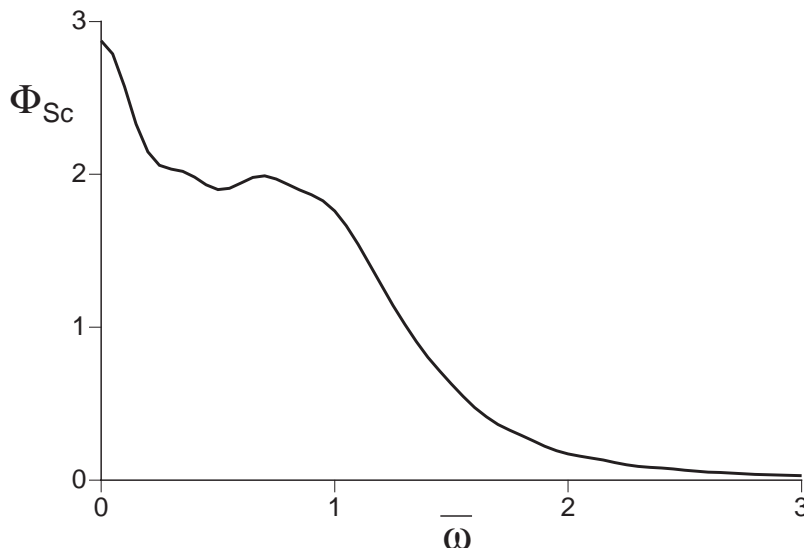
Fig. 6.4. Numerical results of Ref [69] for the scaling function $\Phi_{Sc}(0,\overline{\omega})$ appearing in (6.62).

in the high T limit of the quantum Ising chain in Fig 4.12. For the opposite limit of small $k\xi$, we present the numerical results of Ref [69] for $\Phi_{Sc}(0,\overline{\omega})$ in Fig 6.4. There is a sharp relaxational peak at $\overline{\omega} = 0$, which is again similar to that found in the high T limit of the quantum Ising chain in Fig 4.12. However, there is now a well-defined shoulder at $\overline{\omega} \approx 0.7$ which was not found in the Ising case. This shoulder is a remnant of the large N result (5.22) which predicts a delta function $\omega = \pm m$, with m given by (5.79) in the present large N limit. So $N = 3$ is large enough for this finite frequency oscillation to survive in the high T limit.

There is alternative, helpful way to view this oscillation frequency. Even though we are considering a theory with a unit length field $\mathbf{n}$, correlations of $\mathbf{n}$ decay exponentially on a scale ξ. So if we imagine coarse-graining out to the length ξ, there will be large *amplitude fluctuations* in the coarse-grained field, and it is then useful to visualize an effective field ϕ_α with no length constraint, as we discussed in Section 3.1. As this field ϕ_α is spatially disordered, we expect its effective potential to have a minimum near $\phi_\alpha = 0$. The finite frequency in Fig 6.4 is then due to the harmonic oscillations of ϕ_α about this potential minimum. This is

interpretation is also consistent with the large N limit, in which angular and amplitude fluctuations are not distinguished. The above argument could also have been applied to the quantum Ising chain, but the absence of such a reactive peak at $k = 0$ in Fig 4.12 indicates that $N = 1$ is too far from $N = \infty$ for any remnant of this large N physics to survive. We will meet related phenomena in our study of a quasi-classical wave model for the high T limit in $d = 2$ in Section 8.3.

We turn next to the correlators of $\mathbf{L}$. The long-time behavior of these was examined numerically in Ref [69], and it was found to be consistent with the diffusive form (6.2). We already know the value of the uniform susceptibility χ. For the spin diffusion constant D_s, we can deduce simply from the fact that it has dimension (length)^2/time, and from (6.59) that it must obey

$$D_s = \mathcal{B}\frac{T^{1/2}\varsigma^{3/2}}{\chi_{u\perp}^{1/2}} \tag{6.63}$$

where $\mathcal{B}$ is a universal number. The numerical estimate [69] is $\mathcal{B} \approx xxxxxx$.

6.4 Summary

We summarize the basic properties of the two regimes in Figs 5.1 and 6.1 in Fig 6.5. We also recall that in the low T region, the dynamic structure factor, $S(k, \omega)$, has most of weight in a frequency window about $\omega = \Delta_+$ of width $1/\tau_\varphi$. In the high T region, $S(k, \omega)$ becomes an even function of ω and most of its weight is in a window of width $1/\tau_\varphi$ centered around $\omega = 0$.

6.5 Applications and extensions

We have already seen in Section 5.1.1.1 that the $d = 1$, O(3) quantum rotor model describes the so-called two-leg ladder antiferromagnets [34, 114]. There are materials, like $SrCu_2O_3$ [34], which consist of two adjacent $S = 1/2$ spin chains, with neighboring spins on the two chains coupled to each other like the rungs of a ladder; thus, they are modeled by (5.7) for the case where the sum over i, j extends a simple one dimensional chain. Actually, as we will see in Section 13.3.1, a much broader class of $d = 1$ antiferromagnets is described by the O(3) rotor model, including spin chains in which the individual spins have inte-

Fig. 6.5. Values of the correlation length, ξ (defined from the exponential decay of the equal-time correlations of $\mathbf{n}$), the uniform spin susceptibility, χ_u, the phase coherence time, τ_φ, and the spin diffusion constant, D_s, for the two regimes in Figs 5.1 and 6.1. Results are for $N = 3$, although many results for general $N \geq 3$ appear in the text. There is a large length scale, ξ_c, in the low T region, which was given in (6.21) and does not appear below; this is the spacing between the thermally excited particles.

	Low T Quasi-classical particles	High T Quasi-classical waves
ξ	$\dfrac{c}{\Delta_+}$	$\dfrac{c}{2\pi T} \ln\left(\dfrac{32\pi e^{-(1+\gamma)} T}{\Delta_+} \right)$
χ_u	$\dfrac{1}{c} \left(\dfrac{2\Delta_+}{\pi T} \right)^{1/2} e^{-\Delta_+/T}$	$\dfrac{1}{3\pi c} \ln\left(\dfrac{32\pi e^{-(2+\gamma)} T}{\Delta_+} \right)$
τ_φ	$\dfrac{\sqrt{\pi}}{3T} e^{\Delta_+/T}$	$\left(\dfrac{3\xi\chi_u}{2T} \right)^{1/2}$
D_s	$\dfrac{c^2 e^{\Delta_+/T}}{3\Delta_+}$	$xxxxx\xi \left(\dfrac{T\xi}{\chi_u} \right)^{1/2}$

ger spin S. The mapping to the rotor model requires that all of these antiferromagnets have an energy gap above the ground state.

There have been a very large number of experimental studies of such one-dimensional antiferromagnets. For example, in the neutron scattering study of the $S = 1$ spin chain compound Y_2BaNiO_5, Xu *et al.* [532] present clear evidence for a triplet particle in the low T spectral density, along with the long phase coherence time associated with its presence [532, 1]. Thermodynamic and NMR measurements on $S = 1$ spin chains and spin ladders have been surveyed by Itoh and Yasuoka [243]: a striking feature of the data is that the energy gaps measured in activation plots of the NMR relaxation rate $1/T_1$ are about 1.5 times the measured gap in a thermodynamic measurement of the uniform susceptibility. It was argued in Ref [117] that this feature could be quite generally explained by the picture of low T spin diffusion developed in Section 6.2 and the value of the spin diffusivity in (6.27). Detailed comparisons [117] of the ballistic to diffusive crossover in (6.23) have been made against NMR experiments by Takigawa *et al.* [485] on the $S = 1$ spin chain compound $AgVP_2S_6$.

As we will see in Chapter 13, the high T analysis of Section 6.3 applies to spin chains with larger values of S, or to spin ladders with greater than two legs, at intermediate temperatures; the precise limits on experimental applicability are discussed in Ref [69]. Explicit comparisons of the thermodynamic predictions in Section 6.3 have been made against Monte Carlo data for $S = 2$ chains by Kim *et al.* [271], with reasonable agreement. Experimental studies of $S = 2$ chains have also been undertaken [186] recently, and there are interesting prospects for confrontation between theory and experiments on dynamical properties in future work. Dynamical measurements have been made on two-leg ladder compounds at higher temperatures [268] and the results have an interesting qualitative similarity to (6.63).

7

The $d = 2$, $O(N \geq 3)$ rotor models

The large N limit of quantum rotor models in $d = 2$ was examined in Chapter 5, and led to the phase diagram shown in Fig 5.2. There we claimed that the large N results provided a satisfactory description of the crossovers in the static and thermodynamic observables for $N \geq 3$. We shall establish this claim in this chapter, and also treat the dynamic correlations of $\mathbf{n}$ at nonzero temperatures. The discussion of the dynamics shall take place in a physical framework suggested by the modified version of Fig 5.2 shown in Fig 7.1. The low T region on the quantum paramagnetic side can be described in an effective model of quasi-classical particles which is closely related to those developed in Sections 4.5.2 and 6.2. On the other low T region on the magnetically ordered side, we shall obtain a 'dual' model of quasi-classical waves, which is connected to that developed in Section 6.3. Finally, in the intermediate 'quantum critical' or continuum high T region, neither of these descriptions is adequate: quantum and thermal, particle- and wave-like behavior, all play important roles, and we shall use a menage of these concepts to obtain a complete picture in this, and the following two chapters.

The results for the quasi-classical wave regime described in this chapter will be obtained by a combination of analytical and numerical techniques, which become exact in the low T limit. For the other two regions, we shall use the large N expansion. This approximate approach is satisfactory for most purposes, but fails in the very low frequency regime, $\omega \ll T$. A proper description of the low frequency dynamical correlators of $\mathbf{n}$ must await alternative techniques which will be developed in Chapter 8 and Section 8.3.

The cases $N = 1, 2$, $d = 2$ are special because they permit phase transitions at non-zero temperatures, and their crossover phase diagrams
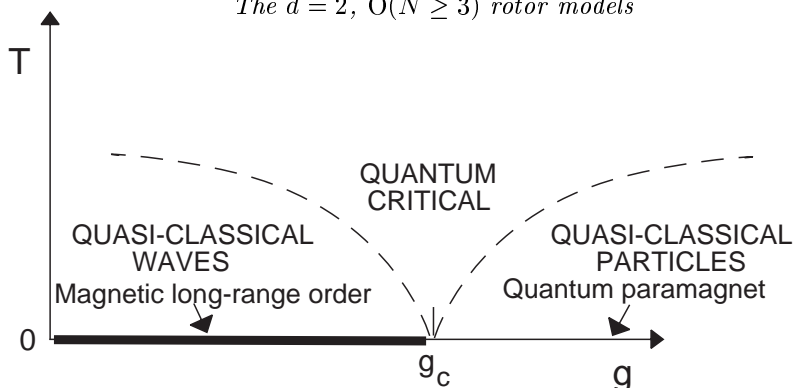
Fig. 7.1. Modified version of Fig 5.2 for the crossovers for the rotor model (5.1,5.16) for $d = 2$, $N \geq 3$. While quasi-classical descriptions of the dynamics and transport can be developed in the two low T regions, the behavior in the 'quantum critical' or 'continuum high T' region is more complex, with thermal and quantum, and particle- and wave-like phenomena playing equal roles. We shall show in Section 8.3 that, to leading order in $\epsilon = 3 - d$, the low frequency correlators of $\mathbf{n}$ in the quantum critical region are described an effective quasi-classical wave model. On the other hand, the transport of the conserved $\mathbf{L}$ in the quantum critical region is dominated by higher energy excitations, and requires a particle-like description in a quantum Boltzmann equation which will be discussed in Chapter 9.

are of the form in Fig 5.3: we will not treat the ordered phases, or the vicinity of the nonzero temperature transition, in this chapter, but defer their discussion to Chapter 8. In principle, the results obtained for the low T region on the quantum paramagnetic side, and for the continuum high T region (see Fig 5.3), apply for all N, including $N = 1, 2$. However, the caveats mentioned in the previous paragraph on the failure of the large N expansion at low frequencies apply even more strongly to $N = 1, 2$, and the dynamics for these cases is best understood using the methods of Chapters 8 and 9. Nevertheless, we will quote our results in this chapter for these two regions for all values of N.

We shall not consider time-dependent correlations of the angular momentum $\mathbf{L}$ in this chapter. The conservation of the total $\mathbf{L}$ implies that its low frequency dynamics obeys the diffusive form (6.2). So the problem reduces to the determination of a 'transport coefficient' (the spin diffusion constant D_s), and we shall defer discussion of the transport problem to Chapter 9.

The main purpose of this chapter shall be a more complete description of the basic scaling forms for nonzero temperature correlations of $\mathbf{n}$

introduced in Section 5.4. In $d = 2$, on the magnetically ordered side
($g < g_c$), the scaling ansatz (5.60) is

$$\chi(k, \omega) = \frac{Z}{T^{(2-\eta)}} \Phi_- \left(\frac{ck}{T}, \frac{\omega}{T}, \frac{\rho_s}{NT} \right) \tag{7.1}$$

where we have set $z = 1$ and used the expression (5.54) for Δ_-, which
in $d = 2$ is simply

$$\Delta_- = \rho_s / N; \tag{7.2}$$

i.e., the $T = 0$ spin stiffness ρ_s is an energy which serves as a measure of
the deviation of the magnetically ordered ground state from the quantum
critical point; the factor of $1/N$ (7.2) is for future convenience, as ρ_s is
naturally of order N in the large N limit. Clearly ρ_s is defined only
for the case of models with a continuous symmetry, and so (7.1) applies
only for $N \geq 2$. For $g > g_c$ we have

$$\chi(k, \omega) = \frac{Z}{T^{(2-\eta)}} \Phi_+ \left(\frac{ck}{T}, \frac{\omega}{T}, \frac{\Delta_+}{T} \right) \tag{7.3}$$

characterizing the nonzero temperature behavior on the quantum para-
magnetic side for all N.

We will begin in Section 7.1 by treating the low T region on the mag-
netically ordered side of the $d = 2$ phase diagram in Fig 5.2; notice
that in this figure the magnetic long-range disappears at any non-zero
T: this will be shown below to happen for all $N \geq 3$, and we will only
consider these cases. The following Section 7.2 will then consider dy-
namical properties of the continuum high T and quantum-paramagnetic
low T regions of Fig 5.2 and 5.3, and describe the structure of the scaling
function in (7.3); in principle, these results apply for all N.

7.1 Low T on the magnetically ordered side, $T \ll \rho_s$

As noted above, we will only consider the case where magnetic order
disappears at any non-zero T, and this happens (as shown below) for all
$N \geq 3$. Recall that the quantum Ising chain, considered in Chapter 4,
also had the feature of losing magnetic order at any non-zero T (compare
the phase diagrams in Fig 4.3 and 5.2): we shall find here that the static
and dynamic properties of the $d = 2$ $N \geq 3$ rotor models in this low T
region are very similar to those discussed earlier for the corresponding
region of the quantum Ising chain in Section 4.5.1. However, our analysis
shall use techniques which are very similar to those developed earlier in
the 'classical wave' description of the high T region of the $d = 1$ rotor

model in Section 6.3. The reader is urged to review these sections before proceeding.

The key property of this region is the very large value of the correlation length, obtained earlier in (5.83) in the large N limit:

$$\xi_c \sim (c/T) \exp(2\pi\rho_s/NT). \tag{7.4}$$

We can use an argument similar to that following (6.31) for the $d = 1$ model, to establish the effective classical wave behavior of the system in this region; indeed the subscript c in (7.4) anticipates this. The typical wave excitations of the **n** field will have an energy $\sim c\xi_c^{-1}$, and therefore a thermal occupation number

$$\frac{1}{e^{c\xi_c^{-1}/T} - 1} \approx \frac{T}{c\xi_c^{-1}} \approx \exp\left(\frac{2\pi\rho_s}{NT}\right) \gg 1. \tag{7.5}$$

Therefore, as in Section 6.3, we can treat these waves classically. Note that the classical thermal fluctuations are exponentially preferred, unlike the much weaker logarithmic preference in Section 6.3. The exponential preference is similar to that found for the quantum Ising chain in Section 4.5.1, although there the reason was the energy gap towards creation of domain walls.

This low T region was studied in the influential paper of Chakravarty, Halperin and Nelson [83], where they called it "renormalized classical", as seems natural from the reasoning above. We have not used this name here to prevent confusion with other types of effectively classical behavior which appear in different regions of the phase diagram.

As in the Ising case, we can expect that static and dynamic correlations obey a reduced scaling form of two arguments. The analog of the expression (4.89) turns out to be

$$C(x, t) = N_0^2 \left(\frac{T}{\rho_s}\right)^{\frac{(N-1)}{(N-2)}} \Phi_c \left(\frac{x}{\xi_c}, \frac{t}{\tau_\varphi}\right) \tag{7.6}$$

where N_0 is the ground state ordered moment, Φ_c is a completely universal function to be determined by some effective classical model, and as before, τ_φ, is a characteristic phase coherence time which will be determined below. Unlike the Ising case, it is not possible to determine Φ_c exactly, although most of its qualitative properties can be described. There is an additional prefactor of a power of T/ρ_s in (7.6) which is not present in (4.89); note that this is a rather weak prefactor on the scale of ξ_c as $\ln \xi_c \sim \rho_s/T$. As we will discuss below, its origin is in the 'wavefunction renormalization' of the $D = 2$ nonlinear σ-model, which also

led to the logarithmic prefactor in (6.58) in the classical wave region of the $d = 1$ quantum rotor model. It is also easy to check from (5.62) that (7.6) is consistent with the global scaling form (7.1). Finally, note that (7.6) is consistent with the large N result obtained from (5.22), (5.48), and (5.58). Also, by matching scaling forms at $N = \infty$ we obtain the value $\tau_\varphi = \xi_c/c$; however, we had no damping in the dynamic suscepti- bility (5.22) at $N = \infty$, and so τ_φ cannot even be interpreted as a phase coherence time. We shall find that the value of the phase coherence time at finite N is different—$\tau_\varphi \sim (\rho_s/T)^{1/2}\xi_c/c$; this result is actually quite similar to that for the quantum Ising chain, where we obtained in (4.80) and (4.88), $\tau_\varphi \sim (\Delta/T)^{1/2}\xi_c/c$.

We will describe the computation of the exact values of ξ_c and τ_φ in the following subsections. A description of the function Φ_c will then follow.

7.1.1 Computation of ξ_c

The exact value of ξ_c, in the limit $T \ll \rho_s$, was obtained by Hasenfratz and Niedermayer [217] building upon foundations laid in Ref [83]. Here we shall obtain the result by a different method which has the advantage of connecting with results already obtained for the $d = 1$ case, and also allowing for a streamlined discussion of dynamic properties in subsequent subsections.

We begin by precisely defining ξ_c: the definition (7.6) leaves it unde- fined up to an overall constant which could be absorbed into a redefini- tion of Φ_c. It is then clear that demanding

$$\lim_{|\overline{x}| \to \infty} \Phi_c(\overline{x}, 0) \sim \frac{e^{-\overline{x}}}{\sqrt{\overline{x}}} \tag{7.7}$$

fixes ξ_c as the exponential decay rate of the long-distance equal-time correlations. The $\overline{x}$ dependent prefactor in (7.7) is the familiar 'Ornstein- Zernicke' form expected in the long-distance decay of a classical, two- dimensional disordered system (the expression (5.33) is of this form in $D = d + 1$ dimensions). The missing coefficient in (7.7) is universal, but its value is not known exactly: estimates have been made in the $1/N$ expansion [97] and in numerical simulations [462, 83].

As in Section 6.3, the inequality (7.5) suggests that we develop an effective action for the $\omega_n = 0$ component of $\mathbf{n}$ to describe its equal time correlations. A simple argument then suggests the form of the effective action. Recall that we have true long-range order in $\mathbf{n}$ at $T = 0$,

and we have denoted the exact spin stiffness of this ordered state as ρ_s (Section 5.3.3). The energy cost of any sufficiently slowly-varying static deformation $\mathbf{n}(x)$ can be computed using this stiffness, and so we obtain the following partition function for the equal-time correlations:

$$\mathcal{Z} = \int \mathcal{D}\mathbf{n}(x)\delta(\mathbf{n}^2 - 1) \exp\left(-\frac{\rho_s}{2T} \int d^2x \, (\nabla\mathbf{n})^2\right). \qquad (7.8)$$

This has the same form as the $d = 1$ classical wave model (6.34). The relationship of ρ_s to the couplings in the underlying quantum action (5.16) is not known exactly, and in general, quite difficult to determine. At $N = \infty$ we obtained the relationship specified by (5.58) and (5.25). For our purposes here, it will be useful to have an expression for ρ_s of the quantum model (5.16) in powers of g. Such an expansion can be obtained by a simple extension of the methods of Section 6.1. We take for $\mathbf{n}_<$ in (6.5) an externally imposed, long-wavelength, static deformation of $\mathbf{n}$, and then account for the quantum fluctuations by integrating out π fields at all wavevectors and frequencies at $T = 0$. The energy cost of such a deformation defines ρ_s, and this is obtained by the generalization of (6.7):

$$\rho_s = \frac{cN}{g}\left[1 - \frac{(N-2)g}{N}\int^\Lambda \frac{d^3p}{(2\pi)^3}\frac{1}{p^2} + \mathcal{O}(g^2)\right] \qquad (7.9)$$

where, as in Section 5.2, $p \equiv (\vec{k}, \omega/c)$, and the nature of the ultraviolet cutoff, Λ, was discussed below (5.16). We shall not need to specify the precise form of this cutoff, for the scaling properties of the quantum-critical point at $g = g_c$ imply that all observables become cut-off independent once expressed in terms of ρ_s and the ordered moment N_0, in place of the bare couplings in (5.16). So we shall really require the inverse of (7.9): a series for g in powers of $1/\rho_s$, which can, of course, be easily generated from (7.9). Notice also that the large N limit of (7.9) is consistent with (5.58) and (5.25).

Having determined ρ_s, let us return to the properties of the effective partition function (7.8) for the static fluctuations in $d = 2$. A little thought exposes a crucial difference from the corresponding model (6.34) in $d = 1$. In the latter case, the continuum theory (6.34) was ultraviolet finite and needed no short-distance regularization, and so the exact correlation length appeared as a coupling constant in (6.34), and completely specified the equal-time correlations of $\mathbf{n}$. In contrast, (7.8) is not well-defined as it stands. Indeed, the action (7.8) has precisely the same form as the $d = 1$ *quantum* rotor model at $T = 0$ studied in Section 6.1,

and was shown there to require some short-distance regularization (see the expression (6.10) for the energy gap). In the present situation, we do not have the luxury of choosing the form of this regularization. The partition function (7.8) is only an effective classical theory, and cannot be applied at distances so short that quantum effects become important. In particular, it cannot hold at wavevectors larger than where the energy of a spin wave $\sim ck$ becomes of order T. So quantum mechanics acts as an underlying high-momentum regularization of (7.8), at momenta of order $\Lambda_c \sim T/c$. We have added a subscript c to emphasize that this a cutoff for the classical theory; Λ_c is completely unrelated to the cutoff of the quantum theory Λ noted in (7.9). The latter has a non-universal nature, while the cutoff at momenta of order Λ_c has a universal form which will be elucidated below.

An important property of the model (7.8) emerged in the renormalization group analysis of Chapter 6. We showed that its long-distance properties did not depend separately upon its coupling ρ_s/T and its cutoff $\sim \Lambda_c$, but only upon a single renormalization group invariant $\Lambda_{\overline{MS}}$. Therefore the central task facing us is the determination of a precise expression for $\Lambda_{\overline{MS}}$ as a function of ρ_s/T and the momentum scale T/c. With this at hand, we obtain ξ_c by the analog of the Bethe-ansatz relation [215, 216] (6.45)

$$\xi_c^{-1} = \Lambda_{\overline{MS}} \frac{(8/e)^{1/(N-2)}}{\Gamma(1 + 1/(N-2))},\tag{7.10}$$

as the gap of the $d = 1$ quantum model at $T = 0$ becomes the exponential decay rate of correlations of the $d = 2$ classical model (7.8). We could also proceed, in principle, to use (7.8) to determine the entire function $\Phi_c(\overline{x}, 0)$.

One way to determine $\Lambda_{\overline{MS}}$ is to return to the underlying quantum model (5.16) and to directly compute the long-distance form of its equal-time correlators. This gives an expression for ξ_c in terms of c, g, and Λ; re-expressing g in terms of ρ_s using the inverse of (7.9), and matching against (7.10) we could then obtain the needed expression for $\Lambda_{\overline{MS}}$. This is clearly an intractable route, as it involves the physics of (7.8) in its strong-coupling regime. Instead, we shall use a simple trick which does the matching between the two theories in a weak-coupling regime.

Recall our discussion in Chapter 6 that the theory (7.8) is strongly-coupled at length scales longer than $\Lambda_{\overline{MS}}^{-1}$, and weakly-coupled at shorter scales. Clearly, we should do the matching between (7.8) and (5.16) in the latter regime. To do this, imagine restricting the spatial co-

ordinate, x, of both theories to an infinite cylinder of circumference L (the temporal direction of (5.16) remains unchanged). If we choose $L \ll \Lambda_{\overline{MS}}^{-1}$ then we will be in the weak-coupling regime, and can compute properties of both theories using perturbation theory. At the same time, we have to ensure that $L \gg c/T$ so that all length scales are longer than the inverse classical cutoff Λ_c^{-1}, we remain in the regime of effective classical behavior in model (5.16). Because $\Lambda_{\overline{MS}}^{-1} \sim \xi_c$ is exponentially large in $1/T$, these two conditions are easily compatible. Thus we have modified (7.8) to

$$\mathcal{Z} = \int \mathcal{D}\mathbf{n}(x)\delta(\mathbf{n}^2 - 1)\exp\left(-\frac{\rho_s}{2T}\int dx_1 \int_0^L dx_2\,(\nabla\mathbf{n})^2\right), \qquad (7.11)$$

with periodic boundary conditions on $\mathbf{n}$ along the x_2 direction. However, precisely such a model, in the regime $L \ll \Lambda_{\overline{MS}}^{-1}$, was studied in Section 6.3: we simply have to identify x_2 with the imaginary time direction τ of a fictitious $d = 1$ quantum model, and the then L is just its inverse temperature. This model was analyzed by a further dimensional reduction: we integrate out all modes of $\mathbf{n}$ which have a non-zero wavevector along the x_2 direction, and obtain an effective *one*-dimensional model:

$$\mathcal{Z} = \int \mathcal{D}\mathbf{n}(x_1)\delta(\mathbf{n}^2 - 1)\exp\left(-\frac{(N-1)\xi_c(L)}{4}\int dx_1\,(\partial_{x_1}\mathbf{n})^2\right), \quad (7.12)$$

We have written the co-efficient of the gradient coupling in a form such that $\xi_c(L)$ is precisely the correlation length of two-point $\mathbf{n}$ correlator along the x_1 direction (this follows from (2.68). Indeed, we can read off the value of $\xi_c(L)$ as a function of $\Lambda_{\overline{MS}}$ and L from the result (6.44):

$$\xi_c(L) = \frac{L(N-2)}{\pi(N-1)}\ln\left(\frac{\mathcal{C}}{L\Lambda_{\overline{MS}}}\right) + \ldots \qquad (7.13)$$

where $\mathcal{C}$ is the constant defined in (5.80). We expect a universal scaling form $\xi_c(L) = LF(L\Lambda_{\overline{MS}})$ for general L, and (7.13) specifies the leading term in the small u limit of $F(u)$. The $u \to \infty$ limit is the strong-coupling regime, with $\xi_c \equiv \xi_c(L \to \infty)$ given by the Bethe ansatz result (7.10).

Let us compute the expression corresponding to (7.13) for the quantum model (5.16). We will do this by performing the dimensional reduction to (7.12) in one-step, in a perturbation theory in g, *i.e.,* we will integrate out all modes with either a non-zero wavevector in the x_2 direction, or a non-zero frequency in the τ direction, but not both. By a simple generalization of (6.7) or (6.35) to this spacetime geometry, we

get

$$\xi_c(L) = \frac{2}{(N-1)} \left[\frac{cNL}{gT} - \sum_{n,m}' \int \frac{dk}{2\pi} \frac{(N-2)}{k^2 + (2\pi m/L)^2 + (2\pi nT/c)^2} \right]$$

(7.14)

plus corrections of order g, where the prime indicates the sum is over all integers n, m excluding the single point $n = m = 0$. The integral and summation in (7.14) are badly divergent in the ultraviolet. However, after expressing g in terms of ρ_s using (7.9), the resulting expression is free of divergences, as we now show. The basic technical tool is to lift the denominators in the integrands of (7.9) and (7.14) up into exponentials using the simple identity

$$\frac{1}{a} = \int_0^\infty d\lambda e^{-\lambda a}$$

(7.15)

Then the combination of (7.14) and (7.9) yields, after a suitable rescaling of λ

$$\xi_c(L) = \frac{2L\rho_s}{(N-1)T} \left[1 - \frac{(N-2)T}{4\pi\rho_s} \int_0^\infty \frac{d\lambda}{\sqrt{\lambda}} \left(A(\lambda)A(\lambda v^2) - 1 - \frac{1}{\lambda v} \right) \right]$$

(7.16)

where $v = TL/c$ and the function $A(y)$ was defined in (2.53). By simple use of the identity (2.65) and (2.53) it is easy to show that the λ integral in (7.16) is convergent. As noted earlier, we are interested in the classical regime $L \gg c/T$, and therefore in the $v \to \infty$ limit of the integral in (7.16). It is not difficult to show that the integral $\sim \ln(v)$ in this limit; we determined the additive constant associated with this logarithm numerically and found

$$\xi_c(L) = \frac{2L\rho_s}{(N-1)T} \left[1 - \frac{(N-2)T}{2\pi\rho_s} \ln \left(\frac{LT}{\mathcal{C}c} \right) + \mathcal{O} \left(\frac{T}{\rho_s} \right)^2 \right]$$

(7.17)

where the constant $\mathcal{C}$ (given in (5.80)) was again found to appear.

We are now prepared to perform the matching between the two approaches to computing $\xi_c(L)$. Comparing (7.13) and (7.17) we find that the L dependencies are consistent, as required, and that

$$\Lambda_{\overline{MS}} = \frac{T}{c} \exp \left(-\frac{2\pi\rho_s}{(N-2)T} \right).$$

(7.18)

This is the result to one-loop order. It is possible to improve this result to two-loop order by using the relationship (6.43) between $\Lambda_{\overline{MS}}$ and the

coupling g_R at an arbitrary scale μ. Matching (7.18) with (6.43) by choosing $\mu = T/c$ $(\sim \Lambda_c)$ we find that

$$\frac{1}{g_R(T/c)} = \frac{\rho_s}{NT} + \frac{(N-2)}{4\pi N} \ln \mathcal{C} + \mathcal{O}\left(\frac{T}{\rho_s}\right). \qquad (7.19)$$

Inserting this back into (6.43) we obtain the final result [217]

$$\Lambda_{\overline{MS}} = \frac{T}{c}\left(\frac{2\pi\rho_s}{(N-2)T}\right)^{1/(N-2)} \exp\left(-\frac{2\pi\rho_s}{(N-2)T}\right)\left[1 + \mathcal{O}\left(\frac{T}{\rho_s}\right)\right]$$
$$(7.20)$$

Combined with (7.10), we have the promised exact result for ξ_c.

7.1.2 Computation of τ_φ

We shall follow the same strategy employed in Section 7.1.1 for ξ_c: extend to dynamical properties the static mapping of the model (5.16) on a cylinder of circumference L, $c/T \ll L \ll \Lambda_{\overline{MS}}^{-1}$, onto the effective one-dimensional classical rotor model. By exactly the same arguments as those leading to (6.51), we have to supplement the partition function (7.12) by an additional kinetic energy term for the classical rotors. We therefore consider

$$\mathcal{Z} = \int \mathcal{D}\mathbf{n}(x_1)\mathcal{D}\mathbf{L}(x_1)\delta(\mathbf{n}^2-1)\delta(\mathbf{L}\cdot\mathbf{n})\exp\left(-\frac{\mathcal{H}_c}{T}\right)$$

$$\mathcal{H}_c = \frac{1}{2T}\int dx_1 \left[\frac{(N-1)T\xi_c(L)}{2}\left(\frac{d\mathbf{n}}{dx_1}\right)^2 + \frac{1}{L\chi_{u\perp}(L)}\mathbf{L}^2\right](7.21)$$

where $L\chi_{u\perp}(L)$ is the uniform susceptibility *per unit length* of the model (5.16) on a cylinder of circumference L. The equations of motion of this one-dimensional classical rotor model follow from the Poisson brackets (6.54). The structure of these has been analyzed in Section 6.3, and by (6.59) they imply a characteristic time

$$\tau_\varphi(L) \sim \left(\frac{\xi_c(L)L\chi_{u\perp}(L)}{T}\right)^{1/2} \qquad (7.22)$$

The value of $\tau_\varphi(L)$ is undetermined up to an overall constant which we will choose later at our convenience.

It remains to compute $\chi_{u\perp}(L)$, and then to use scaling arguments to extrapolate perturbative results from the regime $L\Lambda_{\overline{MS}} \to 0$ to the required $L\Lambda_{\overline{MS}} \to \infty$.

The uniform susceptibility follows from a straightforward generalization of (6.48) to the present geometry. We obtain after a rotational average of the two terms in (6.48):

$$\chi_{u\perp}(L) = \frac{N}{cg} \times$$

$$\left[1 - \frac{(N-2)g}{cN} \frac{T}{L} \sum_{\omega_n \neq 0} \sum_m \int \frac{dk}{2\pi} \frac{1}{k^2 + (2\pi m/L)^2 + (\omega_n/c)^2} \right.$$

$$\left. + \frac{(N-2)g}{cN} \frac{T}{L} \sum_{\omega_n \neq 0} \sum_m \int \frac{dk}{2\pi} \frac{k^2 + (2\pi m/L)^2 - (\omega_n/c)^2}{(k^2 + (2\pi m/L)^2 + (\omega_n/c)^2)^2} \right]. \quad (7.23)$$

We can eliminate g in favor of ρ_s using (7.9) and obtain an expression for $\chi_{u\perp}$ in terms of ρ_s, c, T and L. This expression can then be analyzed in a manner very similar to (7.14) and (7.16). We will not describe the details of this, but simply note that an important difference emerges from the structure of the earlier result (7.17): we find that there are no singular logarithmic terms in $\chi_{u\perp}(L)$ in the limit $TL/c \to \infty$. The dependence on TL/c is exponentially small in this limit, and we can therefore explicitly take the $L \to \infty$ limit already in the expression (7.23), by converting the summation over m into an integral. Taking this limit, and carrying out the summation over ω_n we get

$$\chi_{u\perp}(L) = \frac{\rho_s}{c^2} - (N-2) \int \frac{d^2k}{(2\pi)^2} \left(\frac{1}{ck} \frac{1}{(e^{ck/T} - 1)} - \frac{T}{c^2 k^2} \right)$$

$$+ (N-2) \int \frac{d^2k}{(2\pi)^2} \left(\frac{1}{4T \sinh^2(ck/2T)} - \frac{T}{c^2 k^2} \right). \quad (7.24)$$

The two integrals in (7.24) are individually logarithmically divergent, but the combination is finite: this is a verification that the $L \to \infty$ limit was smooth, and that unlike (7.17), it was not necessary to a keep L finite to obtain a finite answer. We can easily carry out the integral over the difference of the integrands in (7.24) and obtain a result $\chi_{u\perp}(L)$ which is independent of L to the accuracy we need

$$\chi_{u\perp}(L) = \frac{\rho_s}{c^2} \left[1 + \frac{(N-2)T}{2\pi\rho_s} + \mathcal{O}\left(\frac{T}{\rho_s}\right)^2 \right]. \quad (7.25)$$

Note that, combined with $\chi_u = (2/N)\chi_{u\perp}$, this result agrees with our earlier large N result (5.84)

We have assembled all the ingredients necessary to estimate τ_φ. Inserting the results (7.13) and (7.25) into (7.22) we get (ignoring numerical

prefactors)

$$\tau_\varphi(L) \sim \left(\frac{\rho_s}{T}\right)^{1/2} \frac{L}{c} \left[\ln\left(\frac{\mathcal{C}}{L\Lambda_{\overline{MS}}}\right)\right]^{1/2} \tag{7.26}$$

for small $L\Lambda_{\overline{MS}}$.

As the final step, we have to extrapolate the result (7.26) from $L\Lambda_{\overline{MS}} \to 0$ to $L\Lambda_{\overline{MS}} \to \infty$. This can be done by a relatively straightforward scaling argument. The phase relaxation time $\tau_\varphi(L)$ is expected to be given by a natural time scale times a dimensionless function of the ratio of the system width L to the only scale, $\Lambda_{\overline{MS}}^{-1}$, which characterized the two-dimensional nonlinear sigma model (7.11); in other words we expect

$$\tau_\varphi = \frac{AL}{c} G(L\Lambda_{\overline{MS}}) \tag{7.27}$$

where A is some prefactor and G is a universal scaling function. Clearly (7.26) is of this form, and the comparison allows us to fix the value of A. In the limit $L\Lambda_{\overline{MS}} \to \infty$ we expect $\tau_\varphi(L)$ to become independent of the system width L, and therefore we must have $G(u \to \infty) \sim 1/u$. Using this, we get our desired final result for $\tau_\varphi \equiv \tau_\varphi(L \to \infty)$ [83]:

$$\begin{aligned}
\tau_\varphi &\sim \left(\frac{\rho_s}{T}\right)^{1/2} \frac{\Lambda_{\overline{MS}}^{-1}}{c} \\
&= \left(\frac{\rho_s}{T}\right)^{1/2} \frac{\xi_c}{c};
\end{aligned} \tag{7.28}$$

in the last step we have arbitrarily chosen the prefactor and the relationship holds as an equality. This is the promised result for τ_φ. As we noted earlier, this result has an interesting similarity to that obtained in corresponding low T region of the quantum Ising chain in Section 4.5.1–there we found in (4.80) and (4.88) that $\tau_\varphi \sim (\Delta/T)^{1/2}\xi_c/c$.

7.1.3 Structure of correlations

We turn to a discussion of the structure of the reduced classical scaling function Φ_c in (7.6).

7.1.3.1 Equal-time correlations

For the equal-time case, $t = 0$, it is possible to make exact analytic statements in certain asymptotic limits, which we will now discuss (the full functional form of $\Phi_c(\overline{x}, 0)$ can be obtained in a $1/N$ expansion, as discussed in Ref [97]). We have already noted the long distance form in (7.7). We will now discuss the behavior as $\overline{x} \to 0$. As we are restricting

ourselves to the classical regime, we do not want to examine distances
shorter than the thermal de Broglie wavelength of the spin waves—we are
therefore examining the regime $c/T \ll x \ll \xi_c$. The overall dependence
upon x in this regime follows immediately from the homogeneity relation
(6.40); indeed by the precise analog of the argument used to obtain
(6.58), but using distances rather than energies, we have

$$C(x,0) \sim [\ln(\xi_c/x)]^{(N-1)/(N-2)} \quad , \quad c/T \ll x \ll \xi_c \qquad (7.29)$$

We can also precisely fix the prefactor of the term in (7.29) by a sim-
ple argument. At the lower boundary $x \sim c/T$ thermal fluctuations
are no longer important, and the model crosses over into its quantum-
fluctuation dominated ground state correlations. As the ground state is
ordered, the correlations are very simple: we must have $C(x,0) = N_0^2/N$
for $x \sim c/T$ (the factor of N comes from the average over all orienta-
tions of the ground state magnetization). Demanding that (7.29) match
smoothly with this criterion, using the value $\xi_c \sim \Lambda_{\overline{MS}}^{-1}$ in (7.20), and
working to leading order in T/ρ_s, we find that the prefactor of the log-
arithm in (7.29) is uniquely determined. The resulting dependence of
$C(x,0)$ obeys the scaling form (7.6) (indeed, it requires the prefactor of
$(T/\rho_s)^{(N-1)/(N-2)}$ in (7.6), and this is the reason for its presence), and
gives us the small $\overline{x} = x/\xi_c$ limit of the scaling function:

$$\Phi_c(\overline{x} \ll 1, 0) = \frac{1}{N}\left[\frac{(N-2)}{2\pi}\ln(1/\overline{x})\right]^{\frac{(N-1)}{(N-2)}}. \qquad (7.30)$$

It is also useful to present these results in momentum space, in terms of
the equal-time structure factor $S(k)$ defined in (4.5):

$$S(k) = \int d^2x\, e^{-i\vec{k}\cdot\vec{x}} C(x,0). \qquad (7.31)$$

For small k, the scaling form (7.6) implies that

$$S(0) \sim N_0^2 \xi_c^2 \left(\frac{T}{\rho_s}\right)^{\frac{(N-1)}{(N-2)}}, \qquad (7.32)$$

where the missing coefficient is a universal number given by the spatial
integral of Φ_c at $t = 0$ (its numerical estimate [507] for $N = 3$ is ≈ 1.06).
For larger k, we Fourier transform (7.30), and find that for $k\xi_c \gg 1$, but
$ck \ll T$ [83, 97],

$$S(k) = \left(\frac{N-1}{N}\right)\frac{TN_0^2}{\rho_s k^2}\left[\frac{(N-2)T}{2\pi\rho_s}\ln(k\xi_c)\right]^{1/(N-2)}. \qquad (7.33)$$

Notice that for $k \sim c/T$, the term in the square brackets evaluates to $1 + \mathcal{O}(T/\rho_s)$, and so

$$S(k) = \left[\frac{N-1}{N} \right] \frac{T N_0^2}{\rho_s k^2} . \quad , \quad k \sim c/T \qquad (7.34)$$

This can be understood in terms of the response (5.57), with an additional factor of $(N-1)/N$ representing the fact that this response appears only in $N-1$ directions transverse to the local ordered state.

It is instructive at this point to assemble all the known results for the equal-time correlator $C(x,0)$ in the present low T region, $T \ll \rho_s$. We have

$$C(x,0) = \begin{cases} a_1 N_0^2 \left[\dfrac{c}{\rho_s x} \right]^{1+\eta} & x \ll \dfrac{c}{\rho_s} \\[2em] \dfrac{N_0^2}{N} & \dfrac{c}{\rho_s} \ll x \ll \dfrac{c}{T} \\[2em] \dfrac{N_0^2}{N} \left[\dfrac{(N-2)T}{2\pi\rho_s} \ln(\xi_c/x) \right]^{(N-1)/(N-2)} & \dfrac{c}{T} \ll x \ll \xi_c \\[2em] a_2 N_0^2 \left(\dfrac{T}{\rho_s} \right)^{(N-1)/(N-2)} \dfrac{e^{-x/\xi_c}}{\sqrt{x/\xi_c}} & \xi_c \ll x \end{cases}$$

$$(7.35)$$

where a_1, a_2 are universal constants known only via $1/N$ expansion or numerical simulations. It is reassuring to note that all four asymptotic forms in (7.35) are perfectly compatible at the boundaries of their regions of applicability. The first result in (7.35) follows from a Fourier transform of (5.41), combined with prefactor constraints implied by (5.60), (5.62) and (5.54): in this region the correlations are those of the $T = 0$ quantum critical point at $g = g_c$, and the η is the anomalous dimension of the $2 + 1$ dimensional theory. The region $c/\rho_s \ll x \ll c/T$ is where the system appears to have the long-range order of the $g < g_c$ ground state: thermal fluctuations have not yet become apparent. A $T = 0$ quantum analysis of (5.16) is required to describe the crossover between these first two regimes. Finally, the last two regimes in (7.35) are those discussed in the present section, and are contained in the reduced classical scaling function Φ_c.

7.1.3.2 Dynamic correlations

Let us turn to unequal time correlations. A reasonable picture has been obtained through numerical simulations, combined with scaling arguments, and matching to limiting weak-coupling regimes [507, 508]; these results are also supported by other analytic approaches [187, 83, 97]. By arguments similar to those in Section 6.3.3, the dynamics can be mapped onto the obvious two-dimensional generalization of the classical non-linear wave problem defined by (6.51) and (6.55). This is a problem of classical rotors with orientation $\mathbf{n}(x, t)$ and angular momentum $\mathbf{L}(x, t)$. The equal time correlations of $\mathbf{n}$, as already discussed, are given by the classical partition function (7.8). Those of $\mathbf{L}$ are defined, as in (6.51), by the kinetic energy term $\mathbf{L}^2/(2\chi_{u\perp})$ with $\chi_{u\perp}$ given by (7.25). An initial condition is chosen from this ensemble, and then evolved deterministically under the equations of motion following from the Poisson brackets (6.54). This classical problem was numerically simulated by Tyc *et al.* [507] and we will now describe their results.

It is convenient to express the results in term of the dynamic structure factor $S(k, \omega)$ defined by (4.4). As in (4.95) and (6.62), we can incorporate the already determined information on the equal time correlations, and the scaling form (7.6), by writing

$$\frac{2T}{\omega}\mathrm{Im}\chi(k,\omega) = S(k,\omega) = S(k)\tau_\varphi \Phi_{Sc}(k\xi_c, \omega\tau_\varphi), \qquad (7.36)$$

where the first relation is the classical fluctuation dissipation theorem (4.92), and the universal scaling function Φ_{Sc} is an even function of frequency, and has a unit integral of frequency, as in (4.96). The function Φ_{Sc} was determined numerically by Tyc *et al.* [507]. They found that over a wide range of frequency and wavevectors, the frequency dependence of the results could be described by the simple functional form

$$\Phi_{Sc}(\overline{k}, \overline{\omega}) = \frac{\gamma(\overline{k})}{(\overline{\omega} - \nu(\overline{k}))^2 + \gamma^2(\overline{k})} + \frac{\gamma(\overline{k})}{(\overline{\omega} + \nu(\overline{k}))^2 + \gamma^2(\overline{k})} \qquad (7.37)$$

where $\nu(\overline{k})$ and $\gamma(\overline{k})$ are functions of wavevector that were determined numerically. This dynamic response consists of a peak at a spin-wave (rescaled) frequency $\nu(\overline{k})$ with a damping rate $\gamma(\overline{k})$.

For small $\overline{k}$, a best fit was obtained with a $\nu(\overline{k}) \to 0$ as $\overline{k} \to 0$, while $\gamma(\overline{k})$ approached a non-zero constant. So the spin-waves are overdamped for $k\xi_c \ll 1$, and the dynamics is purely relaxational. There is no analog of the non-zero frequency 'shoulder' found in Fig 6.4 for the classical wave dynamics in $d = 1$. Thus amplitude fluctuations are weaker in

$d = 2$, and the relaxation is better considered as arising from angular fluctuations about an ordered state. This is physically sensible as it indicates that the **n** field is 'more ordered' in the present $d = 2$, low T region than it was in the $d = 1$ high T region of Section 6.3.

For large $\overline{k}$ (more precisely, for $k\xi_c \gg 1$ and $ck/T \ll 1$) we expect that the system should crossover into the $T = 0$ spin-wave spectrum at $\omega = ck$. Using the values of ξ_c in (7.20), and that of τ_φ in (7.28), it is easy to see that this is consistent with the dimensionless frequency $\overline{\omega} = \nu(\overline{k})$ for $T \ll \rho_s$ only if

$$\nu(\overline{k} \to \infty) = \overline{k}\left[\frac{(N-2)}{2\pi}\ln\overline{k}\right]^{1/2} \tag{7.38}$$

The large $\overline{k}$ limit of the damping $\gamma(\overline{k})$ was examined in a self-consistent perturbation theory in Ref [508] and it was found to be only logarithmically smaller than $\nu(\overline{k})$.

7.2 Dynamics of the quantum paramagnetic and high T regions

We will turn to the dynamical properties of the remaining two universal regions in Fig 5.2 and 5.3. There is no signature of the ordered state in these regions at any length or time scale. Instead, the basic physics is of the critical ground state or the quantum paramagnet eventually losing phase coherence at times longer than τ_φ due to the thermal effects. The qualitative nature of all the physics turns out not to be particularly sensitive to the precise value of N: all of our results below will apply to all N, including the cases $N = 1, 2$ which were excluded in the low T discussion of Section 7.1. Indeed, the physical phenomena also turns out to be essentially identical those in the corresponding regions of the $d = 1$, $N = 1$ quantum Ising chain, which were discussed in Sections 4.5.2 and 4.5.3. The dynamical properties of this latter model were summarized in Fig 4.13, and the 'High T' and 'low T (quantum paramagnetic)' portions of this figure apply unchanged to the $d = 2$ models of interest here for all N. Exact dynamic response functions were obtained in Sections 4.5.2 and 4.5.3 for all the distinct dynamical regimes of the quantum Ising chain. The same response functions of the $d = 2$ models have a very similar form, but it is no longer possible to obtain exact results. In this section, we will demonstrate how this structure emerges at first order in $1/N$. However, as we noted at the beginning of this chapter, the $1/N$ expansion breaks down at very low frequencies, and

for this regime we will provide an alternative approach in Section 8.3. In a sense, the purpose of this section is somewhat technical: the basic physical concepts are perhaps better appreciated in the simpler, and exact, discussion of Sections 4.1.1, 4.5.2 and 4.5.3, which the reader is urged to review.

We also note that the computations for $d = 1$ in Chapters 4, 6 and for $d = 2$ here, treat interactions in opposing limits. In the $N = \infty$, $d = 2$ results of Chapter 5 we found a description in terms of N non-interacting massive particles with a self-consistently determined temperature-dependent energy gap; at first order in $1/N$ we will find that these particles *weakly* scatter off each other with a T-matrix that is of order $1/N$. In contrast, the collisions of the excitations in $d = 1$ are described by the S matrices (4.17,6.13), describing full reflection of particles with a phase shift of π, and these are as far as one can get from the free-particle result $S = 1$, while being consistent with unitarity; the $d = 1$ case is therefore properly considered as a *strong* scattering limit. The qualitative similarity in $\chi(k, \omega)$ of the weak-coupling results below, and the earlier strong-coupling results in $d = 1$, is reassuring and indicates that we have correctly understood the physics.

We begin by setting up the mechanics of the $1/N$ expansion for the dynamic susceptibility. The $N = \infty$ result was given in (5.22). At order $1/N$, it is necessary to including fluctuations in the λ field about the saddle-point of (5.20), which is determined by the solution of (5.21). We insert a source term in the original action (5.18) for **n**, and then expand the modified (5.20) up to cubic order in the deviation of λ about its saddle-point (all higher order terms can be dropped at this order in $1/N$). The term purely quadratic in λ defines a propagator for the λ fluctuations: the structure of this propagator will be discussed in some detail below. We integrate out the λ fluctuations to order $1/N$, and this leads to the corrections to the **n** field correlator, $\chi(k, \omega)$ shown schematically in Fig 7.2. This leads finally to the following expression for $\chi(k, \omega)$, which replaces (5.22) at order $1/N$ [97] (the reader can also consult Refs [30, 491] for more explicit details on the mechanics of computing $1/N$ corrections for related models):

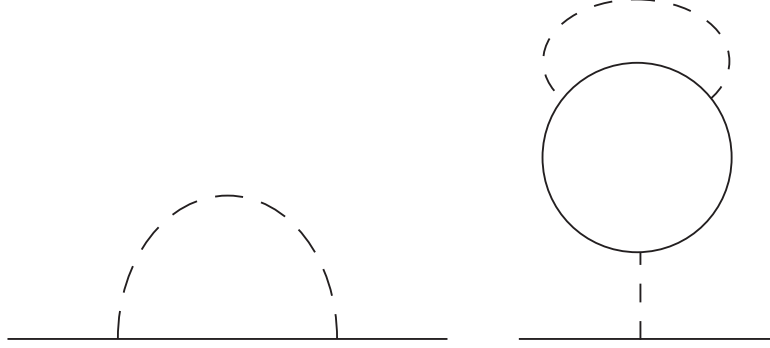$$\chi(k, \omega) = \frac{cg/N}{c^2 k^2 - (\omega + i\epsilon)^2 + m^2 + \Sigma(k, \omega)} \tag{7.39}$$

Fig. 7.2. Feynman diagrams which contributing to the self energy of **n** at order $1/N$. The **n** propagator is a straight line, while the λ propagator, $1/\Pi$, is a dashed line.

where the self energy Σ is given by

$$\Sigma(k, \omega_n) = \widetilde{\Sigma}(k, \omega_n) - \frac{1}{\Pi(0,0)} T \sum_{\epsilon_n} \int \frac{d^2q}{4\pi^2} G_0^2(q, \epsilon_n)\widetilde{\Sigma}(q, \epsilon_n), \quad (7.40)$$

the two terms representing the contributions of the two graphs in Fig 7.2. The frequency and momentum dependent contribution to the self energy is $\widetilde{\Sigma}$ which is given by

$$\widetilde{\Sigma}(k, \omega_n) = \frac{2}{N} T \sum_{\epsilon_n} \int \frac{d^2q}{4\pi^2} \frac{G_0(\vec{k} + \vec{q}, \omega_n + \epsilon_n) - G_0(q, i\epsilon_n)}{\Pi(q, \epsilon)}, \quad (7.41)$$

with $1/\Pi$ the propagator of the λ field,

$$\Pi(q, \epsilon_n) = T \sum_{\Omega_n} \int \frac{d^2q_1}{4\pi^2} G_0(\vec{q} + \vec{q_1}, \epsilon_n + \Omega_n)G_0(q_1, \Omega_n), \quad (7.42)$$

and G_0 is proportional to the susceptibility of **n** at $N = \infty$

$$G_0(k, \omega_n) \equiv \frac{1}{c^2k^2 + \omega_n^2 + m^2}. \quad (7.43)$$

The 'mass' m in the propagators is the saddle-point value of the λ field, and was determined earlier in (5.72) to be

$$m = 2T \ln\left(\frac{e^{\Delta_+/2T} + (4 + e^{\Delta_+/T})^{1/2}}{2}\right) + \mathcal{O}(1/N) \quad (7.44)$$

where, as usual, Δ_+ represents the gap of the quantum-paramagnetic ground state. We also recall the important limiting forms, $m = \Delta_+$ for

$T \ll \Delta_+$ (Eqn (5.76)), and $m = 2\ln((\sqrt{5} + 1)/2)T$ for $T \gg \Delta_+$ (Eqn (5.78)). The value of m we are using in (7.44) is actually precisely the same as in the $N = \infty$ expression (5.72), when expressed in terms of the bare coupling constant g. The $1/N$ correction in (7.44) represents the change necessary because of the new value of the ground state energy gap Δ_+ at this order. At $N = \infty$, the gap Δ_+ was related to the bare coupling constant g in (5.27) and (5.29). The $1/N$ corrections to the value of Δ_+ is obtained by solving the following equation for the location of the pole in the zero momentum $\mathbf{n}$ propagator in (7.39) at $T = 0$

$$m^2 - \Delta_+^2 + \Sigma(0, \omega = \Delta_+). \tag{7.45}$$

The equation relating Δ_+ and the coupling g must then be inverted to express g in terms of Δ_+, and the result inserted into the expression for m. This will lead to the corrections at order $1/N$ in the expression (7.44), and these are crucial in obtaining universal answers for the physical response function $\chi(k, \omega)$.

We will study the properties of (7.39) at $T = 0$ in Section 7.2.1, and at non-zero temperatures in Section 7.2.2.

7.2.1 Zero temperature

The propagator of the λ field in (7.42) can be evaluated in closed form at $T = 0$. We find

$$\Pi(q, \omega) = \frac{1}{4\pi c^2 \sqrt{c^2 q^2 - (\omega + i\epsilon)^2}} \tan^{-1}\left(\frac{\sqrt{c^2 q^2 - (\omega + i\epsilon)^2}}{2\Delta_+}\right) \tag{7.46}$$

Notice that Π is purely real for $|\omega| < \sqrt{c^2 q^2 + 4\Delta_+^2}$, but acquires an imaginary part for larger $|\omega|$. The threshold corresponds to the minimum energy required to create two particles with total momentum q, in agreement with the expression (7.42) for Π as a two particle propagator. We can insert (7.46) into (7.41) and determine the self energy Σ. It is simpler to first consider only its imaginary part: this is obtained by using a spectral representation for $\text{Im}(1/\Pi)$ and evaluating the summation over ϵ_n in the limit of zero T; taking the imaginary part of the result we obtain

$$\text{Im}\Sigma(k, \omega) = \frac{1}{2\pi^2 N} \int \frac{d^2q}{\varepsilon_{\vec{k}+\vec{q}}} \int_0^\infty d\Omega \, \text{Im}\left(\frac{1}{\Pi(q, \Omega)}\right) \delta(\omega - \varepsilon_{\vec{k}+\vec{q}} - \Omega) \tag{7.47}$$

for $\omega > 0$ (for $\omega < 0$ we use the fact that $\text{Im}\Sigma(k,\omega)$ is an odd function of ω), with

$$\varepsilon_{\vec{q}} \equiv \sqrt{c^2 q^2 + \Delta_+^2} \qquad (7.48)$$

the energy spectrum of the quasiparticle. Actually, there is a little subtlety in obtaining (7.47) that we have glossed over: for large Ω, $\text{Im}(1/\Pi(q,\Omega)) \sim \Omega$, and so its Kramers-Kronig transform is not well defined. This issue is discussed more carefully in Ref [97], and it is shown there that for the imaginary part of Σ, the naive result obtained by simply ignoring this potential divergence is in fact correct. Now, the relativistic invariance of the $T = 0$ theory implies that (7.47) is a function only of $c^2 k^2 - \omega^2$, and so its general form can be deduced by evaluating it at $k = 0$. For this case, the q integral can be performed, and then changing variables from Ω to y with $y^2 = 2\omega\Omega - \omega^2 + \Delta_+^2$, we get our final expression for $\text{Im}\Sigma$

$$\text{Im}\Sigma(k,\omega) = -\frac{4\pi}{N\sqrt{\omega^2 - c^2 k^2}} \int_{2\Delta_+}^{\sqrt{\omega^2 - c^2 k^2} - \Delta_+} dy\, y^2$$
$$\times \left[\pi^2 + \ln^2((y + 2\Delta_+)/(y - \Delta_+)) \right]^{-1} \qquad (7.49)$$

for $\omega^2 > c^2 k^2 + 9\Delta_+^2$, and $\text{Im}\Sigma$ is zero otherwise. So we have a threshold at the creation of *three* particles above which $\text{Im}\Sigma$ is non-zero: the $O(N)$ symmetry of the model only allows the N-fold degenerate particle with momentum k and energy ω to decay into a three-particle continuum if its energy is sufficiently large. We also note here the behavior of (7.49) for $\omega^2 - c^2 k^2 \gg \Delta_+^2$:

$$\text{Im}\Sigma(k,\omega) = -\frac{\pi\eta}{2}\left(\omega^2 - c^2 k^2\right) \qquad (7.50)$$

where η is

$$\eta = \frac{8}{3\pi^2 N} \qquad (7.51)$$

In fact, it will turn out that η is precisely the same critical exponent that appeared in (5.41), as will become clear from the discussion below.

Inserting (7.49) into (7.39) we see that the resulting structure in $\text{Im}\chi(k,\omega)$ is identical to that sketched in Fig 4.1 for the quantum Ising chain. Near the quasi-particle energy $\omega = \varepsilon_k$, Σ is purely real, and to there is no broadening of the quasi-particle spectral weight, and it remains a pure delta function as in Fig 4.1. The real part of Σ does contribute a shift in the position of the pole, but this was already accounted for by our defining Δ_+ as the exact $T = 0$ energy gap in (7.45). The next

non-zero spectral weight in χ arises at the three-particle threshold from the imaginary part of Σ discussed above, and is also shown in Fig 4.1. At next order in $1/N$ we will also find a threshold at $5\Delta_+$ and so on.

Let us return to the quasiparticle pole, and consider the value of its residue at order $1/N$. For this we have to evaluate Σ at the pole position. This is most conveniently done by initially going to imaginary frequencies, and explicitly using the relativistic invariance of the theory. In fact, defining $K = \sqrt{k^2 + \omega_n^2/c^2}$, the relativistic invariance implies that Σ is a function only of K: by an angular average of (7.41) in three-dimensional Euclidean spacetime, this function can be reduced to a one-dimensional integral

$$\Sigma(K) = \frac{1}{2\pi^2 cN} \int_0^\Lambda \frac{Q^2 dQ}{\Pi(Q)} \left[\frac{1}{2KQ} \ln \left(\frac{(K+Q)^2 + \Delta_+^2}{(P-Q)^2 + \Delta_+^2} \right) - \frac{2}{Q^2 + \Delta_+^2} \right]$$
(7.52)

where $\Pi(Q)$ is the relativistically invariant, imaginary frequency form of (7.46). A simple analysis shows that the integral is logarithmically divergent at large Q, and so we have introduced a relativistically invariant hard-cutoff at momentum Λ; the same cut-off will appear in other intermediate expressions below, but our final, universal, results will be cut-off independent. Now, from (7.39), the quasiparticle residue $\mathcal{A}$ is given by

$$\mathcal{A} = \frac{cg}{N} \left(1 - \frac{d\Sigma(K^2 = -\Delta_+^2)}{dK^2} \right),$$
(7.53)

i.e., we have to evaluate (7.52) and its derivatives at an imaginary $K = i\Delta_+$; this is quite easily done inside the integral in (7.52), and after a numerical evaluation of the resulting integrand we find

$$\mathcal{A} = \frac{cg}{N} \left(1 - \eta \ln \left(\frac{\Lambda}{\Delta_+} \right) + \frac{\mathcal{X}}{N} \right)$$
(7.54)

with the constant $\mathcal{X} = 0.481740823\ldots$, the same η defined in (7.51) makes an appearance, and we have omitted terms of order Δ_+/Λ which can be neglected in the limit $\Lambda \to \infty$, which will eventually be taken. To order $1/N$, we can rewrite (7.54) as

$$\mathcal{A} = \frac{cg}{N} \left(\frac{\Delta_+}{\Lambda} \right)^\eta \left(1 + \frac{\mathcal{X}}{N} \right),$$
(7.55)

which indicates that the quasi-particle residue vanishes as Δ_+^η as the coupling g approaches g_c from above. That this is the correct form, follows from the general scaling arguments made earlier in Section 5.3.2

which led to the result (5.40), and cannot be completely justified at any finite order in the $1/N$ expansion. The earlier arguments showed how such power laws appear as a general consequence of the vicinity of the system to a scale-invariant critical point. The exponents in the power laws can be expanded in powers of $1/N$, and so are appearing here as logarithms in the computation of observables. We introduce the constant Z, which is precisely that appearing in the basic scaling form (7.3), by writing

$$\mathcal{A} = Z\Delta_+^{\eta}\left(1 + \frac{\mathcal{X}}{N}\right),\tag{7.56}$$

so that by (7.55),

$$Z = \left(\frac{cg}{N}\right)\Lambda^{-\eta},\tag{7.57}$$

and (7.56) corresponds to a particular choice of the numerical constant in (5.61). Notice that Z is a non-universal constant, dependent upon the nature of the cutoff, and it is *non-singular* as the coupling g goes through g_c. However, as neither g nor Λ are measurable, we should regard (7.56) as the definition of Z, where it is related to the $T = 0$ observables $\mathcal{A}$ and Δ_+. Indeed (7.56) is the analog of the relation (4.101) for the quantum Ising chain. In a similar manner, Z can also be related to observables of the ordered ground state (as in (4.78) for the Ising chain); we simply quote the result obtained in Ref [97]

$$\frac{N_0^2}{\rho_s} = Z\left(\frac{\rho_s}{N}\right)^{\eta}(1 + \eta\ln 16)\tag{7.58}$$

We reiterate that while the relations (7.56) and (7.58) relate Z to ground state observables that vanish in a singular manner at the critical point $g = g_c$, Z itself is non-singular and finite.

Now, one of the central implications of universal scaling forms like (7.3) is that when the overall scale of the susceptibility χ is expressed in terms of the quasiparticle residue $\mathcal{A}$, or the closely related non-singular constant Z, the remaining expression becomes universal. In particular, the cutoff dependence in the self energy Σ in (7.52) must disappear. Using the value of Z above, we can rewrite (7.39) as

$$\chi(k,\omega) = ZT^{\eta}\Bigg[c^2k^2 - \omega^2$$

$$+ \lim_{\Lambda\to\infty}\left(m^2 + \Sigma(k,\omega) - \eta(c^2k^2 - \omega^2)\ln\left(\frac{\Lambda}{T}\right)\right)\Bigg]^{-1}\tag{7.59}$$

Provided the limit above exists, it is then evident that (7.59) is precisely
of the scaling form (7.3), and defines the scaling function Φ_+. Conversely
we can use the scaling arguments by which (7.3) was derived to argue
that the limit must exist; indeed, it is not difficult to show explicitly
that the limit exists at this order in $1/N$ at all T. Notice also that
the subtraction in Σ affects only its real part, and this is why we saw
no divergent terms in the computation earlier of its imaginary part.
The constant m^2 has been included within the large Λ limit because
the $\mathcal{O}(1/N)$ corrections in (7.44) are Λ dependent, and these terms are
required to obtain a finite limit.

A complete expression for χ at $T = 0$ is now available by combining
(7.52) and (7.59). The integral over P cannot be simplified further, but
explicit evaluation is however possible in the limit $\Delta_+ \to 0$, which we
now consider. We can view this limit as approaching the critical point
at fixed momenta and frequency, or examining the large energy regime
$\omega^2 - c^2 k^2 \gg \Delta_+$. From the former point of view, we have a picture of
$1, 3, 5, \ldots$ particle continua in the spectral weight coming down in energy,
and we can ask, what does their superposed spectral weight look like?
From (7.52) and (7.46), we have in the limit $\Delta_+ \to 0$

$$
\begin{aligned}
\lim_{\Lambda \to \infty} & \left(\Sigma(K) - \eta \ln \left(\frac{\Lambda}{T} \right) \right) \\
&= \frac{4}{\pi^2 N} \int_0^\infty dQ \left[\frac{Q^2}{K} \ln \left| \frac{K+Q}{K-Q} \right| - 2Q - \frac{2K^2 Q}{3(Q^2 + T^2)} \right] \\
&= K^2 \left[\eta \ln \left(\frac{T}{K} \right) + \frac{8}{9\pi^2 N} \right]
\end{aligned}
\tag{7.60}
$$

Taking the imaginary part of (7.60) for real frequencies, we immediately
get (7.50) for $\omega > ck$: this explains why we parameterized the spectral
weight in terms of the exponent η. Also inserting (7.60) into (7.59) we
get

$$
\chi(k, \omega) = Z \left(1 - \frac{8}{9\pi^2 N} \right) \frac{1}{(c^2 k^2 - \omega^2)^{1 - \eta/2}}
\tag{7.61}
$$

Reassuringly T has dropped out. So as we move to the critical point at
$T = 0$, the resultant of the superposition of the multi-particle continua
is a single critical continuum characterized by the exponent η. This
spectral weight has precisely the form sketched in Fig 4.8 for the Ising
chain (the latter model had $\eta = 1/4$). Indeed the entire structure of the
$T = 0$ crossover from the quasiparticle pole and multiparticle continua

to the critical continuum is essentially identical to that obtained earlier for the Ising model.

7.2.2 Nonzero temperatures

Turning on a nonzero temperature introduces additional thermal damping to the spectral functions computed above, and results in a finite phase coherence time τ_φ. We will find that the structure of these effects is again remarkably similar to those studied earlier for the quantum Ising chain in Sections 4.5.2 and 4.5.3.

First, we note some intermediate steps associated with the mechanics of the computation. We shall be particularly interested in imaginary parts of Green's functions. From (7.42) we get at $T > 0$

$$
\mathrm{Im}\,(\Pi(q,\omega)) = \int \frac{d^2q_1}{16\pi\varepsilon_{\vec{q}_1+\vec{q}}\varepsilon_{\vec{q}_1}} \left[|n(\varepsilon_{\vec{q}_1+\vec{q}}) - n(\varepsilon_{\vec{q}_1})|\delta(\omega - |\varepsilon_{\vec{q}_1+\vec{q}} - \varepsilon_{\vec{q}_1}|) \right.
$$
$$
\left. +(1 + n(\varepsilon_{\vec{q}_1+\vec{q}}) + n(\varepsilon_{\vec{q}_1}))\delta(\omega - \varepsilon_{\vec{q}_1+\vec{q}} - \varepsilon_{\vec{q}_1})\right] \tag{7.62}
$$

where $n(\varepsilon)$ is the Bose function

$$
n(\varepsilon) = \frac{1}{e^{\varepsilon/T} - 1}, \tag{7.63}
$$

and the dispersion spectrum $\varepsilon_{\vec{q}}$ is given by

$$
\varepsilon_{\vec{q}}^2 = c^2 q^2 + m^2 \tag{7.64}
$$

Notice that the T dependence of (7.62) arises from two sources: there is that contained in the Bose function (7.63) reflecting the T-dependent occupation of the modes, and there is that due to the T dependence of the 'mass' m in (7.44) which changes the quasi-particle dispersion. We will also need the generalization of (7.47) to finite temperature where it becomes:

$$
\mathrm{Im}\Sigma(k,\omega) = \frac{1}{2\pi^2 N} \int \frac{d^2q}{\varepsilon_{\vec{k}+\vec{q}}} \int_0^\infty d\Omega \mathrm{Im}\left(\frac{1}{\Pi(q,\Omega)}\right) \Bigg[
$$
$$
|n(\varepsilon_{\vec{k}+\vec{q}}) - n(\Omega)|\delta(\omega - |\varepsilon_{\vec{k}+\vec{q}} - \Omega|)
$$
$$
+(1 + n(\varepsilon_{\vec{k}+\vec{q}}) + n(\Omega))\delta(\omega - \varepsilon_{\vec{k}+\vec{q}} - \Omega)\Bigg] \tag{7.65}
$$

We will first discuss in the physical properties of the above results in the limit $T \ll \Delta_+$, *i.e.*, in the low T regions on the quantum paramagnetic side of Figs 5.2 and 5.3. In this case, it is easy to see from (7.62) and (7.65) that all effects of temperature are exponentially suppressed,

i.e., they are of order $e^{-\Delta_+/T}$ or smaller; also the 'mass' $m \approx \Delta_+$ in this region. This is easy to understand: there is a gap Δ_+ to all excitations above the ground state, and all thermal effects are exponentially suppressed. One of the most important consequences of a non-zero T is the broadening of the quasi-particle pole in $\chi(k,\omega)$ shown in Fig 4.1. We will explicitly describe the nature of this broadening at $k = 0$. The $T = 0$ pole is then at $\omega = \varepsilon_0 = \Delta_+$, and for $\omega \approx \Delta_+$ we can write χ as

$$\chi(k,\omega) = \frac{\mathcal{A}}{2\varepsilon_0} \frac{1}{(\varepsilon_0 - \omega - i/\tau_\varphi)}, \tag{7.66}$$

where

$$\frac{1}{\tau_\varphi} = -\frac{1}{2\varepsilon_0}\mathrm{Im}\Sigma(0,\varepsilon_0). \tag{7.67}$$

Notice the similarity of (7.66) to the Ising chain result (4.106) and the $d = 1$ rotor model result (6.30): as in the previous cases we have chosen to define the inverse phase coherence time, $1/\tau_\varphi$, as the width of the quasiparticle pole. We have included only the T-dependent corrections to $\mathrm{Im}\Sigma$ and neglected those to $\mathrm{Re}\Sigma$: this is because the former are much more important for broadening at $\omega \approx \Delta_+$, while the latter only contribute a negligible correction to the overall spectral weight of the quasi-particle feature. Evaluating $1/\tau_\varphi$ from (7.46), (7.62) and (7.65), we find for $T \ll \Delta_+$

$$\frac{1}{\tau_\varphi} = \frac{2\pi T e^{-\Delta_+/T}}{N} \left[1 + 2 \int_0^\infty dy \frac{e^{-y}}{\pi^2 + \ln^2(8\Delta_+/Ty)} \right] \tag{7.68}$$

Compare this with the exact result (4.88) in the corresponding region of the quantum Ising chain (our definition of τ_φ there was slightly different): the T dependence is essentially identical, and only the numerical prefactors differ. The latter need not agree, of course, as we are comparing models in different dimensions, and the prefactor in (7.68), unlike that in (4.88), is not exact and contains only the leading term in a $1/N$ expansion. There is also a subleading term with a $1/\ln^2(\Delta_+/T)$ dependence in (7.68): this logarithm is due to the T-matrix structure of a dilute Bose gas in two dimensions (which the thermally excited quasiparticles form), and its origin will be understood better in Chapters 9 and 11.

Finally, let us turn to the high T region, $T \gg \Delta_+$. In this case T becomes the most important energy scale and controls the entire structure of the response functions. This is already apparent from the value of m

in this limit: from (7.44) we have

$$m = \Theta T \tag{7.69}$$

where $\Theta = 2\ln[(\sqrt{5}+1)/2] \approx 0.962424\dots$. So the two energy scales which determined spectral functions like (7.62) and (7.65), the mass m and the temperature T in the Bose function, *both* become of order T. As a result, it is evident by a simple rescaling of the variables of integration in (7.62) that the propagator Π satisfies

$$\Pi(k,\omega) = \frac{1}{T}\Phi_\Pi\left(\frac{ck}{T},\frac{\omega}{T}\right) \tag{7.70}$$

Determination of the scaling function Π requires complete evaluation of (7.62), and it is not possible to make any further simplifications: we therefore have to resort to numerical computation. In the limit $ck, \omega \gg T$, however, it is clear that Π reduces to the $\Delta_+ = 0$ limit of (7.46). Very similar considerations also apply to the expression of ImΣ in (7.65). The case of ReΣ is however somewhat more subtle: we already saw this in the computation at $T = 0$ where we encountered a logarithmic cutoff dependence. This was cured by expressing χ is terms of the quasi-particle residue $\mathcal{A}$, or the amplitude Z, which led to the result (7.59) with a subtraction which cancelled the cutoff dependence in ReΣ. Indeed, we can use (7.59) to also evaluate χ for $T > 0$: precisely the same subtraction is still adequate to cancel the cutoff dependence. The expression for (7.59) has to be evaluated numerically, and we will not present the details of this here: they may be found in Ref [97]. The result satisfies the scaling form (7.3) and yields numerical values for the complex-valued scaling function Φ_+ at $\Delta_+/T = 0$.

We show the results of such a numerical evaluation in Fig 7.3. Notice the strong similarity to the corresponding result for the quantum Ising chain in Fig 4.9, for which we had the exact expression (4.114). There are quasi-particle-like peaks with a width of order T: the typical excitation has an energy of order T, and also a width of order T, so the quasi-particles are, strictly speaking, not well defined. At very large $\omega, ck \gg T$, the spectrum crossover to the $T = 0$ result in (7.61), whose form was sketched in Fig 4.8.

It should also be clear from the above discussion, that the phase coherence rate, $1/\tau_\varphi$ is of order T, as it is the only energy scale around. We want to choose definition which yields $\tau_\varphi = \infty$ at $N = \infty$ as there is no damping in this limit. Indeed as quasi-particles are well defined at large, but finite N, even in the high T limit, we may continue to use
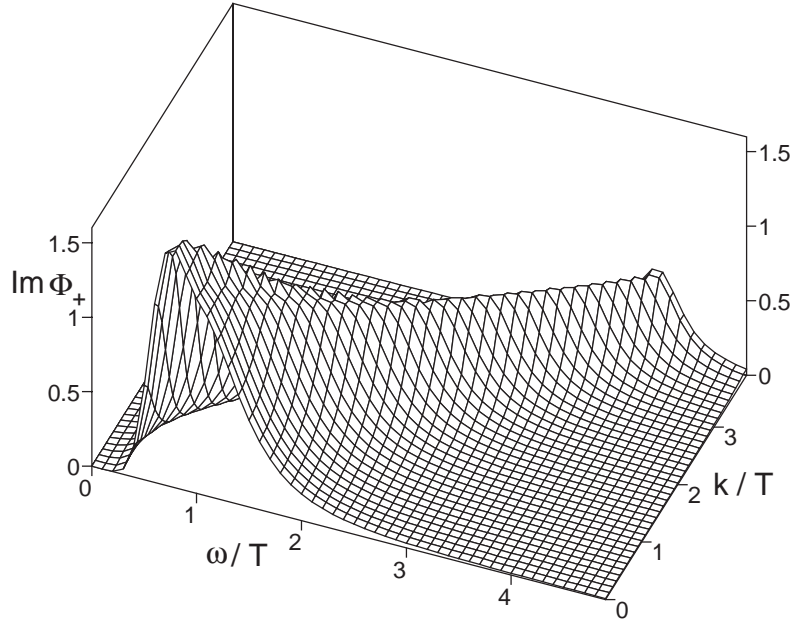
Fig. 7.3. Imaginary part of the scaling function Φ_+ in (7.3) as a function of ck/T and ω/T evaluated in the high temperature limit $\Delta_+/T = 0$. The function was computed in the $1/N$ expansion and evaluated at $N = 3$. Compare with the exact answer for the $d = 1$ Ising model in Fig 4.9.

(7.67) as our definition of τ_φ. Numerical evaluation yields

$$\frac{1}{\tau_\varphi} = 0.904 \frac{k_B T}{N\hbar}. \tag{7.71}$$

where we inserted factor of k_B and $\hbar$ to emphasize that this result depends only on fundamental constants.

Finally, we attempt to use the same expansion above to understand the low frequency behavior of the spectral density $\text{Im}\chi(k, \omega \to 0)$, as was done in Fig 4.10 for the quantum Ising chain. On general grounds, for an interacting system at non-zero temperatures which has an internal relaxational dynamics, we expect that $\chi(k, \omega)$ is analytic as a function of ω at $\omega = 0$; so the odd function $\text{Im}\chi(k, \omega) \sim \omega$, and $\lim_{\omega \to 0} \text{Im}\chi(k, \omega)/\omega$ is nonzero. This was found to be the case for the Ising chain in Fig 4.10. However, the present large N expansion does not obey this requirement; evaluation of (7.65) shows that a low frequency spectral density comes only from collisions of particles with very high momenta, and

Fig. 7.4. Values of the correlation length, ξ (defined from the exponential decay of the equal-time correlations of **n**), the uniform spin susceptibility, χ_u, the phase coherence time, τ_φ, and the spin diffusion constant, D_s, for the two regimes in Figs 5.2 and 7.1. The results in the quasi-classical wave regime are quoted only for $N = 3$, and are asymptotically exact as $T/\rho_s \to 0$; other results are obtained in a $1/N$ expansion, and applicable in principle to all N. The $1/N$ corrections to the values for χ_u and ξ in the high T region were not explicitly computed here, and are taken from Ref [97]. The values for D_s in the quantum critical and quasi-classical particle regimes anticipate results from Chapter 9, and in particular (9.11), (9.65) and (9.69). The order of magnitude of D_s in the quasi-classical wave regime follows from the general scaling arguments in Section 7.1. Finally, χ_u in the quasi-classical particle regime anticipates (9.14).

	Low T (magnetically ordered). Quasi-classical waves	Continuum high T (quantum critical).	Low T (quantum paramagnetic). Quasi-classical particles
ξ	$\dfrac{ec}{16\pi\rho_s}e^{2\pi\rho_s/T}$	$\left[2\ln\left(\dfrac{\sqrt{5}+1}{2}\right)\left(1+\dfrac{0.2373}{N}\right)\dfrac{c}{T}\right]^{-1}$	$\dfrac{c}{|\Delta|}$
χ_u	$\dfrac{2\rho_s}{3c^2}\left[1+\dfrac{T}{2\pi\rho_s}+\dots\right]$	$\dfrac{\sqrt{5}}{\pi}\ln\left(\dfrac{\sqrt{5}+1}{2}\right)\left(1-\dfrac{0.6189}{N}\right)\dfrac{T}{c^2}$	$\dfrac{\Delta_+}{\pi c^2}e^{-\Delta_+/T}$
τ_φ	$\left(\dfrac{\rho_s}{T}\right)^{1/2}\dfrac{\xi}{c}$	$\dfrac{N}{0.904T}$	$\dfrac{N}{2\pi T}e^{\Delta_+/T}$
D_s	$\sim \dfrac{\xi^2}{\tau_\varphi}$	$\dfrac{0.1077N}{\chi_u}$	$\sim \dfrac{1}{\chi_u}$

their contributions are suppressed by exponentially small thermal factors. Specifically, we find [440] $\mathrm{Im}\chi(k,\omega \to 0) \sim \mathrm{sgn}(\omega)\exp(-c/|\omega|)$, for some constant c. This result is an artifact of the $1/N$ expansion, which places undamped intermediate states in the decay rate computation in (7.65). Alternatively stated, *even though the quasiparticles scatter weakly in the large N limit, the low frequency relaxational dynamics of the order parameter* **n** *is strongly-coupled.* This dynamics will be discussed by alternative methods in Section 8.3.

7.3 Summary

As in previous chapters, we summarize the physical properties of the regions of Fig 5.2 and 7.1 in a table in Fig 7.4. The evolution of the

dynamic structure factor $S(k, \omega)$ between the three regimes is quite similar to that discussed for the $d = 1$ Ising model in Section 4.5.4. In the quasi-classical particle regime, we have a narrow peak of width $1/\tau_\varphi$ at a frequency $\omega \approx \Delta_+$. Conversely in the quasi-classical wave regime, $S(k, \omega)$ becomes a symmetric function of ω and is sharply peaked near $k = 0$, $\omega = 0$ with an exponentially large height, and an exponentially small width. In the high T regime there is interesting structure for ω, ck of order T, and this will be discussed in Chapter 8.

7.4 Applications and extensions

The primary application of the $d = 2$ O(3) quantum rotor model has been as a continuum theory of the square lattice Heisenberg antiferromagnet. The connection between these models will become clearer in Chapter 13, but the link between antiferromagnets and quantum rotors has already been motivated in Section 5.1.1.1.

In the low T region, $T \ll \rho_s$, careful tests of the exact results (7.10) and (7.20) for the correlation length have been made. The agreement with neutron scattering measurements on the square lattice insulating antiferromagnets La_2CuO_4 [267] and $Sr_2CuO_2Cl_2$ is impressive. Much higher precision comparisons can be performed against state of the art quantum Monte Carlo simulations and these have been discussed recently in Refs [45] and [269]. The low T dynamical properties discussed in Sections 7.1.2 and 7.1.3.2 were applied to NMR relaxation rates in Ref [84], and compared against measurements in La_2CuO_4 in Ref [238].

We turn next to the 'high T' region of the continuum quantum rotor model. We discussed strong thermodynamic evidence for the existence of this region in the intermediate temperature properties of the $S = 1/2$ square lattice antiferromagnet in Section 5.5. The high T computations discussed in Section 7.2 were used to compute NMR relaxation rates [97, 99] and found to be in good agreement with measurements on La_2CuO_4 [238, 239]. It has been more difficult to disentangle the crossover from low T to high T in experimental measurements of the correlation length, as was pointed early on in Ref [96], and this has been discussed further in Refs [189, 269, 414]. The issue of the 'low T' to 'high T' crossover in square lattice antiferromagnets was also examined in series expansion studies by Sokol *et al.* [467] and Elstner *et al.* [135], and evidence was obtained its existence in a number of static correlators for spin $S = 1/2$. Interestingly, no such evidence was found for the

$S = 1$ case, which (as expected) is clearly too far from the quantum critical coupling.

The computations of this chapter can also be cautiously, but usefully, compared with measurements on lightly doped antiferromagnets [97], the idea being that the primary effect of doping is to change the bare coupling g to a value closer to the quantum critical point [420]. Inelastic neutron scattering measurements [220, 267] have observed a frequency dependent susceptibility which is consistent with the general scaling forms (7.1) and (7.3), for a vanishing value for their third arguments. More recently, exciting new measurements [2] also see high T scaling (with characteristic $\omega \sim T$ and $k \sim T^{1/z}$) at much higher doping, possible due to proximity to a incommensurate charge or spin ordered state. The large N prediction for the scaling function in Fig 7.3 has weight at frequencies $\omega \sim T$ and negligible weight at $\omega \ll T$, implying a 'pseudo-gap' in the spin excitation spectrum. However, this cannot be treated as a reliable experimental prediction yet, as the large N expansion was argued to be invalid for $\omega \ll T$. We will put this issue on a firmer footing in our discussions in Section 8.3 and 8.4.

8

Physics close to and above the upper-critical dimension

We briefly introduced the concept of the upper-critical dimension in Section 5.2: there we saw in a study of the large N limit that physical properties did not satisfy the simplest scaling predictions, and acquired additional cut-off dependencies in physical response functions above spatial dimension $d = 3$. We will show in this chapter that it is possible to describe the physics in $d > 3$ by a relatively straightforward perturbative method. The same perturbative analysis is also useful for $d < 3$ provided

$$\epsilon = 3 - d \tag{8.1}$$

is not too large; the perturbation theory has to be combined with a renormalization group analysis in this case.

The physics described by this perturbative method can, in most cases, also be elucidated by the large N expansion we have developed in the previous chapters. However, there are a number of instances where the underlying principles are most transparently illustrated by studies close to and above $d = 3$. Our specific reasons for undertaking such an analysis are:

- As we have noted earlier, the quantum critical point at $T = 0$, $g = g_c$, extends out to a line of finite temperature phase transitions for the cases $d = 2$, $N = 1, 2$. The ϵ expansion offers a controlled method obtaining the structure of the crossovers in the vicinity of this line.
- We have not yet found a successful description of the low frequency dynamics of the order parameter ($\mathbf{n}$ or σ^z) in the high T regime in $d = 2$, although we did succeed in $d = 1$ in Chapters 4 and 6. We shall show in Section 8.3 that the ϵ-expansion leads to an appealing quasi-classical wave description of this dynamics.

194

- For the quantum rotor models being studied here, the crossovers above the upper-critical dimension, with $d > 3$, are obviously in a physically inaccessible dimension. However the basic structure that will emerge is quite generic to quantum critical points above their upper-critical dimension. The results will therefore be useful in Part 3 where we will consider other models with a lower upper-critical dimension, so that dimensions above the upper-critical can be experimentally studied.
- The following chapter will study transport properties of the quantum rotor models in the high T and quantum-paramagnetic low T regions in $d = 2$. While it is possible to do this within the $1/N$ expansion, the computation is simplest, and most physically transparent, using the ϵ expansion we shall develop here.

The study in this chapter will use the 'soft-spin' formulation of the continuum theory of the vicinity of the quantum critical point that was noted in Section 3.1. The theory is expressed in terms of a N component field $\phi_\alpha(x, \tau)$ ($\alpha = 1 \ldots N$) which is related to the lattice quantum rotor field $\mathbf{n}_i$ by the coarse-graining transformation (3.10); for $N = 1$, a similar relationship holds between the Ising spin $\hat{\sigma}_i^z$ and a one-component field ϕ. We shall study the quantum mechanics of the ϕ_α field as specified by the imaginary time path integral in (3.11), which is reproduced here for completeness

$$\mathcal{Z} = \int \mathcal{D}\phi_\alpha(x, \tau) \exp(-\mathcal{S}_\phi),$$

$$\mathcal{S}_\phi = \int d^d x \int_0^{\hbar/k_B T} d\tau \left\{ \frac{1}{2} \left[(\partial_\tau \phi_\alpha)^2 + c^2 (\nabla_x \phi_\alpha)^2 + r \phi_\alpha^2(x, \tau) \right] \right.$$

$$\left. + \frac{u}{4!} (\phi_\alpha^2(x, \tau))^2 \right\}. \tag{8.2}$$

The structure of this field theory is similar to that of the continuum theory (3.12) or (5.16) for the fixed-length $\mathbf{n}$ field, with the main difference being that the fixed-length constraint has been dropped, and replaced instead by a quartic self-interaction u. The equivalence of the universal properties of these two formulations is a well-established principle in the theory of classical critical phenomena [65, 63]: this equivalence can be expected on general universality grounds, as the two models display a quantum critical point between a magnetically ordered and a quantum-paramagnetic phase with precisely the same symmetry structures and spectrum of low-lying excitations. We will also explicitly see examples of the equivalence in our computations with (8.2) in this chapter. In practical terms, this equivalence means that the susceptibility $\chi(k, \omega)$,

defined as the two-point correlator of the field ϕ_α satisfies, for $d < 3$, the scaling forms (7.1), and (7.3), with precisely the same scaling function $\Phi_\pm$: we shall compute here some features of these scaling functions in an expansion in ϵ, while they were computed in a $1/N$ expansion in Chapter 7. The approaches have been compared in the overlapping region of validity where both ϵ and $1/N$ are small, and exact agreement is found—this shall not be shown explicitly here, however.

The theory (8.2) can also be extended by adding additional terms involving higher powers or gradients of ϕ_α: all of these can be shown to be irrelevant for $d < 3$ using arguments which are very similar to those we discussed in Section 4.3 for the continuum theory of the quantum Ising chain.

We restrict ourselves in this chapter to results to the leading order in ϵ or u: the structure of the quantum/classical crossovers is quite complicated at higher orders, and the reader is referred to discussions in Ref. [427] for a discussion of this subtle issue; alternative approaches are also available [294, 369, 169]. Further, we will limit our discussion to regions of the phase diagram where there is no spontaneous magnetization, and complete $O(N)$ symmetry is preserved (the extension to ordered phases is straightforward). We will therefore be approaching the finite temperature phase boundaries from their high temperature side.

We will begin in Section 8.1 by a discussion of the $T = 0$ properties of (8.2): these are simply related to those obtained by interpreting (8.2) as a classical statistical mechanics problem in $D = d+1$ dimensions. Such results are standard and in-depth reviews are available [550, 247, 63], so Section 8.1 will only contain a brief discussion of the needed concepts. Section 8.2 will then provide a description of the ϵ expansion for the crossovers in the static properties of (8.2) at $T > 0$; this expansion gives a useful qualitative picture, but is not particularly accurate in $d = 2$, and also fails for low frequency dynamical properties. These deficiencies will be repaired in Section 8.2, where we will use the ϵ expansion to motivate an effective model for statics and dynamics which will be solved exactly in $d = 2$.

We will use units in which the velocity $c = 1$ throughout the remainder of this chapter only.

8.1 Zero temperature

We will work in imaginary time throughout this section. We will express the response functions in terms a $D = (d + 1)$-dimensional wavevector

$Q = (i\omega, \vec{q})$. At $T = 0$, all correlators of the action (8.2) are invariant under D-dimensional rotations in Euclidean space, and are therefore only functions of $Q^2 = q^2 + (i\omega)^2 = q^2 - \omega^2$. Dynamic quantum response functions are obtained by analytically continuing to negative Q^2. For positive Q^2 the responses are, of course, those associated with interpreting (8.2) as a classical statistical mechanics problem.

We will begin in subsection 8.1.1 by a discussion of ordinary perturbation theory in u. We will find that the results are adequate for $D > 4$, but suggest that higher-orders have to be resummed for $D < 4$. The resummation will be done using the $1/N$ expansion in subsection 8.1.2, where we will also introduce the important concept of the so-called 'tricritical crossover functions'. Finally, in subsection 8.1.3 we will present a very concise review of the field-theoretic renormalization group approach to resumming the perturbation theory in u.

8.1.1 Perturbation theory

The two-point correlator of ϕ_α under (8.2) defines, as in (5.2), the susceptibility $\chi_{\alpha\beta}(Q)$ (this single argument, D-dimensional susceptibility should not be confused with the static susceptibility of the d-dimensional quantum problem defined in (4.8); the former will always have an argument with a capital letter). In the O(N) symmetric region this satisfies $\chi_{\alpha\beta} = \chi\delta_{\alpha\beta}$. To zeroth order in u, this is

$$\chi(Q) = \frac{1}{Q^2 + r}. \tag{8.3}$$

The static susceptibility diverges at $r = 0$, so to this order in u, the paramagnetic phase is present for $r > 0$, and the quantum-critical point to the ordered phase is at $r = 0$; this is, of course, the familiar mean-field theory result. Indeed, the parameter r shall play a similar role to the tuning parameter g of the fixed-length theory (5.16): the point $g = g_c$ corresponds to $r = r_c$, and to zeroth order in u, we have $r_c = 0$.

Let us discuss corrections due to a non-zero u. As we will see, the theory (8.2) requires a short distance cut-off at a momentum scale Λ, and this cut-off sets a natural scale for u. In D dimensions, simple dimensional analysis of (8.2), shows that ϕ has the engineering dimension of (length)$^{(2-D)/2}$; so u has the engineering dimensions of (length)$^{(D-4)}$, and a natural scale for u is $\Lambda^{(4-D)}$. This suggests that a perturbative approach might be valid for

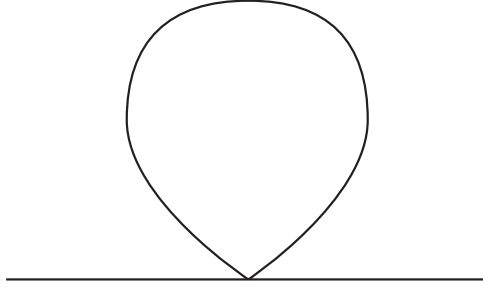$$u \ll \Lambda^{(4-D)}, \tag{8.4}$$

Fig. 8.1. Feynman diagram leading to the first order correction in the susceptibility in (8.5), and to the value of R in (8.24).

and we will assume this condition here. Improving the result (8.3) to first order in u we have from the diagram in Fig 8.1

$$\chi^{-1}(Q) = Q^2 + r + u \left(\frac{N+2}{6} \right) \int^{\Lambda} \frac{d^D K}{(2\pi)^D} \frac{1}{K^2 + r}. \tag{8.5}$$

 The divergence of the susceptibility identifies the quantum-critical point at r_c which to first order in u is

$$r_c = -u \left(\frac{N+2}{6} \right) \int^{\Lambda} \frac{d^D K}{(2\pi)^D} \frac{1}{K^2}. \tag{8.6}$$

Now let us introduce the coupling s

$$s \equiv r - r_c \tag{8.7}$$

which measures the deviation of the system from the critical point. Rewriting (8.5) in terms of s rather than r (we will always use s in favor or r in all subsequent analysis), we have

$$\chi^{-1}(Q) = Q^2 + s + u \left(\frac{N+2}{6} \right) \int^{\Lambda} \frac{d^D K}{(2\pi)^D} \left(\frac{1}{K^2 + s} - \frac{1}{K^2} \right). \tag{8.8}$$

We are interested in the vicinity of the critical point, at which $s \to 0$, and the nature of this limit depends sensitively on whether D is greater than or less than four. For $D > 4$, we can simply expand the integrand in (8.8) in powers of s and obtain

$$\chi^{-1}(Q) = Q^2 + s \left(1 - c_1 u \Lambda^{D-4} \right), \tag{8.9}$$

where c_1 is a non-universal constant dependent upon the nature of the cutoff. So the effects of interactions appear to be relatively innocuous: the static susceptibility still diverges with the mean-field form $\chi(0) \sim$

$1/s$ as $s \to 0$, and the correction to the co-efficient is small, given (8.4). This is in fact the generic behavior to all orders in u, and mean-field critical properties apply for $D > 4$; however, we will see later that there are interesting, universal fluctuation effects at $T > 0$ even for $D > 4$. For $D < 4$, we notice that the integrand in (8.8) is convergent in the ultraviolet, and so under the condition (8.4) it is permissible to send $\Lambda \to \infty$. We then find that the correction first order in u has a universal form

$$\chi^{-1}(Q) = Q^2 + s \left[1 - \left(\frac{N+2}{6} \right) \frac{2\Gamma((4-D)/2)}{(D-2)(4\pi)^{D/2}} \frac{u}{s^{(4-D)/2}} \right]. \quad (8.10)$$

So we notice that no matter how small u is, the correction term eventually becomes important for a sufficiently small s, and indeed diverges as $s \to 0$. The structure of (8.10) can be understood by noting from (8.8) that the correlation length for small u is $\xi_0 = s^{-1/2}$ and this sets a regime $u \ll \xi_0^{-(4-D)}$ over which perturbation theory is valid. So for sufficiently large ξ_0, the mean field behavior cannot be correct, and a sophisticated resummation of the perturbation expansion in u is necessary. When we turn later to an analysis at $T > 0$ however, we will find that the result (8.10) is adequate over a substantial portion of the phase diagram.

8.1.2 Tricritical crossovers

For $D < 4$, the structure of (8.10) suggests that we can express the most important terms at higher-order in u for the static susceptibility in the form

$$\chi^{-1}(Q) = s\,\Psi_D \left(\frac{Q}{s^{1/2}}, \frac{u}{s^{(4-D)/2}} \right) \quad (8.11)$$

where $\Psi_D(q, v)$ is a universal crossover function. This form is consistent with naive dimensional analysis, and the expectation that it is permissible to send $\Lambda \to \infty$ in all the singular terms at higher orders. The result (8.10) gives us the small v behavior of $\Psi_D(q, v)$:

$$\Psi_D(q, v) = q^2 + 1 - \left(\frac{N+2}{6} \right) \frac{2\Gamma((4-D)/2)}{(D-2)(4\pi)^{D/2}} v + \mathcal{O}(v^2) \quad (8.12)$$

To get the critical properties of the model for $D < 4$, however, we need its large v behavior.

The function $\Psi_D(q, v)$ is the so-called "tricritical crossover" function

of Refs. [363, 68]: this terminology is motivated by considerations unrelated to those of interest here, and will not be explained. Computation of $\Psi_D(q, v)$ by various methods are described in the literature [363, 68]: we will simply treat $\Psi_D(q, v)$ as a known function, and will find that some key properties of the $T > 0$ crossovers near the quantum critical point can be expressed in terms of it. For completeness, we note how $\Psi_D(q, v)$ may be computed in the large N limit, with vN fixed. The computation proceeds by a familiar approach: we decouple the quartic term in (8.2) by a Hubbard-Stratanovich field λ so that

$$\mathcal{Z} = \int \mathcal{D}\lambda \mathcal{D}\phi_\alpha(x, \tau) \exp(-\widetilde{\mathcal{S}}_\phi)$$

$$\widetilde{\mathcal{S}}_\phi = \int d^D x \left\{ \frac{1}{2} \left[(\partial_\tau \phi_\alpha)^2 + c^2(\nabla_x \phi_\alpha)^2 + (r + i\lambda)\phi_\alpha^2(x) \right] \right.$$
$$\left. + \frac{3\lambda^2}{2u} \right\}, \tag{8.13}$$

Now, integrate out the ϕ_α fields, which appear only as quadratic terms in (8.13); evaluating the integral over λ as a saddle-point, we obtain the required large N limit. Expressing the result in terms of s using (8.7), we can easily show that $\Psi_D(q, v)$ is given by

$$\Psi_D(q, v) = q^2 + \Pi_D(v), \tag{8.14}$$

where the function $\Pi_D(v)$ is given by the solution of the following nonlinear equation:

$$\Pi_D(v) + Nv \frac{\Gamma((4 - D)/2)}{3(D - 2)(4\pi)^{D/2}} \left[\Pi_D(v) \right]^{(D-2)/2} = 1 \tag{8.15}$$

Notice that as $v \to \infty$, $\Pi_D(v) \sim v^{-2/(D-2)}$, and inserting in (8.11), this implies that $\chi^{-1}(0) \sim s^{2/(D-2)}$ as $s \to 0$. This result agrees with our earlier large N result in (5.34), and the $N = \infty$ relation $\chi^{-1}(0) \sim \Delta_+$.

8.1.3 Field-theoretic renormalization group

The basic ideas behind this approach were already presented in Section 6.3.1 in the context of the $d = 1$ quantum rotor model, along with suggestions for further reading in the literature. Readers who skipped Chapter 6 should now read Section 6.3.1 until Eqn (6.40).

As before, it is advantageous to replace the cut-off Λ by a renormalization scale, μ at which various observable parameters are defined. At the scale μ we introduce renormalized couplings, which then replace the

bare couplings in all expressions for observable quantities: once this sub-
stitution has been performed, it is possible to send the cutoff $\Lambda \to 0$,
order-by-order in an expansion in the non-linearities. In practice, one
never needs to introduce Λ at intermediate stages as all integrals are per-
formed in dimensional regularization in $D = 4 - \epsilon$ dimensions. We will
only work to first order in ϵ here, in which case only two renormalized
couplings are necessary: s_R, a renormalized measure of the deviation
of the system from the quantum critical point, and u_R a renormalized
four-point interaction. The explicit relationship between the bare and
renormalized couplings is [63]

$$
\begin{aligned}
u &= u_R \frac{\mu^\epsilon}{S_D} \left(1 + \frac{N+8}{6\epsilon} u_R \right) \\
s &= s_R \left(1 + \frac{N+2}{6\epsilon} \right)
\end{aligned}
\tag{8.16}
$$

A factor of μ^ϵ has been scaled out u so that u_R is dimensionless, and
$S_D = 2/[\Gamma(D/2)(4\pi)^{D/2}$ is standard phase-space factor, introduced for
notational convenience.

We can state the simple, field-theoretic recipe for computing corre-
lators of (8.2). First, obtain formal expressions for the bare theory in
terms of s and u, leaving integrals unevaluated. Then, perform the sub-
stitution in (8.16) to expressions in terms of u_R and s_R. Now, evaluate
all the integrals in $D = 4 - \epsilon$ dimensions, in powers of ϵ. The constants
in (8.16) have been cleverly chosen so that all poles in ϵ cancel. The
resulting expressions for the correlators of the theory are expressed in
terms of s_R, u_R, and the momentum scale μ.

Exact renormalization group equations for all observables can be ob-
tained by the fact that no physical quantity can depend upon the value
of μ. By studying the behavior of the first equation in (8.16) under
$\mu \to \mu e^\ell$ we obtain the flow equation

$$
\frac{du_R}{d\ell} = \epsilon u_R - \left(\frac{N+8}{6} \right) u_R^2
\tag{8.17}
$$

A simple analysis of this differential equation shows that at long dis-
tances ($\ell \to \infty$), the coupling u_R flows to the attractive fixed point
at

$$
u_R^* = \frac{6\epsilon}{(N+8)}
\tag{8.18}
$$

This implies that a theory with $u_R = u_R^*$ and $s = 0$ does not flow
under rescaling transformations, and is therefore scale-invariant. This

specifies the universal quantum-critical point of theory. Turning on a $s > 0$ induces flow along the leading relevant direction, and therefore determines the $T = 0$ energy gap; deviations in u from u_R correspond to allowing corrections associated with the leading irrelevant operator, and can therefore be ignored in computations of the universal scaling functions.

Let us apply the above approach explicitly to the computation of $\chi(Q)$. We begin with the expression (8.8) and make the substitution in (8.16). Working to linear order in u_R, and evaluating the integrals in an expansion in $\epsilon = 4 - D$, we can write the result in the form

$$\chi(Q) = \frac{1}{Q^2 + \Delta_+^2} \tag{8.19}$$

where Δ_+ is the $T = 0$ gap of the quantum paramagnetic phase with $s > 0$. The explicit expression for Δ_+ is

$$\Delta_+^2 = s_R \left[1 + u_R \frac{(N + 2)}{12} \ln \left(\frac{s_R}{\mu^2} \right) \right], \tag{8.20}$$

where there is no additive term of order u_R associated with the logarithm. Precisely at $u_R = u_R^*$ the scale-invariance of the theory implies that it is permissible to re-exponentiate the logarithm (as was done in the large N expansion in (7.55)), in which case we can write

$$\Delta_+ = \mu \left(\frac{s_R}{\mu^2} \right)^\nu \tag{8.21}$$

where ν is the usual correlation length exponent, defining how the gap vanishes at $s_R = 0$ (recall that this theory has $z = 1$); it is given to this order in ϵ by

$$\nu = \frac{1}{2} + \frac{(N + 2)}{4(N + 8)} \epsilon \tag{8.22}$$

These results imply, from (8.11) that $\Psi_D(v \to \infty) \sim v^{-2(2\nu - 1)/(4 - D)} \sim v^{-(N+2)/(N+8)}$ to leading order in $4 - D$.

8.2 Statics at nonzero temperatures

This section will describes the results of the ϵ expansion on the nonzero temperature properties of (8.2). The results are helpful in exposing the general structure of the theory, but are not expected to be very accurate in $d = 2$ ($\epsilon = 1$). An improved, and quantitatively more accurate

treatment will appear in Section 8.2.1, which will also consider dynamic properties.

We shall describe the $T > 0$ static correlators proceeds [427] by a method adapted from an approach developed by Luscher [312] (related methods were also applied by others to study classical systems in finite geometries [66, 418]). Readers of Chapters 6 and 7 will recall that a similar method was used in Sections 6.3 and 7.1. The main idea is to integrate out the components of $\phi_\alpha(x, \tau)$ with a non-zero frequency along the imaginary time direction by a straightforward ϵ expansion to the vicinity of the quantum critical point. This will result in an effective action for the zero frequency component $\phi_\alpha(x)$ (which is independent of τ), which must subsequently be analyzed more carefully. The correlators of the this zero frequency effective action will yield the static susceptibility, $\chi(k)$. It must be noted that, unlike the situation in Section 4.5.1, this static susceptibility does not yield the equal time correlations, as the relationship (4.92) will not hold in general.

As we are only interested in the universal crossovers in the vicinity of the point $s = 0$, $T = 0$, for $D < 4$, we can set $u_R = u_R^*$ at the outset; further as $u_R \sim \epsilon$, the derivation of the effective action for $\phi_\alpha(x)$ can be performed in an expansion in powers of the non-linear coupling u_R. For $D > 4$ the mean-field behavior of the system at $T = 0$ suggests that an expansion in powers of u should be adequate for $T > 0$, and we shall indeed find that this is the case. A simple, one-loop, perturbative calculation then gives the following effective action for the static correlators:

$$\mathcal{Z} = \int \mathcal{D}\phi_\alpha(x) \exp(-\mathcal{S}_{\phi,\text{eff}})$$

$$\mathcal{S}_{\phi,\text{eff}} = \frac{1}{T} \int d^d x \left\{ \frac{1}{2} \left[(\nabla_x \phi_\alpha)^2 + \widetilde{R} \phi_\alpha^2(x) \right] + \frac{U}{4!}(\phi_\alpha^2(x))^2 \right\}. \quad (8.23)$$

The couplings $\widetilde{R}$ and U can be expressed in terms of the bare couplings in the quantum action (8.2):

$$\widetilde{R} = r + u \left(\frac{N+2}{6} \right) T \sum_{\epsilon_n \neq 0} \int \frac{d^d k}{(2\pi)^d} \frac{1}{\epsilon_n^2 + k^2 + r}$$

$$U = u - u^2 \left(\frac{N+8}{6} \right) T \sum_{\epsilon_n \neq 0} \int \frac{d^d k}{(2\pi)^d} \frac{1}{(\epsilon_n^2 + k^2 + r)^2}. \quad (8.24)$$

The result for $\widetilde{R}$ arises from the diagram in Fig 8.1, and that for U from Fig 8.2, where the internal lines carry only non-zero Matsubara
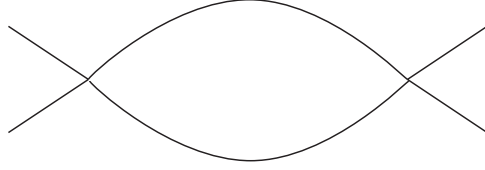
Fig. 8.2. Feynman diagram leading to the coupling U in (8.24).

frequencies. We will discuss the evaluation of these expressions shortly. For the moment, let us simply retain the formal expressions in (8.24), and proceed a bit further. Now notice that the effective action (8.23) has precisely the same form as the original theory (8.2) at $T = 0$: the only, and crucial, difference is that the spacetime dimension D has been replaced by the spatial dimension d. Therefore, the theory (8.23) can be analyzed by the perturbative method of Section 8.1.1, or by the tricritical formulation of Section 8.1.2 simply by performing the replacement $D \rightarrow d$, and by a relabeling of the coupling constants. Using these methods, it is easy to get formal expressions for the equal-time correlators resulting from $\mathcal{S}_{\phi,\mathrm{eff}}$. We first define a shift in the value of the mass, as in (8.6) and (8.7):

$$R = \widetilde{R} + U \left(\frac{N+2}{6} \right) \int \frac{d^d k}{(2\pi)^d} \frac{T}{k^2}. \tag{8.25}$$

Then the equivalence between (8.23) and (8.2) at $T = 0$, and the response function (8.11) of the latter tells us that the static susceptibility, defined in (4.8) is given by

$$\chi(k) = \frac{1}{R} \Psi_d^{-1} \left(\frac{k}{R^{1/2}}, \frac{TU}{R^{(4-d)/2}} \right). \tag{8.26}$$

As noted earlier, we regard Ψ_d as a known function, and so (8.26) construes the final solution of the crossovers of the static observables (8.2) at finite temperature in the region without long-range-order. We emphasize again that Ψ_d has to be computed in the spatial dimension d, and not the spacetime dimensions $D = d + 1$ which was considered in Section 8.1. The large N solution of $\Psi_d(q, v)$ was given in (8.14,8.15), and is valid for all values of v: however, we will find below that the exact perturbative result (8.12) (valid for small v), is in fact sufficient over a substantial portion of the phase diagram.

The transition to the phase with long-range order will be signaled by a divergence in $\chi(k = 0)$. The general structure of (8.26) tells us that

this will happen at a value $R = R_c$, with $R_c \sim (TU)^{2/(4-d)}$ (the missing coefficient is a universal number determined by the function Ψ_d). The $N = \infty$ result (8.15) has $R_c = 0$, and this is also found to leading order in the $4 - d$ expansion for tricritical crossovers. We will assume $R_c = 0$ in our discussion in this section below, and corrections due to a non-zero R_c are higher order in ϵ. So the result (8.26) is valid provided $R > 0$, and the condition $R = 0$ gives the boundary of the finite temperature phase transition to the ordered phase.

It remains to compute the values of the couplings R, U to complete our description of static correlations, and the associated phase diagram of (8.2) in the r, T plane. We will consider the cases $d < 3$ and $d > 3$ separately, as the results are substantially different.

8.2.1 $d < 3$

We first determine the value of R for $d < 3$. The expression for R is given in (8.24) and (8.25), and to evaluate it in the scaling limit, we use precisely the same prescription discussed earlier in Section 8.1.3 for the $T = 0$ computation: the spatial integrals are evaluated in $d = 3 - \epsilon$ dimensions, the couplings are expressed in terms in terms of the renormalized parameters as defined in (8.16), an expansion is made in powers of ϵ, and finally the resulting expression is evaluated at the fixed point value (8.18). Just as at $T = 0$, the poles in ϵ cancel also at $T > 0$, and to first order in ϵ, the result is

$$R = s_R \left[1 + \epsilon \left(\frac{N+2}{N+8} \right) \ln \left(\frac{T}{\mu} \right) \right] + \epsilon T^2 \left(\frac{N+2}{N+8} \right) G \left(\frac{s_R}{T^2} \right) \quad (8.27)$$

where the function $G(y)$ is given by

$$G(y) = \frac{y \ln y}{2} + 4 \int_0^\infty k^2 dk \left(\frac{1}{\sqrt{k^2 + y}} \frac{1}{e^{\sqrt{k^2+y}} - 1} - \frac{1}{k^2 + y} + \frac{1}{k^2} \right) \quad (8.28)$$

We have obtained this expression assuming that $s_R > 0$ (and therefore $y = s_R/T^2 > 0$), and the result for $G(y)$ appears to have some singularity at $y = 0$. We shall shortly establish that this is not the case: a crucial property of the function $G(y)$ is that it is analytic at $y = 0$, and can therefore be analytically continued to $y < 0$. There is an important physical reason for this analyticity, and it is a key step in our analysis. Recall that at $T = 0$, there was a quantum phase transition in (8.2) at $s_R = 0$ ($r = r_c$ from (8.7)), and so all response functions are certainly

non-analytic at $s_R = 0$. However, we are considering the case $T > 0$, and we expect that there is no thermodynamic singularity at $r = r_c$: the critical fluctuations surely get quenched at a non-zero T, and all observables should have a smooth, well-behaved dependence on r at $r = r_c$ for $T > 0$, as we saw in the case of the Ising chain in Chapter 4. There will eventually be a non-zero T phase transition for some $s_R < 0$ ($r < r_c$) as in Fig 5.3, and so there should be a thermodynamic singularity at this point. However, the latter singularity is a property of the scaling function Ψ_d in (8.26), and *not* a singularity in the value of the coupling R. So if our physical interpretation is correct, $G(y)$ should be analytic at $y = 0$, and it should be possible to analytically continue $G(y)$ to all $y < 0$ until the point we hit the transition to the ordered phase where R, as defined in (8.27), first vanishes.

We explicitly demonstrate that the expectation above is indeed satisfied by (8.28) (indeed, our entire analysis of the crossover problem was carefully designed that this would occur). After an integration by parts under the integral in (8.28), and some elementary manipulations, it can be shown that $G(y)$ can be transformed into the following:

$$
G(y) = -\int_0^\infty dk \left[4\ln\left(k\frac{\sinh(\sqrt{k^2 + y}/2)}{\sqrt{k^2 + y}/2} \right) - 2k - \frac{y}{\sqrt{k^2 + 1/e}} \right]
$$
(8.29)

In this form, it is not difficult to see that $G(y)$ is analytic at $y = 0$; the function $\sinh(\sqrt{z})/\sqrt{z}$ is a smooth function of z near $z = 0$, and equals $\sin(\sqrt{|z|})/\sqrt{|z|}$ for $z < 0$, and so there is no singularity in the integrand as y goes through zero. Indeed $G(y)$ is smooth for all $y > -2\pi$, with the singularity arising at -2π when the argument of the logarithm first turns negative. We will find below that the transition to the ordered phase occurs for $y \sim -\epsilon$, so the singularity at $y = -2\pi$ occurs well within the ordered phase where the present results cannot be used, and is therefore of no physical consequence. We also note here some limits of (8.29) which will be useful later

$$
G(y) = \begin{cases} 2\pi^2/3 + 2.45381y & |y| \ll 1 \\ (y/2)\ln y + 2\pi\sqrt{y} + y^{1/4}\sqrt{8\pi}e^{-\sqrt{y}} & y \gg 1 \end{cases}
$$
(8.30)

While we have a fairly complete picture of the function $G(y)$, the result (8.27) for R is still not ready to be used as it involves the unknown momentum scale μ. To remedy this, we recall a basic strategy used throughout this book: all correlators should be expressed in terms of observable parameters characterizing the $T = 0$ ground state. In the

present situation we should clearly replace s_R as a measure of the deviation from the $T = 0$ quantum critical point at $s_R = 0$, by the energy scales $\Delta_\pm$ which were discussed in Chapter 5. We will only do this here for $s_R > 0$ (the case $s_R < 0$ is discussed in Ref [427]): the relationship between s_R and the energy gap of the quantum paramagnet, Δ_+, was obtained in (8.21). Substituting (8.21) into (8.27) we find

$$R = \Delta_+^2 \left[1 + \epsilon \left(\frac{N+2}{N+8} \right) \ln \left(\frac{T}{\Delta_+} \right) \right] + \epsilon T^2 \left(\frac{N+2}{N+8} \right) G \left(\frac{\Delta_+^2}{T^2} \right). \quad (8.31)$$

The dependence on the arbitrary scale μ has disappeared, and we have the required universal dependence of R on Δ_+ and T for $s_R > 0$ ($r > r_c$). A similar relationship exists between the scale Δ_- and R for $r < r_c$ [427].

A closely related computation can be performed for the quartic coupling U in (8.23) using the expression in (8.24). At the fixed point $u_R = u_R^*$ we again find that the μ dependence disappears:

$$U = \frac{6\epsilon T^\epsilon}{S_D(N+8)} \left[1 + \epsilon \frac{20 + 2N - N^2}{2(N+8)^2} + \epsilon G' \left(\frac{s_R}{T^2} \right) \right], \quad (8.32)$$

where $G'(y)$ is derivative of $G(y)$, and we have actually used the expression for u_R^* to order ϵ^2 to obtain the complete result above. For $s_R > 0$ we can simply substitute $s_R = \Delta_+^2$ in the argument of G' to get the universal expression for U.

We have assembled all the ingredients to obtain the full crossover structure for the static susceptibility at $T > 0$: we use the expressions (8.27) or (8.31) for R, and the expression (8.32) for U, substitute them into (8.26), with results for the tricritical crossover function Ψ_d obtained in Section 8.1.2. A straightforward examination of the resulting expressions yields the phase diagram shown in Fig 8.3, which is closely related to the phase diagram obtained earlier in the large N limit in Fig 5.3. The physical properties of the regimes were already discussed in Section 5.4, and we note their properties for small ϵ in turn below.

The low T regime on the quantum paramagnetic side was discussed in Section 5.4.1: it is present for $T \ll \Delta_+ \sim (r - r_c)^\nu$. Using (8.30-8.32), we have for this case

$$
\begin{aligned}
R &\sim \Delta_+^2 \\
U &\sim \epsilon \Delta_+^\epsilon \\
TU/R^{(4-d)/2} &\sim \epsilon T/\Delta_+ \ll 1
\end{aligned}
\qquad (8.33)
$$

The last quantity is that appearing in the argument of the tricritical scaling function, Ψ_d, in (8.26). As it is small, it is evident that a simply
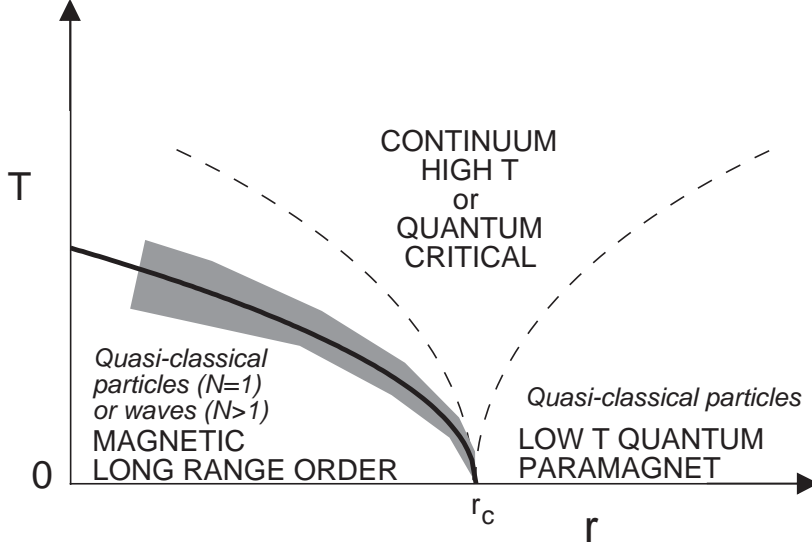
Fig. 8.3. Phase diagram of the theory (8.2) for $d < 3$ (compare with the large N phase diagram in Fig 5.3. The qualitative features are expected to apply to $d > 1$ for $N = 1$, $d \geq 2$ for $N = 2$, and $d > 2$ for $N \geq 3$. The quantum critical point is at $T = 0$ with coupling $r = r_c$ (this is also the coupling where $s = s_R = 0$). All properties are however analytic as a function of r at $r = r_c$ for $T > 0$. The dashed lines are crossovers at $T \sim |r - r_c|^{z\nu}$, as is the full line, which is the locus of finite temperature phase transitions at $T_c(r)$. The shaded region is where the reduced classical scaling functions apply. The region $T > T_c(r)$, but $r < r_c$ is accessed in our calculation by analytic continuation from $r > r_c$, $T > 0$. The simple perturbative expression in (8.10)) can be used in (8.26) for the static susceptibility everywhere in the paramagnetic region, except for the shaded portion. The low T region for $r > r_c$ has a quasi-classical particle description as in Section 4.5.2, and to be discussed in Chapter 9. In the magnetically ordered low T region for $r < r_c$ and $N \geq 2$, the long-wavelength spin waves about the ordered state behave classically, while for $N = 1$, the amplitude oscillations in ϕ_α about its non-zero mean value lead to a quasi-classical particle. As we noted in Fig 7.1, the 'continuum high T' or 'quantum critical' region is more complex, with thermal and quantum, and particle- and wave-like phenomena playing equal roles. In Section 8.3 we shall show that, to leading order in $\epsilon = 3 - d$, the low frequency correlators of ϕ_α in this region are described an effective quasi-classical *wave* model; however, the transport of the conserved angular momentum is dominated by higher energy excitations, and requires a particle-like description in a quantum Boltzmann equation which will be discussed in Chapter 9.

perturbative evaluation of Ψ_d in (8.12) is adequate for analyzing static properties in this regime. Using (8.12) and (8.30-8.32) in (8.26) we get

$$\chi^{-1}(k) = k^2 + \Delta_+^2 + \epsilon \left(\frac{N+2}{N+8} \right) T(8\pi T \Delta_+)^{1/2} e^{-\Delta_+/T}. \qquad (8.34)$$

So there is only a correction of order $e^{-\Delta_+/T}$ to the $T = 0$ response: similar results were obtained in the large N limit in Section 5.4.1. This exponentially small correction arises from the small density of pre-existing thermally excited particles. For the same reasons as those discussed in Section 4.5.2 (and also Section 6.2), we expect that these particles form a Boltzmann gas, whose static and dynamic properties can be described by standard classical methods: we will see this in our discussion of transport properties in Chapter 9.

Next we turn to the high T regime of the continuum theory $T \gg |r - r_c|^\nu$. Now, the analogs of the estimates (8.33) are

$$
\begin{aligned}
R &\sim \epsilon T^2 \\
U &\sim \epsilon T^\epsilon \\
TU/R^{(4-d)/2} &\sim \sqrt{\epsilon} \ll 1.
\end{aligned}
\qquad (8.35)
$$

So again, the second argument of Ψ_d is small, and a perturbative evaluation is permissible. Using (8.12) and (8.30-8.32) in (8.26) we get

$$\chi^{-1}(k) = k^2 + \epsilon \left(\frac{N+2}{N+8} \right) \frac{2\pi^2 T^2}{3} \qquad (8.36)$$

to leading order in ϵ, which implies a correlation length $\xi \sim 1/\sqrt{\epsilon}T$. The almost free nature of this static result suggests that thermal fluctuations are non-critical and can be treated in an effectively Gaussian theory. However, when the present perturbative approach is extended to dynamical properties, one finds that it fails in the low frequency limit [427] (just as we found for the $1/N$ expansion in Section 7.2.2). The strongly coupled dynamical problem will be treated in Section 8.3, and associated transport properties in Chapter 9.

Finally, we turn to a novel part of the analysis using the ϵ expansion: the region of the phase without long-range order for $r < r_c$. Now $s_R < 0$, and it is possible for R to vanish. Using (8.27), we find that this happens at $s_R = s_{Rc}$ given by

$$s_{Rc} = -\epsilon \left(\frac{N+2}{N+8} \right) \frac{2\pi^2 T^2}{3} \qquad (8.37)$$

to leading order in ϵ; this relationship can be translated into a universal

proportionality between T_c and Δ_-, but we will not discuss that here. The value of s_{Rc} determines the phase transition line $T = T_c(r)$ shown in Fig 8.3. The order of magnitude estimates of the couplings in (8.35) remain valid for $T > T_c(r)$ except that the omitted co-efficient in the first expression of R vanishes as one approaches $T_c(r)$ from above. A simple estimate of the dimensionless coupling in the argument of Ψ_d then shows that the perturbative computation of Ψ_d fails when $(T - T_c(r)) \sim \epsilon T_c(r)$. This condition delineates the boundary of the shaded region shown in Fig 8.3. Within this region there is the well-understood classical physics of a finite temperature phase transition in d spatial dimensions: it will described by the appropriate classical singularity of Ψ_d discussed in Section 8.1.3 (we note again that these latter results have to be used in d rather than D dimensions; thus this emergence of classical statistical mechanics is completely unrelated to the $\mathcal{QC}$ mapping of Section 3.2, which mapped d-dimensional quantum mechanics to D-dimensional classical statistical mechanics). From the perspective of the global quantum scaling functions like (5.60), the shaded regime is where the reduced classical scaling functions will apply.

While (8.37) contains the leading prediction of the ϵ expansion for value of the critical temperature $T_c(r)$, the result is not satisfactory in one important respect. Note that we find a $T_c > 0$ for *all N*. This is the correct result for $2 < d < 3$, but is incorrect precisely in $d = 2$, the dimensionality of physical interest. In $d = 2$ we should find $T_c = 0$ for all $N \geq 3$, as we found in the large N expansion in Chapters 5 and 7. This failure suggests that the estimate (8.37) for T_c is not very accurate for $d = 2$, $N = 1, 2$. We will rectify this failure in Section 8.3, where we will treat the effective theory (8.23) *directly in $d = 2$*. This can be done by a variety of analytical and numerical methods [431], which lead to quite accurate results for $d = 2$, $N = 1, 2$.

8.2.2 $d > 3$

This is obviously an unphysical regime, but we discuss it briefly to note the physics of models above their upper-critical dimension. We will later meet models whose quantum-critical points have a lower value for the upper-critical dimension, and their properties will be quite similar to those found here. We will assume here that $d < 4$, so that the classical finite-temperature transition remains below its upper-critical dimension: there is little physical interest in discussing the case where

both the quantum and classical transition are above their respective upper-critical dimensions.

The basic results are already contained in the expression (8.6) for the position of the $T = 0$ critical point, the definition (8.7), and the values (8.24) and (8.25) for the effective coupling R. It will always be sufficient to just use the first order result $U = u$ for the non-linear coupling. It is not necessary to renormalize the values of any coupling, and we can simply express the results in terms of bare parameters. The expressions also have a dependence upon the non-universal upper-cutoff Λ, and the main subtlety in the evaluation of the results is the separation of this non-universality from the T dependence which we shall find is universal. Further this separation of Λ dependence must be done in a manner which maintains analyticity in s at $s = 0$ for $T > 0$.

The first step is the evaluation of the frequency summation in the expressions noted above for R: this leads to form for R closely related to expressions (8.27,8.28) for $d < 3$

$$R = s + u \left(\frac{N+2}{6} \right) \left[\int \frac{d^d k}{(2\pi)^d} \left(\frac{1}{\sqrt{k^2+s}} \frac{1}{e^{\sqrt{k^2+s}/T} - 1} - \frac{T}{k^2+s} \right. \right.$$
$$\left. \left. + \frac{T}{k^2} \right) + \int^\Lambda \frac{d^D K}{(2\pi)^D} \left(\frac{1}{K^2+s} - \frac{1}{K^2} \right) \right]. \tag{8.38}$$

We observe that the cut-off dependence is isolated entirely in the second integrand which is a property of the $T = 0$ theory: this is why the T dependence, which depends only upon the low energy excitations is universal. We can remove this ultraviolet divergence by adding and subtracting s/K^4 to the second-integrand: notice that this correction term is smooth in s so that the analyticity properties of the expression for R in terms of s will not be spoiled. The correction term leads to a cut-off dependent term which is also linear in s, and the remaining integral is convergent at high momenta: in this way we get our final result

$$R = s \left(1 - c_1 u \Lambda^{d-3} \right) + u T^{d-1} \left(\frac{N+2}{6} \right) \widetilde{G}_d \left(\frac{s}{T^2} \right), \tag{8.39}$$

where c_1 is the same non-universal constant which appeared in (8.9), and the universal function $\widetilde{G}_d(y)$ is given by

$$\widetilde{G}_d(y) = S_d \int_0^\infty k^{d-1} dk \left(\frac{1}{\sqrt{k^2+y}} \frac{1}{e^{\sqrt{k^2+y}} - 1} - \frac{1}{k^2+y} + \frac{1}{k^2} \right.$$

$$+\frac{1}{2\sqrt{k^2+y}}-\frac{1}{2k}+\frac{y}{4k^3}\Bigg) . \tag{8.40}$$

Despite appearances, this function is analytic as a function of y at $y = 0$: this can be established by studying the small k behavior of the integrand, and using the fact that the function $1/(e^x - 1) - 1/x + 1/2$ has an expansion about $x = 0$ which involves only positive, odd powers of x. Consequently, (8.40) can also be analytically continued to $y < 0$, but we will not present the details of this.

With the result for R available in (8.39), and the value $U = u$, we obtain the static susceptibility by simply evaluating (8.26), and thence obtain the nonzero T crossovers near the quantum critical point $T = 0$, $s = 0$. The structure of the results is very similar to those obtained in Section 8.2.1, and so we will only state the main conclusions. Provided there is no long-range order the static susceptibility takes the form

$$\chi^{-1}(k) = k^2 + \xi^{-2} \tag{8.41}$$

where ξ is the correlation length. For $s > 0$, and $T \ll \sqrt{s}$ we have

$$\xi^{-2} = s\left(1 - c_1 u \Lambda^{d-3}\right) + u\left(\frac{N+2}{6}\right)\left(\frac{T}{2\pi}\right)^{d/2} s^{(d-2)/4} e^{-\sqrt{s}/T}; \tag{8.42}$$

so the T-dependent correction to the correlation length is exponentially small, as expected for a system with an energy gap. At higher temperatures, $T \gg \sqrt{|s|}$, we have the limiting behavior

$$\xi^{-2} = s\left(1 - c_1 u \Lambda^{d-3}\right) + u T^{d-1}\left(\frac{N+2}{6}\right) S_d \Gamma(d-1)\zeta(d-1) \tag{8.43}$$

where $\zeta(x)$ is the Reimann zeta function; so for $s > 0$ and $\sqrt{s} \ll T \ll (s/u)^{1/(d-1)}$ the first $T = 0$ term in (8.43) dominates, while for higher T the second T-dependent term takes over. For $s < 0$, setting $\xi^{-2} = 0$ gives the us the condition for the transition to the ordered phase, $T_c \sim (|s|/u)^{1/(d-1)}$ which is analogous to the result (8.37) for $d < 3$.

We draw the reader's attention to an important property of the above results. Note that in the high T limit $T \gg \sqrt{|s|}$, the correlation length does *not* obey the relation $\xi \sim T^{-1/z}$ that might be expected from general scaling arguments; instead we have have the result of (8.43) where $\xi \sim T^{-(d-1)/2}$, which agrees with the naive scaling estimate only in the upper-critical dimension $d = 3$. The violations of scaling are a consequence of the prefactor of the irrelevant coupling u in the T-dependent term in (8.43). In the strict scaling limit, we should set this

irrelevant coupling to zero, but then we would have a T-independent correlation length. So, unlike the case for $d < 3$, irrelevant couplings have to included to obtain the leading T dependence. Such couplings which cannot be neglected even though they are formally irrelevant, are called *dangerously irrelevant*. It should also be evident (we will briefly discuss this issue further in the following section) that such violations of scaling also appear in the characteristic time for dynamic fluctuations in the high T regime: they are no longer simply universal numbers times $\hbar/k_B T$, but are proportional to higher powers of $1/T$ times a prefactor involving the non-universal bare value of the coupling u.

8.3 Order parameter dynamics in $d = 2$

We will begin by formulating an effective theory for the low-energy, long-wavelength fluctuations of the order parameter ϕ_α. This model will then be used to compute the behavior of $\mathrm{Im}\chi(k,\omega)$ at small k and ω. An important limitation of the resulting model is that it *cannot* be used to compute universal transport properties (*i.e.* correlators of $\mathbf{L}$, the uniform susceptibility χ_u, and the spin diffusion constant D_s). These turn out to be dominated by larger k and ω, as the small k and ω fluctuations of ϕ_α, while having a large amplitude, carry very little angular momentum current. A separate model for transport properties will be developed in Chapter 9.

We will mostly limit our attention here to dynamics in the continuum high T ('quantum critical') region of Figs 8.3 (which applies to $N = 1, 2$ in $d = 2$) and 7.1 (which applies to $N \geq 3$ in $d = 2$), but consider all values of N. Dynamical properties in this region were studied by large N expansion in Section 7.2, and led to Fig 7.3 for $\mathrm{Im}\chi(k,\omega)$ (which is the analog of Fig 4.9 for the Ising chain). The large N expansion was found to be adequate near the position of the quasi-particle pole ($\omega \approx ck$), but failed badly for $\omega \ll T$, $ck \ll T$. It is this failure we will rectify here; our aim is to obtain the analog of the Ising chain results for $\mathrm{Im}\chi(k,\omega)/\omega$ in Figs 4.10-4.12 for dimension $d = 2$. As we will see, there are some significant, qualitative physical differences between $d = 1$ and $d = 2$.

The basis of our approach depends upon the values of the coupling constants for the effective theory $\mathcal{S}_{\phi,\mathrm{eff}}$ in (8.23) for the static ϕ_α fluctuations obtained in the ϵ-expansion. In particular, this theory is characterized by a renormalized "mass", R (defined in (8.25)), which in the

high T region is (from (8.27) and (8.36))

$$R = \epsilon \left(\frac{N+2}{N+8} \right) \frac{2\pi^2 T^2}{3}. \tag{8.44}$$

The characteristic wavevector and energy of the dominant ϕ_α fluctuations both equal $\sqrt{R}$ (in units with $c = 1$ which we are using in this chapter). Observe that from small ϵ, $\sqrt{R} \ll T$, and so the occupation number of ϕ_α modes with this energy is large

$$\frac{1}{e^{\sqrt{R}/T} - 1} \approx \frac{T}{\sqrt{R}} \sim \frac{1}{\sqrt{\epsilon}} \gg 1; \tag{8.45}$$

The second term above is the classical equipartition value, and suggests that predominant fluctuations are *classical waves* in the magnitude and orientation of ϕ_α.

How can we extend the model (8.23) to describe the dynamics of these classical waves ? (The reasoning is almost identical to that presented in Section 6.3.3 for the high T regime of the $d = 1$ rotor model; readers who have skipped Chapter 6 may wish to read Section 6.3.3 until Eqn (6.55), but this is not essential.) The predominance of fluctuations with energy smaller than T implies that the classical fluctuation dissipation theorem (4.92) applies, and (4.93) allows us to obtain the equal-time correlations of ϕ_α from the static susceptibility of (8.23). For unequal time correlations, we need to account for the kinetic energy of the ϕ_α fluctuations. To this end, we introduce a canonically conjugate momentum, π_α, so that we have the following standard Poisson bracket relations between the ϕ_α, π_α:

$$\begin{aligned}
\{\phi_\alpha(x), \pi_\beta(x')\}_{PB} &= \delta_{\alpha\beta}\delta(x - x') \\
\{\phi_\alpha(x), \phi_\beta(x')\}_{PB} &= 0 \\
\{\pi_\alpha(x), \pi_\beta(x')\}_{PB} &= 0.
\end{aligned} \tag{8.46}$$

The Hamiltonian implied by (8.23) contains only 'potential energy' terms, and it has to be extended to include the kinetic energy. At the low order in ϵ we are working here, there are no renormalizations of the gradient terms in (8.2), and so the kinetic energy is simply the standard $\int d^d x \pi_\alpha^2/2$ implied by the Hamiltonian form of the quantum Lagrangean in (8.2); in this respect, the present situation is simpler than that in Section 6.3.3, where a careful computation of the temperature dependence of the uniform susceptibility was necessary to obtain the proper kinetic energy term. In this manner we are led to the following classical phase

space integral (as in "$\int dq dp$") to generalize the configuration space integral in (8.23):

$$
\mathcal{Z} = \int \mathcal{D}\phi_\alpha(x) \mathcal{D}\pi_\alpha(x) \exp\left(-\frac{\mathcal{H}_c}{T}\right)
$$

$$
\mathcal{H}_c = \int d^d x \left\{ \frac{1}{2} \left[\pi_\alpha^2 + (\nabla_x \phi_\alpha)^2 + \widetilde{R} \phi_\alpha^2 \right] + \frac{U}{4!} (\phi_\alpha^2(x))^2 \right\} . (8.47)
$$

Observe that we can freely integrate out the π_α in a Gaussian integral, and the functional integral over the ϕ_α and its equal-time correlations then reduce to those implied by (8.23), as they should. This argument shows that the couplings $\widetilde{R}$ and U above are precisely those computed in Section 8.2 in the ϵ-expansion.

For unequal time correlations, we compute the Hamilton-Jacobi equations implied by (8.47) and the Poisson brackets (8.46):

$$
\begin{aligned}
\frac{\partial \phi_\alpha}{\partial t} &= \{\phi_\alpha, \mathcal{H}_c\}_{PB} \\
&= \pi_\alpha \\
\frac{\partial \pi_\alpha}{\partial t} &= \{\pi_\alpha, \mathcal{H}_c\}_{PB} \\
&= \nabla_x^2 \phi_\alpha - \widetilde{R}\Phi_\alpha - \frac{U}{6}(\phi_\beta^2)\phi_\alpha . \quad (8.48)
\end{aligned}
$$

Determination of the dynamic correlations now reduces to a problem of the form also discussed in Section 6.3.3. Pick a set of initial conditions for ϕ_α, π_α from the ensemble implied by (8.47). Then evolve forward in time, according to the deterministic equations (8.48). Finally, compute unequal time correlations by averaging products of fields at different times over the set of initial conditions in (8.47).

The scaling structure of the continuum dynamical problem defined above has been discussed carefully in a recent paper [431], but the central result is simple and quite easy to understand. First, let us discuss the equal-time correlations computed in Section 8.2 in a slightly different language. The continuum statistical mechanics problem defined by the functional integral in (8.23) requires some consideration of the dependence of correlators on short-distance cutoff, Λ^{-1}. For $d < 3$, the answer is very simple: introduce a new renormalized 'mass' R as in (8.25), and then send the ultraviolet cutoff, Λ, to infinity—a finite, universal, continuum answer will be obtained, which is, of course, that specified in the tricritical crossover function in (8.26). Notice that the integral in (8.25) is divergent in the ultraviolet for d close to 3: what we are saying is that this is the only short distance singularity in the

problem for $\epsilon = 3 - d > 0$ and small, and this can be removed by a simple, linear shift in the value of the mass R. After such a shift, the continuum limit is well defined, and we can then deduce the form of all correlators by a simple, engineering analysis of dimensions. The claim of Ref [431] (which we accept here without proof) is that this same shift is also sufficient for unequal time correlations; readers who read Chapter 6 will recall that a very similar claim was made in Section 6.3.3.

Let us, then, perform the straightforward engineering analysis of dimensions. We transform to dimensionless spatial, time, and field variables by the substitutions

$$
\begin{aligned}
\overline{x} &= xR^{1/2} \\
\overline{t} &= tR^{1/2} \\
\overline{\phi}_\alpha &= R^{(2-d)/4}T^{-1/2}\phi_\alpha \\
\overline{\pi}_\alpha &= R^{-d/4}T^{-1/2}\pi_\alpha
\end{aligned}
\tag{8.49}
$$

in (8.47) and (8.48). All dimensional couplings in (8.47) and (8.48) disappear, and they acquire a universal form dependent only on a single dimensionless parameter multiplying the quartic (cubic) term in (8.47) ((8.48)), which is

$$
\mathcal{G} \equiv \frac{TU}{R^{(4-d)/2}}.
\tag{8.50}
$$

This is, of course, precisely the dimensionless parameter which appeared in crossover functions like (8.26): we now have given it a separate symbol which represents its role as a 'Ginzburg parameter' [318], controlling the strength of thermal fluctuations. The scaling form (8.26) can now be immediately deduced from the mappings (8.49), but the present approach also allows us to write down the form of the dynamic structure factor in a manner similar to that used in (4.95), (6.62) and (7.36):

$$
\frac{2T}{\omega}\text{Im}\chi(k,\omega) = S(k,\omega) = \frac{T\chi(k)}{\sqrt{R}}\Phi_{Sc}\left(\frac{k}{R^{1/2}}, \frac{\omega}{R^{1/2}}, \mathcal{G}\right).
\tag{8.51}
$$

The first relation is the classical fluctuation-dissipation theorem (4.92), and Φ_{Sc} is a universal scaling function. The prefactor of the static susceptibility, $\chi(k)$, satisfies (8.26), and was already computed in Section 8.2.1; it has been inserted so that the Kramers-Kronig relation (4.10) implies that Φ_{Sc} has a fixed integral over frequency,

$$
\int \frac{d\overline{\omega}}{2\pi}\Phi_{Sc}(\overline{k}, \overline{\omega}, \mathcal{G}) = 1,
\tag{8.52}
$$

as in Fig 4.12 and (4.96).

Our task is now clear. Solve the continuum equations of motion (8.48) for initial conditions specified by (8.47), and so determine the scaling function Φ_{Sc}. For the high T region, this solution should be obtained at the value of $\mathcal{G}$ determined in Section 8.2.1, which is

$$\mathcal{G} = \frac{48\pi\sqrt{3}}{\sqrt{2(n+2)(n+8)}}\sqrt{\epsilon}, \qquad (8.53)$$

and is small for small ϵ. In general, as implied by the discussion in Section 8.2.1, $\mathcal{G}$ is a smooth, dimensionless function of $s_R/T^{1/z\nu}$ (and can be rewritten as a universal function of Δ_+/T on the quantum paramagnetic side, and similarly for the magnetically ordered side); it decreases (increases) from the high T value in (8.53) as we decrease T towards the quantum paramagnetic (magnetically ordered) region. For $\mathcal{G} = 0$, the dynamic problem is one of linear waves, and can be easily solved. For small $\mathcal{G}$, equal-time correlations can be obtained in perturbation theory, and this was already discussed in Section 8.2.1. However, as we have already noted, perturbation theory fails for dynamic properties in the low frequency limit [427] for any non-zero $\mathcal{G}$.

So the only remaining possibility is to numerically solve the strong-coupling dynamical problem specified by (8.47) and (8.48). Formally, we are carrying out an ϵ expansion, and so the numerical solution should be obtained for d just below 3. However, it is naturally much simpler to simulate *directly in $d = 2$*, which is also the dimensionality of physical interest. So the approach to the solution of the dynamic problem in the quantum critical region breaks down into two systematic steps: (*i*) Use the $\epsilon = 3 - d$ expansion to derive an effective classical non-linear wave problem characterized by the couplings R and $\mathcal{G}$. (*ii*) Obtain the exact numerical solution of the classical non-linear wave problem at these values of R and $\mathcal{G}$ directly in $d = 2$. This fracture of the problem into two rather disjointed steps is also physically reasonable: it is primarily the classical thermal fluctuations for which the dimensionality $d = 2$ plays a special role and the cases $N = 1, 2$ and $N \geq 3$ are strongly distinguished, and so it is important to treat these exactly; on the other hand, the $\epsilon = 3 - d$ expansion provides a reasonable treatment of the quantum fluctuations down to $d = 2$ for all N.

Before embarking on a description of this numerical solution, let us make some peripheral remarks. First, the relationship (8.25) between $\widetilde{R}$ and R cannot be used in $d = 2$ because there is now an *infrared*

divergence in the momentum integral. Instead we replace (8.25) by

$$\widetilde{R} = R - U \left(\frac{N+2}{6} \right) \int \frac{d^d k}{(2\pi)^d} \frac{T}{k^2 + R},\tag{8.54}$$

which is a non-linear relationship between $\widetilde{R}$ and $\widetilde{R}$. The change in the propagator makes no difference at large momenta, and so the cancellation of ultraviolet divergences goes through as before [309]. The value of R as computed in the ϵ expansion is now different, but the leading order result (8.44) remains unchanged. The new relationship (8.54) does have some important consequences for the structure of the static properties at large $\mathcal{G}$, but we will not go into this here. In particular, the present approach can be used to reliably obtain physically important crossovers in $d = 2$ (like that in the static susceptibility $\chi(k, \omega = 0)$, and the superfluid density ρ_s for $N = 2$) between the high T and low T regions of Fig 8.3; this is discussed elsewhere [431] in some detail.

Figs 8.4 and 8.5 contain the results of a recent numerical computation of the scaling functions in (8.51) at $k = 0$, *i.e.* for $S(0, \omega)$.   These results are the analog of Fig 4.12 for the Ising chain (and Fig 6.4 for the $d = 1$, $N = 3$ rotor model, for those who have read Chapter 6). As (8.53) evaluates to a moderately large value of $\mathcal{G}$ in $d = 2$, the perturbation theory results of Section 8.2.1 for $\chi(k)$ are no longer accurate, and we also numerically computed the exact values of $\Psi_d(0, \mathcal{G})$ in $d = 2$ (see (8.26)), and these are reported in the captions to the figures. The results show a consistent trend from small values of $\mathcal{G}$ and large values of N to large values of $\mathcal{G}$ and small values of N, and we discuss the physical interpretation of the two limiting cases in turn.

For smaller $\mathcal{G}$ and larger N, we observe a peak in $S(0, \omega)$ at a non-zero frequency. This peak is the remnant of the delta function in the large N result (5.22), where the value of m was given by (5.64,5.72,5.75) (the same peak also appears in the $1/N$ computation in Fig 7.3 in Chapter 7). In the present computation, it is clear that the peak is due to *amplitude fluctuations* as ϕ_α oscillates about the minimum in its effective potential at $\phi_\alpha = 0$. In addition to the peak at finite frequency, there is weight in $S(0, \omega)$ down to zero frequency, with $S(0, \omega) > 0$, and so $\text{Im}\chi(0, \omega) \sim \omega$ for small ω; direct analytic computations of $\text{Im}\chi(0, \omega)$ in either the ϵ or $1/N$ expansions give different, unphysical, low frequency limits for $\text{Im}\chi(0, \omega)$ (as was seen in Section 7.2.2), and so the present exact dynamical computation directly in $d = 2$ with N finite has cured this sickness. Readers of Chapter 6 will also recognize the similarity of
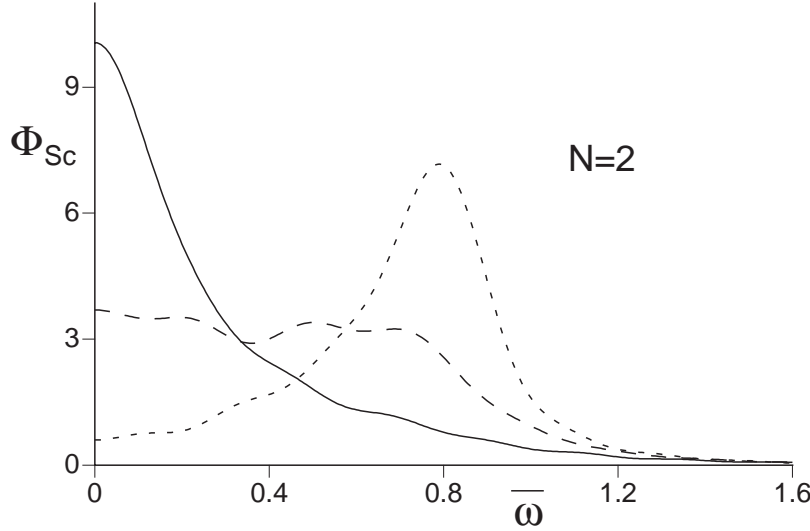
Fig. 8.4. Numerical results from Ref [431] for the zero momentum scaling function $\Phi_{Sc}(0, \overline{\omega}, \mathcal{G})$ appearing in (8.51) for $N = 2$. Results are shown for $\mathcal{G} = 20$ (short dashes), $\mathcal{G} = 30$ (long dashes) and $\mathcal{G} = 40$ (full line). The static susceptibility takes the values (see (8.26)) $R\chi(k) = \Psi_2^{-1}(0, \mathcal{G}) = 1.67$, 2.65, and 4.73 at $\mathcal{G} = 20$, 30, and 40 respectively. The high T limit value of $\mathcal{G}$ in (8.53) evaluates to $\mathcal{G} = 29.2$ at $\epsilon = 1$ and $N = 2$.

this finite frequency peak with the shoulder in Fig 6.4 describing the high T limit of the $d = 1$, $N = 3$ case.

For larger $\mathcal{G}$ and smaller N, the peak in $S(0, \omega)$ shifts down to $\omega = 0$. The resulting spectrum is then closer to the exact solution for $d = 1$, $N = 1$ presented in Fig 4.12. As $\mathcal{G}$ increases further, the zero frequency peak becomes narrower and taller; it has been argued in Ref [431] that this behavior is characteristic of fluctuations of ϕ_α about a minimum in the effective potential which is at a non-zero value of $|\phi_\alpha|$ *i.e.* for $N \geq 2$, the predominant fluctuations are *angular*. Indeed, it has been shown [431] that for $N = 3$ and $\mathcal{G} \to \infty$ the scaling function in (8.51) becomes precisely that in (7.36), which describes the dynamics of a model with fixed $|\phi_\alpha|$.

It is interesting to examine the above results at the value of high T limit for $\mathcal{G}$ in (8.53) evaluated directly in $\epsilon = 1$. We find $\mathcal{G} = 29.2$, 24.9 for $N = 2$, 3, and these values are very close to the position where the crossover between the above behaviors occurs. The $N = 2$ case is closer
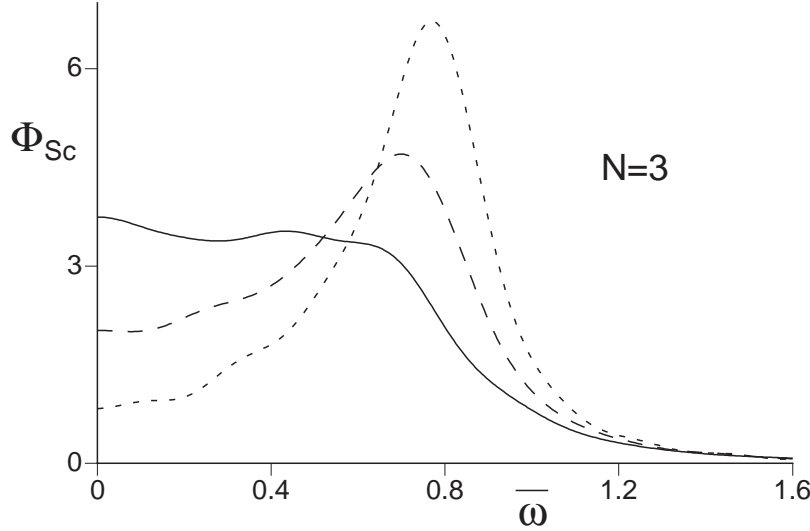
Fig. 8.5. As in Fig 8.4 but for $N = 3$. The values of $\mathcal{G}$ are now $\mathcal{G} = 20$ (short dashes), $\mathcal{G} = 25$ (long dashes) and $\mathcal{G} = 30$ (full line). The static susceptibility takes the values (see (8.26)) $R\chi(k) = \Psi_2^{-1}(0, \mathcal{G}) = 1.73$, 2.17, and 2.75 at $\mathcal{G} = 20$, 25, and 30 respectively. The high T limit value of $\mathcal{G}$ in (8.53) evaluates to $\mathcal{G} = 24.9$ at $\epsilon = 1$ and $N = 3$.

to having a maximum in $S(0, \omega)$ at $\omega = 0$, while there is a more clearly defined finite frequency peak for $N = 3$.

A final parenthetic remark. Readers may recognize a resemblance between the above crossover in dynamical properties as a function of $\mathcal{G}$, and a well-studied phenomenon in dissipative quantum mechanics [302, 525, 303]: the crossover from 'coherent oscillation' to 'incoherent relaxation' in a two-level system coupled to a heat bath . However, here we do not rely on an arbitrary heat bath of linear oscillators, and the relaxational dynamics emerges on its own from the underlying Hamiltonian dynamics of an interacting many-body, quantum system.

8.4 Applications and extensions

Bitko *et al.* [55] have studied the vicinity of the quantum phase transition in the Ising spin system LiHoF$_4$ in the presence of a transverse magnetic field. This Ising spins have long-range dipolar exchange, and this puts the quantum critical point above its upper critical dimension because long-range forces tend to make the mean-field approximation

better. The resulting exponents are therefore mean-field like, and physical properties can be computed in a manner very similar to Section 8.2.2.

We have argued in Section 8.2.1 that for systems below the upper critical dimension with a finite temperature phase transition (the cases $N = 1, 2$, $d = 2$), the critical temperature of the transition is universally related to the ground state energy scale Δ_-. For the case $d = 2$, $N = 2$, we may choose $\Delta_- = \rho_s$, the ground state spin stiffness, and so T_c/ρ_s is a universal constant. Indeed the universality applies to the entire temperature dependence of ρ_s, and so

$$\rho_s(T) = \rho_s \Phi_\rho \left(\frac{T}{\rho_s} \right), \qquad (8.55)$$

where $\rho_s \equiv \rho_s(0)$, and Φ_ρ is a universal function which can be computed by the methods of Section 8.2.1 in a ϵ expansion. The value of T_c is determined by the argument at which Φ_ρ first vanishes. In $d = 2$, the function Φ_ρ will display a discontinuity at $T = T_c$ to allow for the Nelson-Kosterlitz jump [361] in the superfluid density. For experimental comparisons, it is easy to see that (8.55) implies the slightly weaker result

$$\frac{\rho_s(T)}{\rho_s(0)} = \widetilde{\Phi}_\rho \left(\frac{T}{T_c} \right), \qquad (8.56)$$

with the function $\widetilde{\Phi}_\rho$ computable from Φ_ρ. The numerically exact computations in $d = 2$ discussed in Section 8.3 have been used to obtain explicit computations of the functions Φ_ρ, $\widetilde{\Phi}_\rho$ for the model (8.2), and these results contain the jump in the superfluid density. It is quite intriguing that the data [213, 138] on the high temperature superconductors satisfies the relation (8.56), suggesting the proximity of a quantum critical point at which the superfluid density vanishes at $T = 0$.

This last point of view can be further extended by the dynamical results obtained in Section 8.3. There we saw that the high T limit of the $N = 2$ case had a peak in $S(0, \omega)$ at $\omega = 0$, suggesting domination by fluctuations in the phase of the order parameter. We can describe the photo-emission spectrum in such a situation by assuming that the superconducting quasiparticles follow the instantaneous ϕ_α configuration [165, 285], and then a $\omega = 0$ peak in $S(0, \omega)$ is expected to translate into a 'pseudo-gap' in the fermion spectrum.

As we have noted in Sections 4.6 and 7.4, the neutron scattering measurements of Aeppli *et al.* [2] on $La_{2-x}Sr_x CuO_4$ at $x = 0.15$ are consistent with high T limit of scaling forms like (5.60) and (8.51) with $z = 1$,

suggesting proximity to a state with incommensurate spin and charge ordering. The $N = 3$ results of Section 8.3 provide explicit dynamical response functions with which experimental results can be compared; the qualitative features of Fig 8.5 are quite similar to those of the experiments, and more precise comparisons should be made in the future. Notice that, in this case, it is the smaller values of $\mathcal{G}$ (which have a finite frequency peak in Fig 8.5) which lead to a 'pseudo-gap' in the spin excitation spectrum.

Recent light scattering experiments have explored magnetic transitions in double layer quantum Hall systems [377, 378]. As we will discuss in Sections 13.4 and 13.5, the dynamical properties of these systems can be described by models closely related to those studied in Section 8.3. The light scattering spectrum can therefore lead to tests of the dynamic structure factors like those in Fig 8.4 and 8.5.

We have not explicitly considered the case of the upper-critical dimension $d = 3$ in our discussion in this chapter. In this case there are logarithmic corrections, involving a non-universal upper cutoff scale in the argument of the logarithm, which can be computed using renormalization group arguments similar to those considered in Sections 6.3 and 7.1.1. We assume the system begins with a positive coupling u of order unity at a microscopic scale Λ. Then, as in Sections 6.3 and 7.1.1, it pays to use the renormalization group invariance to renormalize to a scale $\mu = T/c$; from the flow equation (8.17) we see that for $\epsilon = 0$ and $T \ll \Lambda$

$$u_R = \left(\frac{6}{N+8} \right) \frac{1}{\ln(c\Lambda/T)}. \tag{8.57}$$

So the non-linearity u is logarithmically small. The $\omega_n \neq 0$ modes can be integrated out by precisely the methods of Section 8.2 to derive an effective action for the $\omega_n = 0$ modes. This step should be carried out at the scale $\mu = T/c$, as this ensures that u_R is small, and also that there are no large logarithms generated in the perturbation theory in u_R (the only scale running through the Feynman diagrams is T, and so dimensionally all logarithms must be order $\ln(c\mu/T)$, which is small). The subsequent analysis of the action for the $\omega_n = 0$ modes then proceeds as before. To lowest order, the physical results can be obtained from the $d < 3$ computation by the replacement $\epsilon \to 1/(\ln(c\Lambda/T))$.

Irkhin and Katanin [241] have applied the methods of this chapter to crossovers in anisotropic magnetic systems, along with comparisons to experimental and numerical data.

We mentioned the proposal of Normand and Rice [366, 367] for the proximity of a $d = 3$, $N = 3$ quantum critical point in $LaCuO_{2.5}$ in Section 5.5. The ground state of this system has Néel order, and these authors argued that there should be a low-lying amplitude fluctuation mode in the spectrum of the ordered phase, in addition to the usual spin-wave modes. The universal properties of such a mode can be obtained directly from the approach developed in this chapter—we examine (8.2) for $r < 0$ in an expansion in the non-linear coupling u, which will be logarithmically small in $d = 3$ as in (8.57). The longitudinal fluctuations in $|\phi_\alpha|$ about a non-zero mean value will lead to a mode whose energy vanishes as $|r| \rightarrow 0$.

9

Transport in $d = 2$

We considered time-dependent correlations of the conserved angular momentum, $\mathbf{L}(x, t)$, of the O(3) quantum rotor model in $d = 1$ in Chapter 6. We found, using effective semiclassical models, that the dynamic fluctuations of $\mathbf{L}(x, t)$ were characterized by a *diffusive* form (see (6.26)) at long times and distances, and were able to obtain values for the spin diffusion constant D_s at low T and high T (see Fig 6.5). The purpose of this chapter is to study the analogous correlations in $d = 2$ for $N \geq 2$; the case $N = 1$ has no conserved angular-momentum, and so no possibility of diffusive spin correlations. Rather than thinking about fluctuations of the conserved angular momentum in equilibrium, we shall find it more convenient here to consider instead the response to an external space and time dependent 'magnetic' field $\mathbf{H}(x, t)$, and to examine how the system transports the conserved angular momentum under its influence.

In principle, it is possible to address these issues in the high T region using the non-linear classical wave problem developed in Section 8.3 in the context of the $\epsilon = 3 - d$ expansion. However, an attempt to do this quickly shows that the correlators of $\mathbf{L}$ contain ultraviolet divergences when evaluated in the effective classical theory. Physically, this is a signal that transport properties are *not* dominated by excitations with energy $\ll T$ (while the order parameter fluctuations, considered in Section 8.3, were), and it is necessary to include fluctuations with higher energy, which must then be treated quantum mechanically. It is this quantum transport problem we will address here. We will show that it is necessary to solve a quantum transport equation for the quantized particle excitations to describe diffusion in the high T and the low T quantum paramagnetic regions.

It is useful to begin by introducing some basic formalism. We shall mostly be using the 'soft-spin' approach to the quantum critical point

discussed in Chapter 8, and so it is useful to setup the machinery of transport theory using its notation. For general N, the 'magnetic' field **H** has $N(N-1)/2$ components (as in (1.18)): this field generates rotations of the ϕ_α order parameter, and the number of components equals the number of ways of choosing independent planes of rotation in the N-dimensional order parameter space. Only for the case $N = 3$ considered earlier, do the order parameter and 'magnetic' field have the same number of components. We will denote this generalized field by H^a, with $a = 1 \ldots N(N-1)/2$. Notice that for $N = 2$, a has only one allowed value and is therefore redundant: we will later apply the $N = 2$ model to the superfluid-insulator transition, and will see there that H^a represents the electrostatic potential. In (5.16), we have already seen the form of the imaginary time effective action for the $N = 3$ rotor model in the presence of a non-zero H^a in the fixed-length **n** field formulation. By the precise analog of the arguments made in Section 5.2 in deriving (5.16), we may conclude that the generalization of the soft-spin theory (8.2) in the presence of an external field H^a is:

$$\mathcal{Z} = \int \mathcal{D}\phi_\alpha(x, \tau) \exp(-\mathcal{S}_\phi)$$

$$\mathcal{S}_\phi = \int d^d x \int_0^{1/T} d\tau \left\{ \frac{1}{2} \left[(\partial_\tau \phi_\alpha - i H^a T^a_{\alpha\beta} \phi_\beta)^2 + c^2 (\nabla_x \phi_\alpha)^2 \right. \right.$$
$$\left. \left. + r\phi_\alpha^2(x) \right] + \frac{u}{4!} (\phi_\alpha^2(x))^2 \right\}. \qquad (9.1)$$

Notice that H^a merely causes a precession of the ϕ_α field: the T^a are $N \times N$ real antisymmetric matrices which generate the O(N) rotation (they are i times the generators of the Lie algebra of O(N)). There are $N(N-1)/2$ such linearly independent matrices: it is convenient to choose the basis in which all but 2 matrix elements of a given T^a are zero, with the non-vanishing elements equaling ± 1. In this functional language, the observable corresponding to the conserved angular-momentum density is given by

$$L^a(x, t) = -\frac{\delta \mathcal{S}_\phi}{\delta H^a(x, t)}. \qquad (9.2)$$

Note that these are $N(N-1)/2$ components of this density, and their spatial integrals are all constants of the motion.

Many of the physical arguments will actually be clearer in a Hamiltonian formalism. For the fixed-length model (5.16), we had the lattice Hamiltonian in (5.1). We can apply the inverse of the transformation used in going from (5.1) to (5.16) to obtain the Hamiltonian form of

(9.1): we interpret ϕ_a as the co-ordinate of a 'particle' with unit mass moving in N dimensions (no longer constrained to move on a sphere), as discussed in Chapter 2, and we obtain the following continuum Hamiltonian

$$\mathcal{H} = \int d^d x \left\{ \frac{1}{2} \left[\pi_\alpha^2 + c^2 (\nabla_x \phi_\alpha)^2 + r\phi_\alpha^2(x) \right] + \frac{u}{4!} (\phi_\alpha^2(x))^2 \right.$$
$$\left. - H^a(x,t) T_{\alpha\beta}^a \pi_\alpha \phi_\beta \right\}. \tag{9.3}$$

Here $\pi_\alpha(x,t)$ is the canonically momentum to the field ϕ_α, which therefore satisfy the equal-time commutation relations

$$[\phi_\alpha(x,t), \pi_\beta(x',t)] = i\delta_{\alpha\beta}\delta(x-x'). \tag{9.4}$$

The Eqns (9.3) and (9.4) are, of course, the quantized Hamiltonian versions of the classical Hamiltonian problem defined by (8.46) and (8.47). The operator representation of the angular momentum density is obtained by the analog of (9.2), and therefore

$$L^a(x,t) = T_{\alpha\beta}^a \pi_\alpha(x,t) \phi_\beta(x,t). \tag{9.5}$$

It can be verified that the fields L^a, ϕ_α satisfy commutation relations which are the continuum limit of the relations (1.19) for the fixed-length rotor model.

The basic purpose of this chapter shall be an analysis of the time evolution of the expectation value of $L^a(x,t)$ in situations close to thermal equilibrium. Let us first examine the exact Heisenberg equation of motion of the operator in (9.5) under the Hamiltonian in (9.3); an elementary computation using the commutation relation (9.4) gives a result which can be written in the form

$$\frac{\partial L^a}{\partial t} = -\vec{\nabla} \cdot \vec{J}^a + f_{abc} H^b L^c, \tag{9.6}$$

where f_{abc} are the structure constants of the Lie algebra of $O(N)$ defined by the commutation relations

$$[T^a, T^b] = f_{abc} T^c. \tag{9.7}$$

These structure constants are totally antisymmetric in a, b, c; for $N = 3$, $f_{abc} = \epsilon_{abc}$, while for $N = 2$, $f_{abc} = 0$. The term proportional to f_{abc} in (9.6) represents the Bloch precession of the angular momentum about the external field. The quantity $\vec{J}^a$ in (9.6) is the angular momentum current. An expression for $\vec{J}^a$ can be easily obtained by generating the equation of motion as noted above; however, as the equations of motion

involve only the divergence of $\vec{J}^a$, this expression will be uncertain up to the curl of arbitrary vector. It is customary to choose this arbitrary vector to obtain the *transport* current $\vec{J}^a_{\mathrm{tr}}$ so that the expectation value $\langle \vec{J}^a_{\mathrm{tr}} \rangle$ vanishes in thermal equilibrium. In this case a non-zero $\langle \vec{J}^a_{\mathrm{tr}} \rangle$ will describe bulk transport of the angular momentum density $\langle L^a \rangle$ across macroscopic distances when the system is driven out of equilibrium by an external perturbation.

Let us introduce some phenomenological considerations for a system close to thermal equilibrium. We imagine that due to weak perturbations from unspecified sources, we deform a thermal equilibrium state into one characterized by a non-zero, space dependent angular momentum density $\langle L^a \rangle$. Further, there is also present a slowly varying 'magnetic' field $H^a(x, t)$. Both these perturbations will tend to induce a non-zero transport current $\langle \vec{J}^a_{\mathrm{tr}} \rangle$, and provided the perturbations are weak and very slowly varying, we can write down the following phenomenological expression for the current:

$$\langle \vec{J}^a_{\mathrm{tr}}(x, t) \rangle = \sigma \vec{\nabla} H^a(x, t) - D_s \vec{\nabla} \langle L^a(x, t) \rangle. \tag{9.8}$$

We have introduced two transport coefficients in the above equation. The first, σ, is the conductivity: a uniform H^a is expected to induce only a non-zero magnetization density, and so any induced current can only be due to gradients of H^a. The second, D_s, is the spin diffusion constant we met in the discussion of the fluctuations of $L^a(x, t)$ in $d = 1$ in Chapter 6: the combination of (9.6) and (9.8) shows that for the external field $H^a = 0$, $\langle L^a(x, t) \rangle$ satisfies the diffusion equation

$$\frac{\partial \langle L^a(x, t) \rangle}{\partial t} = D_s \nabla^2 \langle L^a(x, t) \rangle, \tag{9.9}$$

and identifies D_s as the diffusion constant.

Continuing our phenomenological analysis, we discuss the important Einstein relation between σ and D_s. Imagine we are considering a closed system in which H^a is time-independent, but a slow function of x. Eventually the system will reach thermal equilibrium in which the local angular momentum density is simply given by the equilibrium response to a uniform field

$$\langle L^a \rangle = \chi_u H^a(x), \tag{9.10}$$

where χ_u was defined in (5.3) (we have arranged the initial conditions so that this result is compatible with conservation of the total angular momentum). Under this condition of equilibrium the transport current

should also vanish: this is compatible with the defining transport relation (9.8) only if

$$\sigma = \chi_u D_s \qquad (9.11)$$

This is the basic Einstein relation between the diffusion coefficient characterizing fluctuations, and the conductivity representing the response of the system to an external field.

Using (9.11), we can obtain the basic scaling properties of the conductivity σ. Recall from (5.43) that the scaling dimension of χ_u is $d - z$ (we will henceforth use the value $z = 1$ for the rotor models in the remainder of this chapter), and χ_u satisfies the scaling forms (5.63):

$$\chi_u = \frac{T^{d-1}}{c^d} \Phi_{u\pm} \left(\frac{\Delta_\pm}{T} \right) \qquad (9.12)$$

on the two sides of the quantum critical point (recall that $\Delta_\pm$ are energy scales measuring the deviation of the ground state from the $T = 0$ quantum critical point). In $d = 2$, the $N = \infty$ result for the scaling functions $\Phi_{u\pm}$ can be obtained by inserting (5.64), (5.72) and (5.75) into (5.65). We will note here some asymptotic limits, also mentioned in Fig 7.4: on the ordered side, where $\Delta_- = \rho_s$, the ground state spin stiffness, we have the exact result for $T \ll \rho_s$ obtained in (7.25) which shows that χ_u reaches a non-zero value as $T \to 0$:

$$\chi_u = \frac{2\rho_s}{Nc^2} \left[1 + \frac{(N-2)T}{2\pi\rho_s} + \mathcal{O}\left(\frac{T}{\rho_s} \right)^2 \right] ; \qquad (9.13)$$

on the quantum paramagnetic side, we expect an exponentially small uniform susceptibility for $T \ll \Delta_+$, and we can again obtain an exact result in $d = 2$ by the same dilute gas of quasiparticles argument which led to (6.12):

$$\chi_u = \frac{\Delta_+}{\pi c^2} e^{-\Delta_+/T}; \qquad (9.14)$$

finally, in the high T limit, $T \gg \Delta_\pm$, we must rely on the large N expansion to obtain the value of the constant $\Phi_{u\pm}(0)$, and the $N = \infty$ result is

$$\chi_u = \frac{T}{c^2} \frac{\sqrt{5}}{\pi} \ln \left(\frac{\sqrt{5} + 1}{2} \right) . \qquad (9.15)$$

Turning to the diffusion constant, no explicit scaling results have yet been obtained (indeed, that is the primary purpose of this chapter), but we can deduce its scaling dimension by a simple argument. A glance

at (9.9) shows that D_s has the dimensions of (length)^2/time. There is
no field scale that appears in the definition of D_s, and as the scaling
dimension has to respect the conservation law for L^a, we the scaling
dimensions

$$\dim[D_s] = z - 2$$
$$\dim[\sigma] = d - 2, \qquad (9.16)$$

where the second relation follows from (5.43). Using $\dim[T] = z$, and
matching engineering dimensions with those of c and T, we then see
that D_s must equal c^2/T times a universal function of $\Delta_\pm/T$. Combin-
ing this with (9.11) and (9.12) we have the main scaling form for the
conductivity [159, 157, 78, 527, 422, 116]

$$\sigma(\omega) = \frac{Q^2}{\hbar} \left(\frac{k_B T}{\hbar c} \right)^{d-2} \Phi_{\sigma\pm} \left(\frac{\hbar\omega}{k_B T}, \frac{\Delta_\pm}{k_B T} \right), \qquad (9.17)$$

where $\Phi_{\sigma\pm}$ are completely universal scaling functions. We have momen-
tarily returned to physical units by re-inserting factors of $\hbar$, k_B and and
the charge of the carriers, Q (this had been absorbed into our definition
of H^a; $Q = 2e$ for the superfluid-insulator transition)—we will do this
occasionally below when quoting results for σ. For future use, we have
generalized the conductivity to a dynamical frequency dependent con-
ductivity $\sigma(\omega)$ representing the response in the current at frequency ω
to an external field at the same frequency ($\sigma \equiv \sigma(0)$); the scaling depen-
dence on ω/T then follows from now familiar arguments. We will focus
in this chapter mainly on the high T regime $T \gg \Delta_\pm$, and therefore
on the value of $\Phi_{\sigma\pm}(\omega/T, 0)$. Also notice an important, and remarkable
property of (9.17): in spatial dimension $d = 2$, the prefactor of the power
T disappears, and the conductivity is entirely given by the scaling func-
tion $\Phi_{\sigma\pm}$ times the fundamental constants $Q^2/\hbar$. In the high T limit, we
are then left with the dimensionless scaling function $\Phi_{\sigma\pm}(\omega/T, 0)$ which
depends on no system parameters at all.

    We will work, throughout this chapter, in the high T and quantum
paramagnetic low T regions of Fig 8.3. We will not be studying the
crossover in the shaded classical region of Fig 8.3 near the finite tem-
perature transition for $N = 2$: transport properties in this region are
of considerable practical interest, but the methods developed here are
not adequate to describe them. One consequence of restricting ourselves
out of the shaded region is that we are always in a regime where the
perturbative expansion for the tricritical crossover function in (8.12) is
adequate.

9.1 Perturbation theory

We will begin our computation of σ by a simple perturbative evaluation of the leading order term in both the $\epsilon = 3 - d$ and $1/N$ expansions [116].

First, let us specify more carefully the configuration of the system. We begin, at some time in the remote past, with an infinite d-dimensional quantum rotor system in thermal equilibrium at a temperature T. A small 'magnetic field' with a uniform spatial gradient, and oscillating with a frequency ω, is turned on, also in the remote past. We are interested in the eventual steady state in which there is a spatially uniform angular momentum current present, also oscillating with the frequency ω. The proportionality constant between the current and the field gradient defines the conductivity $\sigma(\omega)$. As the current is spatially uniform, the magnetization density is zero at all times (so the term proportional to D_s in (9.8) is not present).

It should be evident that this physical situation has a translational symmetry. However, in considering the response to the field, we need a uniform gradient, and therefore it appears necessary to consider a response at a non-zero wavevector. This is slightly inconvenient, and so we use an alternative method which should be familiar to most readers in the context of discussion of the Kubo formula in many body systems [146]. The basic point is to note that H^a appears in (9.1) in the same form as the time component of an $O(N)$ non-Abelian gauge field. It is then useful to generalize (9.1) to also introduce a fictitious spatial component of this gauge field, denoted $\vec{A}^a$, by changing only the gradient terms in (9.1) to

$$\frac{1}{2}\left[(\partial_\tau \phi_\alpha + iH^a T^a_{\alpha\beta}\phi_\beta)^2 + c^2(\vec{\nabla}\phi_\alpha - \vec{A}^a T^a_{\alpha\beta}\phi_\beta)^2\right], \qquad (9.18)$$

One advantage of introducing $\vec{A}^a$ is that it can be checked that the current J^a appearing in (9.6) is given by the simple expression

$$\vec{J}^a = -\frac{\delta \mathcal{S}_\phi}{\delta \vec{A}^a}; \qquad (9.19)$$

this result is the analog of (9.2). The action $\mathcal{S}_\phi$ is seen to be invariant under the non-Abelian gauge transformation

$$
\begin{aligned}
\phi_\alpha &\rightarrow& \phi_\alpha + \Omega^a T^a_{\alpha\beta}\phi_\beta \\
\vec{A}^a &\rightarrow& \vec{A}^a + \vec{\nabla}\Omega^a \\
H^a &\rightarrow& H^a + i\partial_\tau \Omega^a
\end{aligned}
\qquad (9.20)
$$

where Ω^a is an arbitrary infinitesimal function of space and time. We

can use this gauge invariance to transform away the field H^a appearing with the time-component and have only a non-zero $\vec{A}^a$. From (9.20) we see that for a system with a non-zero H^a and $\vec{A}^a = 0$, is equivalent to a system with $H^a = 0$ and $\vec{A}^a = \vec{\nabla}\Omega^a$ where $\partial_\tau \Omega^a = iH^a$. So if we have uniform, time-dependent, spatial gradient in H^a, we can define the space-independent $\vec{E}^a = \vec{\nabla}H^a$ and we see, in imaginary frequencies, that $\vec{A}^a(\omega_n) = \vec{E}^a(\omega_n)/\omega_n$ in the gauge-transformed system.

The above mapping allows us to present a simple prescription to compute $\sigma(\omega_n)$. Work with a $\mathcal{S}_\phi$ with $H^a = 0$, and a non-zero space-independent $\vec{A}^a(\omega_n)$: notice that the external source $\vec{A}^a$ is explicitly at zero momentum. Compute the expectation value of (9.19) under this $\mathcal{S}_\varphi$: then the conductivity is given by the linear response to a non-zero $\vec{A}^a$ by

$$\sigma(\omega_n) = -\frac{1}{\omega_n}\frac{\delta}{\delta \vec{A}^a}\left\langle \frac{\delta \mathcal{S}_\phi}{\delta \vec{A}^a}\right\rangle\bigg|_{\vec{A}^a=0} \tag{9.21}$$

It is a simple matter to use (9.21) to compute $\sigma(i\omega_n)$, either to first order in u, or in the $N = \infty$ limit (in this case one simply uses the self-consistent large N propagator in (5.22), and otherwise ignores interactions). In both cases the answer can be written in the following form:

$$\sigma(\omega_n) =$$
$$-\frac{2c^2 T}{\omega_n}\sum_{\epsilon_n}\int \frac{d^d k}{(2\pi)^d}\left[\frac{2c^2 k_x^2}{(\epsilon_n^2 + c^2 k^2 + m^2)((\epsilon_n + \omega_n)^2 + c^2 k^2 + m^2)}\right.$$
$$\left.-\frac{1}{\epsilon_n^2 + c^2 k^2 + m^2}\right]. \tag{9.22}$$

The first term is the so-called 'paramagnetic' contribution, while the second is the 'diamagnetic' term, and these arise from the diagrams shown in Fig 9.1. Here we have taken the gradient of H^a along the x direction and k_x is the x component of the d dimensional momentum $\mathbf{k}$. The "mass" m has been computed in earlier chapters: the ϵ and large N results differ only in their T-dependent values for m. At $N = \infty$ we have the result in (7.44). The ϵ expansion was considered in Chapter 8, and for the high T and quantum paramagnetic low T regions of interest here, we have from (8.26), (8.12) and (8.32) that

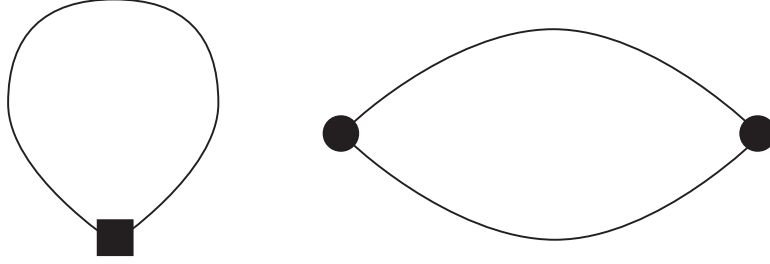$$m^2 = R - \epsilon\left(\frac{N+2}{N+8}\right)2\pi T\sqrt{R} \tag{9.23}$$

Fig. 9.1. Feynman diagrams leading to the two terms in (9.22). The dark circle represents the term linear in $\vec{A}^a$ in (9.18), while the dark square is the term quadratic in $\vec{A}^a$.

where R is given in (8.31); in the high T limit we have $m^2 = \epsilon((N + 2)/(N + 8))2\pi^2 T^2/3$ to leading order in the ϵ expansion.

Now insert $1 = \partial k_x / \partial k_x$ in front of the diamagnetic term in (9.22) and integrate by parts. The surface terms vanish in dimensional or lattice regularization, and the expression for the conductivity becomes

$$\sigma(\omega_n) = -\frac{2c^2}{\omega_n} T \sum_{\epsilon_n} \int \frac{d^d k}{(2\pi)^d} \frac{2c^2 k_x^2}{\epsilon_n^2 + c^2 k^2 + m^2}$$
$$\times \left[\frac{1}{(\epsilon_n + \omega_n)^2 + c^2 k^2 + m^2} - \frac{1}{\epsilon_n^2 + c^2 k^2 + m^2} \right]. \quad (9.24)$$

We evaluate the summation over Matsubara frequencies, analytically continue to real frequencies. The resulting $\sigma(\omega)$ is complex, and we decompose it into its real and imaginary parts $\sigma(\omega) = \sigma'(\omega) + i\sigma''(\omega)$. We will only present results for the real part $\sigma'(\omega)$, and the imaginary part $\sigma''(\omega)$ can be obtained via the standard dispersion relation.

We find that the result for $\sigma'(\omega)$ has two distinct contributions [515, 116] of very different physical origin. We separate these by writing

$$\sigma'(\omega) = \sigma'_I(\omega) + \sigma'_{II}(\omega). \quad (9.25)$$

The first part, $\sigma'_I(\omega)$, is a delta function at zero frequency:

$$\sigma'_I(\omega) = 2\pi c^4 \delta(\omega) \int \frac{d^d k}{(2\pi)^d} \frac{k_x^2}{\varepsilon_k^2} \left(-\frac{\partial n(\varepsilon_k)}{\partial \varepsilon_k} \right), \quad (9.26)$$

where $n(\varepsilon)$ is the Bose function in (7.63) and the excitations have the energy momentum relation ε_k given in (7.64). We will discuss the physical meaning of the delta function in (9.26) below, and obtain a separate and more physical derivation of its weight in Section 9.2. The second
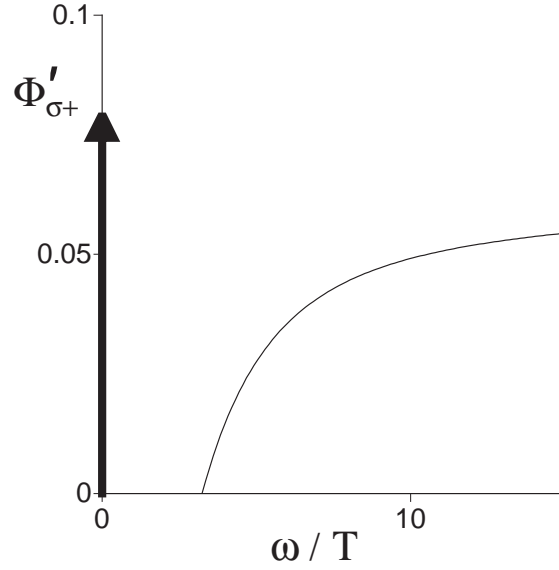
Fig. 9.2. The real part, $\Phi'_{\sigma+}$, of the universal scaling function $\Phi_{\sigma+}$ in the high T limit ($T \gg \Delta_\pm$) (see (9.17)) at the one loop level The numerical values are obtained from (9.26) and (9.27) with $d = 2$ ($\epsilon = 1$). There is a delta function precisely at $\omega/T = 0$ represented by the heavy arrow: the weight of this delta function is given in (9.28) and (9.29). The delta function contributes to σ_I, and the higher frequency continuum to σ_{II}

part, $\sigma'_{II}(\omega)$ is a continuum above a threshold frequency of 2σ:

$$\sigma'_{II}(\omega) = \pi c^4 \int \frac{d^d k}{(2\pi)^d} \frac{k_x^2}{2\varepsilon_k^3} (1 + 2n(\varepsilon_k)) \delta(|\omega| - 2\varepsilon_k)$$

$$= \frac{\pi S_d}{d} \theta(|\omega| - 2m) \left(\frac{\omega^2 - 4m^2}{4\omega^2} \right)^{d/2} [1 + 2n(\omega/2)] \left| \frac{\omega}{c} \right|^{d-2} \quad (9.27)$$

where S_d was defined below (8.16). It can be verified that the above results for $\sigma(\omega)$ obey the scaling form (9.17).

We now discuss the physical and scaling properties of the two components of the conductivity in turn; the results are also sketched in Fig 9.2.

9.1.1 σ_I

This is a zero frequency delta function, and is present only for $T > 0$. It is interpreted as the contribution of thermally excited particles which

propagate ballistically without any collisions with other particles: this will become evident when we rederive this delta function contribution later in Section 9.2 using a transport equation formalism. Indeed, to first order in ϵ (Chapter 8), or at $N = \infty$ (Section 7.2), the excitations are simply undamped particles with an infinite lifetime and energy momentum relation ε_k. As we saw in Section 7.2.2, it is necessary to go to first order in $1/N$, to include collisions which will give the quasiparticles a finite lifetime, and lead to a finite phase coherence time τ_φ; a similar analysis in the ϵ expansion shows that such effects appear at order ϵ^2. We will show in Section 9.3 that these collisions also broaden the delta function in σ_I. The magnitude of the broadening is expected to be determined by the inverse lifetime of the quasiparticles; in the high temperature limit, this inverse lifetime is of order $\epsilon^2 T$ [427] in the ϵ expansion, or of order T/N in the large N theory (see Eqn (7.68)). The typical energy of a quasiparticle at the critical point is of order T, and so the quasiparticles are well-defined, at least within the ϵ or $1/N$ expansion. Notice, however, that the quasiparticle interpretation breaks down at the physically important values of $\epsilon = 1$, $N = 2, 3$.

Let us evaluate the expression (9.26) for σ_I in its limiting regimes.

First, the high T region. Consider first the ϵ expansion. The coefficient of the delta function is a function of the ratio m/T, but notice from (9.23) and below that $m \ll T$ for small ϵ. Evaluating (9.26) in this limit we find for ϵ small

$$\sigma_I'(\omega) = 2\pi c^{2-d} T^{d-1} \delta(\omega) \left[\frac{1}{18} - \frac{m}{8\pi T} + \cdots \right]$$

$$= 2\pi c^{2-d} T^{d-1} \delta(\omega) \left[\frac{1}{18} - \frac{\sqrt{\epsilon}}{8} \left(\frac{2(N+2)}{3(N+8)} \right)^{1/2} + \cdots \right] \quad (9.28)$$

Actually the expression (9.26) is good to order ϵ but we have refrained from displaying the next term as it is rather lengthy. The first term in (9.28) is obtained by evaluating (9.26) at $m = 0$, $d = 3$; the second term is from an integral dominated by small $ck \sim m \ll T$ and hence the Bose function can be replaced by its classical limit. It is important to note that the current carried by the thermally excited carriers is dominated by the leading term of (9.28), which arises from momenta $k \sim T \gg m$ (this is the reason we are not allowed to use the classical wave model of Section 8.2.1 for transport properties). This will be useful to us in the analysis of collisions in Section 9.3 where we will simply be able to set $m = 0$ to obtain the leading term. In the large N theory, the

corresponding expression in $d = 2$ is

$$
\begin{aligned}
\sigma'_I(\omega) &= \frac{T}{2}\delta(\omega)\left[\int_\Theta^\infty d\varepsilon\left(1 + \frac{\Theta^2}{\varepsilon^2}\right)\frac{1}{e^\varepsilon - 1}\right] \\
&= \frac{T}{2}\delta(\omega) \times 0.68940\ldots
\end{aligned}
\tag{9.29}
$$

where $\Theta = 2\ln((\sqrt{5} + 1)/2)$. Notice that as $m \sim T$, we have now been unable to approximate $\varepsilon_k \approx k$ to get the leading result, as was done in the ϵ expansion. The spectral weight of the delta function to leading order in the ϵ expansion is, from (9.28), $\pi T/9 = 0.3491\ldots T$ while the $N = \infty$ $d = 2$ result is $0.3447\ldots T$, which is remarkably close.

Next the low T regime on the quantum paramagnetic side of the transition, $T \ll \Delta_+$. Here both the ϵ and large N expansions give the following result in $d = 2$

$$
\sigma'_I(\omega) = T\left(\frac{\Delta_+ T}{2\pi c^2})\right)^{(d-2)/2} e^{-\Delta_+/T}\delta(\omega)
\tag{9.30}
$$

So the spectral weight of the delta function is exponentially small, since free quasiparticles are thermally activated.

9.1.2 σ_{II}

This is the continuum contribution to σ which vanishes for $\omega < 2m$. At this order in ϵ (or $1/N$) there is a sharp threshold at $\omega = 2m$ but we expect that this singularity will be rounded out when collisions are included at order ϵ^2 $(1/N)$: we will not describe this rounding out here, however. Although they have a strong effect at the threshold, collisions are not expected to significantly modify the form of $\sigma'_{II}(\omega)$ at higher frequencies where the transport is predominantly collisionless. In particular, the $\omega \to \infty$ limit is precisely the $T = 0$ result [78]

$$
\sigma'_{II}(\omega \to \infty) = \frac{\pi S_d}{2^d d}\left|\frac{\omega}{c}\right|^{d-2}
\tag{9.31}
$$

9.2 Collisionless transport equations

The low order perturbative result for $\sigma(\omega)$ in Section 9.1 is clearly not physically satisfactory. Due to the absence of any collisions between the thermally excited particles, we found a singular delta function at $\omega = 0$ and a sharp threshold at $\omega = 2m$. Before we can repair these singularities, we will present an alternative derivation of the delta function

contribution at $\omega = 0$: this will carried out using an equation of motion analysis which clearly exposes the role of collisionless transport of thermally excited particles [116]. The advantage of this new approach is that we will subsequently be able to readily include the effects of collisions.

We saw in the previous section that, at the one-loop level, the only effect of the $(\phi_\alpha^2)^2$ interaction was in inducing the T dependent mass m in the propagators. This suggests that we perform our equation of motion analysis with the following simplification of the Hamiltonian in (9.3):

$$\mathcal{H}' = \mathcal{H}_0 + \mathcal{H}_{\text{ext}} \tag{9.32}$$

The first term, $\mathcal{H}_0$ is the free particle part but with a renormalized mass m

$$\mathcal{H}_0 = \frac{1}{2} \int d^d x \left[\pi_\alpha^2 + c^2 (\nabla_x \phi_\alpha)^2 + m^2 \phi_\alpha^2 \right], \tag{9.33}$$

and $\mathcal{H}_{\text{ext}}$ contains the coupling to the external 'magnetic' field H^a:

$$\mathcal{H}_{\text{ext}} = - \int d^d x H^a(\mathbf{x}, t) T_{\alpha\beta}^a \pi_\alpha(x, t) \phi_\beta(x, t). \tag{9.34}$$

As noted earlier, we shall be interested only in the linear response of the current to the gradient $\vec{E}^a = -\vec{\nabla}_x H^a(x, t)$, and it will be assumed below that $\vec{E}^a$ is independent of x. Notice that, unlike Section 9.1, we are making the gauge choice of coupling to H^a rather than the vector potential $\vec{A}^a$; this is for convenience, and should not change the final gauge-invariant results. Strictly speaking, the renormalized mass m which appears in $\mathcal{H}_0$ also depends upon $\vec{E}^a$: however to linear order in $\vec{E}^a$, and for the case of a momentum-independent interaction, this 'vertex correction' can be neglected, and we will do so here without proof. The explicit form of the angular momentum current $\vec{J}^a$ can be obtained by computing the equation of motion for the angular momentum density and putting it in the form (9.6): in the present situation of a x-independent $\vec{E}^a$, the choice

$$\vec{J}^a = c^2 T_{\alpha\beta}^a \phi_\alpha \vec{\nabla}_x \phi_\beta \tag{9.35}$$

ensures that $\langle \vec{J}^a \rangle$ vanishes when $\vec{E}^a = 0$. Moreover $\langle \vec{J}^a \rangle$ will be independent of x for $\vec{E}^a$ non-zero. For completeness, let us also note here the expression for the total momentum density, $\vec{P}$ of the quantum field theory $\mathcal{H}$; this can be derived by studying the response of the action to translations, as is discussed in standard graduate texts [248]:

$$\vec{P} = \pi_\alpha \vec{\nabla}_x \phi_\alpha. \tag{9.36}$$

Notice that it is quite distinct from $\vec{J}^a$. In particular, in the absence of an external potential, $\vec{P}$ is conserved (*i.e.,* it obeys an equation of the form $\partial_t \vec{P} + \vec{\nabla} \cdot \overset{\leftrightarrow}{Q} = 0$ for some local field $\overset{\leftrightarrow}{Q}$), while $\vec{J}^a$ is not.

The subsequent analysis is simplest in terms of the normal modes which diagonalize $\mathcal{H}_0$. Using the standard approach of diagonalizing harmonic oscillator Hamiltonians we make the mode expansion

$$
\begin{aligned}
\phi_\alpha(x,t) &= \int \frac{d^d k}{(2\pi)^d} \frac{1}{\sqrt{2\varepsilon_k}} \left(a_\alpha(k,t) e^{i\vec{k}\cdot\vec{x}} + a_\alpha^\dagger(\vec{k},t) e^{-i\vec{k}\cdot\vec{x}} \right) \\
\pi_\alpha(x,t) &= -i \int \frac{d^d k}{(2\pi)^d} \sqrt{\frac{\varepsilon_k}{2}} \left(a_\alpha(\vec{k},t) e^{i\vec{k}\cdot\vec{x}} - a_\alpha^\dagger(\vec{k},t) e^{-i\vec{k}\cdot\vec{x}} \right) (9.37)
\end{aligned}
$$

where the $a(\vec{k},t)$ operators satisfy the equal-time commutation relations

$$
\begin{aligned}
\left[a_\alpha(\vec{k},t), a_\beta^\dagger(\vec{k}',t) \right] &= \delta_{\alpha\beta}(2\pi)^d \delta^d(\vec{k}-\vec{k}') \\
\left[a_\alpha(\vec{k},t), a_\beta(\vec{k}',t) \right] &= 0. \qquad\qquad (9.38)
\end{aligned}
$$

It can be verified that (9.4) is satisfied, and $\mathcal{H}_0$ is given by

$$
\mathcal{H}_0 = \int \frac{d^d k}{(2\pi)^d} \varepsilon_k \left[a_\alpha^\dagger(\vec{k},t) a_\alpha(\vec{k},t) + 1/2 \right] \qquad (9.39)
$$

We will also need the expression for the current $\vec{J}^a$ in terms of the a and $a^\dagger$. We will only be interested in the case where the system carries a position-independent current: for this case, inserting (9.37) into (9.35), we find

$$
\begin{aligned}
\vec{J}^a(t) &= \vec{J}_I^a(t) + \vec{J}_{II}^a(t) \\
\vec{J}_I^a(t) &= ic^2 L_{\alpha\beta}^a \int \frac{d^d k}{(2\pi)^d} \frac{\vec{k}}{\varepsilon_k} \left\langle a_\alpha^\dagger(\vec{k},t) a_\beta(\vec{k},t) \right\rangle \\
\vec{J}_{II}^a(t) &= -ic^2 L_{\alpha\beta}^a \int \frac{d^d k}{(2\pi)^d} \frac{\vec{k}}{2\varepsilon_k} \left\langle a_\alpha^\dagger(-\vec{k},t) a_\beta^\dagger(\vec{k},t) \right\rangle + \text{H.c.} (9.40)
\end{aligned}
$$

It should be evident that processes contributing to $\vec{J}_{II}^a$ require a minimum frequency of $2m$, and so $\vec{J}_{II}^a$ only contributes to $\sigma_{II}(\omega)$. We will therefore drop the $\vec{J}_{II}^a$ contribution below and approximate $\vec{J}^a \approx \vec{J}_I^a$. The ease with which the high frequency components of $\sigma(\omega)$ can be separated out is an important advantage of the present formulation of the quantum transport equations. Of course, at this simple free-field level it is not difficult to also include $\vec{J}_{II}^a$, and rederive the complete results for σ_I and σ_{II} obtained in Section 9.1: we will, however not do so in the

interest of simplicity, but urge the reader to carry out this instructive computation.

The central object in our presentation of transport theory shall be the mean, time-dependent occupation number of the normal modes:

$$f_{\alpha\beta}(\vec{k}, t) = \left\langle a_\alpha^\dagger(\vec{k}, t) a_\beta(\vec{k}, t) \right\rangle \tag{9.41}$$

in terms of which the expectation value of current is

$$\left\langle \vec{J}^a(t) \right\rangle = ic^2 T_{\alpha\beta}^a \int \frac{d^d k}{(2\pi)^d} \frac{\vec{k}}{\varepsilon_k} f_{\alpha\beta}(\vec{k}, t). \tag{9.42}$$

The corresponding expression for the momentum density is

$$\left\langle \vec{P}(t) \right\rangle = \int \frac{d^d k}{(2\pi)^d} \vec{k} f_{\alpha\alpha}(\vec{k}, t). \tag{9.43}$$

Notice the difference in the structure of the O(N) indices between (9.42) and (9.43).

For the subsequent analysis it is convenient to choose a definite orientation for the field H^a in the O(N) space. As in Section 6.3, and the discussion above (6.47), we choose the field which generates rotations in the $1 - 2$ plane, *i.e.*, $H^a = 0$ except for the component a which couples to the generator of O(N) with $T_{1,2}^a = -T_{2,1}^a = 1$. We will henceforth denote this non-zero component simply by H, (and $\vec{E} = \vec{\nabla}H$) and the index a will be dropped. Similarly, the current $\vec{J}^a$ is non-zero only for this component, and will be denoted $\vec{J}$. It is also not difficult to see that to linear order in $\vec{E}$, the distribution functions in (9.41) do not get modified for all components $\alpha > 2$: this is because any change in these components must be even in $\vec{E}$. This conclusion is also true to all orders in the interaction u in $\mathcal{H}$. We have therefore

$$f_{\alpha\beta}(\vec{k}, t) = \delta_{\alpha\beta} n(\varepsilon_k) \qquad \alpha > 2 \text{ or } \beta > 2 \tag{9.44}$$

where $n(\varepsilon)$ is the Bose function in (7.63).

The interesting transport phenomena all occur within the $1, 2$ components of $f_{\alpha\beta}(\vec{k}, t)$. Within this subspace, it is helpful to transform to a basis where the external field is diagonal. We therefore define

$$a_\pm(\vec{k}, t) \equiv \frac{a_1(\vec{k}, t) \pm i a_2(\vec{k}, t)}{\sqrt{2}}, \tag{9.45}$$

and we will occasionally refer to a_+ (a_-) as the annihilation operators for the particles (holes). The Hamiltonian $\mathcal{H}_0$ can also be expressed

Particles   **Holes**

$$\vec{P} \qquad \longrightarrow \qquad \longleftarrow$$

$$\vec{J} \qquad \longrightarrow \qquad \longrightarrow$$
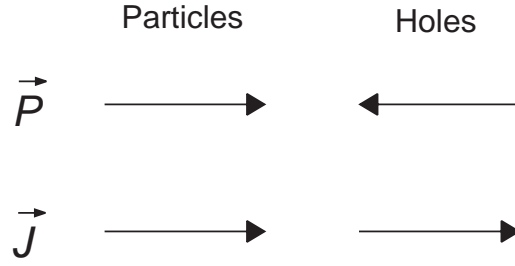
Fig. 9.3. Schematic of the contribution of the particle- and hole-like excitations to the total momentum $\vec{P}$ and the angular momentum current $\vec{J}$. The particles are moving to the right, while the holes are moving to the left. Their contributions to $\vec{P}$ cancel out, while their contributions to $\vec{J}$ add.

in terms of the $a_{\pm}$, and it remains diagonal, with the same form as in (9.33). The current becomes

$$
\begin{aligned}
\left\langle \vec{J} \right\rangle &= \int \frac{d^d k}{(2\pi)^d} \sum_\lambda \lambda \frac{c^2 \vec{k}}{\varepsilon_k} \left\langle a_\lambda^\dagger(\vec{k},t) a_\lambda(\vec{k},t) \right\rangle \\
&= \int \frac{d^d k}{(2\pi)^d} \sum_\lambda \lambda \frac{c^2 \vec{k}}{\varepsilon_k} f_\lambda(\vec{k},t)
\end{aligned}
\tag{9.46}
$$

where the index λ is assumed here and below to extend over the values ± 1, and $f_\lambda \equiv f_{\lambda\lambda}$ are the particle distribution functions (the components of f which are off-diagonal in this λ space can easily be shown to vanish). Let us also note the expression for the momentum density

$$
\vec{P} = \int \frac{d^d k}{(2\pi)^d} \sum_\lambda \vec{k} f_\lambda(\vec{k},t)
\tag{9.47}
$$

An important difference between (9.46) and (9.47) is the λ inside the summation in (9.46) which is absent from (9.47). Thus the angular momentum current is proportional to the difference of the particle and hole number currents, while the momentum density is proportional to their sum; see Fig 9.3.

We have introduced all the basic formalism necessary to introduce the transport equations, which are the equations of motion of the distribution functions $f_\lambda(\vec{k},t)$. These are obtained by computing the Heisenberg equations of motion of $a_{\pm}$ under the Hamiltonian $\mathcal{H}'$ in (9.32). In deriving these equations we make approximations similar to those made for $\vec{J}$: we drop all terms involving the product of two a's or $a^\dagger$'s as these only

contribute to the high frequency σ_{II} (the mixing of these modes with the f_λ can also be neglected to linear order in $\vec{E}$). A straightforward computation then gives the central result of this section

$$\left(\frac{\partial}{\partial t} + \lambda \vec{E}(t) \cdot \frac{\partial}{\partial \vec{k}} \right) f_\lambda(\vec{k}, t) = 0. \tag{9.48}$$

Let us solve (9.46,9.48) in linear response. In the absence of $\vec{E}$, the distribution function has the equilibrium value given by Bose function $f_\lambda(\vec{k}, t) = n(\varepsilon_k)$. We Fourier transform from time, t, to frequency ω, and parameterize to linear order in $\vec{E}$:

$$f_\lambda(\vec{k}, \omega) = 2\pi \delta(\omega) n(\varepsilon_k) + \lambda \vec{k} \cdot \vec{E}(\omega) \psi(k, \omega), \tag{9.49}$$

where we have used the fact that only $\vec{E}$ breaks spatial rotation invariance and O(N) symmetry, to conclude that ψ is independent of $\vec{k}/k$ and λ. Now inserting in (9.48), and using $\partial \varepsilon_k / \partial \vec{k} = \vec{k}/\varepsilon_k$ it is simple to solve for ψ to leading order in $\vec{E}$:

$$\psi(k, \omega) = \frac{c^2}{-i\omega} \frac{1}{\varepsilon_k} \left(-\frac{\partial n(\varepsilon_k)}{\partial \varepsilon_k} \right) \tag{9.50}$$

Finally we insert in (9.46) and deduce the conductivity

$$\sigma(\omega) = \frac{2c^4}{-i\omega} \int \frac{d^d k}{(2\pi)^d} \frac{k_x^2}{\varepsilon_k^2} \left(-\frac{\partial n(\varepsilon_k)}{\partial \varepsilon_k} \right) \tag{9.51}$$

The real part of this agrees with (9.26). Notice that the leading factor of 2 comes from the sum over λ. The current is therefore carried equally by the thermally excited particles and holes: they move in opposite directions to create a state with vanishing momentum but non-zero charge current. We will see in the next section that this charge current can be relaxed by collisions among the particles and holes.

9.3 Collision-dominated transport

We will proceed to improve (9.48) by including collisions among the excitations: these collisions were previously considered in Section 7.2.2 where they led to a finite lifetime for the excitations. Here we will study how the same collisions degrade the transport of angular momentum current.

A full analysis and derivation of the collision contributions to the transport equation is quite lengthy and involved, and beyond the scope of our discussion here. However, the physical interpretation of the final

result is quite straightforward, and with the benefit of hindsight, it is possible to guess the collision terms by a simple application of Fermi's golden rule. We shall follow this latter route here, and omit presentation of a complete, formal derivation. We will begin, in Section 9.3.1, by using the ϵ expansion on the Hamiltonian $\mathcal{H}$ in (9.3). The large N approach will be considered later in Section 9.3.2.

9.3.1 ϵ expansion

The basic idea is to treat (9.48) as a rate equation for the occupation probability of particle states with momentum $\vec{k}$ and polarization λ. The terms present in (9.48) then simply represent the flow of particles with their momenta obeying 'Newton's Law' $d\vec{k}/dt = \lambda\vec{E}$. Collisions can therefore be accounted for by including terms which represents the rate at which particles in state $\vec{k}$ collide with other particles (the 'out' terms) and also the rate at which particles in other states scatter into the state $\vec{k}$ (the 'in' terms). So if there is a matrix element $\mathcal{M}$ for scattering of two particles with momenta and polarizations $\vec{k}$, λ and $\vec{k}_1$, λ_1 into states $\vec{k}_2$, λ_2 and $\vec{k}_3$, λ_3, then Fermi's Golden Rule implies that the right-hand side of the transport equation will acquire the term

$$
\begin{aligned}
-|\mathcal{M}|^2 (2\pi) & \delta(\varepsilon_k + \varepsilon_{k_1} - \varepsilon_{k_2} - \varepsilon_{k_3}) \\
& \times \Big\{ f_\lambda(\vec{k},t) f_{\lambda_1}(\vec{k}_1,t)[1 + f_{\lambda_2}(\vec{k}_2,t)][1 + f_{\lambda_3}(\vec{k}_3,t)] \\
& \quad - f_{\lambda_2}(\vec{k}_2,t) f_{\lambda_3}(\vec{k}_3,t)[1 + f_\lambda(\vec{k},t)][1 + f_{\lambda_1}(\vec{k}_1,t)] \Big\} \quad (9.52)
\end{aligned}
$$

summed over momenta $\vec{k}_{1,2,3}$ and polarizations $\lambda_{1,2,3}$. The expression outside the curly brackets is clearly the collision rate as specified by Fermi's Golden Rule. Inside the curly brackets we have the factors associated with the 'out' and 'in' processes respectively: particles entering into a collision are being annihilated and have associated with them the average Bose matrix element $\langle |\langle n_k - 1|a_k|n_k\rangle|^2 \rangle = f(k)$ (where n_k is the occupation of state k in one realization of the thermal ensemble), while those emerging from a collision have the Bose factor $\langle |\langle n_k + 1|a_k^\dagger|n_k\rangle|^2 \rangle = 1 + f(k)$.

Applying the rules discussed above, a lengthy, but straightforward computation gives us the rather formidable transport equation below [116]; however, the interpretation of the individual terms is quite simple, as

we have already noted.

$$\left(\frac{\partial}{\partial t} + \lambda \vec{E} \cdot \frac{\partial}{\partial \vec{k}}\right) f_\lambda(\vec{k}, t) = -\frac{u^2}{9} \int \frac{d^d k_1}{(2\pi)^d} \frac{d^d k_2}{(2\pi)^d} \frac{d^d k_3}{(2\pi)^d} \frac{1}{16\varepsilon_k \varepsilon_{k_1} \varepsilon_{k_2} \varepsilon_{k_3}}$$

$$\times (2\pi)^d \delta(\vec{k} + \vec{k}_1 - \vec{k}_2 - \vec{k}_3) 2\pi \delta(\varepsilon_k + \varepsilon_{k_1} - \varepsilon_{k_2} - \varepsilon_{k_3}) \Bigg\{$$

$$4\Big\{ f_\lambda(\vec{k}, t) f_{-\lambda}(\vec{k}_1, t)[1 + f_\lambda(\vec{k}_2, t)][1 + f_{-\lambda}(\vec{k}_3, t)]$$

$$- [1 + f_\lambda(\vec{k}, t)][1 + f_{-\lambda}(\vec{k}_1, t)] f_\lambda(\vec{k}_2, t) f_{-\lambda}(\vec{k}_3, t) \Big\}$$

$$+ 2\Big\{ f_\lambda(\vec{k}, t) f_\lambda(\vec{k}_1, t)[1 + f_\lambda(\vec{k}_2, t)][1 + f_\lambda(\vec{k}_3, t)]$$

$$- [1 + f_\lambda(\vec{k}, t)][1 + f_\lambda(\vec{k}_1, t)] f_\lambda(\vec{k}_2, t) f_\lambda(\vec{k}_3, t) \Big\}$$

$$+ (N - 2)\Big\{ f_\lambda(\vec{k}, t) n(\varepsilon_{k_1})[1 + f_\lambda(\vec{k}_2, t)][1 + n(\varepsilon_{k_3})]$$

$$- [1 + f_\lambda(\vec{k}, t)][1 + n(\varepsilon_{k_1})] f_\lambda(\vec{k}_2, t) n(\varepsilon_{k_3}) \Big\}$$

$$+ \frac{(N - 2)}{2}\Big\{ f_\lambda(\vec{k}, t) f_{-\lambda}(\vec{k}_1, t)[1 + n(\varepsilon_{k_2})][1 + n(\varepsilon_{k_3})]$$

$$- [1 + f_\lambda(\vec{k}, t)][1 + f_{-\lambda}(\vec{k}_1, t)] n(\varepsilon_{k_2}) n(\varepsilon_{k_3}) \Big\} \Bigg\} \qquad (9.53)$$

with $\lambda = \pm 1$. The first two pairs of collisions terms represent processes within those with polarizations in the $1 - 2$ plane, while the last two pairs (proportional to $(N - 2)$) represent collisions with particles with polarizations with $\alpha > 2$: in linear response, the latter have their distribution function given simply by the Bose function, as was noted earlier in (9.44).

In writing down (9.53), we have omitted terms associated with collisions which involve creation or annihilation of particle-hole pairs, as they have a negligible contribution in both the high and low T limits in the ϵ expansion (such processes will be included in our later discussion of the $1/N$ expansion). Thus a collision in which, *e.g.*, a positively charged particle of momentum $\vec{k}$ turns into two positively charged particles and a negatively charged hole with momenta $\vec{k}_1$, $\vec{k}_2$, and $\vec{k}_3$ respectively, is permitted by the symmetries of the problem. However, it remains to evaluate the phase space over which such collisions conserve total energy and momentum. In the low T quantum paramagnetic region, we need a particle with energy at least $3\Delta_+$ to have sufficient energy to emit a particle-hole pair, and such particles are exponentially rare. In the opposite high T region, notice that the 'mass' m of the particles/holes

is of order $\sqrt{\epsilon}T$ (below Eqn (9.23)) while their momentum is of order T. So to leading order in ϵ we may just replace the energy momentum relation (7.64) by $\varepsilon_k = ck$ (see also the discussion below (9.28)). The particle-hole pair-creation collision requires that $\vec{k} = \vec{k}_1 + \vec{k}_2 + \vec{k}_3$ and $k = k_1 + k_2 + k_3$. This is only possible if all three momenta are collinear, and this process therefore has vanishing phase space in the high T limit. More generally, for a non-zero m, the phase space vanishes as $\epsilon \to 0$.

We will analyze the solutions of (9.53) separately in the high T and low T paramagnetic regions of Figs 5.2, 5.3 and 8.3.

9.3.1.1 High T, $T \gg \Delta_+$

To obtain the $T \gg \Delta_+$ limit of the scaling results for conductivity as encapsulated in (9.17), it is sufficient to replace the interaction strength u on the right hand side of (9.53) by the fixed point value discussed in Chapter 8 and in (8.18). For the result to leading order in ϵ, we can set

$$u = \frac{48\pi^2 c^3}{(N+8)}\epsilon\mu^\epsilon \qquad (9.54)$$

The prefactor of c^3 has been deduced by dimensional analysis, and did not appear in Chapter 8 because we used units with $c = 1$ there. We expect that in the high T limit, $\mu \sim T/c$, as that is the only natural scale in the problem; in any case, to leading order in ϵ, the precise value of μ is not needed.

The next step is to linearize the transport equation (9.53) by using the ansatz (9.49), and to examine the structure of its solution in the limit of small ϵ. First, we find that the λ dependencies in (9.49) and (9.53) are completely compatible, in that the linearized equation for the unknown function $\psi(k, \omega)$ is independent of λ. Then we perform a simple dimensional analysis of the linear integral equation satisfied by ψ. The dependencies on ϵ (for small ϵ), T and c can all be scaled out, and it is not difficult to show that the solution of the linear integral equation can be written in the form

$$\psi(k, \omega) = \frac{c^2}{\epsilon^2 T^3}\Psi\left(\frac{\omega}{\epsilon^2 T}, \frac{ck}{T}\right), \qquad (9.55)$$

where the dimensionless complex function Ψ satisfies a parameter-free and universal linear integral equation: this equation has to be solved numerically [116], and we will not discuss the details of the numerical analysis here. Finally, computing the current by using (9.46) and (9.49)
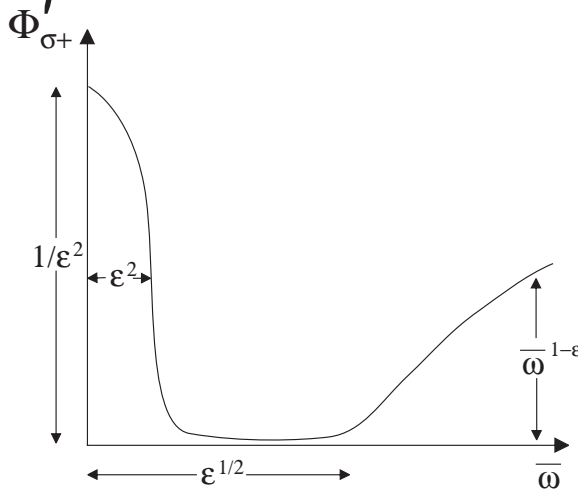
Fig. 9.4. Structure of the real part, $\Phi'_{\sigma+}(\overline{\omega}, 0) = \Phi_{\sigma-}(\overline{\omega}, 0)$, of the universal scaling functions $\Phi_{\sigma\pm}$ in (9.17) in the high T region, $T \gg \Delta_{\pm}$, as a function of $\overline{\omega} = \omega/T$ in the limit of small ϵ. The peak at small $\overline{\omega}$ has a width of order ϵ^2 and a height of order $1/\epsilon^2$: this feature of the conductivity is denoted by σ_I. The collisionless contribution (denoted σ_{II}) begins at $\overline{\omega}$ of order $\epsilon^{1/2}$; as $\overline{\omega} \to \infty$, this contribution is a number of order unity times $\overline{\omega}^{1-\epsilon}$

we see that the conductivity σ_I can be written in the form

$$\sigma_I(\omega) = \frac{(T/c)^{d-2}}{\epsilon^2} \Phi_{\sigma I}\left(\frac{\omega}{\epsilon^2 T}\right) \tag{9.56}$$

where the scaling function $\Phi_{\sigma I}$ is simply related to Ψ. This result is clearly compatible with the scaling form (9.17) for the total conductivity. Notice that the natural frequency scale in (9.55, 9.56) is of order $\epsilon^2 T$—this is the scale over which the delta function in σ'_I was expected to be broadened. Further the peak value of the d.c. conductivity, which diverged at the one-loop level, is seen to be of order $1/\epsilon^2$. (These features are sketched in the schematic of the frequency dependent conductivity in the high T limit in Fig 9.4).

The function $\Phi_{\sigma I}$ therefore defines the smoothening of the delta function in (9.26) and has the same total spectral weight—from (9.28) we see that it satisfies

$$\int_0^\infty d\widetilde{\omega} \mathrm{Re}\Phi_{\sigma I}(\widetilde{\omega}) = \frac{\pi}{18}. \tag{9.57}$$

in the high T limit. It should be noted that this sum rule is special to
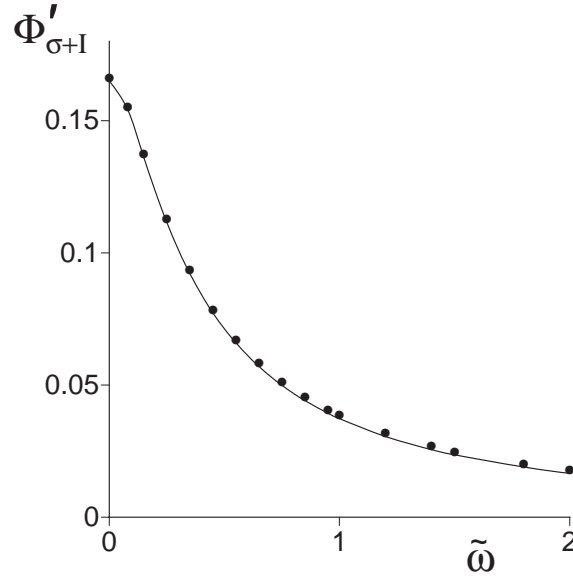
Fig. 9.5. The real part of the universal function $\Phi_{\sigma I}$ as a function of $\widetilde{\omega} = \omega/\epsilon^2 T$, defined in (9.56) in the high T limit $\Delta_+/T = 0$. This function describes the inelastic collision-induced broadening of the $\omega = 0$ delta function in Fig 9.2 at a frequency scale of order $\epsilon^2 T$. The conductivity has an additional continuum contribution $(\sigma_{II}(\omega))$ at frequencies larger than $\omega \sim \epsilon^{1/2} T$ which is not shown above (see Fig 9.4).

the leading order in ϵ being considered here. For ϵ of order unity, there is no sharp distinction between σ_I and σ_{II} and there is no sum rule: indeed the integral in (9.57) when carried out over the total σ will be divergent. For any realistic lattice model there is a large microscopic energy scale ($\sim J$) beyond which the universal scaling results do not apply, and the entire spectral weight (including frequencies beyond J) is not divergent; this latter spectral weight satisfies a sum rule related to non-universal microscopic quantities, and is unrelated to the universal result (9.57).

A complete numerical solution for the function $\Phi'_{\sigma I}$ has been carried out in the high T limit in Ref [116] for the case $N = 2$, and the solution is sketched in Fig 9.5. Most important is the value of $\Phi'_{\sigma I}(0)$ which gives the value of the d.c. conductivity [116]

$$\sigma(0) = \frac{Q^2}{\hbar} \left(\frac{T}{c}\right)^{d-2} \frac{0.1650}{\epsilon^2} \qquad N = 2, T \gg \Delta_\pm. \qquad (9.58)$$

As noted earlier, the result is a pure number times $Q^2/\hbar$ in $d = 2$ (recall that Q is the charge of the carriers, which we usually absorb into the definition of H). These are among the main results for low-frequency transport in this chapter.

9.3.1.2 Low T, $T \ll \Delta_+$

First, we should determine the value of u that must be used in the transport equation (9.53). Now Δ_+ is the largest scale in the problem, and so the generalization of the result (9.54) suggests that

$$u \sim \epsilon c^3 (\Delta/c)^\epsilon. \tag{9.59}$$

However, this result is not adequate, as we will now argue that the limits $T \to 0$ and $\epsilon \to 0$ do not commute. For $T \ll \Delta_+$, as in Sections 4.5.2 and 6.2, all the thermally excited particles are at energies just above the gap, and so we can approximate their dispersion by

$$\varepsilon_k = \Delta_+ + \frac{c^2 k^2}{2\Delta_+}. \tag{9.60}$$

The typical value of the particle momentum is $k \sim \sqrt{\Delta_+ T}/c$. The coupling (9.59) would imply that these quadratically dispersing, slowly moving particles scatter with a T-matrix which is independent of momentum at low momentum. However, we know from elementary quantum mechanics [488], that this Born approximation result is incorrect; the full T-matrix scales as $\sim k^{d-2}$ as the momentum transfer $k \to 0$, and so we should really use a momentum dependent coupling u of order

$$u \sim k^{d-2} \Delta_+^{5-2d} c^{2d-2}, \tag{9.61}$$

where the powers of Δ_+ and c were deduced by a dimensional comparison with (9.59). (Notice that (9.61) diverges as $k \to 0$ in $d = 1$, where the present perturbative transport equation cannot be applied; there, we should instead use the exact S matrix in (6.13), along with the exact transport analysis developed in Section 6.2.) We will not attempt a complete solution of (9.53) with a momentum dependent u here, but will be satisfied with a dimensional analysis which exposes the T dependence of physical observables. By an analysis similar to that leading to (9.55), it is not difficult to show that in the limit $T \ll \Delta_+$, the solution of the linearized integral equation satisfied by ψ takes the form

$$\psi(k, \omega) = \frac{c^2 \tau_\varphi e^{-\Delta_+/T}}{\Delta_+ T} \Psi\left(\omega \tau_\varphi, \frac{ck}{\sqrt{\Delta_+ T}}\right), \tag{9.62}$$

where the particle scattering time, τ_φ, is deduced by a dimensional analysis of the collision term in (9.53) with the momentum dependent coupling u in (9.61):

$$\frac{1}{\tau_\varphi} \sim T \left(\frac{T}{\Delta_+} \right)^{2(d-2)} e^{-\Delta_+/T}. \tag{9.63}$$

Notice that this result for τ_φ. is consistent with the $d = 2$ result in (7.68). Now we can compute the current by inserting (9.62) into (9.46) and (9.49), and the result for σ_I takes the form

$$\sigma_I(\omega) = T\tau_\varphi \left(\frac{\Delta_+ T}{2\pi c^2} \right)^{(d-2)/2} e^{-\Delta_+/T} \Phi_{\sigma+I}(\omega\tau_\varphi) \tag{9.64}$$

Notice that this is consistent with (9.30) in the collisionless limit $\tau_\varphi \to \infty$. The scaling function $\Phi_{\sigma+I}$ is expected to be a constant when its argument vanishes, and so the d.c. conductivity can be obtained from (9.63) and (9.64):

$$\sigma_I(0) \sim \left(\frac{T}{\Delta_+} \right)^{-3(d-2)/2} \left(\frac{\Delta_+}{c} \right)^{(d-2)}. \tag{9.65}$$

This result is valid for $d > 2$, where we see that the d.c. conductivity actually diverges as $T \to 0$. The total spectral weight in the 'Drude' peak of the d.c. conductivity, σ_I, is exponentially small, $\sim e^{-\Delta_+/T}$, but the weak inelastic scattering between the thermally excited particles is also exponentially rare; the two exponential factors cancel each other out, and we get a power-law divergent conductivity. In $d = 2$, because of the logarithmic factors obtained in (7.68), we expect $\sigma_I(0)$ to diverge as $(\ln(\Delta_+/T))^2$; recall that this logarithmic divergence was absence in the high T limit ($T \gg \Delta_+$), where the d.c. conductivity was a completely universal constant in $d = 2$. Finally, as we have already noted, these methods do not apply in $d = 1$, but it is interesting note that the Einstein relation (9.11), when combined with our earlier results (6.12) and (6.27), gives us a d.c. conductivity, $\sigma \sim T^{-1/2}$, which also diverges as $T \to 0$.

9.3.2 Large N limit

A closely related analysis of collisions can also be carried out in the large N limit. It has the advantage of working directly in $d = 2$ at all stages, and so we will briefly discuss its formulation here [430].

The central simplification of the large N limit is apparent by a glance at the right-hand side of (9.53): the $\vec{E}$ field changes the distribution of

particles only with polarization $\alpha = 1, 2$, but their scattering is dominated completely by collisions with particles with polarization $\alpha > 2$ (notice the prefactor of $(N - 2)$ in some of the collision terms). The collisions with these particles actually appear in the form of interactions with the fluctuations of the λ field which were considered in Section 7.2. The propagator, Π of this λ field was given in (7.42), and the upshot of the result (9.44) is that this propagator remains unchanged in the presence of the $\vec{E}$ field. To leading order in $1/N$ we can then simply consider the Gaussian fluctuations of the λ field as a an infinite set of harmonic oscillators with density of modes given by the imaginary part of $1/\Pi$. These harmonic oscillators are coupled to the normal modes of the order parameter $\mathbf{n}$ by the $\lambda \mathbf{n}^2$ vertex in (5.18). The collision terms arise entirely from this vertex, and their form can be deduced from Fermi's Golden Rule as discussed earlier. The resulting generalization of (9.48) is then

$$\left(\frac{\partial}{\partial t} + \lambda \vec{E} \cdot \frac{\partial}{\partial \vec{k}}\right) f_\lambda(\vec{k}, t) = -\frac{2}{N} \int_0^\infty \frac{d\Omega}{\pi} \int \frac{d^2q}{(2\pi)^2} \mathrm{Im}\left(\frac{1}{\Pi(\vec{q}, \Omega)}\right)$$

$$\times \left\{ \frac{(2\pi)\delta(\varepsilon_k - \varepsilon_{|\vec{k}+\vec{q}|} - \Omega)}{4\varepsilon_k \varepsilon_{|\vec{k}+\vec{q}|}} \left[f_\lambda(\vec{k}, t)(1 + f_\lambda(\vec{k} + \vec{q}, t))(1 + n(\Omega)) \right. \right.$$

$$\left. - f_\lambda(\vec{k} + \vec{q}, t)(1 + f_\lambda(\vec{k}, t))n(\Omega) \right]$$

$$+ \frac{(2\pi)\delta(\varepsilon_k - \varepsilon_{|\vec{k}+\vec{q}|} + \Omega)}{4\varepsilon_k \varepsilon_{|\vec{k}+\vec{q}|}} \left[f_\lambda(\vec{k}, t)(1 + f_\lambda(\vec{k} + \vec{q}, t))n(\Omega) \right.$$

$$\left. - f_\lambda(\vec{k} + \vec{q}, t)(1 + f_\lambda(\vec{k}, t))(1 + n(\Omega)) \right]$$

$$+ \frac{(2\pi)\delta(\varepsilon_k + \varepsilon_{|-\vec{k}+\vec{q}|} - \Omega)}{4\varepsilon_k \varepsilon_{|-\vec{k}+\vec{q}|}} \left[f_\lambda(\vec{k}, t)f_{-\lambda}(-\vec{k} + \vec{q}, t)(1 + n(\Omega)) \right.$$

$$\left. \left. - (1 + f_{-\lambda}(-\vec{k} + \vec{q}, t))(1 + f_\lambda(\vec{k}, t))n(\Omega) \right] \right\}, \quad (9.66)$$

where the function Π is defined by analytic continuation from (7.42). Notice that this equation is formulated directly in $d = 2$, and is entirely free of parameters, other than the energy scales T and Δ_+ (through the value of ε_k in (7.64)). So it is already in the scaling limit, and its solution will lead to a σ consistent with the scaling form (9.17).

The equation (9.66) can of course also be formulated in arbitrary d, and it is reassuring to verify that in their overlapping regions of validity

(N large and ϵ small) the results (9.53) and (9.66) are in precise agreement with each other. However, there are important differences between the $d = 2$, large N analysis of (9.66) and the small ϵ analysis of (9.53) discussed earlier. Now we have to use the full dispersion $\varepsilon_k = \sqrt{c^2 k^2 + m^2}$ in (7.64), and in no regime is it possible to approximate it by $\varepsilon_k = ck$. Also, unlike (9.53), (9.66) does contain terms corresponding to collisions which cause production of new particle-hole pairs.

As in the case of the ϵ expansion, it is useful to scale out the small parameter $1/N$ from the transport equation (9.66). Using the ansatz (9.49), and obtaining the linear integral equation for ψ, it can be shown that its solution can be written in the form

$$\psi(k, \omega) = \frac{Nc^2}{T^3} \Psi \left(\frac{N\omega}{T}, \frac{ck}{T}, \frac{\Delta_+}{T} \right) \tag{9.67}$$

where again the dimensionless complex function Ψ satisfies a parameter-free and universal linear integral equation. Computing the current by using (9.46) and (9.49), it follows that the analog of (9.56) and (9.64) is in $d = 2$

$$\sigma_I(\omega) = N \Phi_{\sigma+I} \left(\frac{N\omega}{T}, \frac{\Delta_+}{T} \right). \tag{9.68}$$

The natural frequency scale in (9.67, 9.68) is of order T/N–this is the scale, from (7.71), over which the delta function in σ_I' was expected to be broadened. A schematic of the large N frequency dependent conductivity in the high T limit in Fig 9.6). The sum rule on $\Phi_{\sigma+I}'$ corresponding to (9.57) is specified by (9.29).

A complete numerical solution for the function $\Phi_{\sigma+I}'$ has been carried out in the high T limit in $d = 2$ and the solution is shown in Fig 9.7. The large N value of $\Phi_{\sigma+I}'(0, 0)$ which gives the value of the d.c. conductivity was obtained as

$$\sigma(0) = \frac{Q^2}{\hbar} 0.1077 N \qquad d = 2, T \gg \Delta_\pm. \tag{9.69}$$

These results complement similar results discussed earlier in the ϵ expansion.

9.4 Physical interpretation

This is a convenient point to emphasize some interesting physical features of the above computations of the universal behavior of the conductivity near a quantum-critical point in $d = 2$. The central property is
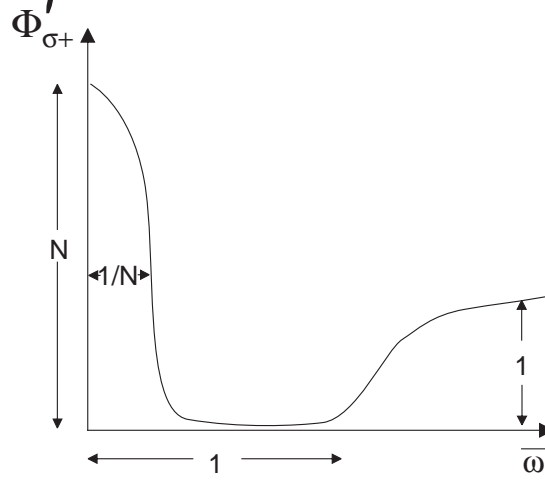
Fig. 9.6. The analog of Fig 9.4 for the large N limit in $d = 2$.

the basic scaling form (9.17) and the above computations have all been aimed at describing the structure in the scaling function $\Phi_{\sigma+}$. A remarkable property of the result emerges in the high T region of Fig 8.3: the dynamical conductivity in $d = 2$ depends upon no material parameters at all, and is given by the pure universal function $\Phi_{\sigma+}(0, \omega/T)$.

Here we focus on two limiting regions of this result in the high T region.

First, consider the high frequency regime $\omega \gg T$. Here we found that the perturbative analysis considered Section 9.1 gave an adequate description of the physics. The main result is contained in (9.31) and has a simple physical interpretation. The system is in its ground state, and the oscillating external field creates a particle-hole pair. The conductivity is then determined by the subsequent motion of this particle-hole pair. As we are effectively at the critical coupling, there is a gapless spectrum, and this particle-hole pair will also create a cascade of lower energy particle hole pairs: such processes lead to corrections to (9.31) which are higher order in ϵ (computed in Ref [143]) or $1/N$ (computed in Ref [78]). It is clear, however, that all these processes are essentially coherent: the system was originally in its phase-coherent ground state, and the particle-hole pairs created move coherently in response to the external field. This coherent transport is characterized by the universal number $\Phi_{\sigma+}(\infty, 0)$.
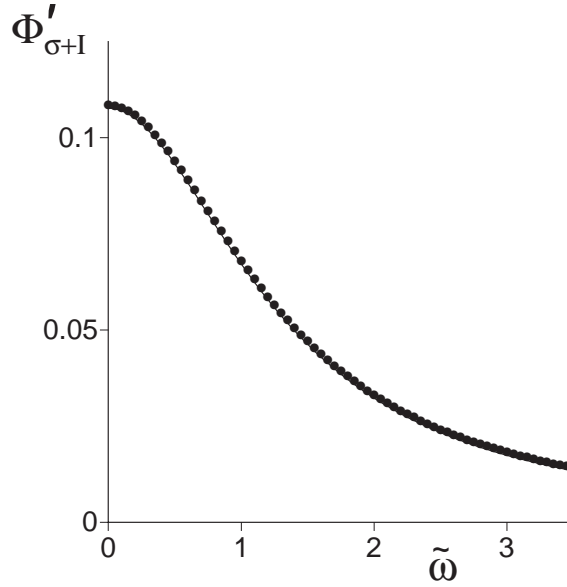
Fig. 9.7. The real part of the large N universal function $\Phi_{\sigma+I}$ as a function of $\widetilde{\omega} = N\omega/T$, defined in (9.68) in the high T limit $\Delta_+/T = 0$. This function describes the inelastic collision-induced broadening of the $\omega = 0$ delta function in Fig 9.2 at a frequency scale of order T/N. The conductivity has an additional continuum contribution ($\sigma_{II}(\omega)$) at frequencies larger than $\omega \sim T$ which is not shown above (see Fig 9.6).

Now, consider the low frequency regime $\omega \ll T$: this also includes the d.c. case. Here, the interpretation is completely different. The system is initially at finite temperature, with an incoherent density of pre-existing of particle-hole pairs already present. The external field accelerates the particles and holes in opposing directions, but their repeated collisions cause them to relax to local equilibrium. The transport is therefore due to a collision dominated drift of these excitations, and is controlled entirely by inelastic processes. Now, clearly, the low frequency transport is entirely incoherent. However, because the collision cross-section between the excitations has a universal form near a quantum critical point, the remarkable fact is that the d.c. conductivity remains universal: it is given by the number $\Phi_{\sigma+}(0,0)$. Results for this number appear in (9.58) in the ϵ expansion, and in (9.69) in the $1/N$ expansion.

The distinct physical interpretations of $\Phi_{\sigma+}(\infty,0)$ and $\Phi_{\sigma+}(0,0)$ make it clear that there is no reason for them to have equal values. This differ-
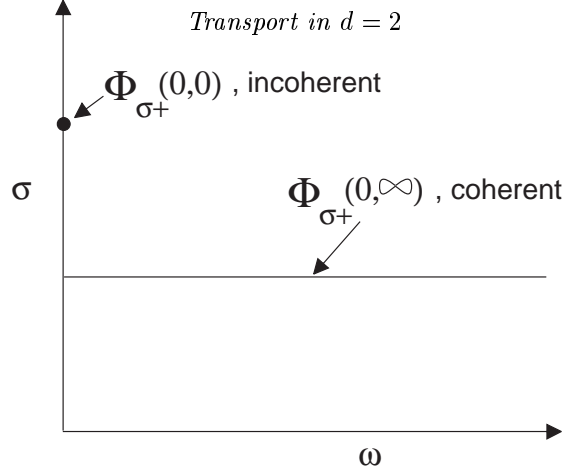
Fig. 9.8. The value of $\sigma(\omega, T \to 0)$ in $d = 2$ at the quantum-critical coupling $s = 0$ (in the notation of Chapter 8) or $g = g_c$ (in the notation of Chapter 5). The value $\Phi_{\sigma+}(0,0)$ characterizes the single point $\omega = 0$.

ence leads to an unusual structure in the $T \to 0$ limit of the conductivity in $d = 2$: in Fig 9.8 we show the universal value of $\sigma(\omega, T \to 0)$. For all $\omega > 0$ we have a frequency independent conductivity given by the number $\Phi_{\sigma+}(\infty, 0)$ describing coherent transport; however only the single point $\omega = 0$ is given by the value $\Phi_{\sigma+}(0, 0)$ which characterizes incoherent transport. For laboratory measurements, we note that a degree Kelvin in temperature converts approximately to 20 Ghz frequency by the factor k_B/h; so even a radio frequency measurement is usually comfortably in the regime $\hbar\omega \ll k_B T$, and will therefore measure $\Phi_{\sigma+}(0, 0)$, given by the isolated $\omega = 0$ point in Fig 9.8.

In physical applications of the $N = 2$ transport analysis of this chapter (discussed a bit more explicitly in Section 9.5), we will interpret σ as the electrical conductivity of carriers of charge Q ($Q = 2e$ for the superconductor-insulator transition); then, in laboratory units, the conductivity is the quantum unit of conductance, $Q^2/\hbar$, times the scaling functions computed here. So, in $d = 2$, the high T region has a d.c. conductivity which is $Q^2/\hbar$ times a universal number. The reader may be familiar with other physical situations in which universal conductances of order e^2/h have been discussed previously: these include Landauer transport in one dimensional microstructures [19], universal conductance fluctuations [17, 300], or critical points in non-interacting electron models of transitions between quantum Hall plateaus [85, 231, 230]. However

in all these cases, the transport is *phase coherent* and the phase-breaking length is assumed to be larger than the sample size. In contrast, the conductivity studied here near an interacting quantum critical point is dominated entirely by *inelastic* processes; it is therefore quite remarkable that the d.c. conductivity is universal despite being entirely incoherent.

9.5 Applications and extensions

An important application of the transport results of this chapter is for the $N = 2$ case, which describes a superfluid to insulator transition in lattice models of bosons. This connection will become clearer in Chapter 10, where it will be discussed further. However, an intuitive understanding can be gained by returning to the lattice Hamiltonian representation in (5.1), and interpreting it as an effective Hamiltonian for a regular two-dimensional array of mesoscopic superconducting quantum dots [129]. For $N = 2$, there is only one component of the angular momentum operator, $\hat{L}_i$ (see (2.56)). We interpret $\hat{L}_i$ as the number operator for bosonic Cooper pairs on a superconducting quantum dot at site i, minus a fixed integer which equals the number of Cooper pairs on an isolated island (the role of this integer will become clearer in Chapter 10). The term proportional to gJ in (5.1) is a caricature of the additional Coulomb energy required for deviation in the number of Cooper pairs on a dot from its optimum value. The angle, θ, defining the orientation of $\hat{\mathbf{n}}$ (as in (2.38)), is taken as the phase of the superconducting order parameter. Then the term proportional to J represents Josephson tunneling of Cooper pairs between neighboring dots. The phase of the rotor model with long range order in $\mathbf{n}$ represents the superfluid, while the quantum paramagnet is the Mott insulator of Cooper pairs. A large number of experiments have measured d.c. transport on granular films, Josephson junction arrays and homogeneously disordered superconductors undergoing a zero temperature transition from a superconductor to an insulator; one of the earliest such experiments was carried out by Strongin *et al.* [482] and reviews of more recent works are in Refs [221] and [308] for reviews. However these experiments cannot be quantitatively modeled by the simple models we have considered here: all experimental systems have an appreciable amount of randomness, and this is surely a relevant perturbation on the simple clean quantum critical point we have studied here. Further, we have entirely ignored fermionic excitations [496, 446], and these could be important near the critical point, although there are indications in recent simulations [178] that the

neglect of fermionic excitations is justified. In some interesting recent experiments [411], a disordered superconducting film was coupled to a tunable, dissipative metallic bath, and some initial theoretical attempts to explain them have also appeared [521]—we will briefly consider the general consequences of fermionic excitations in Chapter 12. Finally, the long-range part of the Coulomb interaction is probably also relevant at the superfluid-insulator transition: this issue has been addressed in Refs [158, 534, 533]. Nevertheless, the scaling forms for the conductivity, and our general discussion on the crossover between coherent and incoherent transport at a frequency scale of order $k_B T/\hbar$, is expected to apply to these more complex systems too.

Dynamical measurements of the conductivity at frequencies of order $k_B T/\hbar$ in systems near a superfluid-insulator transition are not yet available. However, such measurements have been recently made for a system near a metal-insulator transition by Lee *et al.* [298], and nicely exhibit scaling as a function of ω/T. Related measurements [139] have also been made near quantum Hall transitions in $d = 2$, and are again consistent with scaling as a function of ω/T. As we discussed at the conclusion of Section 8.2.2, universal time scales of order $\hbar/k_B T$ require that the quantum critical theory have non-vanishing interactions between its thermal excitations, for otherwise the interactions are "dangerously irrelevant" and the characteristic times are higher powers of $1/T$. These quantum Hall measurements therefore indicate that the non-interacting electron models for these transitions [230, 469] have to be extended to include interactions.

Part three

Other Models

10

Boson Hubbard model

The Hubbard model was originally introduced as a description of the motion of electrons in transition metals, with the motivation of understanding of their magnetic properties. This original model remains a very active subject of research today: important progress has been made in recent years by examining its properties in the limit of large spatial dimensionality [177, 172].

In this chapter, we shall only examine the much simpler "boson Hubbard model", following the analysis in an important paper by Fisher, Weichman, Grinstein and Fisher [160]. As the name implies, the elementary degrees of freedom in this model are spinless bosons, which take the place of the spin-1/2 fermionic electrons in the original model. These bosons could represent Cooper pairs of electrons undergoing Josephson tunneling between superconducting islands, or Helium atoms moving on a substrate. Processes in which the Cooper pair boson decays into a pair of electrons are neglected in this simple model, and this caveat must be kept in mind while discussing experimental applications.

Many of the results discussed in this chapter were also obtained in early literature on quantum transitions in anisotropic magnets in the presence of an applied magnetic field. These are reviewed by Kaganov and Chubukov [258], who also gave an extensive discussion of experimental applications. We will, however, not use their formulation here.

Apart from its direct physical applications, the importance of the boson Hubbard model lies in providing one of the simplest realizations of a quantum phase transition which does not map onto a previously studied classical phase transition in one higher dimension. The continuum theory describing this transition includes complex Berry phase terms, which, in the simplest formulation of the theory, do not become real even after analytic continuation to imaginary time. We shall meet

257

some genuinely new physical phenomena associated with quantum critical points in a relatively simple context, and the insight will be generally applicable to more complicated models in subsequent chapters.

Let us define the degrees of freedom of the model of interest. We introduce the boson operator $\hat{b}_i$ which annihilates bosons on the sites, i, of a regular lattice in d dimensions. These Bose operators and their Hermitian conjugate creation operators obey the commutation relation

$$[\hat{b}_i, \hat{b}_j^\dagger] = \delta_{ij}, \qquad (10.1)$$

while two creation of annihilation operators always commute. It is also useful to introduce the boson number operator $\hat{n}_{bi}$

$$\hat{n}_{bi} = \hat{b}_i^\dagger \hat{b}_i \qquad (10.2)$$

which counts the number of bosons on each site. We allow an arbitrary number of bosons on each site: so the Hilbert space consists of states $|\{m_j\}\rangle$, which are eigenstates of the number operators

$$\hat{n}_{bi}|\{m_j\}\rangle = m_i|\{m_j\}\rangle, \qquad (10.3)$$

and every m_j in the set $\{m_j\}$ is allowed to run over all non-negative integers. This includes the 'vacuum' state with no bosons at all $|\{m_j = 0\}\rangle$.

The Hamiltonian of the boson Hubbard model is

$$H_B = -w \sum_{\langle ij \rangle} \left(\hat{b}_i^\dagger \hat{b}_j + \hat{b}_j^\dagger \hat{b}_i \right) - \mu \sum_i \hat{n}_{bi} + U \sum_i \hat{n}_{bi}(\hat{n}_{bi} - 1). \qquad (10.4)$$

The first term, proportional to w, allows hopping of bosons from site to site ($\langle ij \rangle$ represents nearest neighbor pairs); if each site represents a superconducting grain, then w is the Josephson tunneling which allows Cooper pairs to move between grains. The second term, μ, represents the chemical potential of the bosons: changes in the value of μ changes the total number of bosons. Depending upon the physical conditions, a given system can either be constrained to be at a fixed chemical potential (the grand canonical ensemble), or have a fixed total number of bosons (the canonical ensemble): theoretically it is much simpler to consider the fixed chemical potential case, and results at fixed density can always be obtained from them after a Legendre transformation. Finally, the last term, $U > 0$, represents the simplest possible repulsive interaction between the bosons. We have taken only an on-site repulsion: this can be considered to be the charging energy of each superconducting

grain. Off-site and longer-range repulsion are undoubtedly important in realistic systems, but are neglected in this simplest model.

There is a basic similarity between the boson Hubbard model and the $O(N)$ rotor Hamiltonian H_R in (5.1) which is useful in understanding their respective physical properties, and was indicated in Section 9.5. First, on the issue of symmetries. The rotor Hamiltonian H_R was invariant under global $O(N)$ rotation of the rotor fields $\hat{\mathbf{n}}_i$ and $\hat{\mathbf{L}}_i$; the present H_B is invariant under a global $U(1) \equiv O(2)$ phase transformation under which

$$\hat{b}_i \to \hat{b}_i e^{i\phi}. \tag{10.5}$$

Now notice that the w term in H_B is quite similar to the J term in H_R: both couple neighboring sites in a manner which prefers a state which breaks the global symmetry. However these terms compete with Jg term in H_R, or the U term in H_B, both of which are completely local and prefer states which are invariant under their respective symmetry transformations. So, by analogy with H_R, we may expect a quantum phase transition in H_B as a function of t/U between a state in which the $U(1)$ symmetry (10.5) is unbroken to one in which it is broken.

There is, however, a crucial difference between H_R and H_B which requires a more careful discussion of the symmetries in the two models. Recall that a consequence of the $O(N)$ symmetry of H_R was the conservation of total angular momentum in H_R; similarly we have the conservation of the total number of bosons

$$\hat{N}_b = \sum_i \hat{n}_{bi}; \tag{10.6}$$

it is easily verified that $\hat{N}_b$ commutes with $\hat{H}$. Notice that in H_R the external field $\mathbf{H}$ coupled to the conserved total angular momentum; the term analogous to this is the chemical potential μ in H_B which couples to $\hat{N}_b$. This correspondence also brings out the difference. Recall that all of our analysis of H_R was carried out in zero field $\mathbf{H} = 0$, and we only examined the linear response to an infinitesimal external field $\mathbf{H}$. However, the choice $\mathbf{H} = 0$ was a natural one, as it was *only* for this value that the remainder of H_R was $O(N)$ invariant (at least for $N \geq 3$). In contrast, notice that the μ term in H_B does not break any symmetries, and H_B remains invariant under (10.5) for any value of μ. So there is no natural symmetry criterion by which we can prefer a specific value of μ, and we have no choice but to examine H_B for all μ. (Even for the case $N = 2$, the choice $\mathbf{H} = 0$ for H_R can be made from the requirement

of a "particle-hole" symmetry under which $\mathbf{n}_i \to -\mathbf{n}_i$, while $\mathbf{L}_i$ remains invariant; there is no such corresponding symmetry for H_B.) It will turn out that the results for H_B for general μ, will also allow us to understand H_R for finite non-zero $\mathbf{H}$.

We will begin our study of H_B by introducing a simple mean field theory in Section 10.1. The continuum quantum theories describing fluctuations near the quantum critical points will then introduced in Section 10.2.

10.1 Mean field theory

The strategy, as in any mean field theory, will be to model the properties of H_B by the best possible sum, H_{MF} of single site Hamiltonians:

$$H_{MF} = \sum_i \left(-\mu \sum_i \hat{n}_{bi} + U \hat{n}_{bi}(\hat{n}_{bi} - 1) - \Psi_B^* \hat{b}_i - \Psi_B \hat{b}_i^\dagger \right), \quad (10.7)$$

where the complex number Ψ_B is a variational parameter. We have chosen a mean-field Hamiltonian with the same on-site terms as H_B, and added an additional term with a 'field' Ψ_B which represents the influence of the neighboring sites: this field has to be self-consistently determined. Notice that this term breaks the U(1) symmetry, and does not conserve the total number of particles: this is to allow for the possibility of broken-symmetric phases, while symmetric phases will of appear at the special value $\Psi_B = 0$. As we saw in the analysis of H_R, the state which breaks the U(1) symmetry will have a non-zero stiffness to rotations of the order parameter; in the present case this stiffness is the superfluid density characterizing a superfluid ground state of the bosons.

Another important assumption underlying (10.7) is that the ground state does not spontaneously break a translational symmetry of the lattice, as the mean-field Hamiltonian is the same on every site. Such a symmetry breaking is certainly a reasonable possibility, but we will ignore this complication here for simplicity.

We will determine the optimum value of the mean-field parameter Ψ_B by a standard procedure. First, determine the ground state wavefunction of H_{MF} for an arbitrary Ψ_B: as H_{MF} is a sum of single site Hamiltonians, this wavefunction will simply be a product of single-site wavefunctions. Next, evaluate the expectation value of H_B in this wavefunction. By adding and subtracting H_{MF} from H_B, we can write the
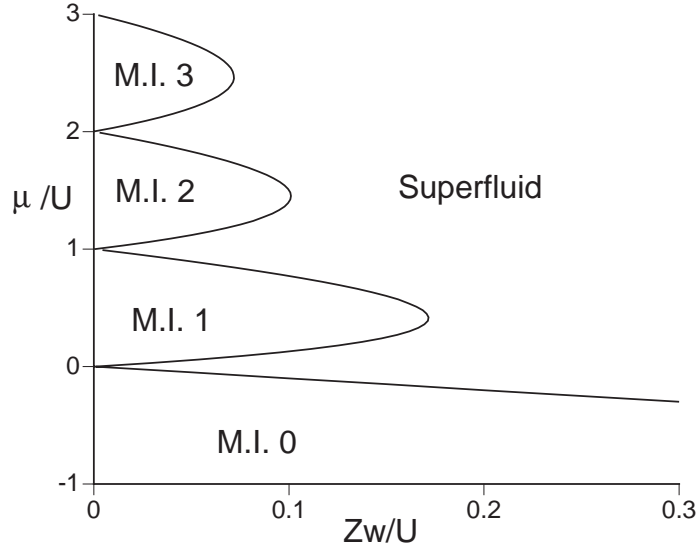
Fig. 10.1. Mean field phase diagram of the ground state of the boson Hubbard model H_B in (10.4). The notation M.I. n refers to a Mott insulator with $n_0(\mu/U) = n$.

mean-field value of the ground state energy of H_B in the form

$$\frac{E_0}{M} = \frac{E_{MF}(\Psi_B)}{M} - Zw\langle\hat{b}^\dagger\rangle\langle\hat{b}\rangle + \langle\hat{b}\rangle\Psi_B^* + \langle\hat{b}^\dagger\rangle\Psi_B \qquad (10.8)$$

where $E_{MF}(\Psi_B)$ is the ground state energy of H_{MF}, M the number of sites of the lattice, Z is the number of nearest neighbors around each lattice point (the 'co-ordination number'), and the expectation values are evaluated in the ground state of H_{MF}. The final step is to minimize (10.8) over variations in Ψ_B. We have carried out this step numerically and the results are shown in Fig 10.1.

Notice that even on a single site, H_{MF} has an infinite number of states, corresponding to the allowed values $m \geq 0$ of the integer number of bosons on each site: the numerical procedure necessarily truncates these states at some large occupation number, but the errors are not difficult to control. In any case, we will show that all the essential properties of the phase diagram can be obtained analytically. Also by taking the derivative of (10.8) with respect to Ψ_B it is easy to show that at the optimum value of Ψ_B

$$\Psi_B = Zw\langle\hat{b}\rangle; \qquad (10.9)$$

this relation, however, does not hold at a general point in parameter space.

First, let us consider the limit $w = 0$. In this case the sites are decoupled, and the mean-field theory is exact. It is also evident that $\Psi_B = 0$, and we simply have to minimize the on-site interaction energy. The on-site Hamiltonian involves only the operator $\hat{n}$, and the solution involves finding the boson occupation number (which are the integer-valued eigenvalues of $\hat{n}$) which minimizes H_B. This is simple to carry out, and we get the ground state wavefunction

$$|m_i = n_0(\mu/U)\rangle \tag{10.10}$$

where the integer-valued function $n_0(\mu/U)$ is given by

$$n_0(\mu/U) = \begin{cases} 0 & \text{for } \mu/U < 0 \\ 1 & \text{for } 0 < \mu/U < 1 \\ 2 & \text{for } 1 < \mu/U < 2 \\ \vdots & \qquad \vdots \\ n & \text{for } n-1 < \mu/U < n \end{cases} \tag{10.11}$$

So each site has exactly the same integer number of bosons which jumps discontinuously whenever μ/U goes through a positive integer. When μ/U is exactly equal to a positive integer, there are two degenerate states on each site (with boson numbers differing by 1) and so the entire system has a degeneracy of 2^M. This large degeneracy implies a macroscopic entropy; it will be lifted once we turn on a non-zero w.

We now consider the effects of a small non-zero w. As is shown in Fig 10.1, the regions with $\Psi_B = 0$ survive in 'lobes' around each $w = 0$ state (10.10) characterized by a given integer value of $n_0(\mu/U)$. Only at the degenerate point with $\mu/U = $ integer, does a non-zero w immediately lead to a state with $\Psi_B \neq 0$. We will consider the properties of this $\Psi_B \neq 0$ later, but now we discuss the properties of the lobes with $\Psi_B = 0$ in some more detail. In mean-field theory, these states have wavefunctions still given exactly by (10.10). However, it is possible to go beyond mean field theory, and make an important exact statement about each of the lobes: the expectation value of the number of bosons in each site is given by

$$\left\langle \hat{b}_i^\dagger \hat{b}_i \right\rangle = n_0(\mu/U), \tag{10.12}$$

which is the same result one would obtain from the product state (10.10) (which, we emphasize, is not the exact wavefunction for $w \neq 0$). There

are two important ingredients behind the result (10.12): the existence of an energy gap and the fact that $\hat{N}_b$ commutes with H_B. First, recall that at $w = 0$, provided μ/U was not exactly equal to a positive integer, there was a unique ground state, and there was a non-zero energy separating this state from all other states (this is the energy gap). As a result, when we turn on a small non-zero w, the ground state will move adiabatically without undergoing any level crossings with any other state. Now the $w = 0$ state is an exact eigenstate of $\hat{N}_b$ with eigenvalue $M n_0(\mu/U)$, and the perturbation arising from a non-zero w commutes with $\hat{N}_b$. Consequently, the ground state will remain an eigenstate of $\hat{N}_b$ with precisely the same eigenvalue, $M n_0(\mu/U)$, even for small non-zero w. Assuming translational invariance, we then immediately have the exact result (10.12). Notice that this argument also shows that the energy gap above the ground state will survive everywhere within the lobe. These regions with a quantized value of the density and an energy gap to all excitations are known as "Mott insulators." Their ground states are very similar to, but not exactly equal to, the simple state (10.10): they involve in addition terms with bosons undergoing virtual fluctuations between pairs of sites, creating 'particle-hole' pairs. The Mott insulators are also known as 'incompressible' because their density does not change under changes of the chemical potential μ or other parameters in H_B:

$$\frac{\partial \langle \hat{N}_b \rangle}{\partial \mu} = 0. \tag{10.13}$$

It is worth re-emphasizing here the remarkable nature of the exact result (10.12). From the perspective of classical critical phenomena, it is most unusual to find the expectation value of any observable to be pinned at a quantized value over a finite region of the phase diagram. However, as we will see quantum field theories of a certain structure allow such a phenomenon, and we will meet different realizations of it in subsequent chapters. The existence of observables like $\hat{N}_b$ which commute with the Hamiltonian is clearly a crucial ingredient.

The numerical analysis shows that the boundary of the Mott Insulating phases is a second order quantum phase transition, *i.e.*, a non-zero Ψ_B turns on continuously. With the benefit of this knowledge, we can determine the positions of the phase boundaries. By the usual Landau theory argument, we simply need to expand E_0 in (10.8) in powers of Ψ_B,

$$E_0 = E_{00} + r|\Psi_B|^2 + \mathcal{O}(|\Psi_B|^4), \tag{10.14}$$

and the phase boundary appears when r changes sign. The value of r can be computed from (10.8) and (10.7) by second-order perturbation theory, and we find

$$r = \chi_0(\mu/U)\left[1 - Zw\chi_0(\mu/U)\right], \qquad (10.15)$$

where

$$\chi_0(\mu/U) = \frac{n_0(\mu/U) + 1}{Un_0(\mu/U) - \mu} + \frac{n_0(\mu/U)}{\mu - U(n_0(\mu/U) - 1)}. \qquad (10.16)$$

The function $n_0(\mu/U)$ in (10.11) is such that the denominators in (10.16) are positive, except at the points at which boson occupation number jumps at $w = 0$. The solution of the simple equation $r = 0$ leads to the phase boundaries shown in Fig 10.1.

Finally, we turn to the phase with $\Psi_B \neq 0$. The mean-field parameter Ψ_B varies continuously as the parameters are varied. As a result all thermodynamic variables also change, and the density does not take a quantized value; by a suitable choice of parameters, the average density can be varied smoothly across any real positive value. So this is a compressible state in which

$$\frac{\partial \langle \hat{N}_b \rangle}{\partial \mu} \neq 0. \qquad (10.17)$$

As we noted earlier, the presence of a $\Psi_B \neq 0$ implies that the U(1) symmetry is broken, and there is a non-zero stiffness to twists in the orientation of the order parameter. The fluctuation analysis to be discussed in the following section can be combined with the methods of Chapter 9 to show that this state is a superfluid, and the stiffness is just the superfluid density.

10.2 Continuum quantum field theories

We will discuss the low energy properties of the quantum phase transitions between the Mott insulators and the superfluid. We will find that it is crucial to distinguish between two different cases, each characterized by its own universality class and continuum quantum field theory. The important diagnostic distinguishing the two possibilities will be the behavior of the boson density across the transition. In the Mott insulator, this density is of course always pinned at some integer value. As one undergoes the transition to the superfluid, depending upon the precise location of the system in the phase diagram of Fig 10.1, there are two

possible behaviors of the density: (A) the density remains pinned at its quantized value in the superfluid in the vicinity of the quantum critical point, or (B) the transition is accompanied by a change in the density. We will show below that case (A) is described by the $N = 2$ case of the quantum rotor field theory (3.11) which was studied in great detail in Part 2 of this book: all universal results for finite T crossovers can be taken over and applied here. Case (B) will lead to a different field theory whose properties will be examined in the following chapter.

It is clear that the critical field theory should be expressed in terms of a spacetime dependent field $\Psi_B(x, \tau)$ which is analogous to the mean field parameter Ψ_B appearing in Section 10.1. Such a field is most conveniently introduced by the well-known Hubbard-Stratanovich transformation. We begin by writing the partition function of H_B, $Z_B = \mathrm{Tr}\, e^{-H_B/T}$, in the standard imaginary-time coherent state path integral for canonical bosons (see the texts by Negele and Orland [360] and Shankar [456] for a careful and complete derivation of this path integral):

$$Z_B = \int \mathcal{D}b_i(\tau)\mathcal{D}b_i^\dagger(\tau) \exp\left(- \int_0^{1/T} d\tau \mathcal{L}_b \right)$$

$$\mathcal{L}_b = \sum_i \left(b_i^\dagger \frac{db_i}{d\tau} - \mu b_i^\dagger b_i + U b_i^\dagger b_i^\dagger b_i b_i \right) - w \sum_{\langle ij \rangle} \left(b_i^\dagger b_j + b_j^\dagger b_i \right) \quad (10.18)$$

We decouple the hopping term proportional to w by introducing an auxiliary field $\Psi_{Bi}(\tau)$ and transforming Z_B to

$$Z_B = \int \mathcal{D}b_i(\tau)\mathcal{D}b_i^\dagger(\tau)\mathcal{D}\Psi_{Bi}(\tau)\mathcal{D}\Psi_{Bi}^\dagger(\tau) \exp\left(- \int_0^{1/T} d\tau \mathcal{L}_b' \right)$$

$$\mathcal{L}_b' = \sum_i \left(b_i^\dagger \frac{db_i}{d\tau} - \mu b_i^\dagger b_i + U b_i^\dagger b_i^\dagger b_i b_i - \Psi_{Bi} b_i^\dagger - \Psi_{Bi}^* b_i \right)$$

$$+ \sum_{i,j} \Psi_{Bi}^* w_{ij}^{-1} \Psi_{Bi}. \quad (10.19)$$

We have introduced the symmetric matrix w_{ij} whose elements equal w if i and j are nearest neighbors, and vanish otherwise. The equivalence between (10.19) and (10.18) (sometimes called the Hubbard-Stratanovich transformation) can be easily established by simply carrying out the Gaussian integral over Ψ_B; this also generates some overall normalization factors, but these have been absorbed into a definition of the measure $\mathcal{D}\Psi_B$. Let us also note a subtlety we have glossed over: strictly speaking, the transformation between (10.19) and (10.18) requires that

all the eigenvalues of w_{ij} be positive, for only then is the Gaussian inte-grals over Ψ_B well defined. This is not the case for, say, the hypercubic lattice which has negative eigenvalues for w_{ij}. This can be repaired by adding a positive constant to all the diagonal elements of w_{ij}, and sub-tracting the same constant from the on-site b part of the Hamiltonian. We will not explicitly do this here as our interest is only in the long-wavelength modes of the Ψ_B field, and the corresponding eigenvalues of w_{ij} are positive.

For our future purposes, it is useful to describe an important symme-try property of (10.19). Notice that the functional integrand is invariant under the following time-dependent U(1) gauge transformation:

$$
\begin{aligned}
b_i &\rightarrow b_i e^{i\phi(\tau)} \\
\Psi_{Bi} &\rightarrow \Psi_{Bi} e^{i\phi(\tau)} \\
\mu &\rightarrow \mu + i\frac{\partial\phi}{\partial\tau}
\end{aligned}
\tag{10.20}
$$

The chemical potential μ becomes time-dependent above, and so this transformation takes one out the of a physical parameter regime; nev-ertheless (10.20) is very useful, as it places important restrictions on subsequent manipulations of Z_B.

The next step is to integrate out the b_i, $b_i^\dagger$ fields from (10.19). This can be done exactly in powers of Ψ_B and Ψ_B^*: the co-efficients are simply products of Green's functions of the b_i. The latter can be determined in closed form because the Ψ_B-independent part of $\mathcal{L}_b'$ is simply a sum of single-site Hamiltonian's for the b_i: these were exactly diagonalized in (10.10), and all single-site Green's functions can also be easily deter-mined. We re-exponentiate the resulting series in powers of Ψ_B, Ψ_B^*, and expand the terms in terms of spatial and temporal gradients of Ψ_B. The expression for Z_B can now be written as [160]

$$
Z_B = \int \mathcal{D}\Psi_B(x,\tau)\mathcal{D}\Psi_B^*(x,\tau) \exp\left(-\frac{V\mathcal{F}_0}{T} - \int_0^{1/T} d\tau \int d^d x \mathcal{L}_B\right)
$$

$$
\mathcal{L}_B = K_1 \Psi_B^* \frac{\partial \Psi_B}{\partial\tau} + K_2 \left|\frac{\partial\Psi_B}{\partial\tau}\right|^2 + K_3 \left|\nabla\Psi_B\right|^2
$$

$$
+ \widetilde{r}|\Psi_B|^2 + \frac{u}{2}|\Psi_B|^4 + \dots
\tag{10.21}
$$

Here $V = Ma^d$ is the total volume of the lattice, and a^d is the volume per site. The quantity $\mathcal{F}_0$ is the free energy density of a system of decoupled sites; its derivative with respect to the chemical potential

gives the density of the Mott insulating state, and so

$$-\frac{\partial \mathcal{F}_0}{\partial \mu} = \frac{n_0(\mu/U)}{a^d}. \tag{10.22}$$

The other parameters in (10.21) can also be expressed in terms of μ, U and w but we will not display explicit expressions for all of them. Most important is the parameter $\widetilde{r}$ which can be seen to be

$$\widetilde{r}a^d = \frac{1}{Zw} - \chi_0(\mu/U), \tag{10.23}$$

where χ_0 was defined in (10.16). Notice that $\widetilde{r}$ is proportional to the mean-field r in (10.15); in particular, $\widetilde{r}$ vanishes when r vanishes, and the two quantities have the same sign. The mean field critical point between the Mott Insulator and the superfluid appeared at $r = 0$, and it is not surprising that the mean field critical point of the continuum theory (10.21) is given by the same condition.

Of the other couplings in (10.21), K_1, the coefficient of the first-order time derivative also plays a crucial role. It can be computed explicitly, but it is simpler to note that the value of K_1 can be fixed by demanding that (10.21) be invariant under (10.20) for small ϕ: a simple calculation shows that we must have

$$K_1 = -\frac{\partial \widetilde{r}}{\partial \mu}. \tag{10.24}$$

This relationship has a very interesting consequence: notice that K_1 vanishes when $\widetilde{r}$ is μ independent; however, this is precisely the condition that the Mott Insulator-superfluid phase boundary in Fig 10.1 have a vertical tangent, *i.e.*, at the tips of the Mott Insulating lobes. This is significant because at the value $K_1 = 0$ it is evident that (10.21) is nothing but the $N = 2$ rotor model field theory action in (3.11), which has been exhaustively studied in Part 2. So the Mott insulator to superfluid transition is in the universality class of the O(2) quantum rotor model phase transition for $K_1 = 0$. In contrast, for $K_1 \neq 0$ we have a rather different field theory: we can now drop the K_2 term as it involves two time derivatives and so is irrelevant with respect to the single time derivative in the K_1 term. The resulting field theory will be examined in some detail in the following chapter.

To conclude this discussion, we would like to correlate the above discussion on the distinction between the two universality classes with the behavior of the boson density across the transition. This can be evaluated by taking the derivative of the total free energy with respect to the

chemical potential, as is clear from (10.4):

$$
\begin{aligned}
\left\langle \hat{b}_i^\dagger \hat{b}_i \right\rangle &= -a^d \frac{\partial \mathcal{F}_0}{\partial \mu} - a^d \frac{\partial \mathcal{F}_B}{\partial \mu} \\
&= n_0(\mu/U) - a^d \frac{\partial \mathcal{F}_B}{\partial \mu},
\end{aligned}
\tag{10.25}
$$

where $\mathcal{F}_B$ is the free energy resulting from the functional integral over Ψ_B in (10.21). We will examine the properties of (10.21) for general K_1, and including fluctuations, in the following chapter: here let us be satisfied by a simple mean field treatment.

In mean-field theory, for $\widetilde{r} > 0$, we have $\Psi_B = 0$, and therefore $\mathcal{F}_B = 0$, implying

$$
\left\langle \hat{b}_i^\dagger \hat{b}_i \right\rangle = n_0(\mu/U) \qquad \text{for } \widetilde{r} > 0.
\tag{10.26}
$$

This clearly places us in a Mott insulator: as argued in Section 10.1, (10.26) is an exact result, and we will another verification of this in our analysis of the fluctuations of (10.21) in Chapter 11.

For $\widetilde{r} < 0$, we have $\Psi_B = \sqrt{-\widetilde{r}/u}$, as follows from a simple minimization of $\mathcal{L}_B$; computing the resulting free energy we have

$$
\begin{aligned}
\left\langle \hat{b}_i^\dagger \hat{b}_i \right\rangle &= n_0(\mu/U) + a^d \frac{\partial}{\partial \mu} \left(\frac{\widetilde{r}^2}{2u} \right) \\
&\approx n_0(\mu/U) + \frac{a^d \widetilde{r}}{u} \frac{\partial \widetilde{r}}{\partial \mu}
\end{aligned}
\tag{10.27}
$$

In the second expression, we ignored the derivative of u as it is less singular as $\widetilde{r}$ approaches 0—we will comment on the consequences of this shortly. So at the transition point at which $K_1 = 0$, by (10.24) we see that the leading correction to the density of the superfluid phase vanishes, and it remains pinned at the same value as in the Mott insulator. So as claimed earlier, the transition with no density change is in the universality class of the O(2) quantum rotor model. Conversely, for the case $K_1 \neq 0$, the transition is always accompanied by a density change: this is a separate universality class which will be considered in the next chapter, and we will see there that we can also consider the density itself as an order parameter for the transition in this case.

We close by commenting on the consequences of the omitted higher order terms in (10.27) to the discussion above. Consider the trajectory of points in the superfluid with their density equal to some integer n. The implication of the above discussion is that this trajectory will meet the Mott insulator with $n_0(\mu/U) = n$ at its lobe. The O(2) quantum

rotor model phase transition then describes the transition out of the Mott insulator into the superfluid along a direction which is tangent to the trajectory of density n. The approximations made above merely amounted to assuming that this trajectory was a straight line.

10.3 Applications and extensions

The fluctuation corrections to the phase diagram in Fig 10.1 have been considered in Refs [166, 167]: they find singularities in the shape of the Mott lobes at the positions of the $z = 1$ transitions. Monte Carlo simulations of the phase diagram have also been carried out [42, 365].

Experimental measurements of the phase diagram have been made in systems such as ^{4}He on graphite [549], flux lines in superconductors with artificial pinning centers [36, 46] and Josephson junction arrays [373].

Extensions of the boson Hubbard model with interactions beyond nearest neighbor can spontaneously break translational symmetry at certain densities. If this coexists with the superfluid order, one can obtain a "supersolid" phase. These issues have been discussed in Refs [43, 168, 20, 355, 513, 514, 471, 182].

11

Dilute Fermi and Bose gases

We will consider a number of different models in this chapter, but they share some important unifying characteristics. They all have a global U(1) symmetry. We shall be particularly interested in the behavior of the conserved density, generically denoted as Q, associated with this symmetry. All the models will exhibit a quantum phase transition between two phases with the a specific $T = 0$ behavior in the expectation value of Q. In one of the phases $\langle Q \rangle$ is pinned precisely at a quantized value, and does not vary as microscopic parameters are varied. This quantization ends at the quantum critical point with a discontinuity in the derivative of $\langle Q \rangle$ with respect to the tuning parameter, and $\langle Q \rangle$ varies smoothly in the other phase; there is no discontinuity in the value of $\langle Q \rangle$, however.

We have already met a transition of the above type in the previous Chapter 10: the Mott insulator to superfluid transition at points excluding the tips of the lobes in Fig 10.1, where the coupling K_1 in (10.21) did not vanish. In this case Q was just the boson density $\hat{b}_i^\dagger \hat{b}_i / a^d$. We will find it convenient to shift the definition of Q by a constant so that the quantized value is zero: so, in this case, Q equals $(\hat{b}_i^\dagger \hat{b}_i - n_0(\mu/U))/a^d$. In this chapter, we will study the universal properties of the continuum theory of this transition, which following (10.21), we write in the following form

$$Z_B = \int \mathcal{D}\Psi_B(x,\tau)\mathcal{D}\Psi_B^*(x,\tau) \exp\left(-\int_0^{1/T} d\tau \int d^d x \mathcal{L}_B\right)$$

$$\mathcal{L}_B = \Psi_B^* \frac{\partial \Psi_B}{\partial \tau} + \frac{1}{2m}|\nabla\Psi_B|^2 - \mu|\Psi_B|^2 + \frac{u}{2}|\Psi_B|^4. \qquad (11.1)$$

We have dropped the second order time derivative (proportional to K_2) from (10.21), and not included any non-linearity beyond the quartic, as

270

these will all be shown to be irrelevant near the transition. We have rescaled Ψ_B by a factor of the square root of K_1 so that the first order time derivative has co-efficient unity: this sets the normalization of the continuum field Ψ_B which will always be consistently maintained in this chapter. This time derivative term is the same as that arising in the coherent state path integral for canonical bosons, where it is the 'Berry phase' associated with the adiabatic evolution of the coherent states: the reader can learn about such path integrals in the book by Negele and Orland [360], and about Berry phases and their relation to coherent state path integrals in the text by Shankar [456] (physically, the Berry phase term here accounts for the Josephson precession in the phase of a condensate of the bosons in the presence of an external chemical potential). So the normalization of Ψ_B is determined by its Berry phase, a feature we will see in other models. With the above rescaling of Ψ_B it is easy to see from (10.24) and (10.21) that, close to the quantum critical point, the co-efficient of the $|\Psi_B|^2$ is the negative of the chemical potential, μ, up to an additive constant: we absorb this unimportant additive constant into a redefinition of μ, and this leads to the $|\Psi_B|^2$ term shown in (11.1). We can also identify the charge Q with $\Psi_B^* \Psi_B$ as

$$\langle Q \rangle = -\frac{\partial \mathcal{F}_B}{\partial \mu} = \langle |\Psi_B|^2 \rangle, \tag{11.2}$$

with $\mathcal{F}_B = -(T/V) \ln Z_B$. With the form of the quadratic term in (11.1), we also see from the mean field results in Chapter 10 that the quantum critical point is precisely at $\mu = 0$ and $T = 0$: we will see in this chapter that there are *no* fluctuation corrections to this location from the terms in $\mathcal{L}_B$ (the K_2 term in (10.21) does lead to shifts in the position of the quantum critical point, but we have already set it to zero here as it is not important for the critical theory). So at $T = 0$, $\langle Q \rangle$ takes the quantized value $\langle Q \rangle = 0$ for $\mu < 0$, and $\langle Q \rangle > 0$ for $\mu > 0$; we will particularly be interested in the nature of the onset at $\mu = 0$, and finite T crossovers in its vicinity. We have also assumed here that $K_1 > 0$, and so, from (10.24) and (10.27), that $\langle Q \rangle$ increases from its quantized value away from the quantum critical point. The opposite case of decreasing Q can be treated after a particle-hole transformation, and has essentially identical properties.

While Z_B in (11.1) shall be the main model of physical interest in this chapter, we find it useful to introduce a closely related model which also displays a quantum phase transition with the same behavior in a conserved U(1) density $\langle Q \rangle$, and many similarities in its physical properties.

The model is exactly solvable, and is expressed in terms of a continuum canonical spinless fermion field Ψ_F; its partition function is:

$$Z_F = \int \mathcal{D}\Psi_F(x,\tau)\mathcal{D}\Psi_F^*(x,\tau) \exp\left(-\int_0^{1/T} d\tau \int d^d x \mathcal{L}_F\right)$$

$$\mathcal{L}_F = \Psi_F^* \frac{\partial \Psi_F}{\partial \tau} + \frac{1}{2m}|\nabla \Psi_F|^2 - \mu |\Psi_F|^2. \tag{11.3}$$

The functional integral is over fluctuations of an anti-commuting Grassman field $\Psi_F(x,\tau)$ (see the discussion in Ref [360] for an introduction to Grassman numbers and their functional integrals). Notice that the terms in $\mathcal{L}_F$ are in one-to-one correspondence with those in $\mathcal{L}_B$ in (11.1), except there is no quartic $|\Psi_F|^4$ term: such a term vanishes because the square of a Grassman number is zero, which is just a mathematical representation of the Pauli exclusion principle. As a result, $\mathcal{L}_F$ is just a free field theory. Like Z_B, Z_F has a quantum critical point at $\mu = 0$, $T = 0$ and we will discuss its properties in this chapter; in particular, we will show that all possible fermionic non-linearities are irrelevant near it. The reader should not be misled by the apparently trivial nature of the model in (11.3); using the theory of quantum phase transitions to understand free fermions might seem like technological overkill. We will see that Z_F exhibits crossovers that are quite similar to those near far more complicated quantum critical points, and observing them in this simple context leads to considerable insight.

In general spatial dimension, d, the continuum theories Z_B and Z_F have different, though closely related, universal properties. However, we will argue here that the quantum critical points of these theories are *exactly* equivalent in $d = 1$: this shall be one of the important results of this chapter. We will see that the bosonic theory Z_B is very strongly coupled in $d = 1$, and present compelling evidence that the solvable fermionic theory Z_F is its exactly universal solution in the vicinity of the $\mu = 0$, $T = 0$ quantum critical point. We shall also be able to make a correspondence between the operators of the two theories, and this will allow us to obtain certain exact results for experimentally measurable bosonic correlation functions of Z_B, including some for the nonzero temperature dynamical properties that are an important focus of this book. Of course, all fermionic correlators of Z_F are exactly known in arbitrary d, but these do not have significant practical interest.

We will begin in Section 11.1 by discussing a simple solvable model in $d = 1$: the spin-1/2 quantum XX chain. This will allow us to motivate the physical origin of the fermionic theory Z_F, and indicate the

relationship between Z_B and Z_F in the context of a lattice model. Then Section 11.2 will present a thorough discussion of the universal properties of Z_F. This will be followed by an analysis of Z_B in Section 11.3: we will use renormalization group methods to obtain perturbative predictions for universal properties. The perturbation theory for Z_B becomes strongly coupled in $d = 1$, but we will be able to obtain exact results for this case by the $d = 1$ mapping between Z_B and Z_F: this will be discussed in Section 11.4. This section will also contain further discussion of the properties of the XX chain of Section 11.1.

11.1 The quantum XX model

This model is obtained by taking the $U \to \infty$ limit of the boson Hubbard model H_B in (10.4): this is then a model of 'hard-core' bosons with an infinite on-site repulsion energy. The only states with a finite energy are those with $\hat{n}_{bi} = 0$ or 1 on every site of the lattice. The Mott insulating states in Fig 10.1 with $n_0 > 1$, have therefore been expelled, and only the two Mott insulators with $n_0 = 0$ or $n_0 = 1$ are permitted. Precisely at $w = 0$, we have the $n_0 = 1$ Mott insulator for $\mu > 0$, while for $\mu < 0$ we have the $n_0 = 0$ Mott insulator, which is a fanciful term for the bare vacuum with no particles.

This model of hard-core bosons can also be written as a magnet of $S = 1/2$ spins with nearest neighbor exchange interactions. The idea is to associate the two states on each site with the up and down states of a $S = 1/2$ spin degree of freedom. In operator language, we can identify

$$
\begin{aligned}
\hat{\sigma}_j^x &= \hat{b}_j + \hat{b}_j^\dagger \\
\hat{\sigma}_j^y &= -i(\hat{b}_j - \hat{b}_j^\dagger) \\
\hat{\sigma}_j^z &= 1 - 2\hat{b}_j^\dagger \hat{b}_j.
\end{aligned}
\tag{11.4}
$$

Then the boson commutation relations (10.1) and the hard-core restriction imply that the $\hat{\sigma}_j^{x,y,z}$ obey the commutation relations of the Pauli matrices, and satisfy $\hat{\sigma}_j^{\alpha 2} = 1$ (no sum over α): we may therefore consider them to be the Pauli matrices. With this mapping, the fully polarized state with all spins up is the $n_0 = 0$ Mott insulator, while that with all spins down is the $n_0 = 1$ Mott insulator. Inverting (11.4), we see that the Hamiltonian H_B in (10.4) becomes (up to an uninteresting additive constant)

$$
H_{XX} = -\frac{w}{2} \sum_{<ij>} \left(\hat{\sigma}_i^x \hat{\sigma}_j^x + \hat{\sigma}_i^y \hat{\sigma}_j^y \right) + \frac{\mu}{2} \sum_i \hat{\sigma}_i^z
\tag{11.5}
$$

This is the so-called XX model which describes spin-1/2 degrees of freedom on the lattice sites with a nearest neighbor ferromagnetic exchange $w/2 > 0$ confined to the x-y plane in spin space, and in a magnetic field $\mu/2$ in the $-z$ direction in spin space. We will argue later that additional exchange in the z-direction in spin space (this corresponds to nearest-neighbor interactions in the boson Hubbard model) will not modify the universal properties of the Mott insulator to superfluid transitions. Note also that both the simple fully-polarized $n_0 = 0$ and $n_0 = 1$ Mott insulators are exact eigenstates of H_{XX} for arbitrary w: for the $n_0 = 1$ state this is a consequence of having sent $U \to \infty$ which eliminates virtual particle-hole pair fluctuations.

Now we specialize to the one-dimensional case $d = 1$: in this case exact expressions for the thermodynamic properties of H_{XX} can be easily obtained. The basic tool is the Jordan-Wigner transformation introduced in Section 4.2 for the solution of the Ising chain in $d = 1$: this transforms the spin-1/2 model into a model of spinless fermions. Inserting (4.24,4.25) into (11.5), we get

$$H_{XX} = -\sum_i \left(w(c_{i+1}^\dagger c_i + c_i^\dagger c_{i+1}) + \mu c_i^\dagger c_i \right) \qquad (11.6)$$

Notice that H_{XX} is simply a free spinless fermion Hamiltonian and its spectrum can therefore be easily determined: adding non on-site interactions to the original H_B would lead to fermion interactions in H_{XX} which will be shown to be irrelevant below. Fourier transforming as in (4.31) we get the simple diagonal form

$$H_{XX} = \sum_k \varepsilon_k c_k^\dagger c_k \qquad (11.7)$$

with the free fermion dispersion $\varepsilon_k = -2w \cos(ka) - \mu$. So for $\mu < -2w$, the energy of all the fermions is positive and the ground state has no fermions present: this is clearly the Mott insulator with $n_0 = 0$; for $\mu > 2w$ all the fermions have negative energy and every fermion state is occupied, leading to the Mott insulator with $n_0 = 1$. At intermediate values of μ there is partial occupation which can be easily computed at $T = 0$:

$$\langle \hat{b}_i^\dagger \hat{b}_i \rangle = \frac{1}{2}(1 - \langle \hat{\sigma}_i^z \rangle) = \langle c_i^\dagger c_i \rangle = \begin{cases} 0 & \mu \leq -2w \\ 1 - (1/\pi)\cos^{-1}(\mu/2w) & |\mu| \leq 2w \\ 1 & \mu \geq 2w \end{cases} .$$
$$(11.8)$$

We show a plot of the boson number as a function of μ in Fig 11.1.
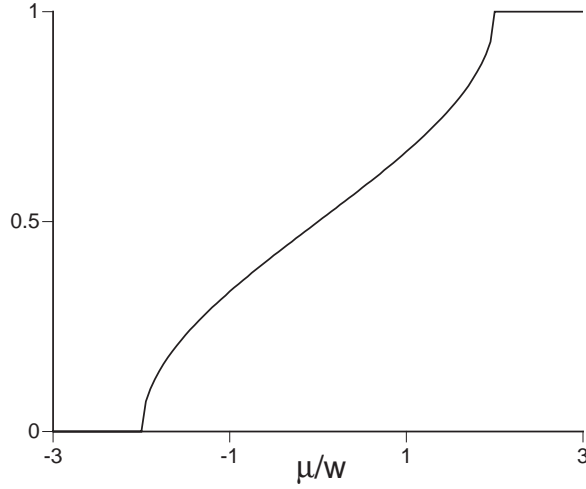
Fig. 11.1. Plot of the boson number per site as a function of the chemical potential μ for the $U \to \infty$ limit of the boson Hubbard model H_B in (10.4) in dimension $d = 1$. There are Mott insulator to superfluid transitions at $\mu = \pm 2w$.

The state with intermediate occupation number has a non-zero superfluid stiffness, but only 'quasi-long range order' in the superfluid order parameter in $d = 1$, as will be discussed in Section 11.4: we will continue to refer to it as a superfluid, however. So the result (11.8) displays two superfluid-Mott insulator transitions: one at $\mu = -2w$ and the other at $\mu = 2w$. We will focus on the one at $\mu = -2w$, where the transition is from a simple vacuum state with no particles (a Mott insulator with $n_0 = 0$) to a low density superfluid.

For μ close to $2w$, the density of bosons is seen to vanish from (11.8) as $\sim (1 + \mu/2w)^{1/2}$. We may identify the power of $1/2$ as an exact critical exponent of the quantum critical point at $\mu = -2w$. Compare this with the mean field result (10.27) which has the value 1 for this critical exponent: we will see that the mean field result applies for $d > 2$.

We can derive a continuum theory for the quantum critical point at $\mu = -2w$, $T = 0$ using an analysis very similar to that in Section 4.3. The low energy fermionic states which are occupied across the transition are near $k = 0$. Therefore we make take the continuum limit simply by taking spatial gradients of the fields. We define the continuum field Ψ_F as in (4.39), and expand H_{XX} is spatial gradients: this leads to the

Hamiltonian

$$H_F = \int dx \left(-\frac{1}{2m} \Psi_F^\dagger(x) \nabla^2 \Psi_F(x) - \mu \Psi_F^\dagger(x) \Psi_F(x) \right) \qquad (11.9)$$

where the fermion mass $m = 1/(2wa^2)$. The coherent state path integral of H_F is, of course, the fermionic theory Z_F (11.3).

We have thus presented evidence that the critical theory of the transition in the XX model in $d = 1$ is given by Z_F: a complete demonstration requires that there are no further relevant perturbations that can appear in H_F: this will be taken up in the following section. Recall also that H_{XX} was derived from the boson Hubbard model (10.4) which was shown to be related to Z_B in (11.1) in Chapter 10. These mappings therefore equate the universal critical properties of Z_B, H_{XX} and Z_F in $d = 1$: these universal correlators will be described explicitly in the subsequent sections.

For dimensions $d > 1$ the analysis of this section and the arguments of Chapter 10 have established that H_{XX} has Mott insulator- superfluid (or between fully polarized and partially polarized spin states) transitions which are described by Z_B. These models are, however, not equivalent to Z_F in this case.

11.2 The dilute spinless Fermi gas

This section will study the properties of Z_F in the vicinity of its $\mu = 0$, $T = 0$ quantum critical point. As Z_F is a simple free field theory, all results can be obtained exactly and are not particularly profound in themselves. Our main purpose is to show how the results are interpreted in a scaling perspective, and to obtain general lessons on the nature of crossovers at $T > 0$. Some of the analysis will be quite similar to that for a different free fermion theory in Section 4.3, and so we can be relatively brief.

First, let us review the basic nature of the quantum critical point at $T = 0$. A useful diagnostic for this is the conserved density Q which in the present model we identify as $\Psi_F^\dagger \Psi_F$. As a function of the tuning parameter μ, this quantity has a critical singularity at $\mu = 0$:

$$\langle \Psi_F^\dagger \Psi_F \rangle = \begin{cases} (S_d/d)(2m\mu)^{d/2} & \mu > 0 \\ 0 & \mu < 0 \end{cases}, \qquad (11.10)$$

where the phase space factor S_d was defined below (8.16). In $d = 1$, this result is clearly the universal continuum limit of (11.8).

We now proceed to a scaling analysis. Notice that at the quantum critical point $\mu = 0$, $T = 0$, the theory $\mathcal{L}_F$ is invariant under the scaling transformations closely related to those in (4.46)

$$
\begin{aligned}
x' &= x e^{-\ell} \\
\tau' &= \tau e^{-z\ell} \\
\Psi'_F &= \Psi_F e^{d\ell/2}
\end{aligned}
\tag{11.11}
$$

provided we make the choice of the dynamic exponent

$$
z = 2.
\tag{11.12}
$$

The parameter m is assumed to remain invariant under the rescaling, and its role is simply to ensure that the relative physical dimensions of space and time are compatible: its role is rather analogous to that of the velocity c in Section 4.3. The transformation (11.11) also identifies the scaling dimension

$$
\dim[\Psi_F] = d/2.
\tag{11.13}
$$

Now turning on a non-zero μ, it is easy to see that μ is a relevant perturbation with

$$
\dim[\mu] = 2.
\tag{11.14}
$$

There will be no other relevant perturbations at this quantum critical point: so by the definition of ν above (4.50) we have

$$
\nu = 1/2
\tag{11.15}
$$

We can now examine the consequences of adding interactions to $\mathcal{L}_F$. A contact interaction like $\int dx (\Psi_F^\dagger(x)\Psi_F(x))^2$ vanishes because of the fermion anti-commutation relation. (A contact interaction is however permitted for a spin-1/2 Fermi gas and its coupling constant has scaling dimension $2 - d$: this is relevant for $d < 2$ and its consequences can be analyzed as done in Section 11.3 for the dilute Bose gas). The simplest allowed term for the spinless Fermi gas is

$$
\mathcal{L}_1 = \lambda \left(\Psi_F^\dagger(x,\tau) \nabla \Psi_F^\dagger(x,\tau) \Psi_F(x,\tau) \nabla \Psi_F(x,\tau) \right)
\tag{11.16}
$$

where λ is a coupling constant measuring the strength of the interaction. However, a simple analysis shows that

$$
\dim[\lambda] = -d.
\tag{11.17}
$$

This is negative and so λ is irrelevant, and can be neglected in the computation of universal crossovers near the point $\mu = T = 0$. In

particular, it will modify the result (11.10) only by contributions which are higher order in μ. The arguments show the sense in which the fermionic theory $\mathcal{L}_F$ is the universal critical theory describing the phase transition in H_{XX} in $d = 1$: additional exchange couplings in the z direction, or further neighbor interactions, can only lead to terms like that in (11.16), and all of these are irrelevant.

Turning to non-zero temperatures, we can write down scaling forms by the same arguments that led to (4.56). Let us define the fermion Green's function

$$G_F(x, t) = \left\langle \Psi_F(x, t) \Psi_F^\dagger(0, 0) \right\rangle ; \qquad (11.18)$$

then the scaling dimensions above imply that it satisfies

$$G_F(x, t) = (2mT)^{d/2} \, \Phi_{G_F} \left((2mT)^{1/2} x, Tt, \frac{\mu}{T} \right) \qquad (11.19)$$

where Φ_{G_F} is a fully universal scaling function. For this particularly simple theory $\mathcal{L}_F$ we can of course obtain the result for G_F in closed form:

$$G_F(x, t) = \int \frac{d^d k}{(2\pi)^d} \frac{e^{ikx - i(k^2/(2m) - \mu)t}}{1 + e^{-(k^2/(2m) - \mu)/T}}, \qquad (11.20)$$

and it is easy to verify that this obeys the scaling form (11.19). Similarly the free energy $\mathcal{F}_F$ obeys the scaling dimension (4.54), and we have

$$\mathcal{F}_F = T^{d/2+1} \Phi_{\mathcal{F}_F} \left(\frac{\mu}{T} \right) \qquad (11.21)$$

with $\Phi_{\mathcal{F}_F}$ a universal scaling function; the explicit result is, of course,

$$\mathcal{F}_F = - \int \frac{d^d k}{(2\pi)^d} \ln(1 + e^{(\mu - k^2/(2m))/T}), \qquad (11.22)$$

which clearly obeys (11.21). The crossover behavior of the fermion density

$$\langle Q \rangle = \langle \Psi_F^\dagger \Psi_F \rangle = -\frac{\partial \mathcal{F}_F}{\partial \mu} \qquad (11.23)$$

follows by taking the appropriate derivative of the free energy. Examination of these results leads to the now familiar crossover phase diagram of Fig 11.2. We will examine each of the regions of the phase diagram in turn, beginning with the two low temperature regions.
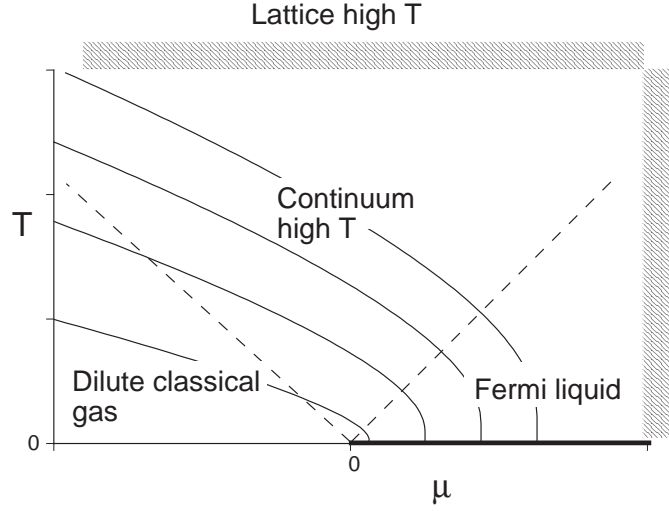
Fig. 11.2. Phase diagram of the dilute Fermi gas Z_F (Eqn (11.3)) as a function of the chemical potential μ and the temperature T. The regions are separated by crossovers denoted by dashed lines, and their physical properties are discussed in the text. The full lines are contours of equal density, with higher densities above lower densities; the zero density line is $\mu < 0$, $T = 0$. The line $\mu > 0$, $T = 0$ is a line of $z = 1$ critical points which controls the longest scale properties of the low T Fermi liquid region. The critical end point $\mu = 0$, $T = 0$, has $z = 2$ and controls global structure of the phase diagram. In $d = 1$, the Fermi liquid is more appropriately labeled a Tomonaga-Luttinger liquid. The hatched region marks the boundary of applicability of the continuum theory and occurs at $\mu, T \sim w$.

11.2.1 Dilute classical gas, $T \ll |\mu|$, $\mu < 0$

The ground state for $\mu < 0$ is the vacuum with no particles. Turning on a non-zero temperature produces particles with a small non-zero density $\sim e^{-|\mu|/T}$. The de Broglie wavelength of the particles is of order $T^{-1/2}$ which is significantly smaller than the mean spacing between the particles which diverges as $e^{|\mu|/dT}$ as $T \to 0$. This implies that the particles behave semiclassically. These properties are quite similar to those of the low T region on the quantum paramagnetic side of the Ising chain in Section 4.5.2. To leading order from (11.20), the fermion Green's function is simply the Feynman propagator of a single particle

$$G_F(x, t) = \left(\frac{m}{2\pi i t}\right)^{d/2} \exp\left(-\frac{imx^2}{2t}\right) \qquad (11.24)$$

and the exclusion of states from the other particles has only an exponentially small effect. Notice that G_F is independent of μ and T and (11.24) is the exact result for $\mu = T = 0$. The free energy, from (11.21) and (11.22), is that of a classical Boltzmann gas

$$\mathcal{F}_F = - \left(\frac{mT}{2\pi} \right)^{d/2} e^{-|\mu|/T} \qquad (11.25)$$

11.2.2 Fermi liquid, $k_B T \ll \mu$, $\mu > 0$

The behavior in this regime is quite complex and rich. As we will see, and as noted in Fig 11.2, the line $\mu > 0$, $T = 0$ is itself a line of quantum critical points. The interplay between these critical points and those of the $\mu = 0$, $T = 0$ critical end point is displayed quite instructively in the exact results for G_F and is worth examining in detail. It must be noted that the scaling dimensions and critical exponents of these two sets of critical points need not, and indeed will not, be the same. The concept of a *reduced scaling function*, used earlier (*e.g.*, in Section 4.5.1 for the quantum Ising chain) to describe the emergence of effective classical models, now comes in useful to obtain the critical behavior of the $\mu > 0$, $T = 0$ critical line out of the global scaling functions of the $\mu = 0$, $T = 0$ critical end point. Precisely the same structure is also present in the physically measurable bosonic correlators of Z_B in $d = 1$ (to be discussed in Section 11.4) but there the results are far more complicated and only available in restricted regimes. In the present case the closed form results (11.20) and (11.22) contain all the structure, and so are worth examining explicitly.

First it can be argued, *e.g.*, by studying asymptotics of the integral in (11.20), that for very short times or distances, the correlators do not notice the consequences of other particles present because of a non-zero T or μ, and are therefore given by the single particle propagator, which is the $T = \mu = 0$ result in (11.24). More precisely we have

$$G(x,t) \text{ is given by (11.24) for } |x| \ll (2m\mu)^{-1/2} \quad |t| \ll \frac{1}{\mu} \qquad (11.26)$$

With increasing x or t, the restrictions in (11.26) are eventually violated and the consequences of other particles due to a non-zero μ become apparent. Notice that as μ is much larger than T, it is the first energy scale to be noticed, and as a first approximation to understand the behavior at larger x we may ignore the effects of T.

Let us therefore discuss the ground state for $\mu > 0$. It consists of a

filled Fermi sea of particles (a Fermi liquid) with momenta $k < k_F = (2m\mu)^{1/2}$. An important property of the this state that it permits excitations at arbitrarily low energies, *i.e.*, it is *gapless*. These low energy excitations correspond to changes in occupation number of fermions arbitrarily close to k_F. As a consequence of these gapless excitations, the points $\mu > 0$ ($T = 0$) form a line of quantum critical points, as claimed earlier. We will now derive the continuum field theory associated with this line of critical points. We are interested here only in x and t which violate the constraints in (11.26), and so in occupation of states with momenta near $\pm k_F$. So let us parameterize, in $d = 1$

$$\Psi(x, \tau) = e^{ik_F x}\Psi_R(x, \tau) + e^{-ik_F x}\Psi_L(x, \tau) \tag{11.27}$$

where $\Psi_{R,L}$ describe right and left moving fermions, and are fields which vary slowly on spatial scales $\sim 1/k_F = (1/2m\mu)^{1/2}$ and temporal scales $\sim 1/\mu$. A similar parameterization can be used for $d > 1$ but we will not explicitly discuss it here; most of the results discussed below hold, with small modifications, in all d (see Refs [457, 229, 286, 359] for more details on a renormalization group analysis of fermions in $d > 1$). Inserting the above parameterization in $\mathcal{L}_F$, and keeping only terms lowest order in spatial gradients, we obtain the "effective" Lagrangean for the Fermi liquid region, $\mathcal{L}_{FL}$ in $d = 1$:

$$\mathcal{L}_{FL} = \Psi_R^\dagger \left(\frac{\partial}{\partial\tau} - iv_F\frac{\partial}{\partial x}\right)\Psi_R + \Psi_L^\dagger \left(\frac{\partial}{\partial\tau} + iv_F\frac{\partial}{\partial x}\right)\Psi_L \tag{11.28}$$

where $v_F = k_F/m = (2\mu/m)^{1/2}$ is the Fermi velocity. The Lagrangean $\mathcal{L}_{FL}$ also describes a massless Dirac field in one spatial dimension, and (like (4.44 for $\Delta = 0$) is invariant under relativistic and conformal transformations of spacetime: these facts shall be of some use to us later. Now notice that $\mathcal{L}_{FL}$ is invariant under a scaling transformation, which is rather different from (11.11) for the $\mu = 0$, $T = 0$ quantum critical point:

$$
\begin{aligned}
x' &= xe^{-\ell} \\
\tau' &= \tau e^{-\ell} \\
\Psi'_{R,L}(x', \tau') &= \Psi_{R,L}(x, \tau)e^{\ell/2} \\
v'_F &= v_F
\end{aligned}
\tag{11.29}
$$

The above results imply

$$z = 1, \tag{11.30}$$

unlike $z = 2$ (Eqn (11.12)) at the $\mu = 0$ critical point, and

$$\dim[\Psi_{R,L}] = 1/2 \qquad (11.31)$$

which actually holds for all d and therefore differs from (11.13). Further notice that v_F, and therefore μ, are *invariant* under rescaling, unlike (11.14) at the $\mu = 0$ critical point. Thus v_F plays a role rather analogous to that of m at the $\mu = 0$ critical point: it simply the physical units of spatial and length scales. The transformations (11.29) show that $\mathcal{L}_{LF}$ is scale invariant for each value of μ, and we therefore have a line of quantum critical points as claimed earlier. It should also be emphasized that the scaling dimension of interactions like λ will also change; in particular not all interactions are irrelevant about the $\mu \neq 0$ critical points. These new interactions are however small in magnitude provided μ is small, *i.e.*, provided we are within the domain of validity of the global scaling forms (11.19) and (11.21), and so we will neglect them here. Their main consequence is to change the scaling dimension of certain operators, but they preserve the relativistic and conformal invariance of $\mathcal{L}_{FL}$: this more general theory of $d = 1$ fermions at low at is known as a Tomonaga-Luttinger liquid, and we will discuss it in Chapter 14.

The action (11.28) and the scaling transformations (11.29) can be considered as defining scaling forms on their on right, independent of any derivation from the original $\mathcal{L}_F$. By complete analogy with the arguments presented earlier, we may deduce that

$$\begin{aligned} G_{R,L}(x,t) &= \langle \Psi_{R,L}(x,t)\Psi_{R,L}^{\dagger}(0,0)\rangle \\ &= \left(\frac{T}{v_F}\right)\phi_{R,L}\left(\frac{Tx}{v_F}, Tt\right) \qquad (11.32) \end{aligned}$$

where the powers of T follow from the scaling dimensions of G, x, and t, the factors of v_F, merely keep track of physical units, and $\phi_{R,L}$ are universal scaling functions. The result is a reduced scaling form of (11.19) in the sense of the discussion in Section 4.5.1; the former has three arguments, and in the limit $\mu/T \to \infty$ it collapses into (11.32) which is itself described the quantum critical theory (11.28).

Explicit expressions for $G_{R,L}$ can of course easily be obtained from the definition (11.32) and the theory $\mathcal{L}_{FL}$ in (11.28); however let us proceed from an instructive derivation from the globally valid expression (11.20). For $|x| \gg (1/2m\mu)^{1/2}$, $|t| \gg 1/\mu$, and $T \ll \mu$, the integral in (11.20) is dominated by contributions near the Fermi points $k = \pm k_F$. So near k_F let us parameterize $k = k_F + p$, expand terms in the integrand to linear order in p, and to leading order let the integral extend over all real p;

a similar procedure can be carried out near $-k_F$. In this manner the expression (11.20) for G_F reduces to

$$G(x,\tau) = e^{ik_F x} \int_{-\infty}^{\infty} \frac{dp}{2\pi} \frac{e^{p(ix - v_F \tau)}}{1 + e^{-v_F p/T}} + e^{-ik_F x} \int_{-\infty}^{\infty} \frac{dp}{2\pi} \frac{e^{p(-ix - v_F \tau)}}{1 + e^{-v_F p/T}}$$
(11.33)

The integrals over p can be evaluated exactly and we obtain

$$G_F(x,t) = e^{ik_F x} G_R(x,t) + e^{-ik_F x} G_L(x,t),$$
(11.34)

with

$$G_{R,L}(x,\tau) = \left(\frac{T}{v_F} \right) \frac{1}{2 \sin(\pi T(\tau \mp ix/v_F))}$$
(11.35)

This result is clearly consistent with the scaling form (11.32). For $T > 0$, the equal time $G_{R,L}$ decay exponentially with a correlation length $\xi = v_F/\pi T$, and the power of T is consistent with the $z = 1$ dynamic exponent of $\mathcal{L}_{FL}$. At $T = 0$, these fermionic Green's functions take the scale-invariant power law decay characteristic of the $\mu > 0$ critical ground state

$$G_{R,L}(x,\tau) = \frac{1}{2\pi v_F (\tau \mp ix/v_F)};$$
(11.36)

note that this is consistent with the scaling transformations (11.29). Notice also that the $T > 0$ result (11.35) and the $T = 0$ result (11.36) of $\mathcal{L}_{FL}$ are related by the mapping (4.64) (with the replacement $c \to v_F$) asserted to be a general property of conformally invariant theories with $z = 1$ in $d = 1$.

11.2.3 High T limit, $T \gg |\mu|$

This is the last, and in many ways the most interesting, region of Fig 11.2. Now T is the most important energy scale controlling the deviation from the $\mu = 0$, $T = 0$ quantum critical point, and the properties will therefore have some similarities to the continuum high T regions discussed in Part 2. chain in Section 4.5.3. As always, it should be emphasized that while the value of T is significantly larger than $|\mu|$, it cannot be so large that it exceeds the limits of applicability for the continuum action $\mathcal{L}_F$: this implies that $T \ll w$.

We discuss first the behavior of the of the fermion density. In the high T limit of the continuum theory $\mathcal{L}_F$, $|\mu| \ll T \ll w$ we have from

(11.22,11.23) the universal result

$$
\begin{aligned}
\langle \Psi_F^\dagger \Psi_F \rangle &= (2mT)^{d/2} \int \frac{d^d w}{(2\pi)^d} \frac{1}{e^{w^2} + 1} \\
&= (2mT)^{d/2} \, \zeta(d/2) \frac{(1 - 2^{d/2})}{(4\pi)^{d/2}} \tag{11.37}
\end{aligned}
$$

This density implies an interparticle spacing which is of order the de Broglie wavelength $= (1/2mT)^{1/2}$: thermal and quantum effects are to be equally important, and neither dominate, as we found in corresponding regions in Chapters 4, 5, and 7.

For completeness, let us also consider the fermion density for $T \gg w$ (the region above the hatched marks in Fig 11.2), to illustrate the limitations on the continuum description discussed above. Now the result depends upon the details of the non-universal fermion dispersion; on a hypercubic lattice with dispersion $\epsilon_k - \mu$, we obtain

$$
\begin{aligned}
\langle \Psi_F^\dagger \Psi_F \rangle &= \int_{-\pi/a}^{\pi/a} \frac{d^d k}{(2\pi)^d} \frac{1}{e^{(\varepsilon_k - \mu)/T} + 1} \\
&= \frac{1}{2a^d} - \frac{1}{4T} \int_{-\pi/a}^{\pi/a} \frac{d^d k}{(2\pi)^d} (\varepsilon_k - \mu) + \mathcal{O}(1/T^2). \tag{11.38}
\end{aligned}
$$

The limits on the integration, which extend from $-\pi/a$ to π/a for each momentum component, had previously been sent to infinity in the continuum limit $a \to 0$. In the presence of lattice cutoff, we are able to make a naive expansion of the integrand in powers of $1/T$, and the result therefore only contains negative integer powers of T. Contrast this with the universal continuum result (11.37) where we had non-integer powers of T dependent upon the scaling dimension of Ψ.

We return to the universal high T region, $|\mu| \ll T \ll w$, and describe the behavior of the fermionic Green's function G_F, given in (11.20). At the shortest scales we again have the free quantum particle behavior of the $\mu = 0$, $T = 0$ critical point

$$
G_F(x, t) \text{ is given by (11.24) for } |x| \ll (2mT)^{-1/2} \quad |t| \ll \frac{1}{T}. \tag{11.39}
$$

Notice that the limits on x and t in (11.39) are different from those in (11.26), in that they are determined by T and not μ. At larger $|x|$ or t the presence of the other thermally excited particles becomes apparent, and G_F crosses over to a novel behavior characteristic of the high T region. We illustrate this by looking at the large x asymptotics of the

equal time G in $d = 1$ (other d are quite similar)

$$G_F(x, 0) = \int \frac{dk}{2\pi} \frac{e^{ikx}}{1 + e^{-k^2/2mT}} \tag{11.40}$$

For large x this can be evaluated by a contour integration which picks up contributions from the poles at which the denominator vanishes in the complex k plane. The dominant contributions come from the poles closest to the real axis, and gives the leading result

$$G_F(|x| \to \infty, 0) = - \left(\frac{\pi^2}{2mT} \right)^{1/2} \exp\left(-(1 - i)\, (m\pi T)^{1/2}\, x \right) \tag{11.41}$$

Thermal effects therefore lead to an exponential decay of equal-time correlations, with a correlation length $\xi = (m\pi T)^{-1/2}$. Notice that the T dependence is precisely that expected from the exponent $z = 2$ associated with the $\mu = 0$ quantum critical point and the general scaling relation $\xi \sim T^{-1/z}$. The additional oscillatory term in (11.41) is a reminder that quantum effects are still present at the scale ξ, which is clearly of order the de Broglie wavelength of the particles.

11.3 The dilute Bose gas

This section will study the universal properties quantum phase transition of the dilute Bose gas model Z_B in (11.1) in general dimensions. We will begin with a simple scaling analysis which will show that $d = 2$ is the upper critical dimension. The first subsection will analyze the case $d < 2$ in some more detail, while the next subsection will consider the somewhat different properties in $d = 3$.

We begin with the analog of the simple scaling considerations presented at the beginning of Section 11.2. At the coupling $u = 0$, the $\mu = 0$ quantum critical point of $\mathcal{L}_B$ is invariant under the transformations (11.11), after the replacement $\Psi_F \to \Psi_B$, and we have as before $z = 2$ and

$$\dim[\Psi_B] = d/2 \quad , \quad \dim[\mu] = 2; \tag{11.42}$$

these results will shortly be seen to be exact in all d. We can easily determine the scaling dimension of the quartic coupling u at the $u = 0$, $\mu = 0$ fixed point under the bosonic analog of the transformations (11.11); we find

$$\dim[u] = 2 - d. \tag{11.43}$$

Thus the free field fixed point is stable for $d > 2$, in which case it is
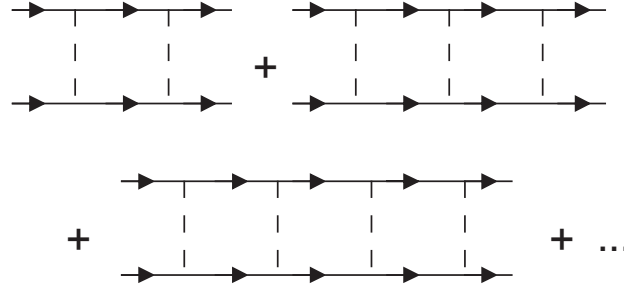
Fig. 11.3. The ladder series of diagrams which contribute the renormalization of the coupling u in Z_B for $d < 2$

suspected that a simple perturbative analysis of the consequences of u will be adequate. However, for $d < 2$, a more carefully renormalization group based resummation of the consequences of u is required, for reasons similar to those presented in Section 8.1.1 for the case of the quantum Ising/rotor models. This identifies $d = 2$ as the upper-critical dimension of the present quantum critical point.

Both here and in the models of Part 2 we have found that the condition for being below the upper-critical dimension is $d + z < 4$; we will find that the same condition also holds in the model of Chapter 12. This common result arises because all of these critical points are described by a bosonic field theory with a quartic non-linearity in which the quantum time dimension scales as z spatial dimensions.

Our analysis of the case $d < 2$ for the dilute Bose gas quantum critical point is very similar to that in Section 8.1.3. However, we will find, somewhat surprisingly, that all the field-theoretic renormalization constants, and the associated flow equations can be determined exactly in closed form. We begin by considering the one-loop renormalization of the quartic coupling u at the $\mu = 0$, $T = 0$ quantum critical point: it turns out that only the ladder series of Feynman diagrams shown in Fig 11.3 need be considered (the T matrix). Evaluating the first term of the series in Fig 11.3 for the case of zero external frequency and momenta, we obtain the contribution

$$-u^2 \int \frac{d\omega}{2\pi} \int \frac{d^d k}{(2\pi)^d} \frac{1}{(-i\omega + k^2/(2m))} \frac{1}{(i\omega + k^2/(2m))}$$
$$= -u^2 \int \frac{d^d k}{(2\pi)^d} \frac{m}{k^2} \tag{11.44}$$

(the remaining ladder diagrams are powers of (11.44) and form a simple

geometric series). Notice the infra-red singularity for $d < 2$, which is cured, as in Section 8.1.1, by moving away from the quantum critical point, or by external momenta. The physical consequences of this singularity can be determined by a field theoretic analysis very similar to that in Section 8.1.3. As in (8.16), we introduce a momentum scale $\widetilde{\mu}$ (the tilde is to prevent confusion with the chemical potential), and express u in terms of a dimensionless coupling u_R by

$$u = u_R \frac{(2m)\widetilde{\mu}^\epsilon}{S_d} \left(1 + \frac{u_R}{2\epsilon}\right). \tag{11.45}$$

Here the prefactor of $(2m)$ has been chosen to make u_R dimensionless, while

$$\epsilon = 2 - d. \tag{11.46}$$

The motivation behind the choice of the renormalization factor in (11.45) is the same as that behind (8.16): the renormalized four-point coupling, when expressed in terms of u_R, and evaluated in $d = 2 - \epsilon$, is free of poles in ϵ as can easily be explicitly checked using (11.44) and the associated geometric series. (Also recall that as in Chapter 8 no such renormalization is necessary above the upper critical dimension (which equals $d = 2$ in the present case), and we can work with bare coupling u.) From the relationship (11.45) we can also derive the flow equation for u_R under the change $\widetilde{\mu} \to \widetilde{\mu}e^\ell$ for fixed u (this is the analog of (8.17)); we obtain [151, 160]

$$\frac{du_R}{d\ell} = \epsilon u_R - \frac{u_R^2}{2} \tag{11.47}$$

Note that for $\epsilon > 0$, there is a stable fixed point at

$$u_R^* = 2\epsilon \tag{11.48}$$

which will control all the universal properties of Z_B.

We now state a very important and surprising feature of the above results, which is not shared by the corresponding calculations in Chapter 8. The renormalization (11.45), the flow equation (11.47), and the fixed point value (11.48) are *exact* to all orders in u_R or ϵ, and it is not necessary to consider u_R dependent renormalizations to the field scale of Ψ_B or any of the other couplings in Z_B. This result is ultimately a consequence of a very simple fact: the ground state of Z_B at the quantum critical point $\mu = 0$ is simply the empty vacuum with no particles. So any interactions which appear are entirely due to particles that have

been created by the external fields. In particular, if we introduce the bosonic Greens function (the analog of (11.20))

$$G_B(x,t) = \left\langle \Psi_B(x,t)\Psi_B^\dagger(0,0) \right\rangle, \tag{11.49}$$

then for $\mu \leq 0$ and $T = 0$, its Fourier transform $G(k,\omega)$ is given exactly by the free field expression

$$G_B(k,\omega) = \frac{1}{-\omega + k^2/(2m) - \mu}. \tag{11.50}$$

The field $\Psi_B^\dagger$ creates a particle which travels freely until its annihilation at (x,t) by the field Ψ_B: there are no other particles present at $T = 0$, $\mu \leq 0$, and so the propagator is just the free field one. The simple result (11.50) implies that the scaling dimensions in (11.42) are exact. Now turning to the renormalization of u, it is clear from the diagram in Fig 11.3 that we are considering the interactions of just two particles: for these, the only non-zero diagrams are the one shown in Fig 11.3, which involve repeated scattering of just these particles. Formally, it is possible to write down many other diagrams which could contribute to the renormalization of u: however all of these vanish upon performing the integral over internal frequencies: there is always one integral which can be closed in one half of the frequency plane where the integrand has no poles. This absence of poles is of course just a more mathematical way of stating that there are no other particles around.

We will consider application of these renormalization group results separately for the cases below and above the upper critical dimension of $d = 2$.

11.3.1 $d < 2$

The approach and analysis here is very similar to that carried out in Chapter 8 below the upper critical dimension ($d < 3$) for the quantum rotor/Ising models.

First, let us note some important general implications of the theory controlled by the fixed point interaction (11.48). As we have already noted, the scaling dimensions of Ψ_B and μ are given precisely by their free field values in (11.42), and the dynamic exponent z also retains the tree level value $z = 2$. All these scaling dimensions are identical to those obtained for the case of the spinless Fermi gas in Section 11.2. Further the presence of a non-zero and universal interaction strength u_R^* in (11.48) implies that the bosonic system is stable for the case

$\mu > 0$ as the repulsive interactions will prevent the condensation of infinite density of bosons (no such interaction was necessary for the fermion case, as the Pauli exclusion was already sufficient to stabilize the system). These two facts imply that the formal scaling structure of the bosonic fixed point being considered here is identical to that of the fermionic one considered in Section 11.2, and that the scaling forms of the two theories are *identical*. In particular, G_B will obey a scaling form identical to that for G_F in (11.19) (with a corresponding scaling function Φ_{G_B}), while the free energy, and associated derivatives obey (11.21) (with a scaling function $\Phi_{\mathcal{F}_B}$). The universal functions Φ_{G_B} and $\Phi_{\mathcal{F}_B}$ can be determined order by order in the present $\epsilon = 2-d$ expansion, and this will be illustrated shortly.

Although the fermionic and bosonic fixed points share the same scaling dimensions, they are distinct fixed points for general $d < 2$. However, the arguments already presented in Section 11.1 suggest that these two fixed points are identical precisely in $d = 1$ [439]. Further evidence for this identity was presented in Ref [115]: there the anomalous dimension of the composite operator Ψ_B^2 was computed exactly in the ϵ expansion, and was found to be identical to that of the corresponding fermionic operator. Assuming the identity of the fixed points, we can then make a stronger statement about the universal scaling function: those for the free energy (and all its derivatives) are identical $\Phi_{\mathcal{F}_B} = \Phi_{\mathcal{F}_F}$ in $d = 1$. In particular, from (11.22) and (11.23) we conclude that the boson density is given by

$$\langle Q \rangle = \langle \Psi_B^\dagger \Psi_B \rangle = \int \frac{dk}{2\pi} \frac{1}{e^{(k^2/(2m)-\mu)/T} + 1} \qquad (11.51)$$

in $d = 1$ only. The operators Ψ_B and Ψ_F are still distinct and so there is no reason for the scaling functions of their correlators to be the same: we will compute numerous exact properties of the scaling function Φ_{G_B} for G_B in the following Section 11.4. The crossover diagram of Fig 11.2 also applies to Z_B in $d = 1$. The critical Fermi liquid state for $\mu > 0$, $T = 0$ is expected to become a critical superfluid state: as we will show in Section 11.4, the bosonic correlation functions decay with a power-law in space implying 'quasi-long-range' superfluid order at $T = 0$. However correlations decay exponentially at any nonzero T implying the absence of any finite T phase transition: this is again consistent with the $T > 0$ behavior of Fig 11.2.

As not all observables can be computed exactly in $d = 1$ by the mapping to the free fermions, we will now consider the $\epsilon = 2 - d$ expansion.

We will present a simple ϵ expansion calculation [438] for illustrative purposes. We focus on density of bosons at $T = 0$. Knowing that the free energy obeys the analog of (11.21), we can conclude that a relationship like (11.10) holds

$$\langle \Psi_B^\dagger \Psi_B \rangle = \left\{ \begin{array}{ll} \mathcal{C}_d (2m\mu)^{d/2} & \mu > 0 \\ 0 & \mu < 0 \end{array} \right. \tag{11.52}$$

at $T = 0$, with $\mathcal{C}_d$ a universal number. The identity of the bosonic and fermionic theories in $d = 1$ implies from (11.10) or from (11.51) that $\mathcal{C}_1 = S_1/1 = 1/\pi$. We will show how to compute $\mathcal{C}_d$ is the ϵ expansion: similar techniques can be used for almost any observable.

Even though the position of the fixed point is known exactly in (11.48), not all observables can be computed exactly: they have contributions to arbitrary order in u_R. The basic recipe is as in Section 8.1.3: compute any physical observable as a formal diagrammatic expansion in u, substitute u in favor of u_R using (11.45), and expand the resulting expression in powers of ϵ. All poles in ϵ should cancel, but the resulting expression will depend upon the arbitrary momentum scale $\widetilde{\mu}$. Finally, substitute the fixed point value u_R^* in (11.48): dependence upon $\widetilde{\mu}$ disappears and a universal answer remains. To compute the boson density for $\mu > 0$, we anticipate that there is condensate of the boson field Ψ_B: so we write

$$\Psi_B(x, \tau) = \Psi_0 + \Psi_1(x, t),) \tag{11.53}$$

where Ψ_1 has no zero wavevector and frequency component. Inserting this into $\mathcal{L}_B$ in (11.1), and expanding to second order in Ψ_1 we get

$$\begin{aligned} \mathcal{L}_1 = &-\mu |\Psi_0|^2 + \frac{u}{2} |\Psi_0|^4 - \Psi_1^* \frac{\partial \Psi_1}{\partial \tau} + \frac{1}{2m} |\nabla \Psi_1|^2 \\ &- \mu |\Psi_1|^2 + \frac{u}{2} \left(4|\Psi_0|^2 |\Psi_1|^2 + \Psi_0^2 \Psi_1^{*2} + \Psi_0^{*2} \Psi_1^2 \right). \end{aligned} \tag{11.54}$$

This is a simple quadratic theory in the canonical Bose field Ψ_1, and its spectrum and ground state energy can be determined by the familiar Bogoliubov transformation. Carrying out this step, we obtain the following formal expression for the free energy density $\mathcal{F}$ as a function of the condensate Ψ_0 at $T = 0$

$$\begin{aligned} \mathcal{F}(\Psi_0) = &-\mu |\Psi_0|^2 + \frac{u}{2} |\Psi_0|^4 \\ &+ \frac{1}{2} \int \frac{d^d k}{(2\pi)^d} \left[\left\{ \left(\frac{k^2}{2m} - \mu + 2u|\Psi_0|^2 \right)^2 - u^2 |\Psi_0|^4 \right\}^{1/2} \right. \end{aligned}$$

$$-\left(\frac{k^2}{2m} - \mu + 2u|\Psi_0|^2\right)\right]. \qquad (11.55)$$

To obtain the physical free energy density, we have to minimize $\mathcal{F}$ with respect to variations in Ψ_0 and to substitute the result back into (11.55). Finally we can take the derivative of the resulting expression with respect to μ and obtain required expression of for the boson density, correct to the first two orders in u:

$$\langle\Psi_B^\dagger\Psi_B\rangle = \frac{\mu}{u} + \frac{1}{2}\int\frac{d^dk}{(2\pi)^d}\left[1 - \frac{k^2}{\sqrt{k^2(k^2+4m\mu)}}\right] \qquad (11.56)$$

We evaluate this expression using the recipe specified at the beginning of this paragraph; at the fixed point $u_R = u_R^*$ we get the universal expression in the form (11.52) with

$$\mathcal{C}_d = S_d\left[\frac{1}{2\epsilon} + \frac{\ln 2 - 1}{4} + \mathcal{O}(\epsilon)\right] \qquad (11.57)$$

11.3.2 $d = 3$

Although we will only discuss the case $d = 3$ here, precisely the same manipulations and results hold for all $2 < d < 4$. The same methods can also be used to compute the logarithmic corrections in $d = 2$, along the lines of the discussion in Section 8.4; related results, obtained through somewhat different methods, are available in the literature [391, 392, 151, 439].

The quantum critical point at $\mu = 0$, $T = 0$ is above its upper critical dimension, and we expect mean-field theory to apply. The analog of the mean field result in the present context is the $T = 0$ relation for the density

$$\langle\Psi_B^\dagger\Psi_B\rangle = \begin{cases} \mu/u + \dots & \mu > 0 \\ 0 & \mu < 0 \end{cases}, \qquad (11.58)$$

where the ellipses represents terms which vanish faster as $\mu \to 0$. Notice that this expression for the density is not universally dependent upon μ: it depends upon the strength of the two-body interaction u (more precisely, it can be related to the s-wave scattering length a by $u = 4\pi a/m$).

We turn to the crossovers and phase transitions at $T > 0$. These are sketched in Fig 11.4. These crossovers were computed by Rasolt *et al.* [399, 524], and also addressed in earlier work [464, 465, 108]; we shall
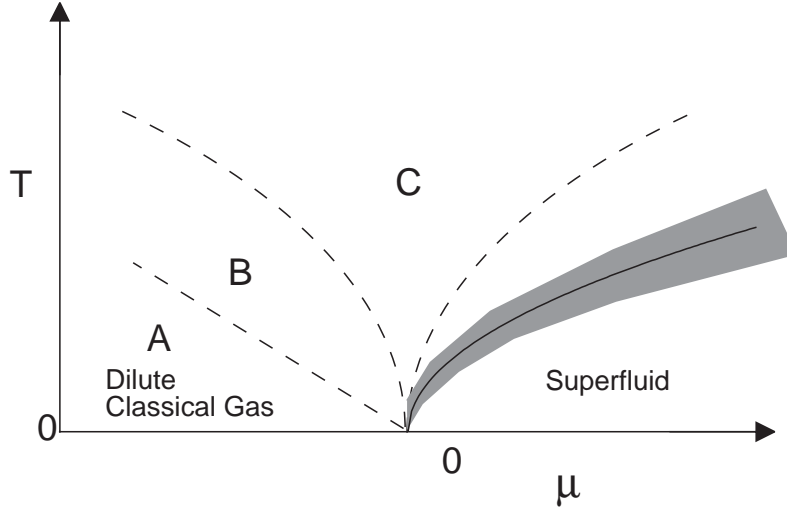
Fig. 11.4. Crossovers of the dilute Bose gas in $d = 3$ as a function of the chemical potential μ and the temperature T. The regimes labeled A, B, C are described in the text. The full line is the finite temperature phase transition where the superfluid order disappears; the shaded region is where the classical $D = 3$, $N = 2$ theory describes thermal fluctuations. The contours of constant density are similar to those in Fig 11.2 and are not displayed.

not follow their approach here, however. Instead, we shall show that the results can be obtained by a direct application of the method used in Section 8.2.2 to study the quantum rotor/Ising models above their upper critical dimension.

The basic approach is one used several times in this book: integrate out the modes with a nonzero Matsubara frequency to obtain an effective action for the static, time-independent modes. In the present situation it is clear that in the non-superfluid phase, the effective action will again have the form of $\mathcal{S}_{\phi,\text{eff}}$ in (8.23) for the case $N = 2$ after the identification

$$\Psi(x) = \sqrt{m}(\phi_1(x) + i\phi_2(x)) \tag{11.59}$$

of the static modes. The values of the couplings, R and U can be obtained by a simple perturbation theory in u: from expressions analogous to (8.24), (8.25) and (8.38) we obtain

$$R = -2m\mu + 4mu \int \frac{d^3k}{(2\pi)^3} \left[\frac{1}{e^{(k^2/2m-\mu)/T} - 1} - \frac{2mT}{k^2 - 2m\mu} + \frac{2mT}{k^2} \right] \tag{11.60}$$

and

$$U = 12m^2 u. \tag{11.61}$$

Armed with the knowledge of the values of R and U we can then proceed precisely as in Section 8.2.2: we simply insert these values into the form (8.26) involving the tricritical crossover function (the susceptibility χ in the present case is the boson Green's function G_B defined in (11.49)), and use the results for the tricritical crossovers in Section 8.1.2 for the case $N = 2$. So a clear understanding of the functional form of R will be useful, and we now discuss this.

Let us first rewrite R in the form analogous to (8.39)

$$R = -2m\mu + 4mu(2mT)^{3/2} K\left(\frac{\mu}{T}\right) \tag{11.62}$$

where the universal function $K(y)$ is given by (compare (8.28) and (8.40))

$$K(y) = \frac{1}{2\pi^2} \int_0^\infty k^2 dk \left(\frac{1}{e^{k^2-y}-1} - \frac{1}{k^2-y} + \frac{1}{k^2}\right). \tag{11.63}$$

Note that the result for R depends explicitly on the bare value of the coupling u, as is expected for a system above its upper-critical dimension, and as we also found in Section 8.2.2. A crucial property of $K(y)$ (as was the case for (8.28) and (8.40)) is that it is analytic as a function of y at $y = 0$: this is clear from the fact that the only possibility singularity of the integrand is the pole at $k^2 = y$, but its residue vanishes because of cancellation between the first two terms in (11.63). We quote some limiting forms for $K(y)$ analogous to (8.30):

$$K(y) = \begin{cases} \zeta(3/2)/(4\pi)^{3/2} - 0.0327826y & |y| \ll 1 \\ \sqrt{|y|}/(4\pi) + e^{-|y|}/(4\pi)^{3/2} & y \ll -1 \end{cases}. \tag{11.64}$$

We have not presented the limiting form for $y = \mu/T \gg 1$ as that will not be needed: this limit puts the system within the superfluid phase (see Fig 11.4) and the present results are only valid for the normal phase.

Inserting the above results into (8.26) and some straightforward analysis allows one to construct the phase diagram in Fig 11.4. We can characterize the non-superfluid regions of Fig 11.4 by the behavior of the zero frequency limit of the boson Green's function G_B; following (8.41) we parameterize this as

$$G_B(k, i\omega_n = 0) = \frac{2m}{k^2 + \xi^{-2}}, \tag{11.65}$$

where ξ can be identified as the correlation length of the superfluid order parameter. An expression for ξ follows from (8.26) and (8.12) at $N = 2$:

$$\xi^{-2} = R - \frac{TU\sqrt{R}}{6\pi}. \qquad (11.66)$$

As in Section 8.2 the condition for the boundary to the ordered super-fluid phase is simply $R = 0$: using (11.62-11.64) we therefore obtain, to leading order in u, the critical temperature

$$T_c = \frac{2\pi}{m} \left(\frac{\mu}{2u\zeta(3/2)} \right)^{2/3} \qquad (11.67)$$

which describes the phase boundary shown in Fig 11.4; notice that $\mu/T_c \sim \mu^{1/3}u^{2/3}m \ll 1$, and so the $\mu/T_c \gg 1$ case of (11.64) was not necessary. Before discussing the various normal state regimes in Fig 11.4 however, we also obtain an expression for the free energy density, $\mathcal{F}$; the boson density then follows immediately from the identity $\langle \Psi_B^\dagger \Psi_B \rangle = -\partial \mathcal{F}/\partial \mu$. The free energy is computed by adding the contribution of the $\omega_n \neq 0$ modes to that of the $\omega_n = 0$ modes as described by $\mathcal{S}_{\phi,\text{eff}}$ in (8.23); we obtain

$$\mathcal{F} = T \int \frac{d^3k}{(2\pi)^3} \ln \left(1 - e^{-(k^2/(2m)-\mu)/T} \right)$$

$$+ T \int_0^\Lambda \frac{d^3k}{(2\pi)^3} \ln \left(\frac{k^2 + \xi^{-2}}{k^2 - 2m\mu} \right). \qquad (11.68)$$

The integral over the $\omega_n \neq 0$ terms yields the first logarithm and the denominator in the argument of the second logarithm: notice that this combination is well-defined even for $\mu > 0$, and the singularity at $k^2 = 2m\mu$ is illusory; the expression (11.68) is analytic at $\mu = 0$, and can be straightforwardly numerically evaluated in the present form both for all real values of μ. The integral over the ϕ_α modes in $\mathcal{S}_{\phi,eff}$ gives the numerator of the second logarithm. Notice also that the second integral requires an large momentum cutoff Λ: the answer will depend partially on the nature of this cutoff, but this is to be expected in a theory above its upper critical dimension. The Λ dependence can be separated out by subtracting a suitable $1/k^2$ term from the second integral: we leave this as a simple exercise for the reader. From the knowledge of $\mathcal{F}$, and therefore of the boson density $\langle \Psi_B^\dagger \Psi_B \rangle$, we can, in principle, convert the μ-T phase diagram in Fig 11.4 into a density-T phase diagram: the constant density contours in Fig 11.4 have a shape quite similar to those in Fig 11.2. However, the theoretical analysis, and the manner in

which the present problem fits into the general theory of crossovers near quantum phase transitions is much more transparent in the μ-T plane, and this representation will continue to be the basis of our remaining discussion. We turn to a separate description of the normal state regions in turn (the discussion will parallel that below (8.41)).

(A) $\mu < 0$, $T \ll |\mu|$, *Dilute classical gas*:
We use the $y \ll -1$ limit of (11.64) in (11.62) and (11.66) to obtain

$$\xi^{-2} = 2m|\mu| + \frac{mu}{2}\left(\frac{2mT}{\pi}\right)^{3/2} e^{-|\mu|/T}. \tag{11.69}$$

So the correlation length is given by its $T = 0$ value and all T dependent corrections are exponentially small. The density of bosons follows from the μ derivative of (11.68) and we obtain

$$\langle \Psi_B^\dagger \Psi_B \rangle = \left(\frac{mT}{2\pi}\right)^{3/2} e^{-|\mu|/T} + \ldots \tag{11.70}$$

The ellipses represent small corrections which depend upon the strength of the weak interaction u, and we invite the reader to work them out from (11.68). This density is very small, and as in Section 11.2.1, the spacing between the particles is much larger than their thermal de Broglie wavelength. We therefore expect an effective classical Boltzmann gas description to apply. While (11.65) and (11.69) give an adequate description of the static correlations, dynamic properties require further analysis following that presented in Chapters 7 and 9 for the quantum rotor models.

(B) $\mu < 0$, $|\mu| \ll T \ll (|\mu|/u)^{2/3}/m$:
As in (A), the correlation length is dominated by its $T = 0$ value of $(2m|\mu|)^{-1/2}$ but the form of the T-dependent corrections is differs from the exponentially small corrections in (A); we have instead, power law corrections which follow from the $|y| \ll 1$ limit of (11.64) inserted in (11.62) and (11.66):

$$\xi^{-2} = 2m|\mu| + \frac{mu}{2}\left(\frac{2mT}{\pi}\right)^{3/2} \zeta(3/2). \tag{11.71}$$

The density is no longer exponentially small, and (11.68) gives

$$\langle \Psi_B^\dagger \Psi_B \rangle = \left(\frac{mT}{2\pi}\right)^{3/2} \zeta(3/2) + \ldots, \tag{11.72}$$

where again the ellipses represent u-dependent corrections which are somewhat messy, but easy to compute from the expressions provided above. For this density the spacing between the particles is of order their thermal de Broglie wavelength, and in this respect this regime is similar to the high T limit of the Fermi gas discussed in Section 11.2.3. Of course, there are non-universal u-dependent corrections here, which were absent for the Bose gas for $d < 2$ and for the spinless Fermi gas in all d. Again, a description of dynamics in this region (B) requires the extension of the computations on Chapters 7 and 9.

(C) $T \gg (|\mu|/u)^{2/3}/m$, High T:

This is of course the true high T limit of the continuum theory Z_B. Its physical properties are similar to those of (B) but with some significant differences. The expression (11.71) for the correlation length still applies, but it is clear that the second T-dependent term is the larger one. So the correlation length $\xi \sim T^{-3/4}$, which does not agree with the naive scaling estimate $\xi \sim T^{-1/z}$; as we discussed in Section 8.2.2, this is because the interaction u is dangerously irrelevant, and its bare value appears in high T limit of (11.71). The leading term in the density is also as in (11.72), but the omitted u-dependent corrections have a rather different structure.

11.4 Correlators of Z_B in $d = 1$

The study of the bosonic correlators of Z_B is of some interest because they can be measured directly in neutron scattering or NMR experiments on spin systems which realize a quantum phase transition of the type studied here. Explicit realizations include the XX chain of Section 11.1 or gapped antiferromagnets in a strong field (to be discussed in Chapter 13). In all of these cases, the bosonic field Ψ_B has a simple, local relationship to the spin operators (as in (11.4)), allowing its correlators to be simply related to measurable quantities. In contrast, the fermionic correlators of Ψ_F (discussed in Section 11.2) have no physical interpretation in such applications.

We have argued in Sections 11.1, 11.2 and 11.3.1 that the theories Z_B and Z_F are equivalent for small μ: the universal expression for the boson density was given in (11.51). Here we will discuss how to map the two theories at the operator level. For the case of the transition from a Mott insulator with $n_0 = 0$, there are no background particles to account for, and we can derive the theory Z_B simply by the naive

continuum limit of the lattice boson coherent state path integral (10.18): such a procedure leads to the exact operator correspondence $\Psi_B = \hat{b}_i/a$. We know from Section 11.1 that $\hat{b}_i = (\hat{\sigma}_i^x + i\hat{\sigma}_i^y)/2$, and further that the Pauli matrices are related to the lattice fermion field by (4.25) and thence to the continuum Fermi field Ψ_F via (4.39). Combining these transformations, and taking the naive continuum limit, we can obtain the formal operator correspondence

$$\Psi_B(x, t) = \exp\left(i\pi \int_{-\infty}^x dy\, \Psi_F^\dagger(y, t)\Psi_F(y, t)\right) \Psi_F(x, t). \qquad (11.73)$$

So our task is, in principle, well defined: all correlators of Ψ_F under $\mathcal{L}_F$ are known—use these to compute those of Ψ_B using the mapping (11.73). In practice, this evaluation cannot be carried out in the continuum as severe short distance divergences appear: we have to return to the underlying lattice degrees of freedom, evaluate the expectation values under the lattice Hamiltonian, and then return to the continuum limit. A calculation such as this was discussed in Section 4.4 for equal time correlators of the quantum Ising model. A very similar analysis can also be performed for the present XX model: we refer the reader to the literature for details [425] and present the main results.

We are interested here in the two-point bosonic correlation function G_B in (11.49). As discussed in Section 11.3.1, we know that this satisfies a scaling form identical to (11.19), but the bosonic scaling function Φ_{G_B} will be quite different from Φ_{G_F}. The large distance limit of the equal time case can be obtained by the methods of Section 4.4. We use the mapping

$$G_B(x, 0) = \frac{1}{2a} \langle \hat{\sigma}_i^x \hat{\sigma}_0^x \rangle \qquad (11.74)$$

where $x = ia$ and the latter expectation value is evaluated under H_{XX} at a temperature T. This can be performed using essentially the same analysis as in Section 4.4, and we obtain for $T > 0$ that [425]

$$\lim_{|x|\to\infty} G_B(x, 0) = \left(\frac{mT}{2}\right)^{1/2} G_X(\mu/T) \exp\left(-F_X(\mu/T)(2mT)^{1/2}|x|\right) \qquad (11.75)$$

where the universal crossover functions $F_X(y)$ and $G_X(y)$ are given by

$$F_X(y) = \int_0^\infty \frac{ds}{\pi} \ln \coth \frac{|s^2 - y|}{2} + \theta(-y)\sqrt{-y}, \qquad (11.76)$$
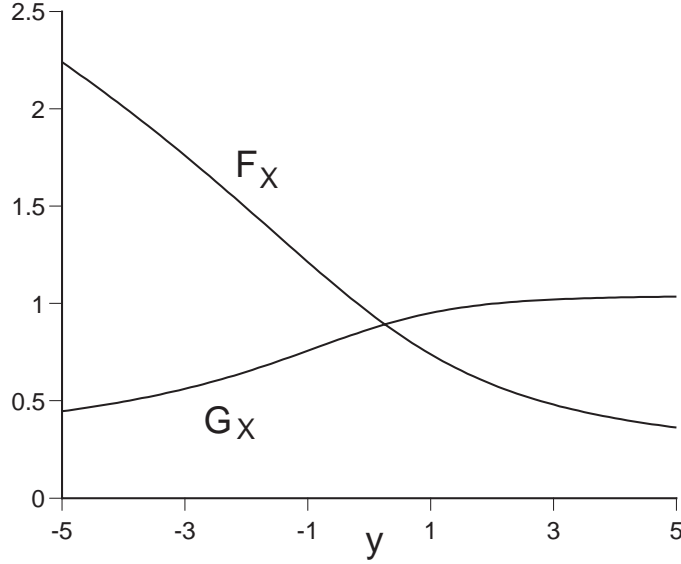
Fig. 11.5. The universal scaling functions $F_X(y)$ for the inverse correlation length and the amplitude $G_X(y)$ (defined in (11.75)), as a function of $y = \mu/T$.

$$\ln G_X(y) = 2 \int_{-\infty}^{-1} ds \left[\left(\frac{dF_X(s)}{ds} \right)^2 + \frac{1}{4s} \right] + 2 \int_{-1}^{y} ds \left(\frac{dF_X(s)}{ds} \right)^2.$$

(11.77)

Notice the similarity of these results to (4.67) and (4.68) for the Ising chain. As in the Ising case, both functions F_X and G_X are analytic (despite appearances) for all real values of y, as must be the case due to the absence of thermodynamic singularities at non-zero T: we show a plot of these functions in Fig 11.5. These results for F_X and G_X have also been obtained in Refs [301, 282, 244, 281] by the rather different, and far more sophisticated, quantum inverse scattering method.

Let us look at the physical implications of the above results for G_B in the different regimes of Fig 11.2.

11.4.1 Dilute classical gas, $T \ll |\mu|$, $\mu < 0$

We need the $y \to -\infty$ limits of the F_X, G_X scaling functions. From (11.76,11.77) we get $F_X(y \to -\infty) = \sqrt{-y}$ and $G_X(y \to -\infty) =$

$1/\sqrt{-y}$, and so have for the equal-time correlator

$$G_B(x, 0) = \frac{T}{2}\left(\frac{2m}{|\mu|}\right)^{1/2} \exp\left(-(2m|\mu|)^{1/2}|x|\right) \quad \text{as } |x| \to \infty. \quad (11.78)$$

This equal time result has a very simple interpretation. It is precisely the Fourier transform of $TG_B(k, \omega_n = 0)$ with the G_B given in (11.65), the prefactor of T coming from the classical limit of the fluctuation-dissipation theorem as in (4.93), and we use the leading low temperature value for ξ in (11.69) $\xi^{-2} = 2m|\mu|$. Classical behavior is of course expected, because, as in Section 11.2.1, the spacing between the particles is much larger than their thermal de Broglie wavelength.

Long time correlators can be obtained by a simple physical argument which relies on the similarity of this regime to the low T regime on the paramagnetic side of the quantum Ising chain, discussed in Section 4.5.2. In that case, and here, we have an exponentially dilute concentration of particles, and are interested in the single-particle boson Green's function. Semiclassical arguments to compute these were advanced in Section 4.5.2, and led to the main result in (4.105): its analog in the present case is

$$G_B(x, t) = G_F(x, t)R(x, t). \quad (11.79)$$

Here G_F is the result given in (11.24) with $d = 1$ (this result is also the Fourier transform of (11.50)), and is the Feynman propagator for a single particle moving quantum mechanically from $(0, 0)$ to (x, t). The factor R represents the consequence of collisions with the exponentially dilute background of thermally excited particles: as argued in Section 4.5.2, G_B picks up a (-1) from the S matrix of each collision, and the result of averaging over such collisions leads to $R(x, t)$ given in (4.86); the only change here is in the dispersion spectrum of the particles $\varepsilon_k = k^2/(2m) + |\mu|$:

$$R(x, t) = \exp\left(-\int \frac{dk}{\pi} e^{-\varepsilon_k/T}\left|x - \frac{d\varepsilon_k}{dk}t\right|\right). \quad (11.80)$$

The explicit structure of the function R was described in Section 4.5.1: equal time correlations decays exponentially in space with the length ξ_c, while equal space correlations decay exponentially in time with the time τ_φ (see (4.87)), and the general function obeys the scaling from (4.90) with the scaling function given in (4.91). The only change is in the specific values of the characteristic scales ξ_c and τ_φ which are given

by

$$\xi_c = \left(\frac{\pi}{2mT}\right)^{1/2} e^{|\mu|/T}$$

$$\tau_\varphi = \frac{\pi}{2T} e^{|\mu|/T} \tag{11.81}$$

Notice that both scales are exponentially large at low T.

The dynamic structure factor can be obtained by a Fourier transform of (11.79), and its physical properties are very similar to those in Section 4.5.2: there is a well defined quasi-particle pole at $\omega = \varepsilon_k$, which is broadened by collisions with other particles on the spatial and temporal scales given in (11.81).

The results (11.79) and (11.80) have also been obtained in Refs [246, 281] by a more rigorous and much lengthier method. The precise agreement gives us confidence that the simple semiclassical arguments used above are essentially exact.

11.4.2 *Tomonaga-Luttinger liquid, $T \ll \mu$, $\mu > 0$*

This is the region labeled a Fermi liquid in Fig 11.2: in $d = 1$ the generic state with interaction among the fermions away from the critical point is a Tomonaga-Luttinger liquid (as we will discuss in Chapter 14), and we will use this more general and standard terminology.

In our discussion of the correlators of Ψ_F this region in Section 11.2.2 we showed that the long-distance properties were described by a line of $z = 1$ critical points at $\mu > 0$, $T = 0$, and that this manifested itself in a collapse of the fermion scaling functions into a reduced scaling form. A similar collapse must also occur for the G_B correlator, and indeed for all other observables. To describe this, we will need the scaling dimension of Ψ_B under the continuum critical theory of this line of critical points, which was $\mathcal{L}_{FL}$ in (11.28).

This dimension can be easily obtained from the equal time results above. Using, from (11.76,11.77), $F_X(y \to \infty) = \pi/4\sqrt{y}$ and $G_X(y \to \infty) = 1.042828\ldots$ we get for $T \ll \mu$

$$G_B(x,0) = G_X(\infty) \left(\frac{mT}{2}\right)^{1/2} \exp\left(-\frac{\pi}{2}\frac{T}{v_F}|x|\right) \quad \text{as } |x| \to \infty \tag{11.82}$$

The prefactor $\sim T^{1/2}$ along with quantities invariant under the scaling transformation (11.29), and the exponent $z = 1$, fixes

$$\dim[\Psi_B] = 1/4 \tag{11.83}$$

along the $\mu > 0$ critical line; recall that $\dim[\Psi_B] = 1/2$ at the $\mu = 0$ critical end point.

The results (11.82) and (11.83) are key, and allow us to deduce the entire space and time dependence of G_B in this regime using a simple argument. The key point is that the long distance and time correlators are controlled by the theory $\mathcal{L}_{FL}$ which is conformally invariant. Then we may use arguments essentially identical to those in Section 4.5.3 where we considered the high T limit of the quantum Ising chain. The latter was controlled by the conformally invariant, $z = 1$, theory $\mathcal{L}_I$ in (4.44) at $\Delta = 0$. As we showed in Section 4.5.2, the $T > 0$ equal-time long-distance decay in (4.111) allowed us to deduce the complete spacetime dependent correlation function in (4.112) and also the exact $T = 0$ correlator at the critical point in (4.108). Proceeding in precisely the same manner here, we may conclude here that the $T = 0$ bosonic correlator obeys for $\mu > 0$

$$G_B(x, \tau) \sim \frac{1}{(x^2 + v_F^2 \tau^2)^{1/4}}, \tag{11.84}$$

where the normalization constant will be fixed shortly. Indeed (11.84) follows simply from (11.83) and the relativistic invariance of $\mathcal{L}_{FL}$. So as announced earlier, the bosonic superfluid correlations decay with a power-law in the $\mu > 0$ ground state. At finite T, the analog of (4.112) is

$$G_B(x, \tau) = \left(\frac{mT}{2}\right)^{1/2} \frac{2^{-1/2} G_X(\infty)}{[\sin(\pi T(\tau + ix/v_F)) \sin(\pi(\tau - ix/v_F))]^{1/4}}. \tag{11.85}$$

Notice that this result obeys the reduced scaling form characteristic of the scaling dimensions of the theory $\mathcal{L}_{FL}$ in (11.29):

$$G_B(x, t) = \left(\frac{mT}{2}\right)^{1/2} \phi_X\left(\frac{Tx}{v_F}, Tt\right) \tag{11.86}$$

From this expression we can also explicitly related the reduced scaling function ϕ_X is related to the global scaling function Φ_{G_B} (this is the scaling function of G_B defined as the bosonic analog of (11.19)) by the $\mu/T \to \infty$ of the latter:

$$\phi_X(\bar{x}, \bar{t}) = \lim_{y \to \infty} \Phi_{G_B}(2\sqrt{y}\bar{x}, \bar{t}, y), \tag{11.87}$$

The physical properties of these dynamical correlations are essentially identical in form to the dynamic responses discussed in Section 4.5.3,

and particularly in Figs 4.8 and 4.9, and so need not be discussed here. Correlations decay exponentially with a length $\xi \sim v_F/T$ and on a phase coherence time $\tau_\varphi \sim 1/T$. Both these scales are those expected in the 'high T' limit of a critical theory with $z = 1$: in the present case this is the theory $\mathcal{L}_{FL}$ characterizing the line of $\mu > 0$ critical points. Remember, though, that the present region is a low T region of the global theory $\mathcal{L}_B$.

11.4.3 High T limit, $T \gg |\mu|$

Now we have from (11.76,11.77)

$$G_B(x,0) = G_X(0) \left(\frac{mT}{2}\right)^{1/2} \exp\left(-F_X(0)\,(2mT)^{1/2}\,|x|\right) \quad \text{as } |x| \to \infty$$

$$(11.88)$$

where $F_X(0) = \zeta(3/2)(1 - 1/\sqrt{8})/\sqrt{\pi} = 0.952781471\ldots$ and $G_X(0) = 0.86757\ldots$ are pure numbers. All scales are set by T, and the correlation length $\sim T^{-1/2}$, as expected from the $z = 2$ value at the $\mu = 0$ critical point. Notice also the similarity of this correlation length to that of the fermionic correlator in (11.41); only the numerical factors are different.

Asymptotics of dynamic correlation functions in this regime have been obtained by Korepin *et al.* [281, 246] by the quantum inverse scattering method. However, this is the one limiting regime where their approach appears indispensable, and an alternative derivation using the simpler physical arguments employed here does not exist; finding such a derivation remains an important open problem. (Korepin *et al.* [281, 246] also give the dynamic analogs of (11.75) containing the crossovers between the different finite T regimes: the methods discussed here cannot give these either). Their results are quite lengthy and will not be reproduced here: we will just be satisfied by noting that, as expected by scaling arguments in the high T regime of a continuum theory, time-dependent correlations decay exponential on a phase coherence time of order $1/T$.

11.4.4 Summary

We summarize all of the structure in the dynamic correlations of Z_B in Fig 11.6; notice the similarity (and some differences) from the corresponding figure for the Ising chain in Fig 4.13. First, in all the three universal regions of Fig 11.2, the short time properties are essentially the same: a free non-relativistic particle propagating quantum mechanically,

Fermi liquid

QUANTUM
RELAXATION
z=1   FERMI
LIQUID   FREE PARTICLE

0   T μ ω

High T

QUANTUM
RELAXATION
z=2   FREE PARTICLE

0   T ω
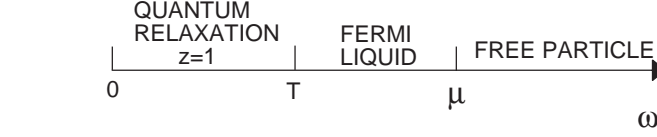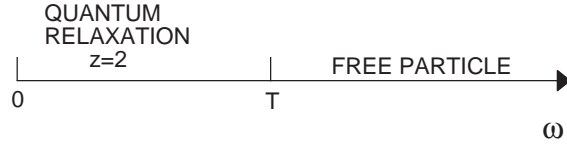
Fig. 11.6. Crossovers as a function of frequency for the boson model Z_B (in (11.1)) in $d = 1$ in the regimes of Fig 11.2; this model is equivalent to Z_F (in (11.3)) in $d = 1$.

without yet having felt the influence of any other particle. The interactions with other particles appear at longer times, and their consequences are rather different in the various regimes.

In the low T regime for $\mu < 0$ ($T \ll |\mu|$), the concentration of other particles is exponentially small, and so the decoherence and spectral line broadening due to collisions is not felt until the very long time $\tau_\varphi \sim (1/T)e^{|\mu|/T}$.

In the opposing low T regime for $\mu > 0$ ($T \ll \mu$) the behavior is rather different. Now the particles are dense and degenerate, and at times longer than $1/\mu$, the Pauli exclusion principle leads to the quantum coherence of a Fermi liquid ground state (more generally for large μ, a Tomonaga-Luttinger liquid, see Chapter 14). This state is described by the separate $z = 1$ theory $\mathcal{L}_{FL}$ in (11.28), and for a while the systems appears to be in the ground state of $\mathcal{L}_{FL}$. However, eventually thermal effects cause decoherence and relaxation at a time $\tau_\varphi \sim 1/T$ and a length scale $\xi \sim 1/T$. This last crossover is entirely a property of $\mathcal{L}_{FL}$ and is characterized by its $z = 1$ critical exponents.

Finally in the high T regime, we have a completely different behavior. Now the value of μ is unimportant, and we may as well set $\mu = 0$. The crossover from the free particle behavior to relaxational dynamics happens at a time $\tau_\varphi \sim 1/T$ and a length scale $\xi \sim 1/\sqrt{T}$, which are characteristic of the $z = 2$ critical point at $\mu = 0$. The mean spacing

between the particles is of order their de Broglie wavelength, and thermal and quantum effects are equally important.

11.5 Applications and extensions

The dilute Fermi gas theory should describe the transition in an interacting electron system (possibly described by a Hubbard-like model) from a Mott insulator to a metal, driven by a variation in the chemical potential. This transition has been studied numerically [28] but appears to display a dynamic critical exponent of $z \approx 4$; it has been argued that this is due to the presence of anomalously flat bands in the particular model studied, which leads to a $\sim k^4$ dispersion of the excitations above the gap of the Mott insulator [236].

Experiments on the loss of superfluidity of ^{4}He adsorbed in aerogel and Vycor [407, 110, 111] provide a realization of the dilute Bose gas theory in the presence of a random external potential [160]. There are few analytic results on this random problem, although some detailed numerical studies have been undertaken [472, 523]; however, a reconciliation between theory and experiments has not yet occurred. The experiments have been carried out both in bulk ($d = 3$) and in films ($d = 2$).

Quantum antiferromagnets in the presence of an external magnetic field provide some of the best experimental realizations of the dilute Bose gas quantum critical point. We defer discussion of experiments on this case until Chapter 13 where the connection will be explicitly discussed.

Corrections to the T_c of a dilute Bose gas in $d = 3$ beyond the result (11.67) have been studied numerically [193] and by a renormalization group method somewhat different from our analysis here [53]. It would be interesting to compare these results with those obtained here, after accounting for the fact that the critical point is at a nonzero $R_c \sim (TU)^{1/2}$ (see the discussion below (8.26))—this has not yet been done.

Our discussion of crossovers in this chapter explicitly avoided the case of $d = 2$, the upper critical dimension. This can be carried out as discussed in Section 8.4 for the upper critical dimension of the rotor/Ising models. Results, obtained by somewhat different methods, can be found in Refs [391, 392, 151, 439].

12

Phase transitions of Fermi liquids

We will take the low T Fermi liquid state of Section 11.2.2 in dimensions $d \geq 2$ (or its spinful generalization), and examine the nature of its instabilities to other ground states of a dense gas of fermions. Possibilities include ferromagnets, states in which there is spin or charge density wave order (to be defined more precisely below) or various types of superconductors. All of these cases are of considerable practical importance and have numerous experimental applications.

A theoretical treatment of the quantum transition between a Fermi liquid and a magnetically or charge ordered state was given in a paper by Hertz [225], although many important points were anticipated in earlier work [44, 351, 352, 396]. We shall present Hertz's basic arguments in Section 12.1 for the case of a transition between a Fermi liquid and a spin density wave state. We shall not treat the other cases here and will, instead, refer the reader to the literature. There are a number of reasons for this neglect:

(i) Many aspects of these transitions are not fully understood (we will note some below), and are the subject of considerable debate in the literature–it is therefore inappropriate to include them in this introductory treatment.

(ii) We shall only consider systems in spatial dimensions $d \geq 2$ here (the $d = 1$ case requires a separate treatment appropriate to Tomonaga-Luttinger liquids, and will be addressed in Chapter 14). For these dimensions, the quantum critical point is invariably at or above its upper critical dimension. As a result, nonuniversal features abound, and the details of the particular microscopic situation under consideration are often important. A unified treatment of all the cases is hardly possible, and we choose, instead, to focus on a single representative case.

(iii) Details of the topology of the Fermi surface topology often matter,

and this adds to the zoo of experimental possibilities. A single illustration for a particular model is however adequate to make the basic point.

We will consider the nature of the non-zero temperature crossovers near the Fermi liquid-spin density wave quantum critical point in Section 12.2. These were computed by Millis [341] who pointed out the universal features and emphasized the basic similarities of the crossovers to those in the dilute Bose gas; related results, not using the perspective of quantum phase transitions, were also available in the earlier work of Moriya [353, 351, 352, 214], Ramakrishnan [395, 396, 347] and others. We have already studied the dilute Bose gas in Section 11.3.2 where we also noticed the similarity to the quantum Ising/rotor models above their upper critical dimension as treated in Section 8.2.2. Here we shall be able to use the techniques developed in these earlier sections to rapidly arrive at the needed generalization. The study of the finite temperature crossovers shall be restricted here to those above the Fermi liquid state and in the high T regime; the crossovers at low T on the magnetically ordered side are not understood, for reasons that will be discussed.

12.1 Effective field theory

We begin by considering a simple model of interacting spin-1/2 fermions which is expected to display a quantum phase transition to a spin density wave state:

$$H_0 = \int \frac{d^d k}{(2\pi)^d} \left(\varepsilon_k - \mu\right) c_{\vec{k}a}^\dagger c_{\vec{k}a} +$$

$$\frac{1}{2} \int d^d x d^d x' J(x - x') c_a^\dagger(x) \vec{\sigma}_{ab} c_b(x) \cdot c_{a'}^\dagger(x') \vec{\sigma}_{a'b'} c_{b'}(x') + \ldots (12.1)$$

Here $c_a^\dagger$ is the creation operator of spin-1/2 fermion either at the position x or the momentum k. The indices a, b, a', b' represent the fermion spin and can take the two values $\uparrow, \downarrow$ which are implicitly summed over, and the $\vec{\sigma}$ are the Pauli matrices. The fermion dispersion ε_k is determined by the underlying lattice, and μ is the chemical potential. Ignoring interactions, the ground state of H_0 would consist of momentum states with $\varepsilon_k < \mu$ occupied, while the remaining will be empty. The empty and occupied states are separated by a $(d-1)$-dimensional Fermi surface. We allow for a very general set of interactions between the fermions, but have explicitly written down a non-local exchange interaction $J(x - x')$ which favors a spin density wave state. Such a non-local exchange could

perhaps be mediated by other localized electronic degrees of freedom not included in H_0.

For sufficiently weak interactions, the non-interacting Fermi liquid ground state is expected to be stable, apart from innocuous changes in the shape of the Fermi surface. However, for a suitable choice of the exchange J, it is believed that the system will undergo a phase transition to a spin density wave state. Such a state is characterized by a spontaneous broken symmetry which allows for a non-zero expectation value like

$$\langle c_a^\dagger(x)\sigma_{ab}^\alpha c_b(x)\rangle = \phi_\alpha \cos(\vec{K}\cdot\vec{x}) \qquad (12.2)$$

Here ϕ_α $(\alpha = 1, 2, 3)$ is a real, spin density wave order parameter, and $\vec{K} \neq 0$ is the spin density wave ordering wavevector. The ordering in (12.2) clearly corresponds to a *collinear* polarization of the spins oscillating with wavevector $\vec{K}$. This is not the most general possibility: non-collinear ordering is also possible, *e.g.*, the spin polarization could take the configuration of a spiral. Such an ordering would require an order parameter consisting of two vectors $\phi_{1\alpha}$, $\phi_{2\alpha}$; we will not consider it here, although its properties are very similar to the collinear case.

Now imagine approaching a state with the ground state ordering (12.2) from a Fermi liquid. The low energy excitations of the latter consist primarily of fluctuations in the occupation number of fermions just above and below the Fermi surface. It should then not be surprising that the value of the wavevector $\vec{K}$, relative to the geometry of the Fermi surface, is of crucial importance. In particular, it matters whether $\vec{K}$ can connect pairs of points on the Fermi surface or not. Specifying two arbitrary points in momentum space requires $2d$ real numbers, requiring both lie on the Fermi surface imposes 2 conditions, and demanding they are separated by $\vec{K}$ imposes d additional conditions. So the space of such points is at most $d - 2$ dimensional. In $d = 2$ these can therefore be isolated pairs of points on the Fermi surface, while in $d = 3$ they will form pairs of lines. Of course there could simply be no points on the Fermi surface separated by $\vec{K}$: in this case low energy fermionic excitations are not very important for the ordering transition, and the critical properties are not very different from the rotor model transitions considered in Part 2—we will therefore not consider this case further here. A separate, and non-generic case, is that the manifold of Fermi surface points separated by $\vec{K}$ has dimensionality greater than $d - 2$: this situation is referred to as 'nesting' and will also not be considered here–'nesting' leads to some complexity which has been discussed in the

literature [92, 18]. In passing, notice that in $d = 1$ if $\vec{K}$ does connect the Fermi 'surface' points, the above definitions suggest that this case is automatically 'nested': thus, it is not surprising that the $d = 1$ case requires a separate treatment.

The remainder of this chapter will consider the generic case when $\vec{K}$ connects a pair of $d - 2$ dimensional manifold of points on the Fermi surface. We only need to focus on fermionic excitations in the vicinity of these points. In $d = 2$ these are an isolated pair of points: we denote them by $\vec{k}_1$, $\vec{k}_2$, with $\vec{k}_1 - \vec{k}_2 = \vec{K}$. Ignoring all fermions, but those in the vicinity of $\vec{k}_1$, $\vec{k}_2$, we can write

$$c_a(x) = \psi_{1a}(x)e^{i\vec{k}_1 \cdot \vec{x}} + \psi_{2a}(x)e^{i\vec{k}_2 \cdot \vec{x}} \qquad (12.3)$$

where $\psi_{1,2a}(x)$ are fermionic fields which are slowly varying: they are essentially constant on the spatial scale $1/|\vec{K}|$. This condition is necessary to allow us to treat the ψ_{1a} and ψ_{2a} as independent excitations. A closely related parameterization can be carried out in $d = 3$, but we will refrain from explicitly writing it to avoid notational complexity: in this case we will need the fields $\psi_{1,2}(s, x_\perp)$ where s is a label which moves along the line on the Fermi surface, while $x_\perp$ is the spatial co-ordinate in the plane orthogonal to the line. The remaining discussion in this section will apply to both the cases $d = 2, 3$, although for simplicity, we will write out some formulae only in $d = 2$.

On phenomenological grounds, we can write down the effective Hamiltonian which couples the order parameter ϕ_α to the fermion fields $\psi_{1,2}$ in $d = 2$:

$$\begin{aligned}
H_1 = \int \frac{d^2k}{(2\pi)^2} &\left[\vec{v}_1 \cdot \vec{k}\, \psi_{1a}^\dagger(k)\psi_{1a}(k) + \vec{v}_2 \cdot \vec{k}\, \psi_{2a}^\dagger(k)\psi_{2a}(k)\right] \\
+ \int d^2x &\left[\frac{\phi_\alpha^2(x)}{J} + \right. \\
&\left. \phi_\alpha(x)\left(\psi_{1a}^\dagger(x)\sigma_{ab}^\alpha\psi_{2b}(x) + \psi_{2a}^\dagger(x)\sigma_{ab}^\alpha\psi_{1b}(x)\right)\right] .(12.4)
\end{aligned}$$

We have approximated the dispersion of the fermions by a linear momentum dependence in the vicinity of the Fermi surface: the fermion energies vanish at $\vec{k} = 0$, because these points are on the Fermi surface, a consequence of the parameterization (12.3). The vectors $\vec{v}_{1,2}$ are the Fermi velocities at the points $\vec{k}_{1,2}$: $\vec{v}_{1,2} = \vec{\nabla}_k\varepsilon_k\big|_{\vec{k}=\vec{k}_{1,2}}$ — see Figure 12.1. The non-nesting condition requires that $\vec{v}_{1,2}$ be non-collinear. The ϕ_α^2 term in H_1 can be viewed as a phenomenological representation of the exchange interaction in H_0, with the coupling J representing the
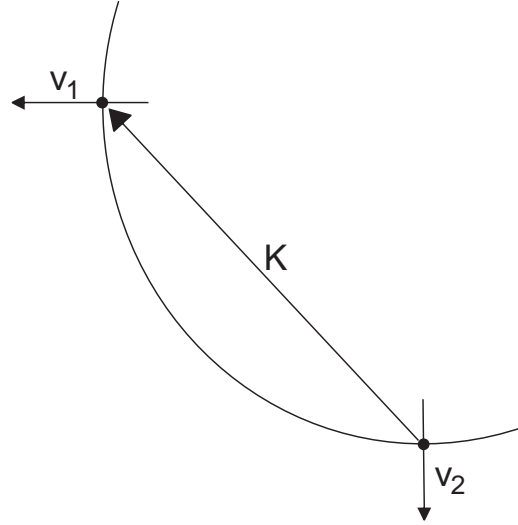
Fig. 12.1. Sketch of a portion of the Fermi surface in $d = 2$, the two selected points with Fermi velocities $\vec{v}_1$ and $\vec{v}_2$; these points are separated by the ordering wavevector $\vec{K}$.

strength of the exchange $J(x - x')$ at the wavevector $\vec{K}$: more literally the terms under the x integral in (12.4) can be obtained by a Hubbard-Stratanovich transformation like that used in Section 10.2 to proceed from (10.18) to (10.19).

We proceed to derive an effective action for the order parameter ϕ_α alone. This requires us to integrate out the fermions $\psi_{1,2}$ from H_1, a potentially dangerous step as the first two fermionic terms in (12.4) allow excitations of arbitrarily small energy (in other words, the fermionic excitations are gapless). Because of these low energy excitations, the resulting terms in the action will have powers of ϕ_α multiplied by coefficients which are non-local in time and space. It is, then, not a priori clear whether it is permissible to truncate this action at any finite order in ϕ_α, or to approximate any of the terms by local interactions. Formally, however, we can integrate out the fermions exactly and obtain the following effective action

$$
\begin{aligned}
\mathcal{S}_0 = & \int d^2 x \int_0^{1/T} d\tau \frac{\phi_\alpha^2(x,\tau)}{J} \\
& + \mathrm{Tr}\ln \begin{pmatrix} \partial/\partial\tau + i\vec{v}_1 \cdot \vec{\nabla}_x & \sigma^\alpha \phi_\alpha(x,\tau) \\ \sigma^\alpha \phi_\alpha(x,\tau) & \partial/\partial\tau + i\vec{v}_2 \cdot \vec{\nabla}_x \end{pmatrix} \quad (12.5)
\end{aligned}
$$

The argument of the logarithm is an operator on the space of functions of space and time which are antiperiodic in τ with period $1/T$—see Ref [360] for a discussion on the definition of such operators. We need to evaluate the $\mathrm{Tr\,ln}$ of such an operator for arbitrary $\phi_\alpha(x,\tau)$: clearly an intractable task required just to obtain the effective action, which must subsequently be integrated over $\vec{\phi}$. However, in the vicinity of the quantum critical point, we expect that ϕ_α will be small and slowly varying, suggesting an expansion in powers and gradients of ϕ_α. This was the strategy followed by Hertz. However before proceeding along this route, we note an important caveat in the following paragraph.

The naive approach is to simply expand the functional determinant in (12.5) in powers of the order parameter $\phi_\alpha(k,\omega_n)$ and also in powers of the wavevectors k and ω_n: such an expansion can, in principle, be carried out to an arbitrarily high order. Given this formal expansion, it is then tempting to believe that the resultant effective action gives an adequate description of the physics everywhere in the phase diagram. In particular, we could attempt to describe the ordered phase by parameterizing

$$\phi_\alpha(k,\omega_n) = N_0 + \phi_{1\alpha}(k,i\omega_n), \tag{12.6}$$

where N_0 is the static polarization of the spin density wave state: we determine N_0 by minimizing the action obtained by expanding in ϕ_α, and then obtain the final effective action for the fluctuations $\phi_{1\alpha}$ about the ordered state. However this procedure is *incorrect*. The reason, simply stated, is that the limits $N_0 \to 0$ and $k,\omega_n \to 0$ in $\mathcal{S}_0$ do not commute. In the procedure just outlined, we have first taken $N_0 \to 0$, then expanded in powers of k, ω_n, and then attempted to impose a nonzero N_0. In reality, we should maintain a non-zero N_0 throughout. Doing this has a very important consequence. For $N_0 \neq 0$, the fermion spectrum of the functional determinant in $\mathcal{S}_0$ undergoes a canonical quantum mechanical band splitting into

$$\frac{\vec{k}\cdot(\vec{v_1}+\vec{v_2})}{2} \pm \left[\left(\frac{\vec{k}\cdot(\vec{v_1}-\vec{v_2})}{2}\right)^2 + N_0^2\right]^{1/2} \tag{12.7}$$

For sufficiently small $\vec{k}$ this implies that there is a *gap* in fermion spectrum: a portion of the Fermi surface in the vicinity of $\vec{k}_{1,2}$ disappears. This gap will however not appear in the expansion of $\mathcal{S}_0$ in powers of ϕ_α, truncated at any finite order. So any such expansion cannot be applied on the ordered side of the transition and it is necessary to return
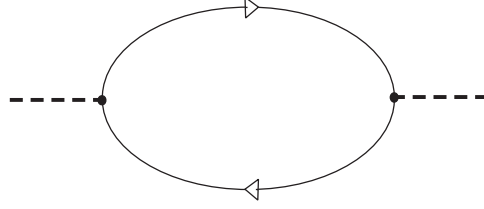
Fig. 12.2. Feynman diagram for the vertex of order ϕ_α^2 generated from the coupling between ϕ_α and the fermion bilinears in (12.4). The full lines are fermion propagators and the wavy lines are the external ϕ_α sources.

to the complete expression in (12.5) [432]. The spectrum in (12.7) is also closely related to the 'pseudo-gap' phenomenon in the high temperature superconductors, and its consequences are an active topic of current research [93, 95].

We return to the route followed by Hertz [225], keeping in mind the caution above about its inapplicability on the ordered side. Expanding the functional determinant in $\mathcal{S}_0$, we focus first on the term quadratic in ϕ_α, represented by the Feynman diagram in Fig 12.2: we parameterize it as $-\chi_0(k, i\omega_n)|\phi_\alpha(k, \omega_n)|^2$, and obtain for χ_0 the familiar Lindhard-like susceptibility

$$
\begin{aligned}
\chi_0(k, \omega_n) &= -T \sum_{\epsilon_n} \int \frac{d^2 p}{(2\pi)^2} \frac{1}{\left(-i(\omega_n + \epsilon_n) + \vec{v}_1 \cdot (\vec{k} + \vec{p})\right)} \frac{1}{\left(-i\epsilon_n + \vec{v}_2 \cdot \vec{p}\right)} \\
&= -\int \frac{d^2 p}{(2\pi)^2} \frac{f(\vec{v}_1 \cdot (\vec{k} + \vec{p})) - f(\vec{v}_2 \cdot \vec{p})}{i\omega_n + \vec{v}_1 \cdot (\vec{k} + \vec{p}) - \vec{v}_2 \cdot \vec{p}} \\
&= \chi_0(0, 0) - c_1 |\omega_n| - c_2 k^2 + \dots .
\end{aligned}
\tag{12.8}
$$

The two factors on the right hand side of the first equation represent the fermion propagators of the lines in Fig 12.2, $f(\varepsilon) \equiv 1/(e^{\varepsilon/T} + 1)$ is the Fermi function, ϵ_n is an odd Matsubara frequency that is summed over, while the frequency, ω_n, carried by the order parameter ϕ_α is even, and c_1 and c_2 are some constants. The most important term above is the $|\omega_n|$ in the expansion of χ_0 at small frequency: as we will see, it represents the damping of order parameter fluctuations due to the coupling to the gapless fermionic excitations in the vicinity of the points $\vec{k}_1$, $\vec{k}_2$ on the Fermi surface connected by the ordering wavevector $\vec{K}$. Its origin is a little easier to see in real frequencies where the corresponding expression in $\chi_0(k, \omega) = \dots + ic_1\omega + \dots$. So, let us examine the imaginary part of

$\chi_0(0, \omega)$, which from (12.8) is

$$
\begin{aligned}
\operatorname{Im}\left[\chi_0(0, \omega)\right] &= \pi \int \frac{d^2 p}{(2\pi)^2}\left[f(\vec{v}_1 \cdot \vec{p}) - f(\vec{v}_2 \cdot \vec{p})\right] \delta\left(\omega + \vec{p} \cdot (\vec{v}_1 - \vec{v}_2)\right) \\
&= \frac{\omega}{4\pi|\vec{v}_1 \times \vec{v}_2|}, \tag{12.9}
\end{aligned}
$$

and tell us that there is a linear in energy density of states of particle-hole excitations which couple to ϕ_α.

Inserting the result (12.8) into (12.5), and rescaling ϕ_α, we finally obtain Hertz's effective action for the Fermi liquid to spin density wave transition:

$$
\begin{aligned}
\mathcal{S}_H = \int \frac{d^d k}{(2\pi)^d} T \sum_{\omega_n} \frac{1}{2}\left[k^2 + \gamma|\omega_n| + r\right]\left|\phi_\alpha(k, \omega_n)\right|^2 \\
+ \frac{u}{4!} \int d^d x\, d\tau\left(\phi_\alpha^2(x, \tau)\right)^2 \tag{12.10}
\end{aligned}
$$

We have added a quartic term obtained from the expansion of the functional determinant, and its k and ω_n dependence has been neglected; this is generated from a fermion loop like in Fig 12.2, but with four external ϕ_α vertices. Phenomenological couplings γ and r have been introduced: γ represents the damping computed in (12.9) while r is the tuning parameter which will take the system from the Fermi liquid ($r > 0$ in the usual mean field theory of $\mathcal{S}_H$) to the spin density wave ($r < 0$). As we have already noted, this action is not to be taken seriously at $r < 0$, $T = 0$ as it does not capture the gap structure on the Fermi surface due to the dispersion (12.7). We will however still be able to use $\mathcal{S}_H$ in the portion of the $r < 0$, $T > 0$ phase diagram which is not too close to the region with spin density wave order. Also notice that $\mathcal{S}_H$ is written for general d dimension: a derivation very similar to the one above also works for $d = 3$. The field ϕ_α will henceforth be allowed to have an arbitrary number of components N; the discussion above was for the case $N = 3$, but other types of ordering lead to different values of N, *e.g.*, charge density wave order corresponds to $N = 1$.

The study of $\mathcal{S}_H$ will occupy the remainder of this chapter. It is useful to compare $\mathcal{S}_H$ with $\mathcal{S}_\phi$ in (3.11) or (8.2), which was studied in Part 2. The only difference is that the ω_n^2 frequency dependence in the quadratic term in the latter has been replaced by the $|\omega_n|$ term in $\mathcal{S}_H$. Also comparing with the dilute Bose gas in (11.1), we see a $-i\omega_n$ frequency dependence in the quadratic term of the boson action. The

$|\omega_n|$ term in the present case changes the nature of the critical quantum and thermal fluctuations, as will be shown in the following section.

12.2 Finite temperature crossovers

Let us first consider some basic scaling results like the value of the upper critical dimension and the scaling dimension of the various coupling. As we just noted, the only difference between $\mathcal{S}_H$ and the dilute Bose gas model analyzed in Section 11.3 is that $\mathcal{S}_H$ contains a $|\omega_n|$ frequency dependence in the quadratic term, while the Bose gas had $-i\omega_n$. Such a change, however, has essentially no effect on the initial scaling analysis of the $u = 0$ theory: the scaling dimension of the frequency dependence is the same in both cases. Therefore, we may immediately borrow some results from Section 11.3: the $u = 0$ theory has dynamic exponent $z = 2$, and the results (11.42) and (11.43) generalize to

$$
\begin{aligned}
\dim[\phi_\alpha] &= d/2 \\
\dim[r] &= 2 \\
\dim[u] &= 2 - d
\end{aligned}
\tag{12.11}
$$

The last result again identifies $d = 2$ as the upper-critical dimension. So above $d > 2$ we can compute physical properties in a perturbation series in u, and the final results will depend upon the microscopic, non-universal value of u. Our discussion below, like that in Section 11.3.2, will be restricted to the cases $2 < d < 4$. We will briefly comment on the case $d = 2$ later.

The computation of the $T > 0$ crossovers is essentially identical to that in Section 11.3.2: it leads to the phase diagram shown in Fig 12.3 [341] which is very similar to Fig 11.4. We integrate out the $\omega_n \neq 0$ modes and obtain an effective action for the static modes which takes the form $\mathcal{S}_{\phi,\text{eff}}$ in (8.23), and is characterized by the couplings R and U. To leading order in u we have $U = u$, while for R we have (analogous to (8.24), (8.25) and (11.60)):

$$
R = r + u \left(\frac{N+2}{6} \right) \int \frac{d^d k}{(2\pi)^d} \left(T \sum_{\omega_n \neq 0} \frac{1}{\gamma |\omega_n| + k^2 + r} + \frac{T}{k^2} \right.
$$
$$
\left. - \int \frac{d\omega}{2\pi} \frac{1}{\gamma |\omega| + k^2} \right)
\tag{12.12}
$$

The next step is the mathematical one of evaluating the frequency and
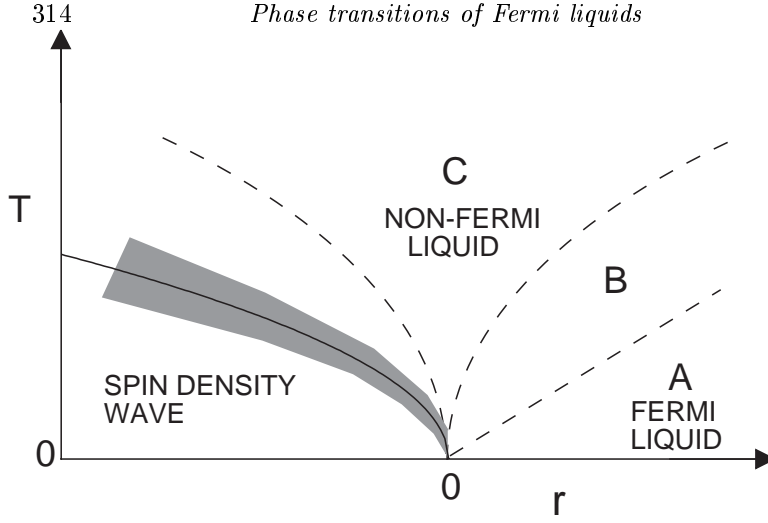
Fig. 12.3. Phase diagram of a Fermi liquid undergoing an instability to a spin density wave state for $2 \leq d < 4$. The regimes A, B, C and their crossover boundaries are described in the text. Compare to Fig 11.4 for the dilute Bose gas.

momentum sums and integrals in (12.12). The main subtlety, like in (8.38), is that while the result does depend upon a large momentum cutoff Λ, the divergent momentum integral can be separated out into a T-independent term. The remaining momentum integrals are convergent in the ultraviolet, and we can safely set $\Lambda \to \infty$ in them at the cost of ignoring some uninteresting and non-critical dependence on T. We show a few intermediate steps on how this separation is performed. The basic idea, as discussed below (5.66), is to subtract from each frequency summation the frequency integral of precisely the same quantity. In this manner we manipulate R into the form

$$R = r + u \left(\frac{N+2}{6} \right) [R_1 + R_2 + R_3] \qquad (12.13)$$

with

$$R_1 = \int \frac{d^d k}{(2\pi)^d} \left(T \sum_{\omega_n} \frac{1}{\gamma |\omega_n| + k^2 + r} - \int \frac{d\omega}{2\pi} \frac{1}{\gamma |\omega| + k^2 + r} \right)$$

$$R_2 = -T \int \frac{d^d k}{(2\pi)^d} \left(\frac{1}{k^2 + r} - \frac{1}{k^2} \right)$$

$$R_3 = \int^\Lambda \frac{d^d k}{(2\pi)^d} \int \frac{d\omega}{2\pi} \left(\frac{1}{\gamma|\omega| + k^2 + r} - \frac{1}{\gamma|\omega| + k^2} \right) \qquad (12.14)$$

It is easy to check that R_1 and R_2 are convergent at large momenta, and all of the cutoff dependence has been isolated in the T-independent term R_3. As discussed below (8.38), we can remove this cutoff dependence by adding and subtracting $r/(\gamma|\omega| + k^2)^2$ to the integrand in R_3: this yields a cutoff dependence term $\sim r\Lambda^{d-2}$. Notice that this cutoff dependence is a smooth linear function of r and so does not effect the remaining universal singular part. After evaluating the terms in (12.14), the final result for R can be written in the scaling form analogous to (8.39) and (11.62)

$$R = r(1 - c_2 u \Lambda^{d-2}) + \frac{u}{\gamma}(\gamma T)^{d/2} \left(\frac{N+2}{6} \right) L \left(\frac{r}{\gamma T} \right) \qquad (12.15)$$

where the universal scaling function $L(y)$ is given by

$$L(y) = \frac{1}{\pi} \int \frac{d^d k}{(2\pi)^d} \left[\ln \left(\frac{k^2}{2\pi} \right) - \psi \left(1 + \frac{k^2 + y}{2\pi} \right) + \frac{\pi + y}{k^2} \right], \qquad (12.16)$$

where ψ is the digamma function. We point out the now familiar property of all such crossover functions: it is analytic at $y = r/\gamma T = 0$ reflecting the absence of any thermodynamic singularity at $r = 0$, $T > 0$ (see Fig 12.3). From (12.16) it is easily seen that $L(y)$ is analytic for $y > -2\pi$; the singularity at $y = -2\pi$ is of no physical consequence as it is within the ordered phase.

Knowing the values of R and U, we can work out the predictions for physical observables. The expression for the order parameter correlations, correct for small u, is (compare (8.41) and (11.65)) is

$$\langle |\phi_\alpha(k, \omega)|^2 \rangle = \frac{1}{-i\omega + k^2 + \xi^{-2}} \qquad (12.17)$$

where from (8.26) and (8.12) we have (compare (11.66))

$$\xi^{-2} = R - Tu \left(\frac{N+2}{6} \right) \frac{2\Gamma((4-d)/2)}{(d-2)(4\pi)^{d/2}} R^{(d-2)/2}. \qquad (12.18)$$

As in (11.68) we can compute the free energy density, and obtain

$$\mathcal{F}(T, r) = \frac{TN}{2} \int \frac{d^d k}{(2\pi)^d} \left[\sum_{\omega_n} \ln(\gamma|\omega_n| + k^2 + r) + \ln \left(\frac{k^2 + \xi^{-2}}{k^2 + r} \right) \right], \qquad (12.19)$$

where the numerator of the second logarithm is the contribution of the $\omega_n = 0$ modes, while the remainder come from the $\omega_n \neq 0$ modes. Notice

that for $T > 0$, the expression (12.19) has no singularity at $r = 0$: this is as expected from the absence of a thermodynamic singularity in the middle of region C in Fig 12.3. It is advantageous to subtract out the free energy of the system at the critical point $r = 0$, $T = 0$ from the above (this was simply 0 for the dilute Bose gas) and evaluate $\Delta \mathcal{F} \equiv \mathcal{F}(T, r) - \mathcal{F}(0, 0)$; for this we get

$$\Delta \mathcal{F} = \frac{TN}{2} \int^{\Lambda} \frac{d^d k}{(2\pi)^d} \left[-\frac{2}{\pi} \int_0^{\infty} \frac{d\Omega}{(e^{\Omega/T} - 1)} \tan^{-1} \left(\frac{\gamma \Omega}{k^2 + r} \right) \right.$$

$$\left. + \frac{k^2 \ln(k^2) - (k^2 + r) \ln(k^2 + r)}{\pi \gamma} + \ln \left(\frac{k^2 + \xi^{-2}}{k^2 + r} \right) \right] + \ldots, (12.20)$$

where we have omitted background terms which are T-independent and only depend upon positive integer powers of r. The momentum integral has a remaining cut-off dependence which cannot be removed and does effect the singular T and r dependence: this is a consequence of being above the upper critical dimension.

We will discuss the implications of the above results for the order parameter susceptibility; thermodynamic properties follow from results like (12.20) and more explicit results are available in the literature [551, 432, 240]. In the low T 'Fermi liquid' region A in Fig 12.3, defined by $T \ll r/\gamma$, the susceptibility is given by (12.17); by evaluating the large y limit of (12.16) and inserting in (12.15) and (12.18) we get for the T dependence of the correlation length

$$\xi^{-2}(T) = \xi^{-2}(T = 0) + \frac{u\gamma}{r^{(4-d)/2}} \frac{(N + 2)\Gamma((4 - d)/2)}{36(4\pi)^{d/2}} T^2. \quad (12.21)$$

Notice the characteristic T^2 dependence of a Fermi liquid. Conversely, in the high T limit, $T \gg r/\gamma$, we take the $y \to 0$ limit of (12.16) and obtain the leading result

$$\xi^{-2}(T) = r + (\gamma T)^{d/2} \frac{(N + 2)u}{6\gamma} L(0) \quad (12.22)$$

where $L(0)$ is a number. In region B of Fig 12.3, $r \ll \gamma T \ll (\gamma r/u)^{2/d}$, the first term in (12.22) dominates, while in region C, $\gamma T \gg (\gamma |r|/u)^{2/d}$, the second T-dependent term is larger. So in the high T region C we have $\xi \sim T^{-3/4}$, which does not agree with the naive scaling estimate $\xi \sim T^{-1/z}$. As we noted in Sections 8.2.2 and 11.3.2, this violation appears because of the presence of a dangerously irrelevant coupling u. Note also that if we insert (12.22) into (12.17), the resulting dynamic

response function does not scale as a function of ω/T, and this is again because the present system is above its upper-critical dimension.

As noted earlier, the results above are analytic at $r = 0$ for $T > 0$, and so apply also for $r < 0$. For this case the correlation length diverges at a critical value of r, and this determines the position of the phase boundary in Fig 12.3 at $T = T_c(r)$, where to leading order in u

$$T_c(r) = \frac{1}{\gamma} \left[-\frac{6\gamma r}{(N+2)u} \right]^{2/d}.$$ (12.23)

Finally, the case of the system being in its upper-critical dimension, $d = 2$, is extremely similar to the corresponding case, $d = 3$, for the rotor/Ising models of Part 2. The renormalization group equations imply that the non-linearity u becomes logarithmically small as in (8.57); the physical properties can then be computed by precisely the same method discussed here, in a two-step integration of the non-zero frequency and then the zero frequency modes, both carried out in an expansion in powers of the effective u in (8.57).

12.3 Applications and extensions

Important applications of the spin density wave to Fermi liquid transition appear in the study of the heavy fermion compounds [23, 341, 504, 103, 104]. A case that has been intensively studied recently is $CeCu_{6-x}Au_x$ [415, 479, 517, 447], and there is also related work on $CeCu_{6-x}Ag_x$ [226]. The Cambridge group [257, 307, 192, 328] has examined a different series of Ce compounds ($CeNi_2Ge_2$, $CePd_2Si_2$ and $CeIn_3$) and these show similar transitions under pressure, but at stoichiometric compositions at which disorder is quite small; recently [328], they have reported the existence of superconductivity near the antiferromagnet/Fermi liquid quantum critical point. A comprehensive study of quantum transitions involving loss of antiferromagnetic order in metallic and insulating phases of V_2O_3 has also been performed recently [37]. A puzzling feature of present experiments in the Ce compounds and V_2O_3 is that while thermodynamic and transport properties are in rough agreement with the theory discussed in this chapter, the dynamic neutron scattering experiments show clear scaling of the response functions as a function ω/T (where ω is the measurement frequency). Such scaling was discussed at length in Part 2, but is *only* a property of quantum critical points below their upper critical dimension; in contrast, the theories used to explain thermodynamic measurements are above

their upper critical dimension, and do not predict scaling of response functions as a function of ω/T—resolving this inconsistency is an important direction for future work. Some recent theoretical work on quantum transitions between spin density waves and Fermi liquids is in Refs [354, 261, 348, 379], and an interesting perspective on open questions has been given by Coleman [102].

The interpretation of the intermediate temperature properties of the un- and lightly doped cuprates in terms of the vicinity of a quantum critical point to an antiferromagnetically ordered state was discussed in Refs [440, 97]. In the same context, the possible relevance of a $z = 2$ spin density wave transition of the type considered here, and its crossover to the $z = 1$ transition studied in Part 2 have been discussed in Refs [432, 40, 434]. More recently, greater interest has focused on the charge degrees of freedom [495, 57], with emerging evidence that the doped holes in the cuprates form striped arrangements, at least over intermediate time scales; this phenomenon has been addressed in $z = 2$ theories of charge density wave formation of the type discussed here [74, 75, 76] or in effective models of electronic motion on fluctuating stripes [140, 541, 275, 542]. The true situation probably involves an intricate interplay of both charge and spin driven effects [512, 505, 506], and a predominance of the $z = 1$ physics of Part 2, as appears to be the case in the latest neutron scattering experiments [2].

In our discussion of the origin of spin density wave order, we assumed that different portions of the Fermi surface were not 'nested'. The nested case has been discussed in Refs [92, 18].

The discussions in this chapter do not apply directly to the case of the Stoner transition [481] from a Fermi liquid to a partially polarized ferromagnet; this is the limiting case of a spin density wave with wavevector $\vec{Q} = 0$. The expansion (12.8) has a different form for this case as was discussed in Refs [225, 341]. The presence of additional wavevector dependent non-analyticities has been pointed out recently by Belitz and Kirkpatrick [273, 519, 49, 48], who have also emphasized that these drastically modify the traditional [225] results. Experimental studies of the ferromagnetic case may be found in the work of the group of Lonzarich [256] and the results are in general agreement with self-consistent Hartree calculations in the spirit of this chapter.

This is also an appropriate point to mention work on quantum transitions of BCS superconductors formed by pairing between the electrons of the Fermi liquids considered here. Fluctuation and finite temperature inelastic effects in the vicinity of a quantum transition between a

superconductor and a Fermi liquid in a clean system have been considered recently [274, 397]. The transition between a BCS superconductor and a Fermi liquid in disordered systems has also been the subject of considerable interest [320, 148, 149]. Some interesting numerical simulations have proposed the existence of a second order quantum transition between a BCS superconductor and an antiferromagnetic Mott insulator [29]; the interplay between these two phases has also been the focus of work on models with higher internal symmetry groups [545, 224].

13
Heisenberg spins: ferromagnets and antiferromagnets

Part 2 of this book dealt with the magnetically ordered and quantum paramagnetic phases of models of N-component quantum rotors. In Chapter 10 we showed how the $N = 2$ rotors could be mapped onto certain boson models in the vicinity of a phase transition between a Mott insulator and a superfluid. In this chapter we shall consider models of Heisenberg spins: these directly represent the spin fluctuations of physical electrons in insulators or other systems with an energy gap towards charged excitations (*e.g.*, certain quantum Hall states). We shall describe the conditions under which certain models of Heisenberg spins reduce to $N = 3$ quantum rotor models, thus providing the long-promised physical motivation for studying the latter models; recall that a preview of this mapping already appeared in Section 5.1.1.1. We shall also discuss the physical properties of Heisenberg spin models under conditions in which they do not map onto the rotor models of Part 2.

We will deal with lattice models with the Hamiltonian

$$H_S = -\sum_{i,j} J_{ij}\hat{\mathbf{S}}_i \cdot \hat{\mathbf{S}}_j - \mathbf{H} \cdot \sum_i \hat{\mathbf{S}}_i. \tag{13.1}$$

Here the magnetic field $\mathbf{H}$ is precisely the same (with no overall scale factor) as that appearing in the rotor Hamiltonian (5.1): $\mathbf{H}$ couples to a conserved total spin (or for the rotors the total angular momentum) which, as we will see, commutes with the rest of the Hamiltonian. The $\hat{\mathbf{S}}_i$ are Heisenberg spin operators whose basic properties were introduced in Section 5.1.1.1: they satisfy the commutation relations (5.8) on each site i, and act on the $2S + 1$ states (5.9) of the spin S representation on each site. The J_{ij} are a set of translationally-invariant exchange interactions between these sites.

We will begin in Section 13.1 by showing how to set up a path integral

for systems with states restricted in the manner (5.9,5.10) on each site. Then Section 13.2 will consider the properties of *ferromagnets* in which all $J_{ij} > 0$, and the ground state is the fully polarized state with all spins parallel and the total spin takes its maximum possible value. The properties of antiferromagnets in which the ground state has negligible total spin will be discussed in Section 13.3–these are likely to arise when all $J_{ij} < 0$. Finally Section 13.4 will consider more complex situations with partial uniform polarization of the spins, which is accompanied by a certain 'canted' order in dimensions $d > 1$.

13.1 Coherent state path integral

We have previously encountered the coherent state path integral in Section 10.2 where we introduced, following Refs [360, 456], a path integral representation of canonical bosons. An important feature of the path integral was the 'Berry phase' term $b^\dagger db/d\tau$ in (10.19) which accounted for the kinematics of ordinary bosons, and played an important role in the structure of the Mott insulating phases and the nature of their transitions to the superfluid. In this section we will present a reasonably complete derivation of the corresponding path integral for the quantum mechanics of the spin states (5.9). Many derivations of this path integral exist in the literature, but we shall follow here the approach used in Ref [400] which has the advantage of explicitly maintaining spin rotation invariance. The reader is also referred to a collection of reprints [277] for further information on coherent states and their relationship to path integrals.

We shall deal in this section with a single Heisenberg spin, and will therefore drop the site index. There is no loss of generality in this, as the same manipulations can be carried out independently on each site. The derivation of any path integral proceeds by the insertion of a complete set of states at infinitesimal intervals in time upon the time evolution operator of the system. It would clearly pay to choose a set of states under which the matrix elements of $\hat{\mathbf{S}}$ are simple: for this reason the states in (5.9) are not convenient. Instead, we shall use the so-called spin-coherent states. These are an infinite set of states $|\mathbf{N}\rangle$, labeled by the points $\mathbf{N}$ on the surface of the unit sphere; so $\mathbf{N}$ is a three-component vector satisfying $\mathbf{N}^2 = 1$. As there are only a total of $2S + 1$ independent states, these states clearly cannot be mutually orthogonal.

They are normalized to unity

$$\langle \mathbf{N}|\mathbf{N}\rangle = 1, \qquad (13.2)$$

$\langle \mathbf{N}|\mathbf{N}'\rangle \neq 0$ for $\mathbf{N} \neq \mathbf{N}'$, and satisfy the completeness relation

$$\int \frac{d\mathbf{N}}{2\pi} |\mathbf{N}\rangle\langle\mathbf{N}| = 1 = \sum_{m=-S}^{S} |S,m\rangle\langle S,m|, \qquad (13.3)$$

where the integral of $\mathbf{N}$ is over the unit sphere. Because of their non-orthogonality, these states are called 'over-complete'. What makes them extremely useful is that the diagonal expectation value of the operator $\hat{\mathbf{S}}$ is very simple:

$$\langle \mathbf{N}|\hat{\mathbf{S}}|\mathbf{N}\rangle = S\mathbf{N}. \qquad (13.4)$$

So the state $|\mathbf{N}\rangle$ is almost like a classical spin of length S pointing in the $\mathbf{N}$ direction; indeed, the spin coherent states are the minimum uncertainty states localized as much in the $\mathbf{N}$ direction as the principles of quantum mechanics will allow, and in the large S limit, $|\mathbf{N}\rangle$ reduces to a classical spin in the $\mathbf{N}$ direction.

The relations (13.2), (13.3), and (13.4) define the spin coherent states. Let us explicitly construct them. For $\mathbf{N} = (0,0,1)$, the state $|\mathbf{N}\rangle$ is easy to determine; we have

$$|\mathbf{N} = (0,0,1)\rangle = |S, m = S\rangle \equiv |\Psi_0\rangle \qquad (13.5)$$

We have labeled this particular coherent state as a reference state $|\Psi_0\rangle$ as it will be needed frequently in the following. Now it should be clear that for other values of $\mathbf{N}$ we can obtain $|\mathbf{N}\rangle$ simply by acting on $|\Psi_0\rangle$ by an operator which performs a $SU(2)$ rotation from the direction $(0,0,1)$ to the direction $\mathbf{N}$. In this manner we obtain the following explicit representation for the coherent state $|\mathbf{N}\rangle$

$$|\mathbf{N}\rangle = \exp\left(z\hat{S}_+ - z^*\hat{S}_-\right)|\Psi_0\rangle \qquad (13.6)$$

where the complex number z is related to the vector $\mathbf{N}$. This relationship is simplest in spherical co-ordinates; if we parameterize $\mathbf{N}$ as

$$\mathbf{N} = (\sin\theta\cos\phi, \sin\theta\sin\phi, \cos\theta) \qquad (13.7)$$

then

$$z = -\frac{\theta}{2}\exp(-i\phi). \qquad (13.8)$$

We leave it as an exercise for the reader to verify that (13.6) satisfies

(13.2), (13.3) and (13.4); this verification is aided by the knowledge that the value of the expression $\exp(-i\mathbf{a} \cdot \hat{\mathbf{S}})\hat{\mathbf{S}}\exp(i\mathbf{a} \cdot \hat{\mathbf{S}})$, where $\mathbf{a}$ is some vector, is determined solely by the spin commutation relations (5.8), and can therefore be worked out by temporarily assuming that the $\hat{\mathbf{S}}$ are twice the Pauli matrices–the result, when expressed in terms of $\hat{\mathbf{S}}$, is valid for arbitrary S.

It will be useful for our subsequent formulation to rewrite the above results in a somewhat different manner, making the $SU(2)$ symmetry more manifest. Define the 2×2 matrix of operators $\hat{\mathcal{S}}$ by

$$\hat{\mathcal{S}} = \begin{pmatrix} \hat{S}_z & \hat{S}_x - i\hat{S}_y \\ \hat{S}_x + i\hat{S}_y & -\hat{S}_z \end{pmatrix}. \tag{13.9}$$

Then Eqn. (13.5) can be rewritten as

$$\langle \mathbf{N}|\hat{\mathcal{S}}_{\alpha\beta}|\mathbf{N}\rangle = SW_{\alpha\beta}, \tag{13.10}$$

where the matrix W is

$$W = \begin{pmatrix} N_z & N_x - iN_y \\ N_x + iN_y & -N_z \end{pmatrix} \equiv \mathbf{N} \cdot \vec{\sigma} \tag{13.11}$$

where $\vec{\sigma}$ are the Pauli matrices. So instead of labeling the coherent states with the unit vector $\mathbf{N}$, we could equally well use the traceless Hermitean matrix W. Furthermore, there is a simple relationship between W and the complex number z. In particular, if we use the spin-1/2 version of the operator in Eqn. (13.6)

$$U = \exp\left[\begin{pmatrix} 0 & z \\ -z^* & 0 \end{pmatrix}\right] \tag{13.12}$$

(U is thus a 2×2 matrix), then we find

$$W = U\sigma_z U^\dagger \tag{13.13}$$

We proceed to the derivation of the coherent state path integral for the partition function

$$Z = \operatorname{Tr}\exp(-H(\hat{\mathbf{S}})/T); \tag{13.14}$$

we will restrict the following discussion to Hamiltonians in which H is a linear function of any given $\hat{\mathbf{S}}$ on a fixed site. The H in Eqn. (13.1) is certainly of this type. The transformation of Z into a path-integral proceeds along the same lines as that discussed in Refs [360, 456] for

bosons. We break up the exponential into a large number of exponentials of infinitesimal time evolution operators

$$Z = \lim_{M \to \infty} \prod_{i=1}^{M} \exp(-\Delta\tau_i H(\hat{\mathbf{S}})), \tag{13.15}$$

where $\Delta\tau_i = 1/MT$, and insert a set of coherent states between each exponential by using the identity (13.3); we label the state inserted at a 'time' τ by $|\mathbf{N}(\tau)\rangle$. We can then evaluate the expectation value of each exponential by use of the identity (13.4)

$$\begin{aligned}
\langle \mathbf{N}(\tau)| \exp(-\Delta\tau H(\hat{\mathbf{S}}))|\mathbf{N}(\tau+\Delta\tau)\rangle \\
\approx \langle \mathbf{N}(\tau)|1 - \Delta\tau H(\hat{\mathbf{S}})|\mathbf{N}(\tau+\Delta\tau)\rangle \\
\approx 1 - \Delta\tau \langle \mathbf{N}(\tau)|\frac{d}{d\tau}|\mathbf{N}(\tau)\rangle - \Delta\tau H(S\mathbf{N}) \\
\approx \exp\left(-\Delta\tau \langle \mathbf{N}(\tau)|\frac{d}{d\tau}|\mathbf{N}(\tau)\rangle - \Delta\tau H(S\mathbf{N})\right). \tag{13.16}
\end{aligned}$$

In each step we have retained expressions correct to order $\Delta\tau$. The coherent states at time τ and $\tau + \Delta\tau$ can in principle have completely different orientations, so, a priori, it is not clear that expanding these states in derivatives of time is a valid procedure. This is a subtlety that afflicts all coherent state path integrals, and has been discussed more carefully by Negele and Orland [360]: the conclusion of their analysis is that except for the single 'tadpole' diagram where a point-splitting of time becomes necessary, this expansion in derivatives of time always leads to correct results. In any case, the resulting coherent state path integral is a formal expression which cannot be directly evaluated, and in case of any doubt one should always return to the original discrete time product in (13.15).

Keeping in mind the above caution, we insert (13.16) into (13.15), take the limit of small $\Delta\tau$ and obtain the following functional integral for Z

$$Z = \int_{\mathbf{N}(0)=\mathbf{N}(1/T)} \mathcal{D}\mathbf{N}(\tau) \exp\left\{-\int_0^{1/T} d\tau \left[\mathcal{S}_B + H(S\mathbf{N}(\tau))\right]\right\}, \tag{13.17}$$

where

$$\mathcal{S}_B = \langle \mathbf{N}(\tau)|\frac{d}{d\tau}|\mathbf{N}(\tau)\rangle \tag{13.18}$$

and $H(S\mathbf{N})$ is obtained by replacing every occurrence of $\hat{\mathbf{S}}$ in the Hamiltonian by $S\mathbf{N}$. The promised Berry phase term is $\mathcal{S}_B$, and it represents

the overlap between the coherent states at two infinitesimally separated times. It can be shown straightforwardly from the normalization condition, $\langle \mathbf{N} | \mathbf{N} \rangle = 1$, that $\mathcal{S}_B$ is pure imaginary. In the remainder of this section we will manipulate $\mathcal{S}_B$ into a physically more transparent form using the expressions above for the coherent states. For the case of the boson coherent state path integral, it is precisely the analog of $\mathcal{S}_B$ which becomes $b^\dagger (\partial b / \partial \tau)$ in (10.19).

Clearly, the τ-dependence of $\mathbf{N}(\tau)$ implies a τ dependent $z(\tau)$ through (13.8). From (13.6) we have therefore

$$\frac{d}{d\tau} |\mathbf{N}(\tau)\rangle = \frac{d}{d\tau} \exp\left(z(\tau)\hat{S}_+ - z^*(\tau)\hat{S}_- \right) |\Psi_0\rangle \tag{13.19}$$

Taking this derivative is however not so simple: notice that if an operator $\hat{O}$ does not commute with its derivative $d\hat{O}/d\tau$ then

$$\frac{d}{d\tau} \exp(\hat{O}) \neq \frac{d\hat{O}}{d\tau} \exp(\hat{O}) \tag{13.20}$$

The correct form of this result is in fact

$$\frac{d}{d\tau} \exp(\hat{O}) = \int_0^1 du \, \exp(\hat{O}(1-u)) \frac{d\hat{O}}{d\tau} \exp(\hat{O}u), \tag{13.21}$$

where u is just a dummy integration variable. This result can be checked by expanding both sides in powers of $\hat{O}$ and verifying that they agree term by term. More constructively, a 'hand-waving' derivation can be given as follows

$$\frac{d}{d\tau} \exp(\hat{O}) = \frac{d}{d\tau} \exp\left(\hat{O} \int_0^1 du \right)$$

$$= \lim_{M \to \infty} \frac{d}{d\tau} \exp\left(\sum_{i=1}^{M} \hat{O} \Delta u_i \right) \quad \text{with } \Delta u_i = 1/M$$

$$\approx \lim_{M \to \infty} \frac{d}{d\tau} \prod_{i=1}^{M} \exp\left(\hat{O} \Delta u_i \right)$$

$$\approx \lim_{M \to \infty} \sum_{j=1}^{M} \prod_{i=1}^{j} \exp\left(\hat{O} \Delta u_i \right) \frac{d\hat{O}}{d\tau} \Delta u_j \prod_{i=j+1}^{M} \exp\left(\hat{O} \Delta u_i \right) \tag{13.22}$$

Finally, taking the limit $M \to \infty$, we obtain the needed result (13.21). Now using (13.19) and (13.21) we find

$$\mathcal{S}_B = \int_0^{1/T} d\tau \, \langle \mathbf{N}(\tau) | \frac{d}{d\tau} | \mathbf{N}(\tau) \rangle$$

$$= \int_0^{1/T} d\tau \int_0^1 du \langle \mathbf{N}(\tau, u)| \left(\frac{\partial z}{\partial \tau} \hat{S}_+ - \frac{\partial z^*}{\partial \tau} \hat{S}_- \right) |\mathbf{N}(\tau, u)\rangle \ (13.23)$$

where $\mathbf{N}(\tau, u)$ is defined by

$$|\mathbf{N}(\tau, u)\rangle = \exp \left(u \left(z(\tau) \hat{S}_+ - z^*(\tau) \hat{S}_- \right) \right) |\Psi_0\rangle \qquad (13.24)$$

From this definition, three important properties of $\mathbf{N}(\tau, u)$ should be apparent

$$\mathbf{N}(\tau, u = 1) \equiv \mathbf{N}(\tau),$$
$$\mathbf{N}(\tau, u = 0) = (0, 0, 1),$$
and $\mathbf{N}(\tau, u)$ moves with u along the great circle
between $\mathbf{N}(\tau, u = 0)$ and $\mathbf{N}(\tau, u = 1) \qquad (13.25)$

We can visualize the dependence on u by imagining a *string* connecting the physical value of $\mathbf{N}(\tau) = \mathbf{N}(\tau, u = 1)$ to the North pole, along which u decreases to 0. Associated with each $\mathbf{N}(\tau, u)$ we can also define a u-dependent $W(\tau, u)$ as in Eqn. (13.11); the analog of (13.25) is $W(\tau, u = 1) \equiv W(\tau)$ and $W(\tau, u = 1) = \sigma_z$. A simple explicit expression for $W(\tau, u)$ is also possible: we simply generalize (13.12) to

$$U(\tau, u) = \exp \left[u \begin{pmatrix} 0 & z \\ -z^* & 0 \end{pmatrix} \right] \qquad (13.26)$$

then the relationship (13.13) gives us $W(\tau, u)$. Now we can use the expression (13.10) to rewrite (13.23) as

$$\mathcal{S}_B = S \int_0^{1/T} d\tau \int_0^1 du \left[\frac{\partial z}{\partial \tau} W_{21}(\tau, u) - \frac{\partial z^*}{\partial \tau} W_{12}(\tau, u) \right], \qquad (13.27)$$

As everything is a periodic function of τ, we may freely integrate this expression by parts and obtain

$$\mathcal{S}_B = -S \int_0^{1/T} d\tau \int_0^1 du \mathrm{Tr} \left[\begin{pmatrix} 0 & z(\tau) \\ -z^*(\tau) & 0 \end{pmatrix} \partial_\tau W(\tau, u) \right]. \qquad (13.28)$$

where the trace is over the 2×2 matrix indices. The definitions (13.13) and (13.26) can be used to easily establish the identity

$$\begin{pmatrix} 0 & z(\tau) \\ -z^*(\tau) & 0 \end{pmatrix} = -\frac{1}{2} W(\tau, u) \frac{\partial W(\tau, u)}{\partial u}, \qquad (13.29)$$

which when inserted into (13.28) yields the expression for $\mathcal{S}_B$ in one of

its final forms

$$\mathcal{S}_B = \int_0^{1/T} d\tau \int_0^1 du \left[\frac{S}{2} \text{Tr} \left(W(\tau, u) \frac{\partial W(\tau, u)}{\partial u} \frac{\partial W(\tau, u)}{\partial \tau} \right) \right] \quad (13.30)$$

An expression for $\mathcal{S}_B$ solely in terms of $\mathbf{N}(\tau, u)$ can be obtained by substituting in (13.11); this yields the final expression for $\mathcal{S}_B$, which when inserted in (13.17) gives us the coherent state path integral for a spin:

$$\mathcal{S}_B = iS \int_0^{1/T} d\tau \int_0^1 du \, \mathbf{N} \cdot \left(\frac{\partial \mathbf{N}}{\partial u} \times \frac{\partial \mathbf{N}}{\partial \tau} \right) \quad (13.31)$$

This expression has a simple geometric interpretation. The function $\mathbf{N}(\tau, u)$ is a map from the rectangle $0 \leq \tau \leq 1/T$, $0 \leq u \leq 1$ to the unit sphere. As $\mathbf{N}$ moves from $\mathbf{N}(\tau)$ to $\mathbf{N}(\tau + \Delta\tau)$ it drags along the string connecting it to the North pole represented by the u dependence of $\mathbf{N}(\tau, u)$ (recall (13.25)). It is easy to see that the contribution to $\mathcal{S}_B$ of this evolution is simply iS times the oriented area swept out by the string. The value of this area clearly depends upon the fact that $u = 0$ end of the string was pinned at the North pole: this was a 'gauge' choice, and by choosing the phases of the coherent states differently, we could have pinned the point $u = 0$ anywhere on the sphere. However when we consider the complete integral over τ in (13.31), the boundary condition $\mathbf{N}(1/T) = \mathbf{N}(0)$ (required by the trace in (13.14) shows that $\mathbf{N}(\tau)$ sweeps out a closed loop on the unit sphere. Then the total τ integral in (13.31) is the area contained within this loop, and is independent of the choice of the location of the $u = 0$ point. Actually this last statement is not completely correct: the 'inside' of a closed loop is not well-defined and the location of the $u = 0$ point makes the oriented area uncertain modulo 4π (which is the total area of the unit sphere). So the net contribution of $e^{\mathcal{S}_B}$ is uncertain up to a factor of $e^{i4\pi S}$. For consistency, we can now demand that this arbitrary factor always equal unity, which, of course, leads to the familiar requirement that $2S$ be an integer.

13.2 Quantized ferromagnets

We turn to the lattice model H_S in (13.1), and consider the case of ferromagnetic interactions where all $J_{ij} > 0$. In this case, the state with all spins parallel $\prod_i |S, S\rangle_i$ is the exact ground state (see, *e.g.*, Ref. [27]; we have assumed that the field $\mathbf{H}$ points along the spin quantization z axis). The adjective 'quantized' in the title refers to the fact that the

magnetization density, M_0, (this is magnitude of the expectation value of the total spin magnetization $\sum_i \hat{\mathbf{S}}_i$ divided by the system volume) is pinned at a simple value which can be determined a priori, and which does *not* vary as the exchange constants J_{ij} are varied. In Section 13.4, we will meet examples of quantized ferromagnets in which the magnetic moment is quantized, but not at a fully polarized value: fractional quantization is also possible, but in every case twice the average total spin moment per unit cell is an integer. The discussion in this chapter will apply to the low energy properties of all such quantized ferromagnets, but will only explicitly refer to the fully polarized case.

Apart from their quantized moment, the characteristic property of a quantized ferromagnet is that the only low-lying excitation which carries spin is a 'spin-wave' which arises from a slow rotation of the orientation of the ordered moment. Many readers may be familiar with the fact that the wave function of a single spin-wave excitation can also be written down exactly for a fully polarized, quantized ferromagnet: these well-known results will also emerge below. The purpose of our discussion shall be two-fold: (*i*) to obtain a continuum field theory of the low-lying excitations of the quantized ferromagnet, and to understand its behavior under a scaling transformation, and (*ii*) to use the continuum theory to systematically enumerate the parameters required describe the low T properties of such ferromagnets.

We begin by constructing the continuum field theory for the low-lying excitations above the fully-polarized ferromagnetic ground state. It is reasonable to expect that these will consist of fluctuations in which the orientations of the spins varies slowly from site to site. We start with the functional integral like (13.17) for the spin orientation $\mathbf{N}_i(\tau)$ on each site i, and perform a gradient expansion by introducing the continuum field $\mathbf{N}(x, \tau)$. Keeping terms up to second spatial derivatives we obtain for the partition function $Z = \mathrm{Tr} e^{-H_S/T}$ [250]:

$$Z = \int \mathcal{D}\mathbf{N}(x, \tau)\delta(\mathbf{N}^2 - 1) \exp\left(-\int_0^{1/T} d\tau \int d^d x \mathcal{L}_F\right)$$

$$\mathcal{L}_F = iM_0 \int_0^1 du \mathbf{N} \cdot \left(\frac{\partial \mathbf{N}}{\partial u} \times \frac{\partial \mathbf{N}}{\partial \tau}\right) - M_0 \mathbf{N} \cdot \mathbf{H} + \frac{\rho_s}{2}(\nabla \mathbf{N})^2, \quad (13.32)$$

where $M_0 \equiv S/v$ is the magnetization density of the ground state, v is the volume per site, and ρ_s is the spin stiffness. We introduced the analogous stiffness for the rotor model in Section 5.3.3; here, the gradient

expansion upon the partition function of H_S gives us

$$\rho_s = \frac{S^2}{2v} \sum_m J_r x_{m1}^2,$$ (13.33)

where the J_m are the set of exchange constants coupling a given site i to the other sites separated from i by $(x_{m1}, x_{m2} \ldots x_{md})$; the sum over m includes separate terms for $\vec{x}_m$ and $-\vec{x}_m$. The continuum theory (13.32) should really be regarded as a convenient schematic representation of the quantum ferromagnet, and we will often need to go back to the underlying lattice model H_S to regulate short distance singularities.

We consider the behavior of $\mathcal{L}_F$ under a rescaling transformation [404] at $T = 0$. The continuum theory is characterized by two dimensionful couplings M_0 and ρ_s, and despite the non-linear constraint in (13.32), some special properties of the quantum theory make it possible to determine their exact renormalization group flow equations (this should be contrasted from the rotor theory (5.16) where no such exact results were available). First, we noticed at the end of Section 13.1 that the single spin Berry phase was uncertain up to an additive constant of $4\pi S$, and this imposed the requirement that S be integer or half-integer. Precisely the same argument applied to the Berry phase of the continuum ferromagnet (13.32) in a hypercubic box of volume L^d, implies $2M_0 L^d$ must be an integer (this is just a fancy way of saying that the continuum ferromagnet must model an integral number of spins). This integer cannot change under any scaling transformation, and as L transform as a physical length, the invariance of $M_0 L^d$ leads to the exact flow equation

$$\frac{dM_0}{d\ell} = dM_0.$$ (13.34)

This equation describes the quantization of the average magnetic moment at its fully saturated value.

A closely related scaling equation holds for ρ_s, and this follows from the exactly known single spin-wave spectrum. To prepare for some future computations, we derive this by going back to the lattice Hamiltonian, H_S, and then taking the continuum limit of the resulting response functions. The most convenient formalism for computations is provided by the Dyson-Maleev transformation [132, 325] from the spin operators $\hat{\mathbf{S}}_i$ to Bose operators $\hat{b}_i$. Explicitly, the mapping is

$$\hat{S}_{+i} = \sqrt{2S}\hat{b}_i^\dagger$$

$$\hat{S}_{-i} = \sqrt{2S}\left(\hat{b}_i - \frac{1}{2S}\hat{b}_i^\dagger\hat{b}_i\hat{b}_i\right)$$

$$\hat{S}_z = -S + \hat{b}_i^\dagger \hat{b}_i. \tag{13.35}$$

Along with the constraint $\hat{b}_i^\dagger \hat{b}_i \leq 2S$, this defines an exact mapping between the Hilbert space of the spin S spins ($2S + 1$ states per spin) and the bosons ($2S + 1$ possible boson occupation numbers); in practice, one does not even have to impose the constraint $\hat{b}_i^\dagger \hat{b}_i \leq 2S$, as all matrix elements out of the physical sector vanish. The reader can verify that the operators in (13.35) do indeed satisfy the commutation relations (5.8). The relations (13.35) do not satisfy the hermiticity requirement $\hat{S}_{+i} = (\hat{S}_{-i})^\dagger$, but this can be repaired by performing a similarity transformation on the space of spin states: the reader should consult Ref [16] for more information, as here we shall mainly use (13.35) as a black-box tool. Inserting (13.35) into (13.1), and Fourier transforming to momentum space by defining $\hat{b}(\vec{k}) = \sqrt{v} \sum_i \hat{b}_i e^{-i\vec{k}\cdot\vec{x}}$ (these Bose operators then satisfy the canonical continuum commutation relations $[\hat{b}(\vec{k}), \hat{b}^\dagger(\vec{k}')] = (2\pi)^3 \delta^d(\vec{k} - \vec{k}')$), the Hamiltonian becomes

$$H_S = \int \frac{d^d k}{(2\pi)^d} \left\{ S\left[J(0) - J(\vec{k}) \right] + H \right\} \hat{b}^\dagger(\vec{k})\hat{b}(\vec{k}) +$$

$$\frac{v}{2} \int \prod_{i=1}^4 \frac{d^d k_i}{(2\pi)^d} (2\pi)^d \delta^d(\vec{k}_1 + \vec{k}_2 - \vec{k}_3 - \vec{k}_4) \left[J(\vec{k}_1) - J(\vec{k}_1 - \vec{k}_4) \right]$$

$$\times \hat{b}^\dagger(\vec{k}_1)\hat{b}^\dagger(\vec{k}_2)\hat{b}(\vec{k}_3)\hat{b}(\vec{k}_4) \tag{13.36}$$

where all momentum integrals are over the first Brillouin zone of the lattice, and

$$J(\vec{k}) = \sum_m J_m e^{-i\vec{k}\cdot\vec{x}_m}. \tag{13.37}$$

This bosonic form for H_S can be analyzed by the methods developed in Chapter 11 for (11.1). The ground state is the vacuum, $|0\rangle$, with no $\hat{b}$ particles (the fully polarized ferromagnet), while the lowest excitations are single boson states, $\hat{b}^\dagger(\vec{k})|0\rangle$, ('spin waves') which are exact eigenstates of H_S with energy $\varepsilon_{\vec{k}} = S(J(0) - J(\vec{k})) + H$. We have $\varepsilon_{\vec{k}} > 0$ for all $\vec{k}$, which indicates that the choice of the no boson state as the ground state is a consistent one. At $T = 0$, the one particle propagator is given exactly by the free particle propagator, as in (11.50), for there are no other particles present. Taking the small momentum limit of this propagator, and using the correspondence between the continuum fields

$$\hat{b}^\dagger(\vec{k}, \omega_n) = (M_0/2)^{1/2} N_+(-\vec{k}, -\omega_n) \tag{13.38}$$

which follows from our definitions above ($N_\pm = N_x \pm i N_y$), we obtain

an exact result for a two-point correlator of (13.32)

$$\left\langle N_-(-\vec{k}, -\omega_n)N_+(\vec{k}, \omega_n) \right\rangle = \frac{2}{-i\omega_n M_0 + \rho_s k^2 + M_0 H}. \tag{13.39}$$

This represents the propagation of spin waves with the exact dispersion $\varepsilon_k = (\rho_s/M_0)k^2 + H$. The consistency of this dispersion with the scaling transformation requires $\dim[H] = z$ (as before in (5.42)), and the exact scaling equation

$$\frac{d\rho_s}{d\ell} = (d + z - 2)\rho_s. \tag{13.40}$$

As the spin-wave disperses quadratically with momentum at small k, it is convenient to choose $z = 2$ (other choices are also permissible, as physical observables will have compensating scale dependence arising from that of ρ_s).

The exact results (13.34), (13.39) and (13.40) are strongly reminiscent of the behavior of the Bose gas in Section 11.8. In both cases, the simplicity is due to the fluctuationless nature of the ground state and the exactly known single particle excitations. For the case of the Bose gas we had an additional non-linearity u, whose renormalization was determined by examining the two-particle scattering amplitude. In the present situation, the dimensionful parameters ρ_s and M_0 determine both the single particle dispersion (13.39) and the strengths of the non-linear couplings. It might therefore seem that the finite T properties of (13.32) must be given by universal functions of T, and the *bare* couplings ρ_s and M_0, consistent with the requirements of scaling and engineering dimensional analysis. However, this will be only the case if a short distance cutoff scale (explicitly present in (13.36) but not in (13.32)) did not influence the low energy properties. Such a scale might be required to cut-off large momentum (ultraviolet) divergences of momentum integrals over virtual excitations. Motivated by the structure of the Bose gas problem in Section 11.3, we look for ultraviolet divergences in the two spin-wave scattering amplitude at $T = 0$ (we need not consider $T > 0$ explicitly as the finite T corrections all involve Bose functions which fall off exponentially at large momentum). For the Bose gas problem we found ultraviolet divergences for $d \geq 2$, and this identified $d = 2$ as the upper critical dimension below which the universality of the continuum theory was robust. We will compute the on-shell T matrix of two spin waves coming in with momenta $\vec{k}_1$ and $\vec{k}_2$, and scattering into spin waves with momenta $\vec{k}_1 + \vec{q}$ and $\vec{k}_2 - \vec{q}$. Conservation of energy requires

$$J(\vec{k}_1) + J(\vec{k}_2) = J(\vec{k}_1 + \vec{q}) + J(\vec{k}_2 - \vec{q}). \tag{13.41}$$

To zeroth order in $1/S$, the Hamiltonian (13.36) gives us the bare T-matrix element $v[J(\vec{k}_1 + \vec{q}) + J(\vec{k}_2 - \vec{q}) - J(\vec{k}_1 + \vec{q} - \vec{k}_2) - J(\vec{q})]$. The first order in $1/S$ correction to the T-matrix is given by the first diagram in Fig 11.3, and by standard quantum mechanical perturbation theory [488], it evaluates to (this expression is the analog of (11.44))

$$\frac{v^2}{S} \int \frac{d^d q_1}{(2\pi)^d} [J(\vec{k}_1 + \vec{q}_1) + J(\vec{k}_2 - \vec{q}_1) - J(\vec{k}_1 + \vec{q}_1 - \vec{k}_2) - J(\vec{q}_1)]$$

$$\times \frac{[J(\vec{k}_1 + \vec{q}) + J(\vec{k}_2 - \vec{q}) - J(\vec{k}_1 + \vec{q} - \vec{k}_2 + \vec{q}_1) - J(\vec{q} - \vec{q}_1)]}{J(\vec{k}_1) + J(\vec{k}_2) - J(\vec{k}_1 + \vec{q}_1) - J(\vec{k}_2 - \vec{q}_1)}. \quad (13.42)$$

To understand the implications of this result for the continuum theory (13.32) we allow the external momenta $\vec{k}_1$, $\vec{k}_2$, $\vec{q}$ to become small, but for the moment allow the internal momentum $\vec{q}_1$ to be large. Then there is a term from (13.42) which is quadratic in external momenta; however this can be seen to vanish after use of the identity $\int d^d q_1 e^{-i\vec{q}_1 \cdot \vec{x}_m} = 0$ (valid because all the $\vec{x}_m \neq 0$)–it is clear that the lattice regularization is crucial in obtaining this result, and it turns out that it is mainly this step which cannot be deduced from the continuum theory (13.32). The next term is *quartic* in external momenta, and it simplifies to

$$\frac{v^2}{S} \int \frac{d^d q_1}{(2\pi)^d} \frac{\left[\sum_m J_m e^{-i\vec{q}_1 \cdot \vec{x}_m} (\vec{k}_1 \cdot \vec{x}_m)(\vec{k}_2 \cdot \vec{x}_m) \right]^2}{\sum_m J_m (1 - e^{-i\vec{q}_1 \cdot \vec{x}_m})}; \quad (13.43)$$

We take the small $\vec{q}_1$ limit of (13.43) and obtain the result for the correction to the two spin-wave T-matrix [284] at low momenta:

$$\frac{4\rho_s}{M_0^3} (\vec{k}_1 \cdot \vec{k}_2)^2 \int \frac{d^d q_1}{(2\pi)^d} \frac{1}{q_1^2}; \quad (13.44)$$

this expression involves only couplings present in $\mathcal{L}_F$ in (13.32) and so could also have been obtained directly from the continuum quantum theory after ignoring ultraviolet divergences in terms lower order in the external momenta. The integral in (13.44) is dominated by the ultraviolet for $d > 2$ and so we have to return to the lattice expression (13.43). However it is ultraviolet finite for $d < 2$, and the continuum theory is insensitive to lattice perturbations; the infrared divergence will of course be cutoff by the external momenta, which have not been kept in the propagator in the above approximation. So as in the case of the dilute Bose gas in Section 11.3, we see the emergence of $d = 2$ as a critical dimension.

It is very useful to interpret (13.44) in renormalization group sense.

If we imagine we are integrating out virtual spin wave fluctuations between momentum scales Λ and $\Lambda e^{-\ell}$ (Λ is a momentum cutoff), then these become the boundaries of the integration in (13.44), and the result generates a four gradient term to $\mathcal{L}_F$. The generated term cannot be quadratic in $\mathbf{N}$, as that would modify the exactly known spin wave dispersion. The simplest terms which modify *only* the two spin-wave scattering amplitude are quartic also in $\mathbf{N}$; by noting the momentum dependence on (13.44), using the low momentum limit of the energy conservation equation (13.41), and imposing the restrictions of rotation invariance of rotational invariance, a simple analysis shows that the generated term is [404]

$$\mathcal{L}_F \to \mathcal{L}_F + \lambda(\nabla_a N_\alpha \nabla_a N_\alpha \nabla_b N_\beta \nabla_b N_\beta - 2\nabla_a N_\alpha \nabla_b N_\alpha \nabla_a N_\beta \nabla_b N_\beta),$$
(13.45)

where λ is a *new* coupling constant of the continuum theory. Converting from scattering amplitudes of b to $\mathbf{N}$ quanta using (13.38), (13.45) and (13.44) imply the flow equation

$$\frac{d\lambda}{d\ell} = (d-2)\lambda + \frac{\rho_s}{M_0}.$$
(13.46)

As with (11.47), this flow equation is believed to be exact. So for $d < 2$, λ is attracted to a universal critical value, and the parameters ρ_s and M_0 completely determine the low energy physics of the continuum theory (13.32). On the other hand, λ becomes large at long distances for $d \geq 2$, and its bare value is important: it is responsible for temperature dependent corrections to the magnetization computed by Dyson [132].

For $d < 2$ these considerations imply that we may write down universal scaling forms for the continuum ferromagnet (13.32). The usual scaling and dimensional considerations imply for the free energy density [404]

$$\mathcal{F} \asymp T M_0 \Phi_{fm}\left(\frac{\rho_s}{M_0^{(d-2)/d}T}, \frac{H}{T}\right),$$
(13.47)

where Φ_{fm} is a universal function; corresponding results follow for observables which are derivatives of the free energy. Actually, our arguments for universality have really been made in an expansion in powers of $1/S$, and so the result (13.47) only holds as an asymptotic expansion in inverse powers of $\rho_s/(M_0^{(d-2)/d}T)$, and this represented by the symbol $\asymp$. Indeed, (13.47) is expected to be true to all orders in $\rho_s/(M_0^{(d-2)/d}T)$, but this is not the same thing as being exactly true. Lattice effects become significant when $T \sim \rho_s/M_0^{(d-2)/d}$, for then the

wavelength of the characteristic spin-wave is of order $M_0^{1/d}$, which is of order a lattice spacing; these effects appear as essential singularities and destroy strict equality for (13.47). Some short distance regularization at the scale $M_0^{1/d}$ is always required for any consistent theory of quantum ferromagnets [203]. Similar considerations apply for expansions in $1/N$ [26, 30, 491], and for ferromagnets with more complicated replica and supersymmetries [194, 195].

Finally, we briefly note that effective classical models for thermal fluctuations in ferromagnets can be derived for $T \ll \rho_s/M_0^{(d-2)/d}$, precisely as was done for the rotor models in Part 2. In $d = 1$ we would get the effective theory (2.68) with $\xi = \rho_s/T$ [484], while in $d = 2$ we would obtain the model (7.8) [280] with a $\Lambda_{\overline{MS}}$ which can be computed from (13.36) by methods parallel to those in Section 7.1.1.

13.3 Antiferromagnets

This section will consider models H_S in (13.1) with all $J_{ij} < 0$. Classically (*i.e.*, in the limit $S \to \infty$), such models will minimize their energies by making nearest neighbor spins acquire an anti-parallel orientation. On bi-partite lattices (*i.e.*, lattices which can be split into two equivalent sublattices so that all nearest neighbors of any site on one sublattice belong to the other sublattice) with nearest neighbor interactions, the anti-parallel constraint is easy to satisfy: the spins simply point in opposite directions on the two sublattices. Notice that any pair of spins is either parallel or antiparallel, and so such an ordering is *collinear*. We will begin by exclusively considering quantum antiferromagnets whose classical ground state is collinear in Section 13.3.1: such an ordering is expected to be present at least over short distances in the quantum case. Non-collinear ordering arises on non-bipartite lattices or even on bipartite lattices with further neighbor interactions: such antiferromagnets are classically frustrated and possess ground states in which the spins are *coplanar* (as on the triangular lattice with nearest neighbor interactions), or in some rare cases, can even form structures which are three-dimensional in spin space. We will consider the non-collinear cases in Section 13.3.2.

13.3.1 Collinear order

For definiteness, we will begin by considering antiferromagnets on a d-dimensional hypercubic lattice with only a nearest neighbor exchange

$J_{ij} = -J < 0$; other collinear antiferromagnets can be treated in a similar manner. In the classical limit of large S, as noted above, the ground state has spins oriented in opposite directions on the two sublattices: this is the so-called Néel-ordered state. For smaller S this orientation should survive at least over a few lattice spacings, suggesting that a continuum description of the quantum antiferromagnet may be possible [204, 3, 4]. We therefore begin by introducing a parameterization of the unit length spin field $\mathbf{N}_i(\tau)$ which captures this local ordering. We write

$$\mathbf{N}_i(x, \tau) = \lambda_i \mathbf{n}(x_i, \tau)) \sqrt{1 - (a^d/S)^2 \mathbf{L}^2(x_i, \tau)} + (a^d/S)\mathbf{L}(x_i, \tau), \quad (13.48)$$

where λ_i equals ± 1 on the two sublattices and a is the lattice spacing. The fields $\mathbf{n}(x_i)$ and $\mathbf{L}(x_i)$ parameterize the staggered and uniform components of the Heisenberg spins. The prefactor of a^d/S has been associated with $\mathbf{L}$ so that the spatial integral of $\mathbf{L}$ over any region is precisely the total magnetization inside it. Both fields are assumed to be slowly varying on the scale of a lattice spacing. This is certainly true as $S \to \infty$, and it is hoped that this assumption remains valid down to $S = 1/2$. So we will treat $\mathbf{n}(x, \tau)$ and $\mathbf{L}(x, \tau)$ as continuum quantum fields which can be expanded in spatial gradients over separations of order a. These continuum fields satisfy the constraints

$$\mathbf{n}^2 = 1 \quad , \quad \mathbf{n} \cdot \mathbf{L} = 0, \quad (13.49)$$

which combined with (13.48) imply that $\mathbf{N}_i^2 = 1$ is obeyed. Further, spins on nearby sites are expected to be predominantly antiparallel, so the uniform component $\mathbf{L}$ should be small; more precisely we have

$$\mathbf{L}^2 \ll S^2 a^{-2d}. \quad (13.50)$$

The field $\mathbf{n}(x, \tau)$ clearly plays the role of the order parameter associated with Néel ordering. Note that although $\mathbf{n}$ varies slowly on the scale of a lattice spacing, values of $\mathbf{n}$ on well separated points can be considerably different, leaving open the possibility of a quantum paramagnetic phase with no magnetic long range order. Magnetic Néel order requires that the time-average orientation of $\mathbf{n}(x, \tau)$ is correlated across the sample: whether this happens will be determined by the effective action for $\mathbf{n}$ fluctuations, which we will now derive.

We insert the decomposition (13.48) for $\mathbf{N}_i$ into $H_S(S\mathbf{N}_i(\tau))$ and expand the result in gradients, and in powers of $\mathbf{L}$. This yields

$$H_S = \int d^d x \left[\frac{JS^2 a^{2-d}}{2} (\nabla_x \mathbf{n})^2 + dJa^d \mathbf{L}^2 - \mathbf{H} \cdot \mathbf{L} \right]$$

$$\equiv \ \frac{1}{2}\int d^d x \ \left[\frac{Nc}{g}(\nabla_x \mathbf{n})^2 + \frac{cg}{N}\mathbf{L}^2 - \mathbf{H}\cdot\mathbf{L}\right]. \tag{13.51}$$

In the second equation we have introduced the couplings $c = \sqrt{2d}JSa$ and $g = (N/S)\sqrt{2d}a^{d-1}$: the notation is suggestive and anticipates our eventual mapping of the present model to the rotor models in (3.12) and (5.16). In the present case $N = 3$, but we introduced a general factor of N for notational consistency with Part 2. If we had used a different form for H_S with modified short-range exchange interactions, the continuum limit of H would have been the same but with new values of g and c.

To complete the expression for the coherent state path-integral of the antiferromagnet in the continuum limit, we also need the expression for $\mathcal{S}_B$ in terms of $\mathbf{n}, \mathbf{L}$. We insert (13.48) into the (13.31) and retain terms up to linear order in $\mathbf{L}$: this yields

$$\mathcal{S}_B = \mathcal{S}_B' + i\int d^d x \int_0^{1/T} d\tau \int_0^1 du \left[\mathbf{n}\cdot\left(\frac{\partial\mathbf{n}}{\partial u}\times\frac{\partial\mathbf{L}}{\partial\tau}\right)\right.$$
$$\left. + +\mathbf{n}\cdot\left(\frac{\partial\mathbf{L}}{\partial u}\times\frac{\partial\mathbf{n}}{\partial\tau}\right) + \mathbf{L}\cdot\left(\frac{\partial\mathbf{n}}{\partial u}\times\frac{\partial\mathbf{n}}{\partial\tau}\right)\right] \tag{13.52}$$

where

$$\mathcal{S}_B' = iS\sum_i \lambda_i \int_0^{1/T} d\tau \int_0^1 du \ \mathbf{n}(x_i)\cdot\left(\frac{\partial\mathbf{n}(x_i)}{\partial u}\times\frac{\partial\mathbf{n}(x_i)}{\partial\tau}\right) \tag{13.53}$$

The evaluation of $\mathcal{S}_B'$ in the continuum limit is a rather subtle matter, as the leading λ_i in (13.53) shows that it is the sum of terms which oscillate in sign on the two sublattices. The naive assumption would be that these oscillating terms just cancel out, and therefore $\mathcal{S}_B' = 0$ in the continuum limit. For some purposes this assumption is in fact adequate, but there are a number of important cases where $\mathcal{S}_B'$ is non-vanishing and is crucial for a complete understanding of the physics. We will postpone a careful evaluation of $\mathcal{S}_B'$ to the following subsections where we will consider its consequences in $d = 1$ and $d = 2$ separately. Let us first simplify the other terms in (13.52) a bit further.

We use the fact that the vectors $\mathbf{L}$, $\partial\mathbf{n}/\partial\tau$, $\partial\mathbf{n}/\partial u$ are all perpendicular to $\mathbf{n}$; hence, they lie in a plane and have a vanishing triple product:

$$\mathbf{L}\cdot\left(\frac{\partial\mathbf{n}}{\partial u}\times\frac{\partial\mathbf{n}}{\partial\tau}\right) = 0. \tag{13.54}$$

Using (13.54) in (13.52) we find

$$\mathcal{S}_B = \mathcal{S}_B' + i\int d^d x \int_0^{1/T} d\tau \int_0^1 du \left[\frac{\partial}{\partial\tau}\left(\mathbf{n}\cdot\left(\frac{\partial\mathbf{n}}{\partial u}\times\mathbf{L}\right)\right)\right.$$

$$+\frac{\partial}{\partial u}\left(\mathbf{n}\cdot\left(\mathbf{L}\times\frac{\partial\mathbf{n}}{\partial\tau}\right)\right)\Bigg] \tag{13.55}$$

The total τ derivative yields 0 after using the periodicity of the fields in τ, while the total u derivative yields a surface contribution at $u=1$. This gives finally

$$\mathcal{S}_B = \mathcal{S}_B' - i\int d^d x \int_0^{1/T} d\tau \mathbf{L}\cdot\left(\mathbf{n}\times\frac{\partial\mathbf{n}}{\partial\tau}\right) \tag{13.56}$$

Putting together (13.51) and (13.56) in (13.17) we obtain the following path-integral for the partition function of the antiferromagnet

$$Z = \int \mathcal{D}\mathbf{n}\mathcal{D}\mathbf{L}\,\delta(\mathbf{n}^2-1)\delta(\mathbf{L}\cdot\mathbf{n})\exp(-\mathcal{S}_B'-\mathcal{S}_n')$$

$$\mathcal{S}_n' = \frac{1}{2}\int_0^{1/T}d\tau\int d^d x\left[\frac{Nc}{g}(\nabla_x\mathbf{n})^2\right.$$

$$\left.+\frac{cg}{N}\mathbf{L}^2 - 2i\mathbf{L}\cdot\left(\mathbf{n}\times\frac{\partial\mathbf{n}}{\partial\tau}-i\mathbf{H}\right)\right] \tag{13.57}$$

The functional integral over $\mathbf{L}$ can be carried out explicitly (after imposing the constraint $\mathbf{L}\cdot\mathbf{n}=0$, *e.g.*, by adding a term $w(\mathbf{L}\cdot\mathbf{n})^2$ to the Hamiltonian, and taking the limit $w\to\infty$ after carrying out the integral) and we obtain the final result of this section [204, 3, 4]

$$Z = \int \mathcal{D}\mathbf{n}\,\delta(\mathbf{n}^2-1)\exp(-\mathcal{S}_B'-\mathcal{S}_n)$$

$$\mathcal{S}_n = \frac{N}{2cg}\int_0^{1/T}d\tau\int d^d x\,\left[c^2(\nabla_x\mathbf{n})^2 + (\partial_\tau\mathbf{n}-i\mathbf{H}\times\mathbf{n})^2\right]. \tag{13.58}$$

Note that $\mathcal{S}_n$ is identical to the rotor model action studied in (5.16). However, before we can carry over all the results of Part 2 here, we have to examine the consequences of $\mathcal{S}_B'$, and this will be done separately in the following two subsections in dimensions $d=1$ and $d=2$ respectively.

13.3.1.1 $d=1$

It is simpler to evaluate S_B' in $d=1$ by a geometric argument, rather than working directly with the formal expression (13.53). We have already argued below (13.31), that the contribution of each site i in (13.53) equals $\lambda_i S$ times the area on the unit sphere contained inside the close loop defined by the periodic time evolution of $\mathbf{n}(x_i,\tau)$: we define this area to equal $\mathcal{A}_i$. Let us examine the contribution of two neighboring sites, i and $i+1$, to $\mathcal{S}_B'$. The weight λ_i will have opposite signs on

these sites, and so the net contribution will be the difference of the areas. We can further assume that the order parameter field $\mathbf{n}(x_i)$ only varies slightly between i and $i + 1$: under these conditions, and using the definition of an area element on the sphere, we have (after defining $\Delta\mathbf{n}(x_i) = \mathbf{n}(x_{i+1}) - \mathbf{n}(x_i)$)

$$
\begin{aligned}
\mathcal{A}_{i+1} - \mathcal{A}_i &\approx \int_0^{1/T} d\tau \mathbf{n}(x_i) \cdot \left(\Delta\mathbf{n}(x_i) \times \frac{\partial\mathbf{n}(x_i)}{\partial\tau} \right) \\
&\approx a \int d\tau \mathbf{n}(x_i) \cdot \left(\frac{\partial\mathbf{n}(x_i)}{\partial x_i} \times \frac{\partial\mathbf{n}(x_i)}{\partial\tau} \right) \quad (13.59)
\end{aligned}
$$

The summation in (13.53) can be carried out over pairs of sites: all terms are of the same sign and therefore the summation can be easily converted into an integral. In this manner we obtain our final result for $\mathcal{S}'_B$ in $d = 1$ [204, 3, 4]:

$$
\mathcal{S}'_B = i\frac{\theta}{4\pi} \int dx \int_0^{1/T} d\tau \mathbf{n} \cdot \left(\frac{\partial\mathbf{n}}{\partial x} \times \frac{\partial\mathbf{n}}{\partial\tau} \right) \quad (13.60)
$$

where $\theta = 2\pi S$. Some comments and/or cautions about the derivation leading up to (13.60) are in order. The arbitrary way in which the sites in (13.59) were paired suggests that the answer is sensitive to the boundary conditions, and upon whether there are an even or odd number of sites in the system. There are indeed interesting boundary effects in the physics of antiferromagnetic spin chains [10, 11, 198], but we will not discuss them here. The overall sign of the answer in (13.60) also depends upon the sign of λ_i, but as we will see shortly, the physics is does not depend upon the sign of θ. Finally the result (13.60) can also be derived by analytic computations from (13.53): we can write the oscillating sum as half the spatial integral of the spatial derivative of the contribution of each site (by the same arguments leading to (13.59))– then using the fact that the triple product of $\partial\mathbf{n}/\partial x$, $\partial\mathbf{n}/\partial\tau$ and $\partial\mathbf{n}/\partial u$ must vanish we can obtain (13.60) using manipulations similar to those leading to (13.56).

In its present form, $\mathcal{S}'_B$ is the so-called topological θ-term, familiar in the particle theory literature. The co-efficient of θ in (13.60) computes a simple topological invariant which, for periodic boundary conditions in space, is always an integer. If we consider the field configuration $\mathbf{n}(x, \tau)$ as a map from two-dimensional spacetime, with periodic boundary conditions, to the surface of a unit sphere, then the topological invariant is simply the number of times spacetime has been wrapped around the

sphere. It is useful to visualize the simplest configuration of $\mathbf{n}(x, \tau)$ corresponding to the topological invariant of unity. Let the unit sphere be placed on an elastic sheet, representing space time. Now fold up the sheet to cover the sphere once: the orientation of $\mathbf{n}$ at (x, τ) is given by the point on the sphere adjacent to the point (x, τ) on the sheet. Such a spacetime configuration represents a tunneling event: deep in the past, or far in the future, $\mathbf{n}$ points to the north pole; however at some time, in a certain compact region of space, the $\mathbf{n}$ orientation tunnels all the way to the vicinity of the south pole and back; configurations with larger topologically invariants can be similarly interpreted. The result (13.23) implies that each such tunneling event yields a factor of $e^{i\theta} = (-1)^{2S}$ to the path integral for the partition function. This is the only consequence of the S'_B term. Of course, the terms in $\mathcal{S}_n$ give the usual positive weights (in imaginary time) also present for the rotor model. Notice that as θ is always an integral multiple of π, the sign of θ does not change the value of $e^{i\theta}$.

We are now able to state our principal conclusions, first reached by Haldane. For integer S, the phase factor with topologically non-trivial tunneling events is simply unity, and the theory reduces to the rotor model action $\mathcal{S}_n$, which has been studied in some detail in Chapters 5 and 6. On the other hand, for half-integer S, there are clearly substantial differences: the present formulation of the theory in (13.58) is however not a particularly convenient way of exploring the physics—it does tell us that the low energy properties of all the half-integer cases are the same, and we will explore the $S = 1/2$ case in the Chapter 14 by alternative methods.

We anticipate these results by sketching the renormalization group flows for the dimensionless coupling g for the cases $\theta = 0$ and $\theta = \pi$ in Fig 13.1. For the case of integer S, where $\theta = 0$, the flow just represents (6.8): all values of g flow eventually to strong coupling, and as we saw in Chapter 6, there is always an energy gap above the ground state. For the case $\theta = \pi$, the perturbative flow at small g is the same as before, as it is independent of θ. However, more sophisticated considerations [9, 5, 544, 142] to be discussed in Chapter 14, show that there is a fixed point at $g = g_c$, of order unity, which attracts all couplings with $g < g_c$. We will also see that the ground state is then a so-called 'Tomonaga-Luttinger liquid' and has gapless, linearly dispersing excitations. For $g > g_c$ (and $\theta = \pi$) the flow is again to strong coupling, and the ground state will be seen to be a 'spin-Peierls' state with an energy gap to all excitations (such a state will be described shortly below for $d = 2$).

θ=0

Quantum paramagnet with an energy gap

0

g

θ=π

0   Tomonaga
Luttinger liquid

g_c

spin-Peierls

g
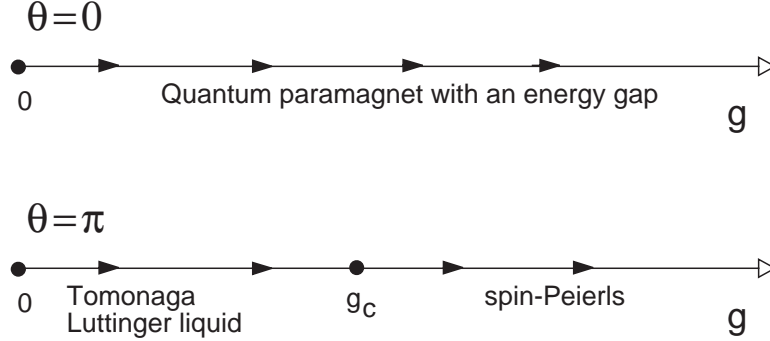
Fig. 13.1. Renormalization group flows for the dimensionless coupling g in (13.58) for $d = 1$ with $\mathcal{S}'_B$ given by (13.60). For $\theta = 0$, the flow is given by (6.8), and there is always an energy gap above the ground state. For $\theta = \pi$, there is a fixed point $g = g_c$, and near it the flow is $dg/d\ell \propto (g - g_c)^2$.

We conclude by reviewing a bit more explicitly the implications of the results of Chapters 5 and 6 for antiferromagnetic chains of integer spins. The mapping between correlation functions of the two theories is provided by (13.48). From this, we see that the correlator χ_u defined in (6.1) also specifies the fluctuations of the magnetization of the spin chain: at wavevector k this is a correlation function of the $\hat{\mathbf{S}}_i$ spins near the wavevector $q = k$. Further the correlations of the order parameter $\mathbf{n}$ given by χ in (5.2) at wavevector k, map onto correlations of $\hat{\mathbf{S}}_i$ at wavevector $q = k + Q$, where $Q = \pi/a$ is the ordering wavevector of the classical antiferromagnetic chain; all of the results for the rotor correlation functions in Chapter 6 can therefore be applied to integer spin antiferromagnets. We saw in Chapter 6 that the $d = 1$, $N = 3$ quantum rotor model always had a gap: the same is therefore true of integer spin antiferromagnetic chains–this is the so-called Haldane gap (we will see in the following chapter that half-integer spin chains can be gapless). The $T = 0$ spectrum of the integer spin antiferromagnets is qualitatively the same as that discussed in the strong coupling expansion in Section 5.1.1: the lowest excited states are a triplet of $S = 1$ particles with infinite lifetime: for the spin chain, this particle appears as a pole in the $\hat{\mathbf{S}}$-$\hat{\mathbf{S}}$ correlation function which has its minimum at $q = \pi/a$. Higher excited states consist of multi-particle continua of this triplet of particles.

13.3.1.2 $d = 2$

We will consider the properties of the theory (13.58) on the $d = 2$ square lattice.

This requires evaluation of the oscillating sum in $\mathcal{S}'_B$ in (13.53). Using techniques very similar to those used in $d = 1$, it is not difficult to establish an important result: $\mathcal{S}'_B$ vanishes for all smooth spacetime configurations of $\mathbf{n}(x, \tau)$. Simply evaluate (13.53) row by row on the square lattice. The sum on each row is precisely the same as that carried out in $d = 1$, and equals (13.60) on each row, up to an overall sign. Moreover, because of the structure of the sublattices, this overall sign will oscillate as we move from row to row. Now, note that the arguments in Section 13.3.1.1 imply that the contribution of each row is quantized in integer multiples of θ. If, as we are assuming, $\mathbf{n}(x, \tau)$ is smoothly varying, the contribution of the rows must also change smoothly as we move from row to row. This is only compatible with the quantization if each row yields precisely the same integer. Hence their oscillating sum appearing in $\mathcal{S}'_B$ vanishes.

However, this is not the end of the story. It turns out there are important *singular* configurations of $\mathbf{n}(x, \tau)$ that do yield a non-vanishing contribution to $\mathcal{S}'_B$. We postpone discussion of the consequences of these contributions until later in this subsection; first, we discuss the implication of the results of Part 2 for square lattice antiferromagnets, assuming that $\mathcal{S}'_B$ vanishes identically for all S.

The properties of the $N = 3$, $d = 2$ quantum rotor model were first discussed using the large N expansion in Chapter 5), and then in some more detail in Chapters 7, 8, and 9. The most significant feature of these results was the existence of a quantum phase transition at a critical value $g = g_c$, separating a magnetically ordered ground state from a quantum paramagnetic ground state.

The magnetically ordered state of the rotor model corresponds to a "Néel" ground state of the antiferromagnet: this is a state in which the spin-rotation invariance of the Hamiltonian (13.1) is broken because of a non-zero, expectation value of the spin operator, which takes opposite signs on the two sublattices: from (13.48) we see

$$\left\langle \hat{\mathbf{S}}_i \right\rangle \propto \lambda_i S \left\langle \mathbf{n}(x_i) \right\rangle = S N_0 \mathbf{e}_z, \tag{13.61}$$

where $\mathbf{e}_z$ is a unit vector pointing the $\mathbf{e}_z$ direction (say) of spin space. Note that there was no state with such a broken symmetry in $d = 1$. The missing proportionality constant in (13.61) depends upon microscopic

details, and is not of any importance: in Part 2 we expressed physical properties of the rotor model on the ordered side in terms of N_0: these can be applied unchanged to the antiferromagnet simply by replacing N_0 by the actual expectation value of $\lambda_i \left\langle \hat{\mathbf{S}}_i \right\rangle$. As in $d = 1$, correlators of $\mathbf{L}$ at wavevector $\vec{k}$ map onto correlators of $\hat{\mathbf{S}}$ at $\vec{q} = \vec{k}$, while correlators of $\mathbf{n}$ at $\vec{k}$ map onto $\vec{q} = \vec{k} + \vec{Q}$, with $\vec{Q} = (\pi/a, \pi/a)$ the ordering wavevector. As was the case for the rotor model, the broken rotational invariance is restored at any non-zero temperature, and the antiferromagnet instead acquires an exponentially large correlation length given by (7.10) and (7.20). In these results, we take for the value of ρ_s the actual $T = 0$ spin stiffness of the quantum antiferromagnet. The non-zero temperature static and dynamic correlations are described by (7.1), with the function Φ_- as described in Chapter 7.

Numerical studies of the square lattice antiferromagnets with nearest neighbor antiferromagnets have shown fairly conclusively that the ground state has Néel order for all values of S including $S = 1/2$ [406, 232]. Thus it appears that all such antiferromagnets map onto the rotor model with $g < g_c$. For $S = 1/2$ it has been argued [96, 97] that the value of g is sufficiently close to g_c so that the universal crossover between the low and high T limits of the continuum rotor field theory shown in Fig 5.2 can be observed with increasing temperature, as we have discussed in Section 5.5. For larger S, the antiferromagnets appear to go directly from the universal low T region on the ordered side of Fig 5.2 to a non-universal lattice high T region [135].

Clearly, it would also be physically interesting to find collinear antiferromagnets which map onto rotor models with $g > g_c$, and therefore do not have Néel order in their ground state. A convenient choice, studied extensively in the literature, has been the square lattice antiferromagnet with first and second neighbor antiferromagnetic exchanges, labeled J_1 and J_2 respectively. The classical limit of this model has collinear Néel order for all J_2/J_1, and so the quantum fluctuations should continue to be described by (13.58). Numerical and series expansion studies [87, 91, 113, 147, 174, 173, 350, 388, 450, 451, 304] for $S = 1/2$ have shown that this model loses the order (13.61) around $J_2/J_1 = J_c \approx 0.4$. So we can identify the point $J_2/J_1 = J_c$ with the quantum critical point $g = g_c$ of the rotor model. The quantum paramagnetic state of the rotor model should therefore yield the characteristics of the antiferromagnet with J_2/J_1 just above J_c: spin rotation invariance is restored, and there

is a gap to all excitations. Nonzero temperature properties are described by (7.3) with Δ_+ the actual energy gap of the antiferromagnet.

One important property of the quantum paramagnetic state of the rotor model deserves special mention, as it has crucial implications for the corresponding antiferromagnet. Recall that the excited states of the rotor model were described in terms of a N-fold degenerate quasiparticle and its multiparticle continua. This lead to the spectrum shown in Fig 4.1 and discussed in the strong-coupling expansion of Section 5.1.1: there is an infinitely sharp delta function in $\mathrm{Im}\chi(k,\omega)$ at the position of the quasi-particle energy $\omega = \varepsilon_k$. For $N = 3$, this is clearly a quasiparticle with total angular momentum $S = 1$; so the dominant excitation of this phase of quantum antiferromagnet is a $S = 1$ particle with its energy minimum at $\vec{q} = \vec{Q}$, and this will lead to a delta function in the dynamic spin susceptibility at wavevectors near $\vec{Q}$. Note that this $S = 1$ particle exists for all values of the spin S of the individual spins of the underlying antiferromagnet. This gapped $S = 1$ excitation should also be contrasted with the spin-wave excitations of the ordered Néel state which are gapless, two-fold degenerate, and do not carry definite total spin (although they are eigenstates of total $\hat{S}_z$, with eigenvalues ± 1 for a Néel state polarized in the z direction).

We conclude this subsection by returning to consideration of $\mathcal{S}'_B$, the consequences of which have been ignored so far. A full computation is quite technical and lengthy, and we will be satisfied here by highlighting some essential features, and refer the reader to the original literature for further details [401, 402]. Before outlining the calculation, let us describe the consequences of $\mathcal{S}'_B$ in simple physical terms. There are important results that emerge:

(i) All of the results above on the nature of the quantum critical point, and on the crossovers in its vicinity on both the Néel ordered and quantum paramagnetic side remain unchanged [356, 440, 97].

(ii) On certain lattices, and for certain values of S, a new spontaneously broken lattice symmetry emerges everywhere in the quantum paramagnet [401] (spin rotation invariance remains unbroken in the quantum paramagnet, and there is no change in the structure of the Néel state). This broken symmetry is associated with the appearance of *spin-Peierls* order, which we will describe momentarily. It is believed that the spin-Peierls order parameter does not play an essential role in the quantum critical point noted in (i), and that its fluctuations only become important at sufficiently low energies and long distances so as not to modify the crossovers of the quantum rotor model computed in Part 2. To

2S (mod 4) = 1,3

2S (mod 4) = 2

2S (mod 4) = 0
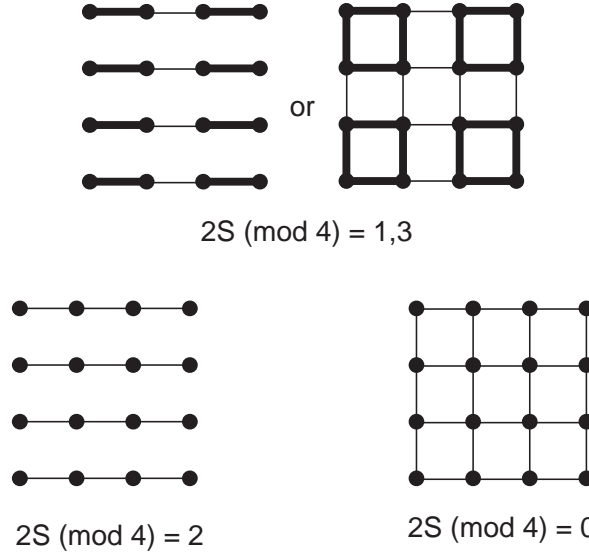
Fig. 13.2. Quantum paramagnetic ground states of the weakly frustrated square lattice antiferromagnet as a function of $2S(\mathrm{mod}\ 4)$. The values of P_{ij} on the nearest neighbor links are schematically indicated by the different kinds of lines on the links; those on thick lines are larger than those on the thin lines, and weakest are on the empty links.

describe the spin-Peierls order, consider the quantity

$$P_{ij} = \left\langle \hat{\mathbf{S}}_i \cdot \hat{\mathbf{S}}_j \right\rangle. \qquad (13.62)$$

Note that P_{ij} is a scalar under spin rotations, and so a non-zero value does not break a spin rotation symmetry. The Hamiltonian H_S in (13.1) is also invariant under a group of lattice symmetries (involving lattice rotation, reflection and translations), and the values of the P_{ij} for all pairs sites i, j should, in general, also respect these symmetries. A spin-Peierls state is one in which the values of P_{ij} break a lattice symmetry; this broken symmetry will be observable experimentally in lattice distortions whose pattern will reflect that in P_{ij}—the distortion arise from the coupling between the spin exchange energy and phonon displacements which have not been included in the Hamiltonians we are considering here. For the case of a square lattice with first and second neighbor interactions, the quantum paramagnet with J_2/J_1 just above J_c possesses spin-Peierls order of the type shown in Fig 13.2. For $S = 1/2$, like values of P_{ij} line up in columns or plaquettes which clearly break symmetry

of rotation by 90 degrees about each lattice point; the ground state is four-fold degenerate, and a similar spin-Peierls ordering is expected for all half-integral S. If it was possible to obtain a quantum paramagnet for $S = 1$ (or other odd integer S) by a continuous transition from a Néel state, then it is predicted to have a two-fold degenerate ground state, with the P_{ij} on the horizontal bonds differing from those on the vertical bonds (see Fig 13.2). Finally, only for even integer S, is the paramagnetic state non-degenerate and breaks no lattice symmetry [10, 11]. Related results exist for quantum paramagnetic states accessed by a continuous transition from other collinear states on the square or other lattices. In all cases there are special values of S for which the quantum paramagnet is non-degenerate and has no spin-Peierls order; these special values extend to all values of S only for lattices with small symmetry groups.

Let us , finally, consider the complete evaluation of $\mathcal{S}'_B$, and discuss its relationship to the spin-Peierls ordering just described. We will consider the case of the square lattice with nearest neighbor exchanges, and possible further neighbor exchanges which do not destroy the collinear, two sublattice ordering of the classical Néel state. We have already argued at the beginning of this subsection that $\mathcal{S}'_B$ vanishes for smooth space-time configurations of $\mathbf{n}(x, \tau)$. We should therefore consider singular configurations, and for the case of 3-component vector order parameter, the only topologically stable possibility is the so-called 'hedgehog' singularity [205]. This is a singularity occurring at point in spacetime and corresponds to a tunneling event in which the 'Skyrmion number', Y, of a given time slice of $\mathbf{n}(x, t)$ changes. The latter is defined by the spatial integral

$$Y(\tau) = \frac{1}{4\pi} \int d^2x\, \mathbf{n} \cdot \left(\frac{\partial \mathbf{n}}{\partial x_1} \times \frac{\partial \mathbf{n}}{\partial x_2} \right). \qquad (13.63)$$

Compare (13.63) to the topological θ term in $d = 1$ of (13.60): the two expressions are identical except that we now have an integral over space only, while earlier we had a spacetime integral. By the same arguments as made below (13.60), Y is an integer for periodic boundary conditions in space. Let us describe a hedgehog tunneling event in which Y changes from 1 to 0, in a pictorial language used by Haldane [205]. As below (13.60) we can represent a configuration with $Y = 1$ as an elastic sheet (now representing space, rather than spacetime) wrapped on a sphere. In reality, the spins lie on a lattice, and so the elastic sheet has a fine square mesh on it. Now imagine a tunneling event in which one square on the mesh expands and allows the sphere to pass through;

the resulting configuration will have its Y changed to 0. It remains to evaluate the summation in (13.53) for the evolution of $\mathbf{n}(x, \tau)$ just described. Actually, we cannot consider hedgehog tunneling events singly, as then the periodic boundary conditions in τ, required for a meaningful evaluation of (13.53), will not be satisfied. We therefore consider a sequence of events at well separated times, centered at the midpoints of plaquettes labeled a, and involving the change in Skyrmion number ΔY_a such that $\sum_a \Delta Y_a = 0$. These events are to be considered as saddle points in the evaluation of the coherent state path integral of the lattice antiferromagnet: the configuration of $\mathbf{n}(x, \tau)$ at the saddle point minimizes the action, and, provided the hedgehogs are well separated, can reasonably be expected to have four-fold rotational symmetry about the plaquette a around which the tunneling occurs. As at the beginning of Section 13.3.1.1, let us write $\mathcal{S}'_B$ as

$$\mathcal{S}'_B = S \sum_i \lambda_i \mathcal{A}_i, \tag{13.64}$$

where $\mathcal{A}_i$ is the contribution of site i. Now we can evaluate $\mathcal{A}_i$ by following the area swept out on the unit sphere by each site on the elastic sheet during the tunneling event: from this it is simple to see the following important intermediate result—the lattice configuration of $\mathcal{A}_i$ has a vortex of strength $4\pi\Delta Y_a$ around plaquette a. As the sum in (13.64) cannot change from smooth changes in the lattice configuration of $\mathcal{A}_i$, we need only take a representative configuration which has the proper vortex singularities; for instance, we can take

$$\mathcal{A}_i = 2 \sum_a \Delta Y_a \arctan\left(\frac{x_{i1} - X_{a1}}{x_{i2} - X_{a2}}\right), \tag{13.65}$$

where $x_{i1,2}$ are the components of the lattice points x_i, and X_a is the position of the center of plaquette a. We have to insert (13.65) into (13.64) and evaluate the sum over i. This is a mathematical step, and the details are given by Haldane [205]: it is not difficult to see that the result takes the form

$$\mathcal{S}'_B = i\pi S \sum_a \Delta Y_a \zeta_a. \tag{13.66}$$

The values of the ζ_a depend upon the co-ordinates of plaquette a; a number of choices for these values are possible, but $e^{-\mathcal{S}'_B}$ remains the same provided $\sum_a \Delta Y_a = 0$. A particular choice is $\zeta_a = 0, 1, 2, 3$ if the co-ordinates X_a are (even,even), (even,odd), (odd,odd), (odd,even).

Now a last step remains: we have to sum over all possible hedgehog

events, while including the phase factors arising from $e^{\mathcal{S}'_B}$ with each such event. Refs [401, 402] showed how such a summation could be carried out systematically in a certain large N expansion: describing this here would take us too far afield, and we refer the reader to Ref [402] for fairly explicit details. The hedgehog events are completely suppressed by the action arising from $\mathcal{S}_n$ for $g < g_c$, and therefore have no significant consequence for the Néel phase. In contrast, for $g > g_c$, these events proliferate, and it was shown in the quoted papers how the Berry phases in (13.66) necessarily led to a spontaneously broken symmetry and the appearance of the spin-Peierls order that has already been described. Note that for S even integer, (13.66) is always an integral multiple of $2\pi i$, and so $\mathcal{S}_B$ has no effect—the properties in this case are therefore the same as the rotor model, and there is no spin-Peierls order [10].

The reader may object that the above arguments for the ubiquity of spin-Peierls order in collinear $S = 1/2$ antiferromagnets rely on theories obtained in a semiclassical large S limit, and could possibly break down at small S. This issue has been addressed by studies designed to directly study $S = 1/2$ quantum antiferromagnets either by phenomenological [276, 412] or large N approaches [400]. Neighboring spins are assumed to form singlet bonds in pairs, and then the low-lying, spin-singlet excitations arise from resonance between different arrangements of the bonds (the 'resonating valence bond' picture [21, 41]). From both approaches, the so-called *quantum dimer model* [412] appears as an effective Hamiltonian for the low energy spin-singlet states. This latter model can be studied quite reliably by a series of duality transformations [547, 402, 163, 435] and an 'instanton' gas model emerges which is, quite remarkably, *equivalent* to the hedgehog gas model obtained above from a semiclassical perspective. In particular, each instanton has a Berry phase which is given precisely by (13.66). In this context, the phases in (13.66) are a consequence of the constraint that each $S = 1/2$ spin can form a valence bond with exactly one of its neighbors, whereas, here we obtained (13.66) from a very different coherent state path integral. The identity of these two distinct approaches reinforces our confidence in the correctness of (13.66), and to the presence of spin-Peierls order for $S = 1/2$, which follows quite robustly [402] from it. The quantum dimer model has also been examined in exact diagonalization studies, and again the evidence for spin-Peierls order is quite convincing [305].

13.3.2 Non-collinear ordering and deconfined spinons

We turn to consideration of quantum antiferromagnets which have more complicated ordered magnetic states than those described so far. We will consider models (13.1) on non-bipartite lattices, or with further neighbor interactions so that simple collinear states are not likely to be the ground states. Throughout, we will only be considering states which do not have a macroscopic magnetic moment, *i.e.*, the expectation value of $\sum_i \hat{\mathbf{S}}_i$ in any low-lying state is not of the order of the number of sites in the system. Such states are expected to be preferred in models with all $J_{ij} < 0$. Also we will only consider the case of $d = 2$ here, as $d = 1$ antiferromagnets are better treated by the methods of the following chapter.

The simplest, and most thoroughly studied example of a non-collinear antiferromagnet is the triangular lattice with a nearest-neighbor antiferromagnetic exchange. In the limit $S \to \infty$, the classical ground state is easy to work out: it is characterized by the expectation value

$$\left\langle \hat{\mathbf{S}}_i \right\rangle = S \left(\mathbf{n}_1 \cos(\vec{Q} \cdot \vec{x}_i) + \mathbf{n}_2 \sin(\vec{Q} \cdot \vec{x}_i) \right), \qquad (13.67)$$

where the ordering wavevector $\vec{Q} = (4\pi/a)(1/3, 1/\sqrt{3})$ on a triangular lattice with $(a, 0, 0)$ one of the vectors connecting nearest-neighbor lattice sites, and $\mathbf{n}_{1,2}$ are arbitrary vectors in spin space satisfying

$$\mathbf{n}_1^2 = \mathbf{n}_2^2 = 1 \quad ; \quad \mathbf{n}_1 \cdot \mathbf{n}_2 = 0 \qquad (13.68)$$

These constraints define two orthogonal unit vectors, and each such pair defines a different classical ground state. This is a key difference from the collinear states in Section 13.3.1.2, where only a *single* unit vector was sufficient to characterize the ground state, as in (13.61). Alternatively stated, the order parameter characterizing the broken symmetry in the classical ground state is a *pair* of orthogonal vectors [206, 128]. One possible ground state is shown in Fig 13.3, for the case where $\mathbf{n}_1$, $\mathbf{n}_2$ lie in the plane of the lattice. Other antiferromagnets with *coplanar* ordering in their classical ground states can be treated in an essentially identical manner. Another important example studied in the literature is the square lattice antiferromagnet with first, second, and third neighbor exchanges (the J_1-J_2-J_3 model). For a range of parameters this model has an incommensurate spiral ground state: such an ordering is described as in (13.67), but the wavevector $\vec{Q}$ is no longer pinned at a precise value, and varies continuously as the values of exchange constants are changed. As we move from site to site in the direction $\vec{Q}$ the
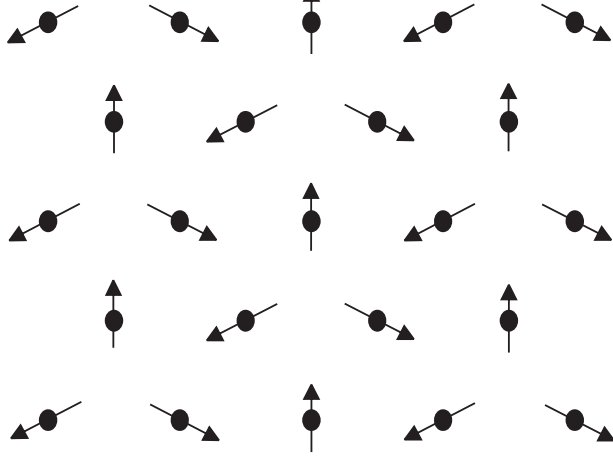
Fig. 13.3. Magnetically ordered ground state on the triangular lattice. The spins have been taken to lie in the plane of the triangular lattice, but this need not generally be the case.

spin orientation rotates by some irrational angle in the plane defined by $\mathbf{n}_1$ and $\mathbf{n}_2$. Finally antiferromagnets in which the spin arrangement is not even coplanar but genuinely three-dimensional can be treated using similar methods, but will not be considered here.

Instead of working with vectors $\mathbf{n}_1$, $\mathbf{n}_2$ which satisfy the constraints (13.68), it is convenient to introduce an alternative parameterization of the space of ground states. It takes 6 real numbers to specify the two vectors $\mathbf{n}_1$, $\mathbf{n}_2$, and the 3 constraints (13.68) reduce the degrees of freedom to 3. We can use these 3 real numbers to introduce two complex numbers z_1, z_2 subject to the single constraint

$$|z_1|^2 + |z_2|^2 = 1. \tag{13.69}$$

We relate these numbers to $\mathbf{n}_1$, $\mathbf{n}_2$ by [24, 98]

$$n_{2\alpha} + in_{1\alpha} = \sum_{a,b,c=1}^{2} \varepsilon_{ac} z_c \sigma_{ab}^{\alpha} z_b, \tag{13.70}$$

where $\alpha = x, y, z$, σ^α are the Pauli matrices, and ε_{ab} is the second-rank antisymmetric tensor $\varepsilon_{12} = -\varepsilon_{21} = 1$, $\varepsilon_{11} = \varepsilon_{22} = 0$. The reader can check that the parameterization (13.70) for $\mathbf{n}_{1,2}$ automatically satisfies (13.68) provided the single constraint (13.69) holds. So we have succeeded in reducing the number of constraints down from 3 to 1. However the mapping from $z_{1,2}$ to $\mathbf{n}_{1,2}$ is not one-to-one but two-to-one; the

two-fold redundancy is apparent from (13.70) as z_a and $-z_a$ correspond to precisely the same $\mathbf{n}_{1,2}$, and therefore the same spin configuration; this redundancy will be crucial to our subsequent considerations. To describe it further, let us decompose z_a into its real and imaginary parts

$$z_1 = m_1 + im_2 \quad ; \quad z_2 = m_3 + im_4. \tag{13.71}$$

Then the order parameter becomes a 4-component, real vector m_ρ ($\rho = 1, 2, 3, 4$) and (13.69) translates into the constraint that this vector has unit length (of course, there is no reason the effective action for m_ρ should be invariant under O(4) rotations in this space–the underlying symmetry is always O(3)). The identity of z_a and $-z_a$ means that m_ρ is a *headless* vector, much like a nematic liquid crystal, which is described by a headless 3-vector.

We can proceed to examine the quantum fluctuations about the above classical states by precisely the same strategy as that followed in Section 13.3.1.2. We allow $\mathbf{n}_{1,2}$, and therefore z_a, to be slowly varying functions of spacetime. We also introduce a slowly varying uniform magnetization field $\mathbf{L}(x,t)$ such that the spatial integral over $\mathbf{L}$ is precisely the total magnetization. Then, following (13.48) we parameterize

$$\mathbf{N}(i,\tau) = \left(\mathbf{n}_1(x_i,\tau) \cos(\vec{Q} \cdot \vec{x}_i) + \mathbf{n}_2(x_i,\tau) \sin(\vec{Q} \cdot \vec{x}_i) \right)$$
$$\times \sqrt{1 - v^2 \mathbf{L}^2(x_i,\tau)} + v\mathbf{L}(x_i,\tau), \tag{13.72}$$

where v is the volume per site. This is to be inserted in the coherent state path integral of H_S in (13.1) and the result expanded in gradients. Finally the uniform magnetization variable $\mathbf{L}$ is to be integrated out as below (13.56). The steps are similar to those in Section 13.3.1.2 and will not be explicitly carried out. Rather, let us try to anticipate the form of the answer on general symmetry grounds.

We list the constraints that must be obeyed by the final effective action:

(i) We must clearly require invariance under spin rotations. These are realized by the global $SU(2)$ transformation

$$\begin{pmatrix} z_1 \\ z_2 \end{pmatrix} \to U \begin{pmatrix} z_1 \\ z_2 \end{pmatrix} \equiv \begin{pmatrix} \alpha & \beta \\ -\beta^* & \alpha^* \end{pmatrix} \begin{pmatrix} z_1 \\ z_2 \end{pmatrix} \tag{13.73}$$

where α and β are complex numbers satisfying $|\alpha|^2 + |\beta|^2 = 1$. Applying this to (13.70), we see that this performs the rotation $n_{1,2\alpha} \to R_{\alpha\beta} n_{1,2\beta}$ where

$$U^\dagger \sigma^\alpha U = R_{\alpha\beta} \sigma^\beta \tag{13.74}$$

(*ii*) Next, we consider the consequences of lattice translations. Any spatial configuration of $\mathbf{n}_{1,2}(x,\tau)$ should have its energy unchanged under translation by a lattice vector $\vec{y}$. By combining (13.70) with (13.72) we see that such a translation is realized by a simple overall phase change of the z:

$$z_a \to e^{-i\vec{Q}\cdot\vec{y}/2} z_a. \tag{13.75}$$

Note that this transformation is not a special case of (13.73), which was restricted to unitary matrices with unit determinant. For the case of the triangular lattices (13.75) requires that the action be invariant under multiplication of z_a by the cube roots of unity. For incommensurate spiral states, by different choices of $\vec{y}$ we see that (13.75) requires invariance under multiplication of z_a by an arbitrary U(1) phase factor.

(*iii*) Finally, let us recall the two-fold redundancy in the mapping from z_a to the $\mathbf{n}_{1,2}$ discussed below (13.70). The change in sign of z_a can vary from point to point in spacetime with no consequence for the $\mathbf{n}_{1,2}$: therefore, we require invariance under the discrete Z_2 gauge transformation

$$z(x,\tau) \to \eta(x,\tau) z(x,\tau) \tag{13.76}$$

where $\eta(x,\tau) = \pm 1$ but can otherwise vary arbitrarily. In the naive continuum limit, the gauge nature of the transformation (13.76) does not impose any additional constraints beyond those arising from a constant η. However, the theory has to be regularized at short scales, and the Z_2 gauge symmetry does impose additional constraints on any effective lattice action. Moreover, the invariance (13.76) will also play a crucial role in the nature of the possible topological defects.

Let us write down the simplest action consistent with the above constraints in the naive continuum limit. Up to second order in spatial gradients, there are only two independent terms: $|\nabla z_a|^2$ and $|z_a^*\nabla z_a|^2$ (a third possibility, $|\varepsilon_{ab}z_a\nabla z_b|^2$ satisfies a simple linear relation with these two). Identical considerations also apply to the terms with two temporal gradients. We are therefore led to the following effective action for the z_a, which plays the role of $\mathcal{S}_n$ in Section 13.3.1.2

$$\mathcal{S}_z = \int d^2x d\tau \sum_{\mu=\vec{x},\tau} \frac{1}{g_\mu} \left[|\partial_\mu z_a|^2 + \gamma_\mu |z_a^*\nabla z_a|^2 \right] \tag{13.77}$$

where g_x, g_τ, γ_x and γ_τ are coupling constants. In addition, as in Section 13.3.1.2, there could be Berry phases, associated with singular

configurations of the z_a. These have to be analyzed on a lattice-by-lattice basis and are not completely understood.

However, even at the level of the action $\mathcal{S}_z$, and ignoring possible Berry phases, open questions remain (in contrast, the action $\mathcal{S}_n$ is believed to be quite thoroughly understood). There are vexing differences between different ways of analyzing $\mathcal{S}_z$: renormalization group analyses using expansions in $(d-1)$, $(3-d)$, or the inverse of the number of z_a components, and numerical simulations[122, 25]. There is little doubt that the fate of the Z_2 gauge symmetry (13.76) plays a crucial role in these differences, as the different approaches treat it in quite inequivalent manners. In particular, the system allows a Z_2 vortex excitation, and the nature of the quantum paramagnet depends upon whether such vortices proliferate or are suppressed. Because of the importance this vortex, let us describe its structure more carefully. The vortex is best visualized in terms of the headless vector m_ρ: as one circles the core of the vortex, m_ρ rotates by 180 degrees about a fixed axis orthogonal to m_ρ. So upon returning to the original point, m_ρ has now turned into $-m_\rho$, but this is acceptable as the overall sign of m_ρ is not significant (in mathematical terms, the order parameter m_ρ belongs to the space S_4/Z_2, and the vortex is associated with its first homotopy group Z_2). An especially clear discussion of such vortices, and their relationship to the Z_2 gauge symmetry has been given by Lammert *et al.* [289] in the context of nematic liquid crystals, and the reader is urged to consult their paper.

We will not survey all earlier approaches to the analysis of $\mathcal{S}_z$ here, but highlight a promising scenario which has some striking consequences for the quantum paramagnet. This scenario emerged first in a direct large N study [403, 436, 419] of the quantum antiferromagnet (13.1) on frustrated lattices, and related results emerge from studies of the continuum theory $\mathcal{S}_z$ in an expansion in the inverse of the number of z_a components, or in an expansion in $(d-1)$ [32, 98, 33, 101]. There are two phases: a magnetically ordered phase and a quantum paramagnet, and these are separated by a second order quantum phase transition. The Z_2 vortices are obviously suppressed in the magnetically ordered phase by the non-zero spin stiffness, but they remain suppressed in the quantum paramagnet, as is also found to be the case in the corresponding phases of the nematic liquid crystal [289]. The physical properties of both phases can be rapidly understood by considering the case $\gamma_\mu = 0$ in (13.77), although this special value will not modify the general form of the following results. For $\gamma_\mu = 0$, we insert (13.71) into (13.77), and see

straightforwardly that the action $\mathcal{S}_z$ is symmetric under O(4) rotations of the m_ρ, and becomes precisely equivalent to the $N = 4$ case of the quantum rotor model $\mathcal{S}_n$ studied intensively in Part 2. The properties of $\mathcal{S}_z$ therefore follow directly from the results of Part 2. The magnetically ordered phase has $3 = 4-1$ linearly dispersing spin wave excitations, and magnetic order disappears at any non-zero temperature. The quantum paramagnetic phase has an energy gap, Δ_+, and the excitations are built out of the Fock space of a 4-fold degenerate particle.

Despite the mapping above to Part 2, there is a crucial distinction in the physical interpretation of the structure of the quantum paramagnet. Its particle excitations are the bosonic quanta of the z_a field, and the transformation (13.73) under spin rotations makes it clear that these bosons carry spin $S = 1/2$. (This accounts for a 2-fold degeneracy of the particle states; an additional factor of 2 comes from accounting for the particle and anti-particle states). This should be contrasted with the $S = 1$ particle that was found in the quantum paramagnetic with collinear correlations in Section 13.3.1.2. These $S = 1/2$ bosonic particles are labeled 'spinons': we can view the $S = 1$ particle as the bound state of two $S = 1/2$ particles, and therefore a quantum transition from a quantum paramagnet with collinear correlations to one with non-collinear correlations can be viewed as one of the deconfinement of spinons: a simple theory for such a transition has been discussed in Refs [403, 436, 419]. Here let us discuss an important physical property of a quantum paramagnet with deconfined spinons: we compute the dynamic susceptibility at the non-collinear ordering wavevector, defined by

$$\chi(k, i\omega_n)\delta_{\alpha\beta} = \frac{v}{M} \sum_{i,j} \int_0^{1/T} d\tau \left\langle \hat{S}_{i\alpha}(i\tau)\hat{S}_{j\beta}(0) \right\rangle e^{-i((\vec{k}+\vec{Q})\cdot(\vec{x}_i - \vec{x}_j) - \omega_n\tau)}.$$

(13.78)

Using (13.70) and (13.72) we see that (ignoring the contribution of **L**, which will only renormalize a pre-factor that can absorbed into a redefinition of the quasiparticle amplitude $\mathcal{A}$):

$$\chi(k, i\omega_n) = \frac{S^2}{6} \sum_{a,b=1}^{2} \int d^2 x \int_0^{1/T} \left\langle z_a(x, i\tau)z_b(x, i\tau)z_a^*(0,0)z_b^*(0,0) \right\rangle.$$

(13.79)

So χ is given by the propagator of *two spinons*, rather than the single particle propagator which appeared in (5.2). As discussed above, the z quanta of the quantum paramagnet have a quasiparticle pole at $T = 0$ as

in (4.99) or (5.30); the contribution of this pole leads to the expression

$$\chi(k, \omega_n) = \mathcal{A}^2 S^2 \Pi(k, \omega_n), \qquad (13.80)$$

where the two-particle propagator Π was discussed in (7.42). At $T = 0$, taking the imaginary part of (7.46) we obtain

$$\mathrm{Im}\chi(k, \omega) = \frac{\mathcal{A}^2 S^2}{8c^2} \frac{\mathrm{sgn}(\omega)}{\sqrt{\omega^2 - c^2 k^2}} \theta \left(|\omega| - (c^2 k^2 + 4\Delta_+^2)^{1/2} \right), \qquad (13.81)$$

where θ is the unit step function. So there is no pole in $\chi(k, \omega)$ as there was for the case of a quantum paramagnet with collinear spin correlations; rather there is a branch cut at frequencies greater than $(c^2 k^2 + 4\Delta_+^2)^{1/2}$, which corresponds to the threshold for the creation of a *pair* of spinons. This branch cut is a characteristic property of the deconfinement of spinons in a quantum paramagnet.

We emphasize that the suppression of the Z_2 vortices was crucial to the existence of the free bosonic spinons in this quantum paramagnet. In the absence of such vortices, it is possible to consistently assign a global phase to a spinon wavefunction without any sign ambiguities. The wavefunction of a spinon changes in sign upon transport around a Z_2 vortex, and so spinons are expected to confine into integer spin excitations when such vortices proliferate [403, 436].

We close this subsection by noting some related issues that have been discussed in the literature.

A spinon-based approach can also be used to describe the collinear antiferromagnets of Section 13.3.1. One obtains the action (13.77), but at the special point $\gamma_\mu = 1$, where the reader can easily check that it is invariant under the $U(1)$ gauge transformation $z_a(x, \tau) \to e^{i\eta(x,\tau)} z_a(x, \tau)$. This theory has been analyzed by a number of methods [529, 112, 401, 402, 70, 100] with the conclusion that the spinons are *confined*, and the resulting spectrum is in agreement with the form already obtained in Section 13.3.1 by other methods.

Another possible quantum paramagnetic state of frustrated antiferromagnets is the "chiral spin liquid" [260, 292, 526, 207] (and the related 'flux phase' [13]). In this state, the local spin correlations are not only non-collinear, but also non-coplanar, and the ground state breaks parity and time-reversal invariance. Classically, it is quite difficult to construct antiferromagnets with non-coplanar spin ordering in the ground states: some rather intricate lattices or multiple spin couplings are usually necessary. The chiral spin liquid would then be accessed by quantum disordering transition from such a magnetically ordered state. The

interest in such a state has been driven primarily by the fact its excitations have rather remarkable properties: they are $S = 1/2$ spinons which obey fractional statistics. Furthermore, it has been predicted that doping such a state would lead to a new type of 'anyonic' superconductivity [291, 292, 89]. However, no experimental realization of this exotic possibility has so far been found. There have also been assertions [292] that $S = 1/2$ spinon excitations of any two dimensional quantum paramagnet should obey fractional statistics, but this does not agree [436] with the bosonic spinon states discussed in the body of this section.

13.4 Partial polarization and canted states

This section will interpolate between the ferromagnetic states studied in Section 13.2, with maximum uniform spin polarization in their ground states, and the antiferromagnets of Section 13.3, which had a thermodynamically negligible spin polarization. One way to do this would be examine the ground states of models H_S in (13.1) at $\mathbf{H} = 0$, but with a set of J_{ij} which can take both signs. Models of this type were examined in Ref [438], and it was argued that they could be described by a ferromagnetic extension of the rotor models studied in Part 2. The properties of such models are quite intricate, and we refer the reader to the original paper for further details. Here, we shall look at a closely related model whose properties are significantly simpler to delineate. We will begin with an antiferromagnet with all $J_{ij} < 0$, and attempt to force in a macroscopic moment by placing it in a strong uniform field $\mathbf{H}$. So the uniform magnetization will not arise spontaneously from ferromagnetic exchange interactions, but will instead be induced by an external field. This will cause important differences in nature of certain spin-wave excitations, which are no longer required to be gapless due to the explicit breaking of rotational invariance in the Hamiltonian. Nevertheless, numerous other features will be very similar to the far more complicated models considered in Ref [438]. Further, the case of an antiferromagnet in a strong uniform field is of direct physical importance, having been investigated in several recent experiments, as we shall discuss in Section 13.5.

The low energy properties of an antiferromagnet in a field $\mathbf{H}$ are described by the action $\mathcal{S}_n$ in (13.58) or (5.16). So far, analyses of these models has been restricted to $\mathbf{H} = 0$, and to linear response to a weak $\mathbf{H}$. Here, we will look at the full non-linear response to a strong $\mathbf{H}$. It should be noted here that, in $d = 1$, closely related results can also be

obtained by the bosonization technique of Chapter 14 [372], while making no reference to the rotor model—we will not follow such an approach here.

We prefer to begin our analysis by placing the continuum model $\mathcal{S}_n$ on a lattice at some short distance scale, and working with the discrete lattice Hamiltonian. This is the inverse of the mapping carried out in Chapter 5, and we therefore obtain the rotor model Hamiltonian H_R in (5.1):

$$H_R = \frac{Jg}{2} \sum_i \hat{\mathbf{L}}_i^2 - J \sum_{\langle ij \rangle} \hat{\mathbf{n}}_i \cdot \hat{\mathbf{n}}_j - \mathbf{H} \cdot \sum_i \hat{\mathbf{L}}_i. \tag{13.82}$$

The lattice sites in this rotor Hamiltonian are not to be identified with the lattice sites of H_S in (13.1); rather each rotor is an effective degree of freedom for a cluster of an even number of spins in the original model. Each such cluster will have a spin singlet ground state for $\mathbf{H} = 0$, as does the on-site Hamiltonian for each rotor in (13.82) - see (2.71). The rotor also has an infinite tower of states with increasing angular momentum in (2.71); in contrast a cluster of p Heisenberg spins with spin S can have a maximum total angular momentum pS. This difference will have some significant consequences for the topology of the phase diagram, but will leave many essential features unaltered–we will comment on this issue later.

We proceed to understanding the properties of H_R in the remainder of this section. The analysis will be quite similar to that discussed for the Boson Hubbard model in Chapter 10, and the results bear some similarity to those in Ref. [258]; indeed, we will find that the phase diagram of H_R is quite similar to that of H_B in (10.4), and the universality classes of the quantum phase transitions reduce either to the models studied in Part 2, or to those in Chapter 11. This similarity is not surprising at one level: the model H_R in the presence of a non-zero $\mathbf{H}$ only has a global U(1) symmetry corresponding to rotations about an axis parallel to the field (rotations about all other axes are not allowed by the non-zero $\mathbf{H}$), and the model H_B also has only a U(1) symmetry. (In the models considered in Ref [438], uniform moments appear spontaneously due to ferromagnetic exchange in a model with full O(3) symmetry, and this reasoning does not hold: however the similarity to H_B persists, with many (but not all) quantum critical points belonging to the same universality classes as those of H_B.)

Most of the physics of H_R already becomes apparent in a mean-field theory similar to that in Section 10.1. As in (10.7), we make a mean-

field ansatz for H_{MF} as the sum of single-site Hamiltonians with initially arbitrary variational parameters:

$$H_{MF} = \sum_i \left(\frac{Jg}{2}\hat{\mathbf{L}}_i^2 - \mathbf{H} \cdot \sum_i \hat{\mathbf{L}}_i - \mathbf{N} \cdot \hat{\mathbf{n}}_i \right). \qquad (13.83)$$

Here the $\mathbf{N}$ are a set of three variational parameters which represent the effects of the exchange J with nearest neighbors in mean-field theory; they play a role similar to that of the complex number Ψ_B in Section 10.1. We have assumed that the $\mathbf{N}$ are site-independent and are therefore excluding the possibility of states with spatial structure: this is for simplicity and it is not difficult to extend our analysis to allow for broken translational symmetries in H_R.

   Now the analysis proceeds as in Section 10.1: determine the ground state wavefunction of H_{MF}, and optimize the expectation value of H_R in this wavefunction towards variations in $\mathbf{N}$. This was done numerically, and leads to the phase diagram in Fig 13.4; we will discuss the properties of each of the phases in turn, and then consider the nature of the transitions between them.

13.4.1 Quantum paramagnet

The optimum value of the variational parameter is $\mathbf{N} = 0$. For this value, H_{MF} is exactly diagonalizable–the eigenstates are simply the rotor eigenstates $|\ell, m\rangle$ of (5.4) and have eigenvalues $Jg\ell(\ell+1)/2 - Hm$. The quantum paramagnet appears when parameters are such that the minimum energy state has $\ell = m = 0$: this happens for small H/J and large g. This quantum paramagnet is precisely the corresponding state of the rotor model studied in Part 2–the field $\mathbf{H}$ couples only to the total spin which is identically zero in the spin singlet ground state: as a result the wavefunction and all equal time correlations are unaffected by a non-zero $\mathbf{H}$. The energy of the spin triplet particle excitations does change as was shown in (5.6), but their wavefunctions also remain unaffected.

13.4.2 Quantized ferromagnets

These phases also have $\mathbf{N} = 0$, and so the eigenenergies of H_{MF} are those listed above. The minimum energy state has $m = \ell$, and the different quantized ferromagnets are identified by the different positive integer values of ℓ as shown in Fig 13.4. The analogy between these phases and
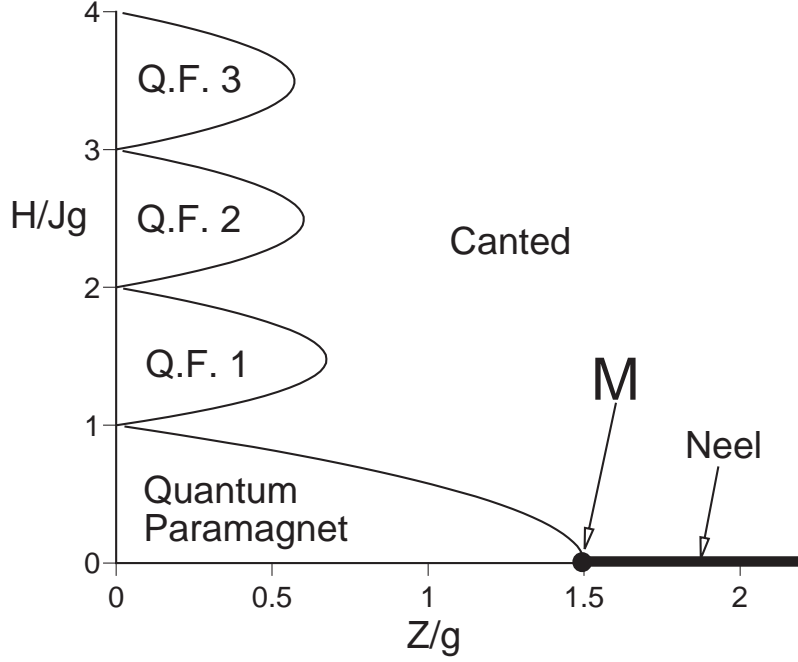
Fig. 13.4. Mean field phase diagram of H_R (in (13.82)), the O(3) quantum rotor model in a field **H**. The notation Q.F. ℓ refers to a quantized ferromagnet with $\langle \hat{L}_z \rangle = \ell$. Compare with the phase diagram of the boson Hubbard model in Fig 10.1: in the latter case, there is no special meaning to the vertical co-ordinate $= 0$, and the vertical axis is unbounded below. The positions of the phase boundaries follow from (13.85). The multicritical point M is precisely the critical point of the O(3) quantum rotor model studied in Part 2.

the Mott-insulating phases of Section 10.1 should be clear: the boson number n_0 corresponds to the integer ℓ. We argued in Section 10.1 that the quantization of n_0 was not an artifact of mean field theory but an exact statement about the full interacting model. Precisely the same arguments apply here to $\langle \hat{L}_z \rangle$ (we are assuming **H** is oriented in the z direction), as the total angular momentum in the z direction commutes with H_R. Such quantized ferromagnetic phases also appear in the models of Ref [438] where ferromagnetism was induced by exchange interactions: in this case complete rotational symmetry of the underlying Hamiltonian implies that the there are gapless spin-wave excitations of the type considered in Section 13.2 with dispersion $\varepsilon_k = (\rho_s/M_0)k^2$. In the present model H_R the spin wave modes acquire a gap from the

external field, and we have $\varepsilon_k = (\rho_s/M_0)k^2 + H$. In these respects these quantized ferromagnets are identical to the fully-polarized ferromagnets of Section 13.2: we simply have to set M_0 equal to the actual quantized value of the ground state magnetization density.

Let us also note some aspects of the interpretation of these quantized ferromagnet phases for underlying spin models like H_S. We noted above that each rotor was an effective degree of freedom for an even number, p, of Heisenberg spins. Such a cluster has maximum spin pS, and so the quantized ferromagnets with $\ell > pS$ clearly cannot exist, and are artifacts of the mapping to the rotor model which introduced an infinite tower of states on each site. Also, for some antiferromagnets, making clusters of p spins may involving reducing the symmetry of the underlying lattice. In this case the quantized ferromagnets with $0 < \ell < pS$ necessarily involve a spontaneously broken translational symmetry: each spin has an average fractional moment of ℓ/p and this can be quantized only if p spins spontaneously group together and carry a total moment ℓ together. This spontaneously broken symmetry will effect the critical theory of the transition out of the quantized phase, but we will not discuss this further here. Finally, the rotor with $\ell = p$ is a fully polarized ferromagnet which can exist without any broken translational symmetry.

It should also be noted that very similar considerations apply for the case of p odd: then we have to work with rotors which carry half integral angular momenta [459, 438].

13.4.3 Canted and Néel States

These states both have $\mathbf{N} \neq 0$, and are thus the analogs of the superfluid state of the boson model of Section 10.1. The Néel state occurs precisely at $\mathbf{H} = 0$, and the full rotational invariance of the Hamiltonian then implies that the direction of $\mathbf{N}$ is immaterial. The *canted* state occurs at non-zero $\mathbf{H}$. If we write $\mathbf{H} = H\mathbf{e}_z$, the numerical optimization of the mean-field Hamiltonian (13.83) shows that the vector $\mathbf{N}$ prefers to lie in the x-y plane; the direction within the plane is immaterial, reflecting the U(1) symmetry of the problem. This orientation of the Néel order parameter in a plane perpendicular to an applied uniform field is quite generic, and the reasons for it will become more evident in Section 13.4.4 below. We choose $N_x \neq 0$ and $N_y = 0$. The resulting canted state is characterized by the non-zero expectation values

$$\langle \hat{n}_x \rangle = N_x/(JZ) \neq 0 \qquad \langle \hat{L}_z \rangle \neq 0, \qquad (13.84)$$
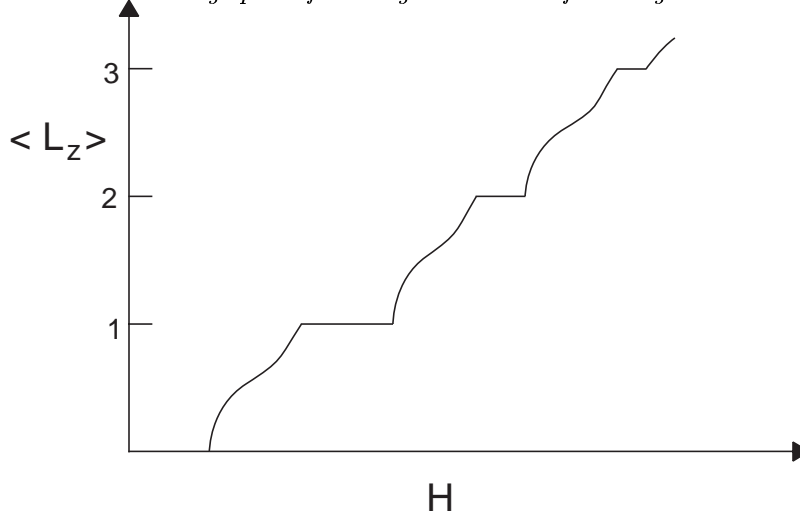
Fig. 13.5. Schematic of the magnetization, $\langle \hat{L}_z \rangle$, as a function of the field **H** for the rotor model (13.82). It is assumed that the value of Z/g in Fig 13.4 is small enough that a vertical line will intersect the Q.F. ℓ phases for $\ell \leq 3$. The magnetization is initially pinned at 0 when the system is in the quantum paramagnet, and is subsequently pinned at ℓ in the Q.F. phases. The magnetization interpolates between these plateaus in the canted or 'unquantized ferromagnet' phase.

and all other components of $\hat{\mathbf{n}}$ and $\hat{\mathbf{L}}$ have vanishing expectation values. The first relation in (13.84) should be compared with (10.9)–its origin is the same. Both non-zero expectation values in (13.84) vary continuously as a function of J, g or H, and nothing is pinned at a quantized value; as there is a non-zero, continuously varying ferromagnetic moment in the canted phase, this is an example of an *'unquantized' ferromagnet*. The results (13.84) also make the origin of term 'canted' clear, as shown in illustration within the canted region of Fig 13.6. In terms of the underlying Heisenberg spins, a non-zero $\langle \hat{n}_x \rangle$ implies antiferromagnetic ordering within the x direction in spin space, while a non-zero $\langle \hat{L}_z \rangle$ implies a uniform ferromagnetic moment in the z direction.

We show a plot of the H dependence of the $T = 0$ magnetization $\langle \hat{L}_z \rangle$ in Fig 13.5. Notice that there are plateaus in the magnetization while the system is in the quantum paramagnetic or quantized ferromagnetic phases. In between these phases is the canted phase, or the unquantized ferromagnet, in which the magnetization continuously interpolates between the quantized values.

The excitation structure of the canted phase is easy to work out. We simply follow the same procedure as that used to the Néel state in Section 5.1.2. Examining equations of the motion of small fluctuations about the ordered state one finds a gapless spin wave excitations with energy $\varepsilon_k \sim k$ corresponding to rotations of the $\hat{\mathbf{n}}$ in the x-y plane. For the case where the canted state appears in a model with full O(3) symmetry, there is an additional gapless mode with dispersion $\varepsilon_k \sim k^2$ [438].

The mean field boundary between the canted/Néel states and the quantized ferromagnets/quantum paramagnet can be computed analytically, using the same analysis leading up to (10.14) for the boson model. We expand the ground state energy of the quantized ferromagnet/quantum paramagnet in powers of N_x and demand that the co-efficient of the N_x^2 vanish. This leads to the analog of the condition $r = 0$ with the expressions (10.15), (10.16); in the present situation we find the condition

$$\frac{g}{Z} = \frac{\dfrac{\ell+1}{(2\ell+3)(\ell+1-H/Jg)} - \dfrac{\ell}{(2\ell+1)(\ell-H/Jg)}}{\dfrac{1}{(2\ell+1)(2\ell+3)(\ell+1+H/Jg)}} \tag{13.85}$$

for the instability of the quantized ferromagnet/quantum paramagnet with $\langle \hat{L}_z \rangle = \ell$ (the denominators in (13.85) are always positive over the range of applicability for a given value of ℓ). Simple application of (13.85) led to Fig 13.4.

An important feature of the above results deserves special mention. Notice that the only phase with a continually varying uniform magnetic moment (an unquantized ferromagnet) is the canted phase. This phase has a broken symmetry in the x-y plane and an associated gapless mode. This result is believed [438] to be a general principle: phases with continuously varying values of a ferromagnetic moment must have gapless spin modes in addition to the usual ferromagnetic spin-waves that are present for the case of a spontaneously generated moment; moreover, unlike the spin-waves, these gapless modes do not acquire a gap in the presence of a uniform field $\mathbf{H}$. In $d \geq 2$, for the rotor models considered here, the gapless modes are associated with the broken symmetry leading to canted order in such phases. In $d = 1$, the analysis in Chapter 11 shows that the order in the x-y plane becomes quasi long-range but the gapless mode survives.

(For completeness, we also note here another physical example of an

unquantized ferromagnet: the Stoner ferromagnet [481] of an interacting Fermi gas, in which there are two Fermi surfaces, one each for up and down spins, with unequal Fermi wavevectors $k_{F\uparrow} \neq k_{F\downarrow}$. The values of $k_{F\uparrow}$ and $k_{F\downarrow}$ can vary continuously as the interaction strength is varied (provided they are both non-zero), and so can the mean magnetic moment. Consistent with the general principle above, in addition to the ferromagnetic spin-waves, this system has low energy spin-flip excitations at finite wave-vectors involving particle-hole pairs near the two Fermi surfaces.)

13.4.4 Zero temperature critical properties

It is clear that the $\mathbf{H} = 0$ transition between the quantum paramagnet and the Néel state is precisely the same as $N = 3$ model intensively studied in Part 2; this critical point is denoted M in Fig 13.4. We will show that the generic $\mathbf{H} \neq 0$ transition between the quantized ferromagnet/quantum paramagnet and the canted state is in the universality class of the dilute Bose gas field theory in (11.1), which was thoroughly studied in Chapter 11. We will do this by examining the line of second order transitions coming into the point M; the remaining portions of the phase boundary can be analyzed in a similar manner. It should also be noted that there are also special 'particle-hole' symmetric points at the tips of the lobes surrounding the quantized ferromagnet phases where the $z = 1$ theory of Part 2 will apply, just as was the case for the Boson Hubbard model in Sections 10.1 and 10.2.

The promised result is most easily established by using the 'soft-spin' theory of the point M studied in Chapter 8. In the presence of a field $\mathbf{H} = H\mathbf{e}_z$ the generalization of the $N = 3$ version of (8.2) is

$$
\mathcal{S}_\phi = \int d^d x \int_0^{1/T} d\tau \left\{ \frac{1}{2} \left[(\partial_\tau \phi_x - iH\phi_y)^2 + (\partial_\tau \phi_y + iH\phi_x)^2 \right. \right.
$$

$$
\left. \left. + (\partial_\tau \phi_z)^2 + c^2 (\nabla_x \vec{\phi})^2 + r\phi_\alpha^2 \right] + \frac{u_0}{4!} (\phi_\alpha^2)^2 \right\} \qquad (13.86)
$$

The uniform magnetic moment density is given by

$$
\frac{1}{v} \langle \hat{L}_z \rangle = -\frac{\partial \mathcal{F}}{\partial H} \qquad (13.87)
$$

where v is the volume per rotor, and $\mathcal{F}$ is the free energy density associated with the action $\mathcal{S}_\phi$.

Let us first discuss the mean field properties of $\mathcal{S}_\phi$, obtained by minimizing the action, while ignoring all spatial and time dependence of
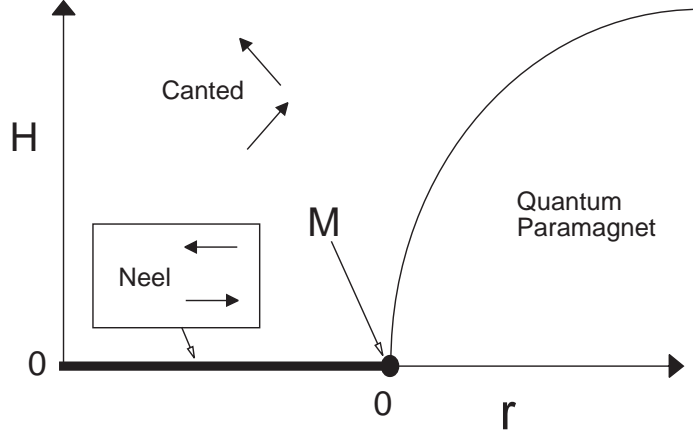
Fig. 13.6. Mean field phase diagram of $\mathcal{S}_\phi$ (in (13.86)) at $T = 0$. The arrows denote the relative orientation of the spins in the corresponding phases of double layer systems, which map onto the rotor model as discussed in Section 5.1.1.1; the field $\mathbf{H}$ is assumed to point towards the top of the page. The multi-critical point M is the $N = 3$ case of the quantum critical point studied in Part 2. Notice that the vicinity of M is similar to that in Fig 13.4.

ϕ_α; this will reproduce the structure in the vicinity of the point M in Fig 13.4 obtained earlier using the mean-field Hamiltonian (13.83). Notice that the components ϕ_x, ϕ_y have a quadratic term with coefficient $r - H^2$, while ϕ_z has the usual coefficient r; so ordering is preferred in the x-y plane, and this was the reason for the choice in the orientation of the $\mathbf{N}$ vector in Section 13.4.3. For $r - H^2 > 0$, the ground state has $\langle \phi_\alpha \rangle = 0$, and is therefore in the quantum paramagnetic phase. For $r - H^2 < 0$, the ground state has $\langle \phi_\alpha \rangle \neq 0$ and in the x-y plane. This is the C phase and the fields have the expectation values

$$\phi_\alpha = \left(\left(\frac{6(H^2 - r)}{u_0} \right)^{1/2}, 0, 0 \right) \qquad \frac{1}{v} \langle \hat{L}_z \rangle = \frac{6H(H^2 - r)}{u_0}, \quad (13.88)$$

or any rotation of ϕ_α in the $x - y$ plane. Notice that $\langle \hat{L}_z \rangle$ vanishes for $H = 0$, and therefore the line $r < 0$, $H = 0$ is the Néel state. The resulting mean field phase diagram is shown in Fig 13.6 and is identical to the vicinity of the point M in Fig 13.4. Let us focus on the vicinity of the generic transition between the quantum paramagnet and the canted phase: this corresponds to the regime $|r - H^2| \ll |r|$. In

this region we can neglect ϕ_z fluctuations and focus only on the $\phi_x + i\phi_y$ which is undergoing Bose condensation. Further, the second-order time derivative in $\mathcal{S}_\phi$ can be dropped as the low energy properties are dominated by the more relevant first order time derivative that appears by expanding the first two terms in $\mathcal{S}_\phi$. Making these approximations, and defining

$$\Psi = \frac{\phi_x + i\phi_y}{\sqrt{H}}, \tag{13.89}$$

we see that $\mathcal{S}_\phi$ reduces to

$$\mathcal{S}_\Psi = \int d^2x \int_0^{1/T} d\tau \left[\Psi^* \frac{\partial \Psi}{\partial \tau} + \frac{c^2}{2H} |\nabla_x \Psi|^2 \right.$$
$$\left. + \frac{(r - H^2)}{2H} |\Psi|^2 + \frac{u_0}{24H^2} |\Psi|^4 \right]. \tag{13.90}$$

This is precisely the theory (11.1), establishing the claim made at the beginning of this subsection.

13.5 Applications and extensions

There has been a great deal of theoretical work on possible quantum paramagnetic ground states of two dimensional, $S = 1/2$ Heisenberg antiferromagnets. On the square lattice, we have already noted the studies on the $J_1 - J_2$ and $J_1 - J_2 - J_3$ models which show clear evidence for the existence of a quantum paramagnetic ground state in a window around $J_2/J_1 \approx 0.5$, $J_3 = 0$. Some of these studies [174, 173, 350, 388, 450, 304] also show reasonable evidence for the existence of columnar spin-Peierls order of the type discussed in Section 13.3.1.2 and shown in Fig 13.2, as was predicted from the Berry phase analyses of Refs [401, 402, 403, 436]. More recently, Zhitomirsky and Ueda have suggested that the plaquette state in Fig 13.2 may be the lowest energy one: this possibility was not thoroughly tested in the earlier work.

The weight of the evidence on the triangular lattice is that the model with only nearest neighbor interactions has long range Néel order of the type shown in Fig 13.3 [94, 283, 50]; other types of magnetic order appear upon including further neighbor exchanges [296]. However, the introduction of multiple spin ring exchanges can induce quantum paramagnetic ground states [346], and these are candidates for exhibiting deconfined spinon excitations in two dimensions. The latter case of

multiple spin exchange appears to have an experimental realization in experiments on an adsorbed ^{3}He layer on graphite [413].

The nearest neighbor $S = 1/2$ antiferromagnet on the kagome lattice has also been intensively studied: here it is virtually certain that the ground state is a quantum paramagnet with a gap towards excitations with non-zero spin. However, there appear to be a large number of low-lying, singlet excitations. These could possibly be described by an effective quantum dimer model [412] and arguments have been advanced [419] that this model should have a gap on the kagome lattice. The current situation, along with earlier references to the literature, has been discussed by Waldtmann *et al.* [522].

The most precise study of the quantum critical point between an ordered Néel state and a quantum paramagnet has been carried out by Troyer *et al.* [497] on a depleted square lattice. All universal properties are in agreement with those of the O(3) quantum rotor model of Part 2, supporting the irrelevancy of the Berry phase terms, discussed in Section 13.3.1.2, for the critical phenomena.

An important experimental candidate for a gapped quantum paramagnetic ground state in two dimensions in CaV_4O_9. The experimental measurements [487] clearly indicate the presence of a spin gap, but there remains a debate upon the nature of the microscopic spin Hamiltonian needed to explain the observations [176, 384, 266].

The analyses of Section 13.4 should make it clear that the dilute Bose gas quantum critical point of Chapter 11 describes the closing of a spin gap of an antiferromagnet by a strong external magnetic field [448, 6, 7, 502, 470, 439, 90]. This critical point has been intensively studied recently in spin ladder organic compound $Cu_2(C_5H_{12}N_2)_2Cl_4$ [79, 80, 81, 209, 137]. The onset of magnetization plateaus at a finite field (as in Fig 13.5) is also described by the same quantum critical point, and such plateaus have been observed recently in experiments on one-dimensional spin chains [358, 463].

A novel realization of the $d = 2$ continuum quantum ferromagnets of Section 13.2 is provided by magnetization studies of single layer quantum Hall systems at filling factor $\nu = 1$ [468, 145, 264, 265]. These are electronic systems with a gap towards charged excitations, and a strong ferromagnetic exchange between the electronic spins. As a result, the low-lying spin excitations are well described by the continuum theory (13.32). The magnetization of this system for different T and H has been measured in NMR [39] and optical [14, 326] experiments, and the results have been interpreted by computations on (13.32) [26, 404, 491].

Exciting recent developments have appeared in studies of double layer quantum Hall systems, when two single layer systems in a ferromagnetic quantum Hall state with a charge gap, are brought close to each other [385, 377, 445, 378, 310]. There is an antiferromagnetic exchange pairing between the layers [546], which suggests that we may consider the two layers to be similar to the two sublattices of an antiferromagnet, and that there is an effective rotor model description of the spin excitations. Indeed, it has been argued [120, 121] that the system maps precisely onto the model studied in Section 13.4. Detailed light scattering studies have mapped out the phase diagram of the system [378], and the results are consistent with Figs 13.4 and 13.6. Specific quantitative predictions for quantum critical behavior have been made in Refs [120, 121, 498, 331, 431], and these and dynamical results like those in Section 8.3 could be tested in future experiments.

14
Spin chains: bosonization

This chapter has two central aims. The first is to describe a particular class of $S = 1/2$ antiferromagnets in $d = 1$ and to understand their properties in the context of the general discussion of antiferromagnets in Chapter 13. The second is to introduce the technical tool of bosonization, and to illustrate its utility in the solutions of the models noted. The powerful bosonization method has been used extensively in recent years to understand a wide variety of systems in one dimension. We shall not attempt to survey this vast literature here, but refer the reader to a number of available reviews: a description of some important current topics appears in articles by Schulz [449] and Affleck [5]. However, most of the basic ideas and general principles will make an appearance in our treatment here. The author benefited from unpublished Trieste lecture notes of T. Giamarchi in preparing this chapter.

The antiferromagnetic chain we shall study [202] has the Hamiltonian

$$H_{12} = J_1 \sum_i \left(\hat{\sigma}_i^x \hat{\sigma}_{i+1}^x + \hat{\sigma}_i^y \hat{\sigma}_{i+1}^y + \lambda \hat{\sigma}_i^z \hat{\sigma}_{i+1}^z \right)$$

$$+ J_2 \sum_i \left(\hat{\sigma}_i^x \hat{\sigma}_{i+2}^x + \hat{\sigma}_i^y \hat{\sigma}_{i+2}^y + \hat{\sigma}_i^z \hat{\sigma}_{i+2}^z \right), \qquad (14.1)$$

where the $\hat{\sigma}_i^\alpha$ are Pauli matrices representing a $S = 1/2$ spin at site i, and the subscript 12 on H indicates the presence of first and second neighbor interactions. For $\lambda = 1$ this reduces to the $S = 1/2$ Heisenberg Hamiltonian H_S in (13.1), with first ($J_1 > 0$) and second ($J_2 > 0$) neighbor exchange in $d = 1$, which was studied in the continuum limit of the coherent state path integral in Chapter 13. We have introduced the anisotropy parameter λ to make contact with the quantum XX chain studied in Sections 11.1 and 11.4 by rather different methods; for $\lambda = 0$ and $J_2 = 0$, (14.1) reduces to the XX Hamiltonian in (11.5). We

shall use these latter methods here, and show how they can be combined
with bosonization to examine the more general model (14.1). Recall that
the XX chain had a global U(1) symmetry, and an associated conserved
charge $Q = (1/2) \sum_i \hat{\sigma}_i^z$: this U(1) symmetry is also present in H_{12} for
general λ. Only the point $\lambda = 1$ has the full Heisenberg $SU(2)$ symmetry.

   We will begin by re-examining the XX model in Section 14.1, and
re-obtain the results of Section 11.4 by introducing the bosonization
method. The same method will be used to describe the phases and low
T properties of H_{12} in Section 14.2. Finally in Section 14.3 we will
rectify an omission from Part 2: we will examine that $N = 2$ $d = 1$
quantum rotor model, and show how it can be understood by a simple
adaptation of the methods introduced in this chapter.

14.1 The XX chain revisited: bosonization

This section will examine the model H_{12} at $\lambda = 0$ and $J_2 = 0$. Then,
as noted earlier, H_{12} reduces to the Hamiltonian H_{XX} in (11.5). For
antiferromagnetic exchange $J_1 > 0$, we obtain H_{XX} with a coupling
$w < 0$; it is somewhat inconvenient to work with a $w < 0$, but we can
map to $w > 0$ by changing the signs of the $\hat{\sigma}^x \hat{\sigma}^x$ and $\hat{\sigma}^y \hat{\sigma}^y$ terms in H_{12}
by rotating every second spin by 180 degrees about the z axis. We used
the Jordan-Wigner transformation to map H_{XX} onto a model of free
spinless fermions, and with the staggered rotation, the transformation
(4.24,4.25) becomes

$$
\begin{aligned}
\hat{\sigma}_i^z &= 1 - 2c_i^\dagger c_i \\
\hat{\sigma}_i^+ &= (-1)^i \prod_{j<i} \left(1 - 2c_j^\dagger c_j\right) c_i \\
\hat{\sigma}_i^- &= (-1)^i \prod_{j<i} \left(1 - 2c_j^\dagger c_j\right) c_i^\dagger..
\end{aligned}
\tag{14.2}
$$

Inserting (14.2) into (14.1) we find

$$
\begin{aligned}
H_{12} = -\sum_i & \Big[2J_1 (c_{i+1}^\dagger c_i + c_i^\dagger c_{i+1}) + J_1\lambda(2c_i^\dagger c_i - 1)(2c_{i+1}^\dagger c_{i+1} - 1) \\
& + J_2(2c_i^\dagger c_i - 1)(2c_{i+2}^\dagger c_{i+2} - 1) \\
& - 2J_2\left(c_i^\dagger(2c_{i+1}^\dagger c_{i+1} - 1)c_{i+2} + c_{i+2}^\dagger(2c_{i+1}^\dagger c_{i+1} - 1)c_i\right)\Big]
\end{aligned}
\tag{14.3}
$$

So for $J_2 = 0$, $\lambda = 0$ we see that H_{12} reduces to the free fermion form
(11.6) of H_{XX} with $w = 2J_1$ and $\mu = 2w$.

   The spin correlations of H_{XX} were examined in Section 11.4, and we

were then especially interested in the quantum phase transition which occurred when the density of fermions in the ground state went from being pinned at zero to a non-zero value. As discussed in Section 11.1 and Fig 11.1, this transition occurred at $\mu = 0$. Here we are interested in the case $\mu = 2w$, when the density of fermions is non-zero and large; by Fig 11.1 the fermion band is exactly half-filled. So we are well away from the quantum critical point of interest in Chapter 11, and are solely interested in the finite ground state fermion density region. This places us exclusively within the Tomonaga-Luttinger liquid region of Section 11.4.2: this is the region labeled "Fermi liquid" in Fig 11.2, which applies to general d. We gave a complete derivation of the asymptotic form of the $T > 0$, equal-time correlators of the Tomonaga-Luttinger liquid region in Section 11.4.2, and then deduced the ground state correlators in (11.84,11.85) by appealing to a mapping based on conformal invariance. The analysis there was specialized to the case $\mu > 0$, but $|\mu| \ll w$, but precisely the same methods also work for $\mu = 2w$. Using the same steps as those leading up to (11.85) (or to (4.112) for the quantum Ising chain), we can obtain the following $T = 0$ correlators of H_{12} at $\lambda = 0$, $J_2 = 0$ [333, 425]:

$$\langle \hat{\sigma}_i^x \hat{\sigma}_{i+n}^x \rangle = \langle \hat{\sigma}_i^y \hat{\sigma}_{i+n}^y \rangle = (-1)^n \frac{8(G_I(0))^2}{(2\pi n)^{1/2}} \quad \text{as } n \to \infty, \qquad (14.4)$$

where the numerical constant $G_I(0)$ was defined in (4.68) and its value was quoted above (4.111). The leading $(-1)^n$ prefactor is as expected from the staggered spin correlations in an antiferromagnet; technically it arises from the staggered rotation of the spins in (14.2). We can also directly use the first mapping in (14.2) to obtain correlators of $\hat{\sigma}^z$ quite simply:

$$\langle \hat{\sigma}_i^z \hat{\sigma}_{i+n}^z \rangle = \delta_{n,0} + (1 - \delta_{n,0}) \left(-\frac{2}{\pi^2 n^2} + \frac{2\cos(\pi n)}{\pi^2 n^2} \right). \qquad (14.5)$$

This section will obtain the power-law decays in (14.4) and (14.5) by the bosonization method [480, 492, 315, 314]. However, this approach abandons attempts to keep track of most of the prefactors (only the prefactor of the non-oscillating $1/n^2$ decay of the conserved z-component of the spin in (14.5) will be obtained exactly). This 'sloppiness' is compensated by the important advantage that the method applies for non-zero λ and J_2. Further, the validity of the conformal mapping between $T > 0$ and $T = 0$ correlators noted above will be explicitly demonstrated.

We begin by taking the continuum limit of H_{12} in (14.3) at $J_2 = \lambda = 0$

in precisely the same manner as discussed in Section 11.2.2 for the 'Fermi liquid' region of Fig 11.2. With lattice spacing a, we introduce the continuum Fermi field $\Psi_F(x, \tau)$ as in (4.39), and then parameterize it in terms of left (Ψ_L) and right (Ψ_R) moving excitations in the vicinity of the Fermi points as in (11.27): the fermion band is half-filled, and so in this case $k_F = \pi/a$. The fields $\Psi_{L,R}$ are described by the simple Hamiltonian

$$H_{FL} = -iv_F \int dx \left(\Psi_R^\dagger \frac{\partial \Psi_R}{\partial x} - \Psi_L^\dagger \frac{\partial \Psi_L}{\partial x} \right), \tag{14.6}$$

which corresponds to the Lagrangean $\mathcal{L}_{FL}$ in (11.28); the Fermi velocity given by $v_F = 4J_1 a$.

We will examine $\mathcal{L}_{FL}$ a bit more carefully, and show, somewhat surprisingly, that it can also be interpreted as a theory of free relativistic bosons. The mapping can be rather precisely demonstrated by placing $\mathcal{L}_{FL}$ on a system of finite length L. We choose to place anti-periodic boundary conditions of the Fermi fields $\Psi_{L,R}(x + L) = -\Psi_{L,R}(x)$: this arbitrary choice will not effect the thermodynamic limit $L \to \infty$, which is ultimately all we are interested in. We can expand $\Psi_{L,R}$ in Fourier modes

$$\Psi_R(x) = \frac{1}{\sqrt{L}} \sum_{n=-\infty}^{\infty} \Psi_{Rn} e^{i(2n-1)\pi x/L}, \tag{14.7}$$

and similarly for Ψ_L. The Fourier components obey canonical Fermi commutation relations $\{\Psi_{Rn}, \Psi_{Rn'}^\dagger\} = \delta_{nn'}$, and are described by the simple Hamiltonian

$$\widetilde{H}_R = \frac{\pi v_F}{L} \sum_{n=-\infty}^{\infty} (2n - 1) \Psi_{Rn}^\dagger \Psi_{Rn} - E_0, \tag{14.8}$$

where the superscript in $\widetilde{H}_R$ has been introduced to prevent confusion with the rotor Hamiltonian (5.1), and E_0 is an arbitrary constant setting the zero of energy, which we adjust to make the ground state energy of H_R exactly equal to 0; very similar manipulations apply to the left-movers Ψ_L. The ground state of H_R has all fermions states with $n > 0$ empty, while those with $n \leq 0$ are occupied. We also define the total fermion number ('charge'), Q_R, of any state by the expression

$$Q_R = \sum_n\ :\Psi_{Rn}^\dagger \Psi_{Rn}: \tag{14.9}$$

The colons are the so-called 'normal-ordering' symbol—they simply indicate that the operator enclosed between them should include a c-number

subtraction of its expectation value in the ground state of $\widetilde{H}_R$, which of course ensures that $Q_R = 0$ in the ground state. Note that Q_R commutes with $\widetilde{H}_R$ and so we need only consider states with definite Q_R, which allows us to treat Q_R as simply an integer. The partition function, Z_R, of $\widetilde{H}_R$ at a temperature T is then easily computed to be

$$Z_R = \prod_{n=1}^{\infty} (1 + q^{2n-1})^2 \qquad (14.10)$$

where

$$q \equiv e^{-\pi v_F / TL} \qquad (14.11)$$

The square in (14.10) arises from the precisely equal contributions from the states with n and $-n+1$ in (14.8) after the ground state energy E_0 has been subtracted out.

We will provide an entirely different interpretation of the partition function Z_R. Instead of thinking in terms of occupation numbers of individual fermion states, let us focus instead on 'particle-hole' excitations. We create a particle-hole excitation of 'momentum' $n > 0$ above any fermion state by taking a fermion in an occupied state n' and moving it to the unoccupied fermion state $n' + n$. Clearly the energy change in such a transformation is $2n\pi v_F/L$, and is independent of the value of n'. This independence on n' is a crucial property, and is largely responsible for the results that follow: it is a consequence of the linear fermion dispersion in (11.27), and of being in $d = 1$. We will interpret the creation of such a particle-hole excitation as being equivalent to the occupation of a state with energy $2n\pi v_F/L$ created by the canonical boson operator $b_{Rn}^{\dagger}$. We can place an arbitrary number of bosons in this state, and we will now show how this is compatible with the multiplicity of the particle-hole excitations that can be created in the fermionic language.

The key observation is that there is a precise one-to-one mapping between the fermionic labeling of the states and those specified by the bosons creating particle-hole excitations. Take any fermion state, $|F\rangle$, with an arbitrary set of fermion occupation numbers and 'charge' Q_R. We will uniquely associate this state with a set of particle-hole excitations above a particular fermion state we label $|Q_R\rangle$; this is the state with the lowest possible energy in the sector of states with charge Q_R, *i.e.*, $|Q_R\rangle$ has all fermion states with $n \leq Q_R$ occupied, and all others
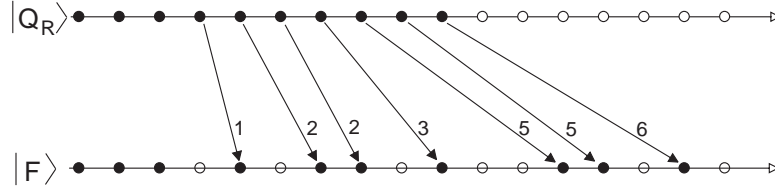
Fig. 14.1. Sequence of particle-hole excitations (bosons b_{Rn}) by which one can obtain an arbitrary fermion state $|F\rangle$ from the state $|Q_R\rangle$, which is the lowest energy state with charge Q_R. The filled (open) circles represent occupied (unoccupied) fermion states with energies that increase in units of $2\pi v_F/L$ to the right. The arrows represent bosonic excitations, b_{Rn}, with the integer representing the value of n. Note that the bosons act in descending order in energy upon the descending sequence of occupied states in $|Q_R\rangle$.

unoccupied. The energy of $|Q_R\rangle$ is

$$
\frac{\pi v_F}{L} \sum_{n=1}^{|Q_R|} (2n-1) = \frac{\pi v_F Q_R^2}{L} \tag{14.12}
$$

Now to obtain the arbitrary fermion state, $|F\rangle$, with charge Q_R, first take the fermion in the 'topmost' occupied state in $|Q_R\rangle$, (*i.e.*, the state with $n = Q_R$) and move it to the topmost occupied state in $|F\rangle$ (See Fig 14.1). Perform the same operation on the fermion in $n = Q_R - 1$ by moving it to the next lowest occupied state in $|F\rangle$. Finally, repeat until the state $|F\rangle$ is obtained. This order of occupying the boson particle-hole excitations ensures that the $b_{Rn}^\dagger$ act in descending order in n. Such an ordering allows one to easily show that the mapping is invertible and one-to-one: given any set of occupied boson states, $\{n\}$, and a charge Q_R, we start with the state $|Q_R\rangle$ and act on it with the set of Bose operators in the same descending order—their ordering ensures that it is always possible to create such particle-hole excitations from the fermionic state, and one is never removing a fermion from an unoccupied state or adding it to an occupied state. The gist of these simple arguments is that the states of the many-fermion Hamiltonian $\widetilde{H}_R$ in (14.8) are in one-to-one correspondence with the many boson Hamiltonian

$$
\widetilde{H}_R' = \frac{\pi v_F Q_R^2}{L} + \frac{2\pi v_F}{L} \sum_{n=1}^{\infty} n b_{Rn}^\dagger b_{Rn} \tag{14.13}
$$

where Q_R can take an arbitrary integer value. It is straightforward to

compute the partition function of $\widetilde{H}'_R$ and we find

$$Z'_R = \left[\prod_{n=1}^{\infty} \frac{1}{(1-q^{2n})} \right] \left[\sum_{Q_R=-\infty}^{\infty} q^{Q_R^2} \right]. \tag{14.14}$$

Our pictorial arguments above are a proof that we must have $Z_R = Z'_R$: that this is the case is an identity from the theory of elliptic function—the reader is invited to verify that the expressions (14.10) and (14.14) generate identical power series expansions in q.

The above gives an appealing picture of bosonization at the level of states and energy levels, but we want to extend it to include operators. To this end, we consider the operator $\rho_R(x)$ representing the normal-ordered fermion density:

$$\rho_R(x) =: \Psi_R^\dagger(x) \Psi_R(x) := \frac{Q_R}{L} + \frac{1}{L} \sum_{n \neq 0} \rho_{Rn} e^{i2n\pi x/L}, \tag{14.15}$$

where the last step is a Fourier expansion of $\rho_R(x)$; the zero wavevector component is Q_R/L, while non-zero wavevector terms have coefficient ρ_{Rn}. The commutation relations of the ρ_{Rn} are central to our subsequent considerations, and require careful evaluation; we have

$$\begin{aligned}
[\rho_{Rn}, \rho_{R-n'}] &= \sum_{n_1, n_2} [\Psi_{Rn_1}^\dagger \Psi_{Rn_1+n}, \Psi_{Rn_2}^\dagger \Psi_{Rn_2-n'}] \\
&= \sum_{n_2} \left(\Psi_{Rn_2+n}^\dagger \Psi_{Rn_2-n'} - \Psi_{Rn_2}^\dagger \Psi_{Rn_2+n-n'} \right) (14.16)
\end{aligned}$$

It may appear that a simple of change of variables in the summation over the second term in (14.16) ($n_2 \to n_2 + n$) shows that it equals the first, and so the combined expression vanishes. However, this is incorrect because it is dangerous to change variables on expressions which involve the summation over all integer values of n_2, and are therefore individually divergent; rather, we should first decide upon a physically motivated large momentum cutoff which will make each term finite, and then perform the subtraction. We know that the linear spectrum in (14.8) holds only for a limited range of momenta, and for sufficiently large $|n|$ lattice corrections to the dispersion will become important. However, in the low-energy limit we are interested in, the high fermionic states at such momenta will be rarely, if ever, excited from their ground state configurations. We can use this fact to our advantage by explicitly subtracting the ground state expectation value ('normal-order') from every fermionic bilinear we consider; the fluctuations will then be practically zero for the

high energy states in both the linear spectrum model (14.8) and the actual physical systems, and only the low energy states, where (14.8) is actually a good model, will matter. After such normal-ordering, the summation over both terms in (14.15) is well-defined and we are free to change the summation variable. As a result, the normal-ordered terms then do indeed cancel, and the expression (14.16) reduces to

$$
\begin{aligned}
[\rho_{Rn}, \rho_{R-n'}] &= \delta_{nn'} \sum_{n_2} \left(\langle \Psi^\dagger_{Rn_2-n} \Psi_{Rn_2-n} \rangle - \langle \Psi^\dagger_{Rn_2} \Psi_{Rn_2} \rangle \right) \\
&= \delta_{nn'} n.
\end{aligned} \tag{14.17}
$$

This key result shows that the only non-zero commutator is between ρ_{Rn} and ρ_{R-n}, and that it is simply the number n. By a suitable rescaling of the ρ_{Rn} it should be evident that we can associate them with canonical bosonic creation and annihilation operators. We will not do this explicitly, but will simply work directly with the ρ_{Rn} as a set of operators obeying the defining commutation relation (14.17), without making explicit reference to the fermionic relation (14.15). We assert that the Hamiltonians $\widetilde{H}_R$, $\widetilde{H}'_R$ are equivalent to

$$
\widetilde{H}''_R = \frac{\pi v_F Q_R^2}{L} + \frac{2\pi v_F}{L} \sum_{n=1}^{\infty} \rho_{R-n} \rho_{Rn}. \tag{14.18}
$$

This assertion is simple to prove. First, it is clear from the commutation relations (14.17) that the eigenvalues and degeneracies of (14.18) are the same as those of (14.13) (the individual states are however not the same: there is a complicated linear relation between them, which is not difficult to reconstruct from our definitions of the operators ρ_{Rn} and b_{Rn}). Second, the definition (14.18), and the commutation relations (14.17) imply that

$$
[\widetilde{H}''_R, \rho_{R-n}] = \frac{2\pi v_F n}{L} \rho_{R-n}; \tag{14.19}
$$

Precisely the same commutation relation follows from the fermionic form (14.8) and the definition (14.15).

We have completed a significant part of the bosonization program: we have the 'bosonic' Hamiltonian in (14.18) in terms of the operators ρ_{Rn} which obey (14.17) and also have the simple explicit relation (14.15) to the fermionic fields. Before proceeding further, we introduce some notation which allows us to recast the results obtained so far in a compact, local, and physically transparent notation. We combine the operators ρ_{Rn} and ρ_{Ln} (the Fourier components of the left-moving fermions Ψ_L)

into two local fields $\phi(x)$ and $\theta(x)$, defined by

$$
\begin{aligned}
\phi(x) &= -\phi_0 + \frac{\pi Q x}{L} - \frac{i}{2} \sum_{n \neq 0} \frac{e^{i 2 n \pi x / L}}{n} \left[\rho_{Rn} + \rho_{Ln} \right] \\
\theta(x) &= -\theta_0 + \frac{\pi J x}{L} - \frac{i}{2} \sum_{n \neq 0} \frac{e^{i 2 n \pi x / L}}{n} \left[\rho_{Rn} - \rho_{Ln} \right], \quad (14.20)
\end{aligned}
$$

where $Q = Q_R + Q_L$ is the total charge, $J = Q_R - Q_L$, and ϕ_0 and θ_0 are a pair of angular variables which are canonically conjugate to J and Q respectively, *i.e.*, the only non-vanishing commutation relations between the operators on the right-hand sides of (14.20) are (14.17) and $[\phi_0, J] = i$ and $[\theta_0, Q] = i$. Our objective in introducing these is that a number of simple and elegant results follow. First, using (14.20), and the commutators just noted, we have

$$
[\nabla \phi(x), \theta(y)] = [\nabla \theta(x), \phi(y)] = i \pi \delta(x - y). \quad (14.21)
$$

Second, (14.18) can now be written in the compact, local form

$$
\widetilde{H}_R'' + \widetilde{H}_L'' = \frac{v_F}{2\pi} \int_0^L dx \left[\frac{1}{K} (\nabla \phi)^2 + K (\nabla \theta)^2 \right], \quad (14.22)
$$

where the dimensionless coupling K has been introduced for future convenience; in the present situation $K = 1$, but we will see later that moving away from H_{XX} to more general H_{12} will lead to other values of K. The expressions (14.22) and (14.21) can be taken as defining relations, and we could have derived all the properties of the ρ_{Rn}, ρ_{Ln}, θ_0, ϕ_0 as consequences of the mode expansions (14.20), which follow after imposition of the periodic boundary conditions

$$
\phi(x + L) = \phi(x) + \pi Q \qquad \theta(x + L) = \theta(x) + \pi J. \quad (14.23)
$$

These conditions show that $\phi(x)$ and $\theta(x)$ are to be interpreted as angular variables. Our final version of the bosonic form of $\widetilde{H}_R + \widetilde{H}_L$ in (14.8) is contained in the (14.21), (14.22) and (14.23), and the two formulations are logically exactly equivalent. The Hilbert space splits apart into sectors defined by the integers $Q = Q_R + Q_L$, $J = Q_R - Q_L$ (and so $(-1)^Q = (-1)^J$), which measure the total charge of the left and right moving fermions. All fluctuations in each sector are defined by the fluctuations of the local angular bosonic fields $\phi(x)$ and $\theta(x)$, or equivalently by the fermionic fields $\Psi_R(x)$ and $\Psi_L(x)$.

We are going to make extensive use of the fields $\phi(x)$, $\theta(x)$ in the following, and so their physical interpretation would be useful. First,

the field ϕ has nothing to do with the O(N) order parameter ϕ_α used in other chapters of this book: both notations are standard, and the context should prevent confusion. The meaning of ϕ follows from the derivative of (14.20), which with (14.15) gives

$$\nabla\phi(x) = \pi\rho(x) \equiv \pi(\rho_R(x) + \rho_L(x)). \qquad (14.24)$$

So the gradient of ϕ measures the total density of particles, and $\phi(x)$ increases by π each time x passes through a particle. The expression (14.24) also shows that we can interpret $\phi(x)$ as the displacement of the particle at position x from a reference state in which the particles are equally spaced as in a crystal, *i.e.*, $\phi(x)$ is something like a phonon displacement operator whose divergence is equal to the local change in density. Turning to $\theta(x)$, one interpretation follows from (14.21) which shows that $\Pi_\phi(x) \equiv -\nabla\theta(x)/\pi$ is the canonically conjugate momentum variable to the field $\phi(x)$. In other words, Π_ϕ^2 is the kinetic energy associated with the 'phonon' displacement $\phi(x)$. Using this interpretation, we can easily apply the methods of Chapter 2 to obtain the Lagrangean form of (14.22):

$$\mathcal{S}_{TL} = \frac{1}{2\pi K v_F} \int dx d\tau \left[(\partial_\tau\phi)^2 + v_F^2(\nabla\phi)^2 \right], \qquad (14.25)$$

where the subscript TL represents Tomonaga-Luttinger. This is just the action of a free, massless, relativistic scalar field. Conversely, we also have a 'dual' formulation of $\mathcal{S}_{TL}$ in which we interpret $\theta(x)$ as the fundamental degree of freedom, and $\Pi_\theta \equiv -\nabla\phi/\pi$ as its canonically conjugate momentum; then we obtain the same action but with $K \to 1/K$

$$\mathcal{S}_{TL} = \frac{K}{2\pi v_F} \int dx d\tau \left[(\partial_\tau\theta)^2 + v_F^2(\nabla\theta)^2 \right], \qquad (14.26)$$

for $\widetilde{H}_R + \widetilde{H}_L$. In this approach a direct physical interpretation of $\theta(x)$ is lacking; we will see below that we can interpret it as an angular variable corresponding to the O(2) order-parameter correlations associated with the antiferromagnet H_{XX} in (11.5). In particular we will find $\hat{\sigma}_+ \sim (\hat{\sigma}_x + i\hat{\sigma}_y) \sim (\phi_1 + i\phi_2) \sim (n_1 + in_2) \sim e^{i\theta}$ (here we have used the notations of Part 2, where $\vec{\phi}$ and $\mathbf{n}$ represent an O(2) order parameter). So a slowly-varying θ corresponds to ordering in the x-y plane in the original antiferromagnet. Also, if, as in Section 11.1 we interpret the $S = 1/2$ antiferromagnet as a hard-core Bose gas, then $e^{i\theta}$ is the superfluid order parameter. Another important property of θ is obtained by taking the

gradient of (14.20), and we obtain the analog of (14.24):

$$\nabla\theta(x) = \pi(\rho_R(x) - \rho_L(x)), \qquad (14.27)$$

so gradients of θ measure the difference in density of right and left moving particles.

The final links in the bosonization procedure are expressions for the fermionic fields $\Psi_{R,L}(x)$ in terms of $\phi(x)$ and $\theta(x)$. The details of such a representation depend upon microscopic features of the particular model under consideration. These have been worked out explicitly for a fermion Hamiltonian known as the Luttinger model [200]; here we are considering H_{XX}, and for this more general case we will be satisfied by an operator correspondence which gets the correct long distance behavior, but abandons attempts to get prefactors like those in (14.4) correct (for recent progress in computing prefactors for H_{12} at $J_2 = 0$ see Refs [311, 8]). With this limited aim, the basic result can be obtained by some simple general arguments. First note that if we annihilate a particle at the position x, from (14.24) the value of $\phi(y)$ at all $y < x$ has to be shifted by π. Such a shift is produced by the exponential of the canonically conjugate momentum operator Π_ϕ:

$$\exp\left(i\pi\int_{-\infty}^x \Pi_\phi(y)dy\right) = \exp\left(-i\theta(x)\right). \qquad (14.28)$$

However, it is not sufficient to merely create a particle: we are creating a fermion, and the fermionic antisymmetry of the wavefunction can be accounted for if we pick up a minus sign for every particle to the left of x, *i.e.*, with a Jordan-Wigner like factor

$$\exp\left(im\pi\int_{-\infty}^x \Psi_F^\dagger(y)\Psi_F(y)dy\right) = \exp\left(imk_Fx + im\phi(x)\right), \qquad (14.29)$$

where m is any odd integer, and $\Psi_F^\dagger\Psi_F$ measures the *total* density of fermions (see (4.39)), including the contributions well away from the Fermi points. In the second expression in (14.29), the term proportional to k_F represents the density in the ground state, while $\phi(x)$ is the integral of the density fluctuation above that. Combining the arguments leading to (14.28) and (14.29) we can assert the basic operator correspondence [199, 200, 201]

$$\Psi_F(x) = \sum_{m \text{ odd}} A_m e^{imk_Fx + im\phi(x) - i\theta(x)}, \qquad (14.30)$$

where the A_m are a series of unknown constants which depend upon

microscopic details. We will see shortly that the leading contribution to (14.30) comes from the terms with $m = \pm 1$, and the remaining terms are subdominant at long distances. Comparing with (11.27) it is clear that we may make the operator identifications for the right and left moving continuum Fermion fields

$$\Psi_R \sim e^{-i\theta + i\phi} \qquad \Psi_L \sim e^{-i\theta - i\phi}. \qquad (14.31)$$

The other terms in (14.30) arise when these basic fermionic excitations are combined with particle-hole excitations at wavevectors which are integer multiples of $2k_F$.

Similar arguments, and the above expressions, can also be applied to spin operators $\hat{\sigma}^\alpha$ via the relations (14.2). For $\hat{\sigma}^+$ the arguments are as above except that the 'string' factor in (14.2) exactly compensates for the change in sign discussed above: we have then

$$\hat{\sigma}_j^+ = (-1)^j \sum_{m \text{ even}} B_m e^{imk_F x_j + im\phi(x_j) - i\theta(x_j)}, \qquad (14.32)$$

for some unknown B_m. The most important term in this expansion is $m = 0$, so that

$$\hat{\sigma}_j^+ \sim (-1)^j e^{i\theta}, \qquad (14.33)$$

establishing our earlier claim of $e^{i\theta}$ as the order parameter for x-y spin correlations. Finally, $\hat{\sigma}^z$ is related to the fermion density: the slowly varying component of that can be reconstructed from (14.24), while additional contributions come from evaluating $\Psi_F^\dagger(x)\Psi_F(x)$ using (14.30)

$$\frac{\hat{\sigma}_j^z}{a} = -\frac{2}{\pi}\nabla\phi(x_j) + \sum_{m \neq 0, \text{even}} C_m e^{imk_F x_j + im\phi(x_j)}, \qquad (14.34)$$

for some C_m, with a the lattice spacing. Note that the coefficient of the slowly varying term (which does not oscillate at a multiple of the wavevector k_F) is precisely determined: this is ultimately related to the fact $\sum_j \hat{\sigma}_j^z = -2Q$ commutes with the Hamiltonian.

We have completed our derivation of the bosonization technology, and are ready to apply it to obtain new results. The basic result is the equivalency of the fermionic Hamiltonian (14.8), and its left-moving partner, to the bosonic theory defined by (14.21), (14.22) and (14.23). Also key are the operator correspondences in (14.24), (14.30), (14.32) and (14.34).

We turn to the evaluation of the correlators of the spin operators, (14.32) and (14.34), under the theory (14.22), (14.25) or (14.26). These

can be obtained by use of the basic identity

$$\langle e^{i\mathcal{O}} \rangle = e^{-\langle \mathcal{O}^2 \rangle/2} \tag{14.35}$$

where $\mathcal{O}$ is an arbitrary linear combination of ϕ and θ fields at different spacetime points; this identity is a simple consequence of the free-field (Gaussian) nature of (14.22). In particular, all results can be reconstructed by combining (14.35) with repeated application of some elementary correlators. The first of these is the two-point correlator of ϕ

$$\frac{1}{2} \left\langle (\phi(x,\tau) - \phi(0,0))^2 \right\rangle = \pi v_F K \int \frac{dk}{2\pi} T \sum_{\omega_n} \frac{1 - e^{i(kx - \omega_n \tau)}}{\omega_n^2 + v_F k^2}$$

$$= \frac{K}{4} \ln \left[\frac{\cosh(2\pi T x/v_F) - \cos(2\pi T \tau)}{(2\pi T/v_F \Lambda)^2} \right], \tag{14.36}$$

where Λ is a large momentum cutoff. Similarly, we have for θ, the correlator

$$\frac{1}{2} \left\langle (\theta(x,\tau) - \theta(0,0))^2 \right\rangle = \frac{1}{4K} \ln \left[\frac{\cosh(2\pi T x/v_F) - \cos(2\pi T \tau)}{(2\pi T/v_F \Lambda)^2} \right]. \tag{14.37}$$

To obtain the θ, ϕ correlator we use the relation $\Pi_\phi = -\nabla\theta/\pi$, and the equation of motion $\Pi_\phi = \partial_\tau \phi/(\pi v_F K)$ which follows from the Hamiltonian (14.22); then by an integral and differentiation of (14.36) we can obtain

$$\langle \theta(x,\tau)\phi(0,0) \rangle = \frac{1}{2} \arctan \left[\frac{\tan(\pi T \tau)}{\tanh(\pi T x/v_F)} \right] \tag{14.38}$$

Applying (14.35) and (14.37) to (14.33) we get

$$(-1)^j \langle \hat{\sigma}_j^+(\tau) \hat{\sigma}_0^-(0) \rangle \sim \left[\frac{T^2}{\sin(\pi T(\tau + ix_j/v_F)) \sin(\pi T(\tau - ix_j/v_F))} \right]^{\frac{1}{4K}}. \tag{14.39}$$

At the value $K = 1$ for H_{XX}, this agrees precisely with the result claimed earlier in (11.74) and (11.85). In this previous case we had obtained the $T > 0$ crossover functions by appealing to the mapping (4.64) between $T = 0$ and $T > 0$ correlators, which was claimed to be a consequence of the conformal invariance of the low-energy theory. Here we have shown that the low energy theory is given by (14.25) or (14.26), and that its $T = 0$ and $T > 0$ correlators are indeed related by (4.64). Very similar arguments can also be advanced by a bosonization analysis of the quantum Ising chain to establish (4.64) for the model of Chapter 4.

At $T = 0$, (14.39) gives an equal time correlator which decays as $1/\sqrt{x}$ which is in agreement with the exact result (14.4). We can also obtain the form of the subleading terms by considering the correlators of the complete expression (14.32): at $T = 0$ we have the following structure in the asymptotic expansion of the equal-time correlators

$$(-1)^j \langle \hat{\sigma}_j^+ \hat{\sigma}_0^- \rangle = \sum_{m=0}^{\infty} \frac{\widetilde{B}_m}{(x_j)^{2m^2 K + 1/(2K)}} \cos(2m k_F x_j) \qquad (14.40)$$

for some unknown coefficients $\widetilde{B}_m$. Notice, as claimed earlier, the $m > 0$ terms all decay faster than the dominant $m = 0$ term.

Precisely the same methods can be applied to the correlators of $\hat{\sigma}^z$. From (14.34), the analog of the expansion (14.40) for the $T = 0$ equal-time correlator is

$$\frac{1}{a^2} \langle \hat{\sigma}_j^z \hat{\sigma}_0^z \rangle = -\frac{2}{\pi^2 x^2} + \sum_{m=1}^{\infty} \frac{\widetilde{C}_m}{(x_j)^{2m^2 K}} \cos(2m k_F x_j), \qquad (14.41)$$

for some unknown $\widetilde{C}_m$. Note that the leading, non-oscillating, term agrees precisely with the first term in (14.5). For the special case of H_{XX}, $K = 1$, and the oscillating terms in (14.41) are in agreement with that in (14.5) for the special values $\widetilde{C}_1 = 2/\pi^2$ and $\widetilde{C}_{m>1} = 0$. The subleading terms in (14.41) do not appear for this special free fermion point, but there is no reason for them to vanish in the general case which will be considered in the following section.

14.2 Phases of H_{12}

We are ready to address the properties of the Hamiltonian H_{12} in (14.1) for the case of general J_1, J_2 and λ [202]. We will use exactly the same bosonization procedure developed in Section 14.2 for H_{XX} but apply it to the more interacting fermion Hamiltonian in (14.3). The first step, as in Section 14.1, is to focus on the low energy degrees of freedom which consist of fermionic excitations near the wave-vectors $\pm k_F$. This is facilitated by taking the continuum limit of (14.3) by inserting the parameterization (4.39) and (11.27). Before doing this it is important to 'normal-order' the terms in (14.3); in other words, we first perform a Hartree-Fock factorization to obtain the suitably renormalized one-particle Hamiltonian. In this manner we obtain the following continuum limit of H_{12}

$$H_{12} = H_{FL} + H_a + H_b \qquad (14.42)$$

where H_{FL} was considered earlier in (14.6), and H_a and H_b are the two new terms arising from non-zero λ and J_2. The first of these has the form

$$H_a = 8(J_1\lambda + 2J_2)a \int dx \left[(\rho_R + \rho_L)(\rho_R + \rho_L)\right] \qquad (14.43)$$

where ρ_R was defined in (14.15), and similarly for ρ_L; this term involves interactions in which left or right moving fermions scatter off each other while exchanging small momenta near the respective Fermi points. The second term, H_b, is more subtle: its appearance relies on the special value of $k_F = \pi/2a$ which is demanded by a half-filled fermion band [202]. For this value of k_F, two right-moving fermions at k_F have a total momentum $2k_F = \pi/a$, which differs from the total momentum of two left moving fermions $(-2k_F = -\pi/a)$, by a reciprocal lattice vector, $2\pi/a$. Hence it is possible to have an 'umklapp' scattering event between these, as in

$$H_b = 4(J_1\lambda - 6J_2) \int dx \left[\Psi_R^\dagger \nabla \Psi_R^\dagger \Psi_L \nabla \Psi_L + \Psi_L^\dagger \nabla \Psi_L^\dagger \Psi_R \nabla \Psi_R \right]. \qquad (14.44)$$

Note that this is the only instance in this chapter where the precise value of k_F has been important–all other expressions apply for general k_F and have been written as such.

We proceed to bosonize H_a and H_b using the prescriptions of Section 14.1. The case of H_a is straightforward: we use (14.24) to write H_a as

$$H_a = \frac{8(J_1\lambda + 2J_2)}{\pi^2} \int dx (\nabla\phi)^2. \qquad (14.45)$$

This can be easily absorbed into the bosonized version of H_{FL} in (14.22) by a redefinition of v_F and K. In this way we have shown that the Hamiltonian $H_{FL} + H_{12}$ is equivalent to (14.22) but with the parameters

$$v_F \approx 4a \left[J_1 \left(J_1 + \frac{4(J_1\lambda + 2J_2)}{\pi} \right) \right]^{1/2}$$

$$K \approx \left[1 + \frac{4(J_1\lambda + 2J_2)}{J_1\pi} \right]^{-1/2}. \qquad (14.46)$$

The values of the parameters only hold for small λ and J_2; however the general result of a renormalization of v_F and K, but with no other change, is expected to hold more generally. Notice that $K \neq 1$, but the results in Section 14.1 were quoted for general K and can now be used.

The consequences of H_b are a little more non-trivial. We insert the expansions (14.30) into H_b and generate a number of terms; the most

important of these arises from simply using the leading terms in (14.31) which yields

$$H_b = -v \int dx \cos(4\phi(x)) + \ldots \qquad (14.47)$$

where $v \sim (J_1\lambda - 6J_2)$. This is an important interaction modifying the simple Gaussian action in (14.22). The final bosonized version of H_{12} is then given by the action

$$\mathcal{S}_{SG} = \int dx d\tau \left[\frac{1}{2\pi K v_F} \left((\partial_\tau \phi)^2 + v_F^2 (\nabla\phi)^2 \right) - v \cos(4\phi) \right] \qquad (14.48)$$

This action represents the so-called sine-Gordon model and its properties will be examined in the following subsection.

For now, let us note the physical implication of the $\cos(4\phi)$ term and some related issues. Recall from the commutation relations (14.21) that $\nabla\phi$ is canonically conjugate to the x-y order represented by the angular variable θ–see the relation above (14.26) that $\Pi_\theta = -\nabla\phi/\pi$. So we can write the $\cos(4\phi)$ term as

$$\exp\left(-4\pi i \int_{-\infty}^x \Pi_\theta(y) dy \right) + H.c. \qquad (14.49)$$

In this form it is clear that this operator translates $\theta \to \theta + 4\pi$ for all $y < x$. But this is the same as inducing a 4π *vortex* in the angular order parameter θ. Thus the effect of the $\cos(4\phi)$ term is to allow for 4π vortex tunneling events between different winding number sectors of the angular variable θ representing spin ordering in the x-y plane. This interpretation is also consistent with (14.27) and (14.44): in the latter equation we see that H_b turns two left-moving particles into two right-moving particles, and so by the former equation there must be a step of 4π in θ at the point this happens.

It is interesting there is no 2π vortex event allowed above in H_{12}. We will see shortly that absence of such single vortices, and the presence only of double vortices this has some important consequences. The single 2π vortices are certainly permitted on general topological grounds, but to induce them it turns out to be necessary to modify H_{12}. One possibility is a *staggered* exchange interaction

$$H_{12} \to H_{12} + J_3 \sum_i (-1)^i \vec{\sigma}_i \cdot \vec{\sigma}_{i+1}. \qquad (14.50)$$

To obtain the bosonized version of this additional term, examine the structure of $\hat{\sigma}_i^+ \hat{\sigma}_{i+1}^-$ under the mapping (14.32); the staggering of the

exchange means that we have to pick up the co-efficient of $(-1)^i = e^{i2k_F x_i}$—this gives us the term $\int dx \sin(2\phi)$. The same term also arises from the corresponding mapping using (14.34) of the $\hat{\sigma}^z_i \hat{\sigma}^z_{i+1}$ term. So we have the operator correspondence

$$(-1)^i \vec{\hat{\sigma}}_i \cdot \vec{\hat{\sigma}}_{i+1} \sim \sin(2\phi). \qquad (14.51)$$

A second possibility is a staggered field in the z direction; by a very similar argument from (14.34) we obtain the operator correspondence

$$(-1)^i \hat{\sigma}^z_i \sim \cos(2\phi). \qquad (14.52)$$

The arguments in the previous paragraph show that adding either of the $\sin(2\phi)$ or $\cos(2\phi)$ terms to $\mathcal{S}_{SG}$ will allow 2π vortex tunneling events. It is also interesting to note the fermionic form of these 2π tunneling events: by reversing the bosonization mapping, it is simple to see that (14.51) and (14.52) correspond single fermion scattering terms that turn left to right movers and vice versa, and change total momentum by $2k_F$. In contrast, the original scattering term in (14.44) scattered two particles and changed momentum by $4k_F$.

14.2.1 Sine-Gordon Model

We will discuss some important properties of the sine-Gordon field theory $\mathcal{S}_{SG}$ in (14.48) as a function of the dimensionless coupling K and the dimensionful parameter v. The velocity v_F simply sets the relative scales of time and space, but does not otherwise modify physical properties.

We have already obtained results for $\mathcal{S}_{SG}$ along the line $v = 0$: the model is a free, gapless, Gaussian field theory characterized by the following $T = 0$ equal-time correlators

$$\langle e^{ip\theta(x)} e^{-ip'\theta(0)} \rangle \sim \delta_{pp'}/x^{p^2/2K} \quad ; \quad \langle e^{ip\phi(x)} e^{-ip'\phi(0)} \rangle \sim \delta_{pp'}/x^{p^2 K/2}; \qquad (14.53)$$

for $p = p'$ these results follow directly from (14.35-14.37), while for $p \neq p'$ application of (14.35) leads to an infrared divergent integral in the exponent, and so the correlator vanishes. Note that these correlators are both power-laws, indicating that the theory is scale invariant along the line $v = 0$ (indeed it is conformally invariant). From (14.53) we see that this is a line of critical points along which the exponents vary continuously as a function of the dimensionless parameter K. The technology of renormalization group scale transformations can therefore be applied

freely at any point along this line. We can talk of scaling dimensions of operators, and the results (14.53) show that

$$\dim[e^{ip\theta}] = \frac{p^2}{4K} \quad ; \quad \dim[e^{ip\phi}] = \frac{p^2K}{4}. \quad (14.54)$$

Also the relativistically invariant structure of the derivative terms in $\mathcal{S}_{SG}$ makes it clear that the dynamic exponent $z = 1$. Using this, and the scaling dimensions (14.54) for $p = 4$, we immediately obtain the scaling dimension $\dim[v] = 2 - 4K$ along the $v = 0$ line. This can be written as a renormalization group flow equation under the rescaling $\Lambda \to \Lambda e^{\ell}$:

$$\frac{dv}{d\ell} = (2 - 4K)v. \quad (14.55)$$

So the critical fixed line $v = 0$ is stable for $K < 1/2$. However, this flow equation is not the complete story, especially when K approaches $1/2$. For $|K - 1/2| \sim |v|$ we see that the term on the right hand side is not linear in the small parameter v, but quadratic. To be consistent, then, we also have to consider other terms of order v^2 which might arise in the flow equations: as we will see below, there is a renormalization of K that appears at this order.

The flow equations at order v^2 are generated using an approach similar to that used in Section 6.1 for the $N \geq 3$ rotor model in $d = 1$. As in (6.5), we decompose the field $\phi(x, \tau)$ into a background slowly varying component $\phi_<(x, \tau)$ and a rapidly varying component $\phi_>(x, \tau)$ which will be integrated out to order v^2:

$$\phi(x, \tau) = \phi_<(x, \tau) + \phi_>(x, \tau), \quad (14.56)$$

where $\phi_<$ has spatial Fourier components at momenta smaller than $\Lambda e^{-\ell}$, while $\phi_>$ has components between $\Lambda e^{-\ell}$ and Λ. Inserting (14.56) into (14.48), to linear order in v we generate the following effective coupling for $\phi_<$:

$$v \int d^2X \, \langle \cos(4\phi_<(X) + 4\phi_>(X)) \rangle_0$$

$$= v \int d^2X \, \cos(4\phi_<(X)) \left\langle e^{i4\phi_>(X)} \right\rangle_0$$

$$= v \int d^2X \, \cos(4\phi_<(X)) e^{-8\langle \phi_>^2 \rangle_0}$$

$$\approx v \left(1 - 4K\frac{d\Lambda}{\Lambda} \right) \int d^2X \, \cos(4\phi_<(X)), \quad (14.57)$$

where $X \equiv (x, \tau)$ is a spacetime co-ordinate, the subscript 0 indicates

an average with respect to the free $v = 0$ Gaussian action of $\phi_>$, and $d\Lambda = \Lambda(1 - e^{-\ell})$. When combined with a rescaling of co-ordinates $X \to Xe^{-\ell}$ to restore the cut-off to its original value, it is clear that (14.57) leads to the flow equation (14.55). The same procedure applies to quadratic order in v: as the algebra is a bit cumbersome, we will only schematically indicate the steps. We generate terms like

$$v^2 \int d^2X d^2Y \cos(4\phi_<(X) \pm 4\phi_<(Y)) \exp\left(\mp 16\langle \phi_>(X)\phi_>(Y)\rangle_0\right)$$

$$= v^2 \int d^2X d^2Y \cos(4\phi_<(X) \pm 4\phi_<(Y)) \exp\left(\mp f(X - Y)d\Lambda\right) \text{(14.58)}$$

where $f(X - Y)$ is some regularization dependent function which decays on spatial scale $\sim \Lambda^{-1}$. For this last reason we may expand the other terms in (14.58) in powers of $X - Y$. The terms with $+$ sign then generate a $\cos(8\phi)$ interaction: we will ignore this term as the analog of the arguments used to obtain (14.55) show that this term is strongly irrelevant for $K \sim 1/2$. The terms with the $-$ sign generate gradients on $\phi_<$ and therefore lead to a renormalization of K. In this manner we obtain the flow equation

$$\frac{dK}{d\ell} = -\delta v^2 \tag{14.59}$$

where δ is a positive, regularization dependent constant (it also depends upon K, but we can ignore this by setting $K = 1/2$ in δ at this order).

A fairly complete understanding of the properties of $\mathcal{S}_{SG}$ follows from an analysis of the equations (14.55) and (14.59). The flow trajectories are shown in Fig 14.2: they lie along the hyperbolae $4\delta v^2 - (2 - 4K)^2 = $ constant. There are three distinct possibilities on the ultimate long-distance fate of the couplings, leading to three separate phases of $\mathcal{S}_{SG}$. We will consider each of these phases in the following subsections, followed by a discussion of the critical lines and points between them. We also show the implications of the properties of $\mathcal{S}_{SG}$ for a phase diagram of H_{12} in Fig 14.3, with some needed justification to follow in the subsections below.

14.2.2 Tomonaga-Luttinger liquid

For $K \geq 1/2$ and $|v| \leq (2K - 1)/\sqrt{\delta}$, the flow is into the fixed line $v = 0$, $K \geq 1/2$. This line is described by the free Gaussian theory in (14.22) or (14.25) or (14.26). The ground state is a spin singlet (total $S_z = 0$) and there are gapless excitations with a linear dispersion
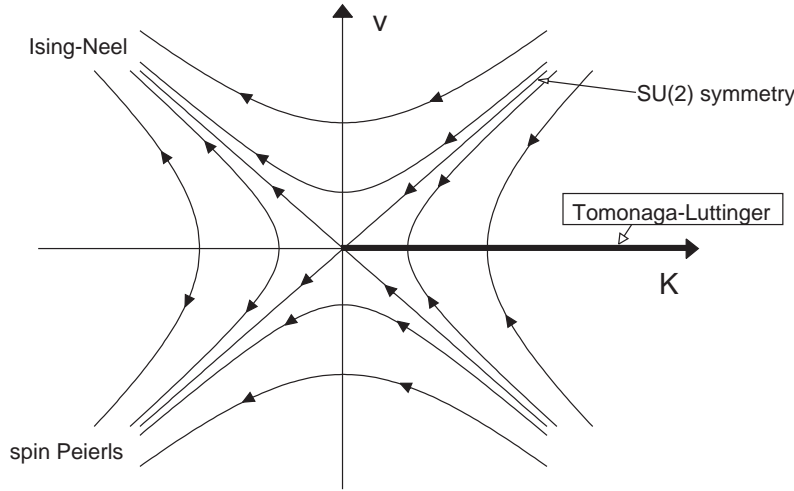
Fig. 14.2. Renormalization group flow trajectories and phase diagram of the sine-Gordon model $\mathcal{S}_{SG}$ in (14.48), as obtained from (14.55) and (14.59). The origin is at $K = 1/2$, $v = 0$. The attractive fixed line $v = 0$, $K \geq 1/2$ controls the Tomonaga-Luttinger liquid phase which is described in Section 14.2.2. The points flowing off to $v \to -\infty$ are in the spin-Peierls phase described in Section 14.2.3. Finally, the points flowing to $v \to \infty$ are in a Ising-Néel state discussed in Section 14.2.4. The separatrices between these regions are $v = \pm(2K - 1)/\sqrt{\delta}$. The line $v = (2K - 1)\sqrt{\delta}$ corresponds to the $SU(2)$ symmetric H_{12} with $\lambda = 1$; different points on this line are accessed by varying J_2/J_1.

which lead to the $T = 0$ power-law decay of correlators in (14.40) and (14.41). The dynamic finite T properties follow from correlators like (14.39) whose properties were discussed in some detail in Section 4.5.3 where we considered the critical point of the quantum Ising chain: the only change is that we now have a general exponent K (compare (14.39) with (4.112)) but this does not make a qualitative change to the physical discussion—only some quantitative factors change, and these can be easily computed for arbitrary K.

14.2.3 Spin-Peierls order

In this case the flow is towards $v = -\infty$: this happens for all $K \leq 1/2$ and $v < 0$, and for $K > 1/2$, $v < (1 - 2K)/\sqrt{\delta}$ (see Fig 14.2).

The flow of $|v|$ to large values indicates that the $\cos(4\phi)$ term in $\mathcal{S}_{SG}$ (Eqn (14.48)) dominates the long distance properties. A good first step is to assume that this is the dominant term, which then indicates that the
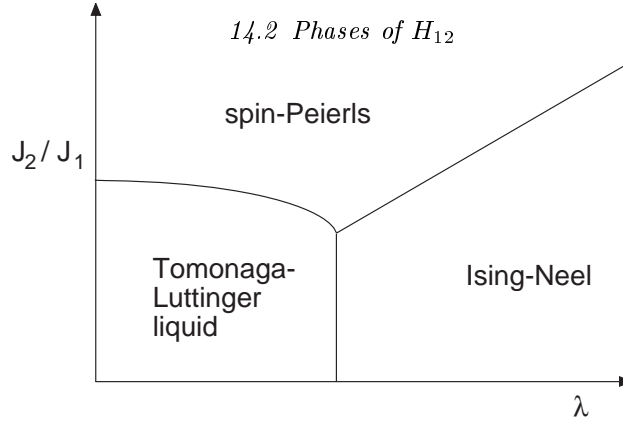
Fig. 14.3. Phase diagram of H_{12} (Eqn (14.1)) deduced from the flows in Fig 14.2 by Ref [202]. The vertical line $\lambda = 1$ has $SU(2)$ symmetry and maps onto the line $v = (2K - 1)/\sqrt{\delta}$ in Fig 14.2. The multicritical point where all three phases meet is the point $v = 0$, $K = 1/2$ in Fig 14.2.

values of ϕ will be pinned predominantly at the minima of the $\cos(4\phi)$ potential. For $v < 0$ these are at

$$\phi = \phi_n = (2n + 1)\pi/4 \tag{14.60}$$

where n is an arbitrary integer. In principle, each value of n labels a different ground state of $\mathcal{S}_{SG}$. However ϕ is an angular variable, and physical observables depend only upon gradients or trigonometric functions of ϕ; one observable which can distinguish between the different ϕ_n is the staggered bond exchange energy in (14.51) as

$$\left\langle (-1)^i \vec{\sigma}_i \cdot \vec{\sigma}_{i+1} \right\rangle \sim \sin(2\phi_n) = (-1)^n \tag{14.61}$$

So there are only two distinct ground states, corresponding to even or odd values of n. There is a spontaneously broken translational symmetry in either of these states due to the appearance of a staggering in the bond exchange energy. This is known as a spin-Peierls ordering, as discussed for the $d = 2$ case in Section 13.3.1.2: a schematic of these spin-Peierls states is shown in Fig 14.4. We emphasize that this ordering appears spontaneously in H_{12} and is not induced by a staggering of the exchange constants as in (14.50); the latter requires an explicit $\sin(2\phi)$ term in the action, which have not included.

We consider the excitations above either of the ground states. From the framework of the sine-Gordon theory it appears natural to parameterize $\phi(X) = \phi_n + \widetilde{\phi}(X)$, and to expand the action in powers of $\widetilde{\phi}$. At
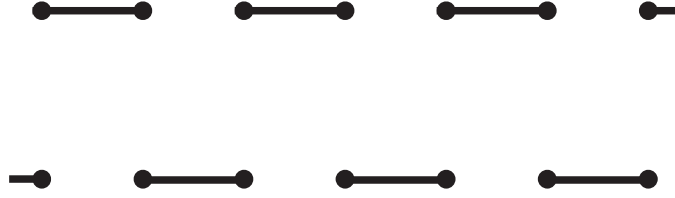
Fig. 14.4. Schematic of the two spin-Peierls ground states of H_{12}. The thick lines represent larger values of $\langle \vec{\sigma}_i \cdot \vec{\sigma}_{i+1} \rangle$, while the unmarked near-neighbor pairs have smaller values.

quadratic order the curvature at the minimum of the $\cos(4\phi)$ potential will give rise to a $\widetilde{\phi}^2$ mass term, and so we can expect that there is a gap and the lowest-lying excitation is a massive $\widetilde{\phi}$ particle. This expectation turns out to be incorrect, and there is an alternative massive excitation with a lower energy. For reasons we shall not fully discuss here, the most important excitation turns out to be a 'soliton': the reader can consult the book by Rajaraman [394] for further details. This is a topological excitation consisting of a localized lump at which ϕ interpolates between the two ground states: so, *e.g.*, we have $\phi(x \to \infty) = \phi_n$ and $\phi(x \to -\infty) = \phi_{n-1}$, and $\phi(x)$ moves between the two limits in the immediate vicinity of some point $x = x_0$. The disturbance around x_0 can move, and this constitutes a quantum particle of mass Δ/v_F^2. This solitonic particle has a lower energy than the $\widetilde{\phi}$ particle for $K > 1/8$, and so, in keeping with the general notation in this book, we have used the symbol Δ for the energy gap of the spin-Peierls state (the action $\mathcal{S}_{SG}$ is relativistically invariant and so the energy-momentum dispersion of the solitonic particle is $\varepsilon_k = (\Delta^2 + v_F^2 k^2)^{1/2}$). The $\widetilde{\phi}$ particle can be considered as a soliton/anti-soliton bound state, and is found to be stable towards decay into a pair of widely separated soliton and anti-soliton particles only for $K < 1/4$. In any case, the low temperature properties are dominated by those of a dilute gas of solitons and anti-solitons for all $K > 1/8$.

It is also useful to have an interpretation of the soliton in terms of the underlying spin Hamiltonian H_{12} [460]. Notice that each soliton involves a change $\Delta\phi = \pm\pi/2$. By the relation (14.24) between gradients of ϕ and the charge density, we see that each soliton carries a charge $Q = \pm 1/2$. This is to be contrasted with the charge $Q = \pm 1$ carried by the underlying Jordan-Wigner fermion Ψ_F. Of course this charge is also equal to the total spin S^z, and so the soliton is a $S_z = \pm 1/2$ particle–a
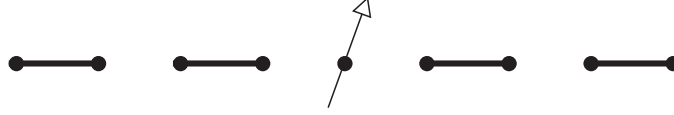
Fig. 14.5. Schematic of a $Q = 1/2$ spinon excitation interpolating between the two spin-Peierls ground states of Fig 14.4.

spinon, in the terminology of Section 13.3.2. This suggests the simple pictorial representation shown in Fig 14.5: the domain between the two spin Peierls states requires a shift in the singlet bonds by one site, leading to a free $S_z = 1/2$ spin at the boundary.

Note that the $\cos(4\phi)$ in the action, representing tunneling only by $\pm 4\pi$ vortices, was crucial for the existence of free spinons. If we had an explicit staggering of the exchange constants, as in (14.50), the resulting action would allow $\pm 2\pi$ vortices with a corresponding $\cos(2\phi)$ term in the action, and a solitonic analysis similar to the one above would show that excitations were particles with *integer* spin. This confinement of spinons is also easy to understand from the pictorial representation in Fig 14.5, as the explicit staggering would lead to an energy cost proportional to the length of the 'wrong' domain between two spinons.

We turn to the low temperature static and dynamic properties of this spin-Peierls phase. As already noted, these are dominated by a dilute gas of $S_z = \pm 1/2$ particles. The latter system can be analyzed using a method essentially identical to that employed in Section 6.2 for the low temperature properties of the $d = 1$ O(3) quantum rotor model. In the latter case, we had particles with $S_z = 1, 0, -1$; this is the one of the main substantive differences, and presence here of particles with $S_z = 1/2, -1/2$ only leads to simple changes in various numerical prefactors– the physical properties of the transport of magnetization density are identical to those discussed in Section 6.2. In particular, the spinon collisions are described by the low-momentum S matrix in (6.13), with the m_1, m_2, m'_1, m'_2 now taking the values $\pm 1/2$: the arguments for this key property are the same as those presented below (6.13). A second important difference is that the spin structure factor is not given by a single particle propagator as in (6.28-6.30); instead we have to consider a convolution of two single particle propagators, as in (13.78-13.81).

An explicit demonstration of the existence of the $S_z = \pm 1/2$ spinons

in this phase can be given at the special value $K = 1/4$. This relies on a commonly used trick of 'refermionization' of sine-Gordon-like field theories in $d = 1$, and this appears to a be convenient occasion to introduce it. Consider the fermionic fields

$$\psi_R \sim e^{-i\theta/2+i2\phi} \qquad\qquad \psi_L \sim e^{-i\theta/2-i2\phi}. \qquad (14.62)$$

Note that $\theta/2$ and 2ϕ obey the same commutation relations as those in (14.21), and so by working backwards through the arguments leading to (14.31), we see that $\psi_{R,L}$ are indeed fermionic operators annihilating particles with a linear dispersion. By the same arguments as those leading to (14.22) we may conclude that

$$-iv_F \int dx \left(\psi_R^\dagger \frac{\partial \psi_R}{\partial x} - \psi_L^\dagger \frac{\partial \psi_L}{\partial x} \right)$$
$$= \frac{v_F}{2\pi} \int dx \left[4(\nabla\phi)^2 + \frac{1}{4}(\nabla\theta)^2 \right]. \qquad (14.63)$$

However this is precisely the Hamiltonian corresponding to the gradient terms in $\mathcal{S}_{SG}$ at $K = 1/4$. Furthermore, it is easy to see from (14.62) that the cosine term in $\mathcal{S}_{SG}$ can be obtained by *bilinear* combinations of the $\psi_{L,R}$. So we have the remarkable result that, at $K = 1/4$, $\mathcal{S}_{SG}$ is equivalent to the free fermion Hamiltonian

$$\int dx \left(-iv_F \psi_R^\dagger \frac{\partial \psi_R}{\partial x} + iv_F \psi_L^\dagger \frac{\partial \psi_L}{\partial x} + \frac{\Delta}{v_F}(\psi_R^\dagger \psi_L + \psi_L^\dagger \psi_R) \right), \quad (14.64)$$

where $\Delta \sim v$ multiplies a term arising from $\cos(4\phi)$ in $\mathcal{S}_{SG}$. However, (14.64) describes a free massive Dirac particle in $d = 1$. Also note that identity analogous to (14.24) is

$$\frac{1}{2} \left(: \psi_R^\dagger \psi_R : + : \psi_L^\dagger \psi_L : \right) = \frac{1}{\pi} \nabla \phi; \qquad (14.65)$$

the leading $1/2$ shows that the Dirac particle/anti-particles carry charges $\pm 1/2$, and identifies them as the spinons.

An important caution about the discussion above at $K = 1/4$ is in order. While the free Dirac particle mapping gives an appropriate picture of the elementary excitations above the ground state, its naive extension to $T > 0$ properties is quite misleading. In particular, if the spinons were really free, their two-particle S matrix for the collision in Fig 6.2) would take the form

$$S_{m_1', m_2'}^{m_1, m_2} = (-1)\delta_{m_1 m_2}\delta_{m_1' m_2'}; \qquad (14.66)$$

here we have included the (-1) arising from the exchange of two fermions

explicitly in the S matrix. Comparing this with (6.13), we see a crucial difference in the structure of the spin indices: the spins are now 'passing through' the collision, rather than 'bouncing off'. In fact (14.66) is never the appropriate result for any realistic condensed-matter system, and (6.13) always applies at low momenta. The important point is that it is not possible to ignore additional 'irrelevant' terms not explicitly included in $\mathcal{S}_{SG}$. When these terms are carried through the refermionization above, they will invariably lead to some four-fermion scattering terms; such terms are always important in the scattering of massive particles in $d = 1$, as discussed below (6.13), and lead to the 'super-universal' S matrix in (6.13).

14.2.4 Néel order

Now the flow is towards $v = +\infty$: this happens for all $K \leq 1/2$ and $v > 0$, and for $K > 1/2$, $v > (2K - 1)/\sqrt{\delta}$ (see Fig 14.2).

The reasoning then closely parallels that in Section 14.2.3 for $v \to -\infty$. The important minima of the $\cos(4\phi)$ potential are at

$$\phi = \widetilde{\phi}_n = n\pi/2. \tag{14.67}$$

The physical properties of these minima are distinguished by the expectation value

$$\left\langle (-1)^i \hat{\sigma}_i^z \right\rangle \sim \cos(2\phi_n) = (-1)^n. \tag{14.68}$$

Thus there is a spontaneously broken symmetry characterized by a staggered expectation value in the z component of the spins. This is a Néel state with an Ising symmetry; it is to be contrasted with the Néel state in Section 13.3.1.2 in which the staggered moment could point in any direction in spin space. Here the anisotropy in the Hamiltonian picks out the z direction as a preferred one, and there is only a two-fold degeneracy in the resulting Ising/Néel ground state. (Note that a fully isotropic Néel state is not possible in $d = 1$, as was indicated in Section 13.3.1.1, and will be discussed further below in Section 14.2.5.)

Apart from the shift in the minima of the cosine potential from (14.60) to (14.67) (and the resulting difference in the physical interpretation of the broken symmetry of the ground state), there is essentially no difference in the analysis of the fluctuations here from that in Section 14.2.3; indeed we can map $v \to -v$ in $\mathcal{S}_{SG}$ by the shift $\phi \to \phi + \pi/4$. For $K > 1/8$ the lowest lying excitations are massive $S_z = \pm 1/2$ spinons

which interpolate between the two Ising/Néel ground states. Their collisions are described at low momenta by (6.13) and the low T properties are as in Section 6.2 with the modifications noted above in Section 14.2.3.

14.2.5 Models with $SU(2)$ (Heisenberg) symmetry

Here we focus on the special point $\lambda = 1$ in H_{12}, where the Hamiltonian has full $SU(2)$ symmetry. We have argued in Sections 13.3.1 and 13.3.1.1 that this model should also be described by the $d = 1$ O(3) non-linear sigma model (13.58) with an additional topological term (13.60) at $\theta = \pi$ (this θ represents the co-efficient of the topological term, and should not be confused with the angular bosonization field θ used elsewhere in this chapter). The latter model is characterized by a single dimensionless coupling g (apart from the momentum cutoff Λ), and we will answer the following important question: to what trajectory in the v-K phase diagram of $\mathcal{S}_{SG}$ in Fig 14.2 does the $d = 1$ O(3) non-linear sigma model at $\theta = \pi$ map onto as a function of g ?

A first guess would be to simply set $\lambda = 1$ in the values of the couplings in (14.46) and in the value of v below (14.47). However, these results hold for small λ and J_2 and are not acceptable for $\lambda = 1$. A strategy which works is the following: let us focus on the Tomonaga-Luttinger phase of Section 14.2.2 and ask if there is any trajectory within it which corresponds to $\lambda = 1$. If there was such a trajectory, then $SU(2)$ symmetry demands that the $\hat{\sigma}^z \hat{\sigma}^z$ and $\hat{\sigma}^+ \hat{\sigma}^-$ correlators should decay with the same exponent. We compare the expansions in (14.40) and (14.41) and notice that their leading terms coincide only at $K = 1/2$ (the first subleading term also coincides at this value of K). So one point with $SU(2)$ symmetry in Fig 14.2 is the very symmetrical point in the center $v = 0$, $K = 1/2$. Now if the renormalization group respects the underlying symmetry of the Hamiltonian, points flowing into and away from $v = 0$ and $K = 1/2$ could also be $SU(2)$ symmetric. By examining the trends in (14.46), and in the value of v below (14.47), we are then led to assert the following important result:

$$\text{the line } v = (2K - 1)/\sqrt{\delta} \text{ has } SU(2) \text{ symmetry,} \qquad (14.69)$$

and therefore corresponds to $\lambda = 1$ in H_{12}; we access different points on this line by varying J_2/J_1, and increasing J_2/J_1 corresponds to decreasing v and K. This line also maps onto the O(3) non-linear sigma model at $\theta = \pi$, and increasing g also corresponds to decreasing v and K. The renormalization group flow along this line is easily deduced from either

(14.55) or (14.59), and we have

$$\frac{dv}{d\ell} = -2\sqrt{\delta}v^2. \tag{14.70}$$

This flow has a fixed point at $v = 0$, which corresponds to some critical value of $J_2/J_1 = J_{2c}$ or $g = g_c$, as in Fig 13.1. The O(3) non-linear sigma model also has an additional unstable fixed point at $g = 0$, but that is inaccessible in the present sine-Gordon theory: this fixed point corresponds to the classical limit $S \to \infty$ (as $g \sim 1/S$) and so it is not surprising it does not appear in an analysis set up explicitly for $S = 1/2$. Presumably, the $g = 0$ fixed point is present somewhere in the large K, v region of Fig 14.2.

All points with $v > 0$ ($J_2/J_1 < J_{2c}$ or $g < g_c$) flow into $v = 0$ (Figs 13.1 and 14.2): for these values the ground state is a Tomonaga-Luttinger liquid with correlations given by (14.40) and (14.41) at $K = 1/2$. The flow into the fixed point is logarithmically slow ($v(\ell) \sim 1/\ell$ for large ℓ), and this leads to logarithmic corrections to the correlators in a manner rather similar to the $d = 3$ quantum rotor model examined in Chapter 8. This critical state at $v = 0$, $K = 1/2$ is the closest a spin model in $d = 1$ can get to achieving long-range Néel order - the equal-time order parameter correlations decay as $1/x$. Without the topological term in the non-linear sigma model, the correlations decay even faster (exponentially) as discussed in Chapters 5 and 6.

Points with $v < 0$ ($J_2/J_1 > J_{2c}$ or $g > g_c$) flow away to large negative values of v. This puts us in the gapped spin-Peierls phase already discussed in Section 14.2.3. Additional support for this identification comes from an interesting exact result of Majumdar and Ghosh [322, 460]. They noted that at the special $SU(2)$ symmetric point, $\lambda = 1$, $J_2 = J_1/2$, it is possible to write down the exact wavefunction of the ground state of H_{12}: it can be checked that the following simple ansatz consisting of a product of pairs of singlet bonds is an exact eigenstate of H_{12},

$$\ldots \mathcal{B}_{12}\mathcal{B}_{34}\mathcal{B}_{56}\mathcal{B}_{78}\ldots, \tag{14.71}$$

where $\mathcal{B}_{ij} = (|\uparrow\rangle_i|\downarrow\rangle_j - |\uparrow\rangle_j|\downarrow\rangle_i)/\sqrt{2}$; this state is degenerate with its symmetry-related partner

$$\ldots \mathcal{B}_{23}\mathcal{B}_{45}\mathcal{B}_{67}\mathcal{B}_{89}\ldots. \tag{14.72}$$

Arguments proving that these are also the ground states are given by Majumdar and Ghosh. It should be clear that these are precisely the spin-Peierls states sketched in Fig 14.4. (We also note that there are

some interesting generalizations of the Majumdar-Ghosh construction of exact ground states to antiferromagnets on the square lattice [461, 59] (one of which has found a recent experimental realization [259, 349]), but these are for cases where the Hamiltonian does not have the full square lattice symmetry.)

We can also use the flow equation (14.70) to deduce how the energy gap vanishes, or the spin-Peierls order disappears, as $v \nearrow 0$ (or $g \searrow g_c$ or $J_2/J_1 \searrow J_{2c}$. The runaway flow for $v < 0$ from the $v = 0$ fixed point in (14.70) has precisely the same structure as the flow in (6.8) for the $d = 1$ O(3) rotor model. Using precisely the same arguments as those presented in Section 6.1 we may conclude here that the energy gap $\Delta \sim \exp(-1/(2\sqrt{\delta}|v|))$ for small $|v|$. Also from (14.54), the spin-Peierls order parameter in (14.61) has scaling dimension $\dim[\sin(2\phi)] = 2^2 K/2 = 1$; so its expectation value vanishes as $\langle \sin(2\phi) \rangle \sim \Delta \sim \exp(-1/(2\sqrt{\delta}|v|))$.

14.2.6 Critical properties near phase boundaries

There are three phase boundaries in Fig 14.3 and we will consider properties in their vicinity in turn. The multicritical point where all three phases meet will not be considered: this point lies on the $SU(2)$ symmetric line $\lambda = 1$ and has therefore already been described in Section 14.2.5.

We first consider the transition from the Tomonaga-Luttinger liquid to the Néel phase. We cross the phase boundary by moving the initial values of v and K in Fig 14.2 across the separatrix $v = (2K - 1)/\sqrt{\delta}$. Notice that last point within the Tomonaga-Luttinger liquid is on the separatrix, which was asserted earlier to have $\lambda = 1$ and $SU(2)$ symmetric correlations. To understand the growth of the Néel order parameter, we have to examine the flows from an initial point just across the separatrix, *i.e.*, from the point $v = (2K - 1 + \epsilon)/\sqrt{\delta}$ for small ϵ. To facilitate the integration of the flow equations (14.55) and (14.59) we change variables to

$$y_{1,2} = \sqrt{\delta}v \mp (2K - 1). \tag{14.73}$$

Then the Eqns (14.55) and (14.59) become

$$\frac{dy_1}{d\ell} = y_1(y_1 + y_2)$$
$$\frac{dy_1}{d\ell} = -y_2(y_1 + y_2). \tag{14.74}$$

It is clear from these equations that one integral is simply $y_1 y_2 = C$

where C is a constant determined by the initial conditions; the first equation is then easily integrated to give

$$\tan^{-1}\frac{y_1(\ell)}{\sqrt{C}} - \tan^{-1}\frac{y_1(0)}{\sqrt{C}} = \sqrt{C}\ell \qquad (14.75)$$

By the usual scaling argument, the characteristic energy gap, Δ, in the Néel phase is of order $e^{-\ell^*}$ where ℓ^* is the value of ℓ over which y_1 grows from an initial value of order $\epsilon \ll 1$ to a value of order unity. From the initial conditions, we expect the constant C to also be of order ϵ, and so let us choose $C = \epsilon$; then a straightforward analysis of (14.75) gives us

$$\Delta \sim \exp\left(-\frac{\pi}{2\sqrt{\epsilon}}\right). \qquad (14.76)$$

This singularity, and the flow analysis above, are characteristic of a "Kosterlitz-Thouless" transition which occurs in a variety of physical situations in both classical and quantum systems–the reader may find more details in the book by Itzykson and Drouffe [247]. Also note the difference between this singularity, and that found for the $SU(2)$ case in Section 14.2.5–there was no square root within the exponential in the latter case. By arguments similar to those presented in Section 14.2.5, we may also conclude here that the order parameter grows as $\sim \Delta$.

The transition between the Tomonaga-Luttinger liquid and the spin-Peierls phase is essentially identical to the above case, and little needs to be said: the energy gap in the spin-Peierls phase obeys (14.76) near the phase boundary, and the spin-Peierls order parameter vanishes as $\sim \Delta$. We note that the terminus of the Tomonaga-Luttinger liquid again has $K = 1/2$, $SU(2)$ symmetric exponents because the flow is again into the $v = 0$, $K = 1/2$ point; this happens even though the underlying model has $\lambda < 1$ (see Figs 14.2 and 14.3).

Finally, let us consider the phase boundary between the spin-Peierls and Néel phases. This coincides with the line $K < 1/2$, $v = 0$ in Fig 14.2. Along this line correlations of both order parameters decay with a power law determined by their common scaling dimension (from (14.51), (14.52) and (14.54)) $\dim[\sin(2\phi)] = \dim[\cos(2\phi)] = K$, *i.e.*, equal-time correlators decay as x^{-2K}. For non-zero v an energy gap appears, and its magnitude is determined by the relevant flow away from the $v = 0$ line in (14.55): this flow equation tells that $1/\nu = \dim[v] = (2 - 4K)$, and as $z = 1$, the energy gap, Δ behaves as

$$\Delta \sim |v|^{1/(2-4K)}. \qquad (14.77)$$

The scaling dimensions of the order parameters above show that they vanish as Δ^K on either side of the phase boundary.

One interesting feature of this last phase boundary deserves further comment. Notice that we have distinct broken symmetries on either side of the transition, characterized by very different order parameters, spin-Peierls and Néel. If we had attempted to construct a generic Landau-like mean field theory for such distinct order parameters, we would have concluded that the two phases would not be separated by a second order transition: a first order line or co-existence between the two phases is generic. Nevertheless, we have found here a second order transition across a line with continuously varying exponents: this is clearly a consequence of the strong quantum fluctuations in a low-dimensional system, and mean field theory is not a suitable guide for the expected behavior. Recall also that a generic second order phase boundary between Néel and spin-Peierls phases has also been proposed in certain collinear antiferromagnets in $d = 2$, as discussed in Section 13.3.1.2.

14.3 O(2) rotor model in $d = 1$

In Part 2 we examined the quantum/Ising rotor models in all spatial dimensions d and for all values of the number of rotor components, N. Only one case was omitted, as noted in Chapter 6, $d = 1$ and $N = 2$. For completeness, we will discuss this case here, as only a simple extension of the methods already introduced is necessary.

We consider a chain of O(2) quantum rotors (defined in Section 2.2 and (2.58)) with the Hamiltonian

$$H_R = \frac{Jg}{2} \sum_i \hat{L}_i^2 - J \sum_i \hat{\mathbf{n}}_i \cdot \hat{\mathbf{n}}_{i+1}, \qquad (14.78)$$

where $\hat{\mathbf{n}}_i$ are 2 component unit vectors, there is only a single generator of O(2) rotations $\hat{L}_i$ on each site, and these operators obey the on-site commutation relations (2.57).

Let us parameterize

$$\mathbf{n}_i = (\cos\theta_i, \sin\theta_i), \qquad (14.79)$$

and take the naive continuum limit of (14.78). This can be done using the methods discussed in Chapter 2; we obtain a continuum $d = 1$ quantum field theory for θ which has precisely the same action as $\mathcal{S}_{TL}$

in (14.26) but with the couplings

$$K \approx \frac{\pi}{\sqrt{g}} \qquad v_F \approx \sqrt{g}Ja. \tag{14.80}$$

Under this action, equal time correlators, from (14.53), decay as

$$\langle \hat{\mathbf{n}}_i \cdot \hat{\mathbf{n}}_j \rangle \sim \frac{1}{|x_i - x_j|^{1/(2K)}}. \tag{14.81}$$

However, this is clearly not the complete story. This naive continuum limit has explicitly prevented the introduction of vortices in the angular θ field: these are tunneling events in which the spatial winding number

$$\frac{1}{2\pi} \int dx \nabla \theta \tag{14.82}$$

changes between integer values. Such vortices can be conveniently introduced in the dual ϕ field formulation, as discussed below (14.49). In the present situation elementary 2π vortices are certainly allowed by the lattice Hamiltonian (14.78), and so by the arguments just before and after (14.49) we obtain the dual action

$$\widetilde{\mathcal{S}}_{SG} = \int dx d\tau \left[\frac{1}{2\pi K v_F} \left((\partial_\tau \phi)^2 + v_F^2 (\nabla \phi)^2 \right) - \widetilde{v} \cos(2\phi) \right]. \tag{14.83}$$

The most important difference from $\mathcal{S}_{SG}$ in (14.48) is that we have a $\cos(2\phi)$ rather than a $\cos(4\phi)$ term. Much of the analysis of $\mathcal{S}_{SG}$ in Section 14.2.1 can now be applied: the renormalization group equations (14.55) and (14.59) are modified to

$$\begin{aligned} \frac{d\widetilde{v}}{d\ell} &= (2 - K)\widetilde{v} \\ \frac{dK}{d\ell} &= -\widetilde{\delta}\widetilde{v}^2 \end{aligned} \tag{14.84}$$

This leads to a renormalization group flow diagram as in Fig 14.2, but in the vicinity of the point $K = 2$, $v = 0$ (instead of $K = 1/2$, $v = 0$). The model H_R therefore has a Kosterlitz Thouless transition from a gapless phase with correlations decaying as (14.81), to a gapped phase (the gap increases as in (14.76)) and equal-time correlations decay exponentially as in (1.24). The exponent K takes the value $K = 2$ at this critical point: this is the most important difference from the corresponding transition in H_{12} where we had $K = 1/2$. As a result, the critical order parameter correlators decay as $1/x^{1/4}$. Also the excitations in the gapped phase carry charges $Q = \pm 1$: this is a consequence of the transition being driven by single 2π vortices.

14.4 Applications and extensions

There is a great deal of experimental and theoretical work on $S = 1/2$ spin chains, and a complete survey will not be attempted here. For a discussion mainly of neutron scattering experiments see the recent review articles by Cowley [105] and Broholm [67]. Nuclear magnetic resonance experiments have also been important in measuring thermodynamic and low frequency spin relaxation properties; a discussion of these may be found in Refs [448, 133, 421, 474, 475, 486]. The spin-Peierls phase of Section 14.2.3 has an experimental realization in the intensively studied compound $CuGeO_3$, although the coupling between the spins and the phonon excitations [109] almost certainly has to be considered for a complete understanding of the experiments; a neutron scattering analysis may be found in Ref [15] and a discussion of some theoretical issues in Ref [31, 191].

The bosonization method has also had an important application in the study of the edge states of quantum Hall systems: see the review by Kane and Fisher [262].

15

Magnetic ordering transitions of disordered systems

by T. Senthil and S. Sachdev

This chapter has been adapted from the Ph. D. thesis of T. Senthil, submitted to Yale University (1997), unpublished.

The last two chapters of this book will move beyond the study of regular Hamiltonians which have the full translational symmetry of an underlying crystalline lattice, and consider the physically important case of disordered systems described by Hamiltonians with couplings which vary from point to point in space. By the standards of the regular systems we have already discussed, the quantum phase transitions of disordered systems are very poorly understood, and only a few well-established results are available: a large amount of theoretical effort has been expended towards unraveling the complicated phenomena that occur, and they remain active topics of current research. The aims of our discussion here will therefore be rather limited– we will highlight some important features which are qualitatively different from those of non-disordered systems, make general remarks about insights that can be drawn from our understanding of the finite T crossovers in Part 2, and discuss the properties of some simple solvable models.

In keeping with the general strategy of this book, we will introduce some basic concepts by studying the effects of disorder on the magnetic ordering transitions of quantum Ising/rotor models studied in Part 2; we will also make some remarks in Section 15.3.1 on the effects of disorder on the ordering transitions of Fermi liquids considered in Chapter 12.

Models with much stronger disorder and frustrating interactions which have new phases not found in ordered systems will be considered in Chapter 16.

Almost all of this chapter will consider the following disordered Hamiltonians: for the case $N = 1$, we generalize (4.1) to

$$H_{Id} = -\sum_i g_i \hat{\sigma}_i^x - \sum_{<ij>} J_{ij} \hat{\sigma}_i^z \hat{\sigma}_j^z, \qquad (15.1)$$

while for $N \geq 2$, we have the disordered version of (5.1):

$$H_{Rd} = \frac{1}{2} \sum_i g_i \hat{\mathbf{L}}_i^2 - \sum_{<ij>} J_{ij} \hat{\mathbf{n}}_i \cdot \hat{\mathbf{n}}_j, \qquad (15.2)$$

where $<ij>$ represents the sum over nearest-neighbors on the sites, i, of a regular lattice, and the couplings $g_i \geq 0$, $J_{ij} \geq 0$ are random functions of position (note that g_i has the dimensions of energy, unlike the dimensionless g in (4.1) and (5.1), and the non-disordered case obtains with $g_i = gJ$ and $J_{ij} = J$). The restriction that the couplings all be non-negative has an important simplifying consequence: there is no frustration in the exchange terms in (15.1) and (15.2), and so for small enough g_i, there is a magnetically ordered ground state, characterized by the same order parameter used for the non-random case. In the present case we define

$$N_0 = \overline{\langle \hat{\sigma}_i^z \rangle} \qquad T = 0, \qquad (15.3)$$

where the overbar denotes an average over different disorder configurations, and the generalization to $N \geq 2$ is obvious. For a specific realization of the disorder, the value of $\langle \hat{\sigma}_i^z \rangle$ in the magnetically-ordered ground state will vary from point to point due to the microscopic disorder, but there will be an average uniform component which is measured by N_0: this average can be computed by summing $\langle \hat{\sigma}_i^z \rangle$ over all sites i for a specific realization of the disorder, or by performing the disorder average as in (15.3)—the result is expected to be the same. Now as we raise the value of all the g_i (say, by increasing their mean, while keeping their variance fixed), we expect a phase transition at a critical value of $\overline{g} = \langle g_i \rangle$ to a quantum paramagnet with $N_0 = 0$—for sufficiently large g_i, the strong-coupling methods of Sections 4.1.1 and 5.1.1 apply, and show that ground state must be a quantum paramagnet. It is this transition from a magnetically ordered state to a quantum paramagnet which will form the basis of most of our discussion of quantum phase transitions in disordered systems in this chapter.

We will begin in Section 15.1 by discussing a general stability criterion that must be satisfied by a quantum critical point in any disordered system: this leads to the requirement that the correlation length exponent ν satisfy $\nu \geq 2/d$. Further general considerations will appear in Section 15.2 where we discuss the low energy spectrum on the phases away from the critical point: the presence of disorder introduces the so-called Griffiths-McCoy singularities. A first analysis of the models H_{Id} and H_{Rd} will appear in Section 15.3 using the field-theoretic methods of Chapter 8. Two solvable cases of H_{Id} will be considered next: models near the percolation transition in Section 15.4 and in $d = 1$ in Section 15.5. Some concluding remarks then appear in Section 15.6.

15.1 Stability of quantum critical points in disordered systems

Because a random system is intrinsically inhomogeneous, it is not a priori clear that it can display a sharp second-order phase transition at a specific average coupling $\overline{g} = \overline{g}_c$ (say) at which the response functions become singular. After all the couplings vary from point to point, and there will always be localized regions which are well away from the critical point, even though the average coupling is critical; consistency requires that such localized regions don't occur often enough. The restrictions this places on the classical critical point were first considered by Harris [211], who actually looked at the simpler question of whether the classical critical point of the non-random system was stable towards the introduction of a small amount of disorder. However, it is clear that the restrictions that emerge apply also to quantum critical points of random systems: this was discussed by Chayes *et al.* [88] who also presented a rigorous argument.

We will be satisfied here presenting a simple heuristic argument, along the lines of Harris [211]. Let us tune the transition by varying the value of $\overline{g}$. Focus now on a any region of size L; we can define a local critical point $\overline{g}_{c,r}$ at which this region will crossover from a magnetically ordered to a quantum paramagnetic state. The value of $\overline{g}_{c,r}$ will not necessarily equal the global value $\overline{g}_c$—we can expect that local random fluctuations will cause a deviation of order $L^{-d/2}$—this follows from the central limit theorem-like argument that the variance of order $\mathcal{N} = L^d$ independent random numbers (the local values of g_c) is of order $\sqrt{\mathcal{N}}$. Such a deviation is significant if it starts becoming of order $|\overline{g} - \overline{g}_c|$: this will happen at length scales shorter than $L = L_r \sim |\overline{g} - \overline{g}_c|^{-2/d}$. Now if L_r is shorter

than the correlation length ξ, then by the time we renormalize out to the scale $\xi \sim |\overline{g} - \overline{g}|^{-\nu}$, the system has unambiguously decided what its critical point is, and local random fluctuations have been smoothed out. So we now have our stability requirement, $L \ll \xi$, or

$$|\overline{g} - \overline{g}_c|^{-2/d} \ll |\overline{g} - \overline{g}_c|^{-\nu}. \tag{15.4}$$

Consistency of (15.4) leads to the main result of this section

$$\nu \geq \frac{2}{d}, \tag{15.5}$$

an inequality which must be satisfied by all quantum critical points of disordered systems.

In our discussion above we considered the consequences of fluctuations in the local position of the critical point. In a field-theoretic language, we can induce such a fluctuation by perturbing the action with a random coupling multiplying the operator which tunes the system across the transition. More generally, consider the case where the randomness couples to some local operator $O(x, \tau)$ which has a scaling dimension $\dim[O] = \zeta_O$. This means that the effective action for the system will have an additional term

$$\int d^d x \int d\tau r(x) O(x, \tau), \tag{15.6}$$

where $r(x)$ is a fixed random function of space *only*. We will assume that the spatial correlations in $r(x)$ are short-ranged, *i.e.*, $r(x)$ and $r(x')$ are considered as independent random variables for moderate values of $|x - x'|$. In contrast, note that as $r(x)$ is time-independent, there is an infinite correlation 'length' along the imaginary time direction: it is this long-range correlation which makes the effects of randomness particularly severe in quantum systems. Now consider averaging over the disorder using replicas (this method will be discussed briefly in Section 15.3). This generates a term $\delta^2 \int d^d x d\tau_1 d\tau_2 \sum_{ab} O_a(x, \tau_1) O_b(x, \tau_2)$ where δ^2 is the variance of r, and a, b are replica indices. The scaling of δ^2 is given by power counting to be $\dim[\delta'^2] = d + 2z - 2\zeta_O$. This type of randomness is therefore relevant if $d + 2z - 2\zeta_O > 0$. For the case of the energy density, the scaling dimension of the associated coupling constant is $1/\nu$, and so the dimension of the energy operator is $\zeta_O = d + z - 1/\nu$; the criterion for its relevance then becomes $\nu < 2/d$, as expected. Conversely, such random fluctuations are perturbatively irrelevant if $\nu > 2/d$.

15.2 Griffiths-McCoy singularities

In addition to the singularities in the spectrum at the quantum-critical point, all disordered systems have additional "Griffiths-McCoy" (GM) singularities [190, 334, 335] which affect the *phases* on either side of the critical point (related singularities are also present in the statics and dynamics of classical spin systems [124, 125, 398]). The physics behind their appearance is quite different from those of the critical singularities, and the complicated interplay of these two distinct phenomena is at the heart of the difficulty of analyzing quantum phase transitions in disordered systems. One possibility is that GM singularities of the phases are quite weak, and are simply idle spectators which are decoupled from the critical singularities–they are then not part of the universal scaling functions describing the crossover between the phases. At the other end of the possibilities, the GM and critical singularities could be tightly coupled, with no sharp distinction between the two— the GM singularities then become the critical singularities as one approaches the critical point. In any case, theoretical analyses cannot deal with one without considering the other, and unraveling the two is often quite difficult.

The central idea will become clear by considering a specific case: the $N = 1$ model H_{Id} (Eqn (15.1)). We will be interested in the nature of the low energy spectrum ($\omega \to 0$) in the quantum paramagnetic phase ($\overline{g} > \overline{g}_c$) not too far from the critical point—this will be controlled by the GM singularities. (Notice the orders of limits ($\omega \to 0$ followed by $\overline{g} \to \overline{g}_c$) characterizing these singularities: the opposite orders of limits ($\overline{g} \to \overline{g}_c$ first and then $\omega \to 0$) lead to the critical singularities.) In the non-disordered case there was an energy gap $\Delta_+ \sim (g - g_c)^{z\nu}$ and so all spectral densities vanished for $\omega < \Delta_+$. We will now argue, following Refs [152, 154, 489, 405, 197, 540, 410] that there is no such gap for the disordered system, and there is always a non-zero spectral density at arbitrarily low energies. Due to the randomness, there would, in general, be a non-zero probability that any given bond is stronger than the critical bond strength at which the system orders as a whole. This would happen in an entire, compact region of linear size L with probability $P(L) \sim \exp(-cL^d)$ where c is a constant determined by the microscopic couplings, width of the random distribution, etc. Such regions constitute clusters of spins that are coupled strongly enough that if they were infinite in size, they would order. Consider any such cluster of size L. For large L, all the spins in the cluster behave coherently in space, and it is legitimate to treat the cluster as a single giant spin in the

presence of some effective transverse field g_L. Thus the cluster has two low-lying energy levels with an energy difference $2g_L$ well separated from other higher energy levels. This effective field, and hence the splitting between the two levels goes to zero as $L \to \infty$, thus giving rise to broken symmetry and "long-range" order within the cluster. For finite L, g_L can be estimated in perturbation theory in the ratio of the transverse field to the bond strength. To zeroth order of perturbation theory, there is no transverse field, and the cluster has two degenerate ground states (all spins up or down) and other excited states separated by a large energy (of order the bond strength). A non-zero transverse field breaks this ground state degeneracy, and there remains instead a doublet with a non-zero but small splitting. It is clear that this effect will appear only in a large order of the perturbation theory (= number of spins in the cluster) $\sim L^d$. Thus the splitting, and hence g_L are exponentially small in L^d: $g_L \sim \overline{g} \exp(-c_1 L^d)$. Now, we assume that different clusters in the system may be treated independently of one another. Consider the density of low-energy excitations as measured by the disorder-average of the imaginary part of the local dynamic susceptibility, $\mathrm{Im}\chi_L(\omega) = \int d^d k/(2\pi)^d \mathrm{Im}\chi(k,\omega)$, with χ defined in (4.7) and (4.20):

$$\mathrm{Im}\chi_L(\omega) = \overline{\sum_\alpha |\langle \alpha | \hat{\sigma}_i^z | 0 \rangle|^2 \delta(\omega - (E_\alpha - E_0))} \qquad (15.7)$$

where $|\alpha\rangle$ refer to eigenstates of the system with energy E_α, and $|0\rangle$ is the ground state. For low ω in the paramagnetic phase, the only contribution will be from the rare clusters discussed above. Thus

$$\mathrm{Im}\chi_L(\omega) \quad \sim \quad \int dL \; P(L)\delta(\omega - 2g_L) \qquad (15.8)$$

$$\sim \quad \int dL \; e^{-cL^d}\delta(\omega - he^{-c_1 L^d}) \qquad (15.9)$$

$$\sim \quad \frac{\omega^{d/\tilde{z}-1}}{(\ln(1/\omega))^{d/(d-1)}}, \qquad (15.10)$$

where $\tilde{z} = c_1 d/c$. Therefore we have the striking result that the paramagnetic phase is gapless with a singular power law (up to logarithmic corrections) density of states at low energies. The power depends upon the non-universal exponent $\tilde{z}$ and could in principle even lead to a divergent density of states at zero energy: this power law singularity leads to singularities in the thermodynamic properties of the system at low temperature. We have chosen the suggestive notation $\tilde{z}$ for the exponent, as it plays the role of the dynamic exponent for the GM sin-

gularities: the spectral density has units of density per unit energy, or $(\text{length})^{-d}/\text{frequency}$, or the 'scaling' dimension $d - \tilde{z}$ (the quotes emphasize that it is really not appropriate to think of the GM singularities as reflecting some underlying scale invariance).

The value of the exponent $\tilde{z}$ will vary continuously with $\overline{g}$, and its limiting value as $\overline{g} \searrow \overline{g}_c$ is of some interest. However, it is important not to confuse this limiting value with the true critical exponent z of the critical singularities at $g = g_c$: for this we will have, by (5.60)

$$\text{Im}\chi_L(\omega) \sim \omega^{(d-2+\eta)/z}. \tag{15.11}$$

The values of $\lim_{\overline{g} \searrow \overline{g}_c} \tilde{z}$ and z are obtained from $\chi_L''(\omega)$ by different orders of limits, and could, in principle, be distinct. There is numerical evidence in some recent simulations [409] that these two quantities coincide for H_{Id}, but there is no clear physical understanding why this should be so.

We emphasize that the GM singularities arise due to the presence of statistically rare clusters which are anomalously strongly coupled, and hence are unique features of the disordered system. The effect becomes weaker with increasing dimension, ultimately vanishing in the limit of infinite dimension. Increasing the range of the interactions also weakens the effect - for infinite range interactions, there are no singularities. Finally, the effect is strongest for the $N = 1$ model with discrete symmetry: we turn below to the $N \geq 2$ cases and will find much weaker singularities.

The analysis of the $N \geq 2$ case also focuses on the contribution of rare regions of size L which are almost ordered. We found above that such regions had a gap of order $\exp(-c_1 L^d)$ for $N = 1$, and now need the corresponding result for $N \geq 2$. For this, we first offer an alternative interpretation of the magnitude of the gap for $N = 1$: we can model the time evolution of the correlated region of size L as a *one*-dimensional classical Ising chain, as is clear from the arguments in Section 2.1— this chain has an 'exchange' of order L^d, and then the results (2.16) and (2.28) lead to the correct exponentially small gap. The same interpretation also works for $N \geq 2$; we again have an 'exchange' of order L^d, but now, by (2.46) and (2.55), the gap is inversely proportional to the exchange, *i.e.,* it now takes a much larger value of order L^{-d}. This larger gap indicates that the correlated region changes its orientation far more frequently and will be less important for the low energy physics.

Inserting this gap into the analog of (15.10), we get

$$\chi_L''(\omega) \quad \sim \quad \int dL \ e^{-cL^d} \delta(\omega - c_1/L^d) \qquad (15.12)$$

$$\sim \quad \exp(-cc_1/\omega), \qquad (15.13)$$

which is only a very weak essential singularity. It appears unlikely that such a weak GM effect will play an important role in the fluctuations at the quantum critical point.

It should be mentioned here that the above analysis of models with a continuous $O(N)$ symmetry is special to the rotor models, and does not apply to random versions of the Heisenberg spin systems of Chapter 13. The GM of singularities of the latter are quite strong and have been considered in Refs [52, 154].

15.3 Perturbative field-theoretic analysis

In this section, we will attempt to analyze H_{Id} and H_{Rd} for the case of weak disorder, by extending the non-disordered system field-theoretic analysis of Chapter 8.

A first question to ask is whether the non-disordered (or 'pure') fixed point is stable against disorder. The arguments of Section 15.1 show that this will be the case if $\nu_{pure} > 2/d$. For $N = 1$ we know that $\nu_{pure} = \frac{1}{2}$ for $d \geq 3$, and $\nu_{pure} \approx .632$ for $d = 2$ and $\nu_{pure} = 1$ for $d = 1$; thus weak randomness is relevant for all dimensions $d < 4$. A similar result holds for higher N. So for $d > 4$, sufficiently weak disorder should not change the critical properties from those of the pure system. For $d < 4$, we might hope that a renormalization group analysis will allow us to access a stable fixed point at least for small $4 - d$. Such an analysis requires a disordered version of the pure system field theory $\mathcal{S}_\phi$ in (8.2): this is clearly realized by simply allowing all the coupling constants to become random functions of the spatial co-ordinate x. However, as could be expected from the arguments above, the most important spatial dependence is that of the parameter r which controls the position of the critical point; we therefore consider the disordered action

$$\mathcal{S}_{\phi d} = \int d^d x \int d\tau \left\{ \frac{1}{2} \left[(\partial_\tau \phi_\alpha)^2 + c^2 (\nabla_x \phi_\alpha)^2 + \right. \right.$$
$$\left. \left. (r_0 + r(x)) \phi_\alpha^2(x) \right] + \frac{u}{4!} (\phi_\alpha^2(x))^2 \right\} (15.14)$$

with $r(x)$ a random function of position with probability distribution

$P[r(x)] \sim \exp(-\int d^d x r^2(x)/(2\delta^2))$. While it is possible to work directly with $\mathcal{S}_{\phi d}$, the subsequent analysis is made simpler by making an explicit average over disorder using the replica method. We will not discuss this method in any detail here, but refer the reader to introductory discussions in the literature, *e.g.*, in the book by Fischer and Hertz [150]. We are interested here in average correlators of the random system defined by

$$\overline{\int \mathcal{D}\phi e^{-\mathcal{S}_{\phi d}} O/\overline{Z}}, \qquad (15.15)$$

where O is any observable, and notice that the average over disorder must include the disorder-dependent partition function, $\overline{Z} = \int \mathcal{D}\phi e^{-\mathcal{S}_{\phi d}}$, in the denominator. To overcome this technical difficulty, we introduce n replicas of the field, $\phi_{\alpha a}$ ($a = 1 \ldots n$ is the replica index): then if the operator O involves only the field with $n = 1$, the integral over the remaining replicas will give a contribution $\overline{Z}^{n-1}$ in the functional integral over $\mathcal{S}_{\phi d}$. Now note that in the limit $n \to 0$, this yields precisely the factor $\overline{Z}^{-1}$ appearing in (15.15). So the prescription of the replica method is to compute correlators with n arbitrary, and then take the peculiar step of analytically continuing to a system with $n = 0$ field components. The advantage is that this allows us to average over the disorder in $e^{-\mathcal{S}_{\phi d}}$ at an early stage.

Introducing n replicas of (15.14) and then averaging over $r(x)$, we obtain the following translationally invariant action of the field $\phi_{\alpha a}$ ($\alpha = 1 \ldots N$, $a = 1 \ldots n$):

$$\mathcal{S}_{\phi d} = \int d^d x \int d\tau \sum_a \left\{ \frac{1}{2} \left[(\partial_\tau \phi_{\alpha a})^2 + c^2 (\nabla_x \phi_{\alpha a})^2 + r_0 \phi_{\alpha a}^2 \right] \right.$$
$$\left. + \frac{u}{4!} (\phi_{\alpha a}^2)^2 \right\} - \frac{\delta^2}{2} \int d^d x \int d\tau d\tau' \sum_{a,b} \phi_{\alpha a}^2(x,\tau) \phi_{\beta b}^2(x,\tau'), \quad (15.16)$$

where all summations over replica indices are explicitly noted. The renormalization group analysis of this action can be carried out by standard methods—we simply treat n as an arbitrary integer, and only take the $n \to 0$ limit after the scaling equations are obtained. We will perturb the theory in powers of the non-linearities u and δ^2. First, simple power counting at zeroth order gives us the flow equations:

$$\frac{dr_0}{dl} = 2r_0$$
$$\frac{du}{dl} = (3-d)u$$

$$\frac{d\delta^2}{dl} = (4-d)\delta^2 \tag{15.17}$$

Thus δ^2 becomes relevant below 4 dimensions, as expected from the arguments at the beginning of this section. Note that the interaction strength u however remains irrelevant down to $d = 3$. At next order, these flow equations get modified to

$$\frac{dr_0}{dl} = 2r_0 + c_1 u - c_2 \delta^2 \tag{15.18}$$

$$\frac{du}{dl} = (3-d)u - c_3 u^2 + c_4 u\delta^2 \tag{15.19}$$

$$\frac{d\delta^2}{dl} = (4-d)\delta^2 + c_5 \delta^4 - c_6 u\delta^2 \tag{15.20}$$

where the c_i are all positive constants. These equations do not allow for a fixed point for small $4 - d$; instead δ^2 has runaway flows suggesting a fundamental instability in the perturbation theory. This is a disappointing result, and we are unable to obtain any reliable information about the quantum critical point by this approach. Analysis of this problem by the large N expansion [270] also fails, again because of runaway flows for the strength of the randomness. Thus the fixed point theory presumably has a strong amount of randomness. At the level of the non-interacting theory, one expects that the lowest energy modes will be strongly localized. Physically, it is clear then that we cannot ignore the effects of interactions - condensation into a localized state leads to enhancement in interaction effects. It is necessary to include both disorder and interactions in a fundamental way.

An alternative approach was taken by Dorogovstev [130] and Boyanovsky and Cardy [60]. They extended (15.16) to a quantum field theory in d space and ϵ_τ time dimensions; formally this amounts to replacing $\int d\tau$ by $\int d^{\epsilon_\tau}\tau$ and using the standard field theoretic methods of dimensional continuation. The quantum critical point of course corresponds to $\epsilon_\tau = 1$, but these authors suggested making an expansion in small ϵ_τ. The validity of such a procedure is not a priori clear as (15.16) represents the quantum mechanics of a Hamiltonian system only for $\epsilon_\tau = 1$, and it is also clear that a small ϵ_τ suppresses the GM singularities. Simple power counting shows that the equations for r_0 and δ in (15.17) remain unchanged, while that for u gets modified to

$$\frac{du}{d\ell} = (4 - \epsilon_\tau - d)u. \tag{15.21}$$

Now notice that for small ϵ_τ, both u and δ become relevant about the

$u = \delta = 0$ fixed point near $d = 4$: this allows interactions to control the instabilities due to disorder, and raises the possibility that a stable fixed point may be found. This was indeed shown to be the case in Ref [60]: they found a fixed point with non-zero disorder and interactions in a double expansion in ϵ_τ and $(4 - d)$ which exhibited conventional dynamic scaling with exponents

$$z = 1 + \frac{(4 - N)(4 - d) + (2N + 4)\epsilon_\tau}{16(N - 1)}$$

$$\nu = \frac{1}{2} + \frac{(13N + 20)(4 - d) + 4(6N + 11)\epsilon_\tau}{32(N - 1)}, \qquad (15.22)$$

at lowest order for $N > 1$. It would be useful to examine the GM singularities of the paramagnetic phase in this approach, and to compute the value of $\tilde{z}$: this is an interesting possibility for future work, and could lead to further insight on the validity of the ϵ_τ expansion.

15.3.1 Metallic systems

The above field theoretic analysis can be easily extended to the random case of the transitions of metallic systems considered in Chapter 12. The central difference from the Ising/rotor models, as in the pure case, is that the frequency dependent ω^2 term in the propagator for the order parameter gets replaced by a $|\omega|$ term as in (12.10). In this manner, the replicated field theory (15.16) generalizes to

$$\mathcal{S}_{Hd} = \int \frac{d^d k}{(2\pi)^d} T \sum_{\omega_n} \frac{1}{2} \left[k^2 + |\omega_n| + r \right] |\phi_{\alpha a}(k, \omega_n)|^2$$

$$+ \frac{u}{4!} \int d^d x d\tau (\phi_{\alpha a}^2(x, \tau))^2$$

$$- \frac{\delta^2}{2} \int d^d x \int d\tau d\tau' \sum_{a,b} \phi_{\alpha a}^2(x, \tau) \phi_{\beta b}^2(x, \tau'). \qquad (15.23)$$

This theory has been analyzed in a double expansion in $(4 - d)$ and ϵ_τ in Ref [272].

In the following two sections of this chapter we will focus on two simpler models which are amenable to an essentially exact analysis. Both models are restricted to the Ising case $N = 1$ and have very strong GM singularities. We will be able to explicitly follow their evolution upon the approach to the critical point: we will find that in these cases the GM singularities in fact become the critical singularities, and the resulting

dynamic scaling is quite different from the one suggested above in (15.22) by the small ϵ_τ expansion above. Interpretations and attempts at a synthesis will follow in the final section.

15.4 Quantum Ising models near the percolation transition

We will consider here a special limiting case of the quantum Ising model H_{Id} in (15.1). Consider the following probability distribution of the exchange interactions

$$J_{ij} = \left\{ \begin{array}{ll} 0 & \text{with probability } p \\ J & \text{with probability } 1-p \end{array} \right. , \qquad (15.24)$$

and let us choose, for simplicity, all the transverse fields $g_i = g$ site independent (the results discussed below can be shown to also hold for a random distribution of g_i). So two neighboring sites either interact with an exchange J (such sites are 'connected') or they have no direct coupling. Sets of mutually connected sites from clusters, and a lot is known about the geometry of such clusters in d spatial dimensions—this is the geometrical 'percolation' problem, and we will quickly review some needed results for percolation theory in Section 15.4.1. This sharp separation of sites into sets of disconnected clusters is an important simplifying feature, and will allow us obtain a number of exact properties of the quantum critical point for general d: this simplification clearly relies upon the fact J_{ij} becomes precisely zero with probability p. After our review of percolation in Section 15.4.1, we will consider the classical Ising model (with $g = 0$) at non-zero T in Section 15.4.2 and finally consider the non-zero g case in Section 15.4.3.

15.4.1 Percolation theory

Removing bonds on a lattice with probability p (see (15.24)) yields the statistical problem of the geometry of connected clusters on the diluted lattice. This has been reviewed in the book by Stauffer and Aharony [476], and we will quote some needed results. There is a critical p_c, such that for $p > p_c$ there are (in the thermodynamic limit) only connected clusters of a finite size, while for $p < p_c$ there is a thermodynamically large connected cluster. Right at $p = p_c$, there are a large number of clusters with a broad distribution of sizes. These clusters are known to have a fractal structure. Though no cluster is thermodynamically large (*i.e.*, the ratio of the number of sites in any cluster to the

total number of sites in the system tends to zero in the thermodynamic limit), there will be an infinite connected cluster with a fractal dimension $d_f < d$). An important fact about the critical percolating cluster is that it consists of arbitrarily long one-dimensional segments which are crucial for its connectedness. Breaking these segments splits the cluster into two disjoint units.

For $p > p_c$ there is a finite probability that any given site belongs to the infinite cluster; this probability vanishes as $p \searrow p_c$ with the power-law $\sim (p_c - p)^{\beta_p}$. We can also consider the probability, $P(N, p)$ that any site belongs to finite, large cluster of N sites; for p close to p_c this satisfies the scaling form

$$P(N, p) \sim N^{1-\tau} G(N/\xi^{d_f}) \tag{15.25}$$

where $\xi \sim |p - p_c|^{-\nu_p}$ is a characteristic finite cluster size which diverges at $p = p_c$, τ, d_f, and ν_p are universal critical exponents, and G is a universal scaling functions. The exponents and scaling functions have been computed either exactly or numerically in $d = 2$ and 3, and we will simply treat them here as known quantities. For some of our later results, we also need to the limiting form of the function $G(y)$; it approaches 1 for $y \ll 1$, while for $y \gg 1$,

$$
\begin{aligned}
G(y, p > p_c) &\sim y^{-\theta+\tau} e^{-c+y} \\
G(y, p < p_c) &\sim y^{-\theta'+\tau} e^{-c-y^{1-1/d}}
\end{aligned}
\tag{15.26}
$$

where θ and θ' are additional known exponents.

Finally, we will also need information on the correlation between pairs of sites. For $p \geq p_c$ the probability that two sites belong to the same cluster decays for large x as $\sim x^{-d+2-\eta_p} F(x/\xi)$ where η_p is another exponent $(2\beta_p = (d - 2 + \eta_p)\nu_p)$ and F a scaling function.

15.4.2 Classical dilute Ising models

We warm up with a discussion of the properties of the classical Ising model, $g = 0$, and nonzero T; its phase diagram is shown in Fig 15.1. At $p = 0$, as T is increased, there is a phase transition from an ordered state to a disordered one (See Fig 15.1). On the other axis, when $T = 0$ there is a percolation transition at $p = p_c$; this transition coincides with loss of magnetic long range order, as there is no infinite cluster, and hence no spontaneous magnetization for $p > p_c$. The boundary of critical temperatures $T = T_c(p)$ approaches zero at $p = p_c$ as $T_c \sim$
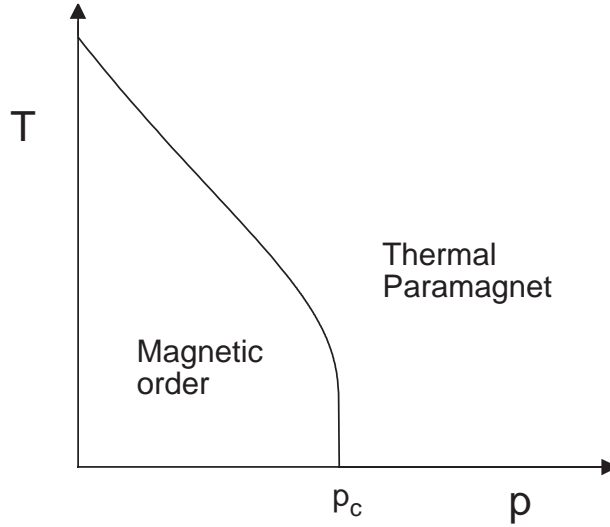
Fig. 15.1. Phase diagram of the classical dilute Ising model at finite temperature. The dilution probability is p. The phase boundary goes to zero as $p \to p_c-$ as $T_c \sim 1/\ln(1/(p_c - p))$.

$\ln(1/(p_c - p))$. These results can be understood in the following way. As we mentioned earlier, the critical percolating cluster consists of a number of arbitrarily large one-dimensional segments. These segments are the weakest links in the cluster; correlations in the cluster will be destroyed if they are destroyed along the segments. From the low temperature behaviour of the classical Ising chain in Section 2.1, we know that any finite T will destroy correlations in a large segment over a length scale ξ_T that is exponentially large in $1/T$. Now consider the infinite cluster at $p < p_c$. This resembles the critical clusters at scales $\ll \xi$, where $\xi \sim (p_c - p)^{-\nu_p}$ is the percolation correlation length. At larger scales, there is a crossover to the geometry of a d-dimensional lattice. Thus thermal effects will destroy correlations in this cluster when $\xi_T \sim \xi$ which leads to $T_c \sim \ln(1/(p_c - p))$.

15.4.3 Quantum dilute Ising models

We are ready to consider the $T = 0$ properties of the quantum Ising model for $g \neq 0$. Its phase diagram as a function of g and p is shown in Fig 15.2. At $p = 0$, as g is increased, there is a $T = 0$ transition from a magnetically ordered ground state to a quantum paramagnetic state
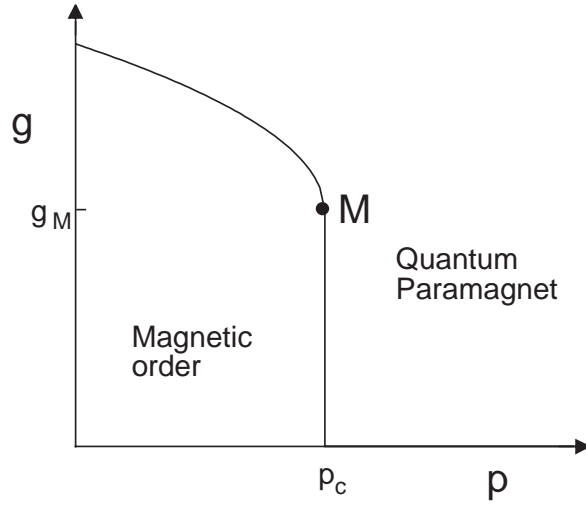
Fig. 15.2. Phase diagram of the dilute Ising model in a transverse field (g) at $T = 0$. The dilution probability is p. The multicritical point M is at $p = p_c$, $g = g_M$. The quantum transition along the vertical phase boundary ($g < g_M$, $p = p_c$) is controlled by the classical percolation fixed point at $p = p_c$, $g = 0$; quantum effects (due to a non-zero g) are dangerously irrelevant, and lead to activated dynamic scaling near the $g < g_M$, $p = p_c$ line.

which is in the universality class of the models of Part 2. On the other axis, when $g = 0$, so that the system is classical, there is a percolation transition at $p = p_c$. For $p < p_c$, for small enough g, the system retains long range order. This is ultimately destroyed for some $g > g_c(p)$, with $g_c(p)$ expected to be a monotonically decreasing function of p. On the other hand, if $p > p_c$, there is no long range order for any g.

We will now argue, as first noted by Harris [212, 478, 131], that the phase boundary of Fig 15.2 remains vertical at $p = p_c$ for a finite range of $g \leq g_M$; we will then show that a number of properties of the quantum phase transition across this vertical phase boundary can be computed exactly, as shown in Ref [455]. The system in fact remains critical along the line $p = p_c$, $g < g_M$; to see this, note that, although there is no thermodynamically large connected cluster at p_c, there still is an infinite connected cluster with a fractal dimension smaller than d. The spins on this cluster align together at $g = 0$. A small but non-zero g is not sufficient to destroy this order on the critical cluster. That this is true can be seen by the following argument: The critical cluster is definitely more strongly connected than a one-dimensional chain of Ising spins.

Even in $d = 1$ where fluctuation effects are strongest, a small g preserves long-range order in the Ising spins, as we know from Chapter 4. Thus a small g will certainly preserve the order in the critical cluster. Note that the effects of quantum fluctuations are thus quite different from the effects of thermal fluctuations that we discussed in the previous section. The root of this difference lies in the observation that while any amount of thermal fluctuations destroy the order in the $d = 1$ Ising chain, it takes a finite strength of quantum fluctuations to do so. In fact, two spins on any sufficiently large finite cluster remain strongly correlated with each other in space for small g. (Of course, for a finite cluster there will be no long-range correlation in time). The critical cluster eventually loses order when g reaches g_M.

Let us consider the equal-time two point spin correlation function $C(x, 0)$ (see (4.2)). Spins at points 0 and x are correlated only if they belong to the same cluster; however, as argued above for $g < g_M$, once two spins are on the same cluster, they have an essentially perfect correlation (normalized to unity) even if they are very far apart. So the disorder-averaged $\overline{C(x, 0)}$ will be simply proportional to the probability that the two spins are on the same cluster; by the results of Section 15.4.1 we can then conclude at $p = p_c$ and for $h < h_M$, $\overline{C(x, 0)} \sim x^{-d+2-\eta_p}$. So this line is critical with exponents given by that of ordinary percolation.

We can also compute a variety of static, dynamic and thermodynamic properties across the $p = p_c$, $g < g_M$ critical line.

First some static properties. By precisely the same arguments as those above for $p = p_c$, we can conclude that for $p \geq p_c$ $\overline{C(x, 0)} \sim x^{-d+2-\eta_p} F(x/\xi)$; so the off-critical exponents and crossover functions are also those of percolation. For $p < p_c$, the spontaneous magnetization, N_0, is simply proportional to the probability that a given site lie on the infinite cluster, and so $N_0 \sim (p_c - p)^{\beta_p}$.

Now consider dynamic correlations. We will compute the low energy part of the contribution to $\chi_L''(\omega)$ by a cluster of N sites: the mean χ_L can then be computed by an average over $P(N, p)$. The energy levels of a cluster of N sites can be described for $g \ll J$ as follows: The two lowest levels correspond to the states of a single effective Ising spin with magnetic moment $\sim N$ in an effective transverse field $g_{\text{eff}, N}$. For large N, $g_{\text{eff}, N}$ can be estimated in N^{th} order perturbation theory to be $\tilde{g} \exp(-cN)$, as discussed in Section 15.2. The quantities $\tilde{g}$ and c are of order h and $\ln(J/g)$ respectively but their precise values depend on the particular cluster being considered. As the distribution of $\tilde{g}$ and c is not expected to become very broad near the transition, we will replace

them by their typical values g_0 and c_0 respectively. Apart from these two lowest levels, there are other levels separated from these by energies $\sim J$. These can be ignored for the low energy physics, and for small $\omega \ll g$, we only need to consider large clusters. Averaging over all sites using $P(N, p)$ as written in (15.25), we obtain

$$
\begin{aligned}
\overline{\chi_L''(\omega)} &\sim \int \frac{dN}{N^{\tau-1}} G(N/\xi^{d_f}) \delta(\omega - g_0 e^{-c_0 N}) \\
&\sim \frac{1}{\omega(\ln(g_0/\omega))^{\tau-1}} G\left(\frac{\ln(g_0/\omega)}{c_0 \xi^{d_f}}\right)
\end{aligned}
\tag{15.27}
$$

This scaling form describing the dynamical properties across the vertical transition line in Fig 15.2 is one of the central results of this section, and reader should pause to consider its implications. Its most striking feature is that the characteristic length ξ scales as a power of the *logarithm* of the frequency ω; this is known as *activated dynamic scaling*, and should be contrasted with the conventional behavior (considered in Section 15.3) where $\omega \sim \xi^{-z}$. The exponent z is effectively infinite if the dynamic scaling is activated. In the present case, the critical point $p = p_c$ contains clusters of all sizes, and as we have already seen, the characteristic excitation energy of a cluster of size L scales as $\exp(-cL^{d_f})$, which indicates the origin of the activated scaling.

The explicit results for the function G in (15.26) allow us to study the low energy spectrum across the transition. For $p > p_c$ we get

$$
\overline{\chi_L''(\omega)} \sim \frac{\omega^{d/\tilde{z}-1}}{(\ln(g_0/\omega))^{\theta-1}}
\tag{15.28}
$$

which, apart from logarithms, is of the form (15.10) discussed earlier as a consequence of GM singularities. The dynamic 'exponent' $\tilde{z}$ can be explicitly computed, and we find

$$
\tilde{z} \sim \xi^{d_f};
\tag{15.29}
$$

i.e., $\tilde{z}$ *diverges* as we approach the quantum critical point. So the value of $\lim_{p \searrow p_c} \tilde{z}$ coincides with the activated dynamic scaling value of $z = \infty$. Precisely at $p = p_c$, the conventional dynamic scaling result (15.11) is replaced here by

$$
\overline{\chi_L''(\omega)} \sim \frac{1}{\omega(\ln(g_0/\omega))^{\tau-1}}.
\tag{15.30}
$$

Finally, on the ordered side with $p < p_c$, the presence of the infinite cluster (and the associated long range order) gives rise to a delta function

at $\omega = 0$; for $\omega \neq 0$, $\chi_L''(\omega)$ is still determined by contributions from the finite clusters, and we find

$$\chi_L''(\omega \neq 0) \sim (1/\omega)(\ln(g_0/\omega))^{1-\theta'} \exp\left(-\kappa(\ln(g_0/\omega))^{1-1/d}\right) \quad (15.31)$$

with $\kappa \sim \xi^{-d_f(1-1/d)}$. Again the system is gapless, reflecting the GM singularities of the ordered phase.

Now we turn to the thermodynamic properties. The magnetization in response to a uniform external applied magnetic field h coupling to $\hat{\sigma}^z$ can be calculated similarly by an average over the response of clusters of size N. For small $h \ll g$, only large clusters contribute, and the magnetization per site is that of an Ising spin of magnetic moment N in a transverse field $g_{\mathrm{eff},N}$, and is therefore given by

$$M_N(h) = \frac{Nh}{((Nh)^2 + g_{\mathrm{eff},N}^2)^{1/2}} \quad (15.32)$$

Thus the total magnetization per site (after subtracting the regular contribution of the infinite cluster for $p < p_c$) is

$$M(h) - M(h = 0) \sim \int dN \frac{1}{N^{\tau-1}} G(N/\xi^{d_f}) M_N(h) \quad (15.33)$$

The singular part therefore has the scaling form

$$M_{\mathrm{sing}}(h) \sim \frac{1}{(\ln(g_0/h))^{\tau-2}} \Phi_M\left(c\frac{\ln(g_0/h)}{\xi^{d_f}}\right) \quad (15.34)$$

with c a non-universal constant, and $\Phi_M(y)$ a universal function which is related to $G(y)$ by $\Phi_M(y) = \int_1^\infty w^{1-\tau} dw G(wy)$. Now the consequence of activated scaling is that a power of the logarithm of the field scales as the correlation length. Using our earlier results for G, we can conclude that for $p > p_c$ rises as a power of H, with a continuously varying exponent which approaches 0 as $p \searrow p_c$, and so the linear susceptibility diverges over a whole region. At $p = p_c$ the magnetization is a power of $\ln(1/h)$. On the ordered side, $p < p_c$, $dM/dh \sim 1/h$ with weak corrections; thus the linear susceptibility diverges in the ordered side as well.

What about the finite T properties of this quantum Ising model ? For the *classical* dilute Ising model at $p = p_c$, the correlation length at finite T behaves as $\exp(\mathrm{constant}/T)$. This is essentially due to the presence of one dimensional segments in the critical percolating clusters. For the quantum problem for $g < g_M$, these one dimensional segments would give rise to a thermal correlation length (ξ_T) with a similar exponential dependence on $1/T$, and a prefactor that is a power-law in T; this is the
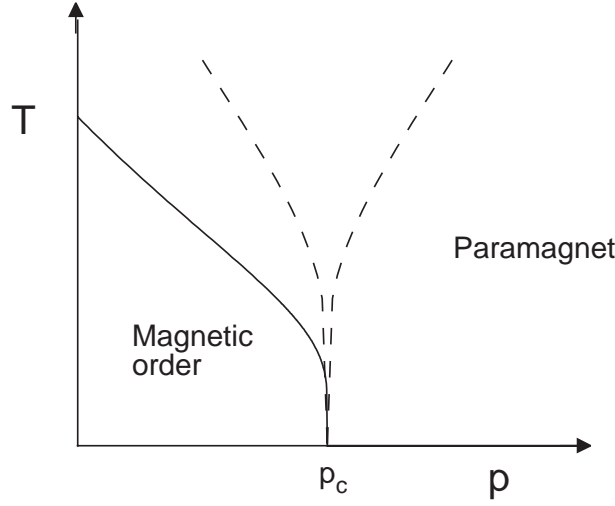
Fig. 15.3. Finite temperature phase diagram for $g < g_M$. The dashed lines $(T \sim 1/\ln(1/|p - p_c|))$ represent crossovers from the high T regime, character-ized by spin fluctuations on the critical infinite cluster, to the low T regimes. The solid line for $p < p_c$ is the phase transition $(T = T_c \sim 1/\ln(1/(p_c - p))$ where long range order is destroyed.

behavior in the "high T" region of Fig 15.3. Away from the critical point, the crossovers are as shown in Fig 15.3. The low T behavior appears when $\xi \sim \xi_T$, or $T \sim \ln^{-1}(1/(|p - p_c|))$. On the paramagnetic side, the low T system is described well as a collection of rigid Ising clusters with effective transverse fields and a size distribution as before; this leads, for instance, to a linear susceptibility $\chi_T \sim T^{-1+\kappa}$ (up to log corrections) with $\kappa \sim \xi^{-d_f}$. On the ordered side, there is a finite temperature phase transition; as in the classical case, as $p \nearrow p_c$, the transition temperature falls to zero as $T_c \sim \ln^{-1}(1/(p_c - p))$. Finally, it would be interesting to understand the real time dynamics at non-zero T, along the lines of our analysis in Part 2: this remains an open problem, of considerable experimental interest.

To summarize, we have presented a simple example of a random quantum transition in dimensions $d > 1$ which exhibits activated dynamics scaling with $\ln(1/\text{energy scale}) \sim \xi^{d_f}$. There were Griffiths-McCoy regions on either side of the transition, with a singular density of states and a diverging susceptibility. Theoretically, an important feature of this transition is that it was controlled by a classical, static, percolation fixed point at $g = 0$, $p = p_c$, with dynamic, quantum fluctuations being

"dangerously irrelevant". To see this, consider again the calculation of the field dependent magnetization at the critical point. At the fixed point with $g = 0$, all the spins in the system align for any strength of the external field and the magnetization per spin would be 1 for any (positive) value of the field. This is however not correct. Quantum fluctuations prevent spins belonging to small clusters from contributing anything to the magnetization. Spins belonging to large clusters however contribute an amount of order 1. The crossover occurs for a cluster size $N_h \sim \ln(1/h)$. The leading scaling result is obtained by aligning all clusters with size bigger than N_h. Similarly for the dynamics, the spin autocorrelation function is clearly just 1 at all times at the fixed point as it is classical. (Hence, we may call such fluctuationless fixed points as static). Again this is not correct, and we need to include the irrelevant quantum fluctuations to get the results we presented earlier.

15.5 The disordered quantum Ising chain

This section will examine H_{Id} in (15.1) in dimension $d = 1$. In this case, as was shown by D.S. Fisher [152, 154], we will find that for a *general* distribution of the couplings g_i, $J_{i,i+1}$ the quantum phase transition exhibits activated dynamic scaling very similar to that introduced in Section 15.4 for models on percolating clusters. This result is established using a renormalization group analysis of the entire probability distributions of the g_i and $J_{i,i+1}$, and relies on the fact that these probability distributions become extremely broad at low energy scales. So if we focus on the response at a given energy scale, ω, all couplings of nearby sites are either much smaller or much larger than ω: this suggests we can set all the small couplings to zero and tightly couple the spins into clusters with the large couplings. This clustering now appears quite similar to the percolation model of Section 15.4, and explains the appearance of activated dynamic scaling in the present situation.

We begin by setting up the renormalization group analysis which will establish the above claims. We will assume that the distribution of couplings is broad to begin with: subsequent analysis shows that this assumption self-consistent, and the resulting renormalized distributions have a large basin of attraction. The basic idea behind the procedure, first used by Dasgupta and Ma[319, 118] in their study of the random antiferromagnetic spin chain, is to successively decimate the strongest

coupling

$$\Omega \equiv \max\{g_i, J_{i,i+1}\}, \tag{15.35}$$

in the chain and get an effective Hamiltonian for the low energy degrees of freedom. Consider the case when the maximum coupling is a field, say g_i. We first solve for the part of the Hamiltonian involving g_i: the ground state is the symmetric combination $|+\rangle_i = (|\uparrow\rangle_i + |\downarrow\rangle_i)/\sqrt{2}$, while the excited state $|-\rangle_i = (|\uparrow\rangle_i - |\downarrow\rangle_i)/\sqrt{2}$ is an energy $2g_i$ higher (see Section 4.1.1). As g_i is the largest energy around, it is legitimate to project the remaining Hamiltonian into the space with the state at i constrained to be $|+\rangle_i$, thereby eliminating the site i. This can be done in a simple perturbation theory in $1/g_i$, and to lowest non-trivial order the result is a new effective bond between the sites $i-1$ and $i+1$ of strength

$$J = \frac{J_{i-1,i}J_{i,i+1}}{g_i} \tag{15.36}$$

We now have a new random quantum Ising chain with one less site, and one less bond.

On the other hand, if the maximum coupling is a bond, say $J_{i,i+1}$, we first solve for the part of the Hamiltonian involving $J_{i,i+1}$. This is just the exchange interaction between the spins at sites i and $i+1$: its ground state is doubly degenerate, $|\uparrow\rangle_i|\uparrow\rangle_{i+1}$ or $|\downarrow\rangle_i|\downarrow\rangle_{i+1}$, and the two excited states with the spins oriented in opposite directions are energy $2J_{i,i+1}$ higher (see Section 4.1.2). Clearly, we may think of the two degenerate ground states as corresponding to the two states of a single effective Ising degree of freedom with a magnetic moment equal to the sum of the moments of the individual spins. For large $J_{i,i+1}$, it is legitimate to project the remaining Hamiltonian into the space with the spins at i and $i+1$ constrained to be in the same state. Again, we do this in second order perturbation theory. The result is that the two sites i and $i+1$ are replaced by a single Ising spin with an effective transverse field of strength

$$g = \frac{g_i g_{i+1}}{J_{i,i+1}} \tag{15.37}$$

To this order of perturbation theory, the interaction of this effective site with the neighboring spins remains unmodified. We now again have a random quantum Ising chain with one less site, and one less bond.

This decimation procedure is the basic renormalization group transformation. The strategy is to iterate this transformation till the maximum

remaining coupling is of the order the energy at which we wish to probe the system. Note that no correlations are introduced between any of the couplings by this procedure. Thus the different bonds and fields continue to be independent random variables, though with probability distributions that are renormalized.

It is convenient to convert these recursion relations into flow equations for the distributions. From the form of the recursion relations, it is clear that it is natural to work in terms of the logarithmic variables: we therefore define

$$
\begin{aligned}
\Gamma &= \ln(\Omega_I/\Omega) \\
\zeta &= \ln(\Omega/J) \geq 0, \\
\beta &= \ln(\Omega/g) \geq 0
\end{aligned}
$$
(15.38)

where Ω_I is the maximum coupling in the initial distributions, and Ω is the maximum at any given stage of the renormalization group. We will denote the normalized probability distribution for the exchange constants by $P(\zeta;\Gamma)$ (satisfying $\int_0^\infty d\zeta P(\zeta;\Gamma) = 1$), and similarly the probability distributions for the transverse field by $R(\beta;\Gamma)$. As we reduce the high energy cutoff Ω, notice that Γ becomes larger. The ultimate low energy is therefore controlled by the limit $\Gamma \to \infty$, and we will be interested in the forms of the distributions P and R in this limit.

This paragraph contains a few intermediate steps showing how to transcribe the transformations (15.36) and (15.37) into partial differential equations for $P(\zeta;\Gamma)$ and $P(\beta;\Gamma)$: readers not interested in the details can move on to the next paragraph. Let $\mathcal{N}(\Gamma)$ be the total number of clusters at scale Γ, $\mathcal{N}_B(\zeta,\Gamma)$ be the total number of bonds of strength ζ at this scale, and $\mathcal{N}_S(\beta,\Gamma)$ the total number of sites with transverse field of strength β. Then, by definition

$$
P(\zeta;\Gamma) = \frac{\mathcal{N}_B(\zeta,\Gamma)}{\mathcal{N}(\Gamma)} \qquad R(\beta;\Gamma) = \frac{\mathcal{N}_S(\beta,\Gamma)}{\mathcal{N}(\Gamma)}
$$
(15.39)

Now perform the basic renormalization group transformation by increasing Γ by an infinitesimal amount $d\Gamma$. This involves eliminating bonds with $\zeta \approx 0$ and sites with $\beta \approx 0$. In terms of Ω_I instead of Ω we have $\zeta = \ln(\Omega_I/J) - \Gamma$, and so when Γ is changed, ζ changes by $d\zeta = -d\Gamma$, and similarly for β. Therefore all bonds and sites with $0 < \zeta, \beta < d\Gamma$ are eliminated which implies

$$
\mathcal{N}(\Gamma + d\Gamma) = \mathcal{N}(\Gamma) - d\Gamma \left[\mathcal{N}_B(0,\Gamma) + \mathcal{N}_S(0,\Gamma)\right].
$$
(15.40)

Now consider the changes in $\mathcal{N}_B(\zeta,\Gamma)$. The transformation (15.36) will

remove two bonds and add a new one: this leads to

$$\mathcal{N}_B(\zeta, \Gamma + d\Gamma) = \mathcal{N}_B(\zeta - d\zeta, \Gamma) + d\Gamma \int d\zeta_1 d\zeta_2 \mathcal{N}_S(0, \Gamma) \times$$

$$P(\zeta_1; \Gamma) P(\zeta_2; \Gamma) [\delta(\zeta - \zeta_1 - \zeta_2) - \delta(\zeta - \zeta_1) - \delta(\zeta - \zeta_2)]; \quad (15.41)$$

the first term within the square brackets represents the new bond which has been created and thus increases the probability (the delta-function multiplying it is the logarithmic version of (15.36)), while the next two terms represent the two eliminated bonds. A very similar result holds for $\mathcal{N}_S$ from the transformation (15.37).

By combining (15.39-15.41) we obtain the required differential equations for the probability distributions

$$\frac{\partial P(\zeta; \Gamma)}{\partial \Gamma} = \frac{\partial P(\zeta; \Gamma)}{\partial \zeta} + P(\zeta; \Gamma)(P(0; \Gamma) - R(0; \Gamma))$$

$$+ R(0; \Gamma) \int d\zeta_1 d\zeta_2 P(\zeta_1; \Gamma) P(\zeta_2; \Gamma) \delta(\zeta - \zeta_1 - \zeta_2)$$

$$\frac{\partial R(\beta; \Gamma)}{\partial \Gamma} = \frac{\partial R(\beta; \Gamma)}{\partial \beta} + R(\beta; \Gamma)(R(0; \Gamma) - P(0; \Gamma))$$

$$+ P(0; \Gamma) \int d\beta_1 d\beta_2 R(\beta_1; \Gamma) R(\beta_2; \Gamma) \delta(\beta - \beta_1 - \beta_2) \quad (15.42)$$

We are now faced with the following applied mathematics problem: given two initial arbitrary distributions $P(\zeta; \Gamma)$ and $R(\beta; \Gamma)$, evolve them with increasing Γ under (15.42)—is it possible to make any general statements about possible universal forms of these distributions in the limit $\Gamma \to \infty$? This problem was solved by Fisher [154] through some rather intricate, but in principle straightforward, mathematical analysis. We shall not be interested in the details of this analysis here, but will simply assert the main results which are then not difficult to verify *a posteriori*.

It was found that for almost all initial conditions, the ultimate flow is towards one of two classes of probability distributions. In the first, most exchange constants are larger than all of the transverse fields, and this clearly represents a system which will then acquire magnetic long-range order in its ground state, as in Section 4.1.2. Conversely, in the second, most transverse fields are larger than all of the exchange constants, and this corresponds to a system with a quantum paramagnetic ground state, as in Section 4.1.1. It is of interest to first examine the critical point between these two classes of solutions, in which case the two distributions P and R turn out to have precisely the same form. Indeed, by setting $P = R$, it can be shown that in the limit $\Gamma \to \infty$

essentially all solutions of (15.42) are attracted to a unique fixed point distribution; this distribution takes the scaling form

$$
\begin{aligned}
P(\zeta; \Gamma) &= \frac{1}{\Gamma} \mathcal{P}\left(\frac{\zeta}{\Gamma}\right) \\
R(\beta; \Gamma) &= \frac{1}{\Gamma} \mathcal{R}\left(\frac{\beta}{\Gamma}\right)
\end{aligned}
\tag{15.43}
$$

and the scaling functions take the simple explicit form

$$
\mathcal{P}(y) = \mathcal{R}(y) = e^{-y}
\tag{15.44}
$$

The reader is invited to verify that (15.44) and (15.43) constitute exact solutions of (15.42). Thus even in terms of the logarithmic variables ζ and β, the distributions become extremely broad at low energies (the width of the distribution is $\sim \Gamma$, which rises indefinitely as we go to lower energies). This broad distribution justifies *a posteriori* the second-order perturbation theory used to obtain (15.36) and (15.37): if we choose the biggest transverse field g_i (say), it is overwhelmingly likely that the exchange couplings $J_{i-1,i}$ and $J_{i,i+1}$ to the neighboring sites will be much smaller. This also suggests that the results obtained by the flow equations (15.42) are asymptotically exact. In terms of the original physical couplings J and g, the fixed point results (15.43) and (15.44) correspond to the distribution

$$
P(J) \sim \frac{1}{J^{1-1/\Gamma}},
\tag{15.45}
$$

and similarly for g. Note that the power in the denominator approaches 1 as Γ approaches ∞. Thus the distribution is highly singular at the origin - in fact for large enough Γ, the expectation value of $1/J$ will be divergent. It is this extreme broadness of the distribution that enables obtaining physical properties of the system with the critical distribution through simple calculations, as we will see shortly.

Let us consider perturbations of this critical solution. Linearizing the flow equations in the vicinity of the fixed point yields, as expected, a single relevant perturbation whose strength we parameterize by the coupling r; thus as in Chapter 8, r will represent the deviation from the critical point, with $r > 0$ putting the system in the quantum paramagnet. Fisher [152, 154] was also able to find a complete solution of (15.42) valid in the limit $\Gamma \to \infty$, $|r| \to 0$, but with $\Gamma|r|$ arbitrary. These

solutions are expressed in scaling forms which generalize (15.43):

$$P(\zeta; \Gamma) = \frac{1}{\Gamma} \mathcal{P}\left(\frac{\zeta}{\Gamma}, r\Gamma\right)$$

$$R(\beta; \Gamma) = \frac{1}{\Gamma} \mathcal{R}\left(\frac{\beta}{\Gamma}, r\Gamma\right), \tag{15.46}$$

and the explicit solutions for the scaling functions are

$$\mathcal{P}(y, y') = \frac{2y'}{e^{2y'} - 1} \exp\left(-\frac{2yy'}{e^{2y'} - 1}\right)$$

$$\mathcal{R}(y, y') = \mathcal{P}(y, -y') \tag{15.47}$$

Again, the reader can verify that (15.46) and (15.47) constitute exact solutions of (15.42). So we have available a family of probability distributions, parameterized by the single tuning parameter r; there is a quantum critical point at $r = 0$ separating the magnetically ordered phase ($r < 0$) from the quantum paramagnetic phase ($r > 0$).

Let us look at the explicit predictions of the above results for the low energy properties of the quantum paramagnet: for this we place ourselves in the paramagnet by fixing $r > 0$, and then access low energies by sending $\Gamma \to \infty$: recall that this was the order of limits discussed in Section 15.2. Then we find the probability distribution of transverse fields to be given by

$$P(g) \sim g^{-1+2\delta}, \tag{15.48}$$

while all exchange constants are essentially at zero energy with $P(J) = \delta(J)$. The spins are therefore effectively decoupled; each site can be independently diagonalized, and has two energy levels separated by $2g$. From this we can determine the leading low energy behavior of the average local spectral density $\overline{\chi_L''(\omega)}$. A naive calculation, using the form (4.20) suggests that

$$\overline{\chi_L''(\omega)} \sim \omega^{-1+1/\tilde{z}}, \tag{15.49}$$

where we have used the notation suggested by (15.10), and the value of the exponent $\tilde{z}$ is given by

$$\tilde{z} = \frac{1}{2r}. \tag{15.50}$$

However, this result is not entirely correct: we also need to know the probability that any given original spin $\hat{\sigma}_i^z$ will be active in the set of effective spins upon which transverse fields given by (15.48) act, *i.e.*, ensure that this spin has not been decimated in the renormalization

group transformation. We do not have the information yet to compute this precisely (although it can be reconstructed from Ref [154]), but it will become clear from the analysis below that the only consequence of rectifying this omission is to change (15.49) by powers of logarithms, as in (15.10). So our result for $\overline{\chi_L''(\omega)}$ is consistent with the general arguments of the GM singularities. Further we have found that the 'dynamic exponent' $\tilde{z}$ *diverges* as we approach the critical point with $r \to 0$. This is also precisely the behavior found in (15.29) for the dilute quantum Ising models in $d > 1$ in Section 15.4. By analogy, we may then expect that the present model also exhibits activated dynamic scaling with the critical dynamic exponent $z = \infty$; further, at the critical point $r = 0$, we may expect from (15.49) that $\overline{\chi_L''(\omega)} \sim 1/\omega$ times powers of $\ln(1/\omega)$, as in (15.30).

To truly establish the existence of activated dynamic scaling, we need information about length scales. In particular, we need to know the average spacing between the spins when we have renormalized down to a characteristic energy scale $\omega \sim \Omega_I e^{-\Gamma}$. We can obtain this information by simply keeping track of the total number of spins, $\mathcal{N}(\Gamma)$, that have not been decimated at a scale Γ. From (15.40) and (15.39) we know that this quantity satisfies the differential equation

$$\frac{d\mathcal{N}(\Gamma)}{d\Gamma} = -(P(0, \Gamma) + R(0, \Gamma))\mathcal{N}(\Gamma). \tag{15.51}$$

Using the result (15.43) we can now conclude that at the critical point $r = 0$

$$\mathcal{N}(\Gamma) \sim \frac{1}{\Gamma^2}. \tag{15.52}$$

So the average spacing between the spins increases as Γ^2; we may identify this as the characteristic length scale, ℓ, and we have

$$\ell \sim \Gamma^2 \sim \left[\ln(1/\omega)\right]^2. \tag{15.53}$$

This is precisely the behavior characteristic of activated dynamic scaling, as exhibited in the scaling form (15.27). We can now also obtain the correlation length, ξ, as the system moves away from criticality. From the scaling (15.46), we know that $\Gamma \sim 1/r$, and therefore from (15.53) we have

$$\xi \sim \Gamma^2 \sim \frac{1}{r^2}. \tag{15.54}$$

This gives us an exponent $\nu = 2$, which saturates the bound (15.5) in

$d = 1$. The length ξ actually sets the scale for the decay of the disorder-averaged correlation functions; typical spin correlations (*i.e.,* the most probable) however decay at a different length scale which diverges with exponent 1 [458]. For the dilute Ising model of Section 15.4, the typical spin correlations were simply zero, as two spins chosen at random typically belong to different clusters.

Fisher [154] has obtained far more precise information on the nature of the spatial correlations. We will not discuss the details of this here, but will review the general strategy and indicate some further results. So far we have only kept track of the probability distributions of the coupling constants, but it is also possible to include additional information about the nature of the renormalized spins as the decimation proceeds. In particular, we can associate with each spin a magnetic moment m_i. Initially, all spins have $m_i = 1$. However when we decimate a large $J_{i,i+1}$, the two spins at i and $i+1$ combine to form a single effective spin with moment $m = 2$. So, in general, parallel with the recursion relation (15.37) for each bond decimation, we have the recursion relation for the magnetic moments

$$m = m_i + m_{i+1}. \tag{15.55}$$

In addition, we can also associate a length, ℓ_B with each bond *and* a length ℓ_S with each spin. We begin with a spin chain with unit lattice spacing: let us associate a length of $1/2$ with each spin and with each bond. Then, when we decimate the bond $J_{i,i+1}$ we get a new spin of length $3/2$. In general, the recursion relation corresponding to the decimation (15.37) is

$$\ell_S = \ell_{S,i} + \ell_{S,i+1} + \ell_{B,i,i+1} \tag{15.56}$$

Similarly, along with the decimation of the spin with transverse field g_i in (15.36) we have the length recursion

$$\ell_B = \ell_{B,i-1,i} + \ell_{B,i,i+1} + \ell_{S,i}. \tag{15.57}$$

We can transcribe (15.55-15.57) into renormalization group flow equations, just as we mapped (15.36) and (15.37) into (15.42). For this we generalize the earlier probability distributions for the couplings, $P(\zeta; \Gamma)$ and $R(\beta; \Gamma)$ into *joint* probability distributions $P(\zeta, \ell_B; \Gamma)$ and $R(\beta, \ell_S, m; \Gamma)$. The joint distributions account for the fact that the length or moment of any given spin is certainly correlated with the size of the transverse field acting on it—a spin with a very weak transverse field must have been obtained after substantial decimation, and is more likely to be longer and

have a larger moment; similarly for the bonds. However, the couplings, lengths and bonds of neighboring spins remain uncorrelated, as they have been obtained by independent decimation steps. The transformations (15.36), (15.37), (15.55), (15.56) and (15.57) imply flow equations for $P(\zeta, \ell_B; \Gamma)$ and $R(\beta, \ell_S, m; \Gamma)$ which are very similar to (15.42); we will not write them out explicitly but note that the first two terms on the right hand sides have essentially the same form (the distributions only have additional obvious arguments), while the last term has additional integrals over ℓ and/or m along with delta functions imposing (15.55)-(15.57).

A thorough analysis of these new flow equations has been carried out by Fisher [154]. Here we simply note that in the limit $\Gamma \to \infty$ the distribution functions satisfy scaling forms which generalize (15.46):

$$
\begin{aligned}
P(\zeta, \ell_B; \Gamma) &= \frac{1}{\Gamma^3} \mathcal{P}\left(\frac{\zeta}{\Gamma}, \frac{\ell_B}{\Gamma^2}, r\Gamma\right) \\
R(\beta, \ell_S, m; \Gamma) &= \frac{1}{\Gamma^{3+\mu}} \mathcal{R}\left(\frac{\beta}{\Gamma}, \frac{\ell_S}{\Gamma^2}, \frac{m}{\Gamma^\mu}, r\Gamma\right).
\end{aligned} \tag{15.58}
$$

The prefactor of the power of Γ can be deduced simply form the requirement that P and R are normalized probability distributions. The scaling $\ell \sim \Gamma^2$ was already obtained in (15.53), but also follows from an analysis of the present flow equations. Finally, there is a non-trivial exponent μ which controls the scaling of m; it differs from that of ℓ because of the difference in the structure of (15.55) from that of (15.56) and (15.57)—it was shown by Fisher that $\mu = (\sqrt{5} + 1)/2$, the golden mean.

We can use these results to analyze the response to a uniform field h coupling to $\hat{\sigma}^z$, as was also done for the dilute Ising model in $d > 1$ below (15.32). Consider (at $T = 0$), the magnetization $M(h, r)$ of the system as a function of external applied field h. In the presence of a magnetic field h, the energy levels of an otherwise-free cluster of magnetic moment m split into two with an energy splitting $E_h = 2mh$. We stop the renormalization when the maximum coupling $\Omega \sim E_h$. The extreme broadness of the distribution implies that almost all the clusters which have already been eliminated have transverse fields considerably bigger than E_h while almost all that are yet to be eliminated have transverse fields considerably smaller than E_h. Therefore, an asymptotically exact expression for $M(h, r)$ is obtained by aligning all the remaining clusters

at $\Omega = E_h$ in the direction of the magnetic field. Thus

$$
\begin{aligned}
M(h,r) \quad = \quad & \bar{m} \times (\text{total number of active spins} \\
& \text{at scale } \Gamma_h = \ln(D_h/h)) + \dots \quad (15.59)
\end{aligned}
$$

where $\bar{m}$ and D_h are non-universal constants. This total number is easily reconstructed from the probability distributions, and we therefore have the scaling form

$$
\begin{aligned}
M(h,r) \quad = \quad & \bar{m}\mathcal{N}(\Gamma_h) \int d\zeta \; d\ell \; dm \frac{m}{\Gamma^{3+\mu}} \mathcal{R}\left(\frac{\zeta}{\Gamma}, \frac{\ell}{\Gamma^2}, \frac{m}{\Gamma^\mu}, r\Gamma\right) \\
= \quad & \bar{m}\Gamma_h^{\mu-2}\overline{\Phi}_M(r\Gamma_h) \\
= \quad & \frac{\bar{m}}{(\ln(D_h/h))^{2-\mu}}\Phi_M\left(\frac{\ln(D_h/h)}{\xi^{1/2}}\right) \quad (15.60)
\end{aligned}
$$

We see that this scaling form is identical in structure to (15.34) of the $d > 1$ dilute Ising model: it is clear that this is another consequence of activated dynamic scaling. Using standard scaling arguments, we can obtain the following results from (15.60): as we approach the transition from the ordered side, the spontaneous magnetization vanishes as $N_0 \sim |r|^\beta$ with $\beta = 2 - \mu$; right at the critical point, $M_{cr}(h) \sim (\ln(D_h/h))^{\mu-2}$. Both forms are identical to those in Section 15.4.3.

Similar arguments can be made to obtain the exact scaling forms for the T dependence of the linear susceptibility χ_h. At the critical point, $\chi_h(T) \sim 1/T(\ln(1/T))^{2-2\mu}$ while it has power-law T dependence in the ordered and disordered phases, reflecting the GM singularities.

15.6 Discussion

We have met two rather distinct scenarios for quantum critical points in random Ising/rotor models in this chapter. Let us review their main properties in turn.

The first was discussed in Section 15.3. For the most part, the scaling structure of the quantum critical point was similar to those discussed in Part 2 for clean systems. Dynamic scaling was conventional, with characteristic length (ℓ) and frequency (ω) scales at the critical point obeying $\omega \sim \ell^{-z}$, with z the usual dynamic critical exponent. The phases flanking the critical point exhibited Griffiths-McCoy singularities in their low energy behavior. For $N \geq 2$ these were only very weak essential singularities. However, they were stronger for $N = 1$, and led to a power-law divergence in the low energy density of states which we

characterized by the exponent $\tilde{z}$. The value of $\tilde{z}$ varied continuously in the phases, and it remains an open question whether it approaches z as we move towards the critical point: there is no obvious mathematical inconsistency with two values remaining different, as they characterize regions of the spectrum reached by distinct orders of limits.

The second scenario of *activated dynamic scaling* was realized in two solvable models in Sections 15.5. This is a special property of the $N = 1$ case and has been argued to occur for the generic $N = 1$ quantum transition in $d = 1$ (Section 15.5); it was also found for a rather special dilute Ising model in all $d > 1$ in Section 15.4, but is only expected to occur for the generic transition only for low values of d, possibly $d = 2$. The characteristic properties of activated dynamic scaling is that the diverging scales ℓ and $1/\omega$ of the critical point are related by $\ln(1/\omega) \sim \ell^{z_a}$, where z_a is now the universal dynamic exponent. There were very strong power-law GM singularities on either side of the transition, and the exponent $\tilde{z}$ diverged as $\tilde{z} \sim \xi^{z_a}$ upon the approach to the critical point.

It is interesting that both solvable models belonged to the second class showing activated behavior. We believe this is not an accident, and the activated scaling is a simplifying physical property which leads to the solvability. In particular, there is a clear separation of scales at which the predominant effects of quantum and disorder-induced fluctuations appear. At any given energy scale, the underlying quantum mechanics mainly serves to separate the system into mutually decoupled clusters of 'active' spins: the subsequent physical properties are then determined by the random geometry and statistics of these active clusters. The spins in each cluster are tightly coupled and each contributes a term of order unity to the magnetization. As we approach the critical point, the contribution of the active spins to the magnetization does not go to zero (as it would if quantum mechanics was playing a more central role); rather the vanishing of the magnetization at the critical point is due to the vanishing of the *number* of active spins at the lower energy scales.

Further progress in this field would be greatly aided by solvable models with disorder and interactions which exhibit conventional dynamic scaling.

15.7 Applications and extensions

The exact results for the random quantum Ising chain in Section 15.5 have been very successfully compared with numerical computations [540,

538, 155]. Closely related methods have also been applied to other one dimensional random spin models: these include $S = 1/2$ Heisenberg and XY spin chains [227, 153, 222], Potts and clock models [454], $S = 1$ antiferromagnetic spin chains [233, 234], and the experimentally realizable case of chains with mixed ferromagnetic and antiferromagnetic exchange [171, 528, 170].

Turning to higher dimensions, the quantum transition in the random Ising model in $d = 2$ has recently been studied in sophisticated Monte Carlo simulations [235, 383, 408], and there are indications that the activated dynamic scaling behavior is generic. As we noted earlier, the large N limit of the random quantum rotor model was studied in Ref [270] by a renormalization group analysis, but no stable fixed point was found; the quantum phase transition of this model has been studied numerically [210] and by an alternative renormalization group defined directly on the saddle-point equations [219].

In three dimensions, random Heisenberg antiferromagnets have been studied by the renormalization group of Section 15.5 and applied to properties of doped semiconductors [52].

Random versions of the boson models of Chapters 10 and 11 have also been studied [160, 179, 472, 523, 324] and are of considerable experimental importance, as was noted in Sections 9.5 and 10.3.

16
Quantum spin glasses

In this chapter, we want to move beyond the simplest disordered models considered in Chapter 15, and consider systems which have magnetically ordered states which are rather more complicated than those in which the average moments are in a regular arrangement, as in (15.3). In the context of the Ising/rotor models, such states can be obtained by relaxing the constraint $J_{ij} > 0$ and allowing the J_{ij} to randomly fluctuate over both negative and positive values (we can always choose the g_i to be positive by a local redefinition of the spin orientations, and will assume this is the case below). In particular, we will be interested here in the magnetically-ordered "spin-glass" state in which orientation of the spontaneous moment varies randomly from site to site, with a vanishing average over sites, $\overline{\langle \hat{\sigma}_i^z \rangle} = 0$ (or $\overline{\langle \hat{\mathbf{n}}_i \rangle} = 0$); such states are clearly special to disordered systems. For classical spin systems, *i.e.*, models (15.1) and (15.2) at $g_i = 0$, such ordered states have been reviewed at length elsewhere [54, 150, 539]. The structure of the ordered spin-glass phases of quantum models is very similar, and so this shall not be the focus of our interest here. Rather, we shall be interested in the quantum phase transition from the spin glass to a quantum paramagnet, and the nature of the finite temperature crossovers in its vicinity, where quantum mechanics plays a more fundamental role.

The quantum Ising/rotor models of Part 2 shall also form the basis of much of our discussion of quantum spin glasses. However, in parallel, we will also consider the appearance of spin-glass order in the metallic systems of Chapter 12. So one of our interests shall be the transition from a paramagnetic Fermi liquid to a *spin density glass* state: such a state is characterized by the analog of the order parameter (12.2) for the ordinary spin density wave state, but now the orientation and magnitude

of ϕ_α varies randomly in space, along with random phase offsets in the cosine.

We begin by introducing the order parameter which characterizes a spin-glass phase [54, 150] using, for now, the familiar terrain of the quantum Ising/rotor models. While a spin-glass has no magnetic moment when averaged over all sites, its characteristic property is that each spin has a definite orientation whose memory it retains for all time. We can use this long-time memory to introduce the Edwards-Anderson order parameter, q_{EA}, defined, for $N = 1$, by

$$q_{EA} = \lim_{t \to \infty} \overline{\langle \hat{\sigma}_i^z(t)\hat{\sigma}_i^z(0) \rangle}, \qquad (16.1)$$

and similarly using rotor variables for $N > 1$. For each site i the long time limit gives the *square* of the local static moment; this is non-negative, and so q_{EA} has a non-zero average in the spin glass phase.

One of the primary objectives of the theory of quantum spin glasses is to understand the nature of dynamics of spin fluctuations in the vicinity of the quantum-critical point where q_{EA} vanishes. As in Chapter 15, we expect Griffiths-McCoy singularities to appear in both the spin glass and quantum paramagnetic phases. Reliable information on these and the critical singularities for low dimensional systems with short-range interactions is so far only available through numerical simulations. A great deal of work has also been done on simplified models with infinite-range interactions which display spin glass phases [82, 185, 509, 58, 340, 535, 364, 279]: the solution of classical infinite-range models was an important step in the development of spin glass theory [54, 150]. Here, we shall restrict our attention to the development of a mean field theory of the quantum critical point (and its vicinity) between a spin glass and a paramagnet in the systems noted earlier. The physical properties of the mean-field theory are closely related to those of the models with infinite-range interactions, but the former also offers a formalism for understanding fluctuations in systems with shorter-range interactions; initial attempts at understanding such fluctuations have been made [405, 437], but shall not be discussed here.

We will present a derivation [535, 405] of the effective action controlling quantum fluctuations of the spin glass order parameter in Section 16.1. The mean field solution of this effective action and its physical properties will then follow in Section 16.2.

16.1 The effective action

We will begin by considering, for definiteness, the appearance of spin-glass order in the quantum rotor Hamiltonian H_{Rd} in (15.2); the results will also apply to the Ising case simply by restricting the O(N) vector indices $\alpha, \beta \ldots$ to just one value. The extension to the metallic systems of Chapter 12 will follow in Section 16.1.1.

We set all the $g_i = g$ and take the J_{ij} to be distributed independently according to the Gaussian probability

$$P(J_{ij}) \sim \exp\left(-\frac{J_{ij}^2}{2J^2}\right). \tag{16.2}$$

We average over this distribution using the replica method, which was introduced briefly in Section 15.3 (see Ref [150] for a more complete treatment). The averaged, replicated partition function becomes

$$\overline{Z^n} = \int \mathcal{D}n_{i\alpha a} \delta(n_{i\alpha a}^2 - 1) \exp\left[-\frac{1}{2g}\int d\tau \sum_{i,a}\left(\frac{\partial n_{i\alpha a}}{\partial \tau}\right)^2\right.$$

$$\left.-\frac{J^2}{2}\sum_{<ij>}\int d\tau_1 d\tau_2 \sum_{ab} n_{i\alpha a}(\tau_1)n_{j\alpha a}(\tau_1)n_{i\beta b}(\tau_2)n_{j\beta a}(\tau_2)\right], \tag{16.3}$$

where i, j are site indices, α, β are O(N) vector indices, and a, b are replica indices; we employ the usual summation convention over repeated O(N) vector indices, but all other summations are explicitly noted. We now want to manipulate this into a form in which the on-site spin correlations responsible for the spin glass order in (16.1) are somehow related to a primary 'order parameter' field; to this end we use the Hubbard-Stratanovich transformation, which we first met in Section 10.2, to decouple the quartic term in (16.3. We choose among the several possible the four spin operators by picking out the one which emphasizes the correlations appearing in (16.1); this gives us

$$\overline{Z^n} = \int \mathcal{D}Q_{i\alpha\beta}^{ab} \exp\left(-\int \frac{d\tau_1 d\tau_2}{2J^2}\sum_{ijab} Q_{i\alpha\beta}^{ab}(\tau_1,\tau_2)K_{ij}^{-1}Q_{j\alpha\beta}^{ab}(\tau_1,\tau_2)\right)$$

$$\times \prod_i Z_i[Q_i] \tag{16.4}$$

where K_{ij} is the connectivity matrix of the lattice (its matrix elements are unity for sites i,j which were coupled by a random exchange, and zero otherwise), and the subsidiary partition function Z_i is a functional

of the values of the field $Q_{i\alpha\beta}^{ab}(\tau_1, \tau_2)$ only on the site i. It is obtained after a functional integral only over the site i quantum field $n_{i\alpha a}$:

$$
Z_i[Q_i] = \int \mathcal{D}n_{\alpha a}\, \delta(n_{\alpha a}^2 - 1) \exp\left[-\frac{1}{2g} \int d\tau \sum_a \left(\frac{\partial n_{\alpha a}}{\partial \tau} \right)^2 \right.
$$
$$
\left. - \int d\tau_1 d\tau_2 \sum_{ab} Q_{i\alpha\beta}^{ab}(\tau_1, \tau_2) n_{\alpha a}(\tau_1) n_{\beta b}(\tau_2) \right]. \tag{16.5}
$$

We have dropped the dummy site index on **n** as this field is integrated over. Notice that functional integral in $Z_i[Q_i]$ is closely related to those considered in Chapter 2 in our study of classical $d = 1$ spin chains. The latter models are exactly soluble, and its known correlators can be used to construct an expansion for $Z_i[Q_i]$ in powers of Q_i for an arbitrary time-dependent Q_i. It should be kept in mind that are n decoupled copies of the classical chain here, and this does lead to interesting and important structure in the resulting action. After evaluating $Z_i[Q_i]$ in this manner, we take the spatial continuum limit and obtain our spin glass partition function, which we write schematically in the form

$$
Z_{sg} = \int \mathcal{D}Q_{\alpha\beta}^{ab}(x, \tau_1, \tau_2) \exp\left(-\mathcal{S}_{sg}[Q] \right). \tag{16.6}
$$

Now the focus of our attention is the field $Q_{\alpha\beta}^{ab}(x, \tau_1, \tau_2)$ which will play the role of an order parameter for the quantum spin glass. Before turning our attention to the structure of the action $\mathcal{S}_{sg}[Q]$, we discuss the physical interpretation of Q. From the structure of the Hubbard-Stratanovich transformation it is clear that we have the correspondence

$$
Q_{\alpha\beta}^{ab}(x_i, \tau_1, \tau_2) \sim n_{i\alpha a}(\tau_1) n_{i\beta b}(\tau_2), \tag{16.7}
$$

where the symbol $\sim$ indicates that correlators of Q are closely related to the corresponding correlators of the right hand side; for simplicity we will assume the proportionality constant is unity and replace (16.7) by an equality. From (16.7) we see that the replica *diagonal* components have the mean value

$$
\lim_{n \to 0} \frac{1}{n} \sum_a \left\langle \left\langle Q_{\alpha\beta}^{aa}(x_i, \tau_1, \tau_2) \right\rangle \right\rangle = \overline{\langle n_{i\alpha}(\tau_1) n_{i\beta}(\tau_2) \rangle}
$$
$$
= \delta_{\alpha\beta} \overline{\chi_L(\tau_1 - \tau_2)}, \tag{16.8}
$$

where the double angular brackets represent averages taken with the translationally invariant replica action $\mathcal{S}_{sg}$ in (16.6) (recall that single

angular brackets represent thermal/quantum averages for a fixed realization of randomness, and overlines represent averages over disorder). So the mean value of Q contains information on the entire time (or frequency) dependence of the average dynamic local susceptibility, which we also considered earlier in (15.7); in a sense, it is the time-dependent χ_L which is the 'order parameter functional' for the quantum spin glass. From (16.1) and (16.8), we see that the Edwards-Anderson order parameter, q_{EA}, can be extracted for the replica diagonal components of Q by taking the long time limit of (16.8) for *real* times t. Precisely at $T = 0$, this long time limit can also be taken along the imaginary time axis (for $T > 0$, $\chi_L(\tau)$ is a periodic function with period $1/T$, and so the long time limit is only defined for real times), and we have

$$q_{EA} = \lim_{\tau \to \infty} \lim_{n \to 0} \frac{1}{n} \sum_a \langle\langle Q^{aa}(x, \tau_1 = 0, \tau_2 = \tau)\rangle\rangle \qquad\qquad T = 0. \quad (16.9)$$

Turning to the replica off-diagonal components, we see by a standard application of replica technology [150, 54] that

$$\lim_{n \to 0} \frac{1}{n(n-1)} \sum_{a \neq b} \langle\langle Q^{ab}_{\alpha\beta}(x_i, \tau_1, \tau_2)\rangle\rangle = \overline{\langle n_{i\alpha}(\tau_1)\rangle \langle n_{i\beta}(\tau_2)\rangle}$$

$$= q_{EA}, \qquad\qquad (16.10)$$

The thermal average in the second step leads to time-independent values, and so the expectation value of the off-diagonal components is independent of both τ_1 and τ_2. In the last step, we have assumed that the thermal ensemble has the "clustering" property, which demands that the long-time limit of the correlator in (16.1) is simply the square of the static magnetic moment on the site, as discussed in Section 1.4; while it is certainly possible to construct states which do not obey clustering, imposing a suitable infinitesimal external field on each site will select the ensemble which does obey (16.10). In (16.10) we have also ignored subtleties that may arise as a consequence of the intricate phenomenon known as 'replica symmetry breaking'. In the simple mean field theory we shall consider below, replica symmetry breaking does not occur; however, it does appear when additional higher order couplings are included [405], but fortunately the structure and analysis of replica symmetry breaking in the spin glass phase turn out to be essentially identical to that discussed elsewhere in the classical case [150, 54]: for these reasons, and also because our interest is primarily in the spin fluctuations in the paramagnetic phase, we will not consider this phenomenon here further.

Returning to our determination the form of $\mathcal{S}_{sg}[Q]$, recall that we noted that the only realistic option was an expansion in powers of Q. It is worthwhile to ponder a bit on the validity of such an expansion. In the vicinity of the quantum critical point, we expect q_{EA} to become small; in the spirit of Landau theory, it would then certainly be appropriate to expand in powers of q_{EA}. However for the quantum transition we need the full time-dependent Q, and not just its long time limit. For very short $|\tau_1 - \tau_2|$, the local on-site spin correlations will certainly be of order unity, and so Q will not be small for these times. What we need to do is to "subtract out" the uninteresting short time part of Q, and focus on only its long time part for which a Landau-like expansion could possibly be valid. To do this we consider the following transformation

$$Q^{ab}_{\alpha\beta}(x, \tau_1, \tau_2) \rightarrow Q^{ab}_{\alpha\beta}(x, \tau_1, \tau_2) - C\delta^{ab}\delta(\tau_1 - \tau_2) \qquad (16.11)$$

where C is a constant, and the delta function $\delta(\tau_1 - \tau_2)$ is a schematic for a function which decays rapidly to zero on a short microscopic time. The value of C should be adjusted so that the resulting Q contains only the interesting long time physics: at this point, it is not clear how this can be done, but we will see shortly that a simple constraint on the effective action allows us to do this quite easily.

Let us consider the expansion of $Z_i[Q_i]$ in (16.5) in powers of Q: we will discuss the nature of the low order terms explicitly, and from these the principles which restrict the structure of the general term will emerge.

The first term is one linear in Q. It is multiplied by a two-point correlator of n which is non-zero only if both replica indices are the same. Further, the subsequent replica-diagonal average will correlate the two time arguments in Q, and we will get an expression like

$$\int d^d x d\tau_1 d\tau_2 Q^{aa}_{\alpha\alpha}(x, \tau_1, \tau_2)\chi^0_L(\tau_1 - \tau_2), \qquad (16.12)$$

where the superscript 0 on the local susceptibility reminds us that this is a bare susceptibility, evaluated without accounting for inter-site correlations. Now an important property of $\chi^0_L(\tau)$ (and all other multi-point correlations of n) is that it decays rapidly to zero over a time τ of order $1/g$. In frequency space, we have in the low frequency limit

$$\chi^0_L(\omega_n) \sim (\omega_n^2 + \Delta_0^2)^{-1} \sim \Delta_0^{-2} - \omega_n^2 \Delta_0^{-4} + \ldots \qquad (16.13)$$

where $\Delta_0 \sim g$ is the gap of the classical chain model $Z_i[Q = 0]$ studied in Chapter 2. If we just take the leading frequency independent term in

(16.13), we have effectively replaced χ_L^0 by a constant and set $\tau_1 = \tau_2$. This is an important principle, which applies also to higher order terms: an even number of replica indices can take the same value, but then the associated time 'indices' must also be set equal, as they can be correlated by quantum fluctuations of the underlying rotors. Subleading corrections will involve derivatives of the difference in times, and it turns out to be necessary to retain the additional ω_n^2 dependence in (16.13) only for the linear term in (16.12).

Moving on to higher order terms, we see that the number of allowed terms proliferates very rapidly. In particular, at n'th order there are terms which can have between 1 and n independent replica indices summed over; associated with each independent replica index will be a time 'index' which is integrated over in the action. So the terms have a variable number of time integrations, and it turns out that most important are those with a maximum number of independent time (and replica) indices: this is not difficult to see from a renormalization group perspective, as each additional time integration increases the scaling dimension of the associated coupling constant.

Proceeding in this manner, we can assert the following results for $\mathcal{S}_{sg}$ for the quantum Ising/rotor spin glass; we have used the benefit of hindsight and retained only this terms which are necessary to obtain the leading critical singularities within mean-field theory:

$$
\begin{aligned}
\mathcal{S}_{sg} = \frac{1}{w} \int d^d x \Bigg\{ & \frac{1}{\kappa} \int d\tau \sum_a \left[\frac{\partial}{\partial \tau_1} \frac{\partial}{\partial \tau_2} + r \right] Q_{\alpha\alpha}^{aa}(x, \tau_1, \tau_2) \Bigg|_{\tau_1 = \tau_2 = \tau} \\
& + \frac{1}{2} \int d\tau_1 d\tau_2 \sum_{ab} \left[\nabla Q_{\alpha\beta}^{ab}(x, \tau_1, \tau_2) \right]^2 \\
& - \frac{\kappa}{3} \int d\tau_1 d\tau_2 d\tau_3 \sum_{abc} Q_{\alpha\beta}^{ab}(x, \tau_1, \tau_2) Q_{\beta\rho}^{bc}(x, \tau_2, \tau_3) Q_{\rho\alpha}^{ca}(x, \tau_3, \tau_1) \\
& + \frac{1}{2} \int d\tau \sum_a \Big[u\, Q_{\alpha\beta}^{aa}(x, \tau, \tau) Q_{\alpha\beta}^{aa}(x, \tau, \tau) \\
& \qquad\qquad + v\, Q_{\alpha\alpha}^{aa}(x, \tau, \tau) Q_{\beta\beta}^{aa}(x, \tau, \tau) \Big] \Bigg\} \\
& - \frac{1}{2w^2} \int d^d x \int d\tau_1 d\tau_2 \sum_{ab} Q_{\alpha\alpha}^{aa}(x, \tau_1, \tau_1) Q_{\beta\beta}^{bb}(x, \tau_2, \tau_2). \quad (16.14)
\end{aligned}
$$

There are 7 terms in the action, but only five coupling constants: w, r, κ, u and v. Rescaling of space and time co-ordinates has allowed us to absorb the other two. The first two terms are linear in Q and are

clearly a transcription of the two terms retained explicitly in (16.13). As the notation suggests, the coupling r will turn out to be relevant tuning parameter which moves the system between its two phases, and we will be interested in the phase diagram in the r,T plane. The spatial gradient term arises from the K^{-1} coupling in (16.4) which couples different sites. This last coupling, and also the expansion of $Z_i[Q]$ also allow the simple quadratic term

$$\int d^d x d\tau_1 d\tau_2 \sum_{ab} \left[Q^{ab}_{\alpha\beta}(x, \tau_1, \tau_2) \right]^2 \qquad (16.15)$$

which we have not included in $\mathcal{S}_{sg}$; instead we have chosen the freedom allowed by the transformation (16.11) to demand that the co-efficient of this term be exactly zero. At the moment, this appears just as a convenient choice, but will be seen later to be exactly the criterion required to focus on only the interesting low frequency behavior of Q. The quadratic terms proportional to u and v have only a single replica index, and account for the non-linear, quantum mechanical interactions of the quantum rotors. We have retained only a single cubic term, proportional to κ/w, the one with the maximum possible three time integrations; other allowed cubic terms are not as important.

Finally, the last term, proportional to $1/w^2$, actually does not appear in the expansion for $\mathcal{S}_{sg}$ as we have chosen to explicitly generate it. To obtain it, we have to allow for *on-site* disorder in the value of g_i as can be schematically seen in a 'soft-spin' approach where randomness in g corresponds to a random mass multiplying $\phi^2 \sim Q^{aa}$; averaging over the random mass will then lead to the last term in (16.14). However, even in the present model with g fixed, the $1/w^2$ term is generated upon any renormalization with the remaining couplings in $\mathcal{S}_{sg}$. In any case, this $1/w^2$ term plays no role in the mean field theory to follow, and so we will not discuss it further. It is, however, important to retain it in any analysis of fluctuations.

16.1.1 Metallic systems

We consider the extension of the analysis of phase transition of Fermi liquids in Chapter 12 to the case of a "spin density glass" [370, 453, 437, 371, 416]. For this we generalize (12.1) to a model with a random

exchange interaction

$$H_{sdg} = \int \frac{d^d k}{(2\pi)^d} (\varepsilon_k - \mu) c_{\vec{k}\mu}^\dagger c_{\vec{k}\mu} - \sum_{<ij>} J_{ij} \hat{\mathbf{S}}_i \cdot \hat{\mathbf{S}}_j \qquad (16.16)$$

where

$$\hat{\mathbf{S}}_i \equiv \frac{1}{2} \sum_{\mu\nu} c_{i\mu}^\dagger \vec{\sigma}_{\mu\nu} c_{i\nu} \qquad (16.17)$$

are the electron spin operators on site i. As was the case for the Ising/rotor models above, we will take the J_{ij} to be independent Gaussian random variables. We refer the reader to a review by the author [428] for the arguments motivating (16.16) as an appropriate low energy model for a large class of disordered metallic systems; a discussion of the strong Griffiths-McCoy singularities in such models [343, 51] may also be found there.

Our analysis of H_{sdg} follows closely the steps presented above for the Ising/rotor models. The field $\mathbf{S}$ replaces $\mathbf{n}$ so now we have

$$Q_{\alpha\beta}^{ab}(x_i, \tau_1, \tau_2) \sim S_{i\alpha a}(\tau_1) S_{i\beta b}(\tau_2), \qquad (16.18)$$

replacing (16.7). Also the on-site action $(\partial n/\partial \tau)^2/(2g)$ is replaced by the first kinetic energy term in (16.16). All other steps are the same, and we obtain an expression identical to (16.4), with the modifications just noted in the definition of $Z_i[Q_i]$. The steps in the derivation of $\mathcal{S}_{sg}$ are also the same, except the functional integral over the metallic electrons leads to differences in the time-dependence of the terms. In particular, from the arguments just above (12.10) we see that the expression (16.13) for the local susceptibility is replaced by

$$\chi_L(\omega_n) \sim A_1 - A_2 |\omega_n| + \ldots \qquad (16.19)$$

for some constants A_1 and A_2. This turns out to be the only significant change in $\mathcal{S}_{sg}$. So the final result takes exactly the form (16.14) except that the single time-derivative term (with co-efficient $1/(w\kappa)$) is replaced by (after a Fourier transform of (16.19)):

$$- \frac{1}{\pi w \kappa} \int d^d x d\tau_1 d\tau_2 \sum_a \frac{Q_{\alpha\alpha}^{aa}(x, \tau_1, \tau_2)}{(\tau_1 - \tau_2)^2} \qquad (16.20)$$

This change in the time derivative term is completely analogous to the change between (8.2) and (12.10) for the case of regular magnetic order.

16.2 Mean field theory

We will now analyze the action $\mathcal{S}_{sg}$ in (16.14), and its metallic extension modification (16.20), in a simple mean field theory. An analysis of the rather complex structure of fluctuations about this mean field has been attempted [405, 437], but we will not discuss it here as the results are quite inconclusive. The mean field theory is useful in that it gives a simple picture of the quantum critical point and the finite temperature crossovers in its vicinity, should serve as a starting point for more sophisticated analyses.

Our strategy will be obtain saddle points of $\mathcal{S}_{sg}$ over variations is a mean field value of the field $Q(x, \tau_1, \tau_2)$. We expect the saddle point to be invariant under translation in space and time, which implies that Q is independent of x and a function only of $\tau_1 - \tau_2$. After Fourier transforming to Matsubara frequencies by

$$
Q_{\alpha\beta}^{ab}(x, \omega_{n1}, \omega_{n2}) = \int_0^{1/T} d\tau_1 \int_0^{1/T} d\tau_2 Q_{\alpha\beta}^{ab}(x, \tau_1, \tau_2) e^{-i(\omega_{n1}\tau_1 + \omega_{n2}\tau_2)},
$$
(16.21)

this motivates the following saddle point ansatz:

$$
Q_{\alpha\beta}^{ab}(x, \omega_{n1}, \omega_{n2}) = \frac{q_{EA}}{T^2}\delta_{\omega_{n1},0}\delta_{\omega_{n2},0}\delta_{\alpha\beta} + \frac{\chi_L(\omega_{n1})}{T}\delta^{ab}\delta_{\omega_{n1}+\omega_{n2},0}\delta_{\alpha\beta}
$$
(16.22)

The first is term is independent of the replica indices, and therefore has been parameterized in terms of the Edwards-Anderson order parameter by (16.10). The second replica diagonal term is related to the local susceptibility by (16.8) (we have dropped the overline representing the disorder average as it is always implied in the present context). Quite independent of these physical interpretations it is clear that (16.22) is the most general replica-symmetric ansatz for Q in terms of the parameters q_{EA} and $\chi_L(\omega_n)$. We insert (16.21) and (16.22) into (16.14) and (16.20) and obtain for the mean field free energy density per replica, $\mathcal{F}/n$:

$$
\begin{aligned}
\frac{\mathcal{F}}{Nn} =\ & \frac{T}{w}\sum_{\omega_n}\left[\left(\frac{M(\omega_n)+r}{\kappa}\right)\chi_L(\omega_n) - \frac{\kappa}{3}\chi_L^3(\omega_n)\right] \\
& + \frac{u+Nv}{2w}\left[q_{EA} + T\sum_{\omega_n}\chi_L(\omega_n)\right]^2 \\
& + \frac{q_{EA}}{w}\left(\frac{r}{\kappa} - \kappa\left[\chi_L(0)\right]^2\right),
\end{aligned}
$$
(16.23)

where

$$M(\omega_n) = \begin{cases} \omega_n^2 & \text{for the Ising/rotor models} \\ |\omega_n| & \text{for the metallic system} \end{cases} . \tag{16.24}$$

There should also be an additional term in (16.23) coming from the last term $1/w^2$ term in (16.14), but it is proportional to n, and therefore does not contribute in the replica limit $n \to 0$. Under these circumstances, the coupling $1/t$ appears only as a prefactor in front of the total free energy, and so the value of w will therefore play no role in the mean field theory. The replica limit $n \to 0$ has also been taken to simplify terms arising from the cubic coupling in $\mathcal{S}_{sg}$. Also, we are considering a metallic system with Heisenberg symmetry, so in this case we should set $N = 3$.

We now determine the saddle point of (16.23) with respect to variations in q_{EA} and $\chi_L(\omega_n)$ for every ω_n; the resulting expressions can be written in the form

$$\begin{aligned} \chi_L(\omega_n) &= -\frac{1}{\kappa}\sqrt{M(\omega_n) + \Upsilon} \\ q_{\text{EA}}\sqrt{\Upsilon} &= 0, \end{aligned} \tag{16.25}$$

where Υ is an intermediate parameter satisfying the equation

$$\Upsilon = r + (u + Nv)\left(\kappa q_{\text{EA}} - T\sum_{\omega_n}\sqrt{M(\omega_n) + \Upsilon}\right) \tag{16.26}$$

The equations (16.25,16.26) clearly have two distinct types of the solutions. The first corresponds to the paramagnetic phase in which the spin glass order parameter vanishes and so

$$q_{\text{EA}} = 0 \tag{16.27}$$

$$\chi_L(\omega_n) = -\frac{1}{\kappa}\sqrt{M(\omega_n) + \Upsilon} \tag{16.28}$$

$$\Upsilon = r - (u + Nv)T\sum_{\omega_n}\sqrt{M(\omega_n) + \Upsilon}; \tag{16.29}$$

the parameter $\Upsilon > 0$ is to be determined from the solution of the nonlinear equation (16.29. The second solution is that of the spin glass phase in which $\Upsilon = 0$, and so

$$\begin{aligned} \chi_L(\omega_n) &= -\frac{1}{\kappa}\sqrt{M(\omega_n)} \\ q_{\text{EA}} &= -\frac{r}{\kappa(u + Nv)} + \frac{T}{\kappa}\sum_{\omega_n}\sqrt{M(\omega_n)} \end{aligned} \tag{16.30}$$

It is clear that for sufficiently large $r > 0$ the paramagnetic solution is the only physically sensible one, and it has a large $\Upsilon > 0$. As we decrease r at fixed T, the value of Υ decreases, and we will have phase transition into the spin glass phase where Υ first vanishes; this will happen at $r = r_c(T)$ which is determined by setting $\Upsilon = 0$ in (16.29):

$$r_c(T) \equiv (u + Nv)T \sum_{\omega_n} \sqrt{M(\omega_n)} \qquad (16.31)$$

The spin glass phase therefore exists for $r < r_c(T)$. It should be clear from this discussion that r plays the role of the relevant tuning parameter for the quantum transition, and this notation is consistent with that of Chapter 8. As in that chapter, it is convenient to shift variables by defining

$$s \equiv r - r_c(0), \qquad (16.32)$$

so the quantum critical point is precisely at $s = 0$, $T = 0$; at $T = 0$ the system is paramagnetic for $s > 0$ and a spin glass for $s < 0$. For $T > 0$ we have phase boundary at $s = s_c(T) < 0$ whose precise shape will be determined shortly below. These considerations lead to the phase diagram shown in Fig 16.1.

Let us briefly discuss the physical properties of the phases found here in mean field theory. In the paramagnetic phase, the local spectral density of the Ising/rotor models (with $M(\omega_n) = \omega_n^2$) is given by

$$\chi_L''(\omega) = \text{sgn}(\omega)\frac{\sqrt{\omega^2 - \Upsilon}}{\kappa}\theta(|\omega| - \sqrt{\Upsilon}); \qquad (16.33)$$

so there is an energy gap, and spectral density increases with a square-root threshold above this gap. Clearly, we can expect that this gap will be filled in at $T = 0$ by Griffiths-McCoy singularities once fluctuation effects are included; for $T > 0$ ordinary thermal fluctuations will be adequate to destroy the gap. The mean-field spectrum becomes gapless precisely at the critical point where $\Upsilon = 0$ and the spectral density vanishes linearly with frequency. The spectral density of the paramagnetic phase of the metallic systems is quite different; now we have $M(\omega_n) = |\omega_n|$, and this leads to

$$\chi_L''(\omega) = \frac{1}{\sqrt{2}\kappa}\frac{\omega}{\sqrt{\Upsilon + \sqrt{\omega^2 + \Upsilon^2}}}; \qquad (16.34)$$

now there is no gap, but the spectral density is linear, $\sim \omega$, for frequencies smaller than Υ, and a square root, $\sim \sqrt{\omega}$ for larger frequencies. We
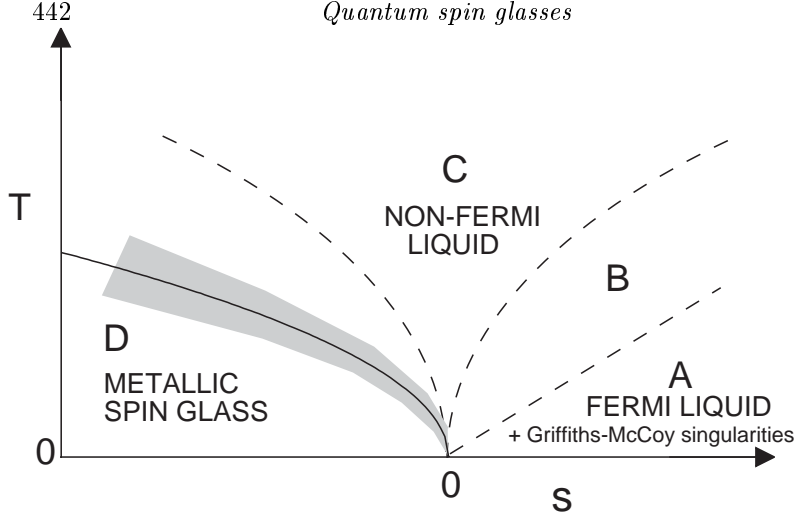
Fig. 16.1. Mean field phase diagram of a metallic spin glass as a function of the ground state tuning parameter s and temperature T. The $T = 0$ state is a metallic spin glass for $s < 0$ and a disordered, paramagnetic Fermi liquid for $s > 0$. The full line is the only thermodynamic phase transition, and is at $s = s_c(T)$ or $T = T_c(s)$ given in (16.44). The quantum critical point is at $s = 0$, $T = 0$. The dashed lines denote crossovers between different finite T regions of the quantum field theory (16.14): the low T regions are A, B (on the paramagnetic side) and D (on the ordered side), while the high T region (C) displays 'non-Fermi liquid' behavior. The crossovers on either side of C, and the spin glass phase boundary $T_c(s)$, all scale as $T \sim |s|^{2/3}$; the boundary between A and B obeys $T \sim s$. The shaded region has classical critical fluctuations described by theories of the type discussed by Refs [54, 150].

will make some further remarks on the physical interpretation of this spectral density below.

Turning to the spin glass phase, it is clear from (16.30-16.32) that the Edwards-Anderson order parameter is given by

$$q_{EA} = \frac{1}{\kappa(u + Nv)} \left[s_c(T) - s \right]. \tag{16.35}$$

The spectral density remains pinned at the $\Upsilon = 0$ case of (16.33) and (16.34) in the entire spin glass phase in the present mean field theory.

An interesting property of the above solutions is that the low frequency limit of the function $\chi_L(\omega_n)$ becomes small as one approaches the phase boundary (for real ω both the real and imaginary parts of χ_L become small), which indicates that expanding in powers of Q was appropriate. This smallness is actually a consequence of the shift (16.11)

used to eliminate the term (16.15) from the action. If we had instead included (16.15) in the present mean field analysis, we would have found a very similar solution, but the resulting χ_L would have an additional frequency-independent contribution to its real part which remained of order unity at the phase boundary. Such a regular frequency-independent term does not modify the interesting long time correlations or the low frequency spectral weight, which actually remain as we have found them here. This is then the promised *a posteriori* justification for the expansion employed in obtaining $\mathcal{S}_{sg}$.

We will discuss the nature of the finite temperature crossovers within the paramagnetic phase of the metallic system, as shown in Fig 16.1; the behavior of the Ising/rotor system is closely related and details may be found elsewhere [405]. The spectral density is given everywhere by (16.34) which depends solely on the energy scale Υ, to be determined by the solution of (16.29). We will present a complete derivation of the universal T and s dependence of Υ in the vicinity of the quantum critical point $T = 0$, $s = 0$; despite the seemingly simple equation (16.29) to be solved, a great deal of structure emerges, including some non-trivial crossover functions. We begin by combining (16.29), (16.31) and (16.32) into

$$\Upsilon + (u + Nv)T\sqrt{\Upsilon} = s - (u + Nv)\left(T \sum_{\omega_n \neq 0} \sqrt{|\omega_n| + \Upsilon} - \int \frac{d\omega}{2\pi}\sqrt{|\omega|} \right).$$
(16.36)

For convenience, we have chosen to move the $\omega_n = 0$ term in the frequency summation from the right hand to the left hand side. To leading order in $u + Nv$, this equation has the simple solution $\Upsilon = s$. To improve this result it turns out to be adequate to simply set $\Upsilon = s$ on the right hand side of (16.36): the minimum value of ω_n in the summation is $2\pi T$ and this always turns out to be much larger than Υ in the interesting universal region, as will become clear from the analysis below. This strategy of separating the $\omega_n = 0$ and $\omega_n \neq 0$ terms, and of treating the $\omega_n = 0$ term with more care, is reminiscent of the approach applied in Chapter 8 for finite T crossovers; we will see below that the resulting crossovers are very similar to those found in Section 8.2.2 for the case when the clean Ising/rotor model was above its upper critical dimension. After making the noted approximation, we can further manipulate (16.36) into

$$\Upsilon + (u + Nv)T\sqrt{\Upsilon} = s + (u + Nv)T\sqrt{s}$$

$$-(u + Nv)\left(T\sum_{\omega_n} \sqrt{|\omega_n| + s} - \int \frac{d\omega}{2\pi}\sqrt{|\omega| + s}\right)$$

$$-(u + Nv)\int \frac{d\omega}{2\pi}\left(\sqrt{|\omega| + s} - \sqrt{|\omega|} - \frac{s}{2\sqrt{|\omega|}}\right)$$

$$-(u + Nv)\int \frac{d\omega}{2\pi}\frac{s}{2\sqrt{|\omega|}}. \tag{16.37}$$

The manipulations above are similar to those discussed below (5.66) and used extensively in Chapter 8: we always subtract from the summation over Matsubara frequencies of any function, the integration of precisely the same function; the difference is then convergent in the ultraviolet, and such a procedure leads naturally to the universal crossover functions [427]. We will now manipulate (16.37) into a form where it is evident that Υ is analytic as a function of s at $s = 0$ for $T > 0$. This analyticity is of course closely related to that discussed in Sections 8.2.1 and 8.2.2, and is due to the absence of any thermodynamic singularity for $T > 0$, $s = 0$ (see Fig 16.1). We use the identity

$$\int_0^\infty \sqrt{\alpha}d\alpha\left(\frac{1}{\alpha + a} - \frac{1}{\alpha + b}\right) = \pi(\sqrt{b} - \sqrt{a}) \tag{16.38}$$

to rewrite (16.37) as

$$\Upsilon + (u + Nv)T\sqrt{\Upsilon} = s\left(1 - \frac{(u + Nv)\Lambda_\omega^{1/2}}{\pi}\right) + (u + Nv)T\sqrt{s}$$

$$+\frac{(u + Nv)}{\pi}\int_0^\infty \sqrt{\alpha}d\alpha\left(T\sum_{\omega_n}\frac{1}{\alpha + |\omega_n| + s} - \int \frac{d\omega}{2\pi}\frac{1}{\alpha + |\omega| + s}\right)$$

$$+\frac{(u + Nv)}{\pi}\int_0^\infty \sqrt{\alpha}d\alpha\int \frac{d\omega}{2\pi}\left(\frac{1}{\alpha + |\omega| + s}\right.$$

$$\left. -\frac{1}{\alpha + |\omega|} + \frac{r}{(\alpha + |\omega|)^2}\right), \tag{16.39}$$

where Λ_ω is an upper cutoff for the frequency. We evaluate the frequency summation by expressing it in terms of the digamma function ψ, and perform all frequency integrals exactly. After some elementary manipulations (including use of the identity $\psi(s + 1) = \psi(s) + 1/s$), we obtain our final result for Υ, in the form of a solvable quadratic equation

for $\sqrt{\Upsilon}$:

$$\Upsilon + (u+Nv)T\sqrt{\Upsilon} = s\left(1 - \frac{(u+Nv)\Lambda_\omega^{1/2}}{\pi}\right) + (u+Nv)T^{3/2}\Phi_{sdg}\left(\frac{s}{T}\right),$$

(16.40)

where the universal crossover function of the spin density glass $\Phi_{sdg}(y)$ is given by

$$\Phi_{sdg}(y) = \frac{1}{\pi^2}\int_0^\infty \sqrt{\alpha}d\alpha\left[\log\left(\frac{\alpha}{2\pi}\right) - \psi\left(1 + \frac{\alpha+y}{2\pi}\right) + \frac{\pi+y}{\alpha}\right].$$

(16.41)

Notice the similarity in the structure of the above results to that of (8.39) and (12.15): in all cases we have universal crossover functions for the characteristic energy scale in the vicinity of a quantum critical point; indeed, for accidental reasons the universal function $\Phi_{sdg}(y)$ is proportional to the universal function L in (12.16) in $d=3$. Also note that the crossovers in (16.40) depend upon the magnitude of the microscopic couplings u, v which represent the quantum mechanical interactions between the rotors or Ising spins. This is also a feature of (8.39) and (12.15), and by analogy we may conclude that the couplings u and v are formally irrelevant at the quantum critical point, but are nevertheless crucial in constructing the crossovers at nonzero temperatures, *i.e.*, they are *dangerously irrelevant*: this expectation is verified by an explicit renormalization group analysis of $\mathcal{S}_{sg}$ [437] which we shall not discuss here.

The above expression for $\Phi_{sdg}(y)$ is clearly analytic for all $y \geq 0$, including $y = 0$, as we hoped to achieve. As was the case for (8.39,8.40), we can use the above result for $y < 0$ until we hit the first singularity at $y = -2\pi$, which is associated with singularity of the digamma function $\psi(s)$ at $s = 0$. However, this singularity is of no physical consequence, as it occurs within the spin glass phase (Fig 16.1), where the above solution is not valid; as shown below, the transition to the spin glass phase occurs for $y \sim -(u+Nv)T^{1/2}$ which is well above -2π. For our subsequent analysis, it is useful to have the following limiting results, which follow from (16.41):

$$\Phi_{sdg}(y) = \begin{cases} \sqrt{1/2\pi}\zeta(3/2) + \mathcal{O}(y) & y \to 0 \\ (2/3\pi)y^{3/2} + y^{1/2} + (\pi/6)y^{-1/2} + \mathcal{O}(y^{-3/2}) & y \to \infty \end{cases}$$

(16.42)

The expression (16.34), combined with the results (16.40) and (16.41) completely specify the s and T dependence of the dynamic susceptibility

in the paramagnetic phase, and allowed us to obtain the phase diagram shown in Fig 16.1, whose details we will now discuss. There is a quantum critical point at $s = 0$, $T = 0$, and the characteristic energy scale Υ vanishes *linearly* upon approach to this point at $T = 0$

$$\Upsilon \sim s \qquad \text{for } s > 0,\ T = 0. \tag{16.43}$$

There is a line of finite temperature phase transitions, denoted by the full line in Fig 16.1, which separates the spin glass and paramagnetic phases; this line is determined by the condition $\Upsilon = 0$, and is at $r = s_c(T)$ (or $T = T_c(s)$), with

$$s_c(T) = -(u+Nv)\Phi(0)T^{3/2} \quad \text{or} \quad T_c(s) = [-s/(u+Nv)\Phi(0)]^{2/3} \tag{16.44}$$

The crossovers within the paramagnetic phase are similar to those found in Section 8.2.2 and 12.2, and we will discuss the characteristics of the different limiting regimes

(A,B) Low T paramagnetic Fermi liquid, $T < [s/(u + Nv)]^{2/3}$

This is the "Fermi liquid" region, where the leading contribution to the characteristic energy scale Υ is its $T = 0$ value $\Upsilon(T) \sim \Upsilon(0) = s$. The leading temperature dependent correction to Υ is however different in two subregions. In the lowest T region A, $T < s$, we have a Fermi liquid-like T^2 power law

$$\Upsilon(T) - \Upsilon(0) = \frac{(u + Nv)\pi T^2}{6\sqrt{s}} \qquad \text{region Ia.} \tag{16.45}$$

At higher temperatures, in region B, $s < T < [s/(u + Nv)]^{2/3}$, we have an anomalous temperature dependence

$$\Upsilon(T) - \Upsilon(0) = (u + Nv)\Phi(0)T^{3/2} \qquad \text{region Ib and II.} \tag{16.46}$$

It is also interesting to consider the properties of regions A, B as a function of observation frequency, ω, as sketched in Fig. 16.2. At large frequencies, $\omega \gg s$, the local dynamic susceptibility behaves like $\chi_L'' \sim \text{sgn}(\omega)\sqrt{|\omega|}$, which is the spectrum of critical fluctuations; at the $T = 0$, $s = 0$ critical point, this spectrum is present at all frequencies. At low frequencies, $\omega \ll s$, there is a crossover (Fig 16.2) to the characteristic Fermi liquid spectrum of local spin fluctuations $\chi_L'' \sim \omega/\sqrt{s}$. Upon consideration of fluctuations beyond mean-field, one finds the appearance of Griffiths-McCoy singularities in this region, as discussed in related contexts in Chapter 15; these are quite important for experimental comparisons at low temperatures, and are further discussed in Refs. [428, 343, 51, 126, 127, 288, 290, 344, 345, 77, 22].

Low T Fermi liquid
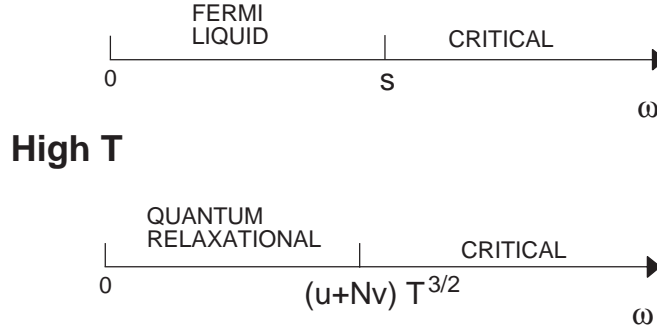
High T

Fig. 16.2. Crossovers as a function of frequency, ω, in the regions of Fig 16.1 of the metallic spin glass. The low T Fermi liquid region is on the paramagnetic side ($s > 0$).

(C) <u>High T region, $T > [|s|/(u + Nv)]^{2/3}$</u>
Here temperature dependent contributions to Υ dominate over those due to the deviation of the coupling d from its critical point, $d = 0$. Therefore thermal effects are dominant, and the system behaves as if its microscopic couplings are at those of the critical ground state. The T dependence in (16.46) continues to hold, as we have already noted, with the leading contribution being

$$\Upsilon \approx (u + Nv)\Phi(0)T^{3/2}. \qquad (16.47)$$

Notice that the characteristic energy scale now does not scale simply as $\sim T$, as it did for the high T region of the models in Part 2 with $d < 3$. Instead all T-dependent corrections arise from the irrelevant coupling u, which leads to the anomalous power-law in (16.47). As in (A,B), it is useful to consider properties of this region as a function of ω (Fig 16.2). For large ω ($\omega \gg (u+Nv)T^{3/2}$) we again have the critical behavior $\chi''_L \sim \text{sgn}(\omega)\sqrt{|\omega|}$; this critical behavior is present at large enough ω in all the regions of the phase diagram. At small ω ($\omega \ll (u + Nv)T^{3/2}$), thermal fluctuations quench the critical fluctuations, and we have relaxational behavior with $\chi''_L \sim \omega/(u + Nv)^{1/2}T^{3/4}$.

(D) <u>Low T region above spin glass, $T < [-s/(u + Nv)]^{2/3}$, $s < 0$</u>
Effects due to the formation of a static moment are now paramount. As one approaches the spin glass boundary (16.44) from above, the system enters a region of purely classical thermal fluctuations, $|T - T_c(s)| \ll$

$(u + Nv)^{2/3} T_c^{4/3}(s)$ (shown shaded in Fig 16.1) where

$$\Upsilon = \left(\frac{s - s_c(T)}{T(u + Nv)} \right)^2 \qquad (16.48)$$

Notice that Υ depends on the *square* of the distance from the finite T classical phase transition line, in contrast to its linear dependence at $T = 0$ in (16.43). It turns out that (16.48) when inserted into the static correlation functions reproduces precisely the critical singularities of the theory of classical spin glasses [405]. Indeed, the reader is invited to show by the methods of Part 2 that the fluctuations in the shaded region of Fig 16.1 are described by precisely the classical critical theories of Refs [54, 150].

The above results for the local dynamic susceptibility can be extended to a number of other experimentally important observables: as the basic methods are similar to those already developed here, we refer the interested reader to the literature [453, 437].

16.3 Applications and extensions

Much of the recent theoretical interest in quantum spin glasses has been driven by the experiments of the group of T. Rosenbaum and G. Aeppli [530, 531] on the insulating, dipolar Ising spin glass $\mathrm{LiHo}_x \mathrm{Y}_{1-x} \mathrm{F}_4$ [530, 531] in a transverse field. These clearly show a crossover between thermal and quantum fluctuation dominated regimes, but the nature of the quantum critical point remains unclear. The vicinity of the spin glass phase is dominated by real time glassy dynamics which drives the system out of equilibrium. On the theoretical side, we have already noted the work on the quantum Ising spin glass in infinite range models. Models with finite range interactions have been studied in imaginary time computer simulations [196, 409] which yield information on thermodynamic properties and critical exponents. However, it is clear that an understanding of the experiments will require a theory of the real time dynamics of quantum spin glasses: we have discussed the real time, nonzero temperature, physics near non-random quantum critical points in Part 2, but there are no corresponding results for the random case. Recent steps towards understanding the real time dynamics include the droplet model picture of Thill and Huse [489] and the infinite-range model studies of Rozenberg and Grempel [417].

A significant application of the concepts discussed here on metallic spin glasses has been in the 'heavy fermion' series of compounds. The

Griffiths-McCoy singularities of the Fermi liquid phase have been the subject of much attention; discussions along with comparisons with experiments may be found in Refs [126, 127, 344, 345, 428, 77, 22]. The anomalous power laws at high T in the vicinity of the quantum critical point [453, 437] have also been examined in recent experimental studies [477].

We have not commented in this chapter on insulating quantum spin glass of Heisenberg spins: such models would generalize those of Chapter 13 to the case of random exchange interactions. These turn out to be considerably more complicated: some work on infinite range models may be found in Refs [61, 441, 278, 452, 188].

As we noted earlier, fluctuation corrections to the mean field theory presented in this chapter have been considered in the literature [405, 437, 453, 452]. The first two [405, 437] focused on spatial fluctuations in the spin-glass order parameter, while the last two [453, 452] considered the quantum fluctuations in the on-site 'quantum impurity' model. These latter works argued that while the mean-field theory of this chapter is an adequate starting point for metallic electronic systems with Ising symmetry, those with full Heisenberg symmetry appear to be controlled by the critical quantum paramagnetic state found in Ref [441] in the study of insulating Heisenberg spin models. The critical state of Ref [441] also appears in a most interesting recent analysis by Parcollet and Georges [375] of a doped Mott insulator with random exchange interactions: the temperature and frequency crossovers found are closely related to those observed in the high temperature superconductors.

References

[1]   Aeppli, G., Broholm C., Di Tusa, J. F., Hayden, S. M., Ito, T.,
        Lee, S.-H., Mason, T. E., Mook, H. A., Oka, K., Perring, T. G.,
        Schröder, A., Takagi, H. & Xu, G. (1997) *Physica B* **237-238**, 30.
[2]   Aeppli, G., Mason, T. E., Hayden, S. M., Mook, H. A. & Kulda, J.
        (1998) *Science* **278**, 1432.
[3]   Affleck, I. (1985) *Nucl. Phys. B* **257**, 397.
[4]   Affleck, I. (1985) *Nucl. Phys. B* **265**, 409.
[5]   Affleck, I. (1990) in *Fields, Strings, and Critical Phenomena, Les
        Houches Summer School Proceedings, Vol 49*, edited by E. Brézin and
        J. Zinn-Justin (North-Holland, Amsterdam).
[6]   Affleck, I. (1990) *Phys. Rev. B* **41**, 6697.
[7]   Affleck, I. (1991) *Phys. Rev. B* **43**, 3215.
[8]   Affleck, I. (1998) cond-mat/9802045.
[9]   Affleck, I. & Haldane, F. D. M. (1987) *Phys. Rev. B* **36**, 5291.
[10]   Affleck, I., Kennedy, T., Lieb, E. H. & Tasaki, H. (1987) *Phys. Rev.
        Lett.* **59**, 799.
[11]   Affleck, I., Kennedy, T., Lieb, E. H. & Tasaki, H. (1988) *Commun.
        Math. Phys.* **115**, 477.
[12]   Affleck, I. & Ludwig, A. W. W. (1991) *Nucl. Phys. B* **360**, 641.
[13]   Affleck, I. & Marston, J. B. (1988) *Phys. Rev. B* **37**, 3774.
[14]   Aifer, A. H., Goldberg, B. B. & Broido, D. A. (1996) *Phys. Rev. Lett.*
        76, 680.
[15]   Ain, M., Lorenzo, J. E., Regnault, L. P., Dhalenne, G.,
        Revcolevschi, A., Hennion, B. & Jolicoeur, Th. (1997) *Phys. Rev.
        Lett.* **78**, 1560.
[16]   Akhiezer, A. I., Bar'yakhtar, V. G. & Peletminskii, S. V. (1968) *Spin
        Waves*, Chapter 8 (North Holland, Amsterdam).
[17]   Altshuler, B. L. (1985) *Pis'ma Zh. Éksp. Fiz.* **51**, 530 (*JETP. Lett.*
        41, 648).
[18]   Altshuler, B. L., Ioffe, L. B. & Millis, A. J. (1995) *Phys. Rev. B* **52**,
        5663.
[19]   Altshuler, B. L., Lee, P. A. & Webb, R. A. eds. (1991) *Mesoscopic
        Phenomena in Solids* (North Holland, Amsterdam).

449

[20] Amico, L., Falci, G, Fazio, R. & Giaquinta, G. (1997) *Phys. Rev. B* **55**, 1100.

[21] Anderson, P. W. (1987) *Science* **235**, 1196.

[22] Andrade, M. C. de, Chau, R., Dickey, R. P., Dilley, N. R., Freeman, E. J., Gajewski, D. A., Maple, M. B., Movshovich, R., Castro Neto, A. H., Castilla, G. E. & Jones, B. A. (1998) cond-mat/9802081.

[23] Andraka, B. & Tsvelik, A. M. (1991) *Phys. Rev. Lett.* **67**, 2886.

[24] Angelucci, A. (1992) *Phys. Rev. B* **45**, 5387.

[25] Antonenko, S. A., Sokolov, A. I. & Varnashev, K. B. (1995) *Phys. Lett. A*, **208**, 161.

[26] Arovas, D. P. & Auerbach, A. (1988) *Phys. Rev. B* **38**, 316.

[27] Ashcroft, N. W. & Mermin, N. D. (1976) *Solid State Physics* (Saunders College, Philadelphia).

[28] Assaad, F. F. & Imada, M. (1996) *Phys. Rev. Lett.* **76**, 3176.

[29] Assaad, F. F., Imada, M. & Scalapino, D. J. (1996) *Phys. Rev. B* **56**, 15001.

[30] Auerbach, A. (1994) *Interacting Electrons and Quantum Magnetism* (Springer-Verlag, New York).

[31] Augier, D., Poilblanc, D., Sorensen, E. & Affleck, I. (1998) cond-mat/9802053.

[32] Azaria, P., Delamotte, B., Delduc, F. & Jolicoeur, Th. (1993) *Nucl. Phys. B* **408**, 485.

[33] Azaria, P., Lecheminant, P. & Mouhanna, D. (1995) *Nucl. Phys. B* **455**, 648.

[34] Azuma, M., Hiroi, Z., Takano, M., Ishida, K. & Kitaoka, Y. (1994) *Phys. Rev. Lett.* **73**, 3463.

[35] Babelon, O. & Bernard, D. (1992) *Physics Letters. B* **288**, 113.

[36] Baert, M., Metlusho, V. V., Jonckheere, R., Moshchalkov, V. V. & Bruynseraede, Y. (1995) *Phys. Rev. Lett.* **74**, 3269.

[37] Bao, W., Broholm, C., Aeppli, G., Carter, S. A., Dai, P., Rosenbaum, T. F., Honig, J. M., Metcalf, P. & Trevino, S. F. (1998) cond-mat/9804320.

[38] Barouch, E. & McCoy, B. M. (1971) *Phys. Rev. A* **3**, 786.

[39] Barrett, S. E., Dabbagh, G., Pfeiffer, L. N., West, K. W. & Tycko, R. (1995) *Phys. Rev. Lett.* **74**, 5112.

[40] Barzykin, V. & Pines, D. (1995) *Phys. Rev. B* **52**, 13585.

[41] Baskaran, G., Zou, Z., & Anderson, P. W. (1987) *Solid State Commun.* **63**, 973.

[42] Batrouni, G. G., Scalettar, R. T. & Zimanyi, G. T. (1990) *Phys. Rev. Lett.* **65**, 1765.

[43] Batrouni, G. G., Scalettar, R. T., Zimanyi, G. T. & Kampf, A. P. (1995) *Phys. Rev. Lett.* **74**, 2527.

[44] Beal-Monod, M. T. & Maki, K. (1975) *Phys. Rev. Lett.* **34**, 1461.

[45] Beard, B. B., Birgeneau, R. J., Greven, M. & Wiese, U.-J. (1998) *Phys. Rev. Lett.* **80**, 1742.

[46] Beauchamp, K. M., Rosenbaum, T. F., Welp, U., Crabtree, G. W. & Vinokur, V. M. (1995) *Phys. Rev. Lett.* **75**, 3942.

[47] Belitz, D. & Kirkpatrick, T. R. (1994) *Rev. Mod. Phys.* **66**, 261.

[48] Belitz, D. & Kirkpatrick, T. R. (1996) *J. Phys. Cond. Matt.* **8**, 9707.

[49] Belitz, D., Kirkpatrick, T. R. & Vojta, T. (1997) *Phys. Rev. B* **55**, 9452.

[50] Bernu, B., Lecheminant, P., Lhuillier, C. & Pierre, L. (1994) *Phys. Rev. B*, **50**, 10048.

[51] Bhatt, R. N. & Fisher, D. S. (1992) *Phys. Rev. Lett.* **68**, 3072.

[52] Bhatt, R. N. & Lee, P. A. (1982) *Phys. Rev. Lett.* **48**, 344 (1982).

[53] Bijlsma, M. & Stoof, H. T. C. (1996) *Phys. Rev. A.* **54**, 5085.

[54] Binder, K. & Young, A. P. (1986) *Rev. Mod. Phys.* **58**, 801.

[55] Bitko, D., Rosenbaum, T. F. & Aeppli, G. (1996) *Phys. Rev. Lett.* **77**, 940.

[56] Bödeker, D., McLerran, L. & Smilga, A. (1995) *Phys. Rev. D* **52** 4675.

[57] Boebinger, G. G., Ando, Y., Passner, A., Kimura, T., Okuya, M., Shimoyama, J., Kishio, K., Tamasaku, K., Ichikawa, N. & Uchida, S. (1996) *Phys. Rev. Lett.* **77**, 5417.

[58] Boechat, B., dos Santos, R. R. & Continentino, M. A. (1994) *Phys. Rev. B* **49**, 6404.

[59] Bose, I. & Mitra, P. (1991) *Phys. Rev. B* **44**, 443.

[60] Boyanovsky, D. & Cardy, J. L. (1982) *Phys. Rev. B* **26**, 154.

[61] Bray, A. J. & Moore, M. A. (1980) *J. Phys. C* **13**, L655.

[62] Brézin, E. (1982) *J. de Physique* **43**, 15.

[63] Brézin, E., Le Guillou, J. C. & Zinn-Justin, J. (1976) in *Phase Transitions and Critical Phenomena* , **6**, edited by C. Domb and M.S. Green (Academic Press, London).

[64] Brézin, E. & Wallace, D. J. (1973) *Phys. Rev. B* **7**, 1967.

[65] Brézin E. & Zinn-Justin, J. (1976) *Phys. Rev. B* **14**, 3110.

[66] Brézin E. & Zinn-Justin, J. (1985) *Nucl. Phys. B* **257**, 867.

[67] Broholm, C. (1998) in *Dynamical Properties of Unconventional Magnetic Systems, NATO Advanced Study Institute, Series B: Physics*, edited by A. Skjeltorp and D. Sherrington (Kluwer Academic, Norwell MA).

[68] Bruce, A. D. & Wallace, D. J. (1976) *J. Phys. A* **9**. 1117.

[69] Buragohain, C. & Sachdev, S. (1998), cond-mat/xxxxxxx.

[70] Campostrini, M. & Rossi, P. (1993) *Riv. Nuovo Cimento* **16**, 1.

[71] Capel, H. W. & Perk, J. H. H. (1977) *Physica A* **87**, 211.

[72] Cardy, J. L. (1984) *J. Phys. A* **17**, L385.

[73] Castellani, C. & DiCastro, C. (1985) in *Localization and the Metal-Insulator Transition* edited by H. Fritzsche and D. Adler (Plenum, New York).

[74] Castellani, C., DiCastro, C. & Grilli, M. (1995) *Phys. Rev. Lett.* **75**, 4650.

[75] Castellani, C., DiCastro, C. & Grilli, M. (1997) *Z. Phys. B* **103**, 137.

[76] Castellani, C., DiCastro, C. & Grilli, M. (1998) *J. Phys. Chem. Solids*, xxxxx.

[77] Castro Neto, A. H., Castilla, G. E. & Jones, B. A. (1997) cond-mat/9710123.

[78] Cha, M.-C. Fisher, M. P.A., Girvin, S. M. Wallin, Mats & Young, A. P. (1991) *Phys. Rev. B* **44**, 6883.

[79] Chaboussant, G., Crowell, P. A., Levy, L. P., Piovesana, O., Madouri, A. & Mailly, D. (1997) *Phys. Rev. B* **55**, 3046.

[80] Chaboussant, G., Julien, M.-H., Fagot-Revurat, Y., Levy, L. P., Berthier, C., Horvatic, M. & Piovesana, O. (1997) *Phys. Rev. Lett.*

79, 925.

[81] Chaboussant, G., Fagot-Revurat, Y., Julien, M.-H., Hanson, M. E., Berthier, C., Horvatic, M., Levy, L. P. & Piovesana, O. (1998) *Phys. Rev. Lett.* **80**, 2713.

[82] Chakrabarti, B. K., Dutta, A. & Sen, P. (1996) *Quantum Ising Phases and Transitions in Transverse Ising Models* (Springer, Berlin).

[83] Chakravarty, S., Halperin, B. I. & Nelson, D. R. (1989) *Phys. Rev. B* **39**, 2344.

[84] Chakravarty, S. & Orbach, R. (1990) *Phys. Rev. Lett.* **64**, 224.

[85] Chalker, J. T. & Coddington, P. D. (1988) *J. Phys. C* **21**, 2665.

[86] Chamati, H., Pisanova, E. S. & Tonchev, N. S. (1998) *Phys. Rev. B* **57**, 5798.

[87] Chandra, P. & Doucot, B. (1988) *Phys. Rev. B* **38**, 9335.

[88] Chayes, J. T., Chayes, L., Fisher, D. S. & Spencer, T. (1986) *Phys. Rev. Lett.* **57**, 2999.

[89] Chen, Y.-H., Wilczek, F., Witten, E., & Halperin, B. I. (1989) *Int. J. Mod. Phys. B* **3**, 1001.

[90] Chitra, R. & Giamarchi, T. (1997) *Phys. Rev. B* **55**, 5816.

[91] Chubukov, A. V. (1991) *Phys. Rev. B* **44**, 392.

[92] Chubukov, A. V. (1995) *Phys. Rev. B* **52**, R3840.

[93] Chubukov, A. V. (1997) cond-mat/9709221.

[94] Chubukov, A. V. & Jolicoeur, Th. (1992) *Phys. Rev. B* **46**, 11137.

[95] Chubukov, A. V. & Morr, D. K. (1997) *Phys. Rep.* **288**, 355.

[96] Chubukov, A. V. & Sachdev, S. (1993) *Phys. Rev. Lett.* **71**, 169.

[97] Chubukov, A. V., Sachdev, S. & Ye, J. (1994) *Phys. Rev. B* **49**, 11919.

[98] Chubukov, A. V., Sachdev, S. & Senthil, T. (1994) *Nucl. Phys. B* **426**, 601.

[99] Chubukov, A. V., Sachdev, S. & Sokol, A. (1994) *Phys. Rev. B* **49**, 9052.

[100] Chubukov, A. V. & Starykh, O. A. (1995) *Phys. Rev. B* **52**, 440.

[101] Chubukov, A. V. & Starykh, O. A. (1996) *Phys. Rev. B* **53**, R14729.

[102] Coleman, P. (1998) cond-mat/9809436.

[103] Continentino, M. A. (1994) *Phys. Rep.* **239**, 179.

[104] Continentino, M. A. (1996) *Z. Phys. B* **101**, 197.

[105] Cowley, R. A. (1998) in *Dynamical Properties of Unconventional Magnetic Systems, NATO Advanced Study Institute, Series B: Physics*, edited by A. Skjeltorp and D. Sherrington (Kluwer Academic, Norwell MA).

[106] Cox, D. L. & Jarrell, M. (1996) *J. Phys. Cond. Matt.* **8**, 9825.

[107] Cox, D. L. & Zawadowski, A. (1998) *Adv. Phys.*

[108] Creswick, R. J. & Wiegel, F. W. (1983) *Phys. Rev. A* **28**, 1579.

[109] Cross, M. C. & Fisher, D. S. (1979) *Phys. Rev. B* **19**, 402.

[110] Crowell, P. A., van Keuls, F. W. & Reppy, J. D. (1995) *Phys. Rev. Lett.* **75**, 1106.

[111] Crowell, P. A., van Keuls, F. W. & Reppy, J. D. (1995) *Phys. Rev. B* **55**, 12620.

[112] d'Adda, A., Luscher, M. & Di Vecchia, P. (1978) *Nucl. Phys. B* **146**, 63.

[113] Dagotto, E. & Moreo, A. (1989) *Phys. Rev. Lett.* **63**, 2148.

[114] Dagotto, E. & Rice, T. M. (1996) *Science* **271**, 618.

[115] Damle, K. & Sachdev, S. (1996) *Phys. Rev. Lett.* **76**, 4412.
[116] Damle, K. & Sachdev, S. (1997) *Phys. Rev. B*, **56**, 8714.
[117] Damle, K. & Sachdev, S. (1998) *Phys. Rev. B* **57**, 8307.
[118] Dasgupta, C. & Ma, S.-K. (1980) *Phys. Rev. B* **22**, 1305.
[119] Das Sarma, S. & Pinczuk, A. eds. (1997) *Perspectives in Quantum Hall Effects* (Wiley, New York).
[120] Das Sarma, S., Sachdev, S. & Zheng, L. (1997) *Phys. Rev. Lett.* **79**, 917.
[121] Das Sarma, S., Sachdev, S. & Zheng, L. (1998) *Phys. Rev. B* **58**, 4672.
[122] David, F. & Jolicoeur, Th. (1996) *Phys. Rev. Lett.* **76**, 3148.
[123] Devreux, F. & Boucher, J.P. (1987) *J. de Physique* **48**, 1663.
[124] Dhar, D. (1983) in *Stochastic Processes: Formalism and Applications*, edited by G. S. Agarwal and S. DuttaGupta (Springer, Berlin).
[125] Dhar, D. & Barma, M. (1980) *J. Stat. Phys.* **22**, 259.
[126] Dobrosavljevic, V., Kirkpatrick, T. R. & Kotliar, G. (1992) *Phys. Rev. Lett.* **69** 1113.
[127] Dobrosavljevic, V. & Kotliar, G. (1993) *Phys. Rev. Lett.* **71** 3218.
[128] Dombre, T. & Read, N. (1989) *Phys. Rev. B* **39**, 6797.
[129] Doniach, S. (1981) *Phys. Rev. B* **24**, 5063.
[130] Dorogovstev, S. N. (1980) *Phys. Lett.* **76A**, 169.
[131] dos Santos, R. R. (1982) *J. Phys. C* **15**, 3141.
[132] Dyson, F. J. (1956) *Phys. Rev.* **102**, 1230.
[133] Eggert, S., Affleck, I. & Takahashi, M. (1994) *Phys. Rev. Lett.* **73**, 332.
[134] Elliott, R. J., Pfeuty, P. & Wood, C. (1970) *Phys. Rev. Lett.* **25**, 443.
[135] Elstner, N., Glenister, R. L., Singh, R. R. P. & Sokol, A. (1995) *Phys. Rev. B* **51**, 8984.
[136] Elstner, N. & Singh, R. R. P. (1998) *Phys. Rev. B* **57**, 7740.
[137] Elstner, N. & Singh, R. R. P. (1998) cond-mat/9803085.
[138] Emery, V. J. & Kivelson, S. A. (1998) *J. Phys. Chem. Solids* xxxxx.
[139] Engel, L. W., Shahar, D., Kurdak, C. & Tsui, D. C. (1993) *Phys. Rev. Lett.* **71**, 2638.
[140] Eskes, H., Osman, O. Y., Grimberg, R., van Saarloos, W. & Zaanen, J. (1997) cond-mat/9712316.
[141] Faddeev, L. D. & Takhtajan, L.A. (1987) *Hamiltonian Methods in the Theory of Solitons* (Springer-Verlag, Heidelberg).
[142] Fateev, V. A., Onofri, E. & Zamolodchikov, A. B. (1993) *Nucl. Phys. B* **406**, 521.
[143] Fazio, R. & Zappala, D. (1996) *Phys. Rev. B* **53**, R8883.
[144] Fendley, P., Ludwig, A. W. W. & Saleur, H. (1995) *Phys. Rev. B* **52** 8934.
[145] Fertig, H. A., Brey, L., Côté, R. & MacDonald, A. H. (1994) *Phys. Rev. B* **50**, 11018.
[146] Fetter, A. L. & Walecka, J. D. (1971) *Quantum Theory of Many-Particle Systems* (McGraw-Hill, New York).
[147] Figueirido, F., Karlhede, A., Kivelson, S., Sondhi, S., Rocek, M. & Rokhsar, D. S. (1990) *Phys. Rev. B* **41**, 4619.
[148] Finkelstein, A. M. (1987) *Pis'ma Zh. Eksp. Teor. Fiz.* **45**, 37. (*JETP Lett.* **45**, 46.)
[149] Finkelstein, A. M. (1990) *Sov. Sci. Rev. A Phys.* **14**, 1.

[150] Fischer, K. H. & Hertz, J. A. (1991) *Spin Glasses* (Cambridge University Press, Cambridge).

[151] Fisher, D. S. & Hohenberg, P. C. (1988) *Phys. Rev. B* **37**, 4936.

[152] Fisher, D. S. (1992) *Phys. Rev. Lett.* **69**, 534.

[153] Fisher, D. S. (1994) *Phys. Rev. B* **50**, 3799.

[154] Fisher, D. S. (1995) *Phys. Rev. B* **51**, 6411.

[155] Fisher, D. S. & Young, A. P. (1998) cond-mat/9802246.

[156] Fisher, M. E. (1964) *Am. J. Phys.* **32**, 343.

[157] Fisher, M. P. A. (1990) *Phys. Rev. Lett.* **65**, 923.

[158] Fisher, M. P. A. & Grinstein, G. (1988) *Phys. Rev. Lett.* **60**, 208.

[159] Fisher, M. P. A., Grinstein, G. & Girvin, S. M. (1990) *Phys. Rev. Lett.* **64**, 587.

[160] Fisher, M. P. A., Weichman, P. B., Grinstein, G. & Fisher, D. S. (1989) *Phys. Rev. B* **40**, 546.

[161] Forster, D. (1975) *Hydrodynamic Fluctuations, Broken Symmetry, and Correlation Functions* (Benjamin/Cummings, Reading).

[162] Fradkin, E. (1991) *Field Theories of Condensed Matter Systems* (Addison-Wesley, Redwood City).

[163] Fradkin, E. & Kivelson, S. A. (1990) *Mod. Phys. Lett.* **B4**, 225.

[164] Fradkin, E. & Susskind, L. (1978) *Phys. Rev. D* **17**, 2637.

[165] Franz, M. & Millis, A. J. (1998) cond-mat/9805401.

[166] Freericks, J. K. & Monien, H. (1994) *Europhys. Lett.* **26**, 545.

[167] Freericks, J. K. & Monien, H. (1996) *Phys. Rev. B* **53**, 2691.

[168] Frey, E. & Balents, L. (1997) *Phys. Rev. B* **55**, 1050.

[169] Friere, F., O'Connor, D. & Stephens, C. R. (1994) *J. Stat. Phys.* **74**, 219.

[170] Frischmuth, B. & Sigrist, M. (1997) *Phys. Rev. Lett.* **79**, 147.

[171] Furusaki, A., Sigrist, M., Westerberg, E., Lee, P. A., Tanaka, K., B. & Nagaosa, N. *Phys. Rev. Lett.* (1994) **73**, 2622.

[172] Gebhard, F. (1997) *The Mott Metal-Insulator Transition*, Springer Tracts in Modern Physics **137** (Springer, Berlin).

[173] Gelfand, M. P. (1990) *Phys. Rev. B* **42**, 8206.

[174] Gelfand, M. P., Singh, R. R. P. & Huse, D. A. (1989) *Phys. Rev. B* **40**, 10801.

[175] Gelfand, M. P., Zheng, W., Hamer, C. J. & Oitmaa, J. (1998) *Phys. Rev. B* **57**, 392.

[176] Gelfand, M. P., Zheng, W. & Singh, R. R. P. (1996) *Phys. Rev. Lett.* **77**, 2794.

[177] Georges, A., Kotliar, G., Krauth, W. & Rozenberg, J. (1996) *Rev. Mod. Phys.* **68**, 13.

[178] Ghosal, A, Randeria, M. & Trivedi, N. (1998) cond-mat/9806060

[179] Giamarchi, T. & Schulz, H. J. (1988) *Phys. Rev. B* **37**, 327.

[180] Girvin, S. M. & Mahan, G.

[181] Glauber, R. J. (1963) *J. Math. Phys.* **4**, 294.

[182] Glazman, L. I. & Larkin, A. I. (1997) *Phys. Rev. Lett.* **79**, 3736.

[183] Goff, J. P., Tennant, D. A. & Nagler, S. E. (1995) *Phys. Rev. B* **52**, 15992.

[184] Goldenfeld, N. (1992) *Lectures on Phase Transitions and the Renormalization Group* (Addison-Wesley, Reading).

[185] Goldschmidt, Y. Y. & Lai, P.-Y. *Phys. Rev. Lett.* **64**, 2467.

[186] Granroth, G. E., Meisel, M. W., Chaparala, M., Jolicoeur, Th., Ward, B. H. & Talham, D. R. (1996) *Phys. Rev. Lett.* **77**, 1616.

[187] Grempel, D. R. (1988) *Phys. Rev. Lett.* **61**, 1041.

[188] Grempel, D. R. & Rozenberg, M. J. (1998) *Phys. Rev. Lett.* **80**, 389.

[189] Greven, M., Birgeneau, R. J., Endoh, Y., Kastner, M. A., Keimer, B., Matsuda, M., Shirane, G. & Thurston, T. R. (1994) *Phys. Rev. Lett.* **72**, 1096.

[190] Griffiths, R. B. (1969) *Phys. Rev. Lett.* **23**, 17.

[191] Gros, C. & Werner, R. (1988) cond-mat/9804092.

[192] Grosche, F. M., Wilson, N. J., Haselwimmer, R. K. W., Lister, S. J. S., Mathur, N. D., Julian, S. R. & Lonzarich, G. G. (1997) APS preprint aug 27_001.

[193] Grüter, P., Ceperley, D. & Laloë, F. (1997) *Phys. Rev. Lett.* **79**, 3549.

[194] Gruzberg, I. A., Read, N. & Sachdev, S. (1997) *Phys. Rev. B* **55**, 10593.

[195] Gruzberg, I. A., Read, N. & Sachdev, S. (1997) *Phys. Rev. B* **56**, 13218.

[196] Guo, M., Bhatt, R. N. & Huse, D. A. (1994) *Phys. Rev. Lett.* **72**, 4137.

[197] Guo, M., Bhatt, R. N. & Huse, D. A. (1996) *Phys. Rev. B* **54**, 3336.

[198] Hagiwara, M., Katsumata, K., Affleck, I., Halperin, B. I. & Renard, J. P. (1990) *Phys. Rev. Lett.* **65**, 3181.

[199] Haldane, F. D. M. (1980) *Phys. Rev. Lett.* **45**, 1358.

[200] Haldane, F. D. M. (1981) *Phys. Rev. Lett.* **47**, 1840.

[201] Haldane, F. D. M. (1981) *J. Phys. C* **14**, 2585.

[202] Haldane, F. D. M. (1982) *Phys. Rev. B* **25**, 4925.

[203] Haldane, F. D. M. (1982) *J. Phys. C* **15**, L831.

[204] Haldane, F. D. M. (1983) *Phys. Rev. Lett.* **50**, 1153.

[205] Haldane, F. D. M. (1988) *Phys. Rev. Lett.* **61**, 1029.

[206] Halperin, B. I. & Saslow, W. M. (1977) *Phys. Rev. B* **16**, 2154.

[207] Halperin, B. I., March-Russell, J., & Wilczek, F. (1989) **40**, 8726.

[208] Hamer, C. J., Kogut, J. B. & Susskind, L (1979) *Phys. Rev. D* **19**, 3091.

[209] Hammar, P. R., Reich, D. H., Broholm, C. & Trouw, F. (1998) *Phys. Rev. B* **57**, 7846.

[210] Hartman, J. W. & Weichman, P. B. (1995) *Phys. Rev. Lett.* **74**, 4584.

[211] Harris, A. B. (1974) *J. Phys. C* **7**, 1671.

[212] Harris, A. B. (1974) *J. Phys. C* **7**, 3082.

[213] Hardy, W. N., Kamal, S., Liang, R., Bonn, D. A., Homes, C. C., Basov, D. N. & Timusk, T. (1996) in *Proceedings of the 10th Anniversary HTS Workshop on Physics, Materials and Applications* edited by B. Batlogg *et al.* (World Scientific, Singapore), p. 223.

[214] Hasegawa, H. & Moriya, T. (1974) *J. Phys. Soc. Jpn.* **36**, 1542.

[215] Hasenfratz, P., Maggiore, M. & Niedermayer, F. (1990) *Phys. Lett. B* **245**, 522.

[216] Hasenfratz, P. & Niedermayer, F. (1990) *Phys. Lett. B* **245**, 529.

[217] Hasenfratz, P. & Niedermayer, F. (1991) *Phys. Lett. B* **268**, 231.

[218] Hasenfratz, P. & Niedermayer, F. (1993) *Z. Phys. B* **92**, 91.

[219] Hastings, M. B. (1998) cond-mat/9809244.

[220] Hayden, S. M., Aeppli, G., Mook, H., Rytz, D., Hundley, M. F. & Fisk, Z. (1991) *Phys. Rev. Lett.* **66**, 821.

456   *References*

[221]   Hebard, A. F. (1994) in *Strongly Correlated Electronic Materials*,
        edited by K. S. Bedell, Z. Wang, D. E. Meltzer & E. Abrahams
        (Addison-Wesley, Reading, MA).
[222]   Henelius, P. & Girvin, S. M. (1998) *Phys. Rev. B* **57**, 11457.
[223]   Henkel, M. & Hoeger, C. (1984) *Z. Phys. B* **55**, 67.
[224]   Henley, C. M. (1998) *Phys. Rev. Lett.* **80**, 3590.
[225]   Hertz, J. A. (1976) *Phys. Rev. B* **14**, 525.
[226]   Heuser, K., Scheidt, E.-W., Schreiner, T. & Stewart, G. R. (1998)
        Phys. Rev. B **57**, R4198.
[227]   Hirsch, J. E. & José, J. V. (1980) *Phys. Rev. B* **22**, 5355.
[228]   Hohenberg, P. C. & Halperin, B. I. (1977) *Rev. Mod. Phys.* **49**, 435.
[229]   Houghton, A. & Marston, J. B. (1993) *Phys. Rev. B* **48**, 7790.
[230]   Huckenstein, B. (1995) *Rev. Mod. Phys.* **67**, 357.
[231]   Huo, R. E., Hetzel, R. E. & Bhatt, R. N. (1993) *Phys. Rev. Lett.* **70**,
        481.
[232]   Huse, D. A. & Elser, V. (1988) *Phys. Rev. Lett.* **60**, 2531.
[233]   Hyman, R. A., Yang, K., Bhatt, R. N. & Girvin, S. M. (1996) *Phys.
        Rev. Lett.* **76**, 839.
[234]   Hyman, R. A. & Yang, K. (1997) *Phys. Rev. Lett.* **78**, 1783.
[235]   Ikegami, T., Miyashita, S. & Rieger, H. (1998) cond-mat/9803270.
[236]   Imada, M., Assaad, F. F., Tsunetsugu, H. & Motome, Y. (1998)
        cond-mat/9808044.
[237]   Imada, M., Fujimori, A. & Tokura, Y. (1998) *Rev. Mod. Phys.*
[238]   Imai, T., Slichter, C. P., Yoshimura, K. & Kosuge, K. (1993) *Phys.
        Rev. Lett.* **70**, 1002.
[239]   Imai, T., Slichter, C. P., Yoshimura, K., Katoh, M. & Kosuge, K.
        (1993) *Phys. Rev. Lett.* **71**, 1254.
[240]   Ioffe, L. B. & Millis, A. J. (1995) *Phys. Rev. B* **51**, 16151.
[241]   Irkhin, V. Yu & Katanin, A. A. (1998) cond-mat/9801270.
[242]   Ising, E. (1925) *Z. Phys.* **31**, 253.
[243]   Itoh, Y. & Yasuoka, H. (1997) *J. Phys. Soc. Jpn* **66**, 334.
[244]   Its, A. R., Izergin, A. G. & Korepin, V. E. (1991) *Physica D* **53**, 187.
[245]   Its, A. R., Izergin, A. G., Korepin, V. E. & Novokshenov, V. Ju.
        (1990) *Nucl. Phys. B* **340**, 752.
[246]   Its, A. R., Izergin, A. G., Korepin, V. E. & Varzugin, G. G. (1992)
        Physica D **54**, 351.
[247]   Itzykson, C. & Drouffe, J.-M. (1989) *Statistical Field Theory*
        (Cambridge University Press, Cambridge).
[248]   Itzykson, C. & Zuber, J. B. (1980) *Quantum Field Theory*
        (McGraw-Hill, New York).
[249]   Jeon, S. & Yaffe, L. G. (1996) *Phys. Rev. D* **53**, 5799.
[250]   Jevicki, A. & Papanicolaou, N. (1979) *Ann. Phys.* **120**, 107.
[251]   Jepsen, D. W. (1965) *J. Math. Phys.* **6**, 405.
[252]   Johnston, D. C. (1989) *Phys. Rev. Lett.* **62**, 957.
[253]   Jolicoeur, Th. & Golinelli, O. (1994) *Phys. Rev. B* **50**, 9265.
[254]   Jordan, P. & Wigner, E. (1928) *Z. Phys.* **47**, 631.
[255]   Joyce, G. S. (1967) *Phys. Rev.* **155**, 478.
[256]   Julian, S. R., Pfleiderer, C., Grosche, F. M., Mathur, N. D.,
        McMullan, G. J., Diver, A. J., Walker, I. R. & Lonzarich, G. G.
        (1996) *J. Phys. Cond. Matt.* **8**, 9675.

[257] Julian, S. R., Carter, F. V., Grosche, F. M., Haselwimmer, R. K. W., Lister, S. J., Mathur, N. D., McMullan, G. J., Pfleiderer, C., Saxena, S. S., Walker, I. R., Wilson, N. J. W. & Lonzarich, G. G. (1998) *J. Magnetism & Magnetic Matt.* **177-181**, 265.

[258] Kaganov, M. I. & Chubukov, A. V. (1987) *Usp. Fiz. Nauk* **153**, 537 (*Sov. Phys. Usp.* **30**, 1015).

[259] Kageyama, H., Yoshimura, K., Stern, R., Mushnikov, N. V., Kato, M., Kosuge, K., Slichter, C. P., Goto, T. & Ueda, Y. (1998) *Phys. Rev. Lett.* xxxxxxxx.

[260] Kalmeyer, V. & Laughlin, R. B. (1987) *Phys. Rev. Lett.* **59**, 2095.

[261] Kambe, S., Raymond, S., Regnault, L.-P., Flouquet, J., Lejay, P. & Haen, P. (1996) *J. Phys. Soc. Jpn* **65**, 3294.

[262] Kane, C. & Fisher, M. P. A. (1997) in *Perspectives in Quantum Hall Effects*, edited by S. Das Sarma and A. Pinczuk (Wiley, New York).

[263] Kapusta, J. I. (1993) *Finite-Temperature Field Theory* (Cambridge University Press, Cambridge).

[264] Kasner, M. & MacDonald, A. H. (1996) *Phys. Rev. Lett.* **76**, 3204.

[265] Kasner, M., Palacios, J. J. & MacDonald, A. H. (1998) cond-mat/9808186.

[266] Katoh, N. & Imada, M. (1998) *J. Phys. Soc. Jpn.* **67**, 564.

[267] Keimer, B., Belk, N., Birgeneau, R. J., Cassanho, A., Chen, C.Y., Greven, M., Kastner, M. A., Aharony, A., Endoh, Y., Erwin, R. W. & Shirane, G. (1992) *Phys. Rev. B* **46**, 14034.

[268] Kikuchi, J., Yamauchi, T. & Ueda Y. (1997) *J. Phys. Soc. Jpn* **66**, 1622.

[269] Kim, J.-K. & Troyer, M. (1997) *Phys. Rev. Lett.* **80**, 2705.

[270] Kim, Y.-B. & Wen, X. G. (1994) *Phys. Rev. B* **49**, 4043.

[271] Kim, Y.-J., Greven, M., Wiese, U.-J. & Birgeneau, R. J. (1998) *Eur. Phys. J. B* **4**, 291.

[272] Kirkpatrick, T. R. & Belitz, D. (1996) *Phys. Rev. Lett.* **76**, 2571. (**78**, 1197 (E)).

[273] Kirkpatrick, T. R. & Belitz, D. (1996) *Phys. Rev. B* **53**, 14364.

[274] Kirkpatrick, T. R. & Belitz, D. (1997) *Phys. Rev. Lett.* **79**, 3042.

[275] Kivelson, S. A., Fradkin, E. & Emery, V. J. (1997) cond-mat/9707327.

[276] Kivelson, S. A., Rokhsar, D. S., & Sethna, J. P. (1987) *Phys. Rev. B* **35**, 8865.

[277] Klauder, J. & Skagerstam, B. eds. (1985) *Coherent States* (World Scientific, Singapore).

[278] Kopeć, T. K. (1995) *Phys. Rev. B* **52**, 9590.

[279] Kopeć, T. K. (1997) *Phys. Rev. Lett.* **79**, 4266.

[280] Kopietz, P. & Chakravarty, S. (1989) *Phys. Rev. B* **40**, 4858.

[281] Korepin, V. E., Bogoliubov, N. M. & Izergin, A. G. (1993) *Quantum Inverse Scattering Method and Correlation Functions* (Cambridge University Press, Cambridge).

[282] Korepin, V. E. & Slavnov, N. A. (1990) *Commun. Math. Phys.* **129**, 103.

[283] Korshunov, S. E. (1993) *Phys. Rev. B* **47**, 6165.

[284] Kosevich, Y. A. & Chubukov, A. V. (1986) *Zh. Eksp. Teor. Fiz.* **91**, 1105 (*Sov. Phys. JETP* **64**, 654).

[285] Kwon, H.-J. & Dorsey, A. T. (1998) cond-mat/9809225.

[286] Kwon, H.-J., Houghton, A. & Marston, J. B. (1995) *Phys. Rev. B* **52**, 8002.

[287] Kyriakidis, J. & Loss, D. (1998) cond-mat/9803156.

[288] Lakner, M., von Löhneysen, H., Langenfeld, A. & Wolfle, P. (1994) *Phys. Rev. B* **50**, 17064.

[289] Lammert, P. E., Rokhsar, D. S. & Toner, J. (1993) *Phys. Rev. Lett.* **70**, 1650.

[290] Langenfeld, A. & Wolfle, P. (1995) *Ann. Physik* **4**, 43.

[291] Laughlin, R. B. (1988) *Phys. Rev. Lett.* **60**, 2677.

[292] Laughlin, R. B. (1988) *Science* **242**, 525.

[293] Laughlin, R. B. (1997) cond-mat/9709195; xxxxxxx.

[294] Lawrie, I. D. (1978) *J. Phys. C* **11**, 3857.

[295] Lebowitz, J. L. & Percus, J. K. (1969) *Phys. Rev.* **188**, 487.

[296] Lecheminant, P., Bernu, B., Lhuillier, C. & Pierre, L. (1995) *Phys. Rev. B* **52**, 6647.

[297] Leclair, A., Lesage, F., Saleur, H. & Sachdev, S. (1996) *Nucl. Phys. B* **482**, 579.

[298] Lee, H.-L., Carini, J. P., Baxter, D. V. & Gruner, G. (1998) *Phys. Rev. Lett.* **80**, 4261.

[299] Lee, P. A. & Ramakrishnan, T. V. (1985) *Rev. Mod. Phys.* **57**, 287.

[300] Lee, P. A. & Stone, A. D. (1985) *Phys. Rev. Lett.* **55**, 1622.

[301] Lenard, A. (1966) *J. Math. Phys.* **7**, 1268.

[302] Leggett, A. J., Chakravarty, S., Dorsey, A. T., Fisher, M. P. A., Garg, A., Zwerger, W. (1987) *Rev. Mod. Phys.* **59**, 1.

[303] Lesage, F. & Saleur, H. (1997) *Nucl. Phys. B* **493**, 613.

[304] Leung, P. W. & Lam, N.-w. (1995) *Phys. Rev. B* **53**, 2213.

[305] Leung, P. W., Chiu, K. C. & Runge, K. J. (1996) *Phys. Rev. B* **54**, 12938.

[306] Lieb, E., Schultz, T. & Mattis, D. (1961) *Ann. of Phys.* **16**, 406.

[307] Lister, S. J. S., Grosche, F. M., Carter, F. V., Haselwimmer, R. K. W., Saxena, S. S., Mathur, N. D., Julian, S. R. & Lonzarich, G. G. (1997) *Z. Phys. B* **103**, 263.

[308] Liu, Y. & Goldman, A. M. (1994) *Mod. Phys. Lett. B* **8**, 277.

[309] Loinaz, W. & Willey, R. S. (1997) hep-lat/9712008.

[310] Lok, J. G. S., Geim, A. K., Tieke, B., Maan, J. C., Stoddart, S. T., Hyndman, R. J., Gallagher, B. L. & Henini, M. (1998) cond-mat/9804256.

[311] Lukyanov, S. (1998) *Nucl. Phys. B* **522**, 533.

[312] Luscher, M. (1982) *Phys. Lett. B* **118**, 391.

[313] Luscher, M. & Pohlmeyer, K. (1978) *Nucl. Phys.* **B137**, 46.

[314] Luther, A. & Emery, V. J. (1974) *Phys. Rev. Lett.* **33**, 589.

[315] Luther, A. & Peschel, I. (1974) *Phys. Rev. B* **9**, 2911.

[316] Ma, S.-K. (1972) *Phys. Rev. Lett.* **29**, 1311.

[317] Ma, S.-K. (1973) *Rev. Mod. Phys.* **45**, 589.

[318] Ma, S.-K. (1976) *Modern Theory of Critical Phenomena* (Benjamin Cummings, Reading).

[319] Ma, S.-K., Dasgupta, C. & Hu, C.-K. (1979) *Phys. Rev. Lett* **43**, 1434.

[320] Maekawa, S. & Fukuyama, H. (1982) *J. Phys. Soc. Japan* **51**, 1380.

[321] Mahan, G. D. (1990) *Many-Particle Physics* (Plenum, New York).

[322] Majumdar, C. K. & Ghosh, D. K. (1970) *J. Phys. C* **3**, 911 (1970).

[323] Maki, K. (1981) *Phys. Rev. B* **24** 335.

[324] Makivic, M., Trivedi, N. & Ullah, S. (1993) *Phys. Rev. Lett* **71**, 2307.

[325] Maleev, S. (1957) *Zh. Eksp. Teor. Fiz.* **33**, 1010.

[326] Manfra, M. J., Aifer, E. H., Goldberg, B. B., Broido, D. A., Pfeiffer, L. & West, K. (1996) *Phys. Rev. B* **54**, R17327.

[327] Mason, T. E., Schröder, A., Aeppli, G., Mook, H. A. & Hayden, S. M. (1996) *Phys. Rev. Lett.* **77**, 1604.

[328] Mathur, N. D., Grosche, F. M., Julian, S. R., Walker, I. R., Freye, D. M., Haselwimmer, R. K. W. & Lonzarich, G. G. (1998) *Nature* **394**, 39.

[329] Matsuda, T. & Hida, K. (1990) J. Phys. Soc. Jpn **59**, 2223.

[330] Matsushita, Y., Gelfand, M. P. & Ishii, C. (1997) *J. Phys. Soc. Jpn* **66**, 3648.

[331] Matsushita, Y., Gelfand, M. P. & Ishii, C. (1998) cond-mat/9808048.

[332] Mattis, D. C. & Lieb, E. H. (1965) *J. Math. Phys.* **6**, 375.

[333] McCoy, B. M. (1968) *Phys. Rev.* **173**, 531.

[334] McCoy, B. M. (1969) *Phys. Rev. Lett.* **23**, 383.

[335] McCoy, B. M. (1969) *Phys. Rev.* **188**, 1014.

[336] McCoy, B. M., Barouch, E. & Abraham, D. B. (1971) *Phys. Rev. A* **4**, 2331.

[337] McCoy, B. M., Perk, J. H. H. & Shrock, R. E. (1983) *Nucl. Phys. B.* **220**, 35.

[338] McCoy, B. M. & Wu, T. T. (1973) *The Two-Dimensional Ising Model* (Harvard University Press, Cambridge, U.S.A.).

[339] Micnas, R. & Chao, K. A. (1985) *Physics Letters* **110A**, 269.

[340] Miller, J. & Huse, D. A. (1993) *Phys. Rev. Lett.* **70**, 3147.

[341] Millis, A. J. (1993) *Phys. Rev. B*, **48**, 7183 (1993).

[342] Millis, A. J. & Monien, H. (1994) *Phys. Rev. B* **50**, 16606.

[343] Milovanovic, M., Sachdev, S. & Bhatt, R. N. *Phys. Rev. Lett.* (1989) **63**, 82.

[344] Miranda, E., Dobrosavljevic, V. & Kotliar, G. (1996) *J. Phys. Cond. Matt.* **8**, 9871.

[345] Miranda, E., Dobrosavljevic, V. & Kotliar, G. (1997) *Phys. Rev. Lett.* **78**, 290.

[346] Misguich, G., Bernu, B., Lhuillier, C. & Waldtmann, C. (1998) *Phys. Rev. Lett.* **81**, 1098.

[347] Mishra, S. G. & Ramakrishnan, T. V. (1978) *Phys. Rev. B* **18**, 2308.

[348] Mishra, S. G. & Sreeram, P. A. (1998) *Phys. Rev. B* **57**, 2188.

[349] Miyahara, S. & Ueda, K. (1998) cond-mat/9807075.

[350] Moreo, A., Dagotto, E., Jolicoeur, Th., & Riera, J. (1990) *Phys. Rev. B* **42**, 6283.

[351] Moriya, T. & Kawabata, A. (1973) *J. Phys. Soc. Jpn.* **34**, 639.

[352] Moriya, T. & Kawabata, A. (1973) *J. Phys. Soc. Jpn.* **35**, 669.

[353] Moriya, T. (1985) *Spin Fluctuations in Itinerant Electron Magnetism* (Springer Verlag, Berlin).

[354] Moriya, T. & Takimoto, T. (1995) *J. Phys. Soc. Jpn.* **64**, 960.

[355] Murthy, G., Arovas, D. & Auerbach, A. (1997) *Phys. Rev. B*, **55**, 3104.

[356] Murthy, G. & Sachdev, S. (1990) *Nucl. Phys. B* **344**, 557.

[357] Nagler, S. E., Buyers, W. J. L., Armstrong, R. L. & Briat, B. (1983) *Phys. Rev. B* **28**, 3873.

[358] Narumi, Y., Hagiwara, M., Sato, R., Kindo, K., Nakano, H. &
       Takahashi, M. (1998) *Physica B* **246-247**, 509.
[359] Nayak, C. & Wilczek, F. (1996) *Int. J. Mod. Phys. B* **10**, 847.
[360] Negele, J. W. & Orland H. (1988) *Quantum Many-Particle Systems*
       (Addison-Wesley, Redwood City, CA).
[361] Nelson, D. R. & Kosterlitz, J. M. (1977) *Phys. Rev. Lett.* **39**, 1201.
[362] Nelson, D. R. & Pelcovits, R. (1977) *Phys. Rev. B* **16**, 2191.
[363] Nelson, D. R. & Rudnick, J. (1975) *Phys. Rev. Lett.* **35**, 178.
[364] Nieuwenhuizen, T. M. & Ritort, F. (1997) *Physica A* **250**, 8.
[365] Niyaz, P., Scalettar, R. T., Fong, C. Y. & Batrouni, G. G. (1994)
       Phys. Rev. B **50**, 362.
[366] Normand, B. & Rice, T. M. (1996) *Phys. Rev. B* **54**, 7180.
[367] Normand, B. & Rice, T. M. (1997) *Phys. Rev. B* **56**, 8760.
[368] Nozières, P. & Blandin, A. (1980) J. Phys. (Paris) **41**, 193.
[369] O'Connor, D. & Stephens, C. R. (1994) *Int. J. Mod. Phys. A* **9**, 2805.
[370] Oppermann, R. & Binderberger, M. (1994) *Ann. Physik.* **3**, 494.
[371] Oppermann, R. & Mueller, A. (1993) *Nucl. Phys. B* **401**, 507.
[372] Oshikawa, M., Yamanaka, M. & Affleck, I. (1997) *Phys. Rev. Lett.*
       78, 1984.
[373] Oudenaarden, A. v. & Mooij, J. E. (1996) *Phys. Rev. Lett.* **76**, 4947.
[374] Parcollet, O, & Georges, A. (1997) *Phys. Rev. Lett.* **79**, 4665.
[375] Parcollet, O, & Georges, A. (1998) cond-mat/9806119.
[376] Parcollet, O., Georges, A., Kotliar, G. & Sengupta, A. M. (1998)
       Phys. Rev. B **58**, 3794.
[377] Pellegrini, V., Pinczuk, A., Dennis, B. S., Plaut, A. S., Pfeiffer, L. N.
       & West. K. W. (1997) *Phys. Rev. Lett.* **78**, 310.
[378] Pellegrini, V., Pinczuk, A., Dennis, B. S., Plaut, A. S., Pfeiffer, L. N.
       & West. K. W. (1998) *Science* **281**, 799.
[379] Pépin, C. & Lavagna, M. (1985) cond-mat/9803255.
[380] Perk, J. H. H. & Capel, H. W. (1977) *Physica A* **89**, 265.
[381] Perk, J. H. H., Capel, H. W., Quispel, G. R. W. & Nijhoff, F. W.
       (1984) *Physica A* **123**, 1.
[382] Pfeuty, P. (1970) *Ann. of Phys.* **57**, 79.
[383] Pich, C. & Young, A. P. (1988) cond-mat/9802108.
[384] Pickett, W. E. (1997) *Phys. Rev. Lett.* **79**, 1746.
[385] Pinczuk, A., Dennis, B. S., Heiman, D., Kallin, C., Brey, L.,
       Tejedor, C., Schmitt-Rink, S., Pfeiffer, L. N. & West, K. W. (1992)
       Phys. Rev. Lett. **68**, 3623.
[386] Pisarski, R. D. & Tytgat, M. (1997) *Phys. Rev. Lett.* **78**, 3622.
[387] Pohlmeyer, K. (1976) *Comm. Math. Phys.* **46**, 207.
[388] Poilblanc, D., Gagliano, E., Bacci, S. & Dagotto, E. (1991) *Phys.
       Rev. B* **43**, 10970.
[389] Polyakov, A. M. (1975) *Phys. Lett. B* **59**, 87.
[390] Polyakov, A. M. (1987) *Gauge Fields and Strings* (Harwood, London).
[391] Popov, V. N. (1972) *Teor. Mat. Phys.* **11**, 354.
[392] Popov, V. N. (1983) *Functional Integrals in Quantum Field Theory
       and Statistical Physics* (D. Reidel, Dordrecht).
[393] Prange, R. E. & Girvin, S. M. eds (1990) *The Quantum Hall Effect*
       (Springer-Verlag, New York).
[394] Rajaraman, R. (1982) *Solitons and Instantons: An Introduction to
       Solitons and Instantons in Quantum Field Theory* (North-Holland,

Amsterdam).

[395] Ramakrishnan, T. V. (1974) *Solid State Commun.* **14**, 449.

[396] Ramakrishnan, T. V. (1974) *Phys. Rev. B* **10**, 4014.

[397] Ramazashvili, R. & Coleman, P. (1997) *Phys. Rev. Lett.* **79**, 3752.

[398] Randeria, M., Sethna, J. P. & Palmer, R. G. (1985) *Phys. Rev. Lett.* **54**, 1321.

[399] Rasolt, M., Stephen, M. J., Fisher, M. E. & Weichman, P. B. (1984) *Phys. Rev. Lett.* **53**, 798.

[400] Read, N. & Sachdev, S. (1989) *Nucl. Phys. B* **316**, 609.

[401] Read, N. & Sachdev, S. (1989) *Phys. Rev. Lett.* **62**, 1694.

[402] Read, N. & Sachdev, S. (1990) *Phys. Rev. B* **42**, 4568.

[403] Read, N. & Sachdev, S. (1991) *Phys. Rev. Lett.* **66**, 1773.

[404] Read, N. & Sachdev, S. (1995) *Phys. Rev. Lett.* **75**, 3509.

[405] Read, N., Sachdev, S., and Ye, J. (1995) *Phys. Rev. B* **52**, 384.

[406] Reger, J. D. & Young, A. P. (1988) *Phys. Rev. B* **37**, 5978.

[407] Reppy, J. D. (1984) *Physica B* **126**, 335.

[408] Rieger, H. & Kawashima, N. (1998) cond-mat/9802104.

[409] Rieger, H. & Young, A. P. (1994) *Phys. Rev. Lett.* **72**, 4141.

[410] Rieger, H. & Young, A. P. (1996) *Phys. Rev. B* **54**, 3328.

[411] Rimberg, A. J., Ho, T. R., Kurdak, C., Clarke, J. Chapman, K. L. & Gossard, A. C. (1997) *Phys. Rev. Lett.* **78**, 2632.

[412] Rokhsar, D. & Kivelson, S. A. (1988) *Phys. Rev. Lett.* **61**, 2376.

[413] Roger, M., Bäuerle, C., Bunkov, Y. M., Chen, A. S. & Godfrin, H. (1998) *Phys. Rev. Lett.* **80**, 1308.

[414] Rönnow, H. M., McMorrow, D. F. & Harrison, A. cond-mat/9806286.

[415] Rosch, A., Schröder, A., Stockert, O. & von Löhneysen, H. (1997) *Phys. Rev. Lett.* **79**, 159.

[416] Rosenow, B. & Oppermann, R. (1996) *Phys. Rev. Lett.* **77**, 1608.

[417] Rozenberg, M. J. & Grempel, D. R. (1998) cond-mat/9802106.

[418] Rudnick, J., Guo, H. & Jasnow, D. (1985) *J. Stat. Phys.* **41**, 353.

[419] Sachdev, S. (1992) *Phys. Rev. B.* **45**, 12377.

[420] Sachdev, S. (1994) *Phys. Rev. B* **49**, 6770.

[421] Sachdev, S. (1994) *Phys. Rev. B* **50**, 13006.

[422] Sachdev, S. (1994) *Z. Phys. B* **94**, 469.

[423] Sachdev, S. (1995) in *Low dimensional quantum field theories for condensed matter physicists*, edited by Yu Lu, S. Lundqvist and G. Morandi, (World Scientific, Singapore); cond-mat/9303014

[424] Sachdev, S. (1996) in *Proceedings of the 19th IUPAP International Conference on Statistical Physics, Xiamen, China*, edited by B.-L. Hao, (World Scientific, Singapore); cond-mat/9508080.

[425] Sachdev, S. (1996) *Nucl. Phys. B* **464**, 576.

[426] Sachdev, S. (1997) in *Strongly Correlated Magnetic and Superconducting Systems*, edited by G. Sierra and M. A. Martin-Delgado (Springer Verlag, Berlin).

[427] Sachdev, S. (1997) *Phys. Rev. B* **55**, 142.

[428] Sachdev, S. (1998) *Phil. Trans. R. Soc. Lond.* A **356**, 173.

[429] Sachdev, S. (1998) in *Dynamical Properties of Unconventional Magnetic Systems*, NATO ASI Series E: Applied Sciences, Vol. 349, edited by A. Skjeltorp and D. Sherrington (Kluwer Academic, Dordrecht); cond-mat/9705266.

[430] Sachdev, S. (1998) *Phys. Rev. B* **57**, 7157.

[431] Sachdev, S. (1998) cond-mat/xxxxxxx.

[432] Sachdev, S., Chubukov, A. V. & Sokol, A. *Phys. Rev. B*

[433] Sachdev, S. & Damle, K. (1997) *Phys. Rev. Lett.* **78**, 943.

[434] Sachdev, S. & Georges, A. (1995) *Phys. Rev. B* **52**, 9520.

[435] Sachdev, S. & Jalabert, R. (1990) *Mod. Phys. Lett.* **B4**, 1043.

[436] Sachdev, S. & Read, N. (1991) *Int. J. Mod. Phys. B* **5**, 219.

[437] Sachdev, S., Read, N. & Oppermann, R. (1995) *Phys. Rev. B* **52**, 10286.

[438] Sachdev, S. & Senthil, T. (1996) *Ann. Phys.* **251**, 76.

[439] Sachdev, S., Senthil, T. & Shankar, R. (1994) *Phys. Rev. B* **50**, 258.

[440] Sachdev, S. & Ye, J. (1992) *Phys. Rev. Lett.* **69**, 2411.

[441] Sachdev, S. & Ye, J. (1993) *Phys. Rev. Lett.* **70**, 3339.

[442] Sachdev, S. & Young, A. P. (1997) *Phys. Rev. Lett.* **78**, 2220.

[443] Sandvik, A. W. & Scalapino, D. J. (1994) *Phys. Rev. Lett.* **72**, 2777.

[444] Sandvik, A. W., Chubukov, A. V. & Sachdev, S. (1995) *Phys. Rev. B* **51**, 16483.

[445] Sawada, A., Ezawa, Z. F., Ohno, H., Horikoshi, Y., Ohno, Y., Kishimoto, S., Matsukura, F., Yasumoto, M., Urayama, A. (1998) *Phys. Rev. Lett.* **80**, 4534.

[446] Scalettar, R. T., Trivedi, N. & Huscroft, C. (1998) cond-mat/9807008.

[447] Schröder, A., Aeppli, G., Bucher, E., Ramazashvili, R. & Coleman, P. (1998) *Phys. Rev. Lett.* **80**, 5623.

[448] Schulz, H. J. (1986) *Phys. Rev. B* **34**, 6372.

[449] Schulz, H. J. (1995) in *Mesoscopic Quantum Physics, Les Houches Summer School Proceedings, Vol 61* edited by E. Akkermans, G. Montambaux, J. Pichard, and J. Zinn–Justin (North-Holland, Amsterdam)

[450] Schulz, H. J. & Ziman, T. A. L. (1992) *Europhys. Lett.* **18**, 355.

[451] Schulz, H. J., Ziman, T. A. L. & Poilblanc, D. (1996) *J. Physique I* **6**, 675.

[452] Sengupta, A. M. (1997) cond-mat/9707316.

[453] Sengupta, A. M. & Georges, A. (1995) *Phys. Rev. B* **52**, 10295.

[454] Senthil, T. & Majumdar, S. (1996) *Phys. Rev. Lett.* **76**, 3001.

[455] Senthil, T. & Sachdev, S. (1996) *Phys. Rev. Lett.* **77**, 5295.

[456] Shankar, R. (1994) *Principles of Quantum Mechanics*, 2nd ed. (Plenum, New York).

[457] Shankar, R. (1994) *Rev. Mod. Phys.* **66**, 129.

[458] Shankar, R. & Murthy, G. (1987) *Phys. Rev. B* **36**, 536.

[459] Shankar, R. & Read, N. (1990) *Nucl. Phys. B* **336**, 457.

[460] Shastry, B. S. & Sutherland, B. (1981) *Phys. Rev. Lett.* **47**, 964.

[461] Shastry, B. S. & Sutherland, B. (1981) *Physica* **108B**, 1069.

[462] Shenker, S. H. & Tobochnik, J. (1980) *Phys. Rev. B* **22**, 4462.

[463] Shiramura, W., Takatsu, K., Kurniawan, B., Tanaka, H., Uekusa, H., Ohashi, Y., Takizawa, K., Mitamura, H. & Goto, T. (1998) *J. Phys. Soc. Jpn.* **67**, 1548.

[464] Singh, K. K. (1975) *Phys. Rev. B* **12**, 2819.

[465] Singh, K. K. (1978) *Phys. Rev. B* **17**, 324.

[466] Singh, S. & Pathria, R. K. (1985) *Phys. Rev. B* **31**, 4483.

[467] Sokol, A., Glenister, R. L. & Singh, R. R. P. (1994) *Phys. Rev. Lett.* **72**, 1549.

[468] Sondhi, S. L., Karlhede, A., Kivelson, S. A. & Rezayi, E. H. (1993) *Phys. Rev. B* **47**, 16419.

[469] Sondhi, S. L., Girvin, S. M., Carini, J. P. & Shahar, D. (1997) *Rev. Mod. Phys.* **69**, 315.

[470] Sorensen, E. S. & Affleck, I. (1993) *Phys. Rev. Lett.* **71**, 1633.

[471] Sorensen, E. S. & Roddick, E. (1995) *Phys. Rev. B* **53**, 8867.

[472] Sorensen, E. S., Wallin, M., Girvin, S. M. & Young, A. P. (1992) *Phys. Rev. Lett.* **69**, 828.

[473] Stanley, H. E. (1968) *Phys. Rev.* **176**, 718.

[474] Starykh, O. A., Singh, R. R. P. & Sandvik, A. W. (1997) *Phys. Rev. Lett.* **78** 539.

[475] Starykh, O. A., Sandvik, A. W. & Singh, R. R. P. (1997) *Phys. Rev. B* **55** 14953.

[476] Stauffer, D. & Aharony, A. (1992) *Introduction to Percolation Theory* (Taylor and Francis, New York).

[477] Steglich, F., Buschinger, B., Gegenwart, P., Lohmann, M., Helfrich, R., Langhammer, C., Hellmann, P., Donnevert, L., Thomas, S., Link, A., Geibel, C., Lang, M., Sparn, G. & Assmus, W. (1996) *J. Phys. Cond. Matt.* **8**, 9909.

[478] Stinchcombe, R. B. (1981) *J. Phys. C* **14**, L263.

[479] Stockert, O., von Löhneysen, H., Rosch, A., Pyka, N. & Loewenhaupt, M. (1998) *Phys. Rev. Lett.* **80**, 5627.

[480] Stone, M. ed. (1994) *Bosonization* (World Scientific, Singapore).

[481] Stoner, E. C. (1936) *Proc. Roy. Soc. London A* **154**, 656.

[482] Strongin, M., Thompson, R. S., Kammerer, O. F. & Crow, J. E. (1970) *Phys. Rev. B* **1**, 1078.

[483] Suzuki, M. (1976) *Prog. Theor. Phys.* **56**, 1454.

[484] Takahashi, M., Nakamura, H. & Sachdev, S. (1996) *Phys. Rev. B* **54**, R744.

[485] Takigawa, M., Asano, T., Ajiro, Y., Mekata, M. & Uemura, Y. J. (1996) *Phys. Rev. Lett.* **76**, 2173.

[486] Takigawa, M., Starykh, O. A., Sandvik, A. W. & Singh, R. R. P. (1997) *Phys. Rev. B* **56** 13681.

[487] Taniguchi, S., Nishikawa, T., Yasui, Y., Kobayashi, Y., Sato, M., Nishioka, T., Kotani, M. & Sano, K. (1995) *J. Phys. Soc. Jpn.* **64**, (1995).

[488] Taylor, J. R. (1972) *Scattering Theory: the quantum theory of non-relativistic collisions* (Wiley, New York).

[489] Thill, M. J. & Huse, D. A. (1995) *Physica* **A15**, 321.

[490] Thompson, C. J . (1972) in *Phase Transitions and Critical Phenomena* , **1**, edited by C. Domb and M.S. Green (Academic Press, London).

[491] Timm, C., Girvin, S. M., Henelius, P. & Sandvik, A. W. (1998) *Phys. Rev. B* **58**, 1464.

[492] Tomonaga, S. (1950) *Prog. Theor. Phys.* **5**, 544.

[493] Tranquada, J. M., Shirane, G., Keimer, B., Shamoto, S. & Sato, M. (1989) *Phys. Rev. B* **40**, 4503.

[494] Tranquada, J. M., Shirane, G., Keimer, B., Shamoto, S. & Sato, M. (1992) *Phys. Rev. B* **46**, 5561.

[495] Tranquada, J. M., Axe, J. D., Ichikawa, N., Moodenbaugh, A. R. Nakamura, Y. & Uchida, S. (1997) *Phys. Rev. Lett.* **78**, 338.

464 *References*

[496] Trivedi, N., Scalettar, R. T. & Randeria, M. (1996) *Phys. Rev. B* **54**, 3756.
[497] Troyer, M., Imada, M. & Ueda, K. (1997) *J. Phys. Soc. Jpn.* **66**, 2957.
[498] Troyer, M. & Sachdev, S. (1998) cond-mat/9807393.
[499] Troyer, M., Tsunetsugu, H. & Rice, T. M. (1996) *Phys. Rev. B* **53**, 251.
[500] Troyer, M., Zhitomirsky, M. E. & Ueda, K. (1997) *Phys. Rev. B* **55**, R6117.
[501] Tsvelik, A. M. (1987) *Zh. Eksp. Teor. Fiz.* **93**, 385. (*Sov. Phys. JETP* **66**, 221).
[502] Tsvelik, A. M. (1990) *Phys. Rev. B* **42**, 10499.
[503] Tsvelik, A. M. (1996) *Quantum Field Theory in Condensed Matter Physics* (Cambridge University Press, Cambridge).
[504] Tsvelik, A. M. & Reizer, M. (1993) *Phys. Rev. B* **48**, 9887.
[505] Tworzydlo, J., Osman, O. Y., van Duin, C. N. A. & Zaanen, J. (1998) cond-mat/9804012.
[506] Tworzydlo, J., van Duin, C. N. A. & Zaanen, J. (1998) cond-mat/9808034.
[507] Tyc, S., Halperin, B. I. & Chakravarty, S. (1989) *Phys. Rev. Lett* **62**, 835.
[508] Tyc, S. & Halperin, B. I. (1990) *Phys. Rev. B* **42**, 2096.
[509] Usadel, K. D., Büttner, G. & Kopeć, T. K. (1991) *Phys. Rev. B* **44**, 12583.
[510] Varma, C. M., Littlewood, P. B., Schmitt-Rink, S., Abrahams, E. & Ruckenstein, A. E. (1989) *Phys. Rev. Lett.* **63**, 1996.
[511] Varma, C. M. (1997) *Phys. Rev. B* **55**, 14554.
[512] van Duin, C. N. A. & Zaanen, J. (1998) *Phys. Rev. Lett.* **80**, 1513.
[513] van Otterlo, A. & Wagenblast, K.-H. (1994) *Phys. Rev. Lett.* **72**, 3598.
[514] van Otterlo, A., Wagenblast, K.-H., Baltin, R., Bruder, C. Fazio, R. & Schön, G. (1995) *Phys. Rev. B* **52**, 16176.
[515] van Otterlo, A., Wagenblast, K.-H., Fazio, R. & Schön, G. (1993) *Phys. Rev. B* **48**, 3316.
[516] von Delft, J., Ralph, D. C., Buhrman, R. A., Upadhyay, S. K., Louie, R. N., Ludwig, A. W. W. & Ambegaokar, V. (1998) *Ann. Phys.* **263**, 1.
[517] von Löhneysen, H., Neubert, A., Schröder, A., Stockert, O., Tutsch, U., Loewenhaupt, M., Rosch, A. & Wolfle, P. (1998) cond-mat/9802222.
[518] Villain, J. (1975) *Physica* **79B**, 1.
[519] Vojta, T., Belitz, D., Narayanan, R. & Kirkpatrick, T. R. (1997) *Z. Phys. B* **103**, 451.
[520] Voss, D. (1998) *Science* **282**, 221.
[521] Wagenblast, K.-H., van Otterlo, A., Schön, G. & Zimanyi, G. T. (1997) *Phys. Rev. Lett.* **79**, 2730.
[522] Waldtmann, Ch., Everts, H.-U. Bernu, B., Sindzingre, P., Lhuillier, C., Lecheminant, P. & Pierre, L. (1998) cond-mat/9802168.
[523] Wallin, M., Sorensen, E. S., Girvin, S. M. & Young, A. P. (1994) *Phys. Rev. B* **49**, 12115.
[524] Weichman, P. B., Rasolt, M., Fisher, M. E. & Stephen, M. J. (1986) *Phys. Rev. B* **33**, 4632.

[525] Weiss, U. (1993) *Quantum Dissipative Systems* (World Scientific, Singapore).

[526] Wen, X. G., Wilczek, F. & Zee, A. (1989) *Phys. Rev. B* **39**, 11413.

[527] Wen, X. G. & Zee, A. (1990) *Int. J. Mod. Phys. B* **4**, 437.

[528] Westerberg, E., Furusaki, A., Sigrist, M. & Lee P. A. (1997) *Phys. Rev. B* **55**, 12578.

[529] Witten, E. (1979) *Nucl Phys B* **149**, 285.

[530] Wu, W., Ellman, B., Rosenbaum, T. F., Aeppli, G. & Reich, D. H. (1991) *Phys. Rev. Lett.* **67**, 2076.

[531] Wu, W., Bitko, D., Rosenbaum, T. F. & Aeppli, G. (1993) *Phys. Rev. Lett.* **71**, 1919.

[532] Xu, G., DiTusa, J. F., Ito, T., Oka, K., Takagi, H., Broholm, C. & Aeppli, G. (1996) *Phys. Rev. B* **54**, R6827.

[533] Ye, J. (1998) *Phys. Rev. B* **58**, 9450.

[534] Ye, J. & Sachdev, S. (1998) *Phys. Rev. Lett.* **80**, 5409.

[535] Ye, J., Sachdev, S. & Read, N. (1993) *Phys. Rev. Lett.* **70**, 4011

[536] Yoshizawa, H., Hirakawa, K., Satija, S. K. & Shirane, G. (1981) *Phys. Rev. B* **23**, 2298.

[537] Young, A. P. (1975) *J. Phys. C* **8**, L309.

[538] Young, A. P. (1997) *Phys. Rev. B* **56**, 11691.

[539] Young, A. P. ed. (1997) *Spin Glasses and Random Fields* (World Scientific, Singapore).

[540] Young, A. P. & Rieger, H. (1996) *Phys. Rev. B* **53**, 8486.

[541] Zaanen, J. (1998) *J. Phys. Chem. Solids* xxxxx.

[542] Zaanen, J. & van Saarloos, W. (1997) *Physica C* **282-287**, 178.

[543] Zamolodchikov, A. B. & Zamolodchikov, A. B. (1979) *Ann. of Phys.* **120**, 253.

[544] Zamolodchikov, A. B. & Zamolodchikov, A. B. (1992) *Nucl. Phys. B* **379**, 602.

[545] Zhang, S.-C. (1997) *Science* **275**, 1089.

[546] Zheng, L., Radtke, R. J. & Das Sarma, S. (1997) *Phys. Rev. Lett.* **78**, 2453.

[547] Zheng, W. & Sachdev, S. (1989) *Phys. Rev. B* **40**, 2704.

[548] Zhitomirsky, M. E. & Ueda, K. (1996) *Phys. Rev. B* **54**, 9007.

[549] Zimanyi, G. T., Crowell, P. A., Scalettar, R. T. & Batrouni, G. G. (1994) *Phys. Rev. B* **50**, 6515.

[550] Zinn-Justin, J. (1993) *Quantum Field Theory and Critical Phenomena* (Oxford University Press, Oxford).

[551] Zülicke, U. & Millis, A. J. (1995) *Phys. Rev. B* **51**, 8996.

Index